生体分子エンジン素過程の
高速顕微画像解析システムの開発

(研究課題番号　07558227)

平成７年度～平成９年度科学研究費補助金（基盤研究Ａ(2)）

研究成果報告書

平成１０年８月

研究代表者　石　渡　信　一

(早稲田大学理工学部物理学科教授)

はしがき

この報告書は、平成７年度から９年度にわたる３年間で行われた文部省科学研究費基盤研究Ａ２「生体分子エンジン素過程（を研究するための高速顕微画像解析システムの開発」（課題番号０７５５８２２７）の研究成果をまとめたものである。本研究で組み上げた顕微操作・解析装置は、平成８年度と９年度の２年間にわたって並行して行われた文部省科学研究費基盤研究Ｂ２「タンパク質間相互作用の一分子くり返し計測」（課題番号０８４５８２１３）においても活用された。従って本報告書では、そこで得られた研究成果も、併せて記載してある。

本研究の目的を大別すると、

１）　高速撮影・光学顕微鏡デジタル画像処理システムの開発

２）　このシステムに適した生体分子エンジンとその集合体における化学・力学過程実験系の開発

の２つである。１）については装置の基本デザインと試作を主として浜松ホトニクス（株）が行い、２）については早稲田大学において行った。

本研究を通じて得られた成果のほとんどは、口頭発表では公表したが、論文としては未だ準備中の段階にある。それらの主な内容は、「研究成果の概要」としてまとめた。今後、論文として逐一刊行する予定である。

なお本研究は、当研究室の西坂崇之（D3,PDF：現、CREST)、加藤宏一（M2：現、日立基礎研)、藤田英明（現、D3)、伊賀隆志（M2：現、日本ゼオン)、藤木保武（M2：現、王子製紙)、進泉（M2：現、ホロン)、多田隈尚史（現、D2)、新藤嘉明（M2：現、王子製紙)、堀田正幸（M2：現、味の素)、岡部治美（M2：現、東京電力)、高橋真（M2：現、東レ)、寺田尚史（M2：現、ＨＰ社)、川口憲治（現、M2)、齋藤素子（現、M2)、熊木雄一（現、M2)、藤原郁子（現、M1)、増川一（B4卒)、藤田尚（D3,シドニー大：現、山本特許事務所)、福田紀男（現、慈恵医大)、安田賢二（現、日立基礎研）の諸君を中心に行われた。フラッシュ・フォトリシス法については堀内桂輔氏（大分医大）にお世話になった。金属基盤上での分子配向については、佐々木裕次、安田賢二（日立基礎研）両氏と共同研究を行った。微小管、キネシン系の扱いについては、豊島陽子（東大)、神谷律（東大）研究室の方々に相談にのっていただいた。また、慶應義塾大学・理工学部・物理学科の木下一彦研究室とは常日頃からの研究交流を通じて、様々な面でお世話になった。記して感謝します。

平成１０年８月　　研究代表者　　石渡　信一

研　究　組　織

研究代表者

石渡　信一　（早稲田大学・理工学部・物理学科・教授）

研究分担者

伊藤　博康　（浜松ホトニクス（株））

研　究　経　費

平成７年度	９，５００千円
平成８年度	２，７００千円
平成９年度	２，５００千円
計	１４，７００千円

研究業績

研究成果の概要

1）超高感度高速カメラの開発：浜松ホトニクス（株）に依頼し、超高感度高速カメラ（時間分解能 2ms）が開発され、市販品として供給された（製品名：ARGUS/HiSCA）。我々はこれを分子モーターの１分子顕微解析に適したシステムとし、分子モーターの力学・熱力学１分子特性や、筋原線維の収縮・振動のダイナミクスに関する研究に応用した。この研究は、現在も継続されている。

2）温度パルス顕微鏡（ＴＰＭ）法の開発：我々の開発した温度パルス顕微鏡（TPM）法には、光学顕微鏡の試料面上に撒かれた金属粉末の塊（5μm 程度の大きさ）に赤外レーザー光を照射し、これを熱源として直径数十μm にわたって同心円状の温度分布を得る「金属粉末法（下図)」と、ガラス表面上に直径 10μm の円状に蒸着したアルミ金属面を熱源とする「金属蒸着法」との２種類がある。温度の空間分布と時間変化は、アクチンフィラメントに結合した蛍光物質 rhodamine-phalloidin の蛍光強度が温度上昇に伴って減少する性質（熱消光）を画像化することによって行った。この結果、１本のアクチンフィラメント上の温度分布を画像化することができ、約２℃/μm の温度勾配を、「金属粉末法」の場合には 6ms の立ち上がり・立ち下がり時間で可逆的に作り出すことが出来るようになった。「金属蒸着法」は温度分布の再現性は高いが、温度変化の緩和時間は数十 ms と遅かった。TPM 法の最大の長所は、短時間の可逆的な温度上昇と下降が出来ることにある。そのことによって、分子機能が熱変性する前に、通常法では得られないような高温における分子機能を研究することが出来ることである。

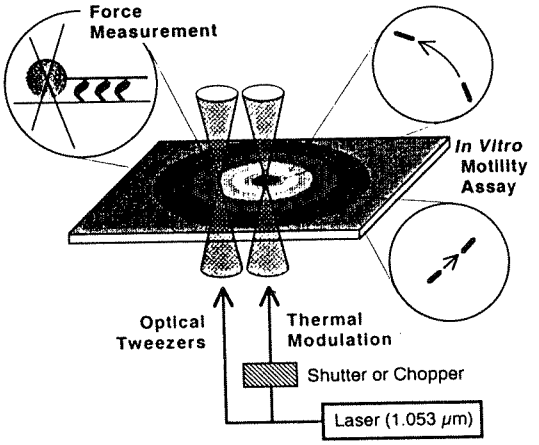

3）ＴＰＭ法によるミオシン分子モーター機能の熱変調・熱励起：「金属粉末法」を用いて，HMM分子上でのアクチンフィラメントの滑り運動速度と滑り力の温度依存性を研究した。その結果、温度上昇に約 6ms 遅れて滑り運動が始まることが分かった。さらに、18℃から約 45℃への温度上昇に伴って、滑り速度は約 4μm/s から約 30μm/s へと可逆的に上昇することが分かった。滑り力も同様に約７倍に上昇した。これらは通常用いられているイオン環境下（25mM KCl）で計測されたが、50mM KCl 存在下では、滑り速度は筋肉から精製したミオシン分子モーターとしては最高の 50μm/s（約 45℃）を記録した。

4）ＴＰＭ法によるキネシン分子モーター機能の熱変調・熱励起：TPM 法を、微小管ーキネシン系に応用した。まずキネシン分子をガラス表面に吸着させ、ATP 存在下で、そのガラス表面上における微小管の滑り運動を観察した。18℃から約 40℃に上昇すると、微小管の滑り速度は約 0.4μ m/s から約 4.0μ m/s へと上昇した。ところでキネシン分子の場合には、一分子での滑り機能を解析することが出来る。プラスチックビーズの表面にキネシン分子を吸着し、ガラス基板に結合した微小管の上でビーズの滑り運動を行わせるのである。その結果、キネシン一分子でも、上の結果と同程度に熱励起されることが確認された。この研究の過程で、キネシン分子の滑り運動機能が熱に対して弱い（高温にさらすと、滑り運動速度が不可逆的に減少する）ことが分かった。従って、キネシン分子モーター機能の熱変調・熱励起の研究にとって TPM 法は最適である。

5）「最小筋肉」システムの開発： 1 分子レベルの研究を進める一方で、我々は筋収縮系の構造と機能を明らかにする目的で、「最小筋肉」系を開発した。それはミオシンフィラメントの束（A 帯）という、横紋筋の筋節構造を保ったものの中を、一本のアクチンフィラメントが滑り運動する実験系である（下図左)。この実験系でアクチンフィラメントに発生する張力とその揺らぎを、イオン強度を（25-150mM）mM KCl と変化させて計測したところ、同じ張力レベルのときには、イオン強度が高いほど張力揺らぎの幅が大きかった。また、この実験系でクロスブリッジ 1 個あたりに発生する張力は、約 1pN であった（下図右)。この実験系はいわゆる in vitro 滑り運動系とは異なって、筋収縮系本来の 3 次元的なフィラメント集合構造を保持しており、生理的な収縮機能を備えた最小のシステムだということが言える。今後はこの実験系を、従来からの筋生理学と 1 分子生理学とを繋ぐ実験系として育てたい。

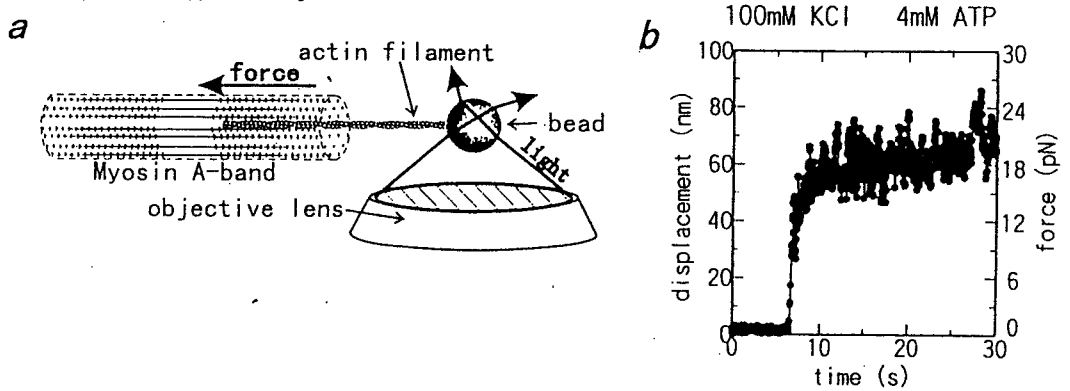

6）単一筋原線維の、caged ATP による張力発生の初期過程高速画像化：ガラス微小針にその両端を保持した単一（骨格筋）筋原線維の、硬直状態から収縮状態に至る力発生の時間経過を、caged ATP 存在下でのフラッシュ・フォトリシス法を用いて室温と低温とで比較検討した。張力の発生と、それに伴う筋節の形態変化の時間経過については、高速カメラを用いて計測・画像化した。その結果、低温では筋節構造を乱すことなく張力が発生するが、その際一過的に張力が減少する（弛緩する）相が存在することを見いだした。

7）アクチンフィラメント・ミオシン分子間結合の破断力：アクチンフィラメントの後端に結合した直径 1μm のポリスチレンビーズを、レーザー光ピンセットによって顕微操作し、アクチンフィラメントとアクチン結合性タンパク質との間の分子間結合に一定の負荷を加え、結合の破断力などを繰り返し顕微計測することができる方法を、この数年の研究によって確立した。この方法を用いて、ATP 非存在下におけるアクチンフィラメントとHMM（双頭または単頭の HMM、あるいは S1）分子の硬直結合について、破断力の１分子計測を行った。その結果、単頭HMMの破断力の分布は約 7pN にピークを持つのに対して、双頭 HMM では数 pN から 20pN にわたって広く分布し、7pN と 10 数 pN とに２つのピークを持った。即ち、アクチン・ HMM 分子の結合破断力は、単頭と双頭とで約２倍異なっていた。

8）アクチンフィラメント・ミオシン分子間硬直結合の寿命：無負荷で熱平衡の状態にあるアクチンフィラメント・ミオシン分子間の硬直結合の寿命について、単頭 HMM 分子と双頭 HMM 分子、それにＳ１分子について比較検討した。非常にまばらにミオシン分子をガラス表面に吸着し、それに一点で結合したアクチンフィラメント（一点で結合しているかどうかは、アクチンフィラメントがその点の周りで旋回ブラウン運動するかどうかで判定した）が時間的に解離していく様子を観察・計測した。その結果、硬直結合の平均寿命は、双頭 HMM 分子の場合には 1000 数百秒であるのに対して、単頭 HMM 分子とＳ１分子の場合には約 100 秒であった。これは溶液系の実験で得られていた値にほぼ一致する。

9）アクチンフィラメント・ミオシン分子間硬直結合の寿命に対する負荷の影響：アクチン・ミオシン分子（S1、HMM）間の硬直結合に対して、光ピンセットを用いて瞬時に（ビデオレート内に）一定の負荷を加え、結合の寿命を１分子ごとに計測した（下図Ａ；２つの矢印の間の時間を計測)。こうして多数の分子についてデータを集めた（下図Ｂ；60s の点線上のデータは、負荷を加えてから 60s 以内には結合が解離しなかったものを表す；▼は HMM 分子、◇印は S1 分子)。

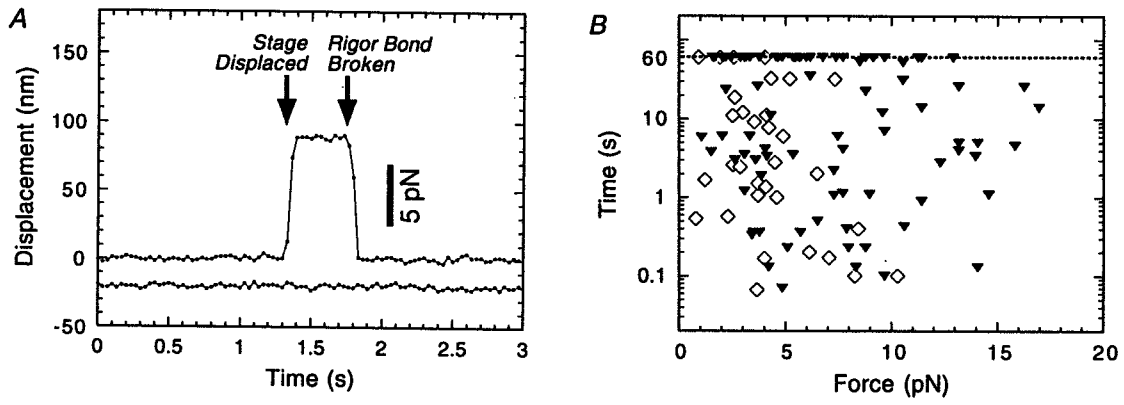

解析の結果、右下図のように、結合寿命τと負荷Fの関係が得られた。S1（◆印）については1つの指数関数τ(F) = τ(0)exp(-Fd/kT)で表されたが(dは相互作用距離で約3nm)、HMMの場合にはτ(F) = τ_1(0)exp(-Fd_1/kT)（▲印）+τ_2(0)exp(-Fd_2/kT)（▼印）と、2つの指数関数の和で表された（d_1とd_2は相互作用距離で2と3nmと見積もられた。kとTは、それぞれボルツマン定数と絶対温度である)。そしてこの関係から得られたτ_1(0)とτ_2(0)はそれぞれ約1000数百秒と約100秒となり、無負荷のときの双頭結合と単頭結合の寿命に対応した。これらのことから、単頭結合と双頭結合との識別が可能になった。

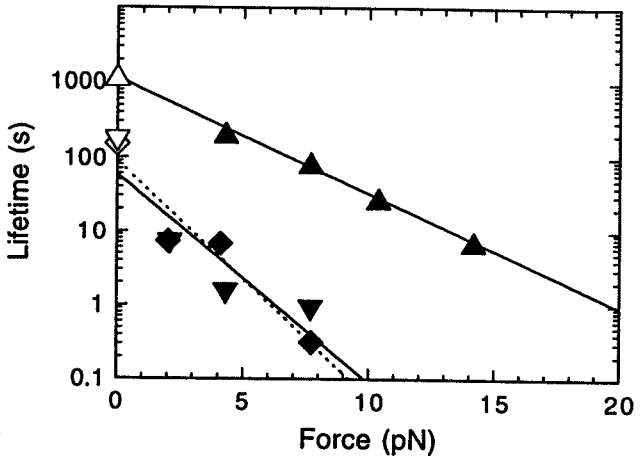

１０）HMM 分子の捻れ弾性率：HMM 1分子に硬直結合したアクチンフィラメントの旋回運動を通して見積もったHMM分子の捻れ弾性率は、平均で$2x10^{-22}$Nm/radであった。この値は、単頭HMMに比べて小さかった。ところが、双頭HMMの場合には旋回運動に幾つもの平衡角（互いに約2π離れた）が存在するように見え、各平衡角の周りで見積もった弾性率は、単頭HMMのものとほぼ一致した。即ち、双頭HMMの場合には、双頭結合（数十秒）→単頭結合（数秒）→双頭結合（数十秒）のように結合様式を変え、結合アクチンフィラメントの平衡角を変化させているように見えた。これは、アクチンフィラメント上でのミオシン分子モーターの滑り運動の様式を解明する上で、示唆に富んだ現象であると期待される。

１１）微小管・キネシン分子間結合の破断力：直径1μmのプラスチックビーズの表面にキネシン分子を共有結合し、ガラス表面上に吸着した微小管にATP非存在下で結合させ、その結合の破断力をビーズを光ピンセットで操作することによって計測した。その結果、10pN程度の破断力が計測された。この値は、アクチンフィラメントーHMM分子間硬直結合の破断力とほぼ同じである。さらに予備実験によって、破断力に方向依存性があるという結果も得られており、キネシン分子の運動性との関連を検討している。

１２）アクチンフィラメント・スペクトリン分子間結合の破断力：赤血球から調製したスペクトリン分子をHMM分子と同様にガラス表面上に吸着させ、アクチンフィラメントとの結合の破断力を1分子計測した。その結果、予備的実験ではあるが、平均3pNという値を得た。これは、アクチン・ミオシン間の硬直結合力（平均9pN）や、アクチンフィラメントとαアクチニンとの結合力（15pN）などと比べて有意に小さい。

研　究　発　表

1．学会誌等

1)Nishizaka,T., Miyata,T., Yoshikawa,H., Ishiwata.S. and Kinosita,Jr.,K. (1995) : *Biophys.J.* 68, 75s.
"Mechanical properties of a single protein motor of muscle studied by optical tweezers."

2)Miyata,T., Hakozaki,H., Yoshikawa,H., Suzuki,N., Furuno,T., Ikegami,A., Kinosita,Jr., K., Nishizaka,T. and Ishiwata,S.(1995) : *Biophys.J.* 68, 286s-290s.
"Mechanical measurements of single actomyosin motor force."

3)石渡信一(1995) : *BME* 9, No.5, 12-20.
" 筋収縮系の力学特性"

4)Nishizaka,T., Miyata,H., Yoshikawa,H., Ishiwata,S. and Kinosita,Jr.,K. (1995) : *Nature* 377, 251-254.
"Unbinding force of a single motor molecule of muscle measured using optical tweezers."

5)Suzuki,N., Miyata,H., Ishiwata,S. and Kinosita,Jr.,K. (1996) : *Biophys.J.* 70, 401-408:
"Preparation of bead-tailed actin filaments: Estimation of the torque produced by the sliding force in an in vitro motility assay."

6)西坂崇之、石渡信一 (1996) : *生物物理* 36, 15-19.
" 分子モーターの力学・ 機能特性を見る"

7)Yasuda,K., Shindo,Y. and Ishiwata,S. (1996) : *Biophys.J.* 70, 1823-1829.
"Synchronous behavior of spontaneous oscillations of sarcomeres in skeletal myofibrils under isotonic conditions."

8)Ishiwata,S., Yasuda,K., Shindo,Y. and Fujita,H. (1996) : *Adv.Biophys.* 33, 135-142.

"Microscopic analysis of the elastic properties of connectin/titin and nebulin in myofibrils.

9)Fujisaki,H., Takahashi,S., Ohzeki,H., Sugisaki,K., Kondo,H., Nagata,H., Kato,H. and Ishiwata,S.(1996) : *J.Microscopy* 182,79-84.
"Soft-X-ray damage to biological samples."

10)Moriyama,Y., Yasuda,K., Ishiwata,S. and Asai,H. (1996) :
Cell Motil.Cytoskel. 34,271-278.
"Ca^{2+}-induced tension development in the stalks of glycerinated Vorticella convallaria."

11)Fujita,H., Yasuda,K., Niitsu,S., Funatsu,T. and Ishiwata,S. (1996) :
Biophys.J. 71,2307-2318.
"Structural and functional reconstitution of thin filaments in the contractile apparatus of cardiac muscle."

12)Fukuda,N., Fujita,H., Fujita,T. and Ishiwata,S. (1996) : *Pflug.Arch.* 433, 1-8.
"Spontaneous tension oscillation in skinned bovine cardiac muscle."

13)Ishiwata,S., Nishizaka,T., Kato,H., Tadakuma,H., Iga,T., Suzuki,N., Miyata,H. and Kinosita,Jr.,K. (1996) : *Neurochem.(Moscow)* 13, 305-313.
"Microscopic analysis of the nature of forces in a single actomyosin motor and its assemblage."

14)Sasaki,Y.C.,Yasuda,K.,Suzuki,Y.,Ishibashi,T.,Satoh,I.,Fujiki,Y.and Ishiwata,S.(1997) : *Biophys.J.* 72, 1842-1848.
"Two-dimensional arrangement of a functional protein by cysteine-gold substrate interaction: Enzyme activity and characterization of a protein monolayer on a gold substrate."

15)石渡信一 (1997) : *ポリファイル* 34, 25-29.
" 生体系材料の分子シンクロナイゼーション"

16)Sase,I., Miyata,H., Ishiwata,S. and Kinosita,Jr.,K. (1997) :
Proc.Natl.Acad.Sci.U.S.A. 94, 5646-5650.

"Axial rotation of sliding actin filaments revealed by single-fluorophore imaging."

17)Ishiwata,S., Miki,M., Shin,I., Funatsu,T., Yasuda,K. and dos Remedios,C.G. (1997) : *Biophys.J.* 73, 895-904.
"Inter-head distances in myosin attached to F-actin estimated by fluorescence energy transfer spectroscopy."

18)石渡信一 (1998) : *科学* 68, 110-113.
" 心筋の収縮と超分子の自己組織化ー化学振動から生物リズムへ2"

19)Kinosita,Jr.,K., Yasuda,R., Noji,H., Ishiwata,S. and Yoshida,M.(1998) : *Cell* 93,21-24.
"F_1-ATPase : A rotary motor made of a single molecule."

20)Fujita,H. and Ishiwata,S. : *Biophys.J.*75: in press. "Spontaneous oscillatory contraction without regulatory proteins in actin filament-reconstituted fibers."

21)Fukuda,N., Fujita,H., Fujita,T. and Ishiwata,S : *J.Muscle Res.Cell Motil.* in press. "Regulatory roles of MgADP and calcium in tension development of skinned cardiac muscle."

22)Suzuki,K., Tanaka,Y., Nakajima,Y., Hirano,K., Itoh,H., Miyata,H., Hayakawa,T. & Kinosita,Jr.,K. (1995) : *Biophys.J.* 68, 739-748.
"Spatiotemporal relationships among early events of fertilization in sea urchin eggs revealed by multiview microscopy"

23)Itoh,H., Ishido,S., Nomura,M., Hayakawa,T. & Mitaku,S.(1996) :
J. Phys.Chem. 100, 21, 9047-9053
"Estimation of the hydrophobicity in microenvironments by pyrene fluorescence measurements : n-β-octylglucoside micelles"

24)Akashi,K., Miyata,H., Itoh, H. & Kinosita,Jr.,K.(1996) : *Biophys.J.* 71, 3242-3250.
"Preparation of giant liposomes in physiological conditions and their characterization under an optical microscope"

25)Itoh,H., Evenzahav,A.,Kinoshita,K., Inagaki,Y., Mizushima,H., Takahashi,A.,

Hayakawa,T. & Kinosita,Jr.,K.(1997) : *SPIE* 2979, 733-740.
"Use of a gain modulating framing camera for time-resolved imaging of cellular phenomena"

26)Itoh,H., Evenzahav,A., Kinoshita,K., Inagaki,Y., Mizushima,H., Takahashi,A., Fukami,T., Hayakawa,T. & Kusumi,A.(1997) : *SPIE* 2980, 12-19.
"Fluorescence lifetime imaging microscopy with a high repetition gated camera and a dual-view assembly for the real time measurement"

27)Akashi,K., Miyata,H., Itoh, H. & Kinosita,Jr.,K.(1998) : *Biophys.J.* 74, 2973-2982.
"Formation of giant liposomes promoted by divalent cations : Critical role of electrostatic repulsion"

2．口頭発表

1)石渡信一，西坂崇之，吉川博，宮田英威，木下一彦：
生体分子のバイオメカニクス（筋タンパク質分子モーターの力学特性）．
第34回日本ME学会大会，東京（1995年5月）

2)Kinosita,Jr.,K., Miyata,H., Sase,I., Yoshikawa,H., Yasuda,R., Suzuki,N., Nishizaka,T. & Ishiwata,S. : "Imaging and manipulating single molecules."
3rd Int. Symp., Maui（1995年7月）

3)石渡信一，西坂崇之，吉川博，宮田英威，木下一彦：
光ピンセットによる分子モーターの顕微操作.
第56回応用物理学会学術講演会，金沢（1995年8月）

4)進泉、安田賢二、石渡信一：制御系存在下でのアクトミオシン硬直結合の構造解析.
日本生物物理学会第33回年会，札幌（1995年9月）

5)佐々木裕次、安田賢二、石橋整、鈴木芳生、藤木保武、石渡信一：
Au基盤表面に化学吸着したミオシンS1単分子膜の評価.
日本生物物理学会第33回年会，札幌（1995年9月）

6)新藤嘉明、安田賢二、石渡信一：
等張性条件下における単一筋原線維SPOCの顕微解析.
7日本生物物理学会第33回年会，札幌（1995年9月）

7)西坂崇之、宮田英威、多田隈尚史、石渡信一、木下一彦：
単一クロスブリッジの寿命と結合エネルギーの顕微計測.
日本生物物理学会第33回年会，札幌（1995年9月）

8)加藤宏一、西坂崇之、石渡信一：
pH感受性蛍光色素を用いた筋収縮系におけるメカノケミカルカップリングの画像化.
日本生物物理学会第33回年会，札幌（1995年9月）

9)藤木保武、石渡信一：in vitroにおける再構成 thin filament の滑り運動の制御－クロスブリッジの数の影響.

日本生物物理学会第 33 回年会，札幌（1995 年 9 月）

10)伊賀隆志、西坂崇之、石渡信一：
単離 A 帯中における単一アクチンフィラメントの滑り力の顕微計測.
日本生物物理学会第 33 回年会，札幌（1995 年 9 月）

11)藤田英明、新藤嘉明、安田賢二、石渡信一：
単一心筋筋原線維における力学特性の顕微解析.
日本生物物理学会第 33 回年会，札幌（1995 年 9 月）

12)木下一彦，佐瀬一郎，吉川博，安田涼平，宮田英威，西坂崇之，石渡信一：
細胞 1 個・分子 1 個を見て操作する.
日本生物物理学会第 33 回年会，札幌（1995 年 9 月）

13)Ishiwata,S., Shindo,Y., Takakura,T. & Yasuda,K. : Microscopic analysis of the elastic properties of connectin and nebulin in myofibrils.
Int. Symp. on Muscle Elastic Proteins，千葉（1995 年 10 月）

14)Fujiki,Y. & Ishiwata,S. : Regulation of sliding movement of reconstituted thin filaments in an in vitro motility assay system.
細胞運動研究会，東京／J.Muscle Res.Cell Motil.vol.17（1995 年 12 月）

15)Shin,I., Yasuda,K. & Ishiwata,S. : Structure of acto-myosin rigor complex analyzed by fluorescence resonance energy transfer.
細胞運動研究会，東京／J.Muscle Res.Cell Motil.vol.17（1995 年 12 月）

16)Ishiwata, S., Nishizaka, T., Miyata, H., Yoshikawa, H. & Kinosita,Jr., K. :
"Mechanical properties of single muscle protein motor studied by optical tweezers."
Takahashi・Kamiya Symp.，東京（ 1995 年 12 月）

17)伊賀隆志、西坂崇之、石渡信一：
A 帯中における単一アクチンフィラメントの滑り力の顕微測定.
生体運動合同班会議，東京（1996 年 1 月）

18)西坂崇之、 宮田英威、木下一彦、石渡信一：
アクトミオシン分子モーターの機能と力学特性の一分子顕微解析.

生体運動合同班会議，東京（1996年1月）

19)Ishiwata,S. : Microscopic analysis of single actomyosin motors and myofibrils.
Texas Univ., Dept.Chem.Seminar, Texas（1996年2月）

20)Ishiwata,S., Miki,M., Shin,I., Funatsu,T., Yasuda,K.& dos Remedios, C. G. :
Distance between myosin heads in rigor complex measured by fluorescence resonance energy transfer.
米国生物物理学会第40回年会／Biophys.J.vol.70, Baltimore（1996年2月）

21)Shindo,Y., Yasuda,K.& Ishiwata,S. : Analysis of spontaneous oscillatory contraction in skeletal myofibrils by isotonic feedback control.
米国生物物理学会第40回年会／Biophys.J.vol.70, Baltimore（1996年2月）

22)多田隈尚史、西坂崇之、石渡信一：単一モーター分子の結合の寿命.
第51回日本物理学会年会，金沢（1996年4月）

23)石渡信一：生体分子モーターの仕組み－1分子と集合体の顕微解析－.
第469回筑波研究フォーラム、筑波（1996年4月）

24)Ishiwata,S. : Structural and functional reconstitution of thin filaments in vitro and in myofibrils.
John Gergely Symposium : Half a Century of Muscle Research, Boston
（1996年7月）

25)Ishiwata, S. : "Microscopic manipulation and analysis of a single actomyosin motor and its assemblage."
UCSF Seminar, San Francisco（1996年7月）

26)佐瀬一郎、西坂崇之、吉川博、安田涼平、宮田英威、石渡信一、木下一彦：
生きた分子を見る.
コンフォーカル488サマーシンポジウム（1996年8月）

27)Nishizaka,T., Tadakuma,H., Kato,H., Miyata,H., Kinosita,Jr.,K. & Ishiwata,S. :
Lifetime of a single actomyosin rigor bond measured using optical tweezers.
Int. Congress of Biophysics, Amsterdam（1996年8月）

28)Ishiwata,S., Nishizaka,T., Kato,H., Tadakuma,H., Iga,T., Suzuki,N., Miyata,H. & Kinosita,Jr.,K. : Microscopic analysis of the nature of forces in a single actomyosin motor and its assemblage.
Workshop on Conformation of Biomacromolecules, Moscow（1996年9月）

29)石渡信一、西坂崇之、多田隈尚史、宮田英威、木下一彦：
アクトミオシン分子モーターの1分子特性.
第10回日本ME学会秋季大会、熊本（1996年10月）

30)石渡信一：筋収縮装置の再構築と自己集合.
JRDC領域探索研究会，東京（1996年11月）

31)堀田正幸、石渡信一：アクチンフィラメントとファロイジンの結合・解離速度.
日本生物物理学会第34回年会，筑波（1996年11月）

32)新藤嘉明、石渡信一：高速カメラを用いた筋原線維の顕微解析.
日本生物物理学会第34回年会，筑波（1996年11月）

33)加藤宏一、西坂崇之、伊賀隆志、木下一彦、石渡信一：
温度パルス顕微鏡によるアクトミオシン分子モーター機能の熱変調の画像化.
日本生物物理学会第34回年会，筑波（1996年11月）

34)多田隈尚史、西坂崇之、石渡信一：
in vitro系における無負荷時のアクトミオシン間単一硬直結合の寿命.
日本生物物理学会第34回年会，筑波（1996年11月）

35)佐々木裕次、安田賢二、石渡信一：
マレイミド基飽和表面に配向したミオシンS1単分子.
日本生物物理学会第34回年会，筑波（1996年11月）

36)藤田英明、石渡信一：
細いFilamentを部分的に再構成した心筋収縮系の収縮・制御能.
日本生物物理学会第34回年会，筑波（1996年11月）

37)寺田尚史、石渡信一：筋原線維自励振動のメカニズム.1.筋節間の協同性.

日本生物物理学会第 34 回年会，筑波（1996 年 11 月）

38)高橋真、石渡信一：アクチン重合過程の画像化とその応用.
日本生物物理学会第 34 回年会，筑波（1996 年 11 月）

39)石渡信一：筋収縮系の構築原理.
第 11 回「生命現象のダイナミクス」シンポジウム，横浜（1996 年 11 月）

40)Hotta,M. & Ishiwata,S. : Temperature dependence of association and dissociation rate constants of rhodamine phalloidin with actin filaments.
細胞運動研究会，東京／J.Muscle Res.Cell Motil.vol.18（1996 年 12 月）

41)Fujita,H. & Ishiwata,S. : Contractility and its regulation of thin filament-reconstituted cardiac muscle fibres: Investigation of the role of regulatory proteins in spontaneous tension oscillation.
細胞運動研究会，東京／J.Muscle Res.Cell Motil.vol.18（1996 年 12 月）

42)石渡信一、加藤宏一、西坂崇之、伊賀隆志、木下一彦：
温度パルス顕微鏡法によるアクトミオシン分子モーター機能の熱励起.
生体運動合同班会議，大阪（1997 年 1 月）

43)Sasaki,Y.,C., Yasuda,K., Suzuki,Y., Ishibashi,T., Satoh,I., Fujiki,Y. & Ishiwata,S. : Two-dimentional arrangement of a functional protein by cysteine-gold interaction: Enzyme activity and characterization of a protein monolayer on gold substrate.
米国生物物理学会第 41 回年会，New Orleans／Biophys.J.vol.71（1997 年 3 月）

44)Kato,H., Nishizaka,T., Iga,T., Kinosita,Jr.,K. & Ishiwata,S. :
Thermal activation of actomyosin motors with temperature-pulse microscopy.
米国生物物理学会第 41 回年会，New Orleans／Biophys.J.vol.71（1997 年 3 月）

45)寺田尚史、石渡信一：筋原線維自励振動における筋節間の協同性.
第 52 回日本物理学会年会、名古屋（1997 年 3 月）

46)Ishiwata, S. : "Actomyosin motors: Manipulation of single molecules and assembly."
Univ. of Penn. Sch. Med., Seminar, Philadelphia（1997 年 3 月）

47)Ishiwata,S., Kato,H., Nishizaka,T., Iga,T., Kumaki,Y., Tadakuma,H. & Kinosita,Jr.,K. : Mechanics and thermodynamics of single actomyosin motors. Symposium on The Molecular Interactions of Actin, Hawaii (1997年4月)

48)Ishiwata,S., Nishizaka,T., Kato,H., Tadakuma,H., Kumaki,Y., Sase,I., Miyata,H. & Kinosita,Jr.,K. : Single-molecule manipulation and analysis of motor proteins under optical microscope.
2nd East Asian Conference of Biophysics, Beijing (1997年5月)

49)Fujita,H. & Ishiwata,S. :
Investigation of SPOC using actin filament-reconstituted cardiac muscle fibers.
2nd East Asian Conference of Biophysics, Beijing (1997年5月)

50)Terada,N. & Ishiwata,S. : Cooperativity observed in spontaneous oscillation of sarcomere length in skeletal myofibrils.
2nd East Asian Conference of Biophysics, Beijing (1997年5月)

51)石渡信一：人工再構築系を用いた筋収縮における分子シンクロナイゼーションの解明.
第15回インテリジェント技術ワークショップ，東京（1997年7月）

52)Ishiwata,S. : Molecular interaction in single motor proteins.
2nd International Workshop on Molecular Interaction at Surfaces, Basel
(1997年7月)

53)Ishiwata, S. : Mechanics and thermodynamics of actomyosin motors: Single molecule manipulation.
MRC at Mill HIll, Seminar, London (1997年7月)

54)石渡信一：はじめに：一分子へ、そして再び集合体へ.
日本生物物理学会第35回年会、京都（1997年10月）

55)高橋真、石渡信一：アクチン重合過程の単一フィラメント顕微解析.
日本生物物理学会第35回年会、京都（1997年10月）

56)熊木雄一、西坂崇之、石渡信一：単一ミオシンモーターの硬直結合力の測定.

日本生物物理学会第35回年会、京都（1997年10月）

57)多田隈尚史、西坂崇之、石渡信一：
アクトミオシン硬直複合体の回転弾性率と結合寿命の顕微解析.
日本生物物理学会第35回年会、京都（1997年10月）

58)寺田尚史、石渡信一：
筋原線維自励振動のメカニズム．Ⅱ．各筋節の力学特性の均一性.
日本生物物理学会第35回年会、京都（1997年10月）

59)福田紀男、藤田英明、石渡信一：心筋スキンド標本の張力振動に及ぼすｐＨの影響.
日本生物物理学会第35回年会、京都（1997年10月）

60)藤田英明、石渡信一：制御系を除いた再構成心筋収縮系におけるＳＰＯＣ.
日本生物物理学会第35回年会、京都（1997年10月）

61)加藤宏一、西坂崇之、伊賀隆志、多田隈尚史、木下一彦、石渡信一：
アクトミオシン分子モーター機能の熱変調の高速画像化.
日本生物物理学会第35回年会、京都（1997年10月）

62)斎藤素子、石渡信一：ＡＴＰアナログ存在下でのアクチンフィラメントの滑り力測定.
日本生物物理学会第35回年会、京都（1997年10月）

63)岡部治美、石渡信一：サブチリシン処理アクチンとミオシンとの相互作用.
日本生物物理学会第35回年会、京都（1997年10月）

64)石渡信一：
生体分子モーターの仕組み－夢と現実.
中央大学講演会（1997年10月）

65)Ishiwata,S., Funatsu,T. & Fujita,H. :
Contractile properties of thin(actin)filament-reconstituted muscle fibers.
Symp. on the mechanism of work production and work absorption in muscle, 箱根（1997年10月）

66)Terada,N. & Ishiwata,S. :

Microsocopic analysis of cooperative properties of SPOC in skeletal myofibrils.
細胞運動研究会，東京／J.Muscle Res.Cell Motil.vol.19（1997年12月）

67)多田隈尚史、西坂崇之、石渡信一：
双頭、単頭結合の比較－単一アクトミオシン硬直結合の寿命、回転、破断力－.
生体運動合同班会議、東京（1998年1月）

68)川口憲治、加藤宏一、石渡信一：
温度パルス顕微鏡によるキネシン分子モーターの熱変調画像化.
生体運動合同班会議、東京（1998年1月）

69)藤田英明、石渡信一：
細いフィラメントの再構成手法を用いた心筋自励振動機能の研究.
第10回バイオエンジニアリング講演会，広島（1998年1月）

70)Ishiwata, S. : "Structural and functional reconstitution of the thin filament in skeletal and cardiac muscle fibers."
The Univ. of Iowa, Dept.Anatomy & Cell Biol., Dept. Seminar, Iowa City
（1998年2月）

71)Takahashi,S. & Ishiwata,S. :
Direct observation of polymerization process of single actin filaments under fluorescence microscope.
米国生物物理学会第42回年会，Kansas City／Biophys.J.vol.74（1998年2月）

72)Kinosita,Jr.K., Yasuda,R., Noji,H., Yoshida,M. and Ishiwata,S. :
A single-molecule rotary motor compared to linear motors.
米国生物物理学会第42回年会，Kansas City／Biophys.J.vol.74（1998年2月）

73)Tadakuma,H., Nishizaka,T., Funatsu,T. and Ishiwata,S. : Direct measurement of lifetime and torsional stiffness of single acto-myosin rigor complex.
米国生物物理学会第42回年会，Kansas City／Biophys.J.vol.74（1998年2月）

74)Fujita,H. & Ishiwata,S. :
Investigation of spontaneous oscillatory contraction (SPOC) using actin filament-reconstituted cardiac muscle fibers.

米国生物物理学会第 42 回年会，Kansas City／Biophys.J.vol.74（1998 年 2 月）

75)福田紀男、栗原敏、石渡信一：
心筋収縮系の自発的振動現象に及ぼす pH の影響.
日本生理学会第 75 回大会，金沢（1998 年 3 月）

76)Itoh,H., Hayakawa,T., Kinoshita,K., Inagaki,Y., Mizushima,H., Takahashi,A., Kher,S. & Kusumi,A. : Use of Framing Camera in Biological Investigations I. High-Repetition Shutter Camera for Fluorescence Lifetime Imaging Microscopes.
3rd Int. Symp. on Innovative Fluorescence Methodologies in Biochemistry and Medicine, Maui（1995 年 7 月）

77)Itoh,H., Hayakawa,T., Kinoshita,K., Inagaki,Y., Mizushima,H.,Takahashi,A., Kher,S. & Kusumi,A. : Use of Framing Camera in Biological Investigations II. Gain Modulating Camera with Significant Depth for Fluorescence Lifetime Imaging.
3rd Int. Symp. on Innovative Fluorescence Methodologies in Biochemistry and Medicine, Maui（1995 年 7 月）

78)明石憲一郎、平野光洋、野口潤、西山修二、伊藤博康、宮田英威、木下一彦：
交流電場中での Giant Liposome の変形.
日本生物物理学会第 33 回年会，札幌（1995 年 9 月）

79)伊藤博康、高橋聡、木下勝之、森博茂：
変調型フレーミングカメラによる寿命分解蛍光イメージング顕微鏡の開発.
日本生物物理学会第 33 回年会，札幌（1995 年 9 月）

80)明石憲一郎、宮田英威、伊藤博康、木下一彦：
Giant Liposome 形成に対する二価アルカリ陽イオンの効果.
日本生物物理学会第 34 回年会，筑波（1996 年 11 月）

81)伊藤博康、Ariella Evenzahav、高橋聡、稲垣喜則、水島廣、木下勝之、早川毅、楠見明弘：実時間寿命分解蛍光イメージ顕微鏡の開発.
日本生物物理学会第 34 回年会，筑波（1996 年 11 月）

82)明石憲一郎、宮田英威、伊藤博康、木下一彦：
複数の連結孔（膜で構成された孔）を有する Giant Liposome.

日本生物物理学会第35回年会，京都（1997年10月）

83)明石憲一郎、宮田英威、伊藤博康、木下一彦：
一枚膜Giant Liposomeを用いた膜間吸着エネルギーの測定.
日本生物物理学会第35回年会，京都（1997年10月）

84)木下勝之、稲垣喜則、高橋聡、伊藤博康、水島廣、早川毅：
超高速・高繰り返しシャッターカメラ.
超高速撮影とフォトニクスに関する総合シンポジウム，東京（1997年12月）

85)Itoh,H., Fukami,T., Kinoshita,K., Inagaki,Y., Mizuxhima,H., Takahashi,A., Hayakawa,T., Kusumi,A. & Kinosita,Jr.,K. :
Fluorescence Lifetime Imaging Microscopy for The Real Time Measurement.
米国生物物理学会第42回年会，Kansas City／Biophys.J.vol.74（1998年2月）

３．出版物

1)柳田敏雄，石渡信一 編(1997)：ナノピコスペースのイメージング
－生物分子モーターのメカニズムを見る－生物物理から見た生命像３ 吉岡書店

2)石渡信一 編著(1997)：生体分子モーターの仕組み
－シリーズ・ニューバイオフィジックス４－ 共立出版

3)石渡信一 (1997)：「生体分子モーターの仕組み
－シリーズ・ニューバイオフィジックス４－」共立出版 pp.1-23.
” 分子モーター研究の新展開”

4)石渡信一 (1997)：「生体分子モーターの仕組み
－シリーズ・ニューバイオフィジックス４－」 共立出版 pp.158-173.
” ミオシン分子モーターの特殊な機能”

5)Ishiwata,S. (1998) : *In* Current Methods in Muscle Physiology-Advantages, Problems and Limitations-. (ed.by H.Sugi) Oxford Univ. Press. pp.199-222.
"Use of fluorescent probes."

6)木下一彦、宮田英威、石渡信一 (1998)：「バイオイメージング
－シリーズ・ニュー バイオフィジックス７－」共立出版 pp.93-104.
” 光ピンセット－１分子を見て操作する”

7)Ishiwata,S., Funatsu,T. and Fujita,H. : *In* Mechanism of work production and work absorption in muscle. (ed. by H.Sugi & G.H. Pollack) Plenum Pub. Corp. in press.” Contractile properties of thin (actin)filament-reconstituted muscle fibers.”

Mechanical Properties of Single Protein Motor of Muscle Studied by Optical Tweezers

Takayuki Nishizaka,* Hidetake Miyata,‡ Hiroshi Yoshikawa,‡ Shin'ichi Ishiwata,* and Kazuhiko Kinosita Jr.‡

*Department of Physics, School of Science and Engineering, Waseda University, Okubo, Shinjuku-ku, Tokyo 169; ‡Department of Physics, Faculty of Science and Technology, Keio University, Hiyoshi, Kohoku-ku, Yokohama 223, Japan

Using optical tweezers and a dual-view (fluorescence and phase-contrast) microscope system, we have succeeded in (1) determining the location of heavy-meromyosin (HMM) molecules adhering to a glass surface precoated with nitrocellulose; and (2) measuring the binding force between an HMM molecule and an actin filament in the absence of ATP, i.e., the tensile strength that is the force needed to break the rigor bond. A polystyrene bead (1 μm in diameter), selectively attached to the rear end of an actin filament through an actin binding protein, gelsolin, was captured by a single light beam of a YAG-laser (wavelength, 1.064 μm). The optical gradient trap force was proportional to the displacement of the bead out to 200 nm. The actin filament (1–10 μm in length) labeled with the fluorescent probe rhodamine phalloidin was observed under a fluorescence microscope using a charge-coupled device camera equipped with an image intensifier.

Fig. 1 shows the single actin filament that was bound to the glass surface precoated with 1 μg/ml HMM. When the bead (arrow in Fig. 1 *A*) was trapped and pulled to the right at a constant rate, a part of the filament was stretched straight from the nodal point (arrowhead in Fig. 1 *B*). As the load imposed by optical tweezers was increased, the nodal point was broken and the actin filament was loosened (Fig. 1 *C*). As the bead was pulled further, the actin filament became taut at another nodal point (arrowhead in Fig. 1 *D*), which broke after a while. Thus, we could directly count the number of HMM molecules that had attached to the filament. We previously reported the stepwise motion of an actin filament under low concentrations of ATP on the surface precoated with 1 μg/ml HMM (Miyata et al., 1994). Using the technique described here, the average number of HMM molecules that had attached to 1 μm actin filament was estimated to be about 1.5, indicating that the stepwise motion was produced by one to several HMM molecules. We measured the tensile strength and the elasticity of an acto-HMM complex by analyzing the position of the bead with the spatial resolution of a nanometer scale under a phase-contrast microscope. When the trap center was moved at 100 nm/s, the average value of the tensile strength was 6.5 $\pm$ 3.7 pN (n = 6). The elasticity, estimated from a steep portion of a stress-strain relation obtained before breaking the rigor bond, was 0.3 $\pm$ 0.2 pN/nm (n = 3). This value is similar to the elasticity of the crossbridge estimated in the muscle fibers (Tawada and Kimura, 1986). On the other hand, the maximum strain (~70 nm) was large compared with the size of the myosin head (20 nm), so that the strain might contain the elongation of the elastic parts in addition to the myosin head. At present, we are conducting the same type of measurements on a silanized glass surface because nitrocellulose might contribute to elasticity. In addition, because a single rigor bond must be broken stochastically, we have started to measure the time required for breaking the rigor bond under a constant load. Those results will be published in the near future.

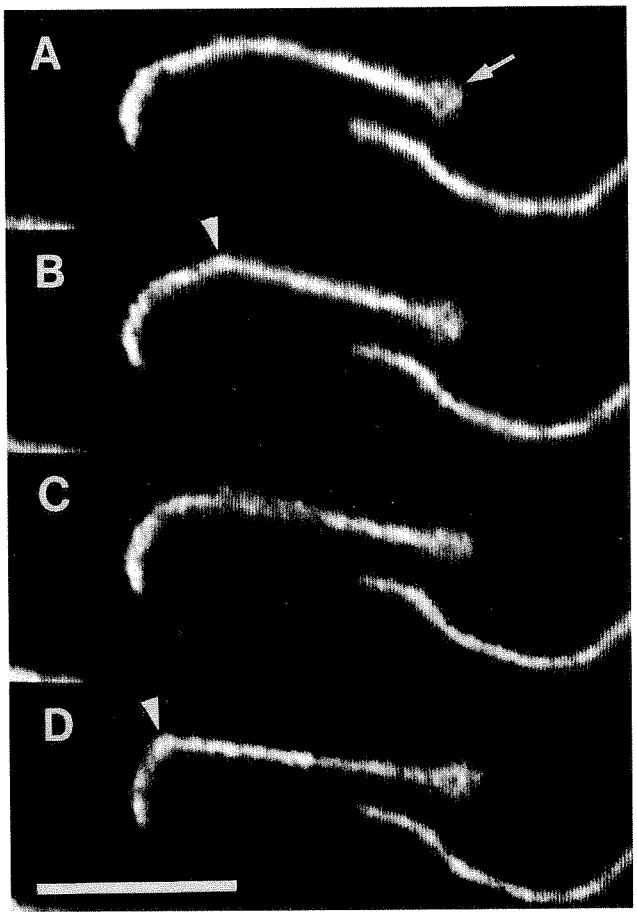

FIGURE 1 A series of micrographs showing the manipulation of an actin filament through a polystyrene bead by using optical tweezers. The position of a single HMM molecule was visualized as a nodal point in the actin filament. Conditions used for the present in vitro assay system was the same as described before (Nishizaka et al., 1993). The glass surface was precoated with nitrocellulose. Scale bar, 5 μm.

REFERENCES

Miyata, H., H. Hakozaki, H. Yoshikawa, N. Suzuki, K. Kinosita Jr., T. Nishizaka, and S. Ishiwata. 1994. Stepwise motion of an actin filament over a small number of heavy meromyosin molecules is revealed in an in vitro motility assay. *J. Biochem.* 115:644–647.

Nishizaka, T., T. Yagi, Y. Tanaka, and S. Ishiwata. 1993. Right-handed rotation of an actin filament in an in vitro motile system. *Nature.* 361:269–271.

Tawada, K., and M. Kimura. 1986. Stiffness of carbodiimide-cross-linked glycerinated muscle fibres in rigor and relaxing solutions at high salt concentrations. *J. Muscle Res. Cell Motil.* 7:339–350.

0006-3495/95/04/75/01 $2.00

Mechanical Measurements of Single Actomyosin Motor Force

Hidetake Miyata,* Hiroshi Yoshikawa*, Hiroyuki Hakozaki,† Naoya Suzuki,§ Taiji Furuno,¶ Akira Ikegami,¶ Kazuhiko Kinosita Jr.,* Takayuki Nishizaka,‖ and Shin'ich Ishiwata‖

*Department of Physics, Faculty of Science and Technology, Keio University, Kohoku-ku, Yokohama 223; †Nikon Corporation, Yokohama Plant, Sakae-ku, Yokohama 244; §Department of Physics, Faculty of Science, Nagoya University, Chikusa-ku, Nagoya 464-01; ¶Department of Physics, Faculty of Medicine, Keio University, Kohoku-ku, Yokohama 223; and ‖Department of Physics, School of Science and Engineering, Waseda University, Shinjuku-ku, Tokyo 169, Japan

ABSTRACT To elucidate the mechanism of force generation by actomyosin motor, a measuring system was constructed, in which an in vitro motility assay was combined with an optical trapping technique. An actin filament of several μm long was attached to a gelsolin-coated polystyrene bead, and was allowed to interact with a small number (~1/1-μm actin filament) of rabbit skeletal heavy meromyosin (an active subfragment of myosin) molecules bound to a nitrocellulose-coated coverglass. The bead position was determined at 33-ms intervals. We measured the force generation event at relatively low (100–400 nM) ATP concentration so that the occurrence of individual force generation events could be detected with our time resolution. The actin-bound bead held in the optical trap moved in a stepwise manner in the direction of the actin filament only in the presence of ATP. At the trap strength of 0.3 pN/nm, the maximum size of the step was 11 nm, and the maximum force associated with the movement was 3.3 pN.

INTRODUCTION

Muscle contraction is driven by cyclic interaction of two contractile proteins, actin and myosin, and this process is fueled by chemical energy of ATP, which is hydrolyzed by individual myosin heads. As one ATP is hydrolyzed by a myosin head, power stroke by the head occurs and actin filament is displaced. Recently, several groups (Finer et al., 1994; Ishijima et al., 1994; Miyata et al., 1994) have carried out experiments to elucidate the molecular mechanism underlying the process. In these experiments an in vitro motility assay was combined with a micromanipulation technique to measure the small force and the displacement; when a small number of myosin heads were allowed to interact with an actin filament that was bound to and manipulated with a microneedle or a μm-sized plastic bead, abrupt motion of the microneedle or the bead was observed in the presence of ATP. Previously, we measured the actomyosin motor force with relatively weak trapping force (trap constant = 0.0063–0.016 pN/nm) and found that the maximum force was about 0.5 pN (Miyata et al., 1994), which was significantly smaller than the value obtained by other groups (~3–5 pN; Finer et al., 1994; Ishijima et al., 1994). From our results it was suggested that the force was larger when the trap was stronger, so that we expected that use of a stronger trap would be necessary to measure larger force. In the experiments reported here we have extended our measurement using a trap stronger than the previous one (up to 0.3 pN/nm).

Address reprint requests to Dr. Hidetake Miyata, Department of Physics, Faculty of Science and Technology, Keio University, 3-14-1 Hiyoshi, Kohoku-ku, Yokohama-shi, 223 Japan. Tel.: 81-45-5631141 ext. 3975; Fax: 81-45-5631761

0006-3495/95/04/286s/05 $2.00

MATERIALS AND METHODS

Materials

Heavy meromyosin (HMM) and actin were prepared from rabbit skeletal muscle. Actin filaments were labeled with rhodamine-phalloidin (Molecular Probes, Inc., Eugene OR). Polystyrene beads (diameter = 0.88 μm) were from Polysciences, Inc. (Warrington, PA). All other chemicals were of analytical grade. A complex of actin filaments and gelsolin-coated polystyrene beads was prepared according to the method described by Suzuki (manuscript in preparation). The length of actin filaments was 3–10 μm.

Methods

The in vitro motility assay was carried out according to the method described by Kron et al. (1991). HMM was bound twice to a nitrocellulose-coated coverglass at 2 μg/ml for 1 min at room temperature. The number of HMM interacting with 1 μm actin filament was ~1 (Miyata et al., 1994). Relatively low ATP concentration (100–400 nM) was maintained with ATP regeneration system (100 μg/ml creatine kinase and 1 mM creatine phosphate). To help the actin filaments bind to a small number of HMM, 0.2% methyl cellulose was added (Uyeda et al., 1991).

To measure the force and motion, an optical trap was integrated into an inverted microscope (TMD, Nikon Tokyo, Japan) (Fig. 1 *a*). Laser light from an yttrium-lithium-fluoride-laser light source (1053 nm, 1 W, OEM 1053–1000p, Amoco Laser Co., Naperville, IL) was focused with an objective lens (numerical aperture = 1.3, 100×, Nikon) to form an optical trap. The trap constant was determined from the distribution of the position of a bead undergoing Brownian motion in the trap potential (for details, see Miyata et al., 1994). The bead position was determined at 33-ms intervals from calculation of the centroid of the phase contrast image of the bead. The potential was found to be axisymmetrical and approximated with that of a Hookean spring up to 200 nm from the trap center, and the trap constant was 0.05–0.3 pN/nm.

In individual experiments an actin-bound bead was held with the optical trap at ~1 μm above the glass surface, and the filament was allowed to interact with the surface-bound HMM (Fig. 1 *b*). The fluorescence image of the bead-bound filament was observed simultaneously with the bead image to ensure that the motion occurred in the filament direction, which is expected if the motion is due to the active interaction of HMM with the actin filament.

In our measurement one actin filament was bound with several myosin heads, and most of the heads were in rigor state, because ATP concentration

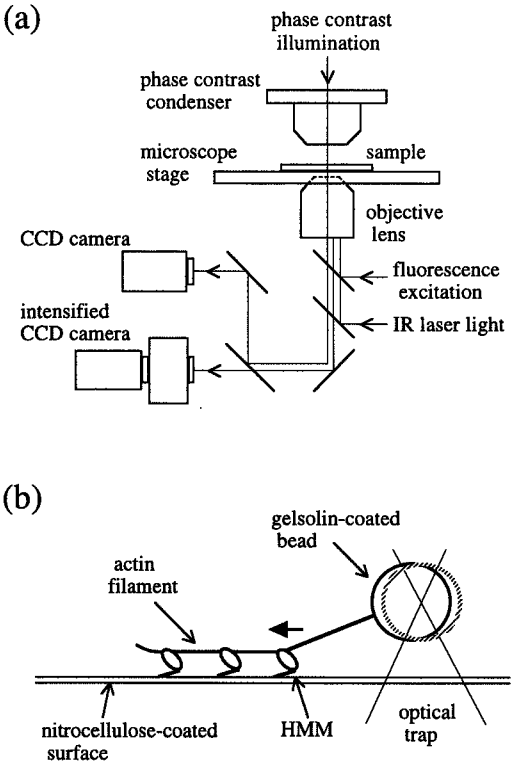

FIGURE 1 Schematic representation of the inverted microscope-based piconewton force measuring system. (*a*) A simplified diagram of the system. The phase contrast and the fluorescence image of the bead and the filament were separated with a dichroic mirror, and were received with a charge-coupled-device (CCD) and an intensified CCD camera, and were electronically combined (not shown). (*b*) A bead-bound actin filament interacting with the HMM molecules bound to a nitrocellulose-coated coverglass. The bead was held with the optical trap at about 1 μm above the surface; thus the filament was tilted when interacting with HMM. Note that the figures are not drawn to scale.

was low. Also for this reason, only one ATP molecule bound to one of those heads at a time. The binding of ATP to one of the heads caused the dissociation of the head from the actin filament, and the force generation (power stroke) immediately followed. This would move the bead: the final bead position is expected to be determined by a balance among the positive and negative force of the heads, and trap force (Miyata et al., 1994). Each event should be easily resolved at a video rate under our experimental condition, because a rate of ATP binding under our condition must be low due to the low ATP concentration, and the small number of HMM interacting with an actin filament. (The bimolecular rate constant of ATP binding to acto-S-1 in solution is $\sim 10^6$/M·s (Goldman, 1987).

RESULTS AND DISCUSSION

Stepwise motion

Fig. 2 (*a–e*) shows several examples of the bead motion (arrows), which we regard as stepwise and as a result of the force generation by individual heads of the surface-bound HMM. These traces were obtained in the presence of 100 and 200 nM ATP at the trap strength of 0.3 pN/nm. In these examples the bead position changed abruptly (within scores of ms). These motions occurred only in the direction of the filament and in the presence of ATP, indicating that the motion was caused by the active interaction between actin and HMM. In the presence of 400 nM ATP, or at different trap strength (0.05 and 0.1 pN/nm), a similar type of motion was observed (not shown).

Under our experimental conditions, binding of ATP to each head initiated the power stroke, which was expected to cause the abrupt change in the bead position. Then, the frequency of the occurrence of the abrupt motion was expected to be equal to the rate of ATP binding. The duration of the motion was on the order of a fraction of a second, which was consistent with the rate of ATP binding. This result further supports the above indication that the abrupt motion was caused by the active interaction of HMM with the actin filament.

To analyze the size of the steps, we selected the abrupt motion with the size $\geq$4 nm. With this criterion, the measured averaged size of the step at 200 nM ATP was 5.8 nm at the trap strength of 0.3 pN/nm, 5.4 nm at 0.1 pN/nm, and 5.3 nm at 0.05 pN/nm, respectively. Occasionally, the bead moved in a gradually ascending manner over several seconds: this type of motion can occur if many myosin heads are interacting with an actin filament and individual heads independently pull the filament for a short distance. However, we could not determine whether this was the case, and no analysis was made on this type of motion.

The magnitude of the force obtained as a product of the averaged size of the step and the trap constant was 1.7, 0.54, and 0.27 pN at each trap strength. The maximum force, 3.3 pN, was obtained at 200 nM ATP and at the trap strength of 0.3 pN/nm. In a few cases a force of about 3 pN was obtained, but in most cases the force was smaller. In our previous study the size of the step at the trap strength of 0.016 pN/nm was around 8 nm: the data shown here indicate that the size of the step showed only ~30% decrease, but the force increased by ~6 times upon increase in the trap force. It seems that it is the size of the step, rather than the magnitude of the force, that is definitive. Definitiveness of the size of the step accords with the proposed mechanism of the power stroke, in which stereospecific interaction between actin protomers and a myosin head is assumed (Rayment et al., 1993).

Effect of the tilt of the actin filament

The maximum force (3.3 pN) was smaller than that obtained by other groups (Finer et al., 1994, Ishijima et al., 1994). The force (i.e., the size of the step $\times$ the trap constant) would be smaller if the size of the step smaller than the actual size of the power stroke. We consider here three factors that can make the step smaller. (1) Tilt of the actin filament: the actin filaments stretched between the bead, and the surface-bound HMM always had some tilt (~30°, under our experimental conditions); thus, the magnitude of the bead motion caused by the displacement in horizontal direction between HMM and actin was smaller by a factor of $\cos^2\theta$, where θ is the tilt angle of the actin filament. Thus, the observed bead displacement was probably ~1.3 times smaller than the actual displacement between HMM and actin filament. (2) Slack of

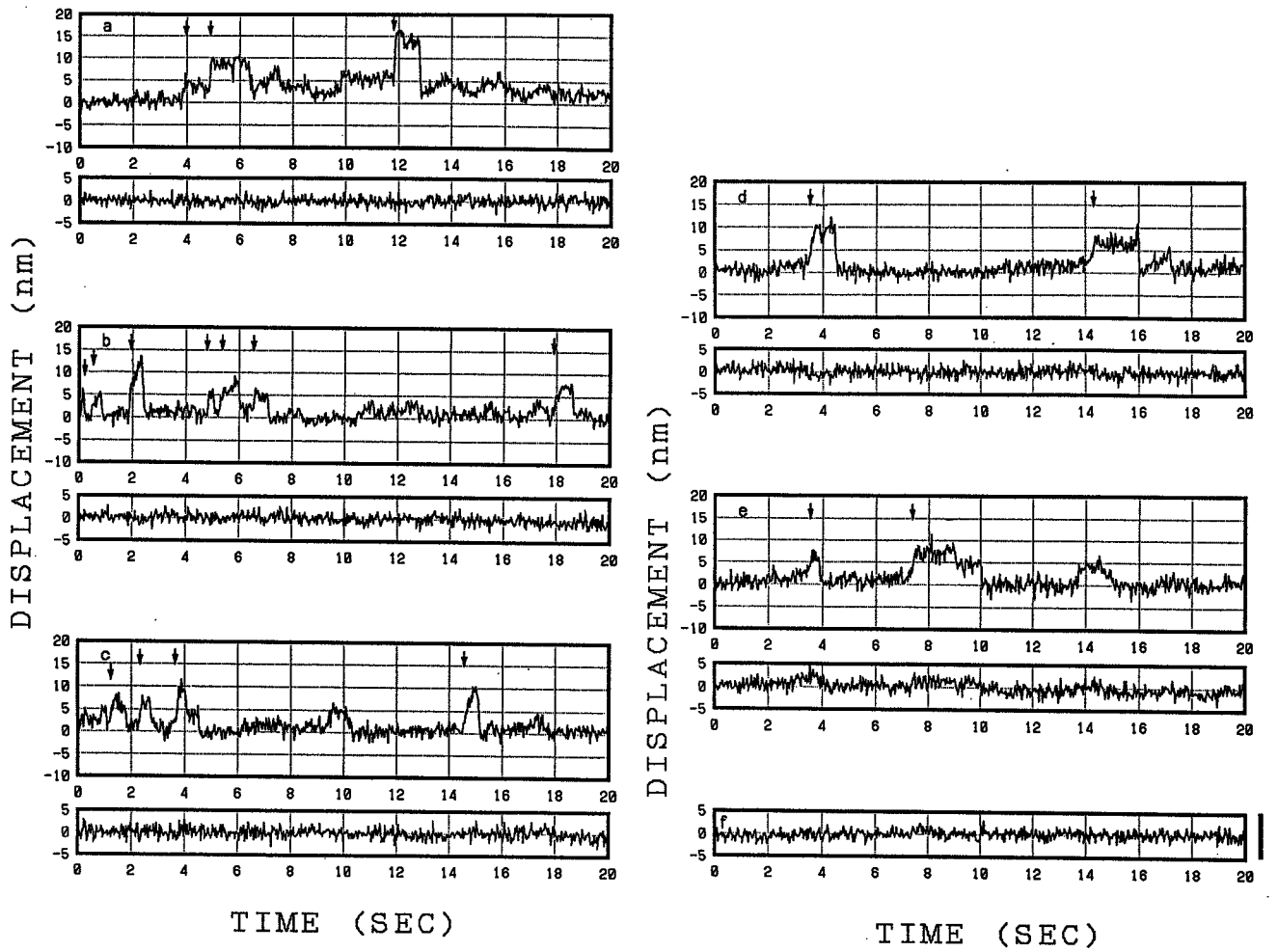

FIGURE 2 Several examples of the stepwise bead motion (indicated by arrows) measured at 0.3 pN/nm trap strength. (*a*) The traces obtained at 100 nM ATP. (*b–e*) The traces at 200 nM ATP. In each set the upper and the lower traces were the record in the direction parallel to and perpendicular to the actin filament direction. In (*e*) the filament direction changed in the middle of the measurement and the slight change in Y direction observed at the beginning almost disappeared in the later stage. (*f*) The trace obtained when the actin did not interact with the surface indicating the level of thermal noise and other types of noise (e.g., mechanical). A bar next to the trace (*f*) indicates 3 pN force.

the actin filament: it is obvious that the power stroke of HMM cannot be effectively transmitted to the bead, if the filament is slack. (3) Existence of large compliance: if large compliance exists somewhere between actin-HMM and HMM-surface linkages (Nishizaka et al., 1995), such compliance makes the bead displacement smaller (Svoboda and Block, 1994).

If we correct the maximum force for factor (1), the force will be ~4.3 pN, closer to the other groups' values, but the averaged force is still smaller: we should also consider factors (2) and (3), but the effect of these factors is more difficult to quantitatively evaluate. We qualitatively consider the effect of the latter two factors in the next section.

The effect of the slack of an actin filament and the compliance

As pointed out above, if the bead-bound actin is slack, or if a large compliance exists, the surface-bound HMM molecules cannot "effectively" pull the bead. When first bound to the HMM molecules, the actin filament itself, or the individual "springs," may not have been sufficiently stretched. (The term "spring" is used hereafter as a substitute for the term "high compliance" for the sake of convenience.) Nevertheless, we did observe the bead motion. This implies that the slack of the filament eventually disappeared, and the springs became more stretched. This seems to be obvious at first, because a small number of HMM can move an actin filament (Uyeda et al., 1991), thereby hauling the filament to achieve these tasks. However, this can only be possible when the HMM molecule nearest to the bead holds the filament throughout the process and the force generation process as well, because dissociation of this HMM would allow the filament to diffuse away and produce again the slack (Fig. 3).

In our experiments the bead motion became observable immediately to ~1 min after the contact of the actin filament with the surface-bound HMM was achieved. This may be explained by variability of the time required for the disappearance of the slack. Even after the motion became observable, the large step and hence the large force was rarely observed. We suspect that this was due to the insufficient stretch of the spring, because one actin filament al-

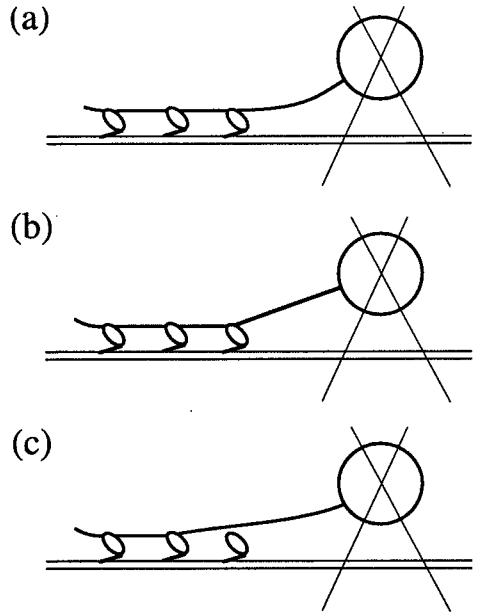

FIGURE 3 The slack of an actin filament and the bead motion. (*a*) When the actin filament (——) is slack, the power stroke of the surface-bound HMM molecules is not effectively transmitted to the bead (○). (*b*) As HMM molecules haul at the filament it eventually becomes straight and the power stroke is effectively transmitted. (*c*) If the HMM nearest to the bead dissociates from the actin, the slack again occurs.

ways interacted with several heads, and it is conceivable that not all the springs had been fully stretched.

The mechanism that enables the hauling process is not clear. Because of the low ATP concentration, it may be that one head of HMM bound the filament in a rigor state while the other head executed a power stroke, or two heads may have alternately functioned as suggested for directional movement of kinesin on a microtubule (Hackney, 1994).

Electron microscopy of HMM

To understand and explain our results in light of the structural change in HMM, we have initiated electron microscopy of HMM molecules. Details will be published elsewhere (T. Furuno, manuscript in preparation). Briefly, a negative-staining solution dissolving HMM was dried on a silicone surface by a spin-coating technique (Furuno et al., 1992), and electron micrographs of the HMM molecules were taken. By preparing the HMM sample in the above manner, we found that the detailed shape of head and tail portion of HMM was well preserved. HMM molecules with straight or slightly curved heads were observed in the absence of MgATP, whereas HMM with sharply bent heads were observed in its presence. It is not clear at the present moment whether this conformational difference in head portion is related to the observed event of force generation, but the above observation seems to be consistent with the result of the analysis of the small-angle x-ray scattering measurements, which has suggested conformational change in S-1 in solution in the presence of ATP (Wakabayashi et al., 1992), as well as the model of the conformational change in S-1 deduced for the x-ray crystallography (Rayment et al., 1993).

This work was supported by a grant-in-aid from the Ministry of Education, Science and Culture of Japan, by Special Coordination Funds for Promoting Science and Technology from the Agency of Science and Technology, and a grant from Keio University.

REFERENCES

Finer, J. T., R. T. Simmons, and J. A. Spudich. 1994. Single myosin molecule mechanics: piconewton forces and nanometre steps. *Nature.* 368: 113–119.

Furuno, T., K. M. Ulmer, and H. Sasabe. 1992. Scanning electron microscopy of negatively stained catalase on a silicone wafer. *Microsc. Res. Tech.* 21:32–38.

Goldman, Y. E. 1987. Kinetics of the actomyosin ATPase in muscle fibers. *Annu. Rev. Physiol.* 49:637–654.

Hackney, D. D. 1994. Evidence for alternating head catalysis by kinesin during microtubule stimulated ATP hydrolysis. *Proc. Natl. Acad. Sci. USA.* 91:6865–6869.

Ishijima, A., Y. Harada, H. Kojima, T. Funatsu, H. Higuchi, and T. Yanagida. 1994. Single-molecule analysis of the actomyosin motor using nano-manipulation. *Biochem. Biophys. Res. Commun.* 199:1057–1063.

Kron, S. J., Y. Y. Toyoshima, T. Q. P. Uyeda, and J. A. Spudich. 1991. Assays for actin sliding movement over myosin coated surfaces. *Methods Enzymol.* 196:399–416.

Miyata, H., H. Hakozaki, H. Yoshikawa, N. Suzuki, K. Kinosita Jr., T. Nishizaka, and S. Ishiwata. 1994. Stepwise motion of an actin filament over a small number of heavy meromyosin molecules is revealed in an *in vitro* motility assay. *J. Biochem.* 115:644–647.

Nishizaka, T., H. Miyata, H. Yoshikawa, S. Ishiwata, and K. Kinosita Jr. 1995. Mechanical properties of single protein motor of muscle studied by otpical tweezers. *Biophys. J.* 68:75s

Rayment, I., H. M. Holden, M. Whittaker, C. B. Yohn, M. Lorenz, M., K. C. Holmes, and R. A. Milligan. 1993. Structure of the actin-myosin complex and its implications for muscle contraction. *Science.* 261:58–64.

Svoboda, K., and S. M. Block. 1994. Force and velocity measured for single kinesin molecules. *Cell.* 77:773–784.

Uyeda, T. Q. P., H. M. Warrick, T. J. Kron, and J. A. Spudich. 1991. Quantitized velocities at low myosin densities in an in vitro motility assay. *Nature.* 352:307–311.

Wakabayashi, K., M. Tokunaga, I. Kohno, Y. Sugimoto, T. Hamanaka, Y. Takezawa, T. Wakabayashi, and Y. Amemiya. 1992. Small-angle synchrotron X-ray scattering reveals distinct shape changes of the myosin head during hydrolysis of ATP. *Science.* 258:443–447.

DISCUSSION

Session Chairperson: Kenneth A. Johnson
Scribe: Michelle Wang

PAUL DRIEZEN: Have you looked at the possible effect that might be caused by pairwise interactions of heavy meromyosin?

HIDETAKE MIYATA: No.

DRIEZEN: Obviously that was a leading question. In a poster presented at this meeting, Umesh Ghodke has shown some evidence that confirms Harrington's original work and

in addition shows that heavy meromyosin under conditions of high Mg-ATP can be regulated in the presence of nucleotides to form low *n*-mers. At high temperatures one can see filament formation, but at lower temperature, such as those that you were working at, we would see low *n*-mers under these conditions of Mg-ATP. These might possibly contribute to some of your force measurements.

MIYATA: Thank you for that information.

AMIT MEHTA: Your optically trapped bead is presumably a few micrometers above that coverslip to which the myosin is bound. So presumably some of the step is being delocalized into the direction perpendicular to the image plane since it is moving at a downward angle. I wondered if this could account for the difference between your results of around 5nm and the 10–17 nm observed by Finer [et al., 1994] and Yanagida [Ishijima et al., 1994].

MIYATA: Yes, probably the downward movement occurs because the actin filament is tilted in our measurements. We have performed a control experiment in which the bead was adsorbed to a coverslip and compared it to the measurements in which the bead held in an optical trap was tied to the surface-bound HMM in the absence of ATP. When we moved the coverslip the same distance using a piezoelectric transducer, we found that the horizontal bead motion in the latter system was about 1.5 times smaller. Thus we think that the geometric consideration could partly explain the difference, but at the present moment we can't totally explain the difference between the Finer group's and the Yanagida group's results and ours.

GERRY POLLACK: Two points, the first is a general comment, and the second a question. For a period of about 10 years we measured stepwise changes in larger scale preparations ranging from whole fibers to small parts of fibers and even to myofibrils. These are really very easy experiments to do in terms of detection of steps relative to the single filament preparation. Now for quite a while these steps were thought to be artifacts, and there was a big controversy. However in the last couple of years there has been confirmation both in Sugi's and Tomiazu's laboratory, the latter of which also finds the steps using different methods. I'm thus not sure that this is necessarily an artifact. If it's true–and their step sizes appear to be roughly the same per half sarcomere as you have been measuring—it may be that larger-scale preparations offer a better opportunity to measure these steps in a more easily controlled environment. The second point is a question, which is a followup from the last comment. If you have a large bead there is a force directed in the *z* axis that is pulling the thin filament upwards, in addition to that pulling along the axis of the filament. Why does the actin filament remain attached to the surface given this upwards directed force?

MIYATA: Thank you very much for the comment. In response to your question, the answer is probably that the HMM nearest the bead kept holding the filament as long as the bead motion was observed. This is possible if one head holds the filament and the other does its work. But we do not know if this particular mechanism was the case.

筋収縮系の力学特性

石渡信一*

1. はじめに

筋肉は自分の手で触れることができるという点で，生体運動を担う器官の中でも特異な存在である．力を出さず弛緩している時には柔らかく，力を出して収縮（強縮）しているときには硬くなるといった，状態の違いによる物性（力学特性）の違いを自ら実感できるという点で際立っている．また，揉みほぐしたり，少々叩いたくらいでは，収縮機能が損なわれたり，筋細胞が壊れたりすることもない．このように考えると，なんとも奇妙な感じがする．さらに想像をたくましくして，1 mm立方の筋肉の塊の中に千兆個もの筋タンパク質が含まれており，百兆個もの分子モーターが整然と配列していることを思うとき，この塊の柔らかさ，硬さを実感できることの奇妙さに心を打たれる．

ところで近年，光学顕微鏡法，レーザー光ピンセットなどの顕微操作法，ビデオ画像解析法などの実験技術の進歩[1]によって，我々は筋肉を構成する直径数十 μm の筋細胞（単一筋線維）のみならず，数十 nm の大きさの分子モーター1個の力学特性さえ研究できるようになってきた．指先に感ずる筋肉の柔らかさと，筋肉を構成する筋タンパク質の柔らかさとが関係づけられようとしている．この小論では，最近開発された実験技術を用いて得られた，横紋筋とそれを構成する分子モーターの力学特性に関する研究成果を，我々の研究を中心にまとめる．

* Ishiwata S　早稲田大学理工学部物理学科

2. 筋収縮系の構造と機能

2.1 階層構造

本論に入る前に，筋収縮系の構造と機能について概観しよう[2]．横紋筋の構造を心筋を例にとって示すと，図1のように 10^{-1} m サイズの心臓という筋組織から 10^{-8} m サイズの単一分子モーターに至る階層構造をとっている．分子モーター（筋収縮系においては，通常ミオシン分子のこと）の働きと力学特性とが有効に加算されるように，筋節中では分子モーターは整然と規則的に配列している．筋収縮系における収縮要素は，ミオシン分子と，これと相互作用するアクチン分子である．ミオシン分子とアクチン分子はそれぞれ太いフィラメントと細いフィラメントと呼ばれる繊維状重合体をなしている．分子モーターはフィラメント上に周期的に配列しているが，筋節が直列（縦方向）に，そして横紋筋という名の由縁でもある並列（横方向）に整然と配列している．

細いフィラメント中のアクチンフィラメントには，制御タンパク質であるトロポミオシンとトロポニン（Ca^{2+} 結合タンパク質）が周期的に結合している．一方，太いフィラメントの骨格をなすミオシンフィラメントにも構造タンパク質が結合しているが，特に分子量300万といわれる巨大タンパク質コネクチン（タイチンとも呼ばれる）がフィラメントの中央部からフィラメントに沿って結合し，さらにフィラメントの端から突き出てZ線に達して結合している（図1には示してないが，

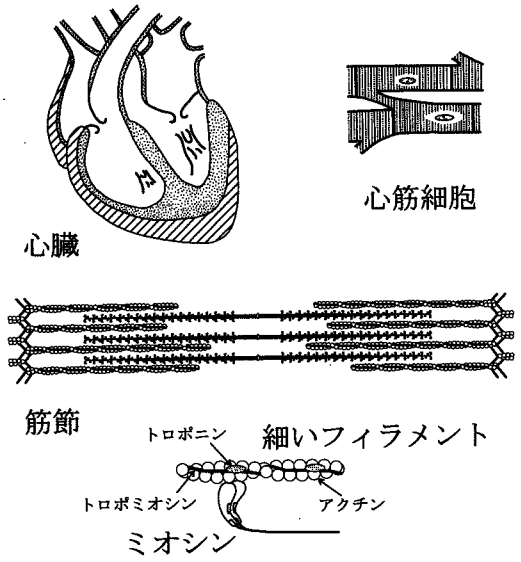

図1　心筋を例にとった横紋筋の階層構造
心筋は多核細胞からなる骨格筋とは異なり，単核細胞である．したがってその構造は筋線維レベルまでは骨格筋と異なる．しかし筋原線維レベルでほぼ一致し，筋節 (sarcomere) レベルとなるとほとんど変わらない．構造上で最も異なる点は，細いフィラメント（アクチンフィラメントにトロポミオシン，トロポニンなどの制御タンパク質が結合している）の長さが一様でない点とZ線の構造が堅固で幅が広い点である．分子モーターであるミオシン分子と，アクチンフィラメントの構造は基本的には心筋，骨格筋に共通している．骨格筋のミオシン分子の頭部（酵素活性断片として調製すると，S1と呼ばれる．一方HMM分子は2個のS1を含む）とアクチン分子の立体構造はすでに明らかになっている[16]．

図4b-dに模式図がある)[3,4]．したがって，太いフィラメントはコネクチン分子の弾性的な性質によって筋節の中央に繋ぎとめられていることになる．さらに骨格筋では，ネブリン（心筋には存在しない[4]）と名づけられた弾性タンパク質が細いフィラメントに沿って結合し，細いフィラメントの構造安定性に寄与しているといわれている[5,6]．

2.2　収縮・弛緩・自励振動[7-9]

筋収縮系は，通常力を発生して収縮する（ON状態）か，力を発生せずに弛緩する（OFF状態）かの2状態をとる（図2）．ON状態における発生張力は，細いフィラメントと結合するモーター分

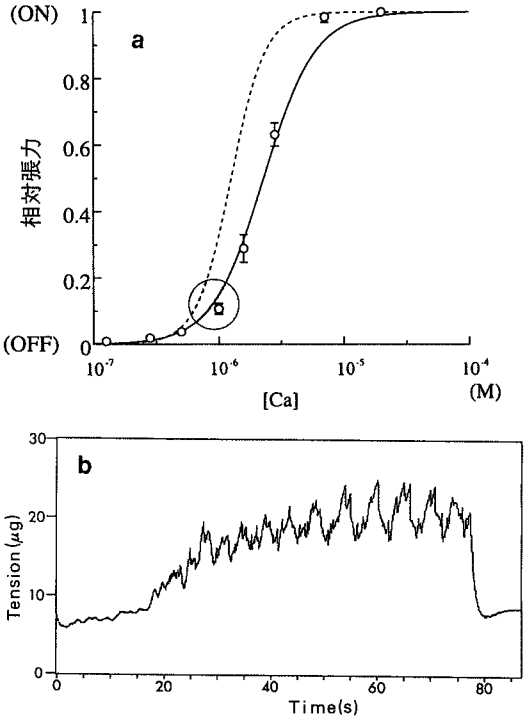

図2　筋収縮系の状態の Ca^{2+} 濃度による制御[7]
(a) 心筋収縮系の場合（実線）には，丸で囲まれた領域で自励振動（Ca-SPOC）が生じる．骨格筋収縮系の場合には，Ca-SPOCは筋タイプによって生じるものと生じないものとがある．すなわち，遅筋では心筋と同様に生じるが，速筋では生じない（破線）．速筋ではON，OFFの転移が鋭く，中間状態が安定には存在しないためらしい．ところが，Ca^{2+} 濃度があまり高くなく，しかもATPと同程度かそれ以上の濃度のADPとPiが共存すると，SPOCは筋タイプによらず生じる（ADP-SPOC）．(b) 骨格筋（速筋）筋原線維に見られるADP-SPOCにおける振動波形の例（ただし，発生張力と同時に平均筋節長も変化する条件でのもの)[10]．

子の数に比例する．力を発生して収縮する際には力学的エネルギーを必要とするが，そのためのエネルギー源としてはATPがADPと無機リン酸(Pi)に加水分解することによって解放される化学的エネルギーの一部が使われる．また2状態間の転移は，遊離の Ca^{2+} 濃度の変化によって起こる．遊離の Ca^{2+} 濃度が1 μMより高いと Ca^{2+} はトロポニン分子に結合し，低いと解離する．これに応じて細いフィラメントはON状態かOFF状態をとる．

ところで心筋の収縮系（筋原線維）の場合には，遊離の Ca^{2+} 濃度が ON・OFF 制御の中点にあたる 1 μM 付近で，筋節長あるいは発生張力が自発的に（自励）振動することが知られている（我々はこの現象を SPOC と呼ぶ；図 2 の丸の中）．骨格筋（速筋）ではこのタイプの SPOC は見られないが，Ca^{2+} 非存在下でも ATP 濃度以上の ADP と Pi が共存すると，同じような自励振動現象が見られることを我々は発見した[7-9]．このような自励振動現象については，その生理的意味も期待されているが，未だに不明な点が多い．ところで通常の収縮条件下では，筋節が伸長するとアクチンフィラメントと相互作用しているモーターの数が減少し，発生張力は減少するはずである．ところが SPOC 状態では筋節長が自発的に短縮，伸長を繰り返し，1 本の筋原線維中に異なる長さの筋節が共存する．SPOC 現象で興味深いのは，通常の収縮時には見られない動的安定性が見られる点である．複数個の分子モーターが関与することにより，細いフィラメントの ON，OFF 状態の制御がタンパク質構造変化の協同性を通じて行われている可能性が高い．

また，非生理的条件ではあるが，ATP 非存在下では，ミオシン分子はアクチンフィラメントと強固に結合し，筋線維は硬直することが知られている．ただし，ATP が存在する生理的条件下であっても，この硬直結合状態は滞在時間は非常に短いが存在するものと考えられている[8]．

3. 高次筋収縮系の力学特性

3.1 筋原線維の顕微操作

高次筋収縮系として，我々は単一筋原線維を取り上げる．単一筋原線維研究の意味は，単一筋原線維こそ，筋線維のもつ規則構造と収縮・力発生機能とを保持している筋収縮系として最小の構造体であり，しかも現在我々が取り扱うことのでき

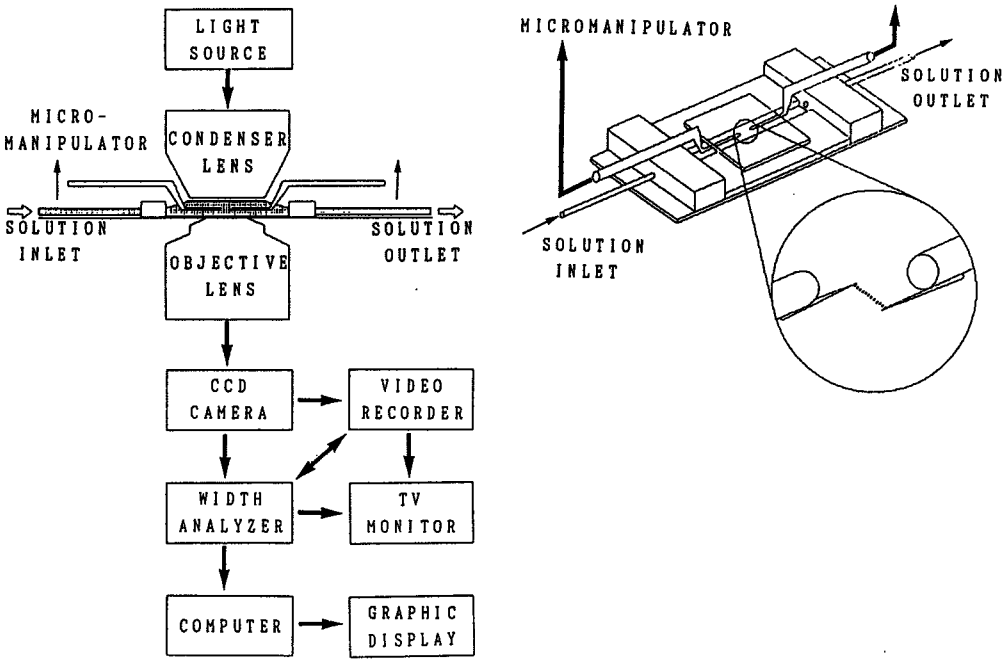

図 3　単一筋原線維の力学特性研究のために開発された顕微解析法の概略[5,10]
まず顕微鏡下で，筋原線維の両端をガラス微小針に巻き付ける．筋原線維の発生力は，柔らかい方の微小針の平衡位置からの変位を位置検出装置（ビデオ画像上で計測）を用いて計測することによって見積もる．この方法を用いて，発生力を nN（ナノニュートン）の精度で計測することができる．

る実験材料であるからである．

そうはいっても，直径1～数 μm の単一筋原線維の取扱いはそう容易ではない．我々はこれを顕微操作・顕微解析する実験法を工夫した[5,10]．計測装置の概略を図3に示す．この方法の利点は，横紋筋の周期構造を実時間で観察しつつ同時に収縮力や弾性率などの力学特性を計測することができる点にある．現在は，実験材料としてはもっぱら骨格筋（ウサギ腸腰筋；速筋タイプ）を用いている．心筋（特に脊椎動物の）は筋細胞間の結合組織が堅牢で，筋原線維を調製しにくいという問題があり，今後解決法を探る必要がある．

3.2 弾性要素と収縮要素の力学特性

上記の筋原線維顕微操作・解析法を用いて，弾性要素であるコネクチンとネブリンの弾性率を計測した．まずコネクチンの弾性率は，ミオシンとアクチンの結合を抑制した弛緩条件か，あるいはアクチンフィラメントの切断タンパク質であるゲルゾリンで処理することによって細いフィラメントを除去した筋モデル（図4a）を用いて計測された[5]．弛緩条件にある筋原線維，あるいは細いフィラメントを除去した筋原線維を引き伸ばすと，太いフィラメントの端とZ線の間を繋いでいるコネクチン分子だけが伸びる[3,4]．したがって，これらの条件下で得られた張力-長さ（筋節長）関係は，コネクチン分子の弾性を反映している．図4aのように，この関係は下に凸の曲線であった．筋節長3.4 μm のときに，1本の太いフィラメントに結合しているコネクチン分子（数分子の束と考えられる）に加わっている力は20 pN，そこでの曲線の傾きから見積もった弾性率は長さ1 μm に換算して0.1 pN/nm であった．

つぎに，我々はネブリンの弾性率を見積もることのできる人工的な筋モデルも開発した[5]．硬直条件下でゲルゾリン処理することによって，細いフィラメントのうちでミオシン分子と結合していない部分だけを切断除去した．この筋モデルでは，除去された細いフィラメントの部分に結合していたネブリン分子の一部がむき出しになった．この筋モデルを伸長するとこの部分だけが伸びる

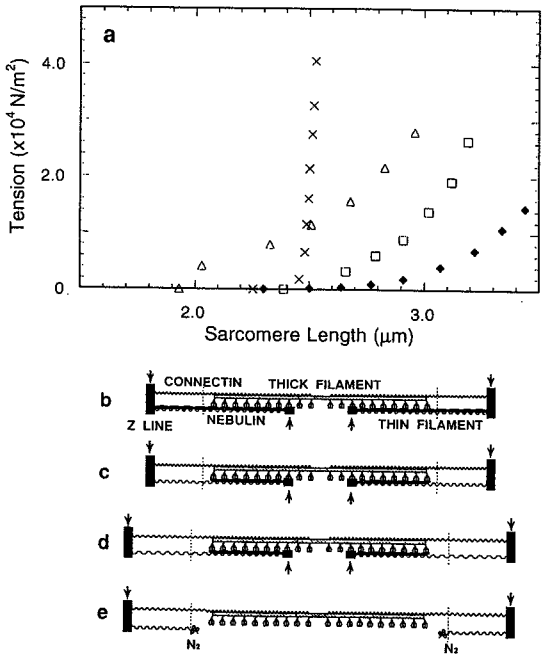

図4 いくつかの条件下での単一筋原線維の力学特性[5]

骨格筋（ウサギ腸腰筋）単一筋原線維を伸長することによって発生する張力－筋節長関係(a)．硬直条件(b)では，ミオシン分子だけでなくアクチンフィラメントの変形も発生張力に寄与する（×印）．弛緩条件（図bで，ミオシン頭部が細いフィラメントと結合していない状態）では，ミオシンフィラメントとZ線を繋いでいる弾性タンパク質コネクチンが伸長する（◆印）．I帯にある細いフィラメントの部分をゲルゾリン処理によって除去することによりネブリン分子をむき出しにし(c, d)，ネブリンのその部分を伸長することによって得られる張力-筋節長関係は上に凸の曲線となる（△印）．細いフィラメントを全て除去すると（e），伸長する部分は再びコネクチンだけとなる（□印）．

ことから，ネブリンとコネクチンとがその伸長の張力を担っていることになる．この筋モデルで見積もられた，長さ1 μm 当りのネブリンの弾性率はおよそ0.01 pN/nm であった．この弾性率は，アクチンフィラメントの弾性率（4.4節参照）よりも3桁以上小さかった．すなわち，ネブリンは細いフィラメントに沿ってその全長にわたって結合し，細いフィラメントの構造安定性に寄与しているものと考えられているが，その弾性率にはほとんど寄与していなかった．

ところで，図4aで最も傾きの大きな曲線は，硬直条件のものである．硬直条件での弾性率には，ミオシン頭部の変形と細いフィラメントの伸びが共に寄与している．この曲線の傾きから見積もったミオシン頭部の曲げの弾性率は，0.1 pN/nm程度であり，単一筋線維を用いて得られた値の数分の一であった．以下で述べる1分子計測の結果は，単一筋線維に近い値を示している．

4. アクトミオシン分子モーターの力学特性

4.1 *In vitro* 滑り運動系

ガラスなどの基盤上に吸着させたミオシン分子の上を，アクチンフィラメントはATPを分解しつつ滑り運動する．アクチンフィラメントは蛍光分子でラベルされているので，その動きは蛍光顕微鏡-超高感度テレビカメラ-ビデオシステムによって観察記録し，画像処理コンピューターによって解析することができる．この *in vitro* 滑り運動系と呼ばれる実験系が開発されたことによって，1個の分子モーターや一本のアクチンフィラメントの力学特性を研究することが可能になった．その成果を二，三紹介しよう．ここで紹介する研究には，ミオシン分子としてその酵素断片であるHMM（heavy meromyosin）分子を用いている．HMM分子はミオシン分子のもつATP分解酵素活性と，アクチンフィラメントに滑り運動を引き起こす分子モーターとしての能力を保持している．

4.2 アクチンフィラメントの回転滑り運動と超ラセン形成[11,12]

分子モーターの働きによって，アクチンフィラメントはその長軸方向に滑り運動する．したがって，分子モーターの発生する滑り力ベクトルは長軸方向を向いているはずである．しかし，その正確な向きは明らかではなかった．そこで我々は，もし滑り力ベクトルがわずかでも長軸方向から傾いていれば，滑り力ベクトルは長軸と垂直な成分を持つことになり，フィラメントをその長軸の回りに回転させるようなトルク成分が存在するはずである点に注目した．では，このトルクの存在の有無を調べるにはどうしたらよいだろうか．一つの方法は，フィラメントの回転運動を直接観察することである．例えばフィラメントの後端部に非対称な形状の物体を結合させておき，*in vitro* 滑り運動系を用いてその回転運動を観察するという方法が考えられる．しかしこの方法では，アクチンフィラメントが数 μm の長さになると曲げの柔らかさが目立つようになり，観察が困難になる．そこで我々は，図5に示すような，回転運動を間接的に示すことのできる，人工的な *in vitro* 滑り運動系を考案した[11]．

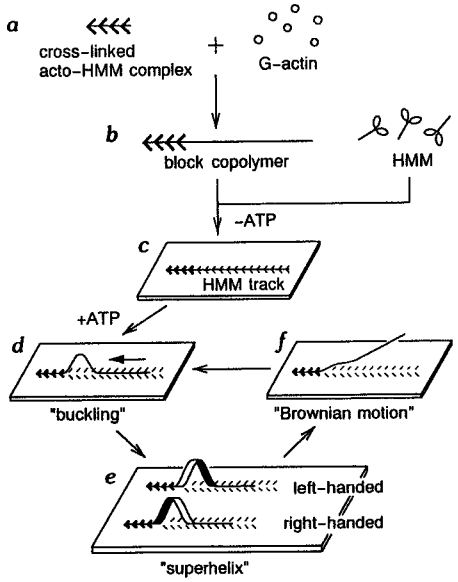

図5 アクチンフィラメントの回転滑り運動を検証するための *in vitro* 滑り運動実験系[11]
アクチンフィラメントの先端部をガラス表面に固定した上で後端部が滑り運動するためにフィラメントの中間部が捻れ，超ラセン（superhelix）が形成された．ラセンが右巻きか，左巻きかを蛍光顕微鏡観察によって決定し，フィラメントの回転の向きを推測した．

アクチンフィラメントの先端部を固定すると，その後方の滑り運動によってフィラメントの中央部分が押されて座屈し横にふくらむ．もし滑り運動にさらに回転運動が伴っていれば，ふくらんだ部分が捻れて超ラセン（superhelix）が形成されるはずである．そして，この超ラセンが右巻きか左

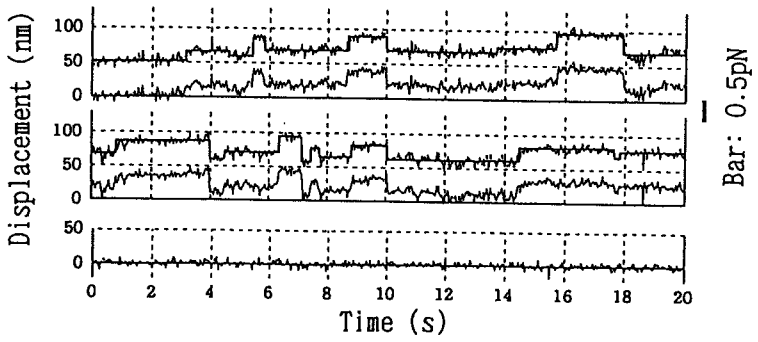

図6　少数個の分子モーターによって発生するアクチンフィラメント滑り運動（ステップ）と滑り力[14]
ガラス表面に吸着するミオシン分子の密度を下げるだけでなく，ATP濃度を0.5 μM以下にすることによって，分子モーターの素動作（ATP 1分子の加水分解に伴う1ステップ）を検出した．

巻きかを蛍光顕微鏡で観察することができれば，右巻きならば左回転，左巻きならば右回転であると結論できる．その結果は，ほとんどの場合に左巻きであった．すなわち結論は，滑り運動は右ネジが進むように生じるというものである．

その後，第一の方法を検討し，次節で述べる方法によってプラスチックビーズをアクチンフィラメントの後端に2個結合させて滑り運動を行わせるという実験系を作り，発生トルクの大きさを検討した[13]．上で述べたような，フィラメントの先端部を固定した上で回転運動を観察するという実験系での検討はまだ行っていない．通常の *in vitro* 滑り運動系では，アクチンフィラメントに垂直な滑り力成分は，フィラメント1 μm当り0.1 pN以下であると見積もられた．

4.3　分子モーターの素動作・発生力

近年，集光したレーザー光の焦点付近に原子・分子・微粒子を捕捉するレーザー光ピンセット法と呼ばれる非接触捕捉法が開発され，生物学研究にも盛んに用いられるようになってきた．我々は，直径1 μmのプラスチックビーズをアクチンフィラメントの後端に結合し[13]，このビーズを光ピンセットで捕捉することによって，アクチンフィラメントの顕微操作やアクチンフィラメントに発生する滑り力の顕微計測を行っている．ビーズに作用する光ピンセットの捕捉力は，フックのバネのように捕捉中心からの距離に比例する．

アクチンフィラメントの後端に結合したビーズを捕捉しつつ 0.5 μM以下のATPを加えたところ，図6に示すようなステップ状の動きがみられるようになった[14,15]．このステップの大きさ（ステップサイズ）は平均10 nmのオーダーであったが，捕捉力を弱めると大きくなる傾向にあった．分子モーターは1分子のレベルで，外力の大きさに応じてその素動作を柔軟に調節しうるようなメカニズムを備えているようにみえる．逆に捕捉力を強めると小さくなるが，あるサイズ以下にはならないようであった．この極限の1ステップで1分子モーターが発生する力は数pNと見積もられた．現在，このような分子モーター1個の素動作はモーターの立体構造が解明されたこともあって，その構造変化によって理解されようとしている[16]．

4.4　分子モーターと細いフィラメントの力学特性

ATP非存在下では，ミオシン分子はアクチンフィラメントと安定な硬直結合を形成する．我々は，*in vitro* 滑り運動系を用いてこの結合1個の破断力を計測した[17-19]．アクチンフィラメントの後端に結合したプラスチックビーズを光ピンセットで顕微操作することによって硬直結合に荷重を加えることができる．荷重を大きくすると結合は破断し，アクチンフィラメントはミオシン分子から離れる．図7にこのような過程を計測した結

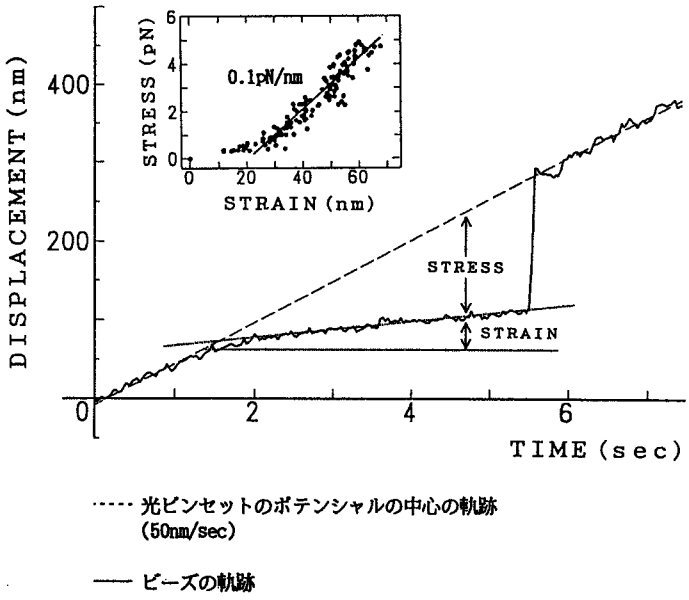

図7 分子モーター1個とアクチンフィラメントとの間の硬直結合（ATP非存在下での結合）の破断力と，分子モーターの弾性率の計測
プラスチックビーズの中心の位置は，画像解析によってnm（ナノメートル）の精度で計測することができる．したがって，光ピンセットの捕捉力の大きさにもよるが，0.1 pNより高い精度で発生力を計測することができる．

果をまとめる(西坂ら，未発表)．破線のように一定の速度（この例では50 nm/sであり，1.5 pN/sに対応する）で光ピンセットの捕捉中心を移動したところ，初めのうちはビーズは捕捉中心とともに移動したが，ある時点でアクチンフィラメントがピンと張るとその時点から捕捉中心からはずれ始めた．その後ビーズには，ビーズの中心と捕捉中心との間隔に比例する力が徐々に加わることになる．そして次に硬直結合が破断すると，ビーズは再び捕捉中心に捉えられた．この時の捕捉中心とビーズ中心との最大距離を求めることによって破断力が見積もられた．その結果，破断力は平均9.2 pNであった[19]．この値は，ATP 1分子の加水分解に伴って1個の分子モーターが発生する滑り力の大きさの数倍にあたる．

ミオシン，アクチン間の硬直結合の大きさは，ガラス微小針法[20]や原子間力顕微鏡法によって計測されたアクチンフィラメントの破断力[21]やアビジン-ビオチン間結合の破断力より一桁小さい．硬直結合の結合定数などからみて破断力が一桁も小さいという結果は，意外である．ミオシン頭部とアクチンフィラメント間結合には幾つもの分子間力が関与しているものと推測されるが，アクチンフィラメントに荷重が加わるとこれらの分子間力が全て一度に破断するのではなく，端から剝されるように徐々に破断するのではなかろうか．これは運動装置としての分子モーターの特徴であるのかもしれない[19]．

さて図7にもどると，ビーズが光ピンセットの捕捉中心から外れた後も，硬直結合が破断するまでの間，わずかではあるが変位したことを見てとることができる．この変位は分子モーター，アクチンフィラメント，ビーズとフィラメントの接合部分などの変形を含んでいる．この変位を横軸に，加えた荷重を縦軸にとると，この分子系の力-変形（stress-strain）関係が得られる．この曲線の傾きがこの分子系の弾性率を表す．最も大きな傾きをとると，平均0.5 pN/nmとなり単一筋

線維で求められたミオシン分子の曲げの弾性率とほぼ一致した．この値を分子モーター1個の弾性率と断定するにはまだ検討の余地があるが，その可能性は十分にある．

一方，アクチンフィラメントの両端にそれぞれ1個のプラスチックビーズを結合し，これを光ピンセットで顕微操作，保持することによってフィラメントに加える力とフィラメントの伸びとを計測しアクチンフィラメント1本の弾性率が見積もられた[22]．それによると，長さ1 μm のアクチンフィラメントの弾性率は 44 pN/nm であった．これにトロポミオシンが結合すると，弾性率は 65 pN/nm に上昇した．フィラメントの弾性率はミオシン分子の結合によっても変化することが知られており，フィラメントの力学特性が収縮・制御機構に密接に関係していることが期待される．

5. 結　　語

筋収縮系の力学特性の研究は，分子モーター1個あるいは筋フィラメント1本の力学特性（力学特性に限らず様々な物性）の研究が可能になったことによって，新しい段階に入った[20]．これまで高次の筋収縮系において明らかになってきた力学特性は，1分子の物性をもとに理解されようとしている．今後は，筋線維や筋原線維の運動生理機能（収縮，自励振動，弛緩）を，1分子の物性を積み上げることによって理解することができるようになるであろう．その中で，分子集合体に固有の協同性などの，生体構造の特徴が浮き彫りになることが期待される．

文　　献

1) 石渡信一(編)：実験生物物理，丸善　東京 1993
2) 石渡信一：筋フィラメントの構造と機能．病態生理 **10**：437-444，1991
3) Funatsu T, Higuchi H, Ishiwata S: Elastic filaments in skeletal muscle revealed by selective removal of thin filaments with plasma gelsolin. J Cell Biol **110**: 53-62, 1990
4) Funatsu T, Kono E, Higuchi H, Kimura S, Ishiwata S, Yoshioka T, Maruyama K, Tsukita S: Elastic filaments *in situ* in cardiac muscle: Deep-etch replica analysis in combination with selective removal of actin and myosin filaments. J Cell Biol **120**: 711-724, 1993
5) Yasuda K, Anazawa T, Ishiwata S: Microscopic analysis of the elastic properties of nebulin in skeletal myofibrils. Biophys J **68**: 598-608, 1995
6) Yasuda K, Fujita H, Fujiki Y, Ishiwata S: Length regulation of thin filaments without nebulin. Proc Japan Acad **70**: 151-156, 1994
7) 石渡信一：収縮構造を解剖する．日本物理学会編，生物物理のフロンティア，培風館　東京 1989，134-145
8) Ishiwata S, Yasuda K: Mechano-chemical coupling in spontaneous oscillatory contraction of muscle. Phase Transitions **45**: 105-136, 1993
9) Ishiwata S, Okamura N, Shimizu H, Anazawa T, Yasuda K: Spontaneous oscillatory contraction (SPOC) of sarcomeres in skeletal muscle. Adv Biophys **27**: 227-235, 1991
10) Anazawa T, Yasuda K, Ishiwata S: Spontaneous oscillation of tension and sarcomere length in skeletal myofibrils. Microscopic measurement and analysis. Biophys J **61**: 1099-1108, 1992
11) Nishizaka T, Yagi T, Tanaka Y, Ishiwata S: Right-handed rotation of an actin filament in an *in vitro* motile system. Nature **361**: 269-271, 1993
12) Tanaka Y, Ishijima A, Ishiwata S: Superhelix formation of actin filaments in an *in vitro* motile system. Biochim Biophys Acta **1159**: 94-98, 1992
13) Suzuki N, Miyata H, Ishiwata S, Kinosita K Jr: Preparation of bead-tailed actin filaments: Estimation of the torque produced by the sliding force in an *in vitro* motility assay. submitted to Biophys J, 1995
14) Miyata H, Hakozaki H, Yoshikawa H, Suzuki N, Kinosita K Jr, Nishizaka T, Ishiwata S: Stepwise motion of an actin filament over a small number of heavy meromyosin molecules is revealed in an *in vitro* motility assay. J Biochem **115**: 644-647, 1994
15) Miyata H, Hakozaki H, Yoshikawa H, Suzuki N, Furuno T, Ikegami A, Kinosita K Jr, Nishizaka T, Ishiwata S: Mechanical measurements of single actomyosin motor force. Biophys J **68**: 2865-2905, 1995
16) Rayment I, Holden HM: The three-dimensional structure of a molecular motor.

Trends Biochem Sci **19**: 129-134, 1994
17) Nishizaka T, Miyata H, Yoshikawa H, Ishiwata S, Kinosita K Jr: Microscopic measurement of the sliding and binding force between muscle proteins with optical tweezers. Optical methods in biomedical and environmental sciences. Ohzu H, Komatsu S eds, Elsevier Sci B V 1994, Amsterdam, 195-198
18) Nishizaka T, Miyata H, Yoshikawa H, Ishiwata S, Kinosita K Jr: Mechanical properties of a single protein motor of muscle studied by optical tweezers. Biophys J **68**: 75S, 1995
19) Nishizaka T, Miyata H, Yoshikawa H, Ishiwata S, Kinosita K Jr: Unbinding force of a single motor molecule of muscle measured using optical tweezers. submitted, 1995
20) Yanagida T, Harada Y, Ishijima A: Nanomanipulation of actomyosin molecular motors *in vitro*: a new working principle. Trends Biochem Sci **18**: 319-324, 1993
21) Kishino A, Yanagida T: Force measurements by micromanipulation of a single actin filament by glass needles. Nature **334**: 93-96, 1988
22) Kojima H, Ishijima A, Yanagida T: Direct measurement of stiffness of single actin filaments with and without tropomyosin by *in vitro* nanomanipulation. Proc Natl Acad Sci USA **91**: 12962-12966, 1994

Unbinding force of a single motor molecule of muscle measured using optical tweezers

Takayuki Nishizaka*, Hidetake Miyata†, Hiroshi Yoshikawa†, Shin'ichi Ishiwata*‡§ & Kazuhiko Kinosita Jr†

* Department of Physics, School of Science and Engineering, and ‡ Advanced Research Center for Science and Engineering, Waseda University, 3-4-1 Okubo, Shinjuku-ku, Tokyo 169, Japan
† Department of Physics, Faculty of Science and Technology, Keio University, 3-14-1 Hiyoshi, Kohoku-ku, Yokohama 223, Japan
§ To whom correspondence should be addressed.

THE unbinding and rebinding of motor proteins and their substrate filaments are the main components of sliding movement[1]. We have measured the unbinding force between an actin filament and a single motor molecule of muscle, myosin, in the absence of ATP, by pulling the filament with optical tweezers[2]. The unbinding force could be measured repeatedly on the same molecule, and was independent of the number of measurements and the direction of the imposed loads within a range of ±90°. The average unbinding force was 9.2 ± 4.4 pN, only a few times larger than the sliding force[3–5] but an order of magnitude smaller than other intermolecular forces[6,7]. From its kinetics[8] we suggest that unbinding occurs sequentially at the molecular interface, which is an inherent property of motor molecules.

In the absence of ATP, a myosin molecule binds to an actin filament forming a crossbridge through a rigor bond. On a glass surface coated with a low concentration of heavy meromyosin (HMM), which is a proteolytic fragment of myosin, short actin filaments (1–2 μm long) rotated around a single point over a range of more than 360° (which is analogous to a microtubule tethered by a single kinesin molecule[9]). Long filaments (5–20 μm long) were attached to the surface at nodal points a few micrometres apart (Fig. 1), between which the filament showed brownian bending motion. These observations suggest that each attachment point corresponds to a single HMM molecule[10], although it is possible that a cluster of HMM molecules may have been involved in some cases.

To measure the unbinding force needed to rupture the rigor bond, we used optical tweezers to impose an external load on the crossbridge by manipulating a polystyrene bead attached to the rear end of an actin filament using gelsolin, an actin binding protein (Fig. 1). The actin filament, once detached, could be reattached by manipulating it into the same position on the surface, provided the front remained attached to the surface by one or more HMM molecules. The reattachment was usually made at a slightly different point on the actin filament indicating that the unbinding had occurred between the actin filament and the HMM molecule, not between the HMM molecule and the glass surface.

The time course of the displacement of the bead is shown in Fig. 2*a*. First, the bead smoothly followed a laser spot moving at a constant rate (along the dotted line), but lagged behind after the actin filament became taut (at 1.4 s; compare with Fig. 1*A*, *a*), so that a load proportional to the distance between the bead and the trap centre was imposed on the rigor bond (labelled 'stress' in Fig. 2*a*). When the rigor bond was ruptured, the bead returned to the trap centre (at 2.9 s in Fig. 2*a*; compare with Fig. 1*A*, *b*), and we could directly determine the unbinding force from this abrupt displacement. The distribution of this unbinding force is shown in Fig. 2*c*: the peak was at 7 pN and the mean value was 9.2 ± 4.4 pN ($n = 168$). This unbinding force is much smaller than other intermolecular forces, for example 110 pN for actin–actin[6], 160 pN for avidin–biotin[7] and >20 pN for actin–gelsolin (judging from the stability observed in the above measurements), but is comparable to the maximum sliding force produced by a single HMM molecule in the presence of ATP[3–5].

Even after the actin filament became taut, the bead was displaced slightly ('strain' in Fig. 2*a*), such that a stress–strain relation could be obtained (Fig. 2*b*). The maximum strain at which the rigor bond was ruptured was 69 ± 27 nm ($n = 30$), larger than a myosin head (20 nm), which indicates that the strain contains

FIG. 1 *A*, A series of fluorescence micrographs showing the measurement of the unbinding force of a rigor bond(s) between a single actin filament and a single HMM molecule. The bead (indicated by the black arrow in *a*) was trapped by a single beam of laser light and moved at a constant rate to the direction indicated by the white arrow, such that the actin filament became taut. The actin filament was attached to the surface by two separate HMM molecules identified as two nodal points (arrowheads in *a*)[10]. As the laser spot was further moved, the load was increased and subsequently one of the two molecules unbound (*b*), such that the filament became nearly straight (c). The actin filament could be reattached to the same HMM molecule repeatedly by manipulating the filament into the same position while the second molecule was still attached, and the external loads could be imposed in any direction, as indicated by the white arrows (*d* and e). Scale bar, 5 μm. *B*, Schematic illustration of *A*: θ is the angle of the applied force, h (<1 μm) is the height of the bead ($\phi \leqslant 10°$).
METHODS. Actin and myosin were prepared from rabbit skeletal white muscle. HMM prepared by chymotryptic digestion of myosin was stored in liquid N_2 (ref. 18). Gelsolin was prepared as described previously[19] and crosslinked to the carboxylated polystyrene bead (1 μm in diameter; Polysciences, PA) with 1-ethyl-3-(3-dimethylaminopropyl)-carbodiimide (N. Suzuki *et al.*, submitted), such that the barbed end of an actin filament was attached to the bead. The average number of actin filaments attached to the bead was controlled by crosslinking an appropriate amount of bovine serum albumin (BSA) to the bead (for example, BSA:gelsolin = 20:1 in weight ratio). A small amount of BSA labelled with rhodamine X maleimide (Molecular Probes, Eugene, OR) was also crosslinked to the bead surface, and the actin filaments were labelled with rhodamine phalloidin (Molecular Probes). The *in vitro* assay system was based on that reported previously[20] but with modifications as follows: the coverslip was exposed to vaporized hexamethyl disilazane (HMDS; Nakalai Tesque, Kyoto) at room temperature overnight. A 50-μm thick flow cell, of which the lower surface was an HMDS-coated coverslip, was filled with assay buffer (25 mM KCl, 4 mM $MgCl_2$, 25 mM imidazole-HCl (pH 7.4), 1 mM EGTA, 1 mM dithiothreitol). Then 2–5 μg ml^{-1} HMM, in assay buffer, was infused from each side of the cell, at an interval of 60 s, and washed with assay buffer containing 0.5 mg ml^{-1} BSA, 10 mM dithiothreitol, 0.22 mg ml^{-1} glucose oxidase, 0.036 mg ml^{-1} catalase and 4.5 mg ml^{-1} glucose (solution B). Finally, bead-tailed actin filaments (20 nM actin and 0.05% (w/v) bead), in solution B, were infused. All experiments were done at 28–30 °C after rinsing the flow cell three times with solution B to wash out ATP (⩽20 nM) carried over from the G-actin solution. An inverted microscope (TMD-300: an oil-immersion objective lens with a phase ring, ×100 NA = 1.3; Nikon, Tokyo) was equipped with optical tweezers based on a 1 W Nd:YLF laser (1053–1000p: $\lambda = 1.053$ μm; Amoco Laser, IL). The linear polarization of the laser light was changed to circular using a quarter waveplate. The trap centre could be moved at a constant rate by controlling a movable mirror with d.c. servo-motors (optmike-e; Sigma Koki, Hidaka, Japan). A phase-contrast image of the bead was digitized and its centroid was calculated with a frame memory computer (DIPS-C2000; Hamamatsu Photonics, Hamamatsu, Japan). A fluorescent image of an actin filament was simultaneously acquired with a modified dual-view microscopy system[21,22]. The trap stiffness used was about 0.1 pN nm^{-1} (at a laser power of 95 mW without the objective) as measured by the following two distinct methods. First, the position of a bead undergoing thermal brownian motion around the trap centre at a low laser power, for example, 0.43 mW, was analysed at a shutter speed of 1/8,000 s with a non-interlace CCD camera (TM-9700; PULNiX, Kyoto). Assuming the Boltzmann distribution for the bead position, the trap stiffness was calculated as 0.44×10^{-3} pN nm^{-1},

the elongation or tilting of some elastic parts in addition to a myosin head. It should be noted, however, that the average elastic modulus, 0.58 ± 0.26 pN nm^{-1} ($n = 17$), estimated at a stress of 8–10 pN (dotted line in Fig. 2*b*), was similar to the elastic modulus of a crossbridge estimated in muscle fibres[1,11].

We could repeatedly measure the unbinding force of the same HMM molecule by selecting long actin filaments attached to the glass surface at more than two points (Fig. 1); short filaments attached at a single point were difficult to reattach after unbinding because of extensive brownian motion at the free end. The unbinding force did not change significantly, even with repetition of the measurements (Fig. 3*a*), indicating that HMM had not been denatured despite the rigor bond being ruptured several times by the external loads.

We also examined whether the unbinding force depends on the direction of the external load (Fig. 1*Aa*, *d*, *e*). The angle (θ in Fig. 1*B*) was limited within the range of ±90°, because filaments forced to bend at angles larger than 90° tended to break at the bend. As shown in Fig. 3*b*, the unbinding force appeared to be independent of the direction of the load. This is due to the flexibility of an HMM molecule, as revealed by the rotation of the attached short actin filaments. In contrast, the sliding force[4]

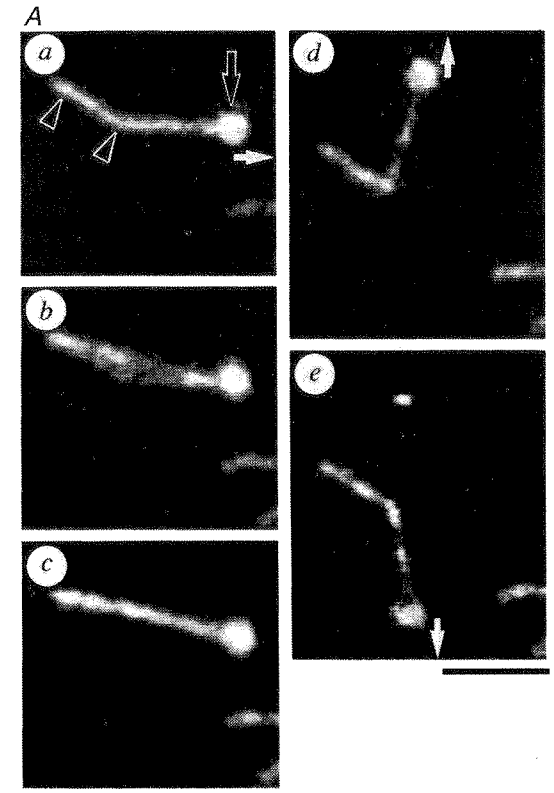

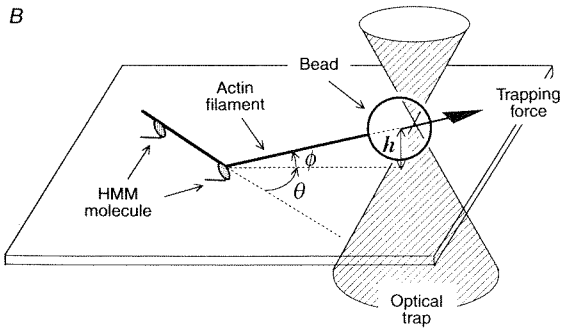

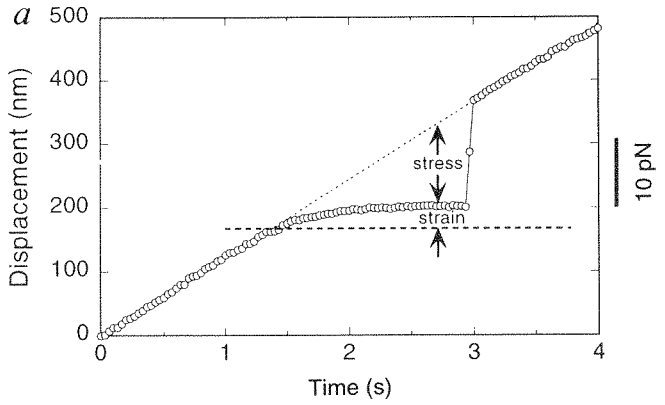

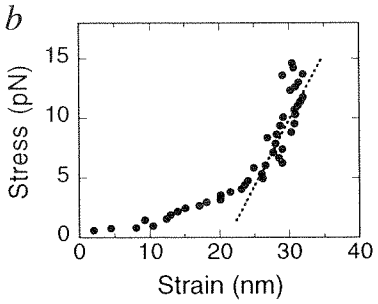

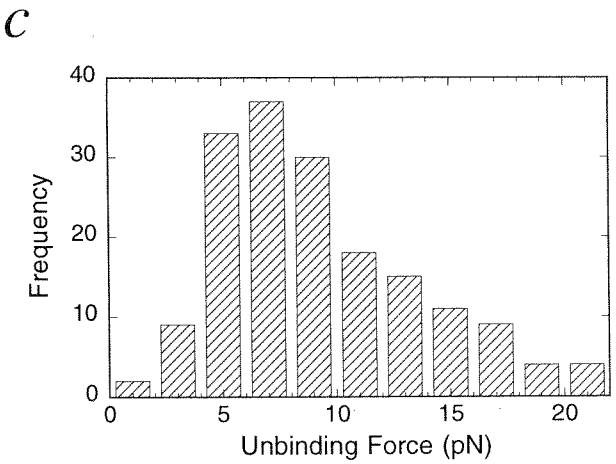

corresponding to 0.097 pN nm^{-1} at 95 mW. The stiffness values thus estimated at $h = 0.5$, 1.5 and 2.5 μm coincided to within ±5%. Second, the flow cell was displaced at a constant rate using a substage with a piezoelectric transducer (L. Pickelmann, Munich, Germany). A bead, trapped at $h = 2.5$ μm so as to make the effects of viscous coupling to the glass surface negligible, was displaced owing to the viscosity of water. The displacement was proportional, to 200 nm, to the force calculated as $F = 6\pi\eta av$, where η is the viscosity of water, a is the radius of the bead (0.5 μm), and v is the velocity of the flow cell. The trap stiffness was 0.095 pN nm^{-1} at 95 mW.

FIG. 2 *a*, Time course of the movement of the trap centre (dotted line, 120 nm s^{-1}, corresponding to about 12 pN s^{-1}) and the bead (circles) to which a single actin filament was attached. From the abrupt displacement at 2.9 s, when the rigor bond was ruptured, the unbinding force between an actin filament and an HMM molecule was estimated. *b*, Stress–strain relation obtained after the actin filament became taut at 1.4 s in *a*. In most samples the elastic modulus increased as the strain became large. The dotted line shows the elastic modulus at the imposed load of 8–10 pN. *c*, Histogram of the unbinding force between a single actin filament and a single HMM molecule.

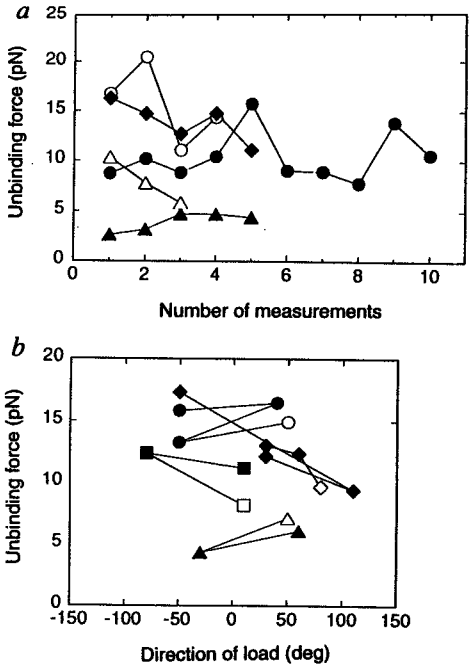

FIG. 3 Effects of the number of measurements (*a*) and the direction (θ defined in Fig. 1*B*) of the external loads (*b*) on the unbinding force measured on the same HMM molecules. Different symbols in each figure represent different HMM molecules. Open and closed symbols in *b* indicate the first and subsequent measurements, respectively, connected by lines.

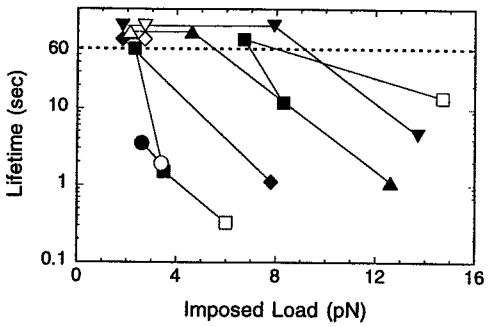

FIG. 4 Effects of the imposed loads on the lifetime of the rigor bond. The flow cell was displaced stepwise within 1/30 s so as to impose a constant external load (2–15 pN) using a piezoelectric substage (p-770.10; Physik Instrumente, Germany) with a function generator (1915; NF Electronic Instruments, Japan). The lifetime was repeatedly measured at various loads for the same HMM molecules. For those rigor bonds not ruptured within 60 s, the lifetimes are plotted above the broken line indicating 60 s. Different symbols represent different HMM molecules, and open and closed symbols indicate the first and subsequent measurements, respectively, connected by lines.

and velocity[12,13] of an actin filament depend largely on the orientation of myosin molecules assembled in a thick filament.

The lifetime of a rigor bond without a load has been reported to be 10^2–10^3 s (refs 14, 15). In our experiments (Fig. 2), HMM molecules detached within 3 s of an external load being imposed (1.5 (=2.9−1.4) in Fig. 2*a*), implying that the external load decreased the lifetime of the rigor bond. To confirm this load dependence, we applied a sudden, constant load and then measured the time that elapsed before unbinding occurred (Fig. 4). Individual lifetimes measured repeatedly on each HMM clearly show that a higher load tends to shorten the lifetime (see lines connecting the symbols in Fig. 4). This is consistent with the observation that the detachment rate of rigor crossbridges in muscle fibres is stress-sensitive[16]. Note that, although variations between different HMM molecules are large, data on individual HMM are relatively consistent (see also Fig. 3).

In our experiments, the actin filament was always 'pulled' in the direction opposite to the 'power stroke' of myosin (the bead being on the rear end of the actin filament), and the reverse pull at ~10 pN accelerated the rate of unbinding of the rigor bond by a factor of 10^2–10^3 (from 10^2–10^3 s to ~1 s (Figs 2 and 4)). This would imply an interaction distance of the order of $(\ln(10^2$–$10^3))k_BT/10$ pN ~ (2–3) nm (where k_B is the Boltzmann constant and T the absolute temperature)[17], which is an order of magnitude greater than the length of individual bonds at the molecular interface. On the other hand, the rate of unbinding of molecular bond(s) having a typical interaction distance (~0.3 nm) would be increased only by a factor of $2 \sim \exp(10\text{ pN} \cdot 0.3\text{ nm}/k_BT)$ (cf. Fig. 3 in ref. 8). This suggests that the reverse pull of the actin filament decreased very efficiently the activation energy barrier for unbinding.

Taken together, our results indicate that pulling an actin filament tends to distort the actin–myosin interface in such a way as to break the bonds at the interface sequentially from one end. This should be a rapid process compared to unbinding without a load, in which all bonds must break almost simultaneously. Conversely, if the myosin molecule in the 'power stroke' prestate could be 'pushed' in the direction of the 'power stroke', that is, towards the rigor-like state, a conformational change(s) that progressively increases the cohesive force between actin and myosin would occur and a longer lifetime would be expected. These properties were predicted on the basis of biochemical data, but our mechanical results suggest that they are inherent to the actin–myosin interaction, and that the role of ATP splitting is to regulate the process of conformational change. □

Received 23 January; accepted 31 July 1995.

1. Huxley, A. F. *Prog. Biophys. biophys. Chem.* **7,** 255–318 (1957).
2. Ashkin, A., Dziedzic, J. M., Bjorkholm, J. E. & Chu, S. *Optics Lett.* **11,** 288–290 (1986).
3. Finer, J. T., Simmons, R. M. & Spudich, J. A. *Nature* **368,** 113–119 (1994).
4. Ishijima, A. *et al. Biochem. biophys. Res. Commun.* **199,** 1057–1063 (1994).
5. Miyata, H. *et al. Biophys. J.* **68,** 286s–290s (1995).
6. Kishino, A. & Yanagida, T. *Nature* **334,** 74–76 (1988).
7. Florin, E., Moy, V. T. & Gaub, H. E. *Science* **264,** 415–417 (1994).
8. Erickson, H. P. *Proc. natn. Acad. Sci. U.S.A.* **91,** 10114–10118 (1994).
9. Hunt, A. J. & Howard, J. *Proc. natn. Acad. Sci. U.S.A.* **90,** 11653–11657 (1993).
10. Nishizaka, T., Miyata, H., Yoshikawa, H., Ishiwata, S. & Kinosita, K. Jr *Biophys. J.* **68,** 75s (1995).
11. Tawada, K. & Kimura, M. *J. Muscle Res. Cell Motil.* **7,** 339–350 (1986).
12. Yamada, A., Ishii, N. & Takahashi, K. *J. Biochem., Tokyo* **108,** 341–343 (1990).
13. Sellers, J. R. & Kachar, B. *Science* **249,** 406–408 (1990).
14. Marston, S. B. *Biochem. J.* **203,** 453–460 (1982).
15. Ishiwata, S. & Yasuda, K. *Phase Transitions* **45,** 105–136 (1993).
16. Schoenberg, M. & Eisenberg, E. *Biophys. J.* **48,** 863–871 (1985).
17. Bell, G. I. *Science* **200,** 618–627 (1978).
18. Nishizaka, T., Yagi, T., Tanaka, Y. & Ishiwata, S. *Nature* **361,** 269–271 (1993).
19. Kurokawa, H., Fujii, W., Ohmi, K., Sakurai, T. & Nonomura, Y. *Biochem. biophys. Res. Commun.* **168,** 451–457 (1990).
20. Toyoshima, Y. Y. *et al. Nature* **328,** 536–539 (1987).
21. Miyata, H. *et al. J. Biochem., Tokyo* **115,** 644–647 (1994).
22. Kinosita, K. Jr *et al. J. Cell Biol.* **115,** 67–73 (1991).

ACKNOWLEDGEMENTS. We thank N. Suzuki and I. Sase for technical assistance in the use of optical tweezers and dual-view microscopy, and T. Iga for preparing the gelsolin. This research was partly supported by Grants-in-Aid for Scientific Research and for Scientific Research on Priority Areas from the Ministry of Education, Science and Culture of Japan. T.N. is a recipient of a JSPS Fellowship for Japanese Junior Scientists.

Preparation of Bead-Tailed Actin Filaments: Estimation of the Torque Produced by the Sliding Force in an In Vitro Motility Assay

Naoya Suzuki,* Hidetake Miyata,* Shin'ichi Ishiwata,‡ and Kazuhiko Kinosita, Jr.*
*Department of Physics, Faculty of Science and Technology, Keio University, 3–14-1, Hiyoshi, Kohoku-ku, Yokohama 223, Japan; and
‡Department of Physics, School of Science and Engineering, Waseda University, 3–4-1, Okubo, Shinjuku-ku, Tokyo 169, Japan

ABSTRACT By coating covalently the surface of a polystyrene bead (diameter = 1 μm) with gelsolin, we have succeeded in attaching the bead selectively at the barbed end of an actin filament and forming a 1:1 bead-actin filament complex. On a layer of heavy meromyosin on a nitrocellulose-coated coverglass, this bead-actin filament complex slid smoothly, trailing the bead at its end. Therefore we called this preparation "bead-tailed" actin filaments. The sliding velocity was indistinguishable from that of nonbeaded filaments. With use of this system, we tried to detect the axial rotation (rotation around the filament axis) in a sliding actin filament. Although a single bead at the tail end did not serve as the marker for the axial rotation, we occasionally found another bead bound to the tail bead. In this case, the orientation of the bead-aggregate could be followed continuously with a video monitor while the filament was sliding over heavy meromyosin. We observed that actin filaments slid over distances of many tens of micrometers without showing a complete turn of the bead-aggregates. On the basis of the calculation of rotational friction drag on the bead-aggregate, we estimate that the rotational component of the sliding force and the torque produced on a sliding actin filament (length $\leq$10 μm) did not accumulate >1 pN and 5 pN · nm, respectively, in the present system of randomly oriented heavy meromyosin lying on a nitrocellulose film without an external load.

INTRODUCTION

To reveal the molecular mechanisms of muscle contraction and cell motility, much attention has been focused on in vitro motility assays (Harada et al., 1990; Huxley, 1990; Vale and Goldstein, 1990; Kron et al., 1991). Recently, several new systems that combine the in vitro motility assays with an apparatus for the simultaneous measurement of nanometer movements (Gelles et al., 1988; Svoboda et al., 1993; Block and Svoboda, 1995) and piconewton forces have been developed (Yanagida et al., 1993; Vale, 1994; Yanagida and Ishijima, 1995). In most of these systems, a bead is used as the handle for trapping with optical tweezers (Ashkin, 1992) and as the reporter of nanometer movements (Kuo and Sheetz, 1993; Svoboda et al., 1993; Finer et al., 1994, 1995; Miyata et al., 1994, 1995; Saito et al., 1994; Svoboda and Block, 1994; Coppin et al., 1995). In actomyosin motility assays, two beads coated with *N*-ethylmaleimide-modified myosin have been bound laterally to an actin filament (Finer et al., 1994, 1995; Saito et al., 1994; Molloy et al., 1995).

We describe here a method to attach a bead selectively to the rear end (barbed end) of an actin filament. The rear end-bound bead provides a relatively convenient means of measuring nanometer movements and piconewton forces with a single optical trap (Miyata et al., 1994, 1995; Nishizaka et al., 1995a,b) compared with the laterally bound beads with two optical traps (Finer et al., 1994, 1995; Saito et al., 1994; Molloy et al., 1995). To make beads designed to be bound to the barbed end of actin filaments, we used gelsolin. Gelsolin has the Ca^{2+}-dependent activity of severing an actin filament, capping the barbed end of the actin filament, and forming a polymerization nucleus as the complex with two actin monomers (Isenberg, 1991). When gelsolin was covalently bound to polystyrene beads (diameter = 1 μm) with EDC or glutaraldehyde, the coated bead was bound specifically to one end of an actin filament. The bead-binding actin filament slid smoothly in an in vitro motility assay, trailing the bead at its end as expected. Therefore, we called this preparation "bead-tailed" actin filaments.

As an application of the bead-tailed actin filaments, we attempted to detect the axial rotation (rotation around the filament axis) in a sliding actin filament. Here we used the tail beads as a marker of the axial rotation. Because an actin filament has a helical structure, the vector of the sliding force may be tilted against the long axis of the filament, and the sliding force has not only a translational component but also a rotational component. In the case of a microtubule and 14S dynein, the axial rotation of the microtubule was directly observed as the rotation of an axoneme attached to the rear end of the microtubule (Vale and Toyoshima, 1988). In the case of an actin filament and myosin, the axial rotation was indicated as a superhelix and a supercoil of the

Received for publication 10 April 1995 and in final form 5 October 1995.

Address reprint requests to Dr. K. Kinosita, Jr., Department of Physics, Faculty of Science and Technology, Keio University, 3–14-1, Hiyoshi, Kohoku-ku, Yokohama 223, Japan. Tel.: 81-45-563-1141, ext. 3975; Fax: 81-45-563-1761.

N. Suzuki's present address: Department of Physics, School of Science, Nagoya University, Furo-cho, Chikusa-ku, Nagoya 464–01, Japan.

Abbreviations used: HMM, heavy meromyosin; BSA, bovine serum albumin; EDC, 1-ethyl-3-[3-(dimethylamino)propyl]carbodiimide; MOPS, 3-morpholinopropanesulfonic acid; TMR, tetramethylrhodamine; DTT, dithiothreitol.

0006-3495/96/01/401/08 $2.00

actin filament (Tanaka et al., 1992; Nishizaka et al., 1993). However, we could not observe a complete turn of the tail beads. This suggests that the accumulated torque is not very high, at least in a usual in vitro motility assay system.

MATERIALS AND METHODS

Preparation of proteins

Acetone-dried powder of rabbit skeletal muscle was prepared according to the method of Ebashi and Maruyama (1965). Actin was extracted and purified by the method of Spudich and Watt (1971). Myosin was prepared from rabbit skeletal white muscle by the method of Perry (1955), with a slight modification described by Holtzer and Lowey (1959). HMM was prepared by α-chymotryptic digestion of myosin as described by Weeds and Taylor (1975). Gelsolin was purified from calf plasma by the method of Funatsu et al. (1990) or Kurokawa et al. (1990). HMM and gelsolin were stored in liquid nitrogen. Protein concentrations were determined spectrophotometrically using the extinction coefficients, $A^{1\%}_{1cm}$ = 6.3 at 290 nm for actin (Houk and Ue, 1974), 6.0 at 280 nm for HMM (Margossian and Lowey, 1978), 6.6 at 280 nm for BSA (A4378; Sigma, St. Louis, MO), and A^{mM}_{1cm} = 117 at 280 nm for gelsolin (Weber et al., 1991). The absorption was corrected for light scattering using the apparent absorption at 320 nm. The molecular weights of proteins were taken as 42,000 for actin, 350,000 for HMM, 83,000 for gelsolin, and 67,000 for BSA.

TMR-labeled BSA was prepared as follows. TMR-maleimide (T-489; Molecular Probes, Eugene, OR) dissolved in *N,N*-dimethylformamide (DMF) was added to BSA solution (~3 mg/ml in 0.1 M KCl and 20 mM MOPS (pH 7.0)) in a molar ratio 3–4:1. The mixture was incubated for 6 h at 0°C in the dark. The reaction was then stopped by adding DTT (141–12; Nacalai Tesque, Kyoto, Japan) to 2 mM. The mixture was dialyzed and applied to a column of Sephadex G-25 (Pharmacia LKB, Uppsala, Sweden). Approximately 70–80% of BSA was labeled by this method.

Gelsolin-coated beads

Covalent coupling of gelsolin to carboxylated polystyrene beads was carried out basically according to the recommended protocol of Polysciences (Warrington, PA), with a slight modification as follows: 0.5 ml of a beads suspension (2.5% carboxylated polystyrene beads, diameter = 1 μm, no. 08226; Polysciences) was placed in a sample tube (1.5 ml capacity). The beads were washed four times with 0.1 M sodium carbonate buffer (pH 9.6) by 5-min centrifugations at 10,000 rpm (TL100, TLA100.3 rotor with an adapter for the sample tube; Beckman, Palo Alto, CA). The beads were then washed four times with 20 mM sodium phosphate buffer (pH 4.5). The beads were resuspended in 0.625 ml of 20 mM sodium phosphate buffer (pH 4.5) and sonicated for 1 min by dipping the sample tube into a sonication bath (Sun cleaner 40kHz; Sun Electron, Tokyo, Japan). EDC (348–0363; Dojindo Laboratories, Kumamoto, Japan) was dissolved to 2% (w/v) in 20 mM sodium phosphate buffer (pH 4.5), and 0.625 ml of the solution was added to the beads suspension. The suspension was mixed continuously and gently for 3.5 h at room temperature. The beads were collected with centrifugation at 10,000 rpm for 7 min and washed four times with 0.1 M borate buffer (pH 8.5). The beads were suspended in 0.7 ml of solution A containing 0.1 M borate buffer (pH 8.5), 0.1 mM $CaCl_2$, and 0.1 mM ATP (519979; Boehringer Mannheim, Mannheim, Germany) and sonicated for 30 s. Four hundred micrograms of proteins (320 μg BSA, 40 μg TMR-labeled BSA, 20 μg G-actin, and 20 μg gelsolin) dissolved in 0.5 ml of solution A was added to the beads suspension. The suspension was mixed continuously and gently for 8–10 h at room temperature in the dark. To stop the reaction, 50 μl of 0.25 M ethanolamine (012–12455; Wako Pure Chemical Industries, Osaka, Japan) was then added and mixed gently for 30 min. The beads were collected with centrifugation at 10,000 rpm for 7 min and resuspended in 1.2 ml of 10 mg/ml BSA in solution A. After sonication for 30 s, the suspension was gently mixed for 30 min. The beads were then washed three times with 10 mg/ml BSA in solution A. The beads were resuspended in 1 ml of a stock solution (150 mM NaCl, 20 mM sodium phosphate buffer (pH 7.4), 0.1 mM $CaCl_2$, 0.1 mM ATP, 10 mg/ml BSA, 5% (v/v) glycerol, and 0.1% (w/v) NaN_3) and stored at 0°C in the dark. The coated beads were usable for about 6 months. In the case of labeling beads of 0.5 μm diameter (no. 09836; Polysciences), three points were altered: centrifugation speed was 17,000 rpm, and 2.6% (w/v) EDC and 500 μg of total protein (with the same mixing ratio (w/w) as described above) were used.

Covalent coupling of gelsolin to amino polystyrene beads was also carried out basically according to the recommended protocol of Polysciences, with a slight modification as follows: 1 ml of a beads suspension (2.5% amino polystyrene beads, diameter = 1 μm, no. 17010; Polysciences) was placed in a sample tube. The beads were washed four times by 8-min centrifugations at 10,000 rpm with PBS containing 0.15 M NaCl and 20 mM sodium phosphate buffer (pH 7.4). The beads were mixed in 1.2 ml of 8% (v/v) glutaraldehyde (EM grade, 071-02031; Wako Pure Chemical Industries) in PBS and sonicated for 30 s. The suspension was mixed continuously and gently for 8 h at room temperature. The beads were then washed five times with PBS. In this washing process, the beads were sonicated for 30 s before each centrifugation. The beads were resuspended in 0.7 ml of solution B (0.15 M NaCl, 20 mM sodium phosphate buffer (pH 7.4), 0.1 mM ATP, and 0.1 mM $CaCl_2$) and sonicated for 30 s. Four hundred fifty micrograms of proteins (350 μg BSA, 50 μg TMR-labeled BSA, 25 μg G-actin, and 25 μg gelsolin) dissolved in 0.5 ml of solution B was added to the beads suspension. The suspension was mixed continuously and gently for 4.5 h at room temperature in the dark. The beads were collected with centrifugation at 10,000 rpm for 10 min. To stop the reaction, 1.2 ml of 0.5 M ethanolamine was added to the beads, and the suspension was sonicated for 30 s and mixed gently for 40 min. The beads were collected with centrifugation at 10,000 rpm for 10 min and resuspended in 1.2 ml of 10 mg/ml BSA in solution B. After sonication for 30 s, the suspension was gently mixed for 30 min. The beads were then washed three times with 10 mg/ml BSA in solution B. The beads were suspended in 1 ml of the stock solution and stored at 0°C in the dark. The coated beads were usable for about 6 months.

Bead-tailed actin filament

The gelsolin-coated beads stock (0.1 ml) was transferred into a sample tube, and 0.1 ml of solution C (25 mM imidazole-HCl (pH 7.4), 25 mM KCl, 4 mM $MgCl_2$, 0.1 mM $CaCl_2$, 0.1 mM ATP, 1 mM DTT, and 0.04% NaN_3) was added and sonicated for 30 s. The suspension was centrifuged at 6000 rpm for 4 min in a microcentrifuge. The beads were washed four times (six times for amino beads) with 0.2 ml of solution C. The beads were resuspended in 40 μl of solution C, and 10 μl of 10 μM F-actin labeled with TMR-phalloidin (Molecular Probes) (Yanagida et al., 1984) was added to the suspension. After gentle mixing, the suspension was incubated overnight at 0°C in the dark. The suspension was then diluted 1:50 with 2 mg/ml BSA in solution C and incubated for more than 2 h at 0°C. The diluted suspension was diluted further with a motility assay solution and used in an in vitro motility assay described below.

In vitro motility assay

The motility assay system we used was the same as that used by Kron et al. (1991), except for a slight modification as follows. We used Ca^{2+}- containing solutions: CaAB (25 mM imidazole-HCl (pH 7.4), 25 mM KCl, 4 mM $MgCl_2$, 0.1 mM $CaCl_2$, 1 mM DTT, and 0.04% (w/v) NaN_3), CaAB/BSA (2 mg/ml BSA in CaAB), CaAB/BSA/GOC (0.03 mg/ml catalase (C-10; Sigma), 0.15 mg/ml glucose oxidase (G-2133; Sigma), and 4.5 mg/ml glucose in CaAB/BSA), and CaAB/BSA/GOC/ATP (2 mM ATP in CaAB/BSA/GOC). We prepared a nitrocellulose-coated coverglass as follows: 2% collodion in isoamyl acetate (Ohken Industry, Tokyo, Japan) was diluted to 0.1% (v/v) in isoamyl acetate (019–03636; Wako Pure Chemicals Industries). Drops of diluted collodion were applied over a coverglass

(24 × 36 mm). The coverglass was tilted, the excess collodion was absorbed with a piece of filter paper, and the coverglass was air-dried. An experimental flow cell (depth = ~100 μm) was made of the collodion-coated coverglass and a noncoated coverglass (18 × 18 mm). We infused 90 μl of ~30 μg/ml HMM solution into the flow cell from one side, and immediately applied 90 μl of 0.5 mg/ml BSA in CaAB from the same side.

Observation system

TMR-labeled actin filaments and beads were observed with an inverted fluorescence microscope (TMD; Nikon, Tokyo, Japan) equipped with epifluorescence optics, an NCF Fluor DL ×100 objective (oil immersion, N.A. = 1.3; Nikon), a 100-W mercury arc lamp, and a G-2A filter cassette (Nikon). Fluorescence images were recorded on a videotape with an image intensifier (KS-1381; Video Scope, Washington, DC), a CCD camera (CCD-72; DageMTI, Michigan, IN), and a video recorder (S-VHS type; A-VS1 Toshiba or NV-FS1000 National, Tokyo, Japan). Movements were analyzed using a digital image processor (C2000; Hamamatsu Photonics, Hamamatsu, Japan).

RESULTS

Bead-tailed actin filaments

We used EDC for carboxylated beads and glutaraldehyde for amino beads as cross-linkers between gelsolin and beads. In both cases, we succeeded in preparing bead-tailed actin filaments. The results described below were essentially the same for both preparations.

We optimized two parameters in preparing the gelsolin-coated beads. One was the weight percentage of gelsolin to total protein (w/w) in the protein solution mixed with the activated beads. We used gelsolin as a 1:2 complex with monomeric actin; we maintained a 1:1 weight ratio of actin to gelsolin in all protein solutions. When the percentage was 50% (maximum percentage we examined, i.e., activated beads were mixed with the protein solution containing actin and gelsolin without BSA), many actin filaments bound to a single bead. When the percentage was too low (<1%), actin filaments scarcely bound to the beads. To maximize the number of actin filaments carrying a single bead, we usually adjusted the amount to several percent. However, this parameter depended on the age of gelsolin. With freshly prepared gelsolin, 1–2% was optimum. With aging of the gelsolin, the ability to bind the actin filament declined.

The other parameter was the weight percentage of TMR-labeled BSA to the total protein in the protein solution. The beads were visualized by staining them with TMR-labeled BSA, whereas actin filaments were labeled with TMR-phalloidin. The fluorescence brightness of the two should be approximately the same. This was achieved when the weight percentage was ~10%.

Fig. 1 shows the fluorescence images of the bead-tailed actin filaments in a rigor state. There were three types of bead-tailed actin filaments. The major type was a single actin filament carrying a single bead (Fig. 1 *a*). Another was a single actin filament carrying double (or more) beads (Fig. 1 *b*). We used this type of bead-tailed actin filaments to detect the axial rotation of a sliding actin filament. The bead-aggregate served as an asymmetric marker of the rotation around the filament axis. The last type was a single bead to which two (or more) actin filaments were bound (Fig. 1 *c*).

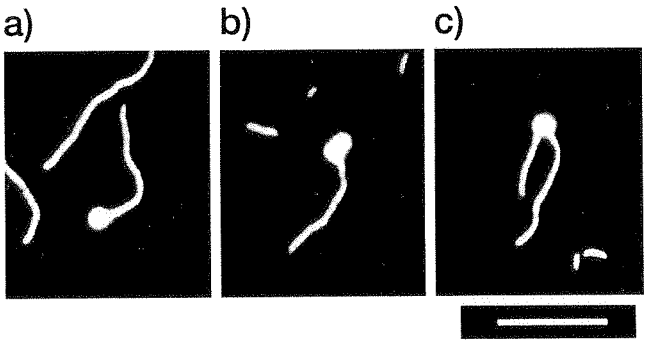

FIGURE 1 Fluorescence images of three types of bead-tailed actin filaments in a rigor state. Type (*a*), a single bead-tailed actin filament; type (*b*), a double bead-tailed actin filament; type (*c*), a single bead-tailed double actin filament. The diameter of the bead was 1.16 μm. Bar, 10 μm.

To confirm the specific binding of actin filaments to gelsolin on the beads, we performed two control experiments. In one, beads were covalently coated with BSA alone; in the other, the gelsolin-coated beads were mixed with F-actin without Ca^{2+} (1 mM EGTA was added to CaAB). In both cases, actin filaments were scarcely bound to the beads.

Sliding bead-tailed actin filaments

If the beads themselves have some nonspecific interaction with the HMM-coated glass surface, sliding of bead-tailed actin filaments must be obstructed. Unfortunately, the gelsolin-coated beads we prepared bound to the HMM-coated glass surface in the solution CaAB (in the rigor state without BSA). From the observations that addition of ATP did not detach the binding beads and the binding was suppressed by addition of BSA, we concluded that this binding was caused by nonspecific interaction (not by the specific interaction between actin on the beads and HMM coated on the glass). We found that the addition of BSA at 2 mg/ml was sufficient to reduce this nonspecific interaction to a negligible level. Therefore, all of the solutions for the sliding experiment contained 2 mg/ml BSA.

Fig. 2 shows the fluorescence images of a sliding bead-tailed actin filament. The bead-tailed actin filament slid smoothly, trailing the bead at its end. The sliding speed of the bead-tailed actin filaments was indistinguishable from that of the nonbeaded filaments (Fig. 3). This suggests that the trailing bead applied only a negligible load to the sliding actin filament.

When two actin filaments were bound to a single bead, each filament slid in its own direction. The two actin filaments formed a straight line, in opposite directions, and a pulling contest began between the opposing actin filaments (Fig. 4 *a*). When more than two actin filaments were bound to a single bead, all filaments slid away from the bead and

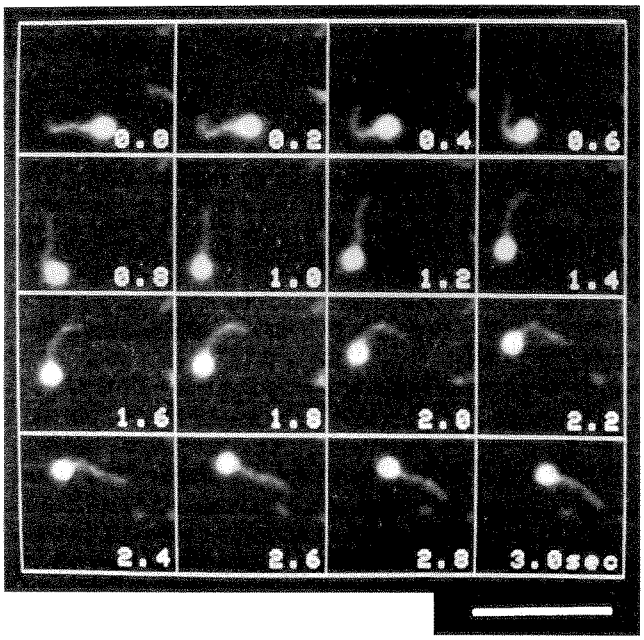

FIGURE 2 Fluorescence images, at 0.2-s intervals, of a sliding single bead-tailed actin filament in the in vitro motility assay (see Materials and Methods). The bead-tailed actin filament slid smoothly, trailing the bead at its end. The diameter of the bead was 1.16 μm. Bar, 10 μm.

were radially straightened from the bead (Fig. 4 *b*). These observations indicate that every actin filament bound to the gelsolin-coated bead had the same polarity; it was always the barbed end that was anchored to the bead.

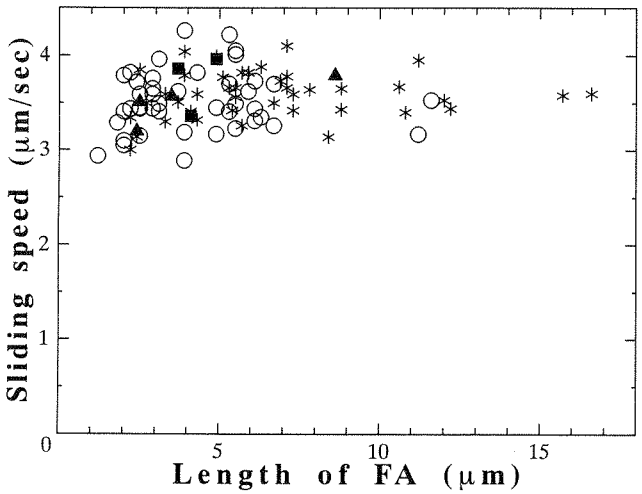

FIGURE 3 Sliding speeds of bead-tailed actin filaments and non-beaded actin filaments in the in vitro motility assay (see Materials and Methods) at 24°C. The diameter of the bead was 1.16 μm. The average sliding speeds ± SD (n = number of data, average length of actin filaments ± SD) were 3.59 ± 0.25 μm/s (n = 41, 6.60 ± 3.45 μm) for nonbeaded actin filaments (*asterisks*), 3.51 ± 0.32 μm/s (n = 43, 4.25 ± 2.25 μm) for single bead-tailed actin filaments (○), 3.52 ± 0.24 μm/s (n = 4, 4.25 ± 2.94 μm) for double bead-tailed actin filaments (▲), and 3.73 ± 0.32 μm/s (n = 3, 4.23 ± 0.61 μm) for triple bead-tailed actin filaments (■).

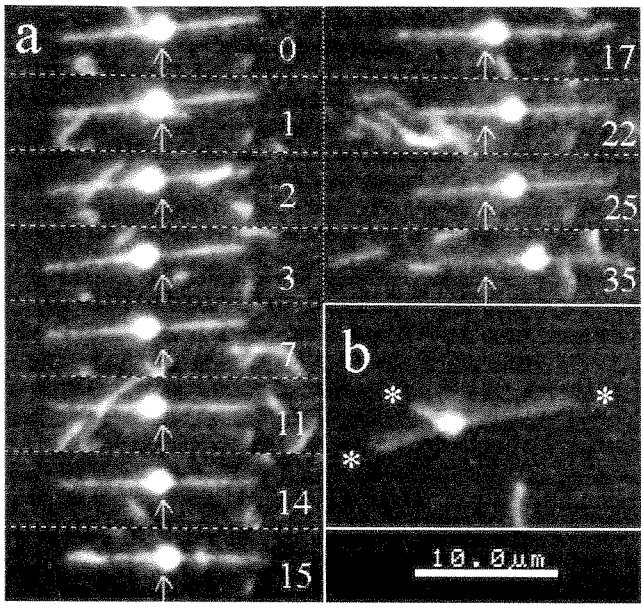

FIGURE 4 Single bead-tailed multiple actin filaments having the same polarity. (*a*) When two actin filaments were bound to a single bead, each filament pulled the bead. The two actin filaments formed a straight line, in opposite directions, and a pulling contest began between the opposing filaments. The arrows indicate the starting position of the pulling contest. The numbers are the elapsed time from the start of the pulling contest in seconds. (*b*) When three actin filaments were bound to a single bead, each filament (indicated by the *asterisks*) pulled the bead and was radially straightened from the bead. The diameter of the bead was 1.16 μm. Bar, 10 μm.

Attempt to detect the rotational motion during sliding

To detect the rotation of an actin filament around its long axis, we observed the sliding of the bead-tailed actin filaments. The orientation of the bead-aggregate (Fig. 5 *a*) was continuously followed by using a video monitor. The orientation fluctuated as seen in Fig. 5 *b*, but the fluctuations failed to accumulate into a turn. We observed a total of 58 filaments, 47 with double beads and 11 with triple beads, each for a continuous period of ~1 min. The total observation period was >1 h, corresponding to a total sliding distance of >12,000 μm. In these continuous runs, the bead-aggregate did not show a continuous rotation or a complete turn as an accumulation of fluctuations. Because of the quenching of fluorescence, the longest continuous observation time was 210 s. In this case, the filament slid over a distance as long as 700 μm without showing a complete turn of the tail beads.

The observed fluctuations of the orientation of the bead-aggregate, relative to the actin filament, suggested that the range of rotational angular fluctuations was ~90° (i.e., ±45°) during the observation period of ~1 min (Fig. 5 *b*). This value was estimated by eye (and therefore is not precise) and represents four times the standard deviation, 4σ ($\pm 2\sigma$). The relatively small angular range might have resulted from steric hindrance (collision with the glass surface), particularly if the bead-aggregate had tended to rotate in a preferred direction. Therefore, in 25 filaments carrying double beads we examined

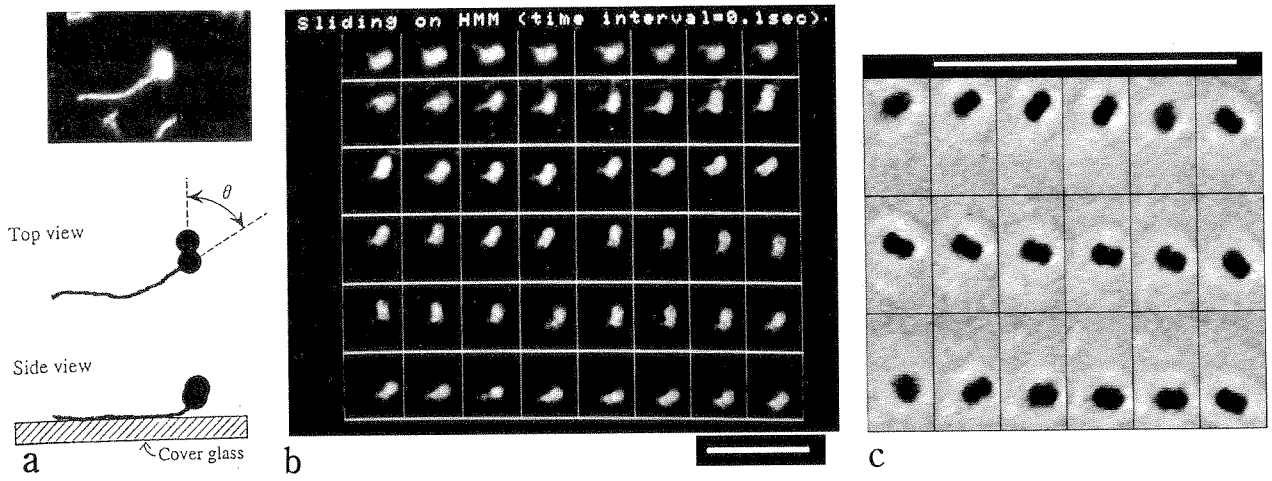

FIGURE 5 Images of a sliding double bead-tailed actin filament in the in vitro motility assay at 25°C (see Materials and Methods). (*a*) Fluorescence image of a sliding double bead-tailed actin filament and its schematic illustrations from the side and top. The diameter of each bead was 1.16 μm. The sliding speed was 4.0 μm/s. (*b*) A snapshot of the pulled double bead at 0.1-s intervals from left to right and top to bottom. If the double bead rotates around the actin filament, we can detect it as the change in the orientation of the bead-aggregate relative to the actin filament (θ in (*a*)). The snapshot shows that the range of angular fluctuations was ~90°. (*c*) A snapshot of phase contrast images, at 1/30-s intervals, of the double bead (bead diameter, 0.55 μm) pulled by an actin filament. The sequence, from left to right and top to bottom, shows a counterclockwise half turn followed by a clockwise half turn. Bars, 10 μm.

whether the second bead attached to the tail bead was located to the right or to the left of the sliding filament. In 8 of the 25 video sequences, the second bead predominantly resided on the right side. In 7, the second bead was on the left, and for the remaining 10, the second bead was found mainly on the filament axis (basically on top of the tail bead). Thus, collision of the second bead with the glass surface does not explain the small angular range, and it is not the reason why we failed to observe a complete turn of the bead-aggregate.

Hydrodynamic friction impedes the bead rotation in proportion to the cube of the bead radius (see Discussion). To reduce the friction, we tested beads with a diameter of 0.55 μm. Examination of 33 bead-tailed filaments, each for a continuous period of ~50 s, also failed to reveal a continuous rotation of the bead-aggregate. In the fluorescence images, however, it was difficult to ascertain whether a filament carried a double or a triple bead. Also, the orientation of the small bead-aggregate was not always unambiguous. Therefore, we observed seven bead-tailed filaments in phase-contrast images, in which double beads were clearly seen. Even in the phase images, the bead-aggregate went out of focus for a frame or two. Thus, the average unambiguous monitoring period was ~10 s. The double bead with the small diameter fluctuated considerably with an angular range of ≤180°. Occasionally, the bead-aggregate made a fast half turn. The fluctuations including such half turns, however, did not accumulate to make up a complete turn (Fig. 5 *c*).

Rotation of the tail beads relative to the actin filament

Although axial rotation in a sliding filament was observed as a superhelix by Nishizaka et al. (1993), we could not detect a complete turn of the bead-aggregate. One possible reason for the present result is that gelsolin (and the actin filament) was connected to the bead through only a single covalent bond around which the actin filament and the bead could rotate independently. To check this possibility, we observed rotational Brownian motion of bead-aggregates while the actin filaments were fixed on the glass surface through sparsely coated HMM in the rigor state. The sparse binding was achieved by perfusing a nitrocellulose-coated observation cell with an HMM solution at 0.3–3.0 μg/ml, 1/10–1/100 the concentration used in the motility assay (Nishizaka et al., 1995a). When bead-tailed actin filaments without ATP were introduced, the tail beads exhibited rotational Brownian motion whose amplitude depended on the length of the free actin tail. The range of angular fluctuations for an observation period of ~2 min was ~45° when the length of the filament between the bead surface and the first fixed point (HMM site) was ≤1 μm (n = 6), ~90° for 1–2 μm (n = 7), and ~180° for 3–4 μm (n = 4) (Fig. 6). This length dependence is consistent with the torsion of the free actin tail (see Discussion). Also, bead-aggregates at the tail never showed free rotational Brownian motion. Thus, we excluded the possibility of a single-bond linkage between gelsolin and the bead.

DISCUSSION

Bead-tailed actin filaments

Brown and Spudich (1979) reported that polylysine-coated polystyrene beads nucleated the polar assembly of G-actin to F-actin. They showed that the polarity of these filaments was uniform; the barbed end was away from the bead. Their preparation, however, was a multiple actin filament-bead

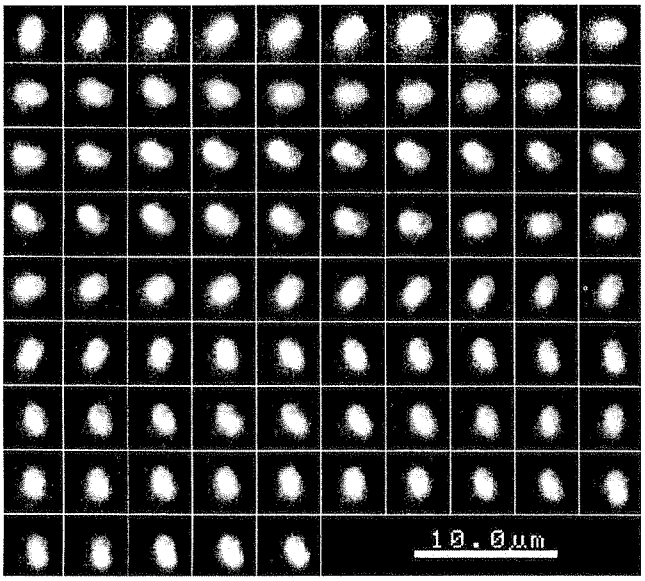

FIGURE 6 A snapshot of fluorescence images of rotational Brownian motion of a double bead at 2/30-s intervals from left to right and top to bottom. The actin filament was fixed on the glass surface through sparsely coated HMM in the rigor state. The length of the free actin filament tail (the length between the bead surface and the first fixed point) was ~3 μm. The range of the angular fluctuations was 180°; however, we never observed the free rotational motion of the bead-aggregate.

complex. They reported that the average number of filaments bound to a single bead was ~30 for the 1.1-μm beads and ~8 for the 0.1-μm beads (Brown and Spudich, 1981). In the present study, we succeeded in preparing a 1:1 polar complex of an actin filament with the gelsolin-coated bead. Our method may be applicable to the preparation of other types of polar complexes: for example, "bead-headed" actin filaments using pointed-end capping proteins such as a fraction of a β-actinin preparation (Funatsu et al., 1988), tropomodulin (Fowler et al., 1993), and so on (for a review see Pollard and Cooper, 1986). We tried DNase I (D4527; Sigma) as a candidate (Podolski and Steck, 1988) but failed in preparing a bead-headed actin filament; actin filaments did not bind to the DNase I-coated beads.

In vitro motility assay using bead-tailed actin filaments

To analyze the actomyosin motor force using bead-tailed actin filaments (Miyata et al., 1994, 1995), the bond between actin and gelsolin must be stronger than that force. Nishizaka et al. (1995b) measured the strength of a rigor bond between a bead-tailed actin filament and a single HMM molecule by pulling the tail bead with optical tweezers. The rigor bond was broken when pulled at 9.2 ± 4.4 pN, whereas the filament was not detached from the bead. This implies that the actin-gelsolin bond was stronger than 10 pN. In a similar experiment (T. Nishizaka, unpublished data) in which many myosin heads held an actin filament, the filament was detached from the bead at 49 ± 16 pN (n = 5), and in two cases the filament remained bound even at 70 pN. Thus, the actin-gelsolin bond is an order of magnitude stronger than a rigor bond.

The average translational component of the sliding force per micrometer of a single actin filament interacting with randomly oriented myosin and myosin subfragment-1 adsorbed on a silicone-coated surface was reported to be 9.6 and 5.4 pN, respectively (Kishino and Yanagida, 1988). We also measured the translational component of the sliding force produced by actomyosin interaction in our system using an optical trap technique and obtained a value of ~1 pN/μm of actin filament when 30 μg/ml of HMM was adsorbed on the nitrocellulose-coated surface (Kinosita et al., 1993). On the other hand, the frictional force against the translational movement of the bead is calculated using the Stokes equation: $F = 6\pi\eta r v$ (F, force; η, viscosity of the medium; r, radius of the bead; and v, sliding velocity). In the typical case in which a bead with a diameter of 1.16 μm is pulled at 4 μm/s, the frictional force is 0.044 pN. Thus, the frictional force is negligible compared with the translational component of the sliding force. This is consistent with the results in Fig. 3, in which the sliding velocity of the bead-tailed actin filaments was indistinguishable from that of nonbeaded actin filaments.

Torque for axial rotation of actin filament produced by actomyosin

A possible reason that continuous rotations of the bead-aggregates could not be detected is the hydrodynamic friction operating on them. The frictional moment against rotational motion of a single bead around its center is calculated by using the following equation: $N = 8\pi\eta r^3\omega$ (N, frictional torque on the single bead; η, viscosity of the medium; r, radius of the bead; ω, angular velocity) (Fig. 7 *a*). When another bead is bound to the side of the bead farthest from the rotational axis (Fig. 7 *c*), the frictional moment is ~5 × N, and this is the maximum frictional moment on a double bead. The frictional moment on a double bead is in the range 2 × N (Fig. 7 *b*) to 5 × N (Fig. 7 *c*). In the case in which double beads, each with a diameter of 1.16 μm, rotate at one turn per second, the range of required torque is calculated to be 62–154 pN · nm. In the case of 0.55-μm beads at the same speed, it is 6.6–16.0 pN · nm. The maximum diameter of an actin filament is estimated as 9–9.5 nm (Holmes et al., 1990). Therefore, at the surface of an actin filament, the rotational component of the sliding force that would produce the torque is 13–33 pN for the 1.16-μm beads and 1.4–3.5 pN for the 0.55-μm beads. The friction against rotation is significant compared with the translation because the torque has to be generated at the surface of the thin actin filament.

Rotation at one turn per second should be detected easily, yet we did not observe it even with the 0.55-μm beads. Therefore, we estimate that the rotational component of the sliding force and the torque produced on a sliding actin

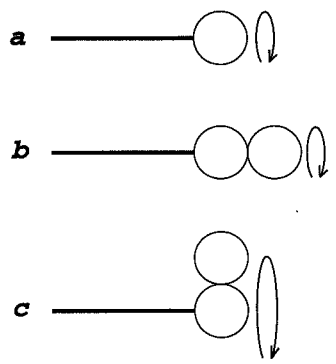

FIGURE 7 Hydrodynamic frictional moments against rotational motion of a double bead. The thick lines and open circles represent actin filaments and beads, respectively. (*a*) The frictional moment on a single bead is calculated using the equation $8\pi\eta r^3\omega$ (= N) (η, viscosity of the medium; r, radius of the bead; ω, angular velocity); (*b*), the minimum frictional moment on a double bead is calculated using the equation $2 \times 8\pi\eta r^3\omega$ (= $2N$); and (*c*) the maximum frictional moment on a double bead is calculated using the equation $8\pi\eta r^3\omega + 8\pi\eta r^3\omega + 6\pi\eta r(2r)^2\omega$ (= $5N$). The second and third terms of the latter equation show the contributions from the rotation and the translation of the outer bead, respectively. In the calculation for the double bead, we neglected the hydrodynamic interaction between the two beads.

filament (length ≤ 10 μm) in the present system of randomly oriented HMM lying on a nitrocellulose film without an external load did not accumulate >1 pN and 5 pN · nm, respectively.

We postulate that the torque produced by the sliding force accumulates with the torsion of the actin filament. After the torsional stress reaches a maximum, the actin-myosin interface slips, and the stress is released from the free front end of the sliding actin filament. The amount of torsion in a sliding filament is estimated as follows. The torsional rigidity of an actin filament has recently been estimated as $(2.6–3.7) \times 10^4$ pN · nm^2 from a normal-mode analysis of the atomic structure of F-actin (Ben-Avraham and Tirion, 1995). Direct observation of the torsional Brownian motion of F-actin has indicated similar values of $(2–10) \times 10^4$ pN · nm^2 (R. Yasuda, H. Miyata, and K. Kinosita, Jr., submitted for publication). The rotational Brownian motion of the tail beads observed in the present work also supports these values. Thus, the root mean squares of the torsional angular fluctuations $\Delta\gamma$ is related to the torsional rigidity C by $C(\Delta\gamma)^2/(2L) = k_BT$ in which L is the length of the filament and k_BT is the thermal energy (Barkley and Zimm, 1979). The angular range we report in this work is $4\Delta\gamma$, which is calculated for $C = 3 \times 10^4$ pN · nm^2 and $T = 298$ K as 84°, 120°, and 168° for $L = 1$ μm, 2 μm, and 4 μm, respectively. The observed values of 45°, 90°, and 180° are in accord with the expected values when limited precision is taken into account. For $C = 3 \times 10^4$ pN · nm^2, the estimated maximal torque of 5 pN · nm above would twist an actin filament with a length of 10 μm by a quarter of a turn (Barkley and Zimm, 1979). Thus, a sliding filament is unlikely to contain a large torsional strain.

The superhelix observed by Tanaka et al. (1992) and the supercoil observed by Nishizaka et al. (1993) indicated that an actin filament was twisted one turn and more than three turns, respectively. The accumulated torsional stress on the actin-myosin interface may not be very high, however, because it will be released by the formation of the superhelix and the supercoil. Therefore, we conclude that these observations are not inconsistent with the present result.

The last important point we must consider is that the sliding force depends on the load. The reason we did not detect the rotational motion of the actin filament may be concerned with this point. In the experiments performed by Nishizaka et al. (1993) and Tanaka et al. (1992), the observed actin filament slid under a translationally loaded condition because the sliding of the front part of it was stopped or reduced. In our system, however, bead-tailed actin filaments slid without a translational load, as indicated by the small translational friction estimated above and shown in Fig. 3. Under a loaded condition, actomyosin produces more sliding force, and its torque might be accumulated more efficiently.

Our results do not deny the axial rotation in the sliding actin filament, but they show that forward movement occurs at the same speed as that of a nonbeaded actin filament even when a large axial torque load is imposed by the hydrodynamic friction. Also, in the case of a microtubule and 14S dynein, Vale and Toyoshima (1988) reported that forward movement occurred even when rotation was suppressed by steric interference. These observations that the translocation and the rotation are not tightly coupled offer an important key for understanding the sliding mechanism.

This study was supported in part by a Grant-in-aid for the Encouragement of Young Scientists and by Grants-in-aid for the General Scientific Research from the Ministry of Education, Science and Culture of Japan, and in part by Special Coordination Funds for Promoting Science and Technology from the Agency of Science and Technology of Japan.

REFERENCES

Ashkin, A. 1992. Forces of a single-beam gradient laser trap on a dielectric sphere in the ray optics regime. *Biophys. J.* 61:569–582.

Barkley, M. D., and B. H. Zimm. 1979. Theory of twisting and bending of chain macromolecules: analysis of the fluorescence depolarization of DNA. *J. Chem. Phys.* 70:2991–3007.

Ben-Avraham, D., and M. M. Tirion. 1995. Dynamic and elastic properties of F-actin: a normal-modes analysis. *Biophys. J.* 68:1231–1245.

Block, S. M., and K. Svoboda. 1995. Analysis of high resolution recordings of motor movement. *Biophys. J.* 68:230s–241s.

Brown, S. S., and J. A. Spudich. 1979. Nucleation of polar actin filament assembly by a positively charged surface. *J. Cell Biol.* 80:499–504.

Brown, S. S., and J. A. Spudich. 1981. Mechanism of action of cytochalasin: evidence that it binds to actin filament ends. *J. Cell Biol.* 88:487–491.

Coppin, C. M., J. T. Finer, J. A. Spudich, and R. D. Vale. 1995. Measurement of the isometric force exerted by a single kinesin molecule. *Biophys. J.* 68:242s–244s.

Ebashi, S., and K. Maruyama. 1965. Preparation and some properties of α-actinin-free actin. *J. Biochem. (Tokyo).* 58:20–26.

Finer, J. T., A. D. Mehta, and J. A. Spudich. 1995. Characterization of single actin-myosin interactions. *Biophys. J.* 68:291s–297s.

Finer, J. T., R. M. Simmons, and J. A. Spudich. 1994. Single myosin molecule mechanics: piconewton forces and nanometre steps. *Nature (Lond.).* 368:113–119.

Fowler, V. M., M. A. Sussmann, P. G. Miller, B. E. Flucher, and M. P. Daniels. 1993. Tropomodulin is associated with the free (pointed) ends of the thin filaments in rat skeletal muscle. *J. Cell Biol.* 120:411–420.

Funatsu, T., Y. Asami, and S. Ishiwata. 1988. β-actinin: a capping protein at the pointed end of thin filaments in skeletal muscle. *J. Biochem. (Tokyo).* 103:61–71.

Funatsu, T., H. Higuchi, and S. Ishiwata. 1990. Elastic filaments in skeletal muscle revealed by selective removal of thin filaments with plasma gelsolin. *J. Cell Biol.* 110:53–62.

Gelles, J., B. J. Schnapp, and M. P. Sheetz, 1988. Tracking kinesin-driven movements with nanometer-scale precision. *Nature (Lond.).* 331: 450–453.

Harada, Y., K. Sakurada, T. Aoki, D. D. Thomas, and T. Yanagida. 1990. Mechanochemical coupling in actomyosin energy transduction studied by in vitro movement assay. *J. Mol. Biol.* 216:49–68.

Holmes, K. C., D. Popp, W. Gebhard, and W. Kabsch. 1990. Atomic model of the actin filament. *Nature (Lond.).* 347:44–49

Holtzer, A., and S. Lowey. 1959. The molecular weight, size and shape of the myosin molecule. *J. Am. Chem. Soc.* 81:1370–1377.

Houk, Jr., T. W., and K. Ue. 1974. The measurement of actin concentration in solution: a comparison of methods. *Anal. Biochem.* 62:66–74.

Huxley, H. E. 1990. Sliding filaments and molecular motile systems. *J. Biol. Chem.* 265:8347–8350.

Isenberg, G. 1991. Actin binding proteins-lipid interaction. *J. Muscle Res. Cell Motil.* 12:136–144.

Kinosita, Jr., K., N. Suzuki, S. Ishiwata, T. Nishizaka, H. Itoh, H. Hakozaki, G. Marriott, and H. Miyata. 1993. Orientation of actin monomers in moving actin filaments. *In* Mechanism of Myofilament Sliding in Muscle Contraction. H. Sugi and G. H. Pollack, editors. Plenum Publishing, New York. 321–329.

Kishino, A., and T. Yanagida. 1988. Force measurements by micromanipulation of a single actin filament by glass needles. *Nature (Lond.).* 334:74–76.

Kron, S. J., Y. Y. Toyoshima, T. Q. P. Uyeda, and J. A. Spudich. 1991. Assays for actin sliding movement over myosin-coated surfaces. *Methods Enzymol.* 196:399–416.

Kuo, S. C., and M. P. Sheetz. 1993. Force of single kinesin molecules measured with optical tweezers. *Science.* 260:232–234.

Kurokawa, H., W. Fujii, K. Ohmi, T. Sakurai, and Y. Nonomura. 1990. Simple and rapid purification of brevin. *Biochem. Biophys. Res. Commun.* 168:451–457.

Margossian, S. S., and S. Lowey. 1978. Interaction of myosin subfragments with F-actin. *Biochemistry.* 17:5431–5439.

Miyata, H., H. Hakozaki, H. Yoshikawa, N. Suzuki, K. Kinosita, Jr., T. Nishizaka, and S. Ishiwata. 1994. Stepwise motion of an actin filament over a small number of heavy meromyosin molecules is revealed in an in vitro motility assay. *J. Biochem. (Tokyo).* 115:644–647.

Miyata, H., H. Yoshikawa, H. Hakozaki, N. Suzuki, T. Furuno, A. Ikegami, K. Kinosita, Jr., T. Nishizaka, and S. Ishiwata. 1995. Mechanical measurements of single actomyosin motor force. *Biophys. J.* 68:286s–290s.

Molloy, J. E., J. E. Burns, J. C. Sparrow, R. T. Tregear, J. Kendrick-Jones, and D. C. S. White. 1995. Single-molecule mechanics of heavy meromyosin and S1 interacting with rabbit or *drosophila* actins using optical tweezers. *Biophys. J.* 68:298s–305s.

Nishizaka, T., H. Miyata, H. Yoshikawa, S. Ishiwata, and K. Kinosita, Jr. 1995a. Mechanical properties of single protein motor of muscle studied by optical tweezers. *Biophys. J.* 68:75s.

Nishizaka, T., H. Miyata, H. Yoshikawa, S. Ishiwata, and K. Kinosita, Jr. 1995b. Unbinding force of a single motor molecule of muscle measured using optical tweezers. *Nature (Lond.).* 377:251–254.

Nishizaka, T., T. Yagi, Y. Tanaka, and S. Ishiwata. 1993. Right-handed rotation of an actin filament in an in vitro motile system. *Nature (Lond.).* 361:269–271.

Perry, S. V. 1955. Myosin adenosine triphosphatase. *Methods Enzymol.* 2:582–588.

Podolski, J. L., and T. L. Steck. 1988. Association of deoxyribonuclease I with the pointed ends of actin filaments in human red blood cell membrane skeletons. *J. Biol. Chem.* 263:638–645.

Pollard, T. D., and J. A. Cooper. 1986. Actin and actin-binding proteins. A critical evaluation of mechanisms and functions. *Annu. Rev. Biochem.* 55:987–1035.

Saito, K., T. Aoki, T. Aoki, and T. Yanagida. 1994. Movement of single myosin filaments and myosin step size on an actin filament suspended in solution by a laser trap. *Biophys. J.* 66:769–777.

Spudich, J. A., and S. Watt. 1971. The regulation of rabbit skeletal muscle contraction. I. Biochemical studies of the interaction of the tropomyosin-troponin complex with actin and the proteolytic fragments of myosin. *J. Biol. Chem.* 246:4866–4871.

Svoboda, K., and S. M. Block, 1994. Force and velocity measured for single kinesin molecules. *Cell.* 77:773–784.

Svoboda, K., C. F. Schmidt, B. J. Schnapp, and S. M. Block. 1993. Direct observation of kinesin stepping by optical trapping interferometry. *Nature (Lond.).* 365:721–727.

Tanaka, Y., A. Ishijima, and S. Ishiwata. 1992. Super helix formation of actin filaments in an in vitro motile system. *Biochim. Biophys. Acta.* 1159:94–98.

Vale, R. D. 1994. Getting a grip on myosin. *Cell.* 78:733–737.

Vale, R. D., and L. S. B. Goldstein. 1990. One motor, many tails: an expanding repertoire of force-generating enzymes. *Cell.* 60:883–885.

Vale, R. D., and Y. Y. Toyoshima. 1988. Rotation and translocation of microtubules in vitro induced by dyneins from tetrahymena cilia. *Cell.* 52:459–469.

Weber, A., M. Pring, S.-L. Lin, and J. Bryan. 1991. Role of the N- and C-terminal actin-binding domains of gelsolin in barbed filament end capping. *Biochemistry.* 30:9327–9344.

Weeds, A. G., and R. S. Taylor. 1975. Separation of subfragment-1 isoenzymes from rabbit skeletal muscle myosin. *Nature (Lond.).* 257: 54–56.

Yanagida, T., and A. Ishijima. 1995. Forces and steps generated by single myosin molecules. *Biophys. J.* 68:312s–320s.

Yanagida, T., Y. Harada, and A. Ishijima. 1993. Nano-manipulation of actomyosin molecular motors in vitro: a new working principle. *Trends Biochem. Sci.* 18:319–324.

Yanagida, T., M. Nakase, K. Nishiyama, and F. Oosawa. 1984. Direct observation of motion of single F-actin filaments in the presence of myosin. *Nature (Lond.).* 307:58–60.

特集

分子モーターの力学・機能特性を見る

早稲田大学 理工学部 物理　西坂崇之，石渡信一

We summarize the mechanical and functional properties of a motor molecule of muscle studied with a new type of an *in vitro* motility assay system and a multi-imaging microscope system. First, supercoiling of an actin filament is shown, suggesting that the filament moves forward like a right-handed screw. Second, we describe the unbinding force and the lifetime of a rigor bond between a single myosin molecule and an actin filament measured by using optical tweezers. From these results, the mechanism of sliding and force generation of the motor molecule is discussed.

acto-myosin motor / supercoiling of an actin filament / optical tweezers / unbinding force / lifetime of an acto-myosin bond

1. はじめに

顕微計測技術の発展により，生体運動を担うミオシンやキネシン・ダイニンなどの分子モーターの研究が1分子レベルで進められるようになった．それぞれの分子モーターの基質フィラメントであるアクチンフィラメントや微小管が1本で可視化され，その滑り運動を直接観察することのできる*in vitro*滑り運動系が開発された．さらにガラス微小針[1),2)]や光ピンセット[3)-5)]を用いてモーターの発生する滑り力が直接計測されるようになった．その結果，微小管上での1個のキネシンによるステップ状の運動[5)]や，1個のミオシン分子上でのATP加水分解の可視化（本特集船津の項参照）など，力発生と化学反応の素過程が光学顕微鏡下で直接捉えられるようになってきた．その一方でミオシンやアクチンの立体構造が解かれ，滑り運動の分子メカニズムの研究は質的に変化しつつある．

こうした中で，我々は*in vitro*滑り運動系に独自の工夫を加え，筋蛋白分子モーターの持つ機能と力学特性の可視化を試みてきた．幾つかの成果を紹介し，近い将来を展望したい．

2. アクチンフィラメントの超らせん（supercoil）形成[6)]

個々のミオシン分子モーターの滑り力ベクトルは正確にアクチンフィラメントの長軸方向を向いているか，傾いているかはこれまで明らかにされていなかった．アクチンフィラメントは右らせん構造をとっているが，例えば滑り力ベクトルがそのらせんに沿っていれば，フィラメントには右巻きのトルクが発生するはずである[7)]．この問題を明らかにする目的で，我々はアクチンフィラメントの先頭部分を固定し，後部の滑り運動によってフィラメントの中央部分がどのように変形するかを調べることにした．滑り力に右巻きのトルク成分が存在すればフィラメントは右回転し，先頭部分を固定したことによって左巻きの超らせんが形成されると考えたのである．

実験結果を図1に示す．アクチンフィラメントは蛍光標識してあり，先頭（写真の上側）の部分がガラス面に固定されている．相互作用するHMM分子（ミオシンの酵素活性断片）は顕微鏡下では見えないが，帯状に配列している（HMMトラック；*b*においてフィラメントが直線状になっている箇所）．フィラメント

Mechanical and functional properties of single motor molecules

Takayuki NISHIZAKA and Shin'ichi ISHIWATA
Department of Physics, School of Science and Engineering, Waseda University

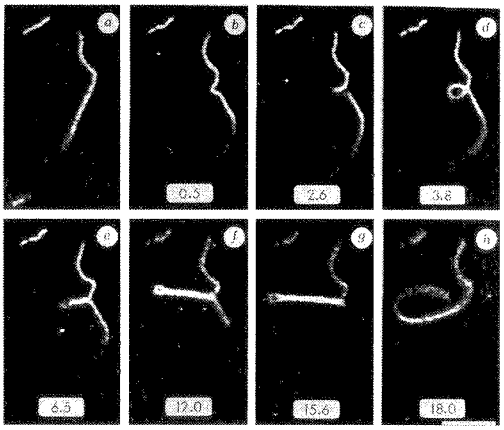

図1　トラック状に配列したHMM分子（写真では見えない）上での滑り運動により，蛍光顕微鏡下で単一アクチンフィラメントが超らせん（supercoil）を作る様子．アクトミオシン系における回転滑り運動が初めて示された．数字は滑り運動が始まってからの時間（秒）．Scale bar, 5μm[6]．

の後ろ側の部分は初めブラウン運動をしているが（*a*），HMMトラックに接触する（時刻0）と滑り運動を開始する．その結果中央部分がたわみ（*b*），さらに後ろ側が進むことで1重の超らせんを形成し（*c*），ループ（*d*）を経て多重の超らせん（*e-g*）へと移行した．後端がねじれの根元に達すると，アクチンフィラメントはトラックから外れてねじれは瞬時にほどけた（*h*）．フィラメントの回転運動の向きは1重の超らせんの向きから判定したが，結果は73例中2例の例外を除きすべて左らせんであった．このことは滑り力には右巻きのトルク成分が存在することを示している．他の分子モーターに関しても，ダイニンやキネシンによる微小管の回転滑り運動が直接可視化されており[8),9)]，さらに超らせんの形成も報告されている[10)]．したがってトルク成分は分子モーターに共通する特性であると考えられ，これが滑り運動メカニズムとどう関連するか興味深い．一方，アクチンフィラメントや微小管に見出された多重の超らせん構造が，非筋細胞の機能に一役買ってはいないか，機会があれば探ってみたい気がする．

3. 光ピンセット法と多画像顕微鏡

顕微操作の手法には従来からガラス針が広く用いられてきたが，我々は光ピンセットを用いた．光ピンセットは，赤外などのレーザー光により，ミクロンサイズの粒子や細胞を非接触で捕捉する技術である[11)]．装置は

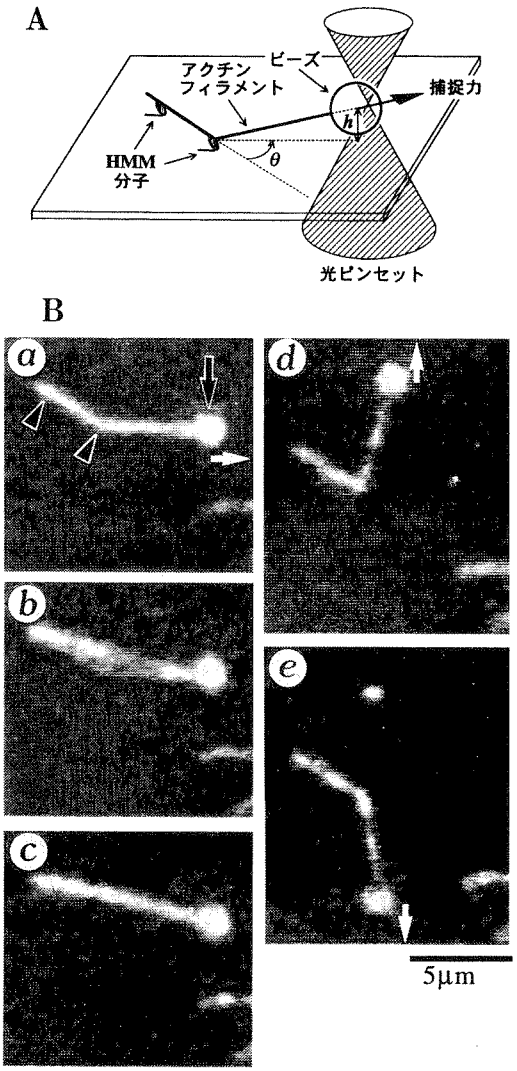

図2　A, 実験の模式図．レーザーの捕捉中心の方向にアクチンフィラメントが張り，1つのHMM分子に負荷が加わっている．B, 光ピンセットを用いたアクチンフィラメントの顕微操作により，ガラス面上のHMM分子の局在が直接わかる．白矢印はレーザーの変位の向き，黒矢印は捕捉しているポリスチレンビーズ，黒三角の先端はHMM分子を指す．Scale bar, 5μm[13)]．

市販の倒立顕微鏡に，レーザー光を導入できる光学系を組み合わせたものである[4),12),13)]．光ピンセットの捕捉力ポテンシャルは，直径1μmのポリスチレンビーズに対して半径200nmの範囲までフックのばね型である（図3におけるばね定数は0.097pN/nm）．顕微操作は容易で，レーザー光の焦点の位置，もしくはステージ

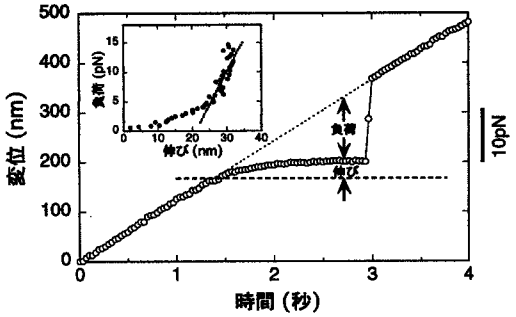

図3　クロスブリッジが破断されるときのビーズの変位の時間経過．HMM1分子とアクチンフィラメントの結合力が直接測定された．点線がレーザーの捕捉中心の位置を表し，白丸はビーズの中心を表す．挿入図はこの測定で測られたクロスブリッジの負荷－伸び関係[13]．

を動かすだけなので実験技術に熟練を要しない．しかし高出力（1W）のレーザーを用いた場合でも最大捕捉力が100pNに満たないこと，小さすぎるサンプルは捕捉できないこと等の制約がある．

太さ8nmのアクチンフィラメントは細すぎるために光ピンセットで捕捉することができない．そこで直径1 μ mのポリスチレンビーズをアクチンフィラメントの一端に付着させ（図2A），そのビーズを捕捉することによって間接的にアクチンフィラメントを顕微操作する方法が開発された[14]．アクチンフィラメント切断蛋白であるゲルゾリンを，架橋剤を用いてビーズの表面に固定し，そこにアクチンフィラメントを加える．ゲルゾリンはアクチンフィラメントのB端に結合するので，ビーズを捕捉すると滑り運動時のフィラメントの後端をつまむことになる．

多画像顕微鏡は，波長や偏光の違いにより光路を分け，異なる情報を同時に画像化する手法である[15]．ここでは蛍光像と位相差像を異なる波長で画像化し，アクチンフィラメントの挙動とビーズの変位を時間的・空間的に対応づけた．観察に適したフィルター類を組み合わせて2つの像に分け，それを超高感度カメラとCCDカメラでビデオ信号とした後に合成する．ビーズの変位については，位相差像を実時間で画像処理コンピューターに取り込んだ後に輝度の重心を計算し，nmオーダーというビデオ画素（40nm）以下の空間分解能を得た[4]．

4. 分子を数える

滑り運動の分子メカニズムを解明するためには，1個の分子モーターの発生張力やステップサイズ（1個のATP加水分解時に滑る距離）などの単位素量を知る必要がある．そのためには1本のアクチンフィラメントに相互作用しているHMM分子の個数を正確に見積もらなくてはならない．我々はアクチンフィラメントを顕微操作することにより，分子の個数を直接数えた[13),16)]．

ATP非存在下ではHMM分子はアクチンフィラメントと硬直結合し，クロスブリッジを形成する．低濃度（1～5 μ g/ml）のHMM分子をガラス表面に吸着させると，フィラメントは数μ mに1点という割合でガラス面に結合し，各HMM分子の位置はブラウン運動をするフィラメントの節として認識できることが分かった．このフィラメントを光ピンセットでガラス面と平行に引くと，ビーズに近い節からまっすぐに張る様子（図2B*a*）が観察された．これを更に強く引くとクロスブリッジが破断してフィラメントは節の部分から瞬時に外れ（*b*），次の別の節から再び張るようになった（*c*）．この手法を用いることでガラス面上のHMM分子の局在が分かり，結合しているモーターの個数を直接数えることができた．

さらに対物レンズの上下方向の動きをピエゾ素子により制御することで，ビーズを一定速度でz軸方向に動かした．その結果，上の方法と比べて高濃度でもモーターの個数を数えることができた．0～15 μ g/mlの範囲ではHMM濃度とフィラメント1 μ m当たりに結合する分子数が比例し，比例係数として0.20分子／μ m･（μ g/ml）が得られた．これを高濃度側に外挿すると，in vitro滑り運動系での滑り運動には1 μ m当たりHMM分子6個以上の相互作用が必要であると推定された（未発表）．

5. 1個の分子モーターの破断力と結合の寿命の測定[13)]

分子モーターは，基質フィラメントと結合・解離を繰り返しながら滑り運動する．そのため，これらの蛋白間に働く結合力の大きさや結合エネルギーの変化は，運動メカニズムに直接結びついているはずである．そこで我々は上記の手法を用いてHMM分子とアクチンフィラメントとの間の硬直結合の破断力と寿命を，1分子のレベルで計測した．

測定にはまずレーザーの捕捉力の中心を一定速度で動かし，クロスブリッジに加わる負荷を時間とともに増加させる方法を用いた．図3にクロスブリッジの破断の前後におけるビーズの変位の時間経過を示す．ビーズは初めレーザーの捕捉中心に追従するが（図3, 0～1.4s），アクチンフィラメントが張る（図3, 1.4s）た

めにほとんど動かなくなる．そのため，移動している捕捉中心とビーズの中心の距離に比例した負荷がクロスブリッジに加わるようになり，あるところで結合は破断する．その時ビーズは先行している捕捉中心に瞬時に移動するが（図3, 2.9s），このビーズの変位を力に換算することで破断直前の負荷の大きさを見積もることができる．こうして測定された破断力の平均は9.2±4.4pN（n＝168）であった．これはガラス微小針を用いて測定されたactin-actin間や原子間力顕微鏡で測定されたavidin-biotin間の破断力に比べてオーダーが1つ小さかった．むしろATP存在下においてHMM1分子が発生する滑り力に近い．

興味深いことに，アクチンフィラメントが張りきった後（図3, 1.4s以降）でも，ビーズの位置は少しずつ変位した．この徐々に増加する負荷と，それに伴うビーズの変位とから，アクチンフィラメント・HMM複合体の負荷-伸び曲線（図3, 挿入図）が得られる．この曲線の傾きから弾性率が求まるが，負荷に応じて大きくなり，破断力（8-10pN）の付近では0.58±0.26pN/nm（n＝17）であった．これは筋線維で見積もられたミオシン頭部の弾性率に近い．しかし結合が破断される直前のビーズの最大変位（69±27nm; n＝30）がミオシン頭部に比べて大きいことから，この負荷－伸び曲線の柔らかい成分はミオシン頭部以外の弾性体の伸びや曲げを含んでいると考えられる．この点については今後さらに検討する必要があるが，いずれにしても，現在の顕微計測技術が，1分子の負荷－伸び関係を直接測定できる段階に来たことは確かである．

次に同じHMM分子の性質を繰り返し調べる実験を行った．光ピンセットを用いて，1度破断したクロスブリッジの位置にアクチンフィラメントを正確に操作すると，アクチンフィラメントを何度でも同じHMM分子に結合させることができる．このようにして強制的な解離と結合を繰り返しても，破断力はほとんど変わらなかった（図4）．しかしながら，破断力の値は個々の分子ごとに異なっているように見えた．1分子を計測することによってそれぞれの分子の個性が現れたと見ることができる．その原因としてはHMM分子のアクチンフィラメントへの結合の向きの違いが考えられるが，フィラメントを引く方向を±90°の範囲で変化させても（図2B*a, d, e*）破断力に有意な差は見られなかった．この他にはHMM分子の分子種の違い（速筋，遅筋など）やガラス面と結合している部位の違い，あるいはフィラメントと結合している頭部の数の違いなどが考えられるが，個性の由来は明らかではない．

以上の実験ではアクチン－ミオシン間相互作用を「力」という面から調べたが，熱揺らぎの下での結合・解離は確率的な現象であるはずであり，解離に要する時間，つまり結合の「寿命」という面から相互作用を調べることもできる．そこで寿命の負荷依存性を見る目的で，フローセルをnmの精度で変位させることによってクロスブリッジにステップ状の負荷を加え，結合が破断するまでに要する時間を計測した（図5）．それぞれの分子に注目すると，高い負荷に応じて寿命が減少していることは明らかである．これら1連のデータも図4同様，分子の個性が見えている．このように分子による違いはあるが，おおよそ無負荷時の10^2-10^3sの寿命が10pNの負荷で1sのオーダーに減少したと見ることができる．

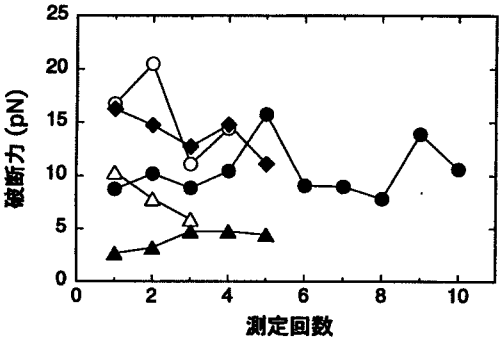

図4　同一のHMM分子の破断力を複数回調べた．それぞれ異なる印は異なるHMM分子を示す．外力により結合・解離を強制的に繰り返しても破断力はほとんど変化しなかった[13]．

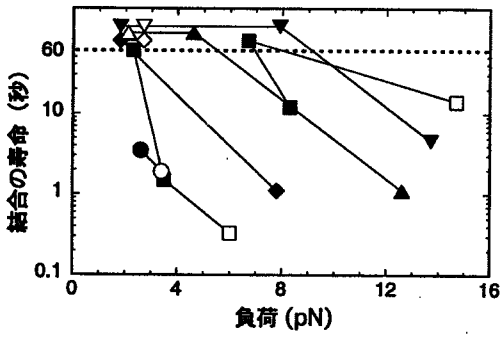

図5　1個の硬直結合にステップ状の負荷をかけ，破断するまでの時間（結合の寿命）を測定した．異なる印は異なるHMM分子を示す．白い印は1回目の測定，黒い印はその後の測定で，測定の順番に線で結んでいる．負荷の増加に応じて結合の寿命が減少した[13]．

さて寿命は結合定数同様，相互作用ポテンシャルを含むボルツマン分布に従うものと考えると，外から10pN加えたことによりアクチンーミオシン間の解離のエネルギー障壁が$k_BT \cdot \ln((10^2\text{-}10^3\text{s})/1\text{s})$ ～ (20-30) pN·nmだけ減少したことになる．これから分子間の相互作用距離を見積もると (2-3) nmとなる．ところがこの値は溶液中における相互作用距離としては長すぎる．逆に通常の値（～0.3nm）ならば，10pNの負荷では$\exp(10\text{pN}\cdot 0.3\text{nm}/k_BT)$ ～2倍程度しか寿命は短くならないはずである．つまりアクチンーミオシンの結合面には，複数の結合が端から次々に外れていくような，弱い負荷で効率よく活性化エネルギーの障壁を減少させる仕掛けがあるのではなかろうか．滑り運動は，このモーター自体に備わった仕掛けが，ATPによって調節されることにより生み出されるのかも知れない．

6. まとめと展望

以上の研究では，1分子レベルでの滑り力の方向性や結合の大きさ・寿命が同じ分子でくり返し調べられた．得られた結果は生体運動の分子メカニズムを解明する上での基礎的な知見となるであろう．蛋白質の性質は，アボガドロ数個の蛋白質の平均的性質としてこれまで捉えられてきた．ところが一挙に分子1個の構造と機能を調べることができるようになったことから，“一分子生理学”と呼ばれる学問の流れが生まれた．この学問の発展には顕微計測技術の一層の進歩が不可欠だが，それと並行して，天然の生理機能に捕らわれることなく，自由な発想で実験系や試料に工夫を加えることが強く望まれる．その中には，例えば遺伝子工学の技法や，分子配列の手法といった人工的な分子操作技術の開発が含まれるだろう．そしてこの学問が，生体分子のもつ機能を人工的に生かすことを目指した“一分子機能学”（むしろ数分子，数十分子の機能学にこそその真髄があるかも知れないが，少数個の代表として敢えて“一”を付けておく）へと発展することも期待される．

(以上の内容は，超らせん形成については田中裕一郎氏（本田技研・和光研究センター），その他については木下一彦氏，宮田英威氏（慶應義塾大学・理工学部）らとの共同研究の成果に基づいている．)

文　献

1) Kamimura, S. and Takahashi, K. (1981) *Nature* **293**, 266-268.
2) Kishino, A. and Yanagida, T. (1988) *Nature* **334**, 74-76.
3) Finer, J. T., Simmons, R. M. and Spudich, J. A. (1994) *Nature* **368**, 113-119.
4) Miyata, H., Hakozaki, H., Yoshikawa, H., Suzuki, N., Kinosita Jr., K., Nishizaka, T. and Ishiwata, S. (1994) *J. Biochem.* **115**, 644-647.
5) Svoboda, K., Schmidt, C. F., Schnapp, B. J. and Block, S. M. (1993) *Nature* **365**, 721-727.
6) Nishizaka, T., Yagi, T., Tanaka, Y. and Ishiwata, S. (1993) *Nature* **361**, 269-271.
7) Tanaka, Y., Ishijima, A. and Ishiwata, S. (1992) *Biochim. Biophys. Acta.* **1159**, 94-98.
8) Vale, R. D. and Toyoshima, Y. Y. (1988) *Cell* **52**, 459-469.
9) Ray, S., Mayhofer, E., Milligan, R. A. and Howard, J. (1993) *J. Cell. Biol.* **121**, 1083-1093.
10) Mimori, Y. and Miki-Noumura, T. (1995) *Cell Motil. Cytoskeleton* **30**, 17-25.
11) Ashkin, A., Dziedzic, J. M., Bjorkholm, J. E. and Chu, S. (1986) *Optics Lett.* **11**, 288-290.
12) Miyata, H., Yoshikawa, H., Hakozaki, H., Suzuki, N., Furuno, T., Ikegami, A., Kinosita Jr., K., Nishizaka, T. and Ishiwata, S. (1995) *Biophys. J.* **68**, 286s-290s.
13) Nishizaka, T., Miyata, H., Yoshikawa, H., Ishiwata, S. and Kinosita Jr., K. (1995) *Nature* **377**, 251-254.
14) Suzuki, N., Miyata, H., Ishiwata, S. and Kinosita Jr., K. (1996) *Biophys. J.*, in press.
15) Kinosita Jr., K., Itoh, H., Ishiwata, S., Hirano, K., Nishizaka, T. and Hayakawa, T. (1991) *J. Cell Biol.* **115**, 67-73.
16) Nishizaka, T., Miyata, H., Yoshikawa, H., Ishiwata, S. and Kinosita Jr., K. (1995) *Biophys. J.* **68**, 75s.

Synchronous Behavior of Spontaneous Oscillations of Sarcomeres in Skeletal Myofibrils under Isotonic Conditions

Kenji Yasuda,* Yoshiaki Shindo,‡ and Shin'ichi Ishiwata‡
*Advanced Research Laboratory, Hitachi, Hatoyama, Saitama 350-03, Japan, and ‡Department of Physics, School of Science and Engineering, Waseda University, 3-4-1 Okubo, Shinjuku-ku, Tokyo 169, Japan

ABSTRACT An isotonic control system for studying dynamic properties of single myofibrils was developed to evaluate the change of sarcomere lengths in glycerinated skeletal myofibrils under conditions of spontaneous oscillatory contraction (SPOC) in the presence of inorganic phosphate and a high ADP-to-ATP ratio. Sarcomere length oscillated spontaneously with a peak-to-peak amplitude of about 0.5 μm under isotonic conditions in which the external loads were maintained constant at values between 1.5×10^4 and 3.5×10^4 N/m^2. The shortening and yielding of sarcomeres occurred in concert, in contrast to the previously reported conditions (isometric or auxotonic) under which the myofibrillar tension is allowed to oscillate. This synchronous SPOC appears to be at a higher level of synchrony than in the organized state of SPOC previously observed under auxotonic conditions. The period of sarcomere length oscillation did not largely depend on external load. The active tension under SPOC conditions increased as the sarcomere length increased from 2.1 to 3.2 μm, although it was still smaller than the tension under normal Ca^{2+} contraction (which is on the order of 10^5 N/m^2). The synchronous SPOC implies that there is a mechanism for transmitting information between sarcomeres such that the state of activation of sarcomeres is affected by the state of adjacent sarcomeres. We conclude that the change of myofibrillar tension is not responsible for the SPOC of each sarcomere but that it affects the level of synchrony of sarcomere oscillations.

INTRODUCTION

The study of the molecular mechanism of muscle contraction has been advanced by the advent of a nanoscopic analysis technique measuring the motion of and generation of force by single molecular motors (cf. Kishino and Yanagida, 1988). From a physiological viewpoint, on the other hand, the structural and functional unit is a single myofibril. To elucidate the mechanisms regulating tension development in the higher-order structure of muscle, we have therefore devised a simple method for investigating both the mechanical properties and fine structure of a single myofibril (cf. Anazawa et al., 1992; Yasuda et al., 1995).

Recently, a new type of spontaneous oscillation of tension and sarcomere length in vertebrate skeletal myofibrils was found and was named SPOC (for spontaneous oscillatory contraction; Okamura and Ishiwata, 1988). The SPOC occurs under conditions intermediate between relaxing and contracting conditions induced either by high concentrations of MgADP and inorganic phosphate in the absence of Ca^{2+} (ADP-SPOC; Ishiwata et al., 1991; Shimizu et al., 1992) or by submicromolar concentrations of free Ca^{2+} (Ca-SPOC). Whereas ADP-SPOC is observed irrespective of the muscle type, Ca-SPOC has not been observed in fast-type skeletal muscle but has been observed in slow-type skeletal muscle (Iwazumi and Pollack, 1981; Stephenson and Williams, 1981, 1982) and cardiac muscle (Fabiato and Fabiato, 1978; Sweitzer and Moss, 1990; Linke et al., 1993).

The SPOC phenomenon has been studied under isometric conditions, where the lengths of constituent sarcomeres oscillate while maintaining the total length of myofibrils (muscle fibers) constant, as well as under auxotonic conditions, in which the tension increases as the sarcomere length decreases such that the external load and the length of myofibrils are inversely related (cf. Anazawa et al., 1992). Under isometric conditions, oscillation of one part of the myofibril does not appear to be related to that of other parts. Under auxotonic conditions, on the other hand, the yielding phase of sarcomeres repeatedly propagates from one end of a myofibril to the other (we previously called this the *organized state of SPOC*; see figure 6 of Anazawa et al., 1992; hereafter we call this *metachronal SPOC*, in contrast to synchronous SPOC). These observations imply that the activation state of sarcomeres is affected by the states of adjacent sarcomeres.

In the present study, we used a newly developed microscopy system to investigate the length-tension relation of SPOC in a single skeletal myofibril under isotonic conditions for the purpose of understanding the role of the external load in SPOC.

MATERIALS AND METHODS

Solutions

Rigor solution A: 60 mM KCl, 5 mM $MgCl_2$, 10 mM Tris-maleate (pH 6.8), and 1 mM EGTA. Rigor solution B: 0.1 M KCl, 5 mM $MgCl_2$, 10 mM 3-(*N*-morpholino)propanesulfonic acid (MOPS) (pH 7.0), and 1 mM EGTA. Relaxing solution: 0.12 M KCl, 4 mM $MgCl_2$, 4 mM ATP, 20 mM MOPS (pH 7.0), and 4 mM EGTA. SPOC solution: 0.12 M KCl, 4 mM $MgCl_2$, 0.2 mM ATP, 4 mM ADP, 4 mM K_2HPO_4, 20 mM MOPS (pH 7.0), and 4 mM EGTA. The pH values were adjusted for each preparation of solution. ATP and ADP were purchased from Boehringer Mannheim

Received for publication 8 August 1995 and in final form 4 January 1996.
Address reprint requests to Dr. K. Yasuda, Advanced Research Laboratory, Hitachi, 2520 Akanuma, Hatoyama, Saitama 350-03, Japan. Tel.: 81-492-96-6111, ext. 6372; Fax: 81-492-96-6006; E-mail: yasuda@harl.hitachi.co.jp.

0006-3495/96/04/1823/07 $2.00

GmbH (Mannheim, Germany); MOPS and EGTA were from Dojindo Laboratories (Kumamoto, Japan). Other chemicals were also of reagent grade.

Preparation of myofibrils

Single myofibrils and small bundles of myofibrils were prepared by homogenizing rabbit psoas fibers glycerinated in 50% (v/v) glycerol containing 0.5 mM $NaHCO_3$, 5 mM EGTA, and 1 mM leupeptin for more than 3 weeks at −20°C as described previously (Ishiwata and Funatsu, 1985). Glycerol and undissolved large aggregates in the suspension of myofibrils were removed by centrifugation at 3000 × *g* in rigor solution A at 4°C.

Microscopy system

The microscopy system and methods for analysis were basically the same as those reported previously (Anazawa et al., 1992; Yasuda et al., 1995), except for a piezo element that was used for feedback control to establish isotonic conditions. The system (Fig. 1) consisted of the following four parts: 1) A temperature-controlled cell (solution capacity of about 200 μl) in which a myofibril was fixed to a pair of glass microneedles, one of which was flexible (Hooke's constant of 10–40 mN/m) and the other of which was rigid (Hooke's constant of 3 N/m). The displacement of the rigid needle was controlled by the piezoelectric element (PSt 150/50/5, Dr. Lutz Pickelmann, Munich, Germany). 2) An inverted phase-contrast microscope (DIAPHOT-TMD; Plan Apo 60× oil DM objective lens (1.40 NA; Nikon Co., Tokyo, Japan) equipped with a CCD camera (C3077H; Hamamatsu Photonics K. K., Hamamatsu, Japan). 3) A feedback control system for keeping the position of the flexible needle constant (i.e., for maintaining the isotonic condition) by controlling the displacement of the rigid needle (cf. Kamimura and Kamiya, 1989; Yagi et al., 1994). 4) A video-computer image analysis system for recording the positions of the microneedles and for making micrographs and density profiles of the myofibrils. The position of the flexible needle was monitored every millisecond by using two opposing elements of a quadrant-type photodiode (S1557; Hamamatsu Photonics K. K.). The position of the rigid microneedle was feedback controlled so as to keep the differential output voltage of the two elements of the photodiode constant. The video-computer system was used to estimate the average sarcomere length by measuring the separation between the inner edges of the two microneedles (i.e., the length of myofibril) by using a double-channel position detector (width analyzer C3161; Hamamatsu Photonics K. K.). The tension developed (strictly, the external load) under isotonic conditions was estimated with the video-computer system by measuring the deflection of the flexible needle. The time resolution for data acquisition by the video analysis system was 33 ms.

Microscopic analysis of SPOC

A single myofibril or a small bundle of myofibrils was held with a pair of glass microneedles according to the procedure reported previously (Anazawa et al., 1992). The cross-sectional area of the myofibrils was estimated to be from 2×10^{-12} to 7×10^{-12} m^2, and the number of sarcomeres per myofibril was between 20 and 30. After the myofibril or myofibril bundle was set on the microneedles, the rigor solution B in the cell was replaced by the relaxing solution. The central area of the quadrant-type photodiode was set at the position of the flexible microneedle by moving the photodiode manually, and feedback control of the rigid microneedle was started. After an appropriate load was imposed by moving the photodiode manually, the relaxing solution was replaced by the SPOC solution. During feedback control of the rigid microneedle, the position of the flexible microneedle was kept in the central area of the photodiode such that the myofibrils were maintained under isotonic conditions. Thus the level of external load was determined by the position of the photodiode and was changed by moving the photodiode.

The spatial resolution for monitoring the position of the microneedle was 51 nm, and when a flexible needle with a Hooke's constant of 2.37×10^{-2} N/m was used, the resolution with which the developed tension was measured was 1.2×10^{-9} N ($(51 \times 10^{-9}$ m) × (2.37×10^{-2} N/m)).

RESULTS

Performance of the feedback system

Figs. 2 and 3 show how accurately isotonic tension was maintained (see *left arrow* in Fig. 2 and *left arrowheads* in Fig. 3) during the shortening and yielding of sarcomeres in SPOC. The feedback control of the rigid needle was rapid enough to follow the change in tension. In Fig. 4 *b*, for example, we can see that the external load imposed on the myofibril was kept almost constant (i.e., within 1.4% of the average tension: 2.15×10^4 N/m^2). The deviation could be

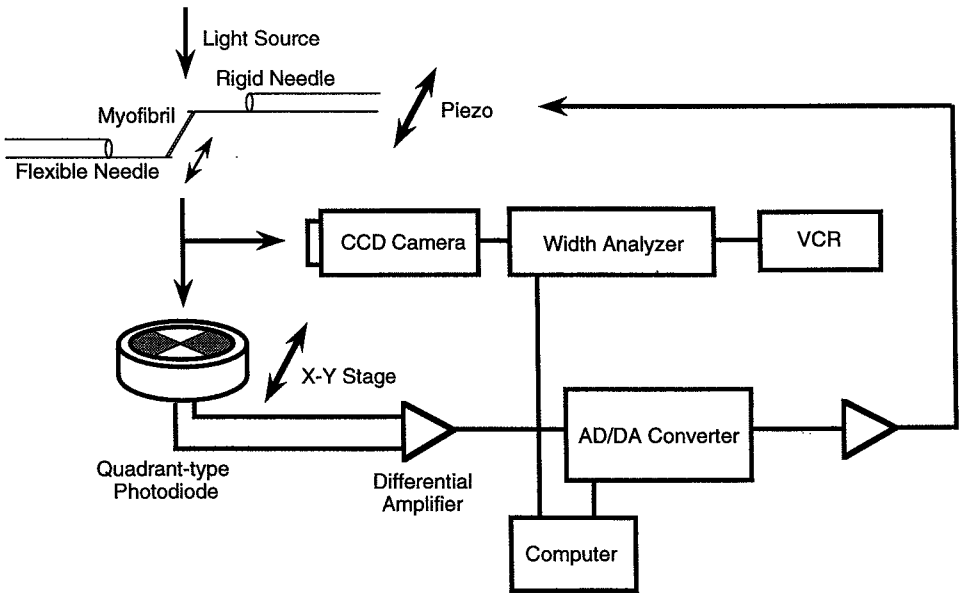

FIGURE 1 The microscopic analysis system. (For details, see Materials and Methods.)

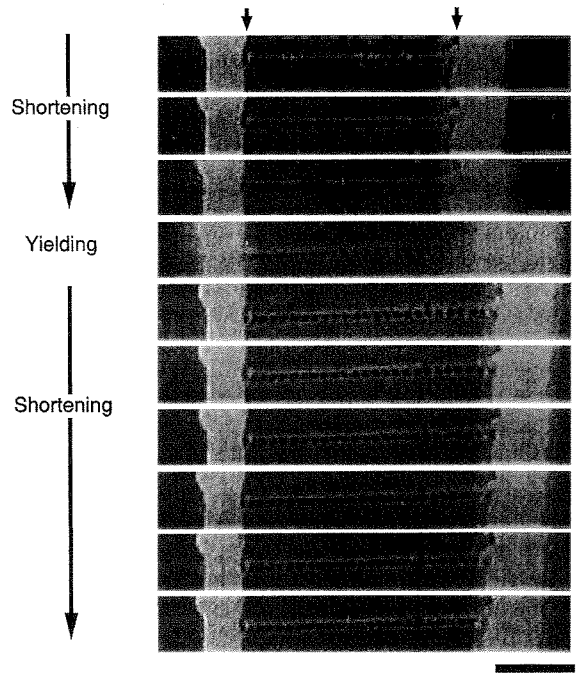

FIGURE 2 Phase-contrast micrographs taken every 33 ms and showing the time course of the isotonic SPOC of a single myofibril. The displacement of the flexible needle (*left arrow*) indicates the level of the external load imposed on the myofibril. At the fourth micrograph from the top, the synchronous yielding of sarcomeres occurred within one video frame (33 ms); note that the flexible microneedle was kept at almost the same position even during the yielding phase. The average external load was 2.17×10^4 N/m^2 (see Fig. 4 *b*). Scale bar, 20 μm.

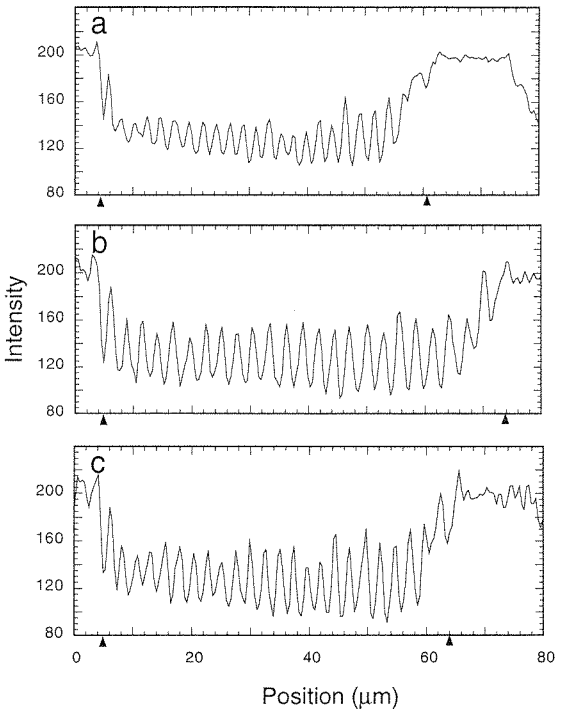

FIGURE 3 Image profiles of myofibrils showing isotonic SPOC. Horizontal and vertical axes represent the position along a myofibril and the brightness of the phase-contrast image. The arrowheads on each side correspond to the inner edges of microneedles (see *arrows* in Fig. 2): (*a*) just before the yielding (the third micrograph from the top in Fig. 2), (*b*) just after the yielding (the fifth micrograph from the top in Fig. 2), and (*c*) during the shortening (micrograph not shown). The flexible needle corresponding to the arrow on the left-hand side was kept at the same position by manipulating the rigid needle with feedback control. Peaks and valleys of the image profile respectively correspond to the I-bands and the A-bands of the sarcomeres.

reduced by increasing the gain of the feedback amplifier but was limited by the 1-ms time resolution of feedback control. Thus in this system we accepted a fluctuation of about 1% of the external load.

The transient response to a sudden change of load was estimated to take place within 10 ms because the image profile of the flexible needle, which is averaged over 33 ms, was broadened only slightly (see the fourth micrograph from the top in Fig. 2).

Microscopic analysis of SPOC

As shown in Figs. 2 and 3, the shortening and yielding of sarcomeres tended to be synchronized along the length of the myofibril (synchronous SPOC). Every sarcomere yielded within 33 ms, and all of them yielded at almost the same time (Fig. 2). This means that the yielding velocity of sarcomeres was greater than 12 μm/s. Such a coordination of yielding was never observed when sarcomeres under auxotonic conditions were investigated (Anazawa et al., 1992). The image profiles of the sarcomeres (Fig. 3) show the uniformity of sarcomere lengths. The average sarcomere length was estimated by dividing the distance between the inner edges of two microneedles by the number of sarcomeres. Because the shortening and yielding of sarcomeres were in concert, this could be regarded as an estimate of the length of each sarcomere. The metachronal SPOC occurred reproducibly without changing the oscillation period when the condition was changed from isotonic to auxotonic (data not shown).

As shown in Fig. 4, synchronous SPOC occurred under isotonic conditions irrespective of the external load, and the time course of the oscillation of sarcomere length displayed a sawtooth waveform similar to that directly observed by phase-contrast microscopy under isometric (cf. Ishiwata et al., 1991) and auxotonic (cf. Anazawa et al., 1992) conditions. Because of the synchronous oscillation, the waveform of the oscillation of sarcomere lengths could be measured more accurately here than in previous studies. The duration of the yielding of sarcomeres was less than 33 ms, such that the yielding phase represented about 1/60 of the total period of oscillation.

Effect of the external load on the synchronous SPOC

Fig. 5 shows the relation between sarcomere length and average shortening velocity under three different external loads, and the track in this relation was triangular and anticlockwise, irrespective of the external load, and the

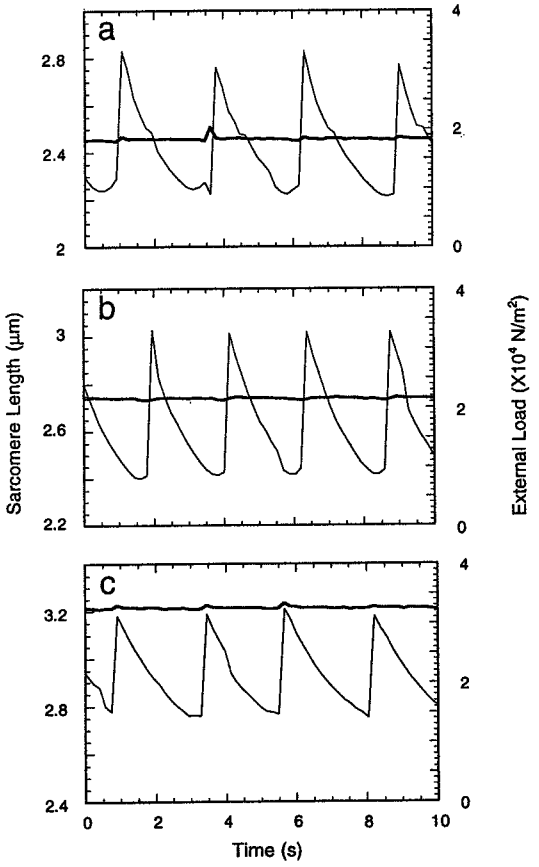

FIGURE 4 Oscillation of average sarcomere length (*thin lines*) during isotonic SPOC under different external loads (*thick lines*). The average external loads were (*a*) 1.83 × 10^4 N/m^2, (*b*) 2.17 × 10^4 N/m^2 (the same as in Figs. 2 and 3), and (*c*) 3.27 × 10^4 N/m^2. The data in these examples were recorded every 150 ms.

same track was followed over many cycles of SPOC (we observed nearly 30 cycles). Just after the yielding of sarcomeres ceased, the shortening of sarcomeres started with its maximum velocity; this initial shortening velocity appears to increase when the external load is reduced. After the start of shortening, the shortening velocity decreased at a nearly constant rate until the shortening stopped. The rate of decrease in shortening velocity was independent of the external load and was about 0.4 μm/s^2.

As summarized in Fig. 6, the peak-to-peak amplitude of the sarcomere length oscillation—that is, the difference between sarcomere length before (*open squares*; shortest length) and after (*open triangles*; longest length) the yielding of sarcomeres—was about 0.50 μm (minimum, 0.40 μm; maximum, 0.58 μm). Developed tension, which should be balanced with the external load at the shortest and the longest sarcomere lengths, increased as sarcomere length increased but was less than tension developed under normal Ca^{2+} contraction ((2–3) × 10^5 N/m^2 at full overlap between thick and thin filaments), even at the greatest sarcomere length. When the external load was less than 1.5 × 10^4 N/m^2 (that is, when the average sarcomere length was less

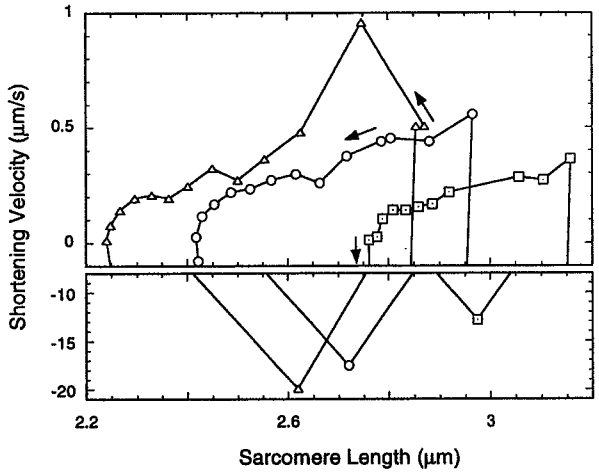

FIGURE 5 Relation between sarcomere length and average shortening velocity of sarcomeres under various external loads. Open triangles correspond to Fig. 4 *a*; open circles, to Fig. 4 *b*; and open squares, to Fig. 4 *c*. Shortening velocities were estimated every 150 ms (actual shortening velocities should be larger than these values; cf. Results). Arrows indicate the direction of each cycle of oscillation.

than 2 μm), synchronous SPOC was not observed and each sarcomere oscillated independently of the others.

We also examined the effects of the transient change of the external load (less than 5% of total load) on SPOC by rapidly (within 10 ms) moving the rigid needle under auxotonic conditions. When we did that, we found that the SPOC waveform was simply shifted to the larger level of tension without a change in the phase or the period of oscillation (data not shown).

Period of isotonic SPOC under various external loads

The period of the SPOC was about 2.3 s (Fig. 7, *open triangles*: minimum period, 1.5 s; maximum period, 2.6 s).

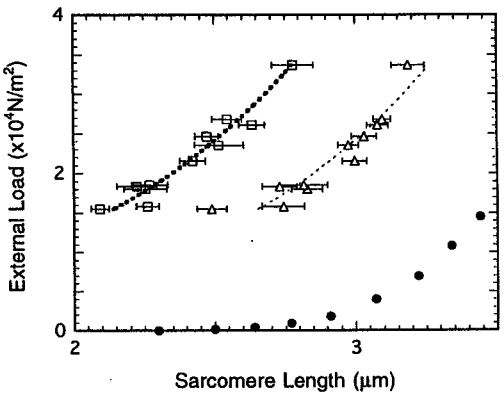

FIGURE 6 Relation between sarcomere length and external load during isotonic SPOC. Open squares and triangles respectively indicate the shortest and the longest sarcomere lengths under various external loads. Error bars indicate the standard deviation of about 15 cycles of oscillation. Closed circles show the resting tension at various sarcomere lengths (taken from figure 7 of Yasuda et al., 1995).

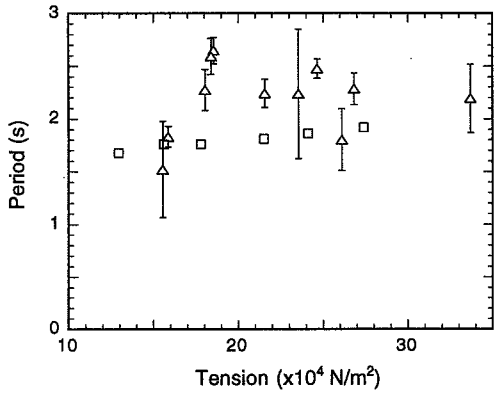

FIGURE 7 Relation between external load and the period of isotonic SPOC. Open triangles indicate average period of sarcomere length oscillation. Error bars indicate the standard deviation of about 15 cycles of oscillation. Open squares indicate average period of auxotonic SPOC (taken from figure 9 of Anazawa et al., 1992).

As shown in Fig. 7, we could not find a clear tension dependence of the period, even when the external load increased by a factor of 2. The period of oscillation for the isotonic SPOC was indistinguishable from that of the auxotonic SPOC (Fig. 7, *open squares*; see figure 9 of Anazawa et al., 1992).

Contribution of connectin (titin) for SPOC

Connectin, an elastic protein of myofibrils, has been shown to have large viscoelastic influence on the mechanical properties of muscle fibers (cf. Magid and Law, 1985). To examine the possible contribution of connectin to SPOC, it was partially digested by adding 0.25 μg/ml trypsin to the SPOC solution under the auxotonic condition. The result (not shown) was that the average tension at an average sarcomere length greater than 2.7 μm gradually decreased with the progress of digestion, but the amplitude of tension oscillation was hardly affected until the level of tension fell by about half.

DISCUSSION

Synchronization of sarcomere oscillations under isotonic conditions

We first observed isometric SPOC in experiments in which both ends of myofibrils were attached to a glass surface (Okamura and Ishiwata, 1988). In such isometric SPOCs, a sawtooth waveform was observed in the oscillation of the length of each sarcomere, but the oscillation was asynchronous or locally metachronal; that is, the yielding phase of sarcomere propagated only locally, extending at most over only several sarcomeres. Thus, in isometric SPOC the oscillation of one part of the myofibril does not appear to be related to that of other parts. Because in those experiments we could neither measure the developed tension nor control the external load, we could not evaluate possible relationships between changes in tension and the oscillation in sarcomere length.

We therefore developed a microscopic analysis system to measure tension and sarcomere length during SPOC under auxotonic conditions (Anazawa et al., 1992). Using that system, we found the organized state of SPOC in which the sarcomere oscillation was not synchronous but in which each sarcomere's oscillation was metachronously related to that of the others. Under auxotonic conditions the yielding of sarcomeres was always accompanied by a decrease in tension and the shortening of sarcomeres was always accompanied by an increase in tension. There was therefore a possibility that the metachronal SPOC was induced by the changes in tension without the boundary condition of isometric SPOC that the total length of myofibril is maintained constant, that is, shortening of one sarcomere should be accompanied by yielding of some other sarcomeres. Thus, clarification of the correlation between the change in tension and SPOC would give us information about the mechanism of synchrony of sarcomere oscillations.

To make the above point clear, we examined the isotonic conditions where the constant external load is always imposed on all sarcomeres in the myofibrils (cf. Schoenberg et al., 1974). As a result, it has been demonstrated that the tendency for the oscillation of adjacent sarcomeres to be synchronized was more pronounced and the synchronous SPOC occurred (Figs. 2 and 3). Thus the metachronal SPOC observed under auxotonic conditions might be regarded as an intermediate state between the asynchronous SPOC under isometric conditions and the synchronous SPOC under isotonic conditions. And the change of the external load during SPOC may cause the decline of synchrony of oscillation from synchronous to metachronal and to asynchronous SPOC.

Under isotonic conditions the period of length oscillation for each sarcomere did not depend on the external load (Fig. 7), and the waveform of each sarcomere in SPOC under isotonic conditions was similar to that under auxotonic and isometric conditions. These results indicate that the change of the myofibrillar tension is not responsible for the SPOC of each sarcomere.

Although the change of the external load may cause the decline of the synchrony of sarcomere oscillations, the transient change of load (mechanical impulse) caused by the delay (1 ms) of our isotonic feedback system might have triggered the synchronous SPOC. We therefore examined the effects of the external impulse by rapidly moving the rigid needle during SPOC; the results show that the synchrony of SPOC is not caused by the impulse.

A possible cause for the synchronization of sarcomeres is the conformational change of the protein components present between half-sarcomeres, such as the Z line and the M line. Linke and his colleagues obtained a dose-dependent decrease of oscillation amplitude by stiffening the Z line structure of cardiac myofibrils through labeling with anti-α-actinin, although the period was not affected (Linke et al., 1993). The structural change of the Z line lattice from

expanded form to contracted form has also been reported to accompany changes in the states of sarcomeres (Goldstein et al., 1988). It has been reported that actin filaments rotate during the sliding movement that occurs when they interact with myosin (Nishizaka et al., 1993). Those observations suggest the following possible mechanism for the transmission of information between adjacent sarcomeres: the generation of active force twists the thin filaments, changing the structure of the Z line lattice (cf. Jarosch, 1987) and thus changing the degree of twist of the thin filaments at the adjacent half-sarcomere. If the twist of thin filaments, for example, accelerates the release of the cross-bridges, it may change the degree of the inhibition of the regulatory proteins. A similar process might occur through the M line. Such a transmission of structural information through the Z line and the M line might be the cause of the metachronal SPOC and the synchronous SPOC. The loss of synchrony during the transition from the synchronous SPOC to the metachronal SPOC may be attributable to the decrease in the external load accompanying the yielding of sarcomeres, which in turn may delay the transmission of structural information to the neighboring sarcomeres. In this respect, we should mention that the transmission of structural information disappeared when the external load was less than a certain threshold value. This is consistent with the idea that the certain degree of strain (such as twist) in constituent proteins is required for the transmission of information that must occur in the organization of SPOC.

The possibility that SPOC is caused by damaged sarcomeres

It has been pointed out that if the tension generation is imbalanced because of damaged sarcomeres, this imbalance might cause a tug-of-war between sarcomeres and, then, SPOC (Iwazumi and Pollack, 1981). The tug-of-war mechanism, however, is excluded by the occurrence of synchronous SPOC because all sarcomeres would not be able to oscillate in concert if tension generation were imbalanced because of the presence of damaged sarcomeres.

Elasticity of connectin (titin) and the mechanism of SPOC

It was previously reported that connectin (titin) is not essential to the SPOC occurring under isometric conditions, because microscopic observation indicated that partial trypsinization of connectin in skeletal myofibril did not affect the oscillation of sarcomere length (Shimizu et al., 1992).

As shown in Fig. 6, the resting tension produced by the elongation of connectin is too small to contribute to the isotonic tension, even under the SPOC condition. This is especially true at sarcomere lengths less than 2.5 μm. There remains a possibility, however, that the large viscoelasticity of connectin may contribute to the tension at the quick yielding phase and thus might determine the greatest sarcomere length during oscillation (cf. Fig. 6, *open triangles*). This possibility was examined by partially digesting connectin, and the result indicates that although the passive tension of connectin may contribute to the level of tension, it is not essential to the oscillation mechanism itself.

The time course of the sarcomere length oscillation during isotonic SPOC was simulated by Smith and Stephenson, who used a model (see figure 11(a) of Smith and Stephenson, 1994) in which the resting tension of connectin was taken into account. The model could reproduce the oscillation of sarcomeres, but the waveform was not of a sawtooth type, and the shortening velocity increased as the shortening of myofibrils proceeded. This change in velocity is opposite that evident in the experimental results shown in Fig. 4.

Finally, we would like to stress that under isotonic conditions the active tension increased as the average sarcomere length increased (Fig. 6). Such a length-tension relation was also observed in the isometric tension analysis under conditions with submicromolar Ca^{2+} concentrations (Endo, 1973; Fabiato and Fabiato, 1978; Iwazumi and Pollack, 1981; Stephenson and Wendt, 1984). Under isotonic conditions, the active tension after yielding (*thin dashed line*) was the same as that before yielding (*thick dashed line*), even though the maximum number of cross-bridges should be smaller. It should be noted that the level of tension under SPOC conditions is much smaller than that in normal Ca^{2+} activation, so that there is room available for a number of force-generating cross-bridges. The number of force-generating cross-bridges may be self-controlled during sarcomere oscillations (cf. Ishiwata and Yasuda, 1993). To confirm this inference, the stiffness of myofibrils should be measured during isotonic SPOC.

We thank Dr. Toshiki Yagi and Dr. Shinji Kamimura of the University of Tokyo for valuable advice, Mr. Tohru Takakura of Waseda University for technical assistance, and Dr. Shin-ichiro Umemura and Dr. Shojiro Asai of Hitachi for their continuous encouragement.

This work was supported in part by Grants-in-Aid for Scientific Research (04402053 to SI) and for Scientific Research on Priority Areas (06213233 to SI) from the Ministry of Education, Sport, Science and Culture of Japan.

REFERENCES

Anazawa, T., K. Yasuda, and S. Ishiwata. 1992. Spontaneous oscillation of tension and sarcomere length in skeletal myofibrils. Microscopic measurement and analysis. *Biophys. J.* 61:1099–1108.

Endo, M. 1973. Length dependence of activation of skinned muscle fibers by calcium. *Cold Spring Harb. Symp. Quant. Biol.* 37:505–510.

Fabiato, A., and F. Fabiato. 1978. Myofilament general tension oscillations during partial calcium activation and activation dependence of the sarcomere length-tension relation of skinned cardiac cells. *J. Gen. Physiol.* 72:667–699.

Goldstein, A. M., L. H. Michael, J. P. Schroeter, and R. L. Sass. 1988. Structural states in the Z band of skeletal muscle correlate with states of active and passive tension. *J. Gen. Physiol.* 92:113–119.

Ishiwata, S., and T. Funatsu. 1985. Does actin bind to the ends of thin filaments in skeletal muscle? *J. Cell Biol.* 100:282–291.

Ishiwata, S., N. Okamura, H. Shimizu, T. Anazawa, and K. Yasuda. 1991. Spontaneous oscillatory contraction (SPOC) of sarcomeres in skeletal muscle. *Adv. Biophys.* 27:227–235.

Ishiwata, S., and K. Yasuda. 1993. Mechano-chemical coupling in spontaneous oscillatory contraction of muscle. *Phase Transitions.* 45: 105–136.

Iwazumi, T., and G. H. Pollack. 1981. The effect of sarcomere non-uniformity on the sarcomere length-tension relationship of skinned fibers. *J. Cell. Physiol.* 106:321–337.

Jarosch, R. 1987. Screw-mechanical models for the action of actin- and tubulin-containing filaments. *In* Nature and Function of Cytoskeletal Proteins in Motility and Transport. K. E. Wohlfarth-Bottermann, editor. Gustav Fischer, Stuttgart. 231–249.

Kamimura, S., and R. Kamiya. 1989. High-frequency nanometre-scale vibration in "quiescent" flagellar axonemes. *Nature.* 340:476–478.

Kishino, A., and T. Yanagida. 1988. Force measurements by micromanipulation of a single actin filament by glass needles. *Nature.* 334:74–76.

Linke, W. A., M. L. Bartoo, and G. H. Pollack. 1993. Spontaneous sarcomeric oscillations at intermediate activation levels in single isolated cardiac myofibrils. *Circ. Res.* 73:724–734.

Magid, A., and D. J. Law. 1985. Myofibrils bear most of the resting tension in frog skeletal muscle. *Science.* 230:1280–1282.

Nishizaka, T., T. Yagi, Y. Tanaka, and S. Ishiwata. 1993. Right-handed rotation of an actin filament in an in vitro motile system. *Nature.* 361:269–271.

Okamura, N., and S. Ishiwata. 1988. Spontaneous oscillatory contraction of sarcomeres in skeletal myofibrils. *J. Muscle Res. Cell Motil.* 9:111–119.

Schoenberg, M., J. B. Wells, and R. J. Podolsky. 1974. Muscle compliance and the longitudinal transmission of mechanical impulses. *J. Gen. Physiol.* 64:623–642.

Shimizu, H., T. Fujita, and S. Ishiwata. 1992. Regulation of tension development by MgADP and Pi without Ca^{2+}. Role in spontaneous tension oscillation of skeletal muscle. *Biophys. J.* 61:187–1098.

Smith, D. A., and D. G. Stephenson. 1994. Theory and observation of spontaneous oscillatory contractions in skeletal myofibrils. *J. Muscle Res. Cell Motil.* 15:369–389.

Stephenson, D. G., and I. R. Wendt. 1984. Length dependence of changes in sarcoplasmic calcium concentration and myofibrillar calcium sensitivity in striated muscle fibers. *J. Muscle Res. Cell Motil.* 5:243–272.

Stephenson, D. G., and D. A. Williams. 1981. Calcium-activated force responses in fast- and slow-twitch skinned muscle fibers of the rat at different temperatures. *J. Physiol.* 317:281–302.

Stephenson, D. G., and D. A. Williams. 1982. Effects of sarcomere length on the force-pCa relation in fast- and slow-twitch skinned muscle fibres from the rat. *J. Physiol.* 333:637–653.

Sweitzer, N. K., and R. L. Moss. 1990. The effect of altered temperature on Ca^{2+}-sensitive force in permeabilized myocardium and skeletal muscle. Evidence for force dependence of thin filament activation. *J. Gen. Physiol.* 96:1221–1245.

Yagi, T., S. Kamimura, and R. Kamiya. 1994. Nanometer scale vibration in mutant axonemes of chlamidomonas. *Cell Motil. Cytoskeleton.* 29: 177–185.

Yasuda, K., T. Anazawa, and S. Ishiwata. 1995. Microscopic analysis of the elastic properties of nebulin in skeletal myofibrils. *Biophys. J.* 68:598–608.

Journal of Microscopy, Vol. 182, Pt 2, May 1996, pp. 79–83.
Received 4 July 1995; accepted 13 December 1995

Soft-X-ray damage to biological samples

H. FUJISAKI,* S. TAKAHASHI,† H. OHZEKI,† K. SUGISAKI,† H. KONDO,* H. NAGATA,* H. KATO‡ & S. ISHIWATA‡

**Nikon Corporation, Tsukuba Research Laboratory, 5-9-1 Tokodai, Tsukuba, Ibaraki 300-26, Japan*

†Nikon Corporation, New Business Development Department, 1-6-3 Nishi-Ohi, Shinagawa, Tokyo 140, Japan

‡Waseda University, Department of Physics, School of Science and Engineering, 3-4-1 Okubo, Shinjuku, Tokyo 169, Japan

Key words. X-ray, soft X-ray, X-ray damage, soft-X-ray damage, X-ray microscope, water window, yeast, myofibril.

Summary

X-ray damage to biological samples was investigated in the wavelength region of 2·7–5 nm, which overlaps the so-called 'water window', the wavelength range of 2·4–4·3 nm usually used in X-ray microscopy. Yeast cells and myofibrils were chosen as representatives of whole cell samples and motile protein systems, respectively. The samples were exposed to X-rays using an apparatus composed mainly of a laser-plasma X-ray source, a Wolter mirror condenser, and a sample cell. The yeast cells lost their dye exclusion ability when the X-ray flux was higher than 1×10^6 photons μm^{-2}, while the myofibrils lost contractility when the X-ray flux was higher than 4×10^5 photons μm^{-2}. These X-ray fluxes are lower than the flux required for the X-ray microscope observation of biological samples at a resolution higher than that of light microscopes.

1. Introduction

The X-ray microscope generally uses X-rays of the wavelength region referred to as the 'water window', that is, 2·4–4·3 nm (soft X-rays), where proteins absorb more X-rays than water does. Further refinement of the X-ray microscope is currently being pursued with the hope that observation of biological samples in water, which is impossible with electron microscopes, can be carried out at a higher resolution than that of light microscopes (Michette *et al.*, 1992).

However, biological samples are thought to be damaged by exposure to soft X-rays during X-ray microscope observation (Sayre *et al.*, 1978; Shinohara & Ito, 1991), although only a few reports of experimental examination are available concerning biological samples in water. Bennett and co-workers examined myofibrils with a scanning transmission X-ray microscope to determine the effects of radiation on their function and structure (Bennett *et al.*, 1992, 1993; Foster *et al.*, 1992). They found that after an exposure to $7{\cdot}5 \times 10^5$ photons μm^{-2} myofibrils would no longer contract, and observed the mass loss of myofibrils. Williams *et al.* (1992, 1993) reported the mass loss of chromosomes during observation by scanning transmission X-ray microscope.

We have investigated X-ray damage to biological samples in the wavelength region of 2·7–5 nm, which overlaps the water window. Yeast cells and myofibrils were chosen as representatives of whole cells and motile protein systems, respectively. The sample, in a vacuum-tight sample cell, was exposed to X-rays from a laser-plasma X-ray source through a titanium membrane filter and a Wolter mirror condenser.

2. Apparatus for exposing biological samples to X-rays

We constructed an apparatus to expose biological samples to soft X-rays. As shown in Fig. 1, this apparatus was composed of a laser-plasma X-ray source, a titanium membrane filter, a Wolter mirror condenser, a vacuum-tight sample cell, a Wolter mirror objective, a CCD image detector (Sony, Tokyo), and a vacuum chamber equipped with evacuation systems. Laser plasmas were generated by a 1-J Nd:YAG laser light focused to a diameter of 100 μm on a motor-driven tungsten target plate 0·1 mm thick and 50 mm square (Nilaco, Tokyo). This Nd:YAG laser (Continuum, San Diego, CA) can emit up to a 2-J laser light, although throughout our experiments the laser energy was

Correspondence: Hisao Fujisaki; Tel +81-298-47-5425, fax +81-298-47-5427, e-mail fujisaki@tsukubagw.nikon.co.jp

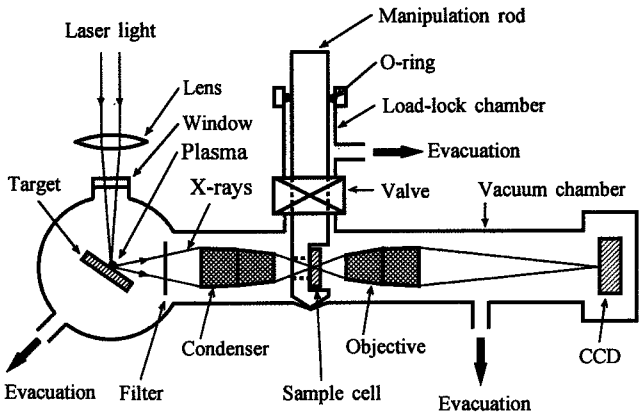

Fig. 1. Apparatus for exposing biological samples to soft X-rays. YAG laser light is focused on the target plate to generate a plasma. X-rays emitted by the plasma are focused on the sample in the sample cell by a Wolter mirror condenser (×1/4). A Wolter mirror objective (×32) and a CCD image detector are used with He–Ne laser light to determine the position of the X-ray focused area on the sample prior to the X-ray exposure.

kept at 1 J. The pulse width was 8 ns. Various numbers of 0·5-μm-thick titanium membranes (Takeuchi Metal Foil and Powder, Tokyo) were layered together and used as a single filter to change the strength of the X-rays to which the samples were exposed. The filter also limited the X-ray wavelengths to the water window region, excluding X-rays whose wavelengths were shorter than 2·7 nm, and visible and ultraviolet light. In addition, it protected the Wolter mirror objective from ions and debris emitted by the plasma.

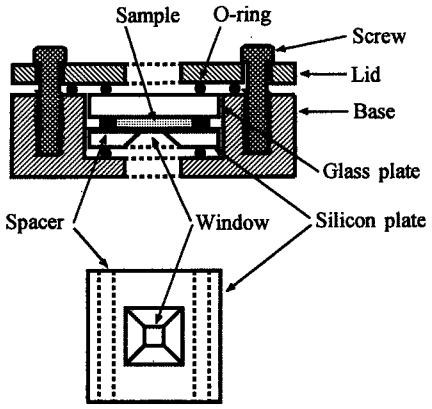

Fig. 2. Vacuum-tight sample cell. The sample solution is held between a 0·5-mm-thick glass plate and a 0·4-mm-thick silicon plate, each 10-mm square. The silicon plate has a 0·2-mm square X-ray-transparent window made of 0·1-μm-thick silicon nitride. Polymethylmethacrylate spacers 10 μm thick on the silicon plate determine the thickness of the sample solution. The glass and silicon plates are put into the base and covered with the lid. Screws and O-rings are used to make the cell vacuum-tight.

The sample cell, schematically shown in Fig. 2, was composed of a stainless-steel base, a stainless-steel lid, a 0·5-mm-thick Pyrex glass plate, and a window plate. The window plate was a 0·4-mm-thick silicon plate coated with a 0·1-μm-thick silicon nitride membrane and back-etched to make a 0·2-mm square X-ray-transparent window. The sample solution was placed between the glass plate and the window plates. Rubber O-rings and screws were used to make the cell vacuum-light.

The Wolter mirror condenser produced a four-times reduced image of the plasma on the image plane where the samples were placed. Using the calibration curve reported by Kinoshita (1985) and partially confirmed by our preliminary experiments, the X-ray strength at the sample position was determined for the optical density of the Kodak 101-01 X-ray film exposed to X-rays and developed according to Kodak's specifications. The optical density was measured with a Konica densitometer PDP-15.

Figure 3 shows the spectrum of the X-rays to which the sample was exposed. The X-rays were generated with a single shot of 1-J YAG laser light. X-rays with wavelengths shorter than 2·7 nm or longer than 5 nm were excluded by the titanium membrane filter.

3. Samples

Dried yeast cells (Nissin, Tokyo) were immersed in water at 30 °C (125 mg mL^{-1}). A dye solution of 0·5% trypan blue (Cosmo Bio, Tokyo) was added to make the yeast

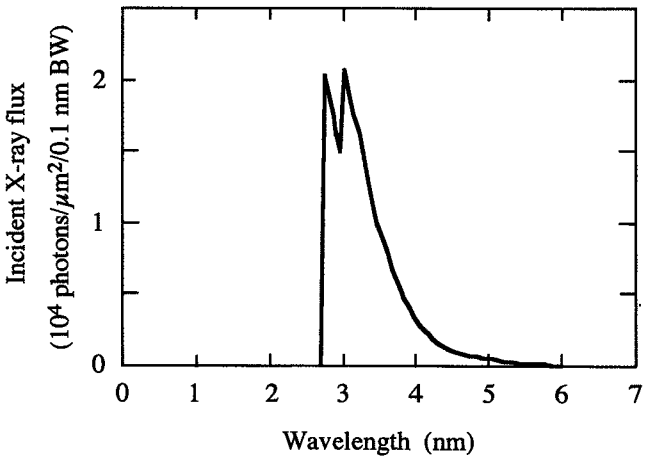

Fig. 3. X-ray spectrum to which the samples were exposed. The filter consisted of two pieces of 0·5-μm-thick titanium membrane. A window plate was set alone in the sample cell and a monochromator was used instead of the objective and the CCD image detector. The monochromator was composed of a stainless-steel plate with a 50-μm slit and a 1000-line mm^{-1} grating. A sheet of X-ray film was placed behind the monochromator and exposed to X-rays emitted by a 1-J-laser-produced plasma. The total flux of the X-rays was $3{\cdot}3 \times 10^5$ photons μm^{-2} per exposure.

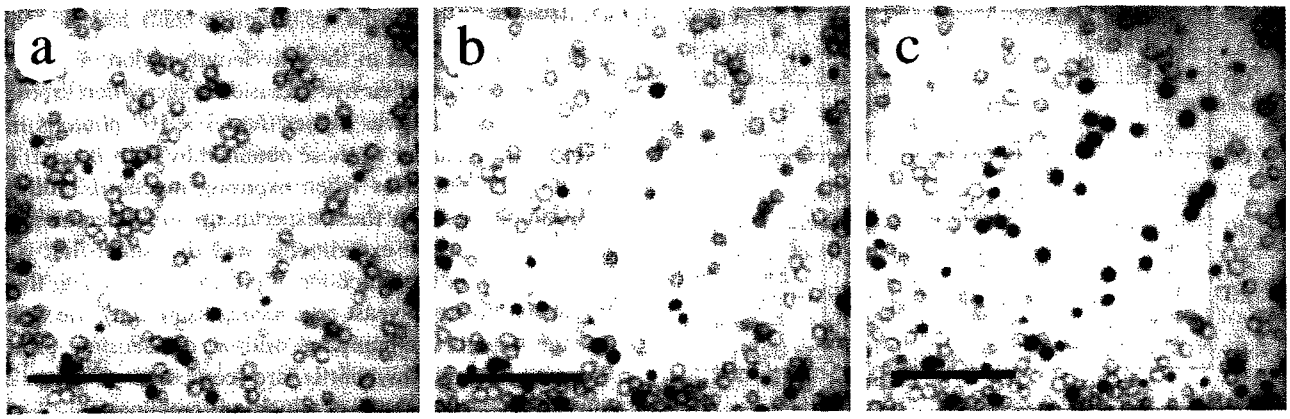

Fig. 4. Staining of yeast cells exposed to soft X-rays in 0·3% trypan blue solution. Photographs were taken under a light microscope (a) before; (b) 3 min after; (c) 30 min after the exposure. The X-rays were generated by 100 shots of 1-J Nd : YAG laser light at 1 Hz. The filter used was composed of five pieces of 0·5-μm-thick titanium membrane. The total incident X-ray photon flux was 1×10^6 μm^{-2} on the sample. The scale bars indicate 50 μm.

concentration 50 mg mL^{-1} and the trypan blue concentration 0·3%. This was so that we could determine if each yeast cell was alive using a light microscope, since living yeast cells exclude this dye while dead ones are stained purple.

When the sample solution was first put into the sample cell and not yet exposed to X-rays, about 10% of the yeast cells were already stained, as shown in Fig. 4(a). These cells did not revive from the dried state. Most of the other cells did not become stained for at least a week. The staining that did occur took place at the very low rate of less than 1% per day.

Myofibrils were prepared from glycerol-treated rabbit psoas muscle according to Ishiwata & Funatsu (1985) and suspended in 60 mM KCl, 5 mM $MgCl_2$ 1 mM EGTA, and 10 mM PIPES at pH 6·8. The ATP solution added to the X-ray-exposed myofibril suspension was 120 mM KCl, 4 mM $MgCl_2$, 1·9 mM $CaCl_2$, 2 mM EGTA, 20 mM MOPS, and 2 mM ATP at pH 7·0 (2 μM free Ca^{2+}).

4. Results

The dye solution containing the yeast cells was placed between the window plate and the glass plate in the sample cell. After observing the sample under a light microscope (Nikon, Tokyo) and taking a photograph with a Polaroid camera (Fig. 4a), the sample cell was set on the manipulation rod. The manipulation rod was inserted into the sample chamber of the X-ray exposure apparatus through a load-lock chamber.

A He–Ne laser light aligned coaxially with the Nd : YAG laser light was focused on the tungsten target plate. The titanium filter was removed from the light path and the scattered light was focused on the sample by the Wolter mirror condenser. The sample was imaged on the CCD by the Wolter mirror objective, and the area on the sample to be exposed to X-rays was determined. The filter was returned to its original position and the Nd : YAG laser light was focused on the tungsten target plate to a diameter of 100 μm to produce a plasma. X-rays emitted by the plasma and passed through the filter were focused in a 1/4× reduction on the sample.

The results shown in Figs. 4(b) and 4(c) were obtained by exposing the sample at the centre of the silicon nitride window to a total X-ray exposure of 1×10^6 photons μm^{-2}. The exposure was completed with 100 shots of 1-J Nd : YAG laser at 1 Hz using a filter consisting of five pieces of 0·5-μm-thick titanium membrane. Figure 4(b) shows the sample observed under a light microscope 3 min after its exposure. Several yeast cells were faintly stained. Figure 4(c) shows the sample observed under a light microscope 30 min after the exposure. Almost all the yeast cells at the centre of the window were darkly stained. The 30 min taken for the complete staining of the yeast cells after their exposure to the X-rays is thought not to be the time the yeast cells survived, but rather the time required for the absorption and accumulation of the dye molecules from the surrounding solution into the yeast cells. Even when the yeast cells were exposed to X-rays whose flux was as high as 3×10^7 photons μm^{-2}, 30 min was still necessary for their complete staining.

Similar exposure experiments were done changing exposure condition. In Fig. 5, results from exposures to low intensity X-rays for long periods and those to high intensity X-rays for short periods are compared. These results depended entirely on the total X-ray photon flux and showed no relationship to the exposure condition. This shows that the damage to the samples seen in these experiments was not due to heat generated by X-ray absorption, but rather due to the effects of X-ray photons on the samples. These effects might include cleavage within molecules or intra- and/or intermolecule cross-linking.

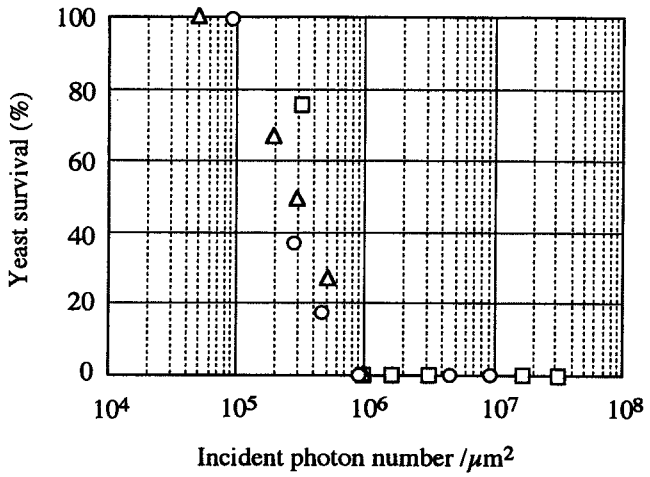

Fig. 5. Survival of yeast cells exposed to various fluxes of soft X-rays. The total incident photon fluxes given on the abscissa were obtained by multiple exposures of the sample to X-rays of $3{\cdot}3 \times 10^5$ (□), $9{\cdot}2 \times 10^4$ (○), or $1{\cdot}0 \times 10^4$ (△) photons μm^{-2} per exposure, using two, three or five pieces of 0·5-μm-thick titanium membrane as a filter, respectively. The exposure frequency was 0·1–1 Hz.

Experiments similar to those above were conducted using myofibrils as the sample in order to compare the performance of our apparatus with that of Bennett *et al.* (1993). Here, instead of a staining test, the contractility of the myofibrils was examined after the X-ray exposure. Both the unexposed myofibrils and those exposed to X-rays of 9×10^4–3×10^5 photons μm^{-2} shortened to become lumps after the addition of the ATP solution. This result differs from the results obtained by Bennett *et al.* (1993), and occurred possibly because our sample cell had not been drained. Therefore, myofibrils did not stick strongly to the silicon nitride window or the glass plate. In the case of Bennett *et al.*, the sample cell was drained once, so that myofibrils might have stuck firmly to the window and shown only the disappearance of stripes in their contraction.

When exposed to X-rays of 3×10^5–3×10^6 photons μm^{-2}, the myofibrils lost their contractility. When exposed to X-rays of 2–4×10^5 photons μm^{-2}, the myofibrils showed ambiguity following the addition of the ATP solution. Their characteristic stripes sometimes deformed and at other times disappeared without any change in length.

The above results are consistent with the observation of Bennett *et al.* (1993) that myofibrils lost their contractility after exposure to $\sim 0{\cdot}75 \times 10^6$ 385-eV X-rays μm^{-2}. This consistency shows that, as long as the wavelengths are within the water window region, X-rays with a broad spectrum have the same effect on the sample as monochromatized X-rays. This may be because the effects of X-rays on biological samples depend only on the total incident photon energy, as seen in Fig. 5.

5. Discussion

Figure 5 shows that in the wavelength region of 2·7–5 nm the yeast cells lost their dye exclusion ability when exposed to X-rays whose flux was higher than 1×10^6 photons μm^{-2}. This value is similar to those obtained by both Bennett *et al.* (1993) and ourselves when exposing myofibrils. Although the samples used in these experiments are different species, the purpose of the experiments was the same; that is, the examination of the functions of proteins. Examining the dye exclusion ability of yeast cells means examining the viability of the membrane-pumping and/or dye-sensing proteins. Correspondingly, myofibrils are composed of actin and myosin molecules, both of which are proteins.

In order to compare with these experimental results, we calculated the X-ray photon flux required to image biological samples with a Wolter-type X-ray microscope using Eq. (A5) (see Appendix). In the calculations, we used the chemical formula of insulin $C_{254}H_{332}O_{78}N_{62}S_6$, as the protein sample, and that of silicon nitride, Si_3N_4, as the X-ray-transparent plate window material. We fixed the X-ray wavelength at 4·3 nm, where the contrast of proteins to water is the largest in the water window wavelength region. The transmittance T necessary in the calculation was obtained as follows:

$$T = \exp(-\mu t), \tag{1}$$

$$\mu = 2R_0\lambda N\rho f_2/M_w. \tag{2}$$

Here, μ is the linear absorption coefficient of each material, and t is each material's thickness. R_0 is the classical electron radius, λ the wavelength of the X-rays, N Avogadro's number, and ρ and M_w the density and molecular weight of each material, respectively; f_2 is the imaginary part of the atomic scattering factor of each material. The atomic scattering factors of the elements composing each material were obtained from the table of Henke *et al.* (1989). The modulation transfer function M and the transmittance T_m of the Wolter mirror objective were assumed to be 0·2 and 0·5, respectively. The detection efficiency E was assumed to be 0·2. The resolution R and the sample thickness were taken to be 50 nm.

The contrast of the protein to water was calculated to be 0·09 using Eq. (A1). The photon number calculated is $6 \times 10^7 \mu m^{-2}$ at this contrast, which is about two orders larger than the value obtained experimentally. This means that it is difficult to make an image of a protein sample at a resolution higher than that of light microscopes without damaging the function of the proteins.

6. Conclusions

X-ray damage to yeast cells and myofibrils was investigated in the wavelength region of 2.7–5 nm. The yeast cells lost their dye exclusion ability when exposed to X-rays whose flux was higher than 1×10^6 photons μm^{-2}, while

myofibrils lost their contractility when exposed to X-rays whose flux was higher than 4×10^5 photons μm^{-2}. These values are lower than the required photon number μm^{-2} estimated for observing biological samples with a Wolter-type X-ray microscope at a resolution of 50 nm. This means that it is difficult to observe biological samples continuously while maintaining their functions. Thus it is inadvisable to employ repeated X-ray exposure for the imaging of biological samples when one must preserve the functional integrity of the sample. An image of a biological sample in its state just before denaturing may be obtained with a single shot of short pulse X-rays strong enough to make an image. Phase-contrast X-ray microscopy might be an alternative solution, albeit a difficult one, in cases where death of the sample must be avoided (Schmahl *et al.*, 1995). The use of free-radical scavengers might also be effective for sample protection (Bennet *et al.*, 1993).

Acknowledgment

We would like to thank members of the Technological Development Department of Nikon Co. for fabricating the Wolter mirrors.

References

Bennett, P.M., Buckley, C.J., Foster, G.F. & Anastasi, P.A.F. (1992) Radiation damage studies on active myofibrils. *X-ray Microscopy III* (ed. by A.G. Michette, G.R. Morrison & C.J. Buckley). Springer Series in Optical Sciences Vol. 67, pp. 400–403. Springer-Verlag, Berlin.

Bennett, P.M., Foster, G.F., Buckley, C.J. & Burge, R.E. (1993) The effect of soft X-radiation on myofibrils. *J. Microsc.* **172**, 109–119.

Foster, G.F., Buckley, C.J., Bennett, P.M. & Burge, R.E. (1992) Investigation of radiation damage to biological specimens at water window wavelengths. *Rev. Sci. Instrum.* **63**, 599–600.

Henke, B.L., Davis, J., Gullikson, E.M. & Perera, R.C.C. (1989) A preliminary report on x-ray photoabsorption coefficients and atomic scattering factors for 92 elements in the 10–10,000 eV region. *Lawrence Berkeley Laboratory Report LBL-26259.*

Ishiwata, S. & Funatsu, T. (1985) Does actin bind to the ends of thin filaments in skeletal muscle? *J. Cell Biol.* **100**, 282–291.

Kinoshita, T. (1985) Absolute measurement of spectra emitted by laser-produced plasmas. *Ph. D. Thesis*, Max Planck Institut für Quantenoptik.

Michette, A.G., Morrison, G.R. & Buckley, C.J. (eds) (1992) *X-ray Microscopy III.* Springer Series in Optical Sciences, Vol. 67. Springer-Verlag, Berlin.

Sayre, D., Kirz, J., Feder, R., Kim, D.M. & Spiller, E. (1978) Assessment of the potential of ultrasoft X-ray microscopy. *Ann. NY Acad. Sci.* **306**, 286–290.

Schmahl, G., Rudolph, D., Guttmann, P., Schneider, G., Thieme, J. & Niemann, B. (1995) Phase contrast studies of biological specimens with the x-ray microscope at BESSY. *Rev. Sci. Instrum.* **66**, 1282–1286.

Shinohara, K. & Ito, A. (1991) Radiation damage in soft X-ray microscopy of live mammalian cells. *J. Microsc.* **161**, 463–472.

Williams, S., Jacobsen, C., Kirz, J., Zhang, X., Van't Hoff, J. & Lamm, S. (1992) Radiation damage to chromosomes in scanning transmission X-ray microscopy. *SPIE Proc.* **1741**, 318–324.

Williams, S., Zhang, X., Jacobsen, C., Kirz, J. & Lindaas, S. (1993) Measurements of wet metaphase chromosomes in scanning transmission X-ray microscopy. *J. Microsc.* **170**, 155–165.

Appendix: incident X-ray photon flux required to make an image with an X-ray microscope using a Wolter mirror objective

Our purpose is to calculate the incident X-ray photon flux, i.e. the photon number per unit area, necessary to image protein samples of volume R^3 suspended in a water layer of thickness R, considering the use of a real X-ray microscope system. Sayre *et al.* (1978) reported a similar calculation under ideal conditions neglecting losses of photons or resolution which actually occur in any system.

When the incident flux is I_0, the contrast C of the X-ray passing through the sample and the water layer is calculated as follows:

$$C = (I_0T_w - I_0T_s)/(I_0T_w + I_0T_s)$$
$$= (T_w - T_s)/(T_w + T_s). \quad \text{(A1)}$$

Here, T_w and T_s are transmittances of the water layer and the sample, respectively.

Under the condition that, in order to distinguish the sample from the background, the difference between their signal intensities, calculated from the area of R^2 for each, is greater than three times the largest noise N,

$$I_0R^2T_w - I_0R^2T_s > 3N. \quad \text{(A2)}$$

Since the largest noise is contained in the largest signal, and T_w is larger than T_s in the 'water window' region,

$$N = (I_0R^2T_w)^{1/2}. \quad \text{(A3)}$$

From Eqs. (A1)–(A3)

$$I_0 > 9(1 + C)^2/(4C^2T_wR^2). \quad \text{(A4)}$$

The incident photon flux should be compensated by the transmittance T_c of the sample cell, the transmittance (reflectance) T_m of the objective, and the detection efficiency E of the image detector. Considering also the modulation transfer function M of the objective, the contrast C should be multiplied by M.

The incident X-ray photon flux I_0 required for a unit area on the sample surface is therefore expressed as

$$I_0 > 9(1 + MC)^2/(4M^2C^2T_wT_cT_mER^2). \quad \text{(A5)}$$

When the water layer is thicker than R, say R', the right-hand side of Eq. (A5) should be divided by the transmittance of the water layer of thickness $R' - R$.

Adv. Biophys., Vol. 33, pp. 135–142 (1996)

MICROSCOPIC ANALYSIS OF THE ELASTIC PROPERTIES OF CONNECTIN/TITIN AND NEBULIN IN MYOFIBRILS

SHIN'ICHI ISHIWATA,*[1] KENJI YASUDA,*[2] YOSHIAKI SHINDO,*[1] AND HIDEAKI FUJITA*[1]

*[1] *Department of Physics, School of Science and Engineering, Waseda University, Shinjuku-ku, Tokyo 169 and* *[2] *Advanced Research Laboratory, Hitachi Ltd., Hatoyama, Saitama 350-03, Japan*

The contractile system of muscle is composed not only of the active components, *i.e.*, a molecular motor consisting of myosin and actin, and the regulatory proteins tropomyosin and troponin, but also of the elastic framework that enables the active components to locate appropriate positions in a sarcomere and perform physiological functions. The main component of the elastic framework is connectin/titin (*1, 2*) which connects the end of thick filaments and the Z line (*3, 4*) and sustains the structure of thick filaments at the center of a sarcomere (*5*). In this report we briefly summarize the elastic properties of connectin/titin and also nebulin obtained by microscopic analysis and manipulation of the model systems of skeletal and cardiac myofibrils (*3, 6, 7*).

I. MYOFIBRIL MODELS

We have developed several models of skeletal and cardiac myofibrils to study the structure, function and mechanical properties of connectin / titin and nebulin. Figure 1 summarizes the strategy used in the present study. We used gelsolin, an actin filament severing protein which was isolated from bovine serum, as a molecular tool to selectively remove thin filaments in the myofibrils. When the myofibrils were treated with gelsolin under

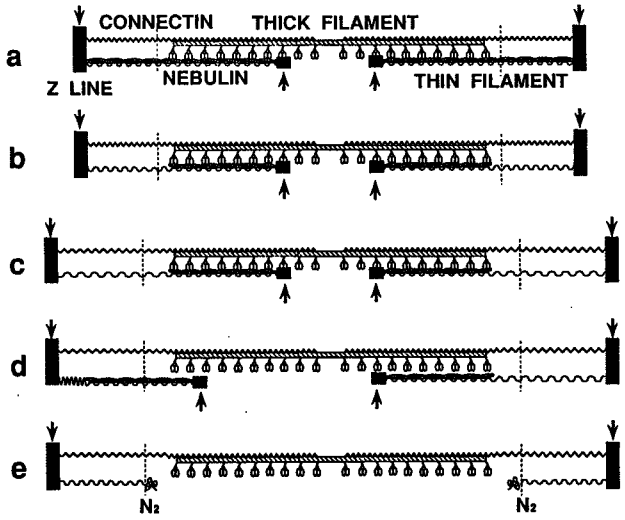

Fig. 1. Schematic illustration of the assumed filament structure of a sarcomere in *skeletal* myofibril models prepared by gelsolin treatment under rigor or contracting conditions. (a) Untreated sarcomere before gelsolin treatment; the fine structures of thick and thin filaments together with connectin/titin and nebulin are depicted schematically. (b and c) RG-treated sarcomere under rigor conditions; the portions of thin filaments located at the I band have been removed, so that a portion of each nebulin molecule is exposed (b; *cf.*, a model of nebulin attached to the thin filament in *20*) and with sarcomere stretching (c) only the I band is elongated without movement of the thin filament fragments remaining at the A band. (d) RG-treated sarcomere under relaxing conditions; the remaining fragments of thin filaments move to the Z line (left half) or stay as in c (right half) depending on whether the exposed portion of the nebulin molecule, which connects the remaining thin filament fragment to the Z line, shrinks. (e) CG-treated sarcomere; thin filaments are removed except the short fragments at the Z line by further treatment of c with gelsolin under contracting conditions, so that the nebulin is free of thin filaments. Portions of the free ends of nebulin appear to be folded and have become entangled in the N_2 line (*3*). Vertical dashed lines indicate the approximate position of the N_2 line. Arrows indicate the position at which rhodamine-phalloidin staining occurs without chemical fixation (taken from 7). In *cardiac* myofibril models, nebulin is absent, so that the remaining fragments of thin filaments at the A band (b and c) are believed to be free of the Z line (the wavy line appearing at the I band is absent) and also the N_2 line does not appear after the removal of thin filaments (*4*); a whole region of thin filaments is stained with rhodamine-phalloidin without chemical fixation (*21*).

rigor (– ATP) conditions containing Ca^{2+}, only the portions of thin filaments located at the I band were removed (RG-treated myofibrils; Figs. 1b, c and 2c); when these RG-treated myofibrils were further treated with gelsolin under contracting conditions, whole portions of thin filaments except small fragments at the Z line were removed (CG-treated myofibrils; Fig. 1e, see Fig. 1c of ref. 7). Instead of using this two-step preparation method, CG-treated myofibrils could be prepared by the gelsolin treatment in the contracting solution containing 2,3-butanedione 2-monoxime (BDM) in addition to MgATP and Ca^{2+}; BDM is a reversible inhibitor for

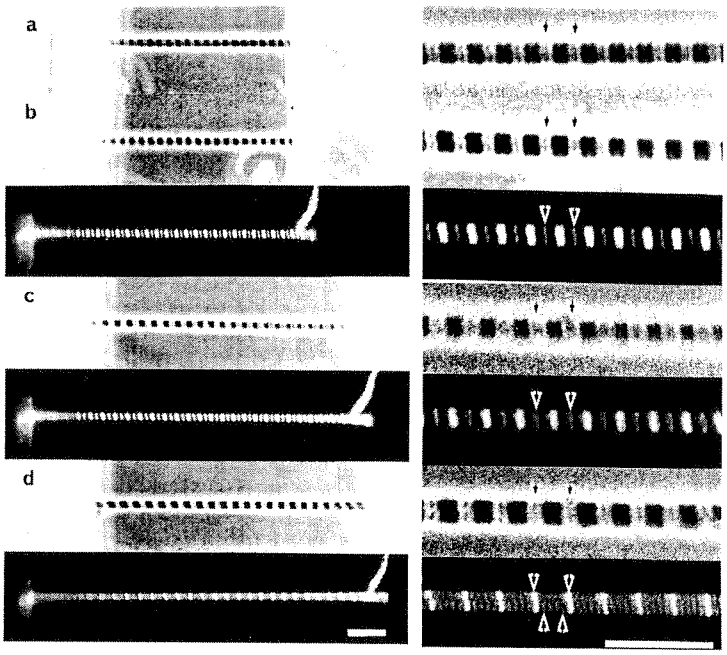

Fig. 2. Phase-contrast and fluorescence micrographs of RG-treated skeletal myofibrils showing the effects of extension under rigor (*cf.* Fig. 1b, c) and relaxing (*cf.* Fig. 1d) conditions. The free ends of thin filaments and the Z line were visualized by rhodamine-phalloidin staining. (a) Untreated myofibril (for method of myofibril preparation, see *18*; for method of microscopic manipulation of single myofibrils, see *6*, *7*, *22*, *23*); (b) myofibril of *a* after RG-treatment; (c) myofibril of *b* that had been stretched under rigor condition; (d) myofibril of c under relaxing condition. The fluorescence micrograph of a was omitted because it was indistinguishable from that of b. Enlarged figures are shown on the right. Arrows pointing from the upper side of myofibrils indicate the positions of the Z lines. Both the central fluorescent doublet (b and c) and the quartet (d) in each sarcomere correspond to the free ends of thin filaments (see arrows in Fig. 1). Arrows pointing from the lower side of the myofibril in *d* indicate the outer pair of quartet bands originating from the central doublet of b or c (see the left half of Fig. 1d). Scale bars, 10 μm (taken from 7).

tension development, so that the CG-treated myofibrils can be prepared without disturbing the ordered structure of sarcomeres (see Fig. 1c of ref. 7). We confirmed that the sarcomere homogeneity was maintained throughout the present work.

II. ELASTIC PROPERTIES OF CONNECTIN/TITIN IN SKELETAL AND CARDIAC MYOFIBRILS

When an untreated myofibril is stretched under relaxing conditions, the passive tension called resting tension is developed as shown in Fig. 3 (a for skeletal and b for cardiac). Even after the thin filaments were completely

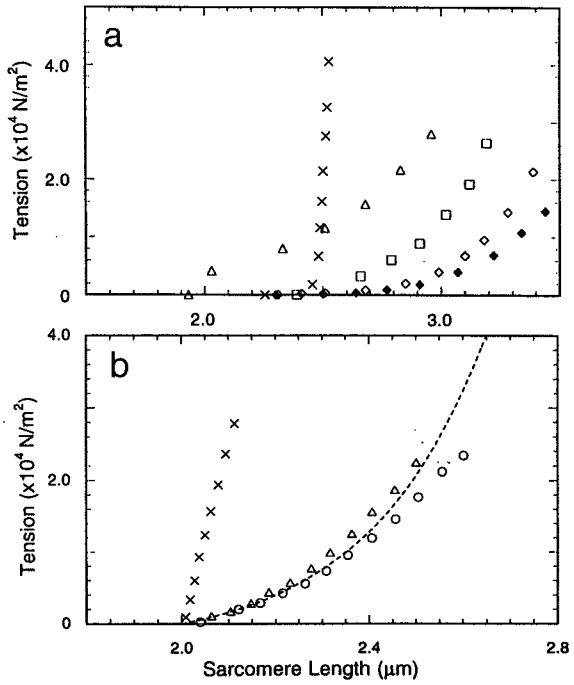

Fig. 3. Passive tension (P) *vs.* extension (L) relation of skeletal (a) and cardiac (b) myofibrils under various conditions before and after gelsolin treatment. First, an untreated myofibril (a few μm thick and about 50 μm long) at an average sarcomere length of 2.47 μm (a) or 2.1 μm (b) was gradually extended in a rigor ($-Ca^{2+}$) solution, and the tension was measured from the deflection of a flexible glass microneedle to which one end of the myofibril was fixed (×); after returning to the initial sarcomere length, it was treated with gelsolin in a rigor ($+Ca^{2+}$) solution (RG-treated myofibril; *cf.* Figs. 1 and 2) and the passive tension was measured stepwise (△) in the rigor ($-Ca^{2+}$) solution starting from a slack length at which no tension was developed (about 1.93 μm for a; about 2.0 μm for b). For the cardiac RG-treated myofibril (b), the passive tension was also measured stepwise in the relaxing solution (○) similarly to the above; note that the P-L relation was nearly the same as that of untreated myofibrils obtained under the relaxing conditions (dashed line). The skeletal RG-treated myofibril (a) was further treated with gelsolin in a contracting solution (CG-treated myofibril) after returning to the initial sarcomere length, and the passive (resting) tension was again measured stepwise in a relaxing solution (□); as a control, the resting tension of an untreated skeletal myofibril with (◆) or without BDM (◇) was also measured using a different specimen (taken from 7).

removed (CG-treated myofibrils), the resting tension *vs.* sarcomere length relation was concave and similar to that of an untreated one, showing that the thin filaments are not responsible for the resting tension. This result is consistent with that obtained using a single skeletal muscle fiber (*3*), although slightly greater tension development was observed in myofibrils. The absolute value of the resting tension per unit cross-sectional area for skeletal myofibrils was nearly equal to those previously obtained using a single fiber, *e.g.*, about 10^4 N/m^2 at sarcomere lengths slightly longer than

3.0 μm (*cf. 8–11*). Thus, we conclude that the resting tension is attributable to the elongation of connectin/titin. It should be noted, however, that the absolute value of the resting tension is an order of magnitude smaller than that of active tension even at sarcomere lengths longer than 3.0 μm.

III. ELASTIC PROPERTIES OF NEBULIN IN SKELETAL MYOFIBRILS

In the RG-treated myofibrils, the portion of nebulin at the I band is expected to be free of the thin filaments (Figs. 1b–d and 2b, c), so that the elastic properties of this portion of nebulin can be examined by applying external force. As shown in Fig. 3a, the passive tension (P) *vs.* sarcomere length (L) relation in the RG-treated myofibrils was very peculiar in the case of skeletal myofibrils; first, the tension was developed accompanying removal of the portion of thin filaments, so that the slack length of a sarcomere was shortened. Second, the P-L relation at shorter sarcomere lengths was convex, which is in contrast to the concave curve observed for CG-treated myofibrils or untreated ones under the relaxing conditions. We confirmed that, in the case of cardiac myofibrils, such a peculiarity did not appear and the P-L relation of RG-treated myofibrils was almost the same as that of untreated ones under relaxing conditions (Fig. 3b); this is probably due to the absence of nebulin in cardiac muscle.

The above results show that the P-L relation for the RG-treated skeletal myofibrils is ascribable to the elastic properties of the exposed portion of nebulin (see Fig. 1). The static elastic modulus of the exposed portion of nebulin per thin filament could be estimated from the slope of the P-L relation at the sarcomere length where the RG-treatment was done, *i.e.*, 2.47 μm in Fig. 3a; the average elastic modulus was about 10 pN (= 10^{-2} pN/nm for the 1 μm long exposed portion of nebulin).

The elastic modulus of an actin filament, on the other hand, has been estimated to be about 2×10^4 pN (= 20 pN/nm for an actin filament 1 μm long and 2 nm in the effective radius of cross section) (*12, 13*), three orders of magnitude greater than that of nebulin. Thus, we conclude that nebulin, at least the portion of the molecule located near the Z line, does not contribute to the static elastic modulus of thin filaments in skeletal muscle. It has been inferred from the amino acid sequence that a large portion of nebulin is composed of α-helix (*14, 15*), of which the elastic modulus is several tens of times larger than that estimated for nebulin. There are at least two possible ways to reconcile this apparent discrepancy: first, the α-helix of nebulin is unfolded when detached from an actin filament or, second, the exposed portion of nebulin is not composed of α-helix alone.

IV. PHYSIOLOGICAL FUNCTIONS OF ELASTIC COMPONENTS

How do the elastic properties of connectin/titin play in the physiological function of myofibrils? To partly answer this question, we examined the effects of disconnection of connectin/titin by mild tryptic digestion on the spontaneous oscillatory contraction (SPOC) of skeletal myofibrils; peak-to-peak amplitude of oscillation of sarcomere lengths during SPOC reaches 0.6 μm, that is, the sarcomere length spontaneously oscillates between, *e.g.*, 2.2 and 2.8 μm (*16–18*). First, we examined the time course of the decrease in the resting tension after the addition of trypsin at three different sarcomere lengths. As shown in Fig. 4, the resting tension decreased nearly independently of the sarcomere lengths (there was a tendency for the decay rate to be larger at shorter sarcomere lengths, consistent with the previous result obtained by a single fiber (*19*)), and was nearly one tenth after the digestion for 200 sec. We confirmed by SDSPAGE that digestion of connectin/titin occurred in parallel with the time course of the decrease in the resting tension, although troponin T/I and even myosin molecules were partly digested.

We examined the effects of tryptic digestion on SPOC at two different sarcomere lengths: 2.1–2.4 μm, where the resting tension does not contribute to the SPOC tension (Fig. 5a), and 2.7–3.0 μm, where the resting tension is still small but contributes to the total tension by nearly 10% (Fig. 5b). As shown in Fig. 5, there seems to be little effect of tryptic digestion for 200 sec on the tension oscillation, especially at shorter sarcomere

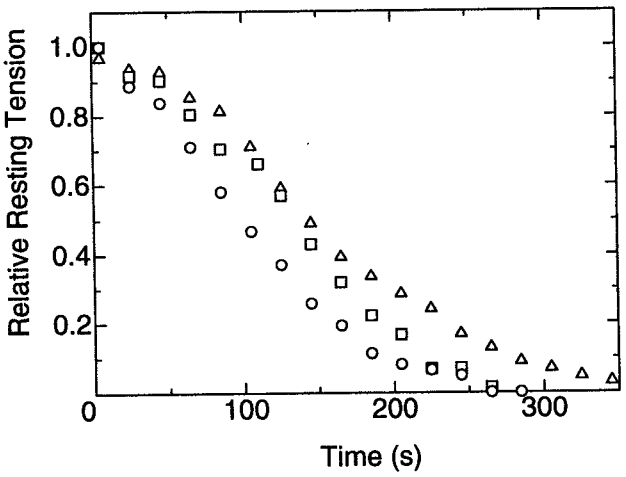

Fig. 4. Effects of tryptic digestion on resting tension of skeletal myofibrils. Time course of the decrease in the resting tension after the addition of trypsin (0.25 μg/ml) to the relaxing solution (0.12 M KCL, 4 mM $MgCl_2$, 4 mM ATP, 20 mM MOP (pH 7.0), 4 mM EGTA, and 20mM BDM) was measured at three different sarcomere lengths (○, 2.8 μm; □, 3.0 μm; △, 3.6 μm) at room temperature.

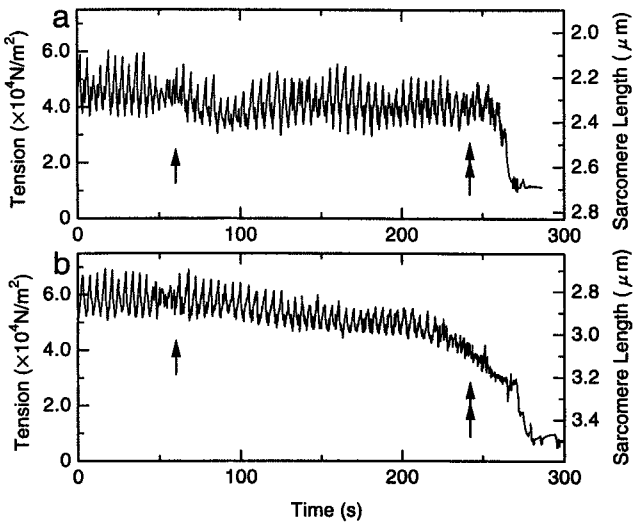

Fig. 5. Effects of tryptic digestion on spontaneous oscillatory contraction (SPOC) of skeletal myofibrils observed under an auxotonic condition (*6*) at two different sarcomere lengths at room temperature. a and b, the initial average sarcomere lengths were, respectively, 2.2 μm and 2.8 μm. Trypsin (0.25 μg/ml) was added to the SPOC solution (0.12 M KCl, 4 mM $MgCl_2$, 0.2 mM ATP, 4 mM ADP, 4 mM K-inorganic phosphate, 20 mM MOPS (pH 7.0), and 4 mM EGTA) at the time shown by an arrow, and the SPOC solution containing trypsin was exchanged for the relaxing solution at the time shown by a double arrow.

lengths; at longer sarcomere lengths, the level of tension gradually decreased (probably due to the disconnection of connectin/titin) together with slight decrease in the oscillation amplitude, but the oscillation itself was not largely affected. Thus, we conclude that the extension of connectin/titin does not play a principal part in SPOC.

Acknowledgments

This work was partly supported by Grants-in-Aid for General Scientific Research and Science Research on Priority Areas from the Ministry of Education, Science, Sports and Culture of Japan.

REFERENCES

1 K. Maruyama, *Biophys. Chem.*, **10**, 333 (1994).
2 K. Wang, "Cell and Muscle Motility," Vol. 6, ed. by J. W. Shay, Plenum Pub. Corp., New York, p. 315 (1985).
3 T. Funatsu, H. Higuchi, and S. Ishiwata, *J. Cell Biol.*, **110**, 53 (1990).
4 T. Funatsu, E. Kono, H. Higuchi, S. Kimura, S. Ishiwata, T. Yoshioka, K. Maruyama, and S. Tsukita, *J. Cell Biol.*, **120**, 711 (1993).
5 R. Horowits and R.J. Podolsky, *J. Cell Biol.*, **105**, 2217 (1987).
6 T. Anazawa, K. Yasuda, and S. Ishiwata, *Biophys. J.*, **61**, 1099 (1992).
7 K. Yasuda, T. Anazawa, and S. Ishiwata, *Biophys. J.*, **68**, 598 (1995).

8 R. Natori, *Jikeikai Med. J.*, **1**, 119 (1954).
9 A. Magid and D.J. Law, *Science*, **230**, 1280 (1985).
10 R.L. Moss and W. Halpern, *Biophys. J.*, **17**, 213 (1977).
11 H.L.M. Granzier and K. Wang, *Biophys. J.*, **65**, 2141 (1993).
12 S. Fujime, "Optical Studies of Muscle Cross-bridges," ed. by R.J. Baskin and Y. Yeh, CRC Press, FL, p. 149 (1987).
13 H. Higuchi, Y. Nakauchi, K. Maruyama, and S. Fujime, *Biophys. J.*, **65**, 1906 (1993).
14 S. Labeit, T. Gibson, A. Kakey, K. Leonard, M. Zeviani, P. Knight, J. Wardale, and J. Trinick, *FEBS Lett.*, **282**, 313 (1991).
15 M. Pfuhl, S.J. Winder, and A. Pastore, *EMBO J.*, **13**, 1782 (1994).
16 N. Okamura and S. Ishiwata, *J. Muscle Res. Cell Motil.*, **9**, 111 (1988).
17 S. Ishiwata, N. Okamura, H. Shimizu, T. Anazawa, and K. Yasuda, *Adv. Biophys.*, **27**, 227 (1991).
18 S. Ishiwata, T. Anazawa, T. Fujita, N. Fukuda, H. Shimizu, and K. Yasuda, "Mechanism of Myofibril Sliding in Muscle Contraction," ed. by H. Sugi and G.H. Pollack, Plenum Press, New York, p. 545 (1993).
19 T. Yoshioka, H. Higuchi, S. Kimura, K. Ohashi, Y. Umazume, and K. Maruyama, *Biomed. Res.*, **7**, 181 (1986).
20 J. Trinick, *FEBS Lett.*, **307**, 44 (1992).
21 K. Yasuda and S. Ishiwata, *Proc. Jpn. Acad.*, **70**, 151 (1994).
22 T. Iwazumi, *Am. J. Physiol.*, **252**, C253 (1987).
23 T. Funatsu, T.Anazawa, and S. Ishiwata, *J. Muscle Res. Cell Motil.*, **15**, 158 (1994).

Cell Motility and the Cytoskeleton 34:271–278 (1996)

Ca^{2+}-Induced Tension Development in the Stalks of Glycerinated *Vorticella convallaria*

Yasushige Moriyama, Kenji Yasuda, Shin'ichi Ishiwata, and Hiroshi Asai

Department of Physics, School of Science and Engineering, Waseda University, Okubo, Shinjuku-ku, Tokyo, Japan

We have developed a method of measuring the isometric tension in glycerinated stalks of *Vorticella convallaria*. Using this method, we measured tension vs. pCa relations in glycerinated *V. convallaria* stalks. The maximum isometric tension was 4×10^{-8} N on average. The Hill's parameter, n, which is the number of calcium ions bound simultaneously and cooperatively to a contractile element (a force generating element), is approximately 3.2 when the Ca^{2+} concentration is increased and 2.5 when it is decreased. In order to estimate the efficiency of the energy conversion of Ca^{2+} binding to mechanical work, we measured the Ca^{2+}-induced Carnot cycle in the *Vorticella* stalk. The energy efficiency was tentatively estimated to be about 7%. With this method, we have also succeeded in measuring the isometric tension of isolated spasmoneme, the rubber-like contractile fibrous organelle in the stalk. The maximum tension of spasmoneme was approximately one tenth that of the glycerinated stalk. We speculate that the isolated spasmoneme was only partially functional due to damage sustained when it was pulled out of the stalk.

Key words: calcium ion, spasmoneme, Hill's parameter, energy efficiency

INTRODUCTION

The peritrich ciliates *Vorticella, Carchesium,* and *Zoothamnium* are composed of zooids and long stalks. In the living state, *Vorticella* can be stimulated mechanically or electrically, causing its stalk to coil spasmodically into a helix. Such stalk coiling is produced by the contraction of spasmoneme. Spasmoneme is an intracellular fibrous organelle which has a helical configuration inside the cylindrical outer sheath of the stalk. Reextension of the stalk is due entirely to the elastic tension of the stalk's outer sheath. Hoffmann-Berling [1958] and other investigators [Amos, 1971; Asai et al., 1978; Ochiai et al., 1979] reported that the stalk of glycerinated *Vorticella* coiled with the addition of Ca^{2+} and uncoiled when Ca^{2+} was subsequently removed by adding a calcium chelator such as EGTA. Since the contraction-extension cycle of the stalk can be repeated many times by changing the free Ca^{2+} concentration in the medium without the hydrolysis of ATP or any other organic substrate [Ochiai et al., 1979], the immediate source of energy for spasmoneme contraction is thought to be the binding energy of Ca^{2+} to certain calcium-binding proteins (called spasmins or spastins) which are the principle components of spasmoneme [Yamada and Asai, 1982]. Thus the motile system of *Vorticellan* spasmoneme is entirely different from those of other motile organs in eukaryotes, e.g., muscle, the mitotic apparatus, flagella, or cilia.

Ochiai et al. [1979] studied the pCa vs. stalk length relations of *Vorticella*. Rahat et al. [1973] reported the contractile properties of *Carchesium*. However, to our knowledge, the pCa vs. isometric tension relations have not previously been examined. Herein, we report correlations between the Ca^{2+} concentration and isometric tension, as well as the efficiency of the energy conversion of Ca^{2+} binding to mechanical work.

Received August 11, 1995; accepted April 15, 1996.

Address reprint requests to Yasushige Moriyama, Room 51-706, Hiroshi Asai Lab., Department of Physics, School of Science and Engineering, Waseda University, Okubo 3-4-1, Shinjuku-ku, Tokyo 169, Japan.

*Dr. Yasuda's current address is Advanced Research Laboratory, Hitachi, Hatoyama, Saitama 350-03, Japan.

MATERIALS AND METHODS

Cell Culture

Vorticella convallaria was cultivated at 20°C in 0.025% "vita-shrimp" infusion [Ochiai et al., 1979], which had previously been inoculated with *Escherichia coli*.

Glycerol Treatment

Following the immersion of several pieces of fishing-line in a *V. convallaria* culture medium, a portion of the swimming zooids adhered to the fishing-line and subsequently developed new contractile stalks. Within a week after immersion, a suitable number of cells had attached to the fishing-line. The fishing-line with cultured *V. convallaria* cells was then immersed in a medium consisting of 0.1% saponin, 4 mM EDTA-2Na, 0.1 M KCl, and 20 mM imidazole, pH 6.8, at 0°C for 45 min, followed by rinsing with a washing solution containing 0.1 M KCl, 4 mM EDTA-2Na, and 20 mM imidazole, at pH 6.8. The fishing-line was then placed in a new medium containing 35% glycerol, 0.1 M KCl, 4 mM EDTA-2Na, and 20 mM imidazole, pH 6.8, at 0°C for 60 min. Glycerinated cells can be preserved in a medium containing 50% glycerol, 0.1 M KCl, 4 mM EDTA-2Na, and 20 mM imidazole, pH 6.8, at −20°C for several weeks at a minimum [Asai et al., 1978]. Before use, the glycerinated cells were washed again with the washing solution to remove the glycerol.

Reaction Mixture

The reaction mixture consisted of Ca^{2+} in a solution of 0.1 M KCl, 4 mM EGTA, and 20 mM MOPS, at pH 6.8. A value of 5×10^5 M^{-1} was employed as the apparent stability constant of Ca^{2+} [Ogawa, 1968] in the solution. The free Ca^{2+} concentrations are indicated on the abscissas of Figures 3, 4, and 5 as $pCa = -\log_{10}[Ca^{2+}]$.

Method of Measuring Isometric Tension

We devised a special measuring glass needle for hooking the zooids of *V. convallaria* (Fig. 1). The fishing-line with the glycerinated *V. convallaria* and the needle were attached to micro-manipulators and placed as shown in Figures 1 and 2, in a Lucite chamber under a dissecting microscope. The microscopic image was monitored with a CCD camera (C3077, Hamamatsu Photonics K.K., Hamamatsu, Japan). The displacements of the fishing-line and the needle were measured by means of a double-channel position detector (Width analyzer C3161, Hamamatsu Photonics K.K.). The developed tension was obtained by a deflection of the needle and Hooke's elastic constant for the needle [Anazawa et al., 1992].

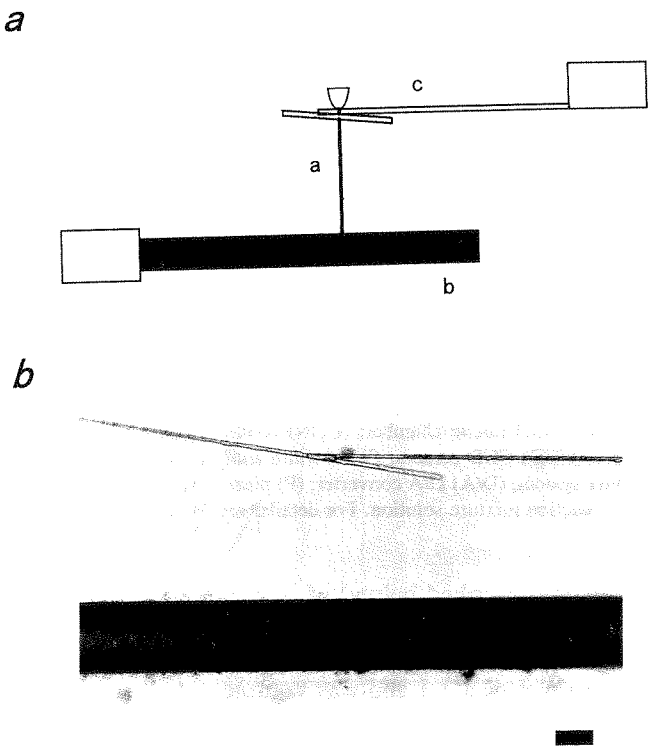

Fig. 1. **a:** Schematic view of the principle used in measuring the tension produced by a glycerinated *Vorticella* stalk. A glycerinated *Vorticella* (a), attached to a fishing-line (b), was hooked with a glass measuring needle (c). **b:** Photomicrographs of a glycerinated *Vorticella* attached to a fishing-line, and hooked with a glass measuring needle. Bar = 100 μm.

Using a computer system and a piezoelectric element we were able to measure the tension generated in the stalk by the addition of Ca^{2+} without changing the initial stalk length, that is to say, isometrically. Namely two positions of the fishing-line and the needle were monitored every 33 msec by the position detector. The displacement of the fishing-line was controlled by the piezoelectric element, and the position of it was feedback controlled so as to keep a constant distance between the fishing-line and the needle (i.e., the length of the stalk) [Yasuda et al., 1996]. The generation of tension of glycerinated *V. convallaria* is slow enough so as to measure it as an isometric tension with this system. After complete replacement of the reaction mixture to another pCa in the Lucite chamber, the new generated isometric tension, which had reached equilibration, was again measured. All experiments at various pCa were performed at room temperature.

RESULTS AND DISCUSSION

Calcium Concentration and Tension Saturation

The isometric tension was measured at various pCa. In Figure 3, the average of the relative isometric

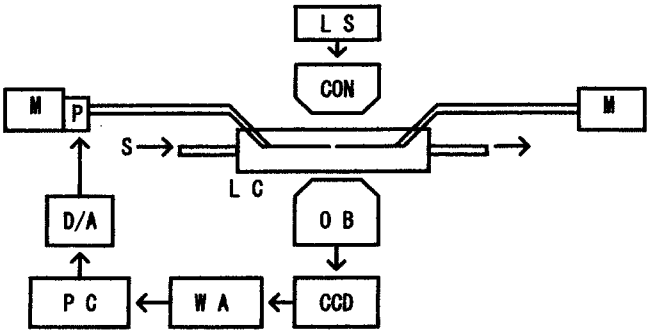

Fig. 2. Schematic diagram showing measurement of the isometric tension generated in a glycerinated stalk of *Vorticella*. (LS) light source; (LC) Lucite chamber; (CON) condenser lens; (OB) objective lens; (CCD) CCD camera; (WA) width analyzer; (PC) personal computer system; (D/A) D/A converter; (P) piezo; (M) micro-manipulator; (S) reaction mixture solution. For details, see Materials and Methods.

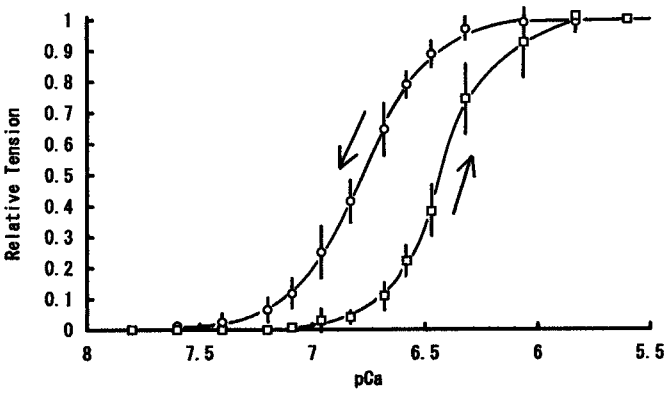

Fig. 3. Relation between the isometric tension in a glycerinated *Vorticella* stalk and the Ca^{2+} concentration. The isometric tension was converted to the average of the relative tension (see text). □, the relative tension when pCa was decreased; ○, the relative tension when pCa was increased; Arrows show the courses of change. The vertical bars indicate S.D. Eleven stalks were used to make the measurements. The increase and subsequent decrease in the Ca^{2+} concentration were made over a period of approximately 1 h.

tension (described below) of 11 stalks is plotted against pCa. When the free Ca^{2+} concentration, was increased stepwise from 7.8 to 5.6, the isometric tension began to develop at pCa 7.1 and was saturated at pCa 5.8. Then, again, the free Ca^{2+} concentration was decreased stepwise. The isometric tension began to decrease at pCa 6.4 and disappeared at pCa 7.6. The relation between the developed tension and pCa was clearly a sigmoidal curve as shown in Figure 3.

Increasing and Decreasing the Free Ca^{2+} Concentration Three Times in the Same Stalk

While measuring the isometric tension generated in a stalk, the free Ca^{2+} concentration was increased (pCa, from 7.8 to 5.6) and then decreased (pCa, from 5.6 to 7.8). This procedure was repeated three times in the same stalk (one of 11 stalks in Fig. 3), leading to successive declines in the maximum isometric tension (Fig. 4a). All curves obtained did, however, have similar sigmoidal shape. The isometric tension was normalized to the relative tension at each time point (Fig. 4b). The relative tension, T_R, is defined so as to normalize the isometric tension between 0 and 1.0 by means of the following equation,

$$T_R = T/T_{max}$$

where T_{max} is the maximum isometric tension of the stalk, and T is the isometric tension at a given pCa. As shown in Figure 4a, and T values of triplicate measurements differed from each other at the same pCa, while T_R values coincided, as illustrated in Figure 4b. The curves of the triplicate measurements were also coincident. Spasmoneme is assumed to consist of an assembly of contractile elements (force generating elements). The present results appear to confirm this assumption. We speculate that the binding of calcium ions to a contractile element induces the development of isometric tension in the contractile element. Over time, some contractile elements are damaged and lose their force developing capacity. Each live contractile element would be expected to have the same relation between force generation and pCa, however, such that the correlation between relative tension and pCa, i.e., the sigmoidal curve, did not differ among the three contractile responses.

Hill's Parameter

If it is assumed that n moles of Ca^{2+} bind to a contractile element in its relaxed state and that this binding brings about force generation in the contractile element, the following equations (Hill's equations) are obtained:

$$[S] + n\,[Ca^{2+}] \rightleftharpoons [S\cdot(Ca^{2+})_n]$$

and

$$\frac{[S]\,[Ca^{2+}]^n}{[S\cdot(Ca^{2+})_n]} = K = K_m^n$$

where [S] is the contractile element in the relaxed state and $[S \cdot (Ca^{2+})_n]$ is the contractile element in the force generating state. The relative tension T_R can be expressed as a function of the free Ca^{2+} concentration $[Ca^{2+}]$,

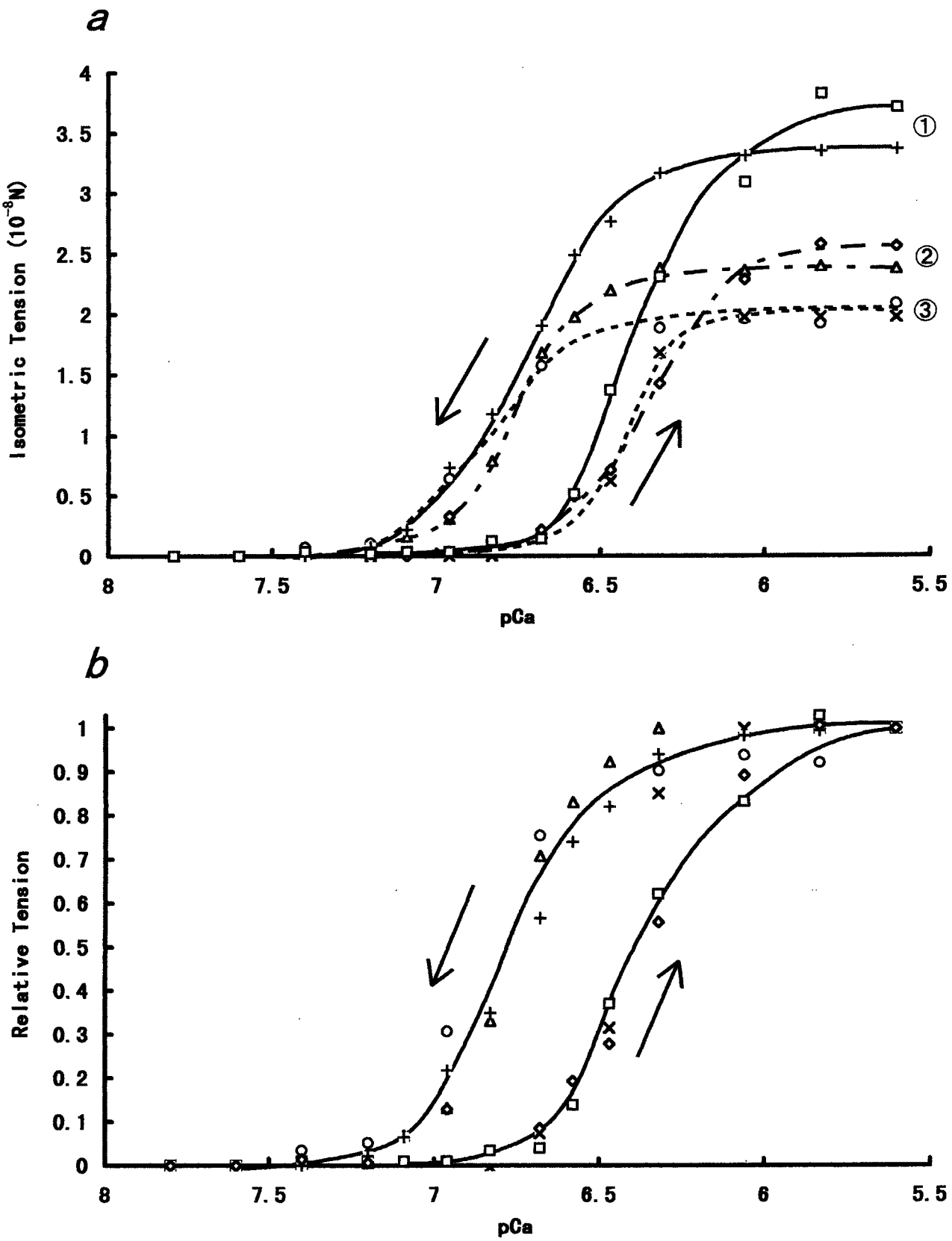

Fig. 4. **a:** Relation between the isometric tension generated in one glycerinated *Vorticella* stalk and the Ca^{2+} concentration changes which were made in triplicate. □, the isometric tension when pCa was decreased for the first time; + the isometric tension when pCa was increased for the first time; ◇ for the second decrease; △ for the second increase; × for the third decrease; ○ for the third increase; ① the measurement of the isometric tension for the first time; ② for the second time; ③ for the third time. Arrows show the courses of change. **b:** Same as **a** but the isometric tension was converted to the relative tension at each time point. In each curve of **a**, the maximum tension generated at pCa 5.6 was normalized to 1. For details, see text.

$$T_R = \frac{[S\cdot(Ca^{2+})_n]}{[S]+[S\cdot(Ca^{2+})_n]} = \frac{1}{1+\left(\frac{K_m}{[Ca^{2+}]}\right)^n}$$

or

$$\log_{10}\frac{T_R}{1-T_R} = n(-\,pCa - \log_{10}K_m)$$

n is called Hill's parameter, and K_m is the apparent dissociation constant, the inverse of the stability constant, in molar units.

As shown in Figure 5, n and K_m are 3.2 and 0.40 μM, respectively, when the free Ca^{2+} concentration is increased, and 2.5 and 0.16 μM, respectively, when the free Ca^{2+} concentration is decreased. This implies that the binding of three calcium ions to a contractile element in the spasmoneme induces a force cooperatively and simultaneously. This result differs from previous observations obtained using the free stalk length measured at various Ca^{2+} concentrations (Hill's parameter, n = 2) [Asai et al., 1978; Ochiai et al., 1979]. The discrepancy might be due to the difference in stalk length between this investigation and previous experiments. The average length of the stalks used in former studies was 300 μm, while in this study the average length was 200 μm. Indeed, the threshold free calcium concentration for the contraction of a portion of the stalk near the zooid is somewhat lower than that near the rootlet attached to the solid support. It is known that the K_m value of the portion of the stalk near the zooid is lower than the value of that near the rootlet, because the spasmoneme near the zooid is constructed later than that near the rootlet. The T_R value in this study and the fractional stalk length in former studies are the average of a large number of normalized overall stalk tensions or lengths. Thus, Hill's parameter was found to be smaller in former studies. The value (Hill's parameter, n = 3.2 or 2.5) in this study is more accurate than that obtained in previous studies.

In earlier studies, the values of Hill's parameter and K_m were calculated from the average equilibrium length of contractile stalks, which was measured at various pCa. The work of the elastic outer sheath tension was included in these measurements. Under the isometric tension measurement conditions employed, no work was produced by either the elastic outer sheath or the spasmoneme. The measurement conditions were, thus, quasi-thermodynamic or most nearly reversible.

It is difficult to assess the mechanism of cooperativity. It was reported that there are three Ca^{2+}-binding proteins in the spasmoneme of *Carchesium* [Yamada and Asai, 1982]. The interaction of these Ca^{2+}-binding proteins may cause cooperativity comparable to that of α chains and β chains in hemoglobin (heme-heme interaction). It is also possible that there are some Ca^{2+}-binding sites which bind Ca^{2+} without conformational changes in one Ca^{2+}-binding protein, such as calmodulin. The calmodulin conformational change is completed upon binding 2 mol of Ca^{2+}/mol of protein, though calmodulin can bind 4 mol of Ca^{2+}/mol of protein [Crouch and Klee, 1980; Dedman et al., 1977; Klee, 1977; Yagi et al., 1978].

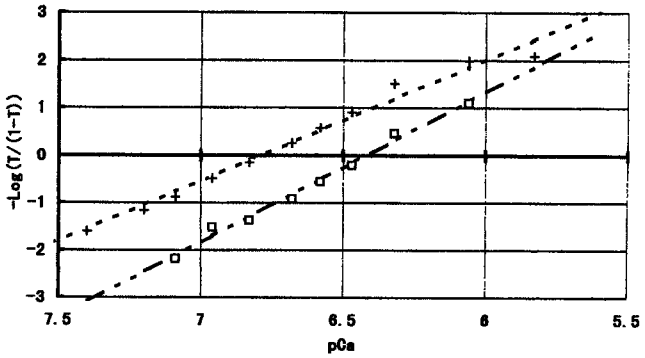

Fig. 5. Hill plot of Figure 3. Hill's parameter is n = 3.2 when the free Ca^{2+} concentration is increased (-□-), and n = 2.5 when it is decreased (-+-).

It is not clear whether Ca^{2+}-binding proteins are themselves the contractile (force generating) element or whether other Ca^{2+}-nonbinding proteins form a contractile element which is regulated by Ca^{2+}-binding proteins [Yamada-Horiuchi and Asai, 1985; Yokoyama and Asai, 1987].

Maximum Isometric Tension

The maximum isometric tension was 4×10^{-8} N on average, with some stalks developing tensions as high as 12×10^{-8} N.

With a spasmoneme diameter 1.0–1.2 μm and a maximum isometric tension of 4×10^{-8} N, the tension per unit cross-sectional area is 35,000–51,000 N/m^2. Rahat et al. [1973] reported a value of 40,000–80,000 N/m^2, which is slightly larger than ours. These authors' measuring method was based on growing *Carchesium* on glass microscope slides and then attaching small pincers just below the zooids. The pincers in turn were attached to a sensitive spring-balance mounted on a micro-manipulator. With this method, they measured the contractile tension of living *Carchesium* specimens. The contractions were evoked by electrical stimuli. Their experiment was, in other words, quite different from ours. Amos [1975] calculated the minimum spasmoneme tension value from the high speed film data of Jones et al. [1970]. When *Vorticella* contracts, the zooid, which may be approximated to a sphere of radius 20 μm, may be pulled 80 μm

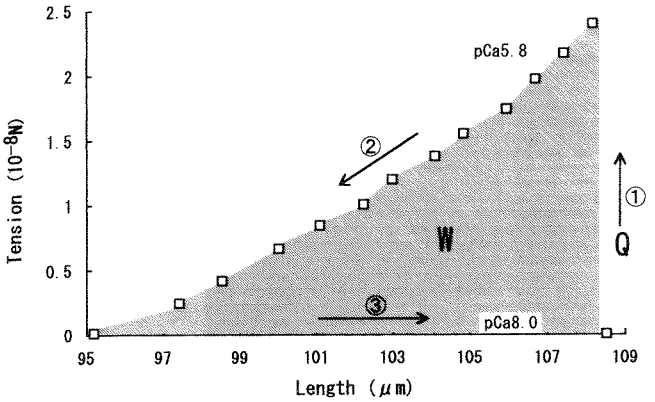

Fig. 6. The Ca^{2+}-induced Carnot cycle. ①, In the first step of the cycle, the stalk generates internal energy, Q, by changing the free Ca^{2+} concentration from pCa 8.0 to 5.8. ②, In the second step of cycle, the stalk does work, W. ③, In the third step of cycle, the stalk is allowed to extend under zero tension by changing the free Ca^{2+} concentration from pCa 5.8 to 8.0.

at an average velocity of 23 mm/sec. Assuming a viscosity of 10^{-3} N sec/m^{-2} (0.01 poise), the viscous drag on the zooid can be calculated from Stokes' formula ($F = 6\pi a \eta v$) as 0.86×10^{-8} N. If the diameter of the spasmoneme is taken as 1.0 μm, the tension per unit cross-sectional area becomes 11,000 N/m^2.

The tension in the spasmoneme is similar to that of striated muscles working at optimal tension for the performance of work [Close, 1965].

Hysteresis

As shown in Figure 3, the isometric tension vs. pCa curves were sigmoidal, but the two curves did not coincide with each other. At the same pCa, the two isometric tensions (one is the tension which developed in response to increasing the free Ca^{2+} concentration, the other to decreasing free Ca^{2+}) also did not coincide. These observations reflect the hysteresis phenomenon. Ochiai et al. [1979] reported the hysteresis phenomenon of the contraction-extension cycle. In the present study, we measured the isometric tension of the stalk, such that the influence of the outer sheath on hysteresis could be ignored. The hysteresis phenomenon, in measurements of isometric tension, is a characteristic of the spasmoneme (described below).

Ca^{2+}-Induced Carnot Cycle and Work Efficiency

To estimate the efficiency of the energy conversion of Ca^{2+} binding to mechanical work, the Ca^{2+}-induced Carnot cycle of a glycerinated stalk of *Vorticella* was measured. Weis-Fogh and Amos [1972] also proposed a cycle of this type. This cycle consists of three processes (see Fig. 6).

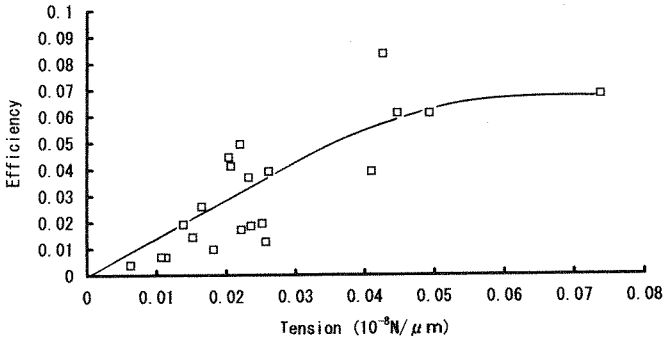

Fig. 7. Work efficiency of the stalk. The abscissa expresses the maximum isometric tension per stalk length. Twenty-one stalks were used for the measurements.

In the first process, a glycerinated stalk was placed in conditions of zero tension in a solution of pCa 8.0. The solution was then changed from pCa 8.0 to 5.8. The stalk generated tension isometrically (maintaining a constant stalk length), producing internal energy, Q, without working. This internal energy, Q, is derived from the chemical potential of the difference in the free Ca^{2+} concentration. The internal energy is calculated as:

$$Q = N \cdot L \cdot RT \ln \frac{[Ca^{2+}]_{high}}{[Ca^{2+}]_{low}}$$

where N is the number of calcium ions binding to spasmoneme per 1 μm length of the spasmoneme, for which we use the Amos' value of $N = 6.6 \times 10^{-18}$ (moles/μm) [1975], L is the original stalk length, R is the gas constant, and T is the absolute temperature.

In the second process, the glycerinated stalk, which is generating isometric tension, is relaxed by allowing it to shorten to zero. During this contraction the stalk does work, W, on the glass needle. The work, W, is calculated from the equation:

$$W = \int (\text{tension of the stalk}) \times \Delta L(\text{change in stalk length})$$

In the third process, the solution is changed from pCa 5.8 to 8.0 and the stalk without the glass needle is allowed to extend under zero tension. The initial state of the stalk is thereby restored.

Through this Ca^{2+}-induced Carnot cycle, the energy efficiency, ε, is:

$$\varepsilon = W/Q$$

Figure 7 shows the results. The abscissa in Figure 7 is the value of the maximum isometric tension per stalk length. In the calculation of the internal energy, Q, the

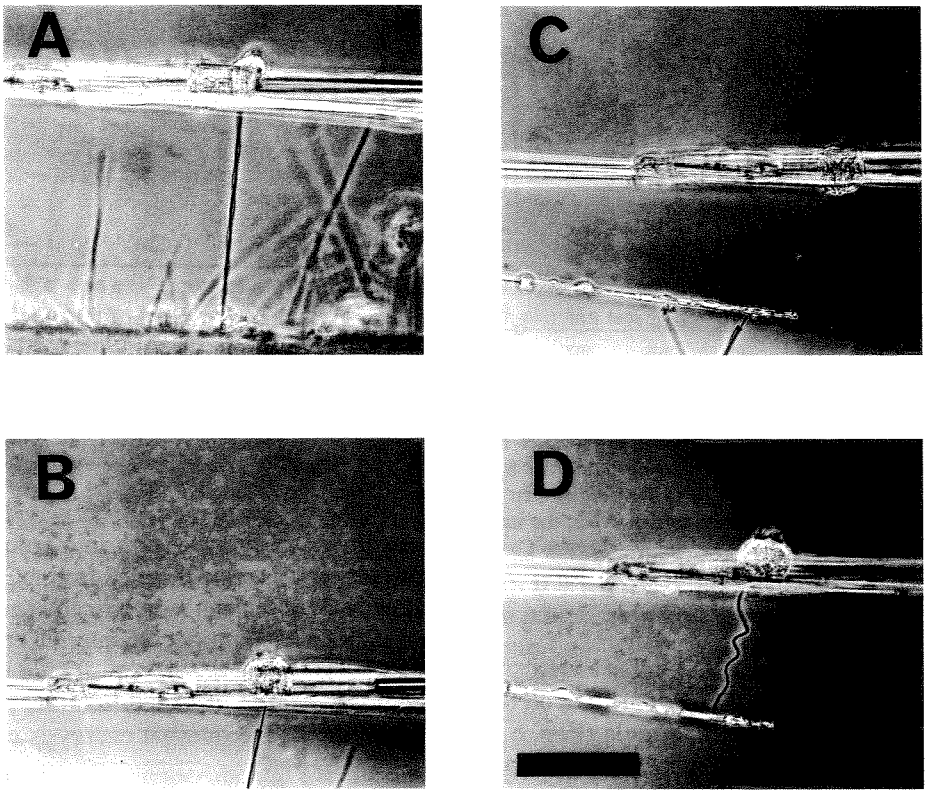

Fig. 8. Photomicrographs depicting the isolation of a spasmoneme from its outer sheath. **A:** A glycerinated *Vorticella* attached to a fishing-line is hooked with a measuring glass needle. **B,C:** The spasmoneme is then slowly pulled out of the outer sheath. **C,D:** The root of the spasmoneme is attached to another solid glass needle. The needle has been coated with polylysine to facilitate bonding to the spasmoneme. Bar = 100 μm.

stalk length was used as the value of L without taking into consideration the maximum isometric tension. The values obtained suggest that some of the samples were damaged. In those samples with values ranging from 0.04×10^{-8}–0.07×10^{-8} N/μm, the energy efficiency was tentatively estimated to be about 7%.

The samples with values of 0.01×10^{-8}–0.03×10^{-8} N/μm, the energy efficiency of which would be 0.01 to 0.05, may have been damaged during experimental manipulations.

Isometric Tension of Isolated Spasmoneme

We have succeeded in measuring the isometric tension of isolated, glycerinated spasmonemes of *Vorticella*. Isolation was achieved by pulling the spasmoneme, out of the stalk, as shown in Figure 8. The spasmoneme is highly extensible, and during isolation, was stretched to more than two times its resting length with elastic recovery. The maximum isometric tension of the isolated spasmoneme was demonstrated to be 2.2×10^{-9} N. The tension of the spasmoneme is about one tenth that of the stalk. It is difficult to avoid damaging the spasmoneme with this method of isolation.

The hysteresis phenomenon was observed in isolated spasmonemes as well as in stalks (data not shown).

Studying the tension generated in isolated spasmonemes contributes to our understanding of biological contractile mechanisms. Further studies are planned to elucidate the mechanism of spasmonemal contraction.

REFERENCES

Amos, W.B. (1971): Reversible mechanochemical cycle in the contraction of *Vorticella*. Nature 229:127–128.

Amos, W.B. (1975): Contraction and calcium binding in the *Vorticellid* ciliates. In Inoue S., and Stephens, R.E., (eds.): Molecules and Cell Movement. New York: Raven Press, pp. 411–436.

Anazawa, T., Yasuda, K., and Ishiwata, S. (1992): Spontaneous oscillation of tension and sarcomere length in skeletal myofibrils. Microscopic measurement and analysis. Biophys. J. 61:1099–1108.

Asai, H., Ochiai, T., Fukui, K., Watanabe, M., and Kano, F. (1978): Improved preparation and cooperative calcium contraction of glycerinated *Vorticella*. J. Biochem. 83:795–798.

Close, R. (1965): Dynamic properties of mammalian skeletal muscles. Physiol. Rev. 52:129–197.

Crouch, T.H., and Klee, C.B. (1980): Positive cooperative binding of calcium to bovine brain calmodulin. Biochemistry 19:3692–3698.

Dedman, J.R., Potter, J.D., Jackson, R.L., Johnson, J.D., and Means, A.R. (1977): Physiochemical properties of rat testis Ca^{2+}-dependent regulator protein of cyclic nucleotide phosphodiesterase. J. Biol. Chem. 252:8415–8422.

Hoffmann-Berling, H. (1958): Der Mechanismus eins neuen, von der Muskelkontraktion verschiedenen Kontraktionszyklus. Biochim. Biophys. Acta 27:247–255.

Jones, A.R., Jahn, T.L., and Fonseca, J.R. (1970): Contraction of protoplasm. IV. Cinematographic analysis of the contraction of some peritrichs. J. Cell Physiol. 75:9–20.

Klee, C.B. (1977): Conformational transition accompanying the binding of Ca^{2+} to the protein activator of 3′,5′-cyclic adenosine monophosphate. Biochemistry 16:1017–1024.

Ochiai, T., Asai, H., and Fukui, K. (1979): Hysteresis of contraction-extension cycle of glycerinated *Vorticella*. J. Protozool. 26: 420–425.

Ogawa, Y. (1968): The apparent binding constant of glycoletherdiamine tetraacetic acid for calcium at neutral pH. J. Biochem. 64:255–257.

Rahat, M., Pri-Paz, Y., and Parnas, I. (1973): Properties of stalk-'muscle' contractions of *Carchesium* sp. J. Exp. Biol. 58:463–471.

Weis-Fogh, T., and Amos, W.B. (1972): Evidence for a new mechanism of cell motility. Nature 236:301–304.

Yagi, K., Yazawa, M., Kakiuchi, S., Ohshima, M., and Uenishi, K. (1978): Identification of an activator protein for myosin light chain kinase as the Ca^{2+}-dependent modulator protein. J. Biol. Chem. 253:1338–1340.

Yamada, K., and Asai, H. (1982): Extraction and some properties of the proteins, spastin B, from the spasmoneme of *Carchesium polypinum*. J. Biochem. 91:1187–1195.

Yamada-Horiuchi, K., and Asai, H. (1985): Circular dichroism studies of the Ca^{2+}-binding proteins from the spasmoneme of *Carchesium*. Comp. Biochem. Physiol. 81B:927–931.

Yasuda, K., Shindo, Y., and Ishiwata, S. (1996): Synchronous behavior of spontaneous oscillations of sarcomeres in skeletal myofibrils under isotonic conditions. Biophys. J. 70 (1823–1829).

Yokoyama, Y., and Asai, H. (1987): Contractility of the spasmoneme in glycerinated *Vorticella* stalk induced by various divalent metal and lanthanide ions. Cell Motil. Cytoskeleton 7:39–45.

Pflügers Arch – Eur J Physiol (1996) 433:1–8

ORIGINAL ARTICLE

Norio Fukuda · Hideaki Fujita · Takashi Fujita
Shin' ichi Ishiwata

Spontaneous tension oscillation in skinned bovine cardiac muscle

Received 19 February 1996 / Received after revision: 16 July 1996 / Accepted: 14 August 1996

Abstract Skinned fibres from bovine ventricles exhibited spontaneous tension oscillations when MgADP and inorganic phosphate (Pi) were added to the solution bathing fibres in the relaxed state (ADP-SPOC). A similar type of oscillation was observed at intermediate concentrations of free Ca^{2+} in the absence of MgADP and Pi (Ca-SPOC). To investigate the correlation between ADP-SPOC and Ca-SPOC, we constructed two-dimensional state diagrams of cardiac muscle using different concentrations of Pi (0–20 mM) and free Ca^{2+} [pCa=around 5 (+Ca^{2+}), pCa=5.15–6.9 and +EGTA (–Ca^{2+})], with varying concentrations of MgADP (0–10 mM), with 2 mM MgATP and 2 mM free Mg^{2+} maintaining ionic strength at 0.15±0.01 M, pH 7.0, 25 °C. The three-dimensional (pCa-Pi-MgADP) state diagram thus obtained was divided into three regions, i.e. the contraction region in which tension oscillation was undetectable, the spontaneous tension oscillation (SPOC) region and the relaxation region. We found that the regions of ADP-SPOC and Ca-SPOC were continuously connected by a single oscillation region sandwiched between the contraction and relaxation regions. The state diagram, which encompasses physiological conditions, shows that the probability of SPOC is higher in cardiac muscle than in skeletal muscle. From these results, we suggest that, despite distinct ionic conditions, the molecular state of cross-bridges during SPOC is common to both ADP-SPOC and Ca-SPOC.

N. Fukuda · H. Fujita · T. Fujita · S. Ishiwata (✉)
Department of Physics, School of Science and Engineering, Waseda University, 3-4-1 Okubo, Shinjuku-ku, Tokyo 169 Japan

S. Ishiwata
Advanced Research Institute for Science and Engineering, Waseda University, 3-4-1 Okubo, Shinjuku-ku, Toyko 169, Japan

N. Fukuda
Pharmacology and Molecular Biology Research Laboratories, Sankyo Co., Ltd., 1-2-58 Hiromachi, Shinagawa-ku, Tokyo 140, Japan

Key words Cardiac muscle · Oscillation · Spontaneous oscillatory contraction · Spontaneous tension oscillation · State diagram of muscle

Introduction

Under unstimulated conditions, cardiac tissues and single cells frequently show spontaneous oscillations [3, 5, 14, 21], which are often manifest as propagating waves [17, 18]. Since these oscillations are abolished by agents that interfere with Ca^{2+} loading and/or release from the sarcoplasmic reticulum (SR), such as ryanodine and caffeine, they are attributable to a Ca^{2+}-induced Ca^{2+} release mechanism. On the other hand, tension and sarcomere length oscillations in chemically skinned cardiac preparations have also been reported [6, 16, 25]. As treatment with a detergent was used in these studies, the contractile system per se was considered to be responsible for the oscillation.

We found that the coexistence of MgADP and inorganic phosphate (Pi) with MgATP induces oscillations in isometric tension and sarcomere length in fast-type skeletal muscle fibres and myofibrils in the absence of Ca^{2+} [2, 10–12, 19, 23, 26], and have termed this phenomenon "SPOC" (spontaneous oscillatory contraction). These observations indicate that MgADP and Pi play a synergistic role in the regulation of thin filaments leading to the induction of oscillations [10, 23], as does Ca^{2+} under partial Ca^{2+} activation [16].

In the present study, we first confirmed, using glycerinated bundles from bovine ventricles, that skinned cardiac muscle preparations exhibit tension oscillations under SPOC conditions, i.e. in the presence of MgADP and Pi under relaxing conditions (ADP-SPOC) and at submicromolar concentrations of free Ca^{2+} in the absence of MgADP and Pi (Ca-SPOC). To clarify the correlation between ADP-SPOC and Ca-SPOC, we constructed a state diagram for various concentrations of MgADP, Pi and Ca^{2+} at a fixed concentration of MgATP (2 mM). The range of conditions examined included physiologi-

cal ionic conditions, such that not only were MgATP and Ca^{2+} present, but also Pi and MgADP. The physiological significance of SPOC phenomena is also discussed.

Preliminary reports of this investigation have been presented elsewhere [7, 8, 12].

Materials and methods

Solutions

The chemical compositions of typical solutions used in this study are summarized in Table 1. The isometric tension was measured with the preparation bathed in solutions containing 2 mM MgATP, 0–10 mM MgADP, 0–20 mM Pi and various concentrations of free Ca^{2+} [pCa=around 5 ($+Ca^{2+}$), pCa=5.15–6.9, and +EGTA ($-Ca^{2+}$)]. The concentration of free Mg^{2+} was maintained at around 2 mM. The ionic strength (IS) was maintained at 0.15±0.01 M by adjusting the KCl concentration. The concentrations of ATP (Na-salt, Boehringer Mannheim, Mannheim, Germany), ADP (K-salt, Boehringer Mannheim), $MgCl_2$, Pi (K-salt), EGTA (Dojindo, Kumamoto, Japan) and other chemicals were calculated by computer using the published values for stability constants [9]. The pH value for each solution was finally adjusted to 7.0±0.02 with 1 N KOH or HCl in the presence of 10 mM 3-(*N*-morpholino)propanesulphonic acid (MOPS; Dojindo) at 25 °C. P^1,P^5-di (adenosine-5′)pentaphosphate (AP_5A; Boehringer Mannheim) was added to inhibit the rephosphorylation of ADP to ATP by myokinase [15]. When required, an ATP-regenerating system composed of 1.0 mg/ml creatine phosphokinase (CPK; Sigma, St. Louis, Mo., USA) and 10 mM creatine phosphate (CP; Boehringer Mannheim) was used. To reduce Pi contamination, 1 unit of sucrose phosphorylase (Sigma, see [20]) containing 10 mM sucrose was added. All chemicals were of reagent grade.

Preparation of skinned muscle

Glycerinated skeletal muscle fibres were prepared from rabbit psoas muscle according to a previously described procedure [23]. Glycerinated cardiac muscle was prepared as follows: at a local slaughterhouse, a bovine heart was quickly extracted and opened for complete blood removal. A muscle bundle of suitable size (about 3 mm wide, 7 mm thick and 70 mm long) was excised, using a surgical knife, from a straight portion of left ventricular papillary muscle while the muscle was still warm. Then, both ends of the bundle were fastened to a glass rod (3 mm diameter) with cotton thread and immediately stored in a glycerol solution [50% (v/v) glycerol, 5 mM EGTA and 0.5 mM $NaHCO_3$ and 2 mM leupeptin] at 0 °C. After 24 h, the preparation was placed in fresh solution and stored at −20 °C. All experiments were carried out using specimens that had been stored for 2–8 weeks. Results obtained during this period were reproducible and consistent.

For the experiments, a glycerinated bundle (40–80 μm wide, 20–40 μm thick and 1.5 mm long) was carefully stripped off with a pair of forceps with the aid of a stereomicroscope just before use; we took special care to make the bundle as thin as possible, because the higher the ATPase activity and the thicker the bundle, the greater was the possibility of ATP depletion occurring while ADP and Pi accumulated inside the muscle [4, 23]. To avoid MgATP depletion at the centre of the bundle we used 2 mM MgATP rather than the concentration of 1 mM used in the majority of our previous experiments. To prepare a suitably thin bundle of glycerinated cardiac muscle, the dissection was done with the preparation in the glycerol solution at about −10 °C. We found that dissection at such a low temperature was essential for stripping off the muscle bundle smoothly; when either the surface of the bundle was not smooth or the thickness of the bundle was not uniform, the initial rate of tension development was slow.

Measurement of tension development

Both ends of the muscle bundle (or the single muscle fibre), from which glycerol had been absorbed with a paper string, were fixed to thin tungsten wires with enamel, one of which was attached to a tension transducer (AE-801, SensoNor, Norway) and the other to a micromanipulator (Narishige, Tokyo, Japan). This procedure was carried out in room air within 15 s without removal of glycerol from the central part of the bundle (for details, see [23]). The muscle thus mounted was immersed in rigor solution for 5 min to remove glycerol and then in rigor solution containing 0.3% (v/v)

Table 1 Compositions of typical solutions used in this study. Values calculated by computer are in *parentheses*. Absence is indicated by –. Ionic strenght (*IS*) was maintained at a nearly constant level, 0.15±0.01 M, by changing the KCl concentration. The pH value was adjusted to 7.0±0.02 for each solution. When the concentration of free Ca^{2+} was adjusted ($-Ca^{2+}$ to pCa=5.15), the Ca^{2+} (0–1.9 mM)/EGTA (2.0 mM) buffer was used; only for the condition indicated by ($+Ca^{2+}$) was the Ca^{2+} (3.95 mM)/EGTA (4.0 mM) buffer used. The pCa values of high- and low-EGTA relaxing solutions were, respectively, higher than 8.5 and 7.5; Ca^{2+} contamination was assumed to be 10 μM. The free Mg^{2+} concentration was maintained at around 2 mM except in the rigor and relaxing solutions. In contraction solution containing the ATP-regenerating system, *IS* was maintained at a constant value by the addition of 82 mM KCl. Only one typical example for ADP-SPOC is shown here; for other ADP-SPOC solutions, the concentration of added ATP (MgATP) was fixed at 2.2 (2.0) mM, while the concentrations of added ADP (MgADP) and Pi were, respectively, changed from 0 to 16.4 (9.7) mM and 20 mM. The concentrations of $MgCl_2$ and KCl were also appropriately adjusted to maintain the free Mg^{2+} concentration at around 2 mM and the *IS* constant. [*ADP-SPOC* spontaneous oscillatory contraction measured in the presence of MgADP and inorganic phosphate (*Pi*) under relaxing conditions]

Solution	Constituent (mM)								
	ATP (MgATP)	ADP (MgADP)	MOPS	EGTA	$CaCl_2$	AP_5A	$MgCl_2$ (Mg^{2+})	Pi	KCl (*IS*)
Rigor	–	–	10	1.0	–	–	5.0	–	120
Relaxation (high-EGTA)	3.8 (3.0)	–	10	4.0	–	–	3.9 (0.9)	–	120 (160)
Relaxation (low-EGTA)	3.8 (3.0)	–	10	0.4	–	–	3.9 (0.9)	–	120 (150)
Contraction ($+Ca^{2+}$)	2.2 (2.0)	–	10	4.0	3.95	0.1	4.2 (2.2)	–	112 (150)
ADP-SPOC	2.2 (2.0)	16.4 (9.7)	10	2.0	–	0.1	14.2 (1.8)	10	41 (150)

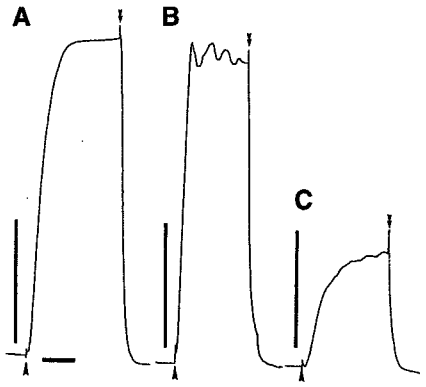

Fig. 1A–C Recordings of tension development in cardiac muscle. An example showing contraction induced by MgADP (**A**) and spontaneous tension oscillation induced by MgADP and inorganic phosphate (*Pi*) (**B** strong oscillation; **C** weak oscillation) in the absence of Ca^{2+}. Solvent condition for **A**: 2 mM MgATP, 10 mM MgADP, 2 mM Mg^{2+} (free), 10 mM MOPS (pH 7.0), 2 mM EGTA, 0.1 mM AP_5A; **B** 10 mM Pi was added to **A** (see ADP-SPOC in Table 1); **C** 2 mM MgADP and 5 mM Pi were added to **B** instead of 10 mM MgADP and 10 mM Pi; *IS* (ionic strength) was maintained at 0.15 M with KCl. *Vertical bars* indicate 5×10^{-5} N (for **A**) or 2.5×10^{-5} N (for **B, C**); *horizontal bar* 30 s (for **A–C**). [AP_5A P^1, P^5-di(adenosine-5′)pentaphosphate]

Fig. 2A, B Effects of Pi on cardiac muscle tension induced by MgADP under various pCa conditions. Conditions: the same as in Fig. 1A except that the free Ca^{2+} concentrations were adjusted with Ca^{2+}-EGTA buffer and 0–20 mM Pi (**A**) or 10 mM Pi (**B**) was added. **A** Relative tension vs Pi concentration at various free Ca^{2+} concentrations (○ $-Ca^{2+}$, △ pCa=6.9, □ 6.55, ◇ 6.3, ◑ 6.0, ◭ 5.8, ◨ 5.55, ◆ 5.15 ● $+Ca^{2+}$). The *dashed line* represents the boundary between regions of oscillation (SPOC) and contraction (without tension oscillation); spontaneous tension oscillation was observed to occur in the region below the *dashed line*. For the extent of tension oscillation, see the state diagram shown in Fig. 5A. The *dashed line* corresponds to the thin line in Fig. 5A, although the two are not exactly the same because several data points were added to construct the state diagram in Fig. 5A. Tension was noramlized with respect to that obtained without Pi in high Ca^{2+} ($+Ca^{2+}$). *Vertical bars* are SD for 3–10 data points. **B** Effects of ryanodine (30 μM) on tension oscillation; **B a** and **B c** −ryanodine, **B b** +ryanodine. *Vertical* and *horizontal bars*, 5×10^{-5} N and 30 s, respectively

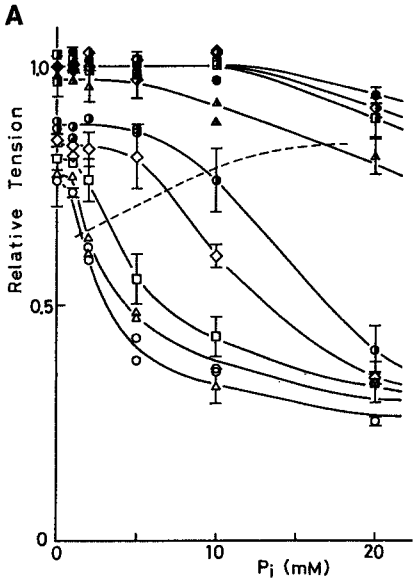

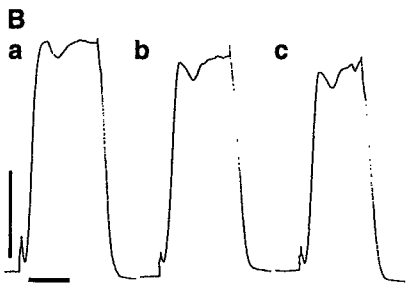

Triton X-100 for 90 s to remove residual portions of the membrane system. After washing out the Triton X-100 with rigor solution, the muscle was immersed in high-EGTA relaxing solution, in which the muscle length was adjusted so that the muscle was slack (sarcomere length, about 2.0 μm). Then, the muscle was transferred to low-EGTA relaxing solution; the concentration of EGTA was set low enough for the muscle to respond rapidly to activating conditions. All procedures were done at room temperature.

The tension measurement was initiated by immersing the muscle bundle (fibre), prepared as described above, in an appropriate activating solution. The relative tension was estimated from the ratio of the developed tension in an assay solution to the average of those in a standard solution obtained before and after the assay measurement. For each series of experiments, the solution in which the highest level of tension had developed was used as the standard solution, such that it usually contained Ca^{2+} (pCa ≈5), as in the cases shown in Figs. 3 and 4; however, when the effect of Pi was examined (Fig. 2), a solution without Pi was used as the standard solution. Two to four data points were obtained from each bundle (fibre). The data were used only when the ratio of the tension before and after the assay measurement was more than 85% and the final tension measured in the standard solution after obtaining two to four data points was more than 70% of the initial tension.

Figure 1 shows typical records of contraction without tension oscillation (Fig. 1A) and with spontaneous tension oscillation (Fig. 1B, C). The magnitude of the tension oscillation was defined as the ratio of the peak-to-peak tension oscillation amplitude to the maximum tension in an individual contraction. Here, oscillation is termed "strong" (Fig. 1B) or "weak" (Fig. 1C) depending on whether the magnitude was larger or smaller than 5%, respectively. When the tension oscillation was too weak to be distinguished, we looked carefully for oscillations of sarcomeres inside the muscle, of which both ends were fixed on a glass slide using double-sided adhesive tape, using a phase-contrast microscope (Biophoto; objective lens, Plan Apo 60×oil DM, NA=1.40; Nikon, Tokyo, Japan).

The measurement chamber routinely used was a silicon-coated aluminium block (10 cm×10 cm×1 cm), with several small holes (≈5 mm in diameter) filled with about 0.4 ml of various solutions, designed for tension measurement [9]. The muscle was immersed in the piled-up portion of the solution, such that only 1–2 s was required for transfer of the muscle from one solution to another. The solution was stirred vigorously with a spherical, Teflon-coated miniature magnetic stirrer 3 mm in diameter. The chamber temperature was maintained at 25.0±0.2 °C by circulating thermo-regulated water (CL-80 Coolnit, Taitec, Saitama, Japan).

Results

Effects of Pi on ADP-induced tension at various free Ca^{2+} concentrations

As previously reported, for skinned fast-twitch skeletal muscle fibres [23], isometric tension developed upon the addition of MgADP under relaxing conditions and reached approximately 70% of the maximal tension obtained under normal Ca^{2+} activation at 6 mM MgADP; thereafter a plateau was reached. Thus, we examined the effects of Pi on tension induced by MgADP (10 mM) in the absence and presence of free Ca^{2+}. As shown in Fig. 2A, the tension decreased with the addition of Pi along an inverse sigmoidal curve; Ca^{2+} competitively suppressed the extent of this tension decrease and increased the Pi concentration required to reduce the tension. At low Ca^{2+} (pCa≥6.55), tension began to drop at around 1 mM Pi, whereas at high Ca^{2+} (pCa≤5.55) the tension change was nearly undetectable in the presence of 10 mM Pi.

Spontaneous tension oscillations reproducibly appeared when the tension decreased upon addition of Pi, as long as the free Ca^{2+} concentrtion was relatively low (pCa≥5.8). The dashed line in Fig. 2A represents the boundary between the contraction region in which tension oscillation was undetectable and the spontaneous tension oscillation (SPOC) region; however, the boundary was not sharp, such that the state gradually changed across the dashed line. Interestingly, there was no absolute tension level below which oscillations could be induced; as illustrated, the boundary was not parallel to the abscissa. No tension oscillation was observed to occur in either the absence of Pi or the presence of high Ca^{2+} concentrations (pCa≤5.55) under the conditions used. Irrespective of the Ca^{2+} concentration, the tension oscillation just below the dashed line was relatively weak (compare with Fig. 1C). We have designated the oscillations that occur in the absence of Ca^{2+} ADP-SPOC, because the tension generation was induced by MgADP rather than Ca^{2+}.

We confirmed, using an optical microscope, that almost all sarcomeres in the muscle bundle oscillated under SPOC conditions (micrographs not shown); in other words, there were no distinct regions in which certain numbers of sarcomeres either did or did not oscillate. On the other hand, there were regions between which oscillations in the length of sarcomeres were out of phase and between which their oscillation periods differed slightly; within each region, the sarcomere oscillations were organized so that the oscillation periods of sarcomeres were the same.

The tension oscillation was not affected by 30 μM ryanodine (Fig. 2B). Thus, the SR is not responsible for ADP-SPOC. In addition, 2 mM NaN_3 had no effect on tension oscillation (data not shown), suggesting that the membrane ATPase does not contribute to ADP-SPOC.

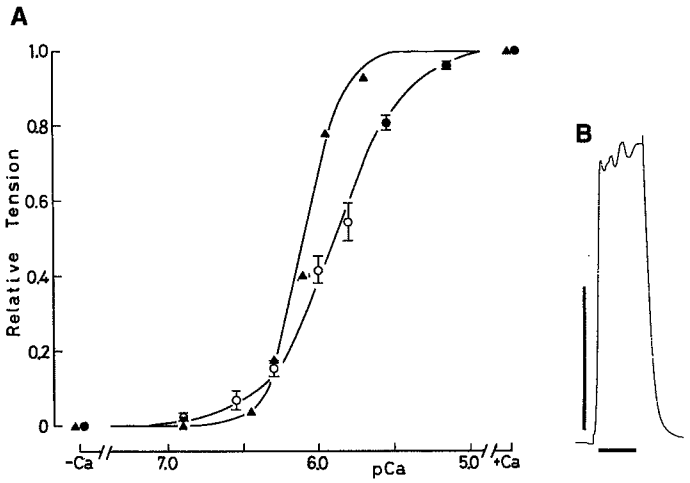

Fig. 3A, B Tension vs pCa relation in cardiac and skeletal muscle under normal conditions without MgADP and Pi. Conditions, the same as in Fig. 2A except that MgADP and Pi were absent and an ATP-regenerating system (10 mM creatine phosphate and 1 mg/ml creatine phosphokinase) was present. (*Circles* Cardiac muscle, *triangles* skeletal muscle). **A** Tension vs pCa relation, at which tension was normalized with respect to that under high-Ca^{2+} (+Ca^{2+}) conditions for each muscle. (*Filled symbols* Relaxation or contraction without tension oscillation, *open symbols* strong tension oscillation, *half-filled symbols* weak tension oscillation). In skeletal muscle, no tension oscillation was observed. *Vertical bars* are SD of 3 data points. **B** Recording of tension oscillation (Ca-SPOC) in cardiac muscle at pCa 6.0. Note that the amplitude and frequency of oscillation are nearly the same as those observed in ADP-SPOC (compare Figs. 1B and 2B). *Vertical* and *horizontal bars* indicate 2.5×10^{-5} N and 30 s, respectively

Spontaneous tension oscillation under partial Ca^{2+} activation

We constructed the isometric tension versus pCa relation of cardiac muscle, as compared with that of skeletal muscle, in the presence of the ATP-regenerating system (Fig. 3A). Spontaneous tension oscillations occurred under conditions of partial Ca^{2+} activation (Ca-SPOC) in cardiac muscle, as previously reported [6, 16, 25].

As shown in Fig. 3B, the amplitude and frequency of oscillations were not distinguishable from those of ADP-SPOC (see Figs. 1B and 2B). Ca-SPOC were observed to occur at pCa values between 6.9 and 5.8, in other words, in the region in which relative tension was between about 10 and 50% of maximal tension. The amplitude and frequency of Ca-SPOC were unaffected by 30 μM ryanodine, as reported previously (see [16]), suggesting that Ca-SPOC are distinct from oscillations due to an oscillating Ca^{2+} concentration coupled with a Ca^{2+}-induced Ca^{2+} release mechanism.

These tension/pCa relations were analysed according to the Hill equation described in Table 2. The pCa value was determined to be 5.89 for cardiac muscle and 6.04 for skeletal muscle, and the Hill coefficient (n_H) was 1.75 for cardiac, and 3.09 for skeletal, muscle. As expected (see [22]), pCa_{50}, an indicator of Ca^{2+} sensitivity, was nearly the same, whereas n_H, an indicator of cooperativity, was lower in cardiac than in skeletal muscle.

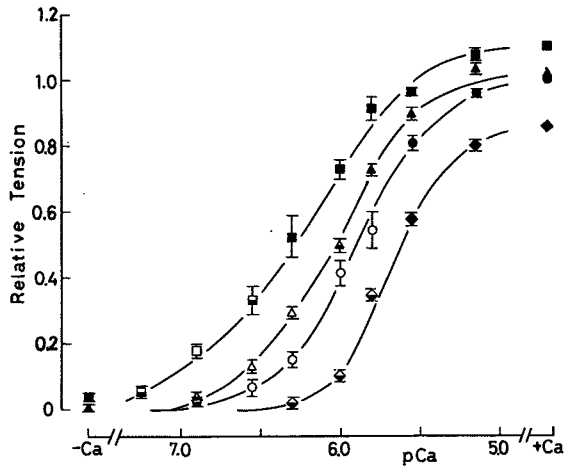

Fig. 4 Effects of MgADP or Pi on the tension vs pCa relation and tension oscillation (Ca-SPOC) in cardiac muscle. Conditions, the same as in Fig. 3 except that MgADP (*triangles* 0.1 mM, *squares* 0.5 mM) or Pi (*diamonds* 1 mM) was present. In the presence of MgADP, the ATP-regenerating system was absent. [*Circles* Without the addition of ADP or Pi as a control (same as the data in Fig. 3A), *filled symbols* relaxation or contraction without tension oscillation, *open symbols* strong tension oscillation, *half-filled symbols* weak tension oscillation]. Tension was normalized with respect to that of the control in high-Ca^{2+} solution (+Ca^{2+}). *Vertical bars* are SD of 3 data points

Effect of MgADP or Pi on Ca-SPOC

In the presence of MgADP (0.1 and 0.5 mM), the tension/pCa curve shifted to the left (Fig. 4); concomitantly, the SPOC region became smaller and diminished to nothing when the concentration of MgADP was higher than 0.5 mM (compare the states of muscle along the abscissae in Fig. 5C, D). On the other hand, the addition of 1 mM Pi shifted the curve to the right (Fig. 4) and, at the same time, considerably weakened tension oscillation. This is not in accordance with results of a previous report of a study of rabbit cardiac myofibrils [16], in which Pi (10 mM) had no effect on sarcomeric oscillations under partial Ca^{2+} activation. The n_H and pCa_{50} values obtained are summarized in Table 2.

State diagrams of cardiac muscle on the Ca^{2+}-Pi plane at various MgADP concentrations

Figure 5A shows a state diagram constructed on the Ca^{2+}-Pi plane; data were measured with the preparation in the presence of 10 mM MgADP. The contraction region within which tension oscillations were undetectable and the SPOC region were separated by a near-straight line with a slope of about 10^4. This line corresponds to the dashed line in Fig. 2A. Such a linear relationship between the critical concentration of Pi and the free Ca^{2+} concentration implies that Pi and Ca^{2+} compete; this competition should occur allosterically because the binding sites differ markedly from each other.

Table 2 Hill coefficients (n_H) and pCa_{50} of cardiac muscle under various conditions. The Hill equation is represented by $\log[P/(1-P)]=n_H(pCa_{50}-pCa)$, where P is the relative tension, n_H the Hill coefficient and pCa_{50} the pCa value at which P=0.5. Only data points below 1.3 of $|\log[P/(1-P)]|$ were used. Conditions, see Figs. 3 (control, without MgADP and Pi) and 4 (MgADP and Pi) from which the parameters were obtained

	Control	MgADP		Pi
		(0.1 mM)	(0.5 mM)	(1 mM)
n_H	1.75	1.69	1.35	2.26
pCa_{50}	5.89	6.04	6.26	5.68

Figure 5B, C shows similar state diagrams constructed from data obtained when the preparation was bathed in 4 and 2 mM MgADP. At 4 mM MgADP, the slope of the initial portion of the boundary was about half that at 10 mM MgADP; at 2 mM MgADP, this feature became more prominent. As the MgADP concentration decreased further to 0.5 mM, the SPOC region reached the abscissa where SPOC occurred in the absence of Pi (see open and half-filled circles on the abscissa in Fig. 5D), and the relaxation region appeared near the ordinate (see closed squares in Fig. 5D); at such a low MgADP concentration, increases in the Pi concentration up to 10–20 mM diminished tension oscillations and the isometric tension decreased to less than 10% of the maximum.

In the absence of MgADP (Fig. 5E), the Ca-SPOC region appeared clearly on the abscissa, where spontaneous tension oscillations occurred in the absence of both MgADP and Pi, requiring only submicromolar concentrations of free Ca^{2+}. As stated above (see Fig. 4), tension oscillations were weakened by 1 mM Pi. Here, MgADP produced by ATP hydrolysis inside the muscle bundle was removed by the ATP-regenerating system. Nonetheless, submillimolar concentrations of Pi may have accumulated inside the muscle. Thus, we examined the effect of sucrose phosphorylase with sucrose, which reduced the concentration of accumulated Pi (see [20]), but the Ca-SPOC region was unaffected (data not shown). Hence, we conclude that the ADP-SPOC and Ca-SPOC regions merge into a single SPOC region.

Discussion

The ionic conditions for inducing ADP-SPOC and Ca-SPOC are distinct from each other. We demonstrated, however, that in cardiac muscle the ADP-SPOC and Ca-SPOC regions are continuously connected through a single SPOC region. The SPOC region was located between the contraction (without tension oscillation) and relaxation regions in a three-dimensional state diagram constructed using different concentrations of free Ca^{2+} (pCa), Pi and MgADP (see Fig. 5), which regulate the proportions of the different chemical states of the cross-bridges.

When the state of the muscle changes from relaxation to contraction, the proportion of non-force generating (or

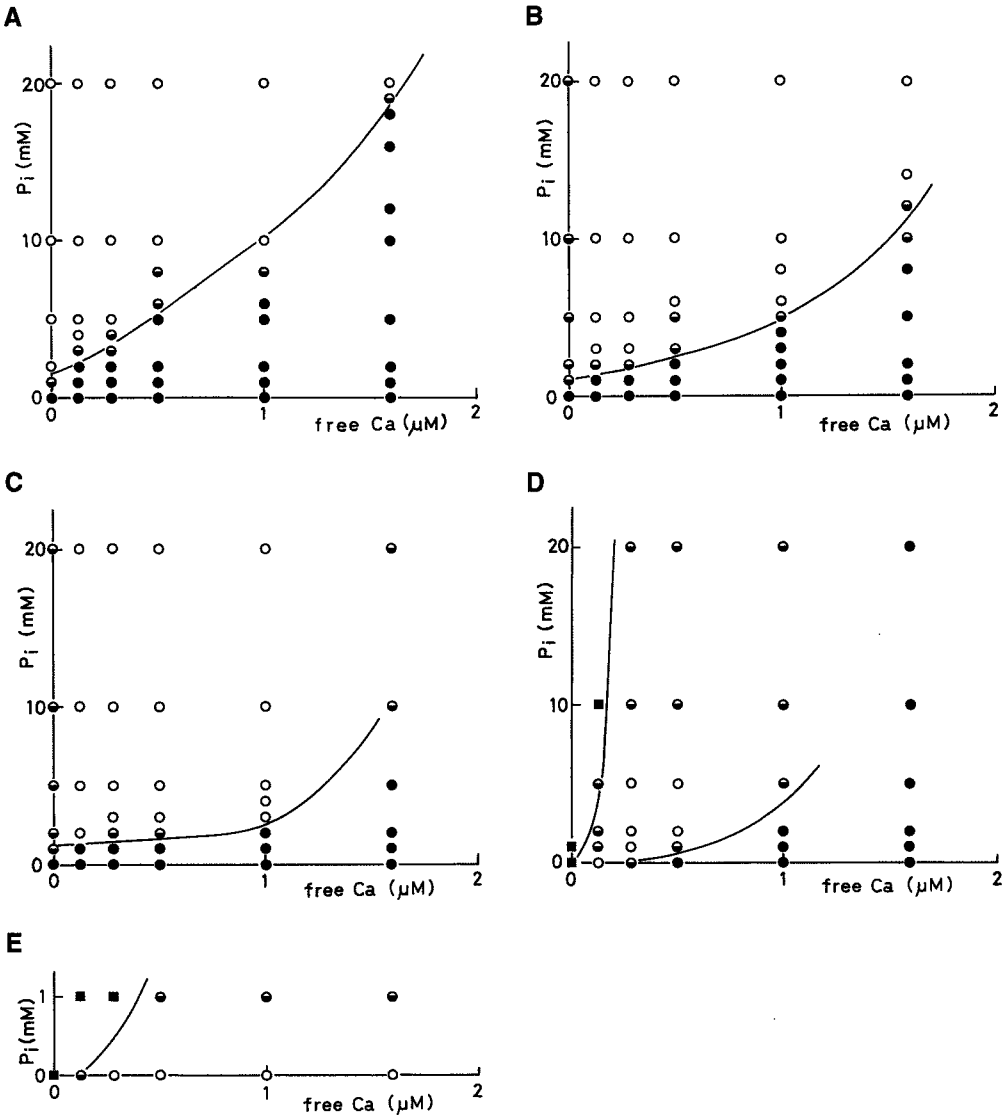

Fig. 5A–E State diagrams on the Ca^{2+}-Pi plane showing all three cardiac muscle states, i.e. contraction without tension oscillation, SPOC and relaxation, at 10 mM (**A**), 4 mM (**B**), 2 mM (**C**), 0.5 mM (**D**) and 0 mM (**E**) MgADP. Other conditions, the same as in Fig. 2A. The data shown in Fig. 2A were used for constructing state diagram **A**; also, the data in Fig. 4 were used for determining the states on the abscissae of Fig. D, E. (*Filled circles* Contraction without tension oscillation, *open circles* strong tension oscillation, *half-filled circles* weak tension oscillation, *filled squares* relaxation or contraction in which the tension developed was less than 2% of the maximum). *Thin lines* indicate the boundaries between two states; the *thin line* in **A** corresponds to the *dashed line* in Fig. 2A. However, the two are not exactly the same because several data points were added to construct the former line

weak) cross-bridges decreases, whereas that of force-generating (or strong) cross-bridges increases, so that either type of cross-bridges is predominant under contraction and relaxation conditions. On the other hand, in an intermediate condition between contraction and relaxation both types of cross-bridges coexist to some extent. Utilizing a model calculation based on an actomyosin ATPase kinetics scheme, we previously proposed that the requirement for induction of SPOC is not the absolute tension level per se, that is, the proportion of force-generating cross-bridges, but rather the coexistence of both types of cross-bridges at levels exceeding a certain threshold proportion (see [10, 12]). From the present results, we suggest that the molecular state of cross-bridges inside muscle is common to ADP-SPOC and Ca-SPOC, although the precise proportion of both types of cross-bridges under each experimental condition has yet to be determined.

With regard to Ca-SPOC, the above-described requirement may be more easily met if the transition between turned-off and turned-on states regulated by the Ca^{2+} concentration is increasingly gradual. In other words, the smaller the Hill coefficient in the tension/pCa relation, the more easily this requirement will be met (see [10, 12]). This appears to be consistent with the observations that: (1) Ca-SPOC occurred in the cardiac but not in skeletal muscle, which has a higher Hill coefficient, and (2) Pi, which increases the Hill coefficient, markedly weakened Ca-SPOC (Fig. 4 and Table 2). The apparent discrepancy with the previous result, i.e. that Pi did not affect the Ca-SPOC [16], should be clarified in future by examining the effects of myofibril thickness, differences among species of muscle, and so on. On the other hand, the SPOC region tended to be diminished with the addition of MgADP, despite the fact that the Hill coefficient was smaller, i.e. approaching 1 (Fig. 4 and Table 2). This observation strongly suggests that a smaller Hill coefficient alone is not sufficient to fulfil the above requirement for SPOC.

A correlation between the Hill coefficient and the occurrence of Ca-SPOC was suggested by Kentish et al.

[13]. However, they observed no tension oscillation under any conditions examined, irrespective of Hill coefficient values (between 2.7 and 4.5; as they mentioned, these values may be too large to meet the above requirement for SPOC). The high Hill coefficient values may be attributable to Pi accumulation (see Fig. 4) and to a decrease in pH inside muscle bundles. In addition, the lack of observable Ca-SPOC can also be ascribed to disorganized oscillation of myofibrils cancelling out tension oscillations of the bundles (see also below), as these investigators used thick bundles (>100 μm). The specimens in which SPOC were observed to occur were thinner than 50 μm (see [6, 16, 25]; see also Materials and methods). We confirmed that tension oscillations were not detectable in bundles thicker than 100 μm, although sarcomere length oscillations were detected with the aid of an optical microscope.

The apparent period of tension oscillation of the muscle bundle, as reported in Figs. 1B, 2B and 3B, was 10–20 s, about five times longer than the period of sarcomere length oscillation observed with the aid of a microscope (micrographs not shown). This was also the case in skeletal muscle; the apparent period of tension oscillation was generally longer than 5 s in a bundle of myofibrils (see Fig. 5 in [2]) or a single fibre (see Fig. 8 in [23]), whereas the period of sarcomere length oscillation was only a few seconds [19]. When the sarcomere oscillations were organized in a single myofibril, the period of tension oscillation became about 2 s, which coincides with the period of sarcomere length oscillation (see Figs. 7 and 9 in [2]; Fig. 4 in [26]). A possible explanation for the long period of tension oscillation observed to occur in muscle bundles is the effect of the interference of a number of oscillations with different periods of sarcomere shortening and relengthening (see [24]).

The physiological or pathological significance of SPOC, especially in cardiac muscle, remains unclear. However, it is noteworthy that the state diagram we constructed shows that the SPOC region encompasses physiological conditions in which not only MgATP and Ca^{2+}, but also Pi and MgADP, coexist. Moreover, the following two points merit emphasis. First, the SPOC region in cardiac muscle is larger than that in skeletal muscle: that is, a Ca-SPOC region exists in cardiac muscle but not in skeletal muscle and, in addition, the ADP-SPOC region in cardiac muscle extends to the side with the lower ADP concentration. This implies that the probability of SPOC occurring is higher in cardiac muscle. Second, in the living heart, rhythm is controlled by a pacemaker such that the contractile system itself is not a determinant of rhythm. On the other hand, it is reasonable to speculate that the contractile system has the properties of a nonlinear oscillator enabling it to respond autonomously to the forced oscillation modulated by a pacemaker with various frequencies. Thus, there may be a correlation between the normal heart rate and the frequency of tension oscillation or sarcomere length oscillation. In this respect, it is tempting to examine the frequencies of SPOC in the cardiac muscle contractile systems of various animal species having different heart rates, e.g. about 50 beats/min for bovine, about 250 beats/min for rabbit and about 350 beats/min for rat hearts (see [1]).

Acknowledgements We thank Mr. Y. Nishizawa (Waseda University) for his preliminary experiments, done in the initial stages of this research. This study was supported in part by Grants-in-Aid for Scientific Research (No. 61580226 and No. 04402053 to S.I.) and Grants-in-Aid for Scientific Research on Priority Areas (No. 04237228, No. 05221234 and No. 06213233 to S.I.) from the Ministry of Education, Science, Sports and Culture of Japan and The Uehara Memorial Foundation.

References

1. Altman P, Dittmer DS (1964) Biology data book. Federation of American Societies for Experimental Biology, Washington DC
2. Anazawa T, Yasuda K, Ishiwata S (1992) Spontaneous oscillation of tension and sarcomere length in skeletal myofibrils. Microscopic measurement and analysis. Biophys J 61:1099–1108
3. Brenner B (1979) An indirect proof of stretch-induced Ca^{2+} release from the sarcoplasmic reticulum in glycerinated skeletal and heart muscle preparations. Basic Res Cardiol 74:177–202
4. Cooke R, Pate E (1985) The effects of ADP and phosphate on the contraction of muscle fibers. Biophys J 48:789–798
5. Fabiato A, Fabiato F (1975) Contractions induced by a calcium-triggered release of calcium from the sarcoplasmic reticulum of single skinned cardiac cells. J Physiol (Lond) 249:487–517
6. Fabiato A, Fabiato F (1978) Myofilament-generated tension oscillations during partial calcium activation and activation dependence of the sarcomere length-tension relation of skinned cardiac cells. J Gen Physiol 72:667–699
7. Fukuda N, Fujita T, Ishiwata S (1991) Effects of ADP, inorganic phosphate and calcium on spontaneous tension oscillation of glycerinated cardiac muscle (abstract). J Muscle Res Cell Motil 12:304
8. Fukuda N, Fujita T, Ishiwata S (1992) Spontaneous tension oscillation in glycerinated cardiac muscle induced by ADP, inorganic phosphate and calcium (abstract). J Muscle Res Cell Motil 13:477
9. Horiuti K (1986) Some properties of the contractile system and sarcoplasmic reticulum of skinned slow fibres from *Xenopus* muscle. J Physiol (Lond) 373:1–23
10. Ishiwata S, Yasuda K (1993) Mechano-chemical coupling in spontaneous oscillatory contraction of muscle. Phase Transi 45:105–136
11. Ishiwata S, Okamura N, Shimizu H, Anazawa T, Yasuda K (1991) Spontaneous oscillatory contraction (SPOC) of sarcomeres in skeletal muscle. Adv Biophys 27:227–235
12. Ishiwata S, Anazawa T, Fujita T, Fukuda N, Shimizu H, Yasuda K (1993) Spontaneous tension oscillation (SPOC) of muscle fibers and myofibrils. Minimum requirements for SPOC. In: Sugi H, Pollack G (eds) Mechanism of myofilament sliding in muscle contraction. Plenum, London, pp 545–556
13. Kentish JC, ter Keurs HEDJ, Ricciardi L, Bucx JJJ, Noble MIM (1986) Comparison between the sarcomere length-force relations of intact and skinned trabeculae from rat right ventricle. Influence of calcium concentrations on these relations. Circ Res 58:755–768
14. Lappé DL, Lakatta EG (1980) Intensity fluctuation spectroscopy monitors contractile activation in "resting" cardiac muscle. Science 207:1369–1371
15. Lienhard GE, Secemski II (1973) P^1, P^5-di(adenosine-5′)pentaphosphate, a potent multisubstrate inhibitor of adenylate kinase. J Biol Chem 248:1121–1123
16. Linke WA, Bartoo ML, Pollack GH (1993) Spontaneous sarcomeric oscillations at intermediate activation levels in single isolated cardiac myofibrils. Circ Res 73:724–734

17. Lundblad A, Gonzales-Serratos H, Inesi G, Swanson J, Paoline P (1986) Patterns of sarcomere activation, temperature dependence, and effect of ryanodine in chemically skinned cardiac fibers. J Gen Physiol 87:885–905
18. Mulder BJM, de Tombe PP, ter Keurs HEDJ (1989) Spontaneous and propagated contractions in rat cardiac trabeculae. J Gen Physiol 93:943–961
19. Okamura N, Ishiwata S (1988) Spontaneous oscillatory contraction of sarcomeres in skeletal myofibrils. J Muscle Res Cell Motil 9:111–119
20. Pate E, Cooke R (1989) Addition of phosphate to active muscle fibers probes actomyosin states within the power stroke. Pflügers Arch 414:73–81
21. Rieser G, Sabbiadini R, Fry M, Inesi G (1979) Sarcomere motion in isolated cardiac cells. Am J Physiol 236:C70–C77
22. Rüegg JC (1988) Calcium in muscle activation. Springer, Berlin Heidelberg New York
23. Shimizu H, Fujita T, Ishiwata S (1992) Regulation of tension development by MgADP and Pi without Ca^{2+}. Role in spontaneous tension oscillation of skeletal muscle. Biophys J 61:1087–1098
24. Smith DA, Stephenson DG (1994) Theory and observation of spontaneous oscillatory contractions in skeletal myofibrils. J Muscle Res Cell Motil 15:136–189
25. Sweitzer NK, Moss RL (1990) The effect of altered temperature on Ca^{2+}-sensitive force in permeabilized myocardium and skeletal muscle. Evidence for force dependence of thin filament activation. J Gen Physiol 96:1221–1245
26. Yasuda K, Shindo Y, Ishiwata (1996) Synchronous behavior of spontaneous oscillations of sarcomeres in skeletal myofibrils under isotonic conditions. Biophys J 70:1823–1829

Biophysical Journal Volume 71 November 1996 2307–2318

Structural and Functional Reconstitution of Thin Filaments in the Contractile Apparatus of Cardiac Muscle

Hideaki Fujita*, Kenji Yasuda,# Shigehiko Niitsu,* Takashi Funatsu,§ and Shin'ichi Ishiwata*¶

*Department of Physics, School of Science and Engineering, Waseda University, Tokyo 169; #Advanced Research Laboratory, Hitachi, Hatoyama, Saitama 350-03; §Yanagida BioMotron Project, Exploratory Research for Advanced Technology, Research Development Corporation of Japan, Mino, Osaka 562; and ¶Advanced Research Institute for Science and Engineering, Waseda University, Tokyo 169, Japan

ABSTRACT The muscle contractile apparatus has a highly ordered liquid crystalline structure. The molecular mechanism underlying the formation of this apparatus remains, however, to be elucidated. Selective removal and reconstitution of the components are useful means of examining this mechanism. In addition, this approach is a powerful technique for examining the structure and function of a specific component of the contractile system. In this study we have achieved the structural and functional reconstitution of thin filaments in the cardiac contractile apparatus. First, all thin filaments other than short fragments at the Z line were removed by treatment with gelsolin. Under these conditions no active tension could be generated. By incorporating exogenous actin into these thin filament-free fibers, actin filaments were reconstituted, and active tension, which was insensitive to Ca^{2+}, was restored. The active tension after the reconstitution of thin filaments reached 135 ± 64% of the original level. The augmentation of tension was attributable to the elongation of reconstituted filaments. As another possibility for augmented tension generation, we suggest the presence of an inhibitory system that was not reconstituted. In any case, the thin filaments of the cardiac contractile apparatus are considered to be assembled so as not to develop the highest degree of tension. Incorporation of the tropomyosin-troponin complex fully restored Ca^{2+} sensitivity without affecting maximum tension. The present results indicate that a muscle contractile apparatus with a higher order structure and function can be constructed by the self-assembly of constituent proteins.

INTRODUCTION

Starting with the tobacco mosaic virus (Fraenkel-Conrat and Williams, 1955), it has been demonstrated that biological supramolecular structures, such as ribosomes (Nomura, 1974), flagella, actin filaments (Oosawa and Asakura, 1975), and so on, can be reconstituted in vitro from exogenous components according to self-assembly mechanisms. Thus a question arises as to whether a higher order biological structure, such as the muscle contractile apparatus, can also be constructed via a similar self-assembly mechanism. The muscle contractile apparatus is composed mainly of two distinct filaments (thick and thin filaments) and the elastic framework that maintains the lattice structure. Muscle contraction is based on mutual sliding between thick and thin filaments, which are arranged in liquid-crystalline arrays (Huxley and Niedergerke, 1954; Huxley and Hanson, 1954).

Actin filaments can be reconstituted by spontaneous polymerization of monomers under appropriate conditions in vitro, but their length distribution is broad and of an exponential type at equilibrium (Oosawa and Asakura, 1975). Thin filaments, which have regulatory systems, can be reconstituted in vitro by incubating the reconstituted actin filaments with tropomyosin and troponin under appropriate conditions (Ishiwata, 1973; Ishiwata and Kondo, 1978). The duration of the incubation period required for reconstitution depends on temperature. Thick filaments can also be reconstituted from myosin molecules under appropriate conditions in vitro, and their length distribution and average length are similar to those in vivo (see review by Katsura and Noda, 1973). Because selective removal of thick filaments can easily be achieved by treatment with a high-salt solution (Huxley and Hanson, 1954), several attempts were made to reconstitute thick filaments using "ghost" fibers or fibrils (Tawada et al., 1976; Taniguchi and Ishikawa, 1982; Maw and Rawe, 1986). Unlike the case with thick filaments, it is difficult to remove thin filaments selectively only by controlling ionic conditions. Recently we succeeded in selectively removing thin filaments in skeletal and cardiac muscle fibers using calf plasma gelsolin, an actin filament-severing protein (Funatsu et al., 1990, 1993; Yasuda et al., 1995). We also succeeded in reconstituting thin filaments by using thin filament-free skeletal muscle fibers and fibrils, but the maximum tension of the reconstituted fibers generated was approximately 20% that of intact fibers (Funatsu et al., 1994). The number density of thin filaments in reconstituted skeletal muscle fibers, based on thin-section electron microscopy, was also about 20% that of intact fibers.

In this investigation we selectively removed and reconstituted thin filaments in the cardiac contractile apparatus. The removal and reconstitution of thin filaments were first examined functionally, according to the ability of the fibers to generate active tension. Reconstitution of regulatory proteins was examined by the pCa-tension relation of the reconstituted fibers. In addition, the removal and reconsti-

Received for publication 31 May 1996 and in final form 16 August 1996.

Address reprint requests to Dr. Shin'ichi Ishiwata, Department of Physics, School of Science and Engineering, Waseda University, 3-4-1 Okubo, Shinjuku-ku, Tokyo 169, Japan. Tel.: 81-3-5286-3437; Fax: 81-3-3200-2567; E-mail: ishiwata@cfi.waseda.ac.jp.

0006-3495/96/11/2307/12 $2.00

tution of thin filaments were examined structurally by laser scanning confocal microscopy after the thin filaments were selectively stained with a fluorescent dye. The reconstituted fibers were observed by thin-section electron microscopy to determine the length, number, and location of reconstituted thin filaments.

The technique and approach described herein are expected to be useful for examining, as an example, the characteristics of genetically altered actin, tropomyosin, and troponin, provided that the thin filaments can be reconstituted by employing these molecules. This technique should also prove useful for clarifying the molecular basis of muscle contraction and its regulation, by incorporating fluorescence-labeled or spin-labeled molecules into the reconstituted thin filaments.

MATERIALS AND METHODS

Muscle fibers and proteins

Bovine cardiac papillary muscle fibers (approximately 5 mm in diameter) or rabbit psoas muscle fibers (3–5 mm in diameter) were tied to a glass rod and incubated in glycerol solution containing 50% (v/v) glycerol, 0.5 mM $NaHCO_3$, 5 mM EGTA, and 2 mM leupeptin at 0°C overnight. Fibers were then stored in fresh glycerol solution at −20°C. Glycerinated fibers were used within 2–8 weeks after storage. Bovine plasma gelsolin was prepared according to the method of Kurokawa et al. (1990); during this preparation, we shortened the incubation time of gelsolin in Ca^{2+}-free buffer as much as possible because the severing activity appeared to be lowered by prolonged incubation in Ca^{2+}-free buffer. Actin was extracted from acetone powder (Kondo and Ishiwata, 1976) of bovine cardiac muscle according to the method of Spudich and Watt (1971). Purified G-actin was stored at 0°C and used within 2 weeks after extraction. The tropomyosin (Tm)-troponin (Tn) complex (nTm) was prepared from bovine cardiac muscle and from rabbit skeletal muscle according to the method of Ebashi and colleagues (1968).

Solutions

The solutions used were: rigor solution, 0.17 M KCl, 1 mM $MgCl_2$, 10 mM 3-(*N*-morpholino)propanesulfonic acid (MOPS) (pH 7.0), 1 mM EGTA; relaxing solution, 117 mM KCl, 5 mM $MgCl_2$, 4 mM ATP, 10 mM MOPS (pH 7.0), 1 mM EGTA, 20 mM 2,3-butanedione 2-monoxime (BDM); contracting solution, 117 mM KCl, 4.25 mM $MgCl_2$, 2.2 mM ATP, 1.9 mM $CaCl_2$, 20 mM MOPS (pH 7.0), 2 mM EGTA. EGTA and MOPS were purchased from Dojindo Laboratories (Kumamoto, Japan); dithiothreitol (DTT) was from Wako Pure Chemical Industries (Osaka, Japan). Other chemicals were of reagent grade.

Selective removal of thin filaments

A glycerinated cardiac muscle fiber, a small bundle of several cardiac cells (~60 μm in width and ~2 mm in length), was stripped from the glycerinated muscle in a cold glycerol solution (Fukuda et al., 1996), and both ends were tied to a thin tungsten wire with enamel, one end of which was attached to a tension transducer (AE-801; SensoNor a.s, Horten, Norway). The volume of the measurement cell was approximately 200 μl. Fibers were chemically skinned with rigor solution containing 1% (v/v) Triton X-100 for 30 min. After a 15-min wash in rigor solution and then in relaxing solution, active tension was measured in contracting solution. Fibers were then immersed in contracting solution containing 20 mM BDM, 2 mM leupeptin, 2 mM diisopropyl fluorophosphate (DFP), and 0.3 mg/ml gelsolin at 0°C (gelsolin treatment). After a 10-min gelsolin treatment, the fibers were washed with relaxing solution and tension was measured to confirm that active tension was reduced upon the removal of thin filaments. The gelsolin treatment and tension measurement were then repeated. All procedures were carried out at 0 ± 2°C; tension was measured at room temperature (25 ± 2°C). Thus the thin-filament-free fibers used for reconstitution experiments were routinely prepared by continuous gelsolin treatment for 80 min at 0°C.

Reconstitution of thin filaments

To reconstitute actin filaments, the thin filament-free fibers were immersed in actin-polymerizing solution (80 mM KI, 4 mM $MgCl_2$, 4 mM ATP, 4 mM EGTA, 20 mM BDM, and 10 mM K-phosphate, pH 7.0) containing 1 mg/ml of purified G-actin that had been mixed just before use. The polymerizing solutions were newly prepared and exchanged every 7 min and kept at 0°C to prevent the effect of spontaneous formation of nuclei. To reconstitute actin filaments associated with regulatory proteins (i.e., thin filaments), the actin filament-reconstituted fibers were immersed in relaxing solution containing tropomyosin and troponin complexes (total protein concentration of 3 mg/ml) for 12 h at 0°C. The active tension of reconstituted fibers was measured at room temperature (25 ± 2°C, whereas the fibers were relaxed at 0°C).

Laser scanning confocal microscopy

Fibers were treated with 3% formaldehyde in relaxing solution for 30 min, for the purpose of chemical fixation, before and after the reconstitution of actin filaments and were mounted on a glass slide. Fibers were then treated with relaxing solution containing 8 μM rhodamine-phalloidin (RhPh) (Molecular Probes, Eugene, OR) overnight at 0°C, and then free RhPh was washed out with relaxing solution containing 100 mM DTT before microscopic observation. Preparations were observed by laser scanning confocal microscopy (LSM-GB200; Olympus Co., Tokyo). The light source was a 25-mW Ar laser of 488 nm. A 550-nm long-pass filter was used to detect the fluorescence of RhPh. A PlanApo 60 × 1.00 W LSM objective lens was used. The scanning time to take one picture was 40 s. The fluorescence intensity was recorded in a 1024 × 768 frame memory with an intensity range of 256 steps. The intensity profile was obtained by scanning along a line with a width of five pixels in the *x-y* plane; the depth of the *x-y* plane was changed along the *z* axis by moving the sample with a piezo stage.

Thin-section electron microscopy

The fibers at each step of reconstitution were tied to a platinum wire (0.3 mm in diameter) and chemically fixed in solution containing 2.5% glutaraldehyde and 100 mM sodium cacodylate (pH 7.2) overnight at 2°C. The fibers were then immersed in a solution containing 0.5% tannic acid for 30 min. After washing with 100 mM sodium cacodylate (pH 7.2), the preparations were postfixed with 1% OsO_4 in the same buffer for 2 h at 2°C, dehydrated with ethanol and acetone, and embedded in Poly/Bed 812 (Polysciences, Warrington, PA). Thin sections were stained sequentially with saturated uranyl acetate and 2.6% lead citrate at 20°C. Electron micrographs were taken with a JEM 1200EX electron microscope (operating voltage, 100 kV; JEOL, Tokyo).

Sodium dodecyl sulfate gel electrophoresis

Cardiac muscle fibers (~60 μm thick, ~1 mm long) removed from the tungsten wires either before or after reconstitution were dissolved in lysis solution (7.5% sodium dodecyl sulfate (SDS), 10% glycerol, 1 mM DTT, and 10 mM Tris-HCl, pH 6.8) and heated for 3 min at 90°C. SDS-polyacrylamide gel electrophoresis (PAGE) was carried out according to the method of Laemmli (1970), with 13% polyacrylamide as the running gel and 5% polyacrylamide as the stacking gel. Protein was stained with silver (Silver Stain II Kit; Wako Pure Chemical Industries).

RESULTS

Removal and reconstitution of thin filaments

Fig. 1 schematically illustrates the filamentous structure of a sarcomere after the removal and reconstitution of thin filaments. Thin-filament-free fibers were prepared from glycerinated bovine cardiac muscle fibers (Fig. 1 *a*) by treatment with plasma gelsolin (Fig. 1 *b*). The fibers were then immersed in a solution containing purified G-actin under polymerization conditions. Actin monomers were po-

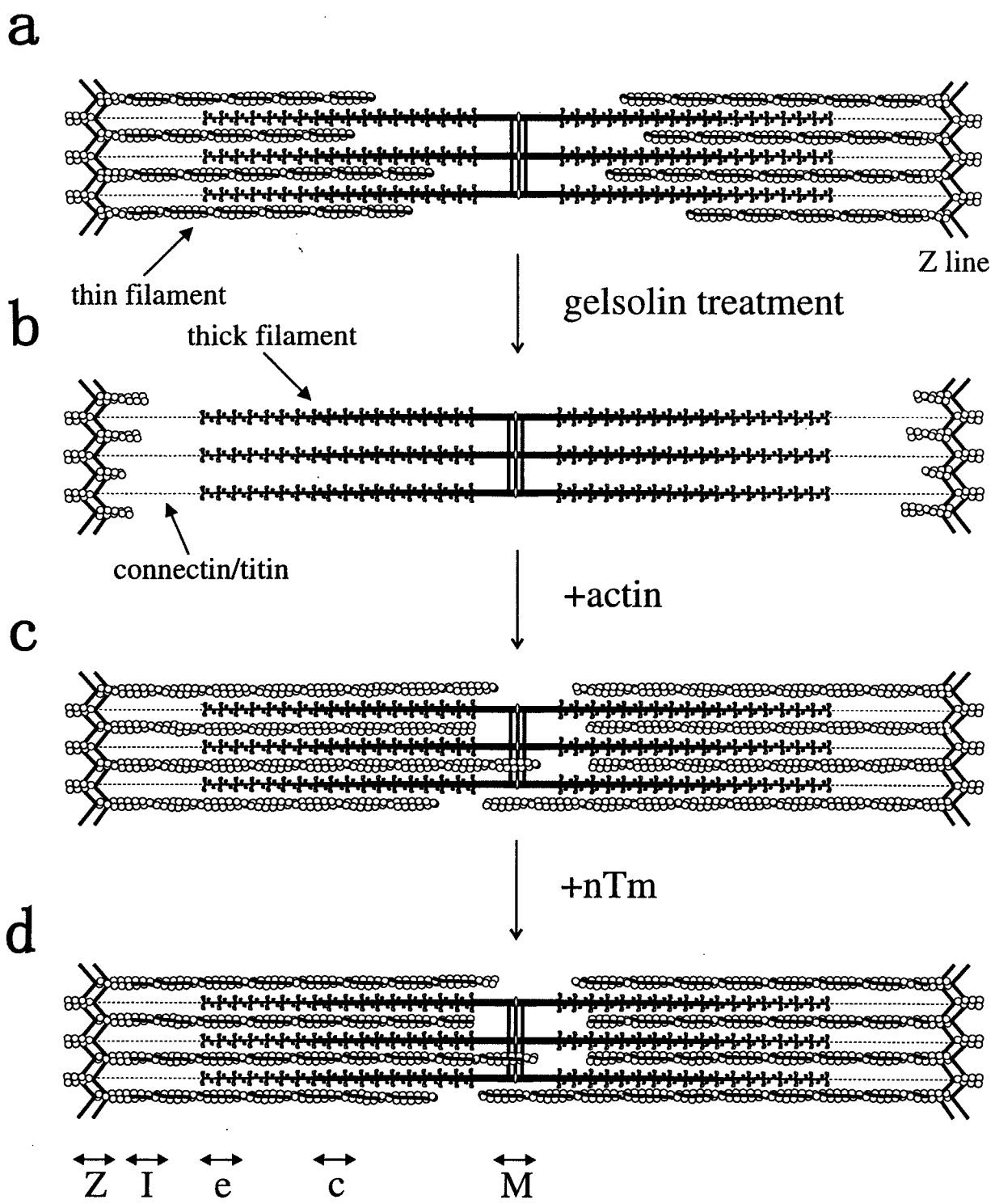

FIGURE 1 A schematic diagram illustrating the removal and reconstitution of thin filaments in a sarcomere. (*a*) Untreated cardiac sarcomere; (*b*) after gelsolin treatment; (*c*) after reconstitution of actin filaments; (*d*) after reconstitution of thin filaments with the addition of nTm. The double-headed arrows labeled Z, I, e, c, and M indicate the regions at which the numbers of thin and thick filaments were counted on electron micrographs (cf. Figs. 4 and 5).

lymerized onto the actin fragments remaining at the Z line (Fig. 1 *c*). To minimize the effects of spontaneous nucleation of actin outside sarcomeres, the fresh actin solution was exchanged every 7 min at 0°C, and a low concentration of KI was used instead of KCl because KI is known to delay nucleus formation (Funatsu et al., 1994). To reconstitute thin filaments, the fibers were immersed in relaxing solution containing tropomyosin-troponin complexes (nTm), and Ca^{2+} sensitivity was measured (Fig. 1 *d*).

The fibers were observed under a laser scanning confocal microscope after staining of the actin filaments with fluorescent RhPh before (Fig. 2 *a*) and after (Fig. 2 *b*) gelsolin treatment and after the reconstitution of thin filaments (Fig. 2 *c*). Fig. 2 *b* shows that all thin filaments, other than short fragments at the Z line, were removed by gelsolin treatment. Fig. 2 *c* shows that the thin filaments were reconstituted at the original position by the addition of exogenous actin. The fluorescence intensity distribution of the confocal images demonstrated the reconstitution of thin filaments around the I band, over the entire region of the fibers. The intensity profile of the thin-filament-reconstituted fiber resembles that of an intact fiber, indicating that the length distribution of thin filaments in reconstituted fibers is similar to that of intact fibers.

SDS-PAGE showed that actin was gradually removed during the course of gelsolin treatment (Fig. 3, lanes 1 and 2) and had essentially been eliminated by 80 min (Fig. 3, lane 3). The extent to which the regulatory proteins were removed together with actin was not clear because of the small quantity of muscle fibers, but the removal of TN-I was detectable; on the other hand, LC1, LC2 and the heavy chain of myosin were confirmed to have remained. In addition, we confirmed that the actin level had recovered after 42 min of reconstitution (7 min × 6) (Fig. 3, lane 4).

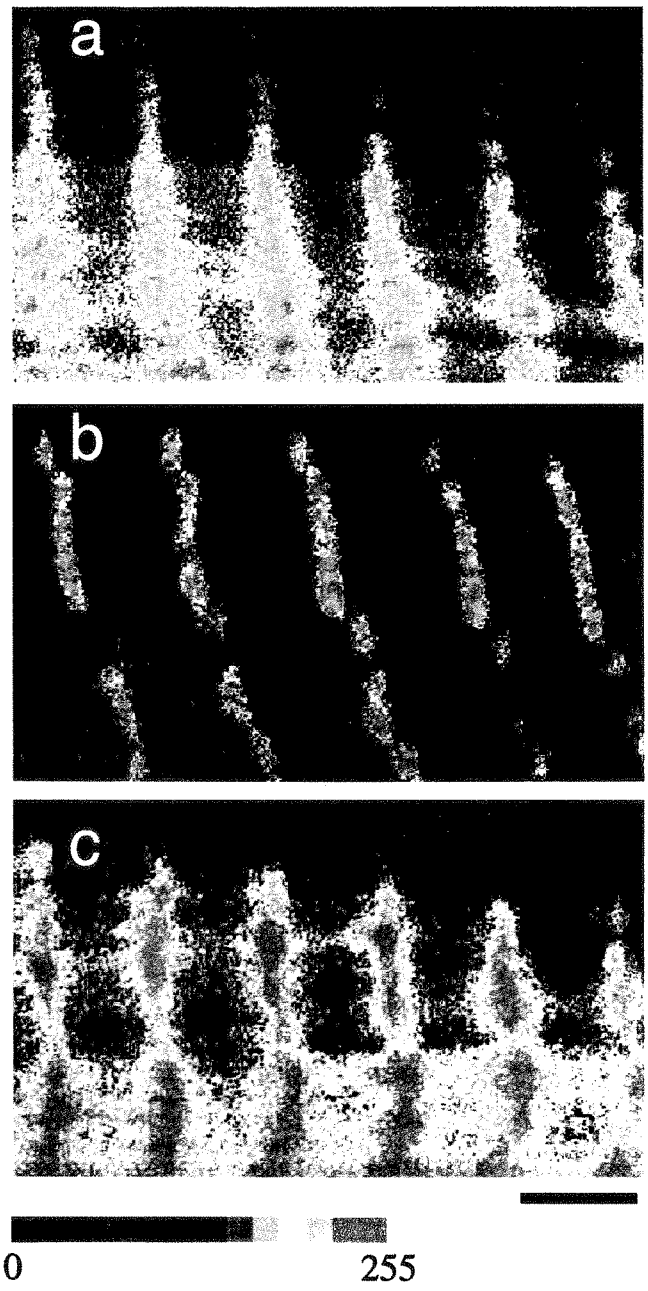

FIGURE 2 Confocal fluorescence images of cardiac muscle at each step in the reconstitution process. (*a*) Untreated cardiac muscle; (*b*) after gelsolin treatment; (*c*) after reconstitution of actin filaments. The images have been pseudocolored using a linear scale of fluorescence intensity of RhPh. The lines of highest intensity (red lines) correspond to the Z lines. Scale bar, 2 μm.

Internal structure of muscle fibers before and after reconstitution of thin filaments

To investigate the postreconstruction internal structure, fibers were observed by thin-section electron microscopy (EM) (Fig. 4). The EM images showed that almost all thin filaments had been removed from the fiber by the gelsolin treatment (Fig. 4 *b, b'*). EM images of longitudinal sections, after reconstitution, revealed the thin filaments to have been reconstituted from the Z line, and cross-sectional images revealed the reconstituted thin filaments to be located inside the hexagonal lattice of thick filaments.

The numbers of thick and thin filaments were counted from cross-sectional EM images. As summarized in Fig. 5, the number densities of thin filaments in untreated and reconstituted fibers were the same at the regions of the Z line (Z) and the I band (I), whereas those in reconstituted fibers were larger than those in untreated fibers at the A-I overlap region (e, c) and the M line (M). This indicates the elongation of thin filaments without a change in the number density of the filaments. The ratio of the numbers of thin and thick filaments at the center of the A-I overlap region (c) was 1.5 in untreated fibers but was increased to 2.0 by reconstitution. The number density of thick filaments in reconstituted fibers was low at the e region, probably because the edges of the thick filaments were misaligned due to slight tension development during reconstitution. The lattice constant (average distance between thick filaments assuming a hexagonal lattice) was decreased from 39 nm to 36 nm by the removal of thin filaments, but was restored to

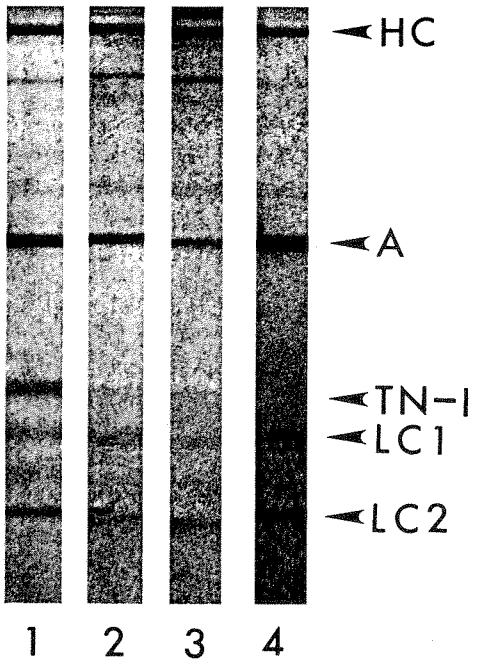

FIGURE 3 SDS-PAGE pattern of cardiac muscle fibers. Lane 1, control muscle fibers. Lanes 2 and 3, muscle fibers treated with 0.3 mg/ml of gelsolin in BDM-contracting solution for 30 min and 80 min, respectively. Lane 4, After gelsolin treatment, the muscle fiber was incubated with 1 mg/ml of actin in the process of polymerization in 80 mM KI, 4 mM $MgCl_2$, 4 mM ATP, 4 mM EGTA, 20 mM BDM, and 10 mM K-phosphate (pH 7.0) for 42 min (7 min × 6). Unbound actin molecules were washed out with relaxing solution containing 20 mM BDM. Arrowheads labeled HC, A, TN-I, LC1 and LC2 indicate the electrophoretic bands of myosin heavy chain, actin, troponin-I, and light chain 1 and light chain 2 of myosin, respectively.

39 nm by reconstitution, as it has been demonstrated in skeletal muscle (Funatsu et al., 1994).

Tension recovery of reconstituted muscle fibers

Active tension decreased exponentially with an increasing duration of gelsolin treatment and was completely absent at 80 min (Fig. 6). To minimize muscle fiber damage during gelsolin treatment, active tension development was suppressed by adding 20 mM BDM, an inhibitor of actin-myosin interactions (Li et al., 1985; Horiuti et al., 1988), and the temperature was kept at 0°C. We confirmed that the resting tension was not affected by gelsolin treatment, showing that connectin/titin remained intact.

During the course of actin filament reconstitution treatment, active tension recovered sigmoidally and reached a plateau after six incubations in actin polymerization solution (Fig. 7). Each tension measurement revealed a 5–10% decrease in tension (cf. Fig. 8 *a*, iii–v, vi, viii), such that the 60% recovery of tension achieved in this experiment suggests more than 100% recovery. To reach a plateau of tension recovery, 42 min (= 7 min × 6) of reconstitution treatment was needed. In the experiment shown in Fig. 7, approximately 7% of active tension persisted after the gelsolin treatment. However, because the magnitude of tension recovery after reconstitution was not affected by the residual tension persisting after the gelsolin treatment (data not shown), we consider the time course of tension recovery to be the same regardless of whether the tension in the initial fiber had been completely abolished by the gelsolin treatment. An example of the tension record at each reconstitution step is shown in Fig. 8 *a*. Active tension became undetectable after 80 min of gelsolin treatment (Fig. 8 *a*, ii). The tension, once abolished, was restored after 42 min (7 min × 6) of reconstitution with pure actin (Fig. 8 *a*, iii). The restored tension was 135 ± 64% (mean ± SD, n = 30) of the original level and ranged from 38% to 248%, as summarized in Fig. 8 *b*.

As a control, we confirmed that the tension in untreated fibers was not affected by consecutive treatments with contracting solution containing BDM without gelsolin and KI solution without actin (data not shown).

Reconstitution of thin filaments with tropomyosin and troponin

Actin filament-reconstituted fibers generated tension in a Ca^{2+}-insensitive manner because of the absence of nTm (Fig. 8 *a*, iii–v). Relaxation was obtained only by adding BDM. After incorporating nTm, however, the actin filament-reconstituted fibers recovered Ca^{2+} sensitivity (Fig. 8 *a*, vi–viii); the Ca^{2+}-insensitive tension decreased with incubation time in the nTm solution and had almost disappeared by 12 h (Fig. 9). The maximum tension in the presence of Ca^{2+} was not appreciably affected by the addition of nTm (compare Fig. 8 *a*, iii–v and vi, viii).

The thin-filament-reconstituted fibers fully regained the original pCa-tension relation (solid lines in Fig. 10). When nTm of skeletal muscle was used instead of cardiac nTm (thick dashed line in Fig. 10), fibers showed a pCa-tension relation resembling that of a skeletal muscle (thin dashed line in Fig. 10). The n_H and pCa_{50} values of the Hill equation were, respectively, 2.5 and 5.6 for cardiac nTm, but 3.5 and 5.9 for skeletal nTm.

DISCUSSION

Structural and functional reconstitution of actin filaments

In the present investigation, full reconstitution of actin filaments in the contractile apparatus was achieved for the first time. In a previous investigation, removal of thin filaments was performed in two steps, that is, the removal of thin filaments at the I band by gelsolin treatment under rigor conditions and then full removal of thin filaments (except the fragments at the Z line) by gelsolin treatment under contracting conditions, because severing of thin filaments at the overlapping region occurs under contracting conditions. Thus tension development during treatment should be minimized to suppress the damage of the sarcomere structure

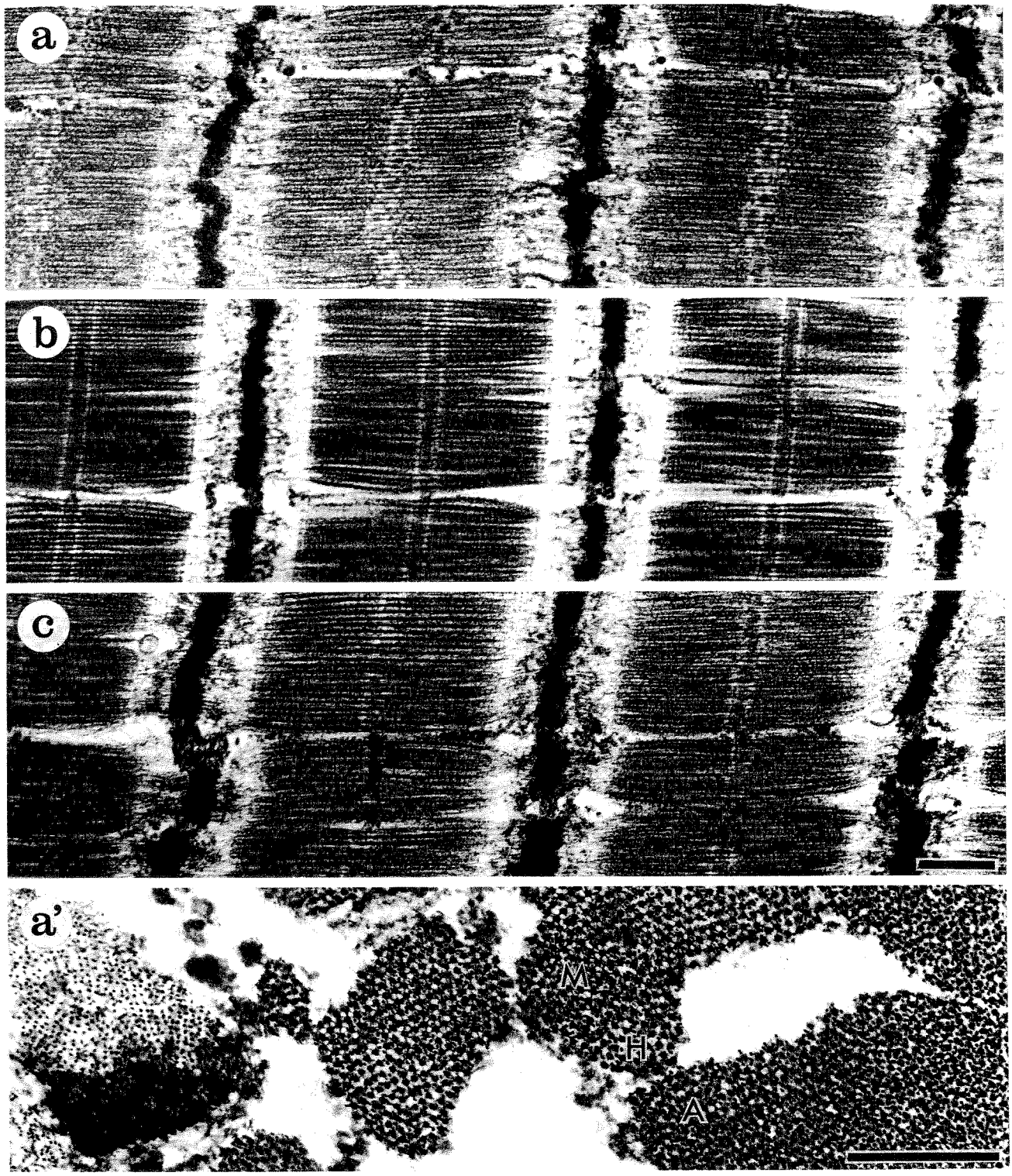

FIGURE 4 Thin-section EM images (a–c, longitudinal section; a'–c', cross section) of cardiac muscle at each step in the reconstitution process. (a and a') Untreated cardiac muscle. (b and b') After gelsolin treatment. (c and c') After reconstitution of thin filaments. M, H, and A, respectively, indicate the cross-sectional areas at the M line; at the pseudo H zone, where myosin heads are absent; and at the A band, where myosin heads are present. Scale bars, 0.5 μm.

(Funatsu et al., 1994). In this study, by adding an inhibitor of actin-myosin interactions, BDM, to the gelsolin solution, the removal of thin filaments was achieved in a single step. BDM was also included in the actin-polymerizing solution to suppress the damage of the sarcomere structure, due to contraction, as fully as possible. Observation by laser scan-

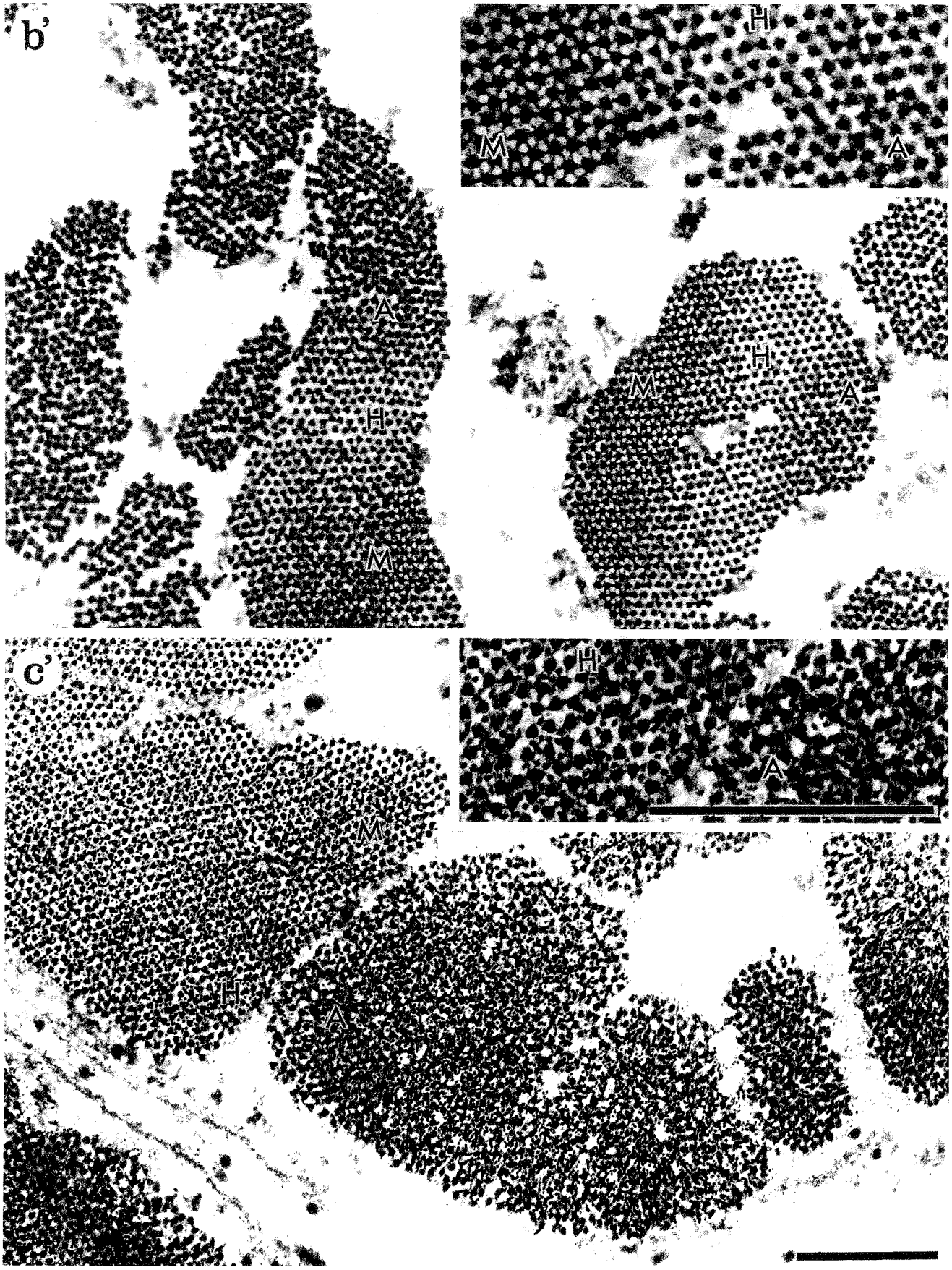

FIGURE 4 *Continued*

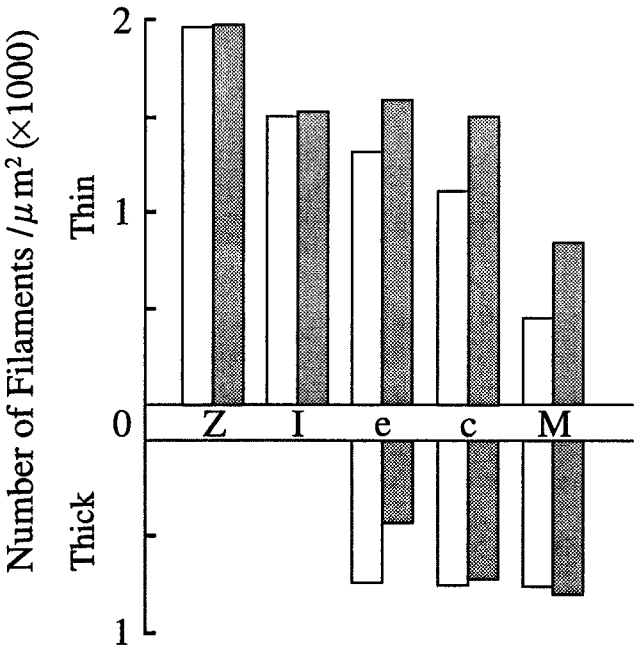

FIGURE 5 The number density of thin (above) and thick (below) filaments in untreated (white bars) and reconstituted (gray bars) fibers. Cross-sectional area measured for each region larger than 1 μm^2. Z, I, e, c, and M, see Fig. 1.

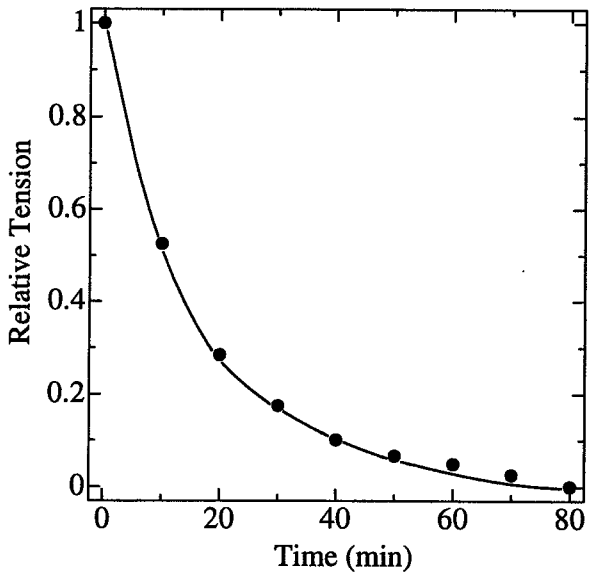

FIGURE 6 Time course of the decrease in active tension with gelsolin treatment. After every 10 min of gelsolin treatment, the active tension was measured on the same muscle bundle. The active tension was normalized with the tension measured before gelsolin treatment.

ning confocal microscopy (Fig. 2) showed that thin filaments had been removed from the fiber without disturbing the ordered arrangement of sarcomeres and that actin filaments were reconstituted at their original positions.

The cross-sectional image on thin-section electron microscopy revealed that actin filaments had been reconstituted inside the hexagonal lattice of thick filaments and that most of the thin filaments were reconstituted at the center of the hexagonal lattice, where intact thin filaments were located. This suggests that this position is the most stable position for actin filaments in the filament lattice.

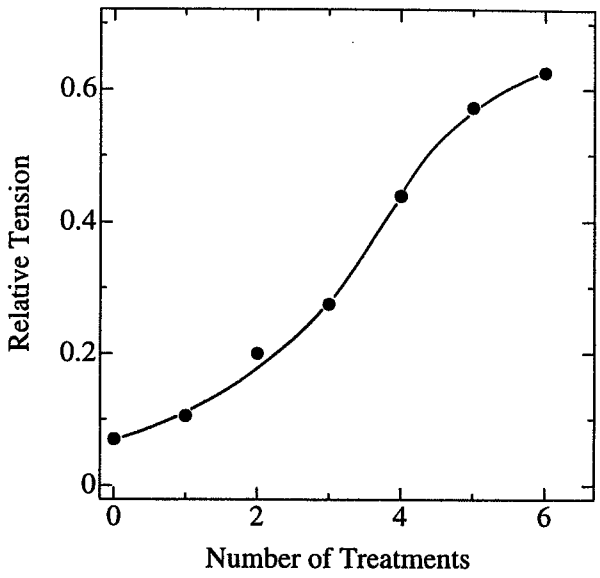

FIGURE 7 Time course of the recovery of active tension with the reconstitution of actin filaments. Fibers were treated with gelsolin for a total of 80 min before reconstitution. After every 7-min reconstitution treatment, the recovered active tension was measured. The active tension was normalized with the tension measured before gelsolin treatment.

In this study, active tension generated by the actin filament-reconstituted fibers reached 135% of that of the intact fibers on average. When reconstitution of actin filaments was performed in skeletal muscle, the active tension recovered was approximately 20% of the tension developed by intact fibers. Cardiac muscle lacks nebulin (Wang and Wright, 1988; Locker and Wild, 1986; Hu et al., 1986) and appears to have a thick, relatively strong, Z-line structure (Yamaguchi et al., 1985); these properties may account for the successful reconstitution of the cardiac contractile apparatus. The entanglement of nebulin at the N2 line, seen in gelsolin-treated skeletal muscle (Funatsu et al., 1990), is thought to disturb the polymerization of actin filaments. The stronger Z-line structure is speculated to play a role in maintaining the number of intact fragments at the Z line after gelsolin treatment. In addition, the stronger Z-line structure would presumably prevent damage of the internal structure due to repeated tension generation.

The gradual increase in and broadening of the fluorescence intensity distributed around the Z line in the reconstituted fibers (Fig. 2) strongly suggest that actin molecules had polymerized onto the short fragments remaining at the Z line. The short actin fragments remaining at the Z line can apparently function as nuclei for actin polymerization, and actin filaments thereby elongate from the Z line. This conclusion is consistent with the observation that tension recovery occurred sigmoidally with an increasing duration of

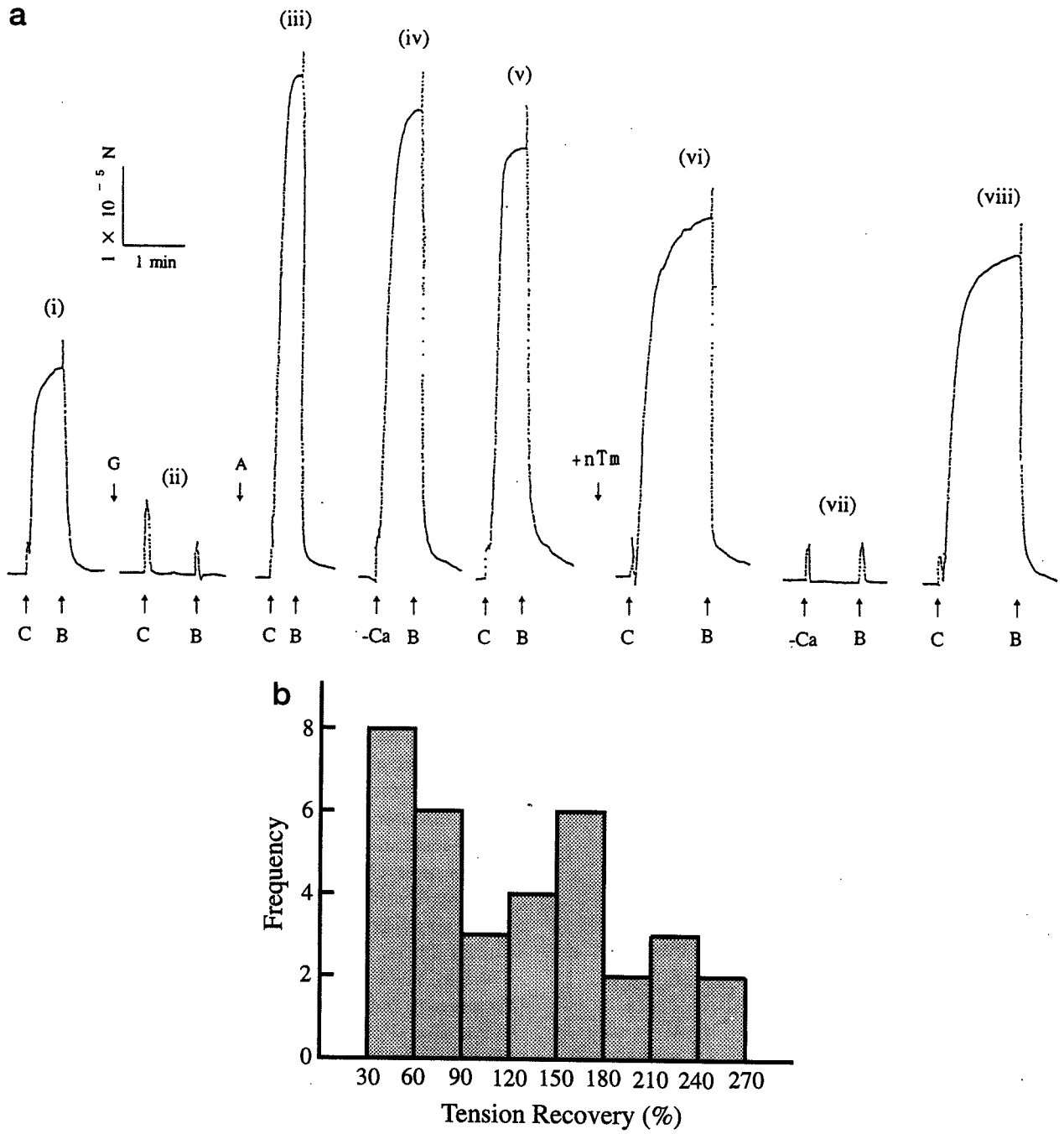

FIGURE 8 Recordings of tension generation at each step of thin filament reconstitution. (*a*) (i) untreated fiber; (ii) after gelsolin treatment; (iii–v) after reconstitution of actin filaments; (vi–viii) after reconstitution of thin filaments (+nTm). All records were taken sequentially from the same fiber. Temperature, 25°C for C, B, and −Ca; 0°C for G, A, and +nTm. Arrows indicate the time at which the solution was exchanged. Spikes observed in the records at each arrow are artifacts due to solution exchange. C, contracting solution; B, relaxing solution; -Ca, contracting solution without Ca^{2+}; G, gelsolin treatment; A, reconstitution of actin filaments; +nTm, addition of the cardiac tropomyosin-troponin complex. (*b*) Distribution of percentages of restored tension in the actin filament-reconstituted fibers. All data shown were obtained from fibers in which active tension had been completely abolished by gelsolin treatment.

actin filament reconstitution treatment (Fig. 7); in the initial lag phase, the reconstituted filaments were probably not long enough to contribute to tension recovery. If the reconstituted actin filaments had attached to connectin/titin, the fluorescent intensity at the I-band region where connectin/titin is exposed must have increased; but this was not the case (Fig. 2).

When actin molecules were directly added to untreated fibers under polymerizing conditions, neither elongation of actin filaments nor tension augmentation was observed

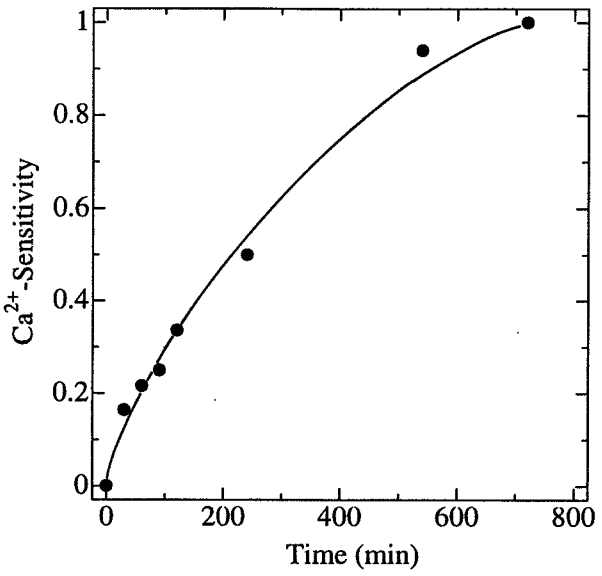

FIGURE 9 Time course of Ca^{2+} sensitivity recovery with incubation of actin filament-reconstituted fibers in relaxing solution containing 3 mg/ml cardiac nTm. Ca^{2+} sensitivity = 1 − (active tension without Ca^{2+})/(active tension with Ca^{2+}).

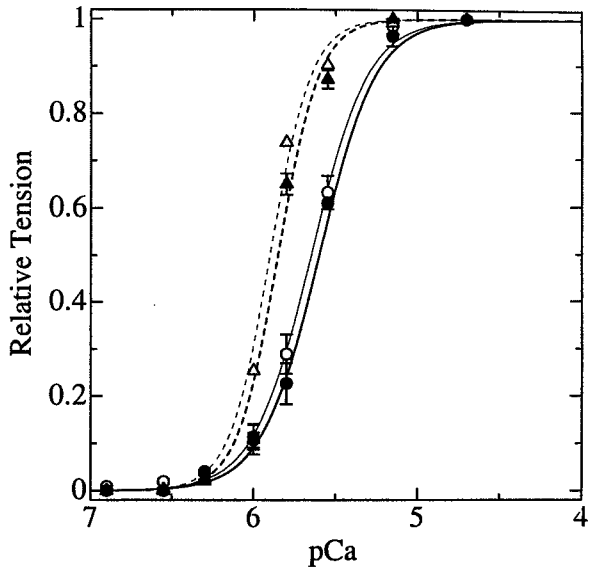

FIGURE 10 pCa-tension relation of intact and thin-filament-reconstituted fibers. ○, thin solid line, untreated cardiac muscle; △, thin dashed line, untreated skeletal muscle; ●, thick solid line, thin filament-reconstituted cardiac muscle fibers using cardiac nTm; ▲, thick dashed line, thin-filament-reconstituted cardiac muscle fibers using skeletal nTm. With the exception of untreated skeletal muscle, SDs of three data points are indicated by vertical bars. Solid and broken lines are fitted, respectively, for cardiac and skeletal nTm's by Hill equations with different Hill coefficients (n_H) and pCa values at half-maximum tension (pCa_{50}). For untreated cardiac muscle, n_H = 2.5, pCa_{50} = 5.6_5; for cardiac muscle reconstituted with cardiac nTm, n_H = 2.5, pCa_{50} = 5.6; for untreated skeletal muscle, n_H = 3.5, pCa_{50} = 5.9; and for cardiac muscle reconstituted with skeletal nTm, n_H = 3.5, pCa_{50} = 5.8_5.

(data not shown). This is attributable to the capping protein tropomodulin (Gregorio et al., 1995), which is located at the pointed ends of thin filaments. It has been reported that the removal of this capping protein results in the ability to bind G-actin to the pointed ends of thin filaments in skeletal muscle (Ishiwata and Funatsu, 1985) and in cardiac myocytes (Gregorio et al., 1995). The capacity of actin filaments to become nuclei for polymerization at their pointed ends does not appear to depend on the length of the fragments remaining at the Z line, because polymerization occurs to the same extent, even at both ends of the I-Z-I brush, in which filament length has been shown to be nearly equal to that of an intact filament (Ishiwata and Funatsu, 1985).

Reconstitution of thin filaments

We have shown that Ca^{2+} sensitivity can be restored only by adding tropomyosin-troponin complexes to the actin filament-reconstituted fibers. As shown in Fig. 10, the cooperativity (n_H) and Ca^{2+} sensitivity (pCa_{50}) of thin-filament-reconstituted fibers were nearly the same as those of intact fibers. The reconstitution of nTm was also confirmed by SDS-PAGE, although we could not estimate the quantity of reconstitution because of a small amount of protein. When nTm from skeletal muscle was used, on the other hand, reconstituted fibers showed a pCa-tension relation resembling that of skeletal muscle fibers. This indicates that the pCa-tension relation is determined only by the type of tropomyosin-troponin complexes used.

In this study, incubation for 12 h in nTm solution was needed to fully restore Ca^{2+} regulation (Fig. 9). This slow reconstitution is attributable mainly to the slow diffusion of nTm in the fiber (Kraft et al., 1995). The recovery time may be shortened by incubation at a higher temperature in the presence of Ca^{2+}, that is, by annealing treatment, at a temperature (e.g., 30°C) at which the functions of the contractile system are not damaged (Ishiwata, 1973; Ishiwata and Kondo, 1978).

We have shown that a muscle contractile apparatus with a higher order structure and function can be constructed by self-assembly of the constituent proteins when the nucleus or the template is located at an appropriate position. It was recently reported that actin filaments appear together with precursors of the Z-line structure in myofibrillogenesis (Rhee et al., 1994; cf. Fischman, 1972). Therefore, the self-assembly of thin filaments as revealed here may play a role in the late stage of I-Z-I brush formation. Furthermore, the splitting and growth of thin filaments may play a role in protein turnover after muscle cell maturation, especially in cardiac muscle, in which nebulin is absent (cf. Imanaka-Yoshida et al., 1993). This absence of nebulin lowers the stability of the thin-filament structure as compared to that of skeletal muscle, which does contain nebulin.

Tension augmentation of thin filament-reconstituted fibers

The present results demonstrate that active tension is not only restored but actually augmented by reconstitution of

actin (thin) filaments. In cardiac muscle, the length distribution of thin filaments is broad and the average length is shorter than that of skeletal muscle (Robinson and Winegrad, 1977; cf. Fig. 5). Therefore, the augmented tension restoration is attributable mainly to the greater length of reconstituted actin filaments; in the case shown in Fig. 5, the number of available cross-bridges is estimated to have increased by 140%, consistent with the degree of tension augmentation.

However, levels of augmentation as high as 250% as shown in Fig. 8 *a* may be at least partially mediated by other mechanisms, including 1) deterioration of tension generation in untreated fibers due to partial dissociation of thin filaments and/or partial removal of TN-C, 2) changes in sarcomere length, and/or 3) the presence of an inhibitory system in untreated fibers that was not restored in the present reconstitution treatment.

As for the first possibility, we confirmed that neither extensive thin-filament dissociation nor TN-C removal occurred during storage in glycerol solution at −20°C, because the tension of untreated glycerinated fibers was estimated to be 86 ± 3 kN/m^2 (mean ± SD, n = 3; the cross-sectional area was determined using confocal images), i.e., it exceeded the average values reported to date (Saeki et al., 1991; Allen and Kentish, 1985). In addition, marked tension augmentation was also observed when fresh fibers, which had been chemically skinned with 1% Triton X-100, were used (data not shown). The second potential mechanism would make a negligible contribution because fully activated tension is minimally affected by sarcomere lengths at around 2.0 μm in skinned cardiac muscle; we confirmed that the tension variation in untreated fibers was only 10% at most between 1.8 and 2.2 μm.

As for the third possibility, an inhibitory system, if one does exist, it must be associated with thin filaments, because other components were observed to be unchanged during the treatments. One possible candidate is nebulette, a recently identified member of the nebulin family. The molecular size of nebulette is, however, small, and it is located near the Z-line (Moncman and Wang, 1995). The cardiac contractile apparatus in vivo is probably specialized so as not to develop the maximum degree of tension.

Application of reconstituted fibers

As an application of this reconstituted system, we examined the effect of RhPh on the tension generation of actin filament-reconstituted fibers without nTm. Recent studies have made it possible to measure the force produced between a single myosin molecule and an actin filament using optical tweezers or a glass microneedle. The technique requires staining of actin filaments with fluorescent dye, usually Rh-Ph, but it is not yet clear whether an actin filament thus stained produces the same amount of force as an unstained filament. Our actin filament-reconstituted system can be applied to measuring both the force produced by an untreated actin filament and that produced after staining with Rh-Ph. Active tension of the actin filament-reconstituted fibers was unaffected by staining with 3.3 μM RhPh in relaxing solution for 2 h at 0°C (data not shown). This result is consistent with that obtained using glycerinated skeletal muscle fibers (Bukatina and Fuchs, 1994).

Finally, we would like to stress that our system is potentially useful for studying the structures and functions of mutant actin and regulatory proteins. Furthermore, reconstitution of thin filaments using fluorescent dye-labeled or spin-labeled proteins will make it possible to study the conformational changes in the constituent proteins of thin filaments accompanying muscle contraction and the molecular mechanisms by which these processes are regulated.

We thank Dr. H. Kanbara of the Central Research Laboratory, Hitachi, for the use of a confocal microscope; Dr. S. Umemura of Advanced Research Laboratory, Hitachi, for encouragement; and Drs. Y. Saeki of Tsurumi University and H. Higuchi of Exploratory Research for Advanced Technology for their critical reading of an early version of the manuscript.

H. Fujita is the recipient of a Research Fellowship from the Japan Society for the Promotion of Science for Young Scientists. This research was partly supported by Grants-in-Aid for Scientific Research (07680728 and 07558227 to SI) and for Scientific Research on Priority Areas (06213233 to SI) from the Ministry of Education, Science, Sports and Culture of Japan and the Uehara Memorial Foundation.

REFERENCES

Allen, D. G., and J. C. Kentish. 1985. The cellular basis of the length-tension relation in cardiac muscle. *J. Mol. Cell Cardiol.* 17:821–840.

Bukatina, A., and F. Fuchs. 1994. Effect of phalloidin on the ATPase activity of striated muscle myofibrils. *J. Muscle Res. Cell Motil.* 15: 29–36.

Ebashi, S., A. Kodama, and F. Ebashi. 1968. Troponin. I. Preparation and physiological function. *J. Biochem.* 64:465–477.

Fischman, D. A. 1972. Development of striated muscle. *In* The Structure and Function of Muscle, Vol. 1, 2nd Ed. G. H. Bourne, editor. Academic Press, New York. 75–148.

Fraenkel-Conrat, H., and R. C. Williams. 1955. Reconstitution of active tobacco mosaic virus from its inactive protein and nucleic acid components. *Proc. Natl. Acad. Sci. USA.* 41:690–698.

Fukada, N., H. Fujita, T. Fujita, and S. Ishiwata. 1996. Spontaneous tension oscillation in skinned bovine cardiac muscle. *Pflügers Arch.* In press.

Funatsu, T., T. Anazawa, and S. Ishiwata. 1994. Structural and functional reconstitution of thin filaments in skeletal muscle. *J. Muscle Res. Cell Motil.* 15:158–171.

Funatsu, T., H. Higuchi, and S. Ishiwata. 1990. Elastic filaments in skeletal muscle revealed by selective removal of thin filaments with plasma gelsolin. *J. Cell Biol.* 110:53–62.

Funatsu, T., E. Kono, H. Higuchi, S. Kimura, S. Ishiwata, T. Yoshioka, K. Maruyama, and S. Tsukita. 1993. Elastic filaments in situ in cardiac muscle: deep-etch replica analysis in combination with selective removal of actin and myosin filaments. *J. Cell Biol.* 120:711–724.

Gregorio, C. C., A. Weber, M. Bondad, C. R. Pennise, and V. M. Fowler. 1995. Requirement of pointed-end capping by tropomodulin to maintain actin filament length in embryonic chick cardiac myocytes. *Nature (Lond.).* 377:83–86.

Horiuti, K., H. Higuchi, Y. Umazume, M. Konishi, O. Okazaki, and S. Kurihara. 1988. Mechanism of action of 2,3-butanedione 2-monoxime on contraction of frog skeletal muscle. *J. Muscle Res. Cell Motil.* 9:156–164.

Hu, D. H., S. Kimura, and K. Maruyama. 1986. Sodium dodecyl sulfate gel electrophoresis studies of connectin-like high molecular weight proteins

of various types of vertebrate and invertebrate muscles. *J. Biochem.* 99:1485–1492.

Huxley, A. F., and R. Niedergerke. 1954. Interference microscopy of living muscle fibres. *Nature (Lond.).* 173:971–973.

Huxley, H. E., and J. Hanson. 1954. Changes in the cross-striations of muscle during contraction and stretch and their structural interpretation. *Nature (Lond.).* 173:973–976.

Imanaka-Yoshida, K., J. M. Sanger, and J. W. Sanger. 1993. Contractile protein dynamics of myofibrils in paired adult rat cardiomyocytes. *Cell Motil. Cytoskeleton.* 26:301–312.

Ishiwata, S. 1973. A study on the F-actin-tropomyosin-troponin complex. I. Gel-filament transformation. *Biochim. Biophys. Acta.* 303:77–89.

Ishiwata, S., and T. Funatsu. 1985. Does actin bind to the ends of thin filaments in skeletal muscle? *J. Cell Biol.* 100:282–291.

Ishiwata, S., and H. Kondo. 1978. Studies on the F-actin·tropomyosin·troponin complex. II. Partial reconstitution of thin filament by F-actin, tropomyosin and the tropomyosin binding component of troponin (TN-T). *Biochim. Biophys. Acta.* 534:341–349.

Katsura, I., and H. Noda. 1973. Assembly of myosin molecules into the structure of thick filaments of muscle. *Adv. Biophys.* 5:177–202.

Kondo, H., and S. Ishiwata. 1976. Uni-directional growth of F-actin. *J. Biochem.* 79:159–171.

Kraft, T., M. Messerli, B. Rothen-Rutishauser, J.-C. Perriard, T. Wallimann, and B. Brenner. 1995. Equilibration and exchange of fluorescently labeled molecules in skinned skeletal muscle fibers visualized by confocal microscopy. *Biophys. J.* 69:1246–1258.

Kurokawa, H., W. Fujii, K. Ohmi, T. Sakurai, and Y. Nonomura. 1990. Simple and rapid purification of brevin. *Biochem. Biophys. Res. Commun.* 168:451–457.

Laemmli, U. K. 1970. Cleavage of structural proteins during the assembly of the head of bacteriophage T4. *Nature (Lond.).* 227:680–685.

Li, T., N. Sperelakis, R. E. Teneick, and J. Solaro. 1985. Effects of diacetyl monoxime on cardiac excitation-contraction coupling. *J. Pharmacol. Exp. Ther.* 232:688–695.

Locker, R. H., and D. J. C. Wild. 1986. A comparative study of high molecular weight proteins in various types of muscle across the animal kingdom. *J. Biochem.* 99:1473–1484.

Maw, M. C., and D. J. C. Rawe. 1986. The reconstitution of myosin filaments in rabbit psoas muscle from solubilized myosin. *J. Muscle Res. Cell Motil.* 7:1473–1484.

Moncman, C. L., and K. Wang. 1995. Nebulette: a 107 kD nebulin-like protein in cardiac muscle. *Cell Motil. Cytoskeleton.* 32:205–225.

Nomura, M. 1974. Assembly of bacterial ribosomes. *J. Supramol. Struct.* 2:163–165.

Oosawa, F., and S. Asakura. 1975. Thermodynamics of the Polymerization of Protein. Academic Press, New York.

Rhee, D., J. M. Sanger, and J. W. Sanger. 1994. The premyofibril: evidence for its role in myofibrillogenesis. *Cell Motil. Cytoskeleton.* 28:1–24.

Robinson, T. F., and S. Winegrad. 1977. Variation of thin filament length in heart muscle. *Nature (Lond.).* 267:74–75.

Saeki, Y., M. Kawai, and Y. Zhao. 1991. Comparison of crossbridge dynamics between intact and skinned myocardium from ferret right ventricles. *Circ. Res.* 68:772–781.

Spudich, J. A., and S. Watt. 1971. The regulation of rabbit skeletal muscle contraction. I. Biochemical studies of the interaction of the tropomyosin-troponin complex with actin and the proteolytic fragments of myosin. *J. Biol. Chem.* 246:4866–4871.

Taniguchi, M., and H. Ishikawa. 1982. In situ reconstitution of myosin filaments within the myosin extracted myofibril in cultured skeletal muscle cells. *J. Cell Biol.* 92:324–332.

Tawada, K., A. Yoshida, and K. Morita. 1976. Myosin-free ghosts of single fibers and an attempt to re-form myosin filaments in the ghost fibers. *J. Biochem.* 80:121–127.

Wang, K., and J. Wright. 1988. Architecture of the sarcomere matrix of skeletal muscle: immunoelectron microscopic evidence that suggests a set of parallel inextensible nebulin filaments anchored at the Z-line. *J. Cell Biol.* 107:2199–2212.

Yamaguchi, M., M. Izumimoto, R. M. Robson, and M. H. Stromer. 1985. Fine structure of wide and narrow vertebrate muscle Z-lines. *J. Mol. Biol.* 184:621–644.

Yasuda, K., T. Anazawa, and S. Ishiwata. 1995. Microscopic analysis of the elastic properties of nebulin in skeletal myofibrils. *Biophys. J.* 68:598–608.

УДК 577.15.591

MICROSCOPIC ANALYSIS OF THE NATURE OF FORCES IN A SINGLE ACTOMYOSIN MOTOR AND ITS ASSEMBLAGE

© 1996 г. SHIN'ICHI ISHIWATA[1,2*], TAKAYUKI NISHIZAKA[1], HIROKAZU KATO[1], HISASHI TADAKUMA[1], TAKASHI IGA[1], NAOYA SUZUKI[3], HIDETAKE MIYATA[4], KAZUHIKO KINOSITA, Jr.[4]

[1] *Department of Physics, School of Science and Engineering, Tokyo, Japan*
[2] *Advanced Research Institute for Science and Engineering, Waseda University, Tokyo, Japan*
[3] *Department of Physics, Faculty of Science, Nagoya University, Nagoya, Japan*
[4] *Department of Physics, Faculty of Science and Technology, Keio University, Hiyoshi, Yokohama, Kanagawa, Japan*

Key words: muscle and nerve cells, myosin motor, optical tweezers, supercoiling of actin filament, in vitro motility assay, SPOC, myofibrils

General mechanisms of motility in many cells including neurons are quite similar to actomyosin motor, that is why the first step in studying of intrinsic mechanisms of sliding movement is to analyse the nature of forces in actomyosin motor. The mechanical and functional properties of a motor proteins were studied utilizing a new type of *in vitro* motility assay system and a microscopic system composed of laser optical tweezers and a multi-imaging system. We describe our recent experimental results on (1) the properties of the right-handed torque component of the sliding force generated by myosin motors in the presence of physiological ATP concentrations (contracting condition), (2) stepwise displacement of actin filament sliding movements, of approximately 10 nm, observed at low ATP concentrations (partial rigor condition), (3) mechanical (e.g., tensile strength and elastic modulus) and thermodynamic (e.g., lifetime of binding and changes in binding energy with external load) properties of the binding force between a single myosin motor and an actin filament in the absence of ATP (rigor condition) and (4) a new type of in vitro motility assay system composed of a single A band (a bundle of thick filaments) and a single actin filament, which is considered to be the minimum unit of motility in different cells. The manipulation and microscopic analysis, at the level of single molecules described here will contribute to the study of higher-ordered functions of motility revealed in the organized structures of muscle, nerve and other types of cells.

Actin, myosin, kinesin and other motor proteins are widely distributed in eukaryotic cells and play essential role in motility functions in cells of many types. For example, actin is able to form microfilaments (diameter 70 A) which take part in such processes as migration of embriotic cells and macrophages. Kinesin and dinein provide transport in axons of nerve cells. Kinesin is a high weight protein which consists of two polypeptide chains; globular ends of the chains being associated with microtubules possess ATPase activity, while fibrillar end is able to bind cell organelles. ATP hydrolysis is coupled with conformational changes of kinesin molecule and as a result transport of vacuoles, mitochondria, etc. takes place in axon. Studies on the nature of forces governing axonal transport may contribute to further elucidation of molecular mechanisms of neurodegeneration and to greater understanding of processes taking part in axons after recovery surgery.

It is interesting that general mechanisms of motility are similar in muscle and different types of non-muscle cells. The mould movement is sliding of actin filaments along myosin molecules coupled with ATP hydrolysis. For example, in axon kinesin slides along microtubules, and this complex (microtubule + specific accosiated protein-translocator) possesses high ATPase activity. This is quite similar to

* Address for correspondence and reprint requests: Department of Physics, School of Science and Engineering, Waseda University, 3–4–1 Okubo, Shinjuku-ku, Tokyo 169, Japan. Tel.: 81–3–5286–3437; Fax: 81–3–3200–2567.

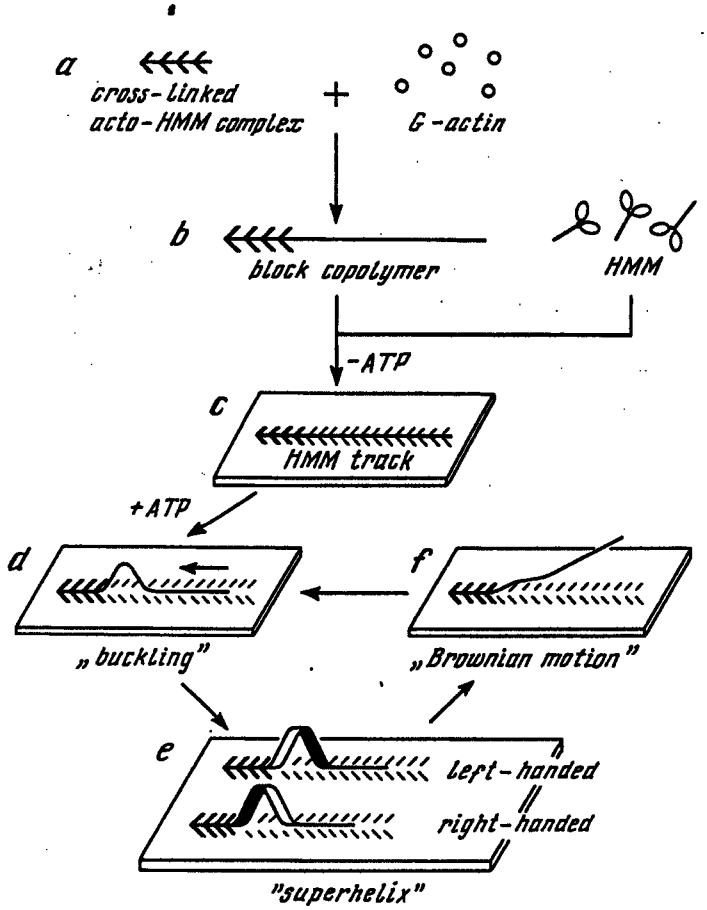

Fig. 1. A flow chart illustrating the arrangements of the artificial in vitro motility assay system, designed to determine the handedness of the torque component of the sliding force (taken from Nishizaka et al., 1993)

actomyosin motor. So, the first step in studying of intrinsic mechanisms of sliding movement in cells of many types is to carry out the microscopic analysis of the nature of forces in actomyosin motor.

At present time in becomes possible to study the molecular mechanism of sliding movement and tension generation literally, at the level of individual molecules under an optical microscope. This possibility is based on several technical breakthroughs: (1) single actin filaments can now be visualized under a fluorescent microscope via binding of a fluorescent probe, rhodamine-phalloidin [1] or by labeling ~~Cys374~~ of actin with fluorescein-isothiocyanate [2], (2) an in vitro motility assay system was designed [3] in which fluorescent actin filaments slide on the proteolytic fragments of myosin molecules (heavy meromyosin (HMM)) absorbed on a glass surface and (3) a microscopic technique, which involves laser optical tweezers [4] that can trap a plastic bead of approximately 1 micrometer in diameter with a trapping force of several tens of pN [5, 6, 7, 8, 9, 10], and a glass microneedle technique [11, 12, 13] have been introduced. Besides, progress has been made in image-processing and optical techniques [14], raising the possibility of determining the displacement of small substances [11, 12].

Supercoiling of actin filaments and the torque component of the sliding force. The sliding movement of actin filaments occurs via the interaction with myosin molecular motors; chemical energy liberated by ATP hydrolysis is effectively utilized as the mechanical energy required for sliding and performing work. Physicochemical properties of the sliding force generated by myosin motors are not, however, fully understood; for example, the sliding force vector is presumably almost parallel to the long axis of an actin filament because the filament slides longitudinally, but the direction of the sliding force developed by a single myosin motor has not been well characterized.

In an *in vitro* motility assay system, the sliding movement of actin filaments is usually smooth, but if for any reason there is an interruption in the movement of the front portion of the filament, several unusual modes of motion are possible [15]: (1) buckling at the middle portion of the filament is occasionally seen when the filament is long and the rear portion continues sliding smoothly, (2) fish-tailed motion of the rear portion of the filament occurs when the filament is not particularly long, and (3)

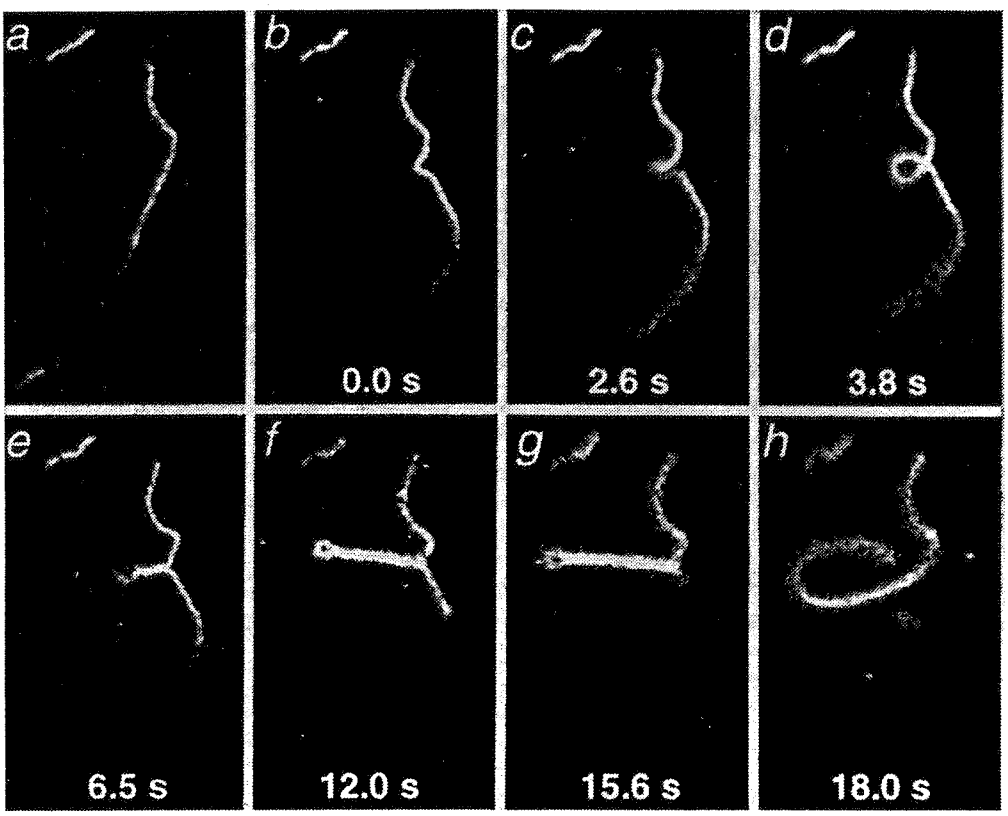

Fig. 2. An example of the supercoiling of an actin filament observed in the artificial *in vitro* motility system illustrated in Fig. 1 (taken from Nishizaka et al., 1993)

rotation on a glass surface around a fixed point, to which the anterior tip of the filament has been attached. In addition, we also noticed that the buckled portion of the filament was on occasion transformed into a single superhelix and then a loop; we speculated that this superhelix formation represents a twist in the filament due to the torque component in the sliding force. We examined the nature of the superhelix; although the proportion of right-handed superhelices predominated (the ratio of right- to left-handed superhelices was approximately 7:3), we could not determine the direction of torque because we had no means of determining which portion of the actin filaments, front or rear, is rotated.

Encouraged by the above observation, we devised an artificial *in vitro* motility system which is schematically illustrated in Fig. 1 [16]. The front portion of an actin filament was fixed on the glass surface through covalently cross-linked HMM molecules preventing the front portion of the filament from rotating. In addition, taking advantage of the preferential polymerization of actin at the rear tip (usually called B-end) of the filament [17], we prepared block co-polymers in which the rear portion of the actin filament was covered with attached HMM molecules such that the sliding movement of that portion occurred on a so-called HMM track [18]. The possibility of the buckled portion adhering to the HMM molecules adsorbed on the glass surface, other than those on the HMM track, was low; thus, the formation of the superhelix was not disturbed.

As demonstrated clearly in Fig. 2, the buckled portion was transformed into a single-turn of the superhelix (Fig. 2c) and a loop (Fig. 2d). After the loop formed, however, a multi-fold supercoil was unexpectedly formed, as shown in Figs. 2e–g. Almost all single-turn superhelices (73 out of 75 cases we observed) formed just before the multi-fold supercoil were identified as being left-handed, strongly suggesting that the rear portion of the filament slides like a right-handed screw. This is attributable to the intrinsic properties of each HMM motor producing a righthanded torque component. A similar supercoil was recently observed in a dynein-microtubule system [19]. Polymorphism of filaments, i.e., multi-fold supercoils, superhelices, loops and rings [15] (we even observed a twisted ring quite similar in appearance to supercoiled DNA [20]) may play an important role in cellular functions.

We then tried to estimate the magnitude of the torque component in a standard in vitro motility assay system, not on the HMM track [8]: first, we prepared a "bead-tailed" actin filament in which a polystyrene bead of 1 micrometer in diameter is specifically attached to the rear tip (a B-end) of the

filament through a B-end capping protein, gelsolin, which is covalently attached to the surface of the bead. The sliding velocity of the bead-tailed actin filament was indistinguishable from that of nonbeaded filaments. On the other hand the torque was not large enough to induce axial rotation of the bead-tailed sliding filament judging from the lack of any sign of rotation of the double beads attached to the B-end of an actin filament. We estimated that the vertical component of the sliding force and the torque produced on an actin filament shorter than 10 micrometer did not exceed 1 pN and 5 pN/nm, respectively, at least in the standard in vitro motility assay system in which HMM molecules are randomly oriented and no external load is imposed. The possibility remains that the torque is large enough to rotate the double beads attached to the B-end of an actin filament on an HMM track on which densely packed HMM molecules are oriented along the actin filament.

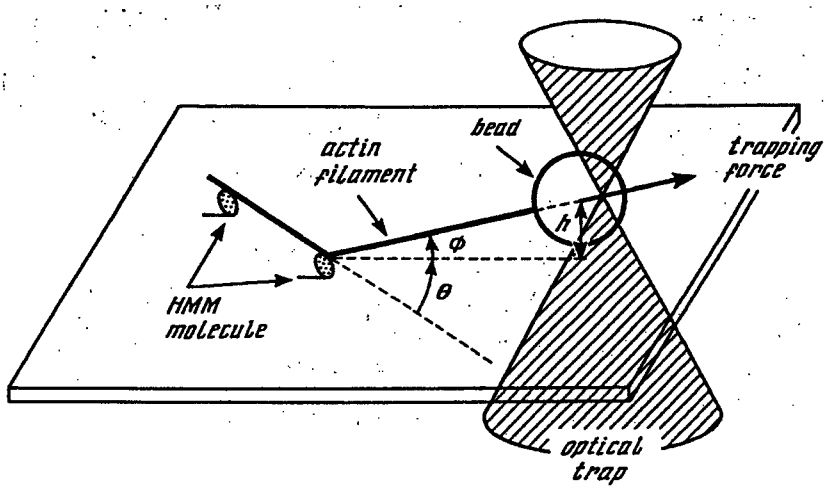

Fig. 3. Schematic illustration showing how to measure the mechanochemical properties of a single rigor bond between a single actin filament and a single HMM molecule (taken from Nishizaka et al., 1995a)

Stepwise sliding movement of actin filaments at low concentrations of ATP. Next, we examined the sliding movement of bead-tailed actin filaments under external loads which were imposed by trapping the polystyrene bead with optical tweezers. We intended to detect stepwise movement of an actin filament accompanied by the hydrolysis of ATP. To achieve this aim, we used ATP concentrations so low that only about one ATP was hydrolyzed every second. A stepwise actin filament movement of approximately 10 nm was, in fact, detectable [21]. This result is consistent with those obtained by other groups [5, 22]. A clearer step was detected by Svoboda et al. [23] in kinesin motor molecules traveling along a microtubule; the step size was 8 nm, being consistent with the size of a doublet of tubulin molecules constituting a microtubule.

Unbinding force of single rigor bond between HMM and actin filament. In the absence of ATP, myosin motor molecules form a strong bond, called a rigor bond, with an actin filament. We measured the unbinding force, the tensile strength, of a single rigor bond, using optical tweezers. An external load was imposed on the rigor bond by trapping and manipulating a polystyrene bead of a bead-tailed actin filament (Fig. 3).

The external load was imposed on a single rigor complex from various directions (Fig. 4); in addition, because the locations of HMM molecules were identifiable, we were able to measure the unbinding force of the rigor bond repeatedly on the same HMM molecule. A typical result from this experiment is shown in Fig. 5; when the external load was increased at a constant rate, i.e., 12 pN/s, the actin-HMM complex was gradually elongated and when about 15 pN was imposed, the rigor bond was broken. From this curve the relation between elongation and external load of the actin-HMM complex was obtained; the elastic modulus of the complex estimated from the slope of this relation was about 0,6 pN/nm, being nearly equal to that of cross-bridges estimated in muscle fiber.

The unbinding force of a single rigor bond thus measured showed somewhat broad distribution (ranging between 1 and 22 pN) with a peak at approximately 7 pN and an average value of 9,2±4,4 pN. We consider the broad distribution to be attributable to the manner in which HMM molecules bind to an

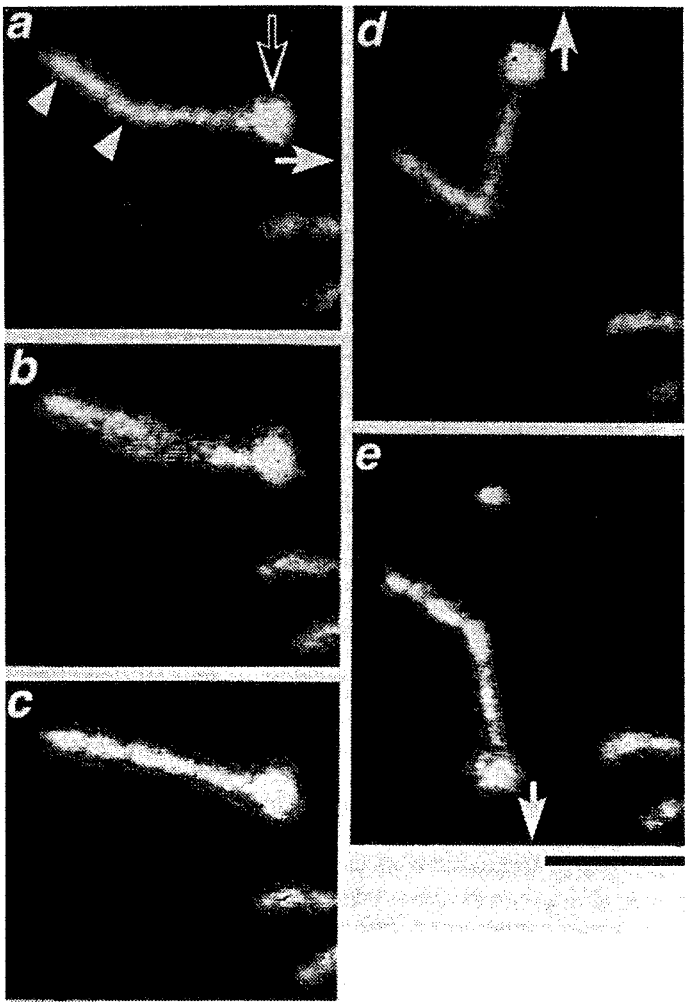

Fig. 4. A series of fluorescence micrographs showing measurement of the unbinding force of a rigor bond between a single actin filament and a single HMM molecule (taken from Nishizaka et al., 1995a)

actin filament being heterogeneous. This heterogeneity is due to attachment of HMM molecules to the glass sufrace and/or because there was an appreciable amount of one-head binding as well as two-head binding as well as two-head binding of HMM molecules.

The repeated measurements of unbinding force for each rigor complex indicate that the properties of the rigor bond were unchanged despite the bond being forcibly broken several times by the external loads (Fig. 6a). Furthermore, the unbinding force did not depend on the external load direction within the range of ±90° (Fig. 6b). These properties are attributable to the presence of rotational freedom at the head-rod junction of HMM molecules. We have noticed that each HMM molecule appeared to have its own characteristics, i.e., individuality, for the unbinding force; the origin of this individuality remains to be elucidated.

Lifetime of single rigor bond between HMM (or S1) and actin filament. Next, we attempted to clarify the thermodynamic properties of a single rigor bond. We examined the effects of external loads on the lifetime of a rigor bond. In this experiment, a sudden stepwise external load was imposed on the rigor bond, and the time that elapsed before unbinding occurred (lifetime of a rigor bond) was measured, repeatedly, on each rigor bond. The results are summarized in Fig. 7; although the variations between HMM molecules were large, as was the case in Figs. 6a and b, it was clear that the lifetime was shortened as the imposed load increased (note the lines sloping downwards to the right in Fig. 7). Here, the aforementioned individuality of HMM molecules was observed again.

The lifetime of a rigor bond without an external load was previously measured in solution and reported to be approximately 10^3 s [24]. The lifetime of an actin-HMM complex of approximately 10^3 s

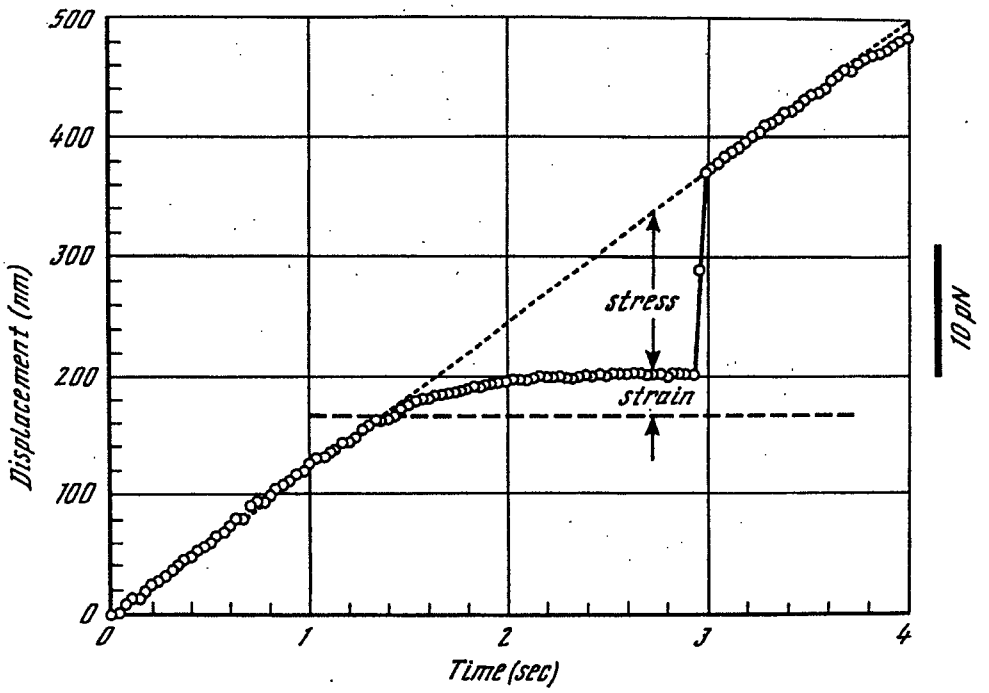

Fig. 5. Example showing measurement of the unbinding force of a single rigor bond between a single HMM molecule and an actin filament, and the elastic modulus of a single acto-HMM complex. Dotted line, movement of the trap center; circles, movement of the bead to which a single actin filament had been attached (taken from Nishizaka et al., 1995a)

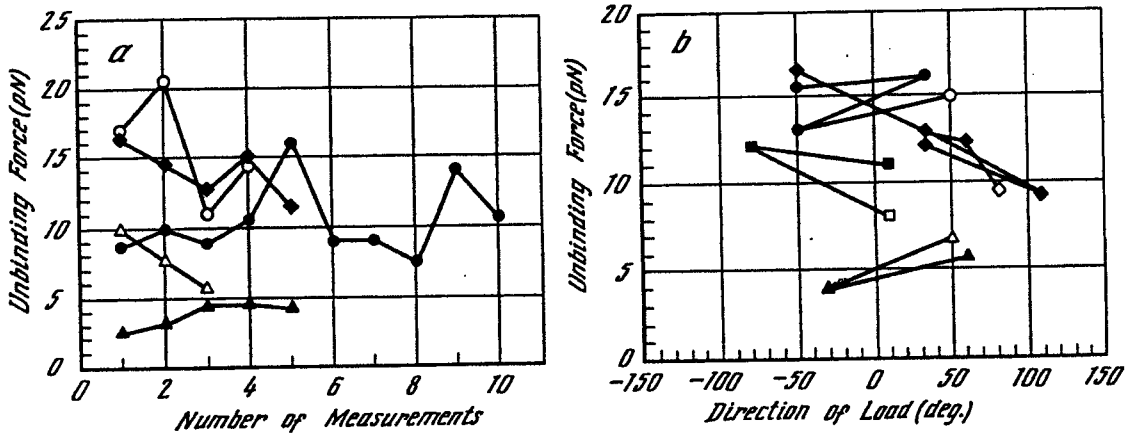

Fig. 6. Effects of the number of measurements (a) and the direction (theta; shown in Fig. 3) of the external loads (b) on the unbinding force measured on the same HMM molecules. Different symbols represent different HMM molecules. Open and closed symbols in (b) indicate the first and subsequent measurements, respectively (taken from Nishizaka et al., 1995a)

was recently confirmed, under conditions identical to those of the present experiment, by measuring the time during which a short actin fragment showed large rotational Brownian movement around a single HMM molecule [25]. The lifetime was found to be decreased to 10^2 s in the case of an actin-S1 complex.

Thus, the lifetime, tau(F), of a rigor bond under the imposed load, F, was decreased to 10^3 of that without a load, tau(0), by imposing an external load on the order of 10 pN, tau(10pN) ~ 1 s; cf. Fig. 7). Because the ratio of the lifetimes, fau(F)/tau(0), is considered to represent the ratio of the probability of binding, it is determined by the Boltzmann factor, that is, tau(F) = tau(0)exp(–Fd/kBT), where d is the interaction distance, kB the Boltzmann constant and T the absolute temperature. Thus, the interaction distance of the rigor bond is about 3 nm (= ln(10^3)kBT/10), being an order of magnitude larger than the distance typically observed. This suggests that the pull of the actin filament in the direction opposite the

power stroke of myosin crossbridges effectively decreased the activation energy barrier for unbinding. Such properties, i.e., intermolecular interactions which are very sensitive to stress, are expected to be characteristic of motor proteins.

Motility assay in a single A band. Recently, we devised a new motility system in which a single actin filament slides and develops tension in a single A band [26]. The single A band was prepared under a phase-contrast microscope from a rabbit psoas glycerinated myofibril, employing several microscopic

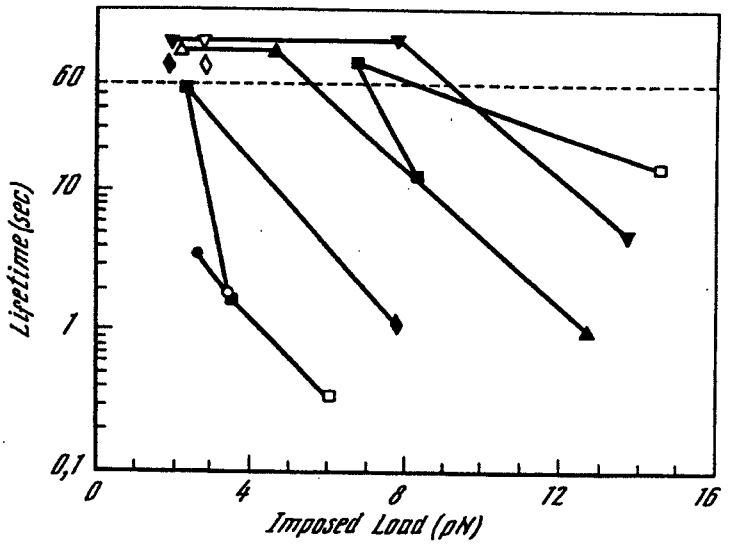

Fig. 7. Effects of the imposed loads on the lifetime of the rigor bond. Meanings of symbols correspond to those in Fig. 6b (taken from Nishizaka et al., 1995a)

techniques to remove organized structures other than the bands, e.g., selective removal of thin filaments by gelsolin treatment [27].

The isolated A band is composed of a bundle of thick filaments, which is considered to maintain the native structure of a thick filament lattice. We consider this to be the minimum functional unit of the skeletal muscle contractile system. It was possible to examine the sliding movement and tension development of a single actin filament under physiological conditions without using methyl cellulose [28] because the actin filament can not escape from the filament lattice even when weakly bound to myosin heads.

We preliminarily examined the tension generated on a single bead-tailed actin filament, using the optical tweezers, at different ionic strengths. The length of the portion of an actin filament entering the A band, i.e., the length of the overlapping region, could be determined by comparing the fluorescent image of the actin filament with the phase-contrast image of the A band, although the estimation error was ±20%, especially with small overlap, because of the limited spatial resolution of fluorescence microscopy. Thus, the average number of interacting cross-bridges could be estimated; it should be noted here that the maximum number of available myosin molecules interacting with the actin filament is about 75 with maximal overlap (about 0,7 micrometer).

The average tension produced by each myosin molecule was estimated to be 0,5 pN at 25 mM KCl (the same solvent condition as that used for the in vitro motility assay) and 0,4 pN at 100 mM KCl, suggesting that the tension decreases as the ionic strength increases. On the other hand, the ratio of the width of tension fluctuation and the average tension appeared to become smaller as the ionic strength increased, suggesting that the average number of interacting cross-bridges decreased with increasing ionic strength. When the laser light was turned off, free sliding of the actin filament could be seen; the initial sliding velocity at 30°C was about 11 micrometer/s.

The A band motility assay system devised here will be useful for studying higher order functions of the muscle contractile system; for example, the spontaneous oscillatory contraction (SPOC) recently recognized in a myofibril [29, 30, 31] is expected to be observable in this minimum unit of a sarcomere (precisely speaking, a half sarcomere). In this sense, the A band motility assay system will serve as a bridge from the single molecule level to that of higher-order physiological systems.

CONCLUSION

Research on molecular motors in muscle, nerve and other cells has entered a new era because it has become possible to manipulate a single protein molecule under an optical microscope and examine its physiological functions and mechanical and thermodynamic properties, literally. We anticipate that the mechano-chemical coupling (relation between mechanical events and chemical reactions) in single molecular motors will soon be elucidated. At the same time, we hope that in the near future, higher-order functions and properties inherent to the organized structure will be elucidated from the physico-chemical properties of single molecules.

ACKNOWLEDGMENTS

This research was supported in part by Grants-in-Aid for Scientific Research from the Ministry of Education, Science, Sports and Culture of Japan. We would like to thank Uehara Memorial Foundation for financial support.

REFERENCES

1. *Yanagida T., Nakase M., Nishiyama K., Oosawa F.* // Nature (Lond.). 1984. V. 307. P. 58–60.
2. *Honda H., Nagashima H., Asakura S.* // J. Mol. Biol. 1986. V. 191. P. 131–133.
3. *Kron S.J., Toyoshima Y.Y., Uyeda T.Q., Spudich J.A.* // Methods Enzymol. 1991. V. 196. P. 399–416.
4. *Ashkin A.* // Biophys. J. 1992. V. 61. P. 569–582.
5. *Finer J.T., Simmons R.M., Spudich J.A.* // Nature (Lond.). 1994. V. 368. P. 113–119.
6. *Miyata H., Hakozaki H., Yoshikawa H., Suzuki N., Kinosita K., Nishizaka T., Ishiwata S.* // J. Biochem. (Tokyo.). 1994. V. 115. P. 644–647.
7. *Saito K., Aoki T., Aoki T., Yanagida T.* // Biophys. J. 1994. V. 66. P. 769–777.
8. *Suzuki N., Miyata H., Ishiwata S., Kinosita K., Jr.* // Biophys. J. 1996. V. 70. P. 401–408.
9. *Nishizaka T., Miyata H., Yoshikawa H., Ishiwata S., Kinosita K., Jr.* // In: Optical methods in biomedical and environmental sciences. H. Ohzu, and S. Komatsu (Eds.). Elsevier Sci. B.V. Amsterdam. 1994. P. 195–198.
10. *Nishizaka T., Miyata H., Yoshikawa H., Ishiwata S., Kinosita K., Jr.* // Nature (Lond.). 1995. V. 377. P. 251–254.
11. *Kamimura S., Takahashi K.* // Nature (Lond.). 1981. V. 293. P. 566–568.
12. *Kishino A., Yanagida T.* // Nature (Lond.). 1988. V. 334. P. 74–76.
13. *Yanagida T., Harada Y., Ishijima A.* // Trends Biochem. Sci. 1993. V. 18. P. 319–324.
14. *Kinosita K., Jr., Itoh H., Ishiwata S., Hirano K., Nishizaka T., Hayakawa T.* // J. Cell Biol. 1991. V. 115. P. 67–73.
15. *Tanaka Y., Ishijima A., Ishiwata S.* // Biochim. Biophys. Acta. 1992. V. 1159. P. 94–98.
16. *Nishizaka T., Yagi T., Tanaka Y., Ishiwata S.* // Nature (Lond.). 1993. V. 361. P. 269–271.
17. *Kondo H., Ishiwata S.* // J. Biochem. (Tokyo). 1976. V. 79. P. 159–171.
18. *Toyoshima Y.Y., Toyoshima C., Spudich J.A.* // Nature (Lond.). 1989. V. 341. P. 154–156.
19. *Mimori, Miki-Noumura T.* // Cell Motil. Cytoskelton. 1995. V. 30. P. 17–25.
20. *Nishizaka T.* Microscopic analysis of function and mechanical properties of acto-myosin motor at single molecular level. Doctoral Dissertation (School of Science and Engineering, Waseda University). 1996.
21. *Miyata H., Yoshikawa H., Hakozaki H., Suzuki N., Furuno T., Ikegami A., Kinosita K., Jr., Nishizaka T., Ishiwata S.* // Biophys. J. 1995. V. 68. P. 286s–290s.
22. *Molloy J.E., Burns J.E., Kendrick-Jones J., Tregear R.T., White D.C.S.* // Nature (Lond.). 1995. V. 378. P. 209–212.
23. *Svoboda K., Schmidt C.F., Schnapp B.J., Block S.M.* // Nature (Lond.). 1993. V. 365. P. 721–727.
24. *Marston S.B.* // Biochem. J. 1982. V. 203. P. 453–460.
25. *Tadakuma H., Nishizaka T., Ishiwata S.* // Abstr. 51st Phys. Soc. Japan. 1996. V. 3. P. 757.
26. *Iga T., Nishizaka T., Ishiwata S.* // Biophysics (Jpn.) Suppl. 1995. V. 35. P. S208.
27. *Funatsu T., Higuchi H., Ishiwata S.* // J. Cell Biol. 1990. V. 110. P. 53–62.

28. *Uyeda T.Q.P., Kron S.J., Spudich J.A.* // J. Mol. Biol. 1990. V. 214. P. 699–710.
29. *Ishiwata S., Yasuda K.* // Phase Transitions. 1993. V. 45. P. 105–136.
30. *Ishiwata S., Okamura N., Shimizu H., Anazawa T., Yasuda K.* // Adv. Biophys. 1991. V. 27. P. 227–235.
31. *Anazawa T., Yasuda K., Ishiwata S.* // Biophys. J. 1992. V. 61. P. 1099–1108.

Поступила в редакцию
15.06.1996

МИКРОСКОПИЧЕСКИЙ АНАЛИЗ ПРИРОДЫ СИЛ, ОБЕСПЕЧИВАЮЩИХ СОКРАЩЕНИЕ АКТОМИОЗИНОВЫХ ВОЛОКОН И ИХ АНСАМБЛЕЙ

Ш. ИШИВАТА[1,2], Т. НИШИЗАКА[1], Х. КАТО[1], Х. ТАДАКУМА[1], Т. ИГА[1], Н. СУЗУКИ[3], Х. МИЯТА[4], К. КИНОШИТА[4]

[1] *Кафедра физики факультета науки и инженерии, Токио, Япония*
[2] *Исследовательский Институт науки и инженерии Университета Васеда, Токио, Япония*
[3] *Кафедра физики научного факультета Университета Нагойя, Нагойя, Япония*
[4] *Кафедра физики факультета науки и технологии Университета Кейо, Хийоши, Канагава, Япония*

Известно, что в основе подвижности, осуществляемой разными клетками, включая и нейроны, лежит работа актомиозинового комплекса. Анализ природы сил, обеспечивающих сокращение актомиозиновых волокон, является первой ступенью на пути изучения общих механизмов подвижности. В настоящей работе исследованы функции и механические свойства белков движения *in vitro*. Рассмотрены: (1) свойства силы скольжения, генерируемой миозиновым мотором в присутствии физиологических концентраций АТФ; (2) ступенчатые (с шагом около 10 нм) перемещения актиновых филаментов при скольжении их в условиях низких концентраций АТФ; (3) механические (сила упругости и эластический модуль) и термодинамические (длительность и энергия связывания с внешним грузом) компоненты взаимодействия актина и миозина в отсутствие АТФ; (4) новая система для оценки подвижности *in vitro*, состоящая из пучка толстых филаментов и одного актинового волокна, которая в настоящее время считается минимальной единицей движения в живых системах.

Детальный микроскопический анализ на уровне единичных молекул может внести значительный вклад в изучение подвижности разных типов клеток (в первую очередь мышечных и нервных) и клеточных органелл.

Two-Dimensional Arrangement of a Functional Protein by Cysteine-Gold Interaction: Enzyme Activity and Characterization of a Protein Monolayer on a Gold Substrate

Yuji C. Sasaki,* Kenji Yasuda,* Yoshio Suzuki,* Tadashi Ishibashi,* Isamu Satoh,# Yasutake Fujiki,§ and Shin'ichi Ishiwata§¶

*Advanced Research Laboratory, Hitachi Ltd., Saitama 350-03, Japan; #Institute for Materials Research, Tohoku University, Sendai 980-77; and §Department of Physics, School of Science and Engineering, and ¶Advanced Research Institute for Science and Engineering, Waseda University, Tokyo 169, Japan

ABSTRACT We have characterized the functional protein, myosin subfragment 1 (S1), attached to a gold substrate by the sulfhydryl groups of cysteine in proteins. The amino groups of the regulatory light chain (RLC) isolated from myosin were labeled with a radioisotope (^{125}I), and the labeled RLC was incorporated into S1 from which the RLC had been removed. The radiation from ^{125}I showed that S1 molecules had attached to the gold and, through the interference effect of the monochromatic radiation from ^{125}I, provided information about the position of labeled RLC sites in the S1 monolayer. The interference fringes showed that the RLC was located close to the gold surface and that all of the adsorbed S1 molecules had the same orientation. We confirmed that the motor function of S1 on the gold surface is maintained by observing sliding movement at low ionic strength and by observing the detachment at high ionic strength of fluorescent actin filaments in the presence of ATP. We also found that the adsorbed S1 molecules were not removed from the Au surface by a reducing agent. Thus the Au-S bond is more stable than the S-S bond.

INTRODUCTION

A two-dimensional arrangement of molecules on a gold surface has recently been investigated through the adsorption of long-chain organic thiols; these thiols formed well-ordered monolayers of molecules by self-assembly driven by the formation of stable gold-sulfide (Au-S) bonds and van der Waals interactions between the side chains of the molecules (Whitesides and Laibinis, 1990). This technique of forming self-assembled monolayers can be used to create new kinds of functionalized surfaces that are suitable, for example, for molecular recognition, which is an essential biological phenomenon.

Two-dimensional arrangements have also been formed when protein molecules were electrostatically adsorbed to a positively charged Langmuir-Blodgett (LB) film (Sasaki et al., 1993, 1994a; Caffrey and Wang, 1995) and hydrophobically adsorbed to a nitrocellulose-coated surface (Kron et al., 1991; Suzuki et al., 1996), a silicone-treated surface (Harada et al., 1990), or a hexamethyldisilazane (HMDS)-treated surface (Nishizaka et al., 1995). Two-dimensional arrangements of protein molecules have also been formed by allowing the molecules to adsorb onto biotin-containing bioreactive surfaces (Muller et al., 1993). These techniques cannot, however, provide protein molecules that have the same orientation, and they are highly dependent on the quality of the modified surfaces. Although organofunctional silane coupling agents on the glass surface also have been successfully used to improve the chemisorption on the surface, the functional sites at the ends of silane coupling agent are also found to interact with the silica surface (Moses et al., 1978; Chiang et al., 1980). Thus the efficiency of the reaction between the proteins and the functional sites is very low.

In the work described in this report, we have characterized the arrangement and enzymatic activity of a functional protein adsorbed onto a gold substrate by direct attachment of the sulfhydryl (SH) groups of cysteine in the protein. This adsorption technique was used because of the stable Au-S reaction between the Au surface, which is an atomically flat and clean single Au surface (Hallmark et al., 1987), and the SH group of cysteine, which is highly reactive, in the protein.

We have chosen myosin molecules as an enzyme that appears to be suitable for applying this technique, because large conformational changes are expected. Myosin is an asymmetrical molecule of about 480 kDa, and it consists of two heavy chains and four light chains. Myosin molecules can be digested into two parts by limited proteolysis with papain: two subfragments, about 130 kDa each (called S1), and one rod-shaped fragment (called myosin rod), with a molecular mass of about 220 kDa. A pair of light chains with molecular masses between 15 and 22 kDa (an essential light chain (ELC) and a regulatory light chain (RLC)), are associated with each S1 molecule. In an in vitro motility assay recently invented to observe the mechano-chemical coupling of molecular motors such as myosin and kinesin, motor molecules are usually bound to a hydrophobic surface on a glass slide. With these methods it is difficult, however, to control the orientation of the motor molecules in this assay, because they have many hydrophobic sites.

Received for publication 3 June 1996 and in final form 8 January 1997.

Address reprint requests to Dr. Yuji C. Sasaki, Advanced Research Laboratory, Hitachi Ltd., Hatoyama, Saitama 350-03, Japan. Tel.: 81-492-96-6111; Fax: 81-492-96-6006; E-mail: ycsasaki@harl.hitachi.co.jp.

0006-3495/97/04/1842/07 $2.00

There have recently been several reports of attempts to arrange motor molecules at a fixed orientation on a glass surface, for example, with the use of specific binding of an avidin-biotin system (Itakura et al., 1993). The direct attachment to a gold surface through the SH group in a certain cysteine residue of a protein is an alternative and powerful technique for arranging the proteins in a vertical direction. The technique of interference pattern from radioisotopes (IPR) can be used to determine the position of a specific site of arranged proteins to which radioisotopes are incorporated (Sasaki et al., 1994a). In the present approach, the vertical movement of the two-dimensionally arranged myosin monolayer may be observed if the conformational changes of myosin molecules occur because of changes in environmental conditions.

MATERIALS AND METHODS

Preparation of the specifically labeled S1 molecules

Myosin prepared from rabbit skeletal white muscle was digested with papain in the presence of Mg^{2+} at 25°C for 8 min to obtain S1, which was purified by high-performance gel filtration (Superose 6; Pharmacia, Piscataway, NJ) (Kron et al., 1991). The regulatory light chain (RLC) was isolated by treating the myosin with 5,5'-dithiobis(2-nitrobenzoic acid) for 10 min at 4°C (Wagner, 1982). The isolated RLC (1.13 mg/ml) was labeled with di[^{125}I]-Bolton-Hunter (BH) reagent (Dupont, DE), which was reacted with amino groups in the protein molecules, in a 5 mM phosphate buffer (pH 8.0) for 1 h at 25°C (Bolton and Hunter, 1973). The isolated RLC (5.1×10^{-10} mole) was labeled with di[^{125}I]-BH reagent (8.0×10^{-11} mole). The ratio between the number of the RLC molecules and radioisotope reagent was approximately 6:1. After ultrafiltration, we confirmed that the ratio between the number of the RLC molecules and labeled radioisotopic reagent was approximately 12:1. On average, about one ^{125}I was incorporated into 12 RLC molecules. The radiolabeled RLC was incubated for 5 min at 25°C in a rigor solution (RS) (0.1 M KCl, 5 mM $MgCl_2$, and 10 mM 3-(*N*-morpholino)propanesulfonic acid; pH 7.0) containing 1 mM thimerosal (mercury-[(*o*-carboxyphenyl)thio]ethyl sodium salt; Sigma Chemical Co., St. Louis, MO), an SH reagent, to block the SH groups (Emoto et al., 1985). After the free thimerosal was removed, the thimerosal-labeled RLC was mixed with S1 from which the RLC had been removed in an EDTA solution (ES) (50 mM KCl, 20 mM EDTA, and 20 mM 3-(*N*-morpholino)propanesulfonic acid, pH 7.0), and was incubated for 2 h at 4°C. The S1 molecules containing the radioiodinated and thimerosal-labeled RLC were incubated on a Au substrate overnight at 4°C in RS and then washed with RS to remove the excess S1.

Preparation of S1 molecules

To check the direct reaction of the Au-S bonds between the gold surface and the S1 molecules, we examined four different preparations of S1: 1) untreated S1(S1); 2) S1 in which the SH groups of the RLC had been modified with thimerosal (S1*); 3) S1, all all the SH groups of which had been modified with thimerosal (S1**); and 4) S1, the most reactive SH group (Cys707 in the heavy chain called SH1) of which had been labeled with 5-eosinylmaleimide (EMI) ($S1^+$). The S1* was prepared as described above. The S1** was prepared by incubating untreated S1 (0.43 mg/ml) in RS containing 1 mM thimerosal for 5 min at 25°C. Four to five SH groups of S1 are thought to be labeled with thimerosal (Emoto et al., 1985). The $S1^+$ was prepared according to the method of Kinosita et al. (1984). The S1, S1*, S1**, and $S1^+$ thus obtained were labeled with di[^{125}I]-Bolton-Hunter reagent in 5 mM phosphate buffer (pH 8.0) for 1 h at 25°C to obtain the radiated S1, S1*, S1**, and $S1^+$, respectively. The radiolabeled S1, S1*, S1**, and $S1^+$ preparations were separately incubated on gold substrates overnight at 4°C in RS and then washed with RS to remove the excess S1s. We found that the S1 molecules did not adsorb to the gold substrate in the buffer containing the reduced form of glutathione, β-mercaptoethanol, or dithiothreitol (DTT) (data not shown). These SH reductants might have prevented the reaction between the S1 and Au surface and therefore were not included in the buffer used when the S1 was bound to the Au surface.

Theory of interference fringes from ^{125}I

This interference effect is generated as a result of the interaction between the direct monochromatic emission from the radioisotopes and the emission totally reflected by the substrate surface (Fig. 1). In other words, it is a Lloyd's-mirror-type interference phenomenon in the x-ray wavelength region (Sasaki et al., 1994b, 1995). Interference fringes can be clearly observed when the take-off angle (θ_t) for electron-capture x-rays emitted from radioisotopes is smaller than the critical angle (θ_c) for x-ray total external reflection. In the theoretical interference pattern from radioisotopes (IPR), we modeled three homogeneous media as stratified media: air, a layer of the myosin S1 molecules labeled with radioactive atoms (^{125}I), and a gold substrate (Fig. 2). Although there is also actually a solution layer and polyimide layer on the sample system, the interference effect of x-rays from ^{125}I is independent of the presence of these solution layers, because their thicknesses (5–7 μm) are greater than the coherence length of the measured electron-capture x-rays. These films only influence the x-ray refraction at each interface. The theoretical IPR from a stratified medium can be obtained on the basis of both the solution of Maxwell's equations for optical electromagnetic waves on each interface and the reciprocity. In other words, the calculation of the x-ray intensity from coordinate z for take-off angle θ_t is identical to that of the incident x-ray field at coordinate z for glancing angle θ_t. When radioactive atoms act as x-ray sources with distribution N, the yield Y is given by

$$I(\theta_t, z) = |E_d + E_r|^2 \tag{1}$$

and

$$Y(\theta_t) = \int N(z) I(\theta_t, z)\, dz, \tag{2}$$

where $I(\theta_t, z)$ is the intensity of x-rays due to interference effects between the direct and totally reflected emissions from coordinate z at the take-off angle (θ_t); E_d and E_r are, respectively, the E-field plane waves of the direct

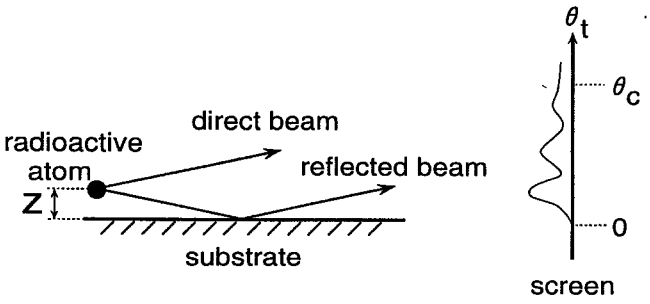

FIGURE 1 Schematic of the interference phenomenon of the electron-capture x-ray from a radioactive atom embedded within a sample. z represents the distance between the radioactive atom and the substrate surface. θ_t is the take-off angle of the electron-capture x-rays. Although emissions from radioisotopes have the form of a spherical wave, a plane wave, which is one of the components of a spherical wave, is observed under the conditions of this experiment. This is because the distance between the observation point and the atomic source points is very long.

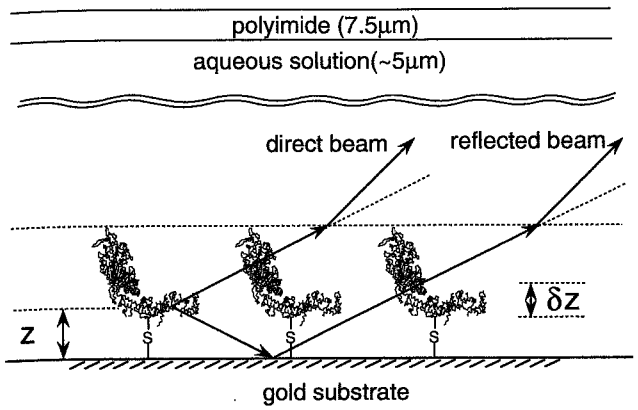

FIGURE 2 Schematic of the cross-sectional view of an ^{125}I-labeled myosin S1 monolayer and the interference phenomenon of a monochromatic radiation from ^{125}I. z and δz represent the distance between the ^{125}I atoms and the substrate surface and the distribution width of the ^{125}I atoms, respectively. There is a refraction effect at the interface between the aqueous solution layer and the S1 molecule layer. The interference fringes between the direct beam and the reflected beam from ^{125}I atoms are influenced by this refraction effect. Thus we can obtain the information about the position of the interface between the aqueous solution layer and the S1 molecule layer. The illustration of S1 was taken from Rayment et al. (1993), but the location of the SH groups is not necessarily accurate.

and reflected emissions; and $N(z)$ is the distribution of labeled atoms, ^{125}I, at a distance z from the substrate surface. In this work we calculated the theoretical angular distribution by considering the interference effect and the refraction effect at each interface of the solution layer and the polyimide film. Thus we could obtain not only the position of ^{125}I (z), but also the total thickness (in other words, the vertical total width of adsorbed S1 molecules) by considering the refraction effect at the interface between the solution layer and the layer of the S1 molecules. The intensity decay of the electron-capture x-rays was ignored by considering the long radioactive decay rate (the half-life time is 60.1 days), whereas the time taken to obtain one datum was about 24 h. In evaluating the theoretical fringes for the normalized yield, we used the following data for the values of 1 (the complex refractive indices) for Te Kα: $(3.2 + 0.0012\,i) \times 10^{-7}$ for the monolayers of protein S1, and $(5.6 + 0.018\,i) \times 10^{-5}$ for the gold substrate in which i is the imaginary unit. Those values for the complex indices of refraction were determined in the χ^2 minimization fitting of the measured interference fringes.

Instrumentation

Fig. 3 is a schematic drawing of the experimental apparatus we used for IPR measurements. The angular distribution of the electron-capture x-rays was measured by scanning the slit along the transversal direction. A slit (30 μm high and 10 mm wide) was placed before a detector at a distance of 200 mm from the sample to determine the take-off angle (θ_t). The angular distribution of electron-capture x-rays was monitored with an energy-dispersive detector (pure Ge detector; EG&G ORTEC, TN). The angular resolution in the measured region was less than 0.3 mradians. All IPR measurements were carried out at 4°C.

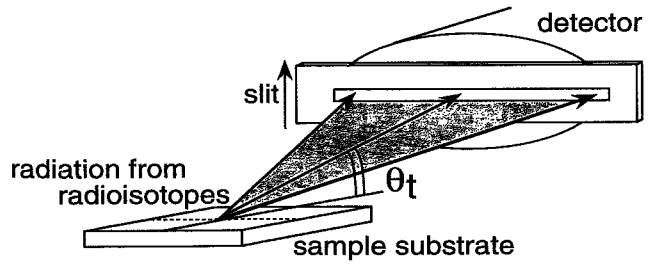

FIGURE 3 Schematic drawing of the experimental apparatus for IPR measurement. The electron-capture x-rays are monitored by a pure Ge detector through a narrow slit.

Fluorescent images of rhodamine-phalloidin-labeled actin filaments

S1 (S1, S1*, or S1**) (2 mg/ml) in RS solution was introduced on both a hexamethyldisilazane (HMDS)-coated glass coverslip and a 100.0-nm-Au-coated glass coverslip. Both of them were used just after the introduction of S1 solution or after the overnight incubation of S1 at 4°C. Just before observation, solution A (25 mM KCl, 25 mM imidazole HCl (pH 7.4), 4 mM $MgCl_2$, 1 mM EGTA, and 10 mM DTT) containing 0.5 mg/ml bovine serum albumin (BSA) was infused into the cell to coat the bare glass surface (Kron et al., 1991). For measuring the attachment of actin filaments to S1 either on the HMDS-coated or Au-coated glass surface, 0.5 μg/ml actin filaments labeled with rhodamine phalloidin in solution A were infused and then washed with solution B (i.e., solution A containing 4.5 mg/ml glucose, 0.2 mg/ml glucose oxydase, and 0.04 mg/ml catalase). The fluorescent images of rhodamine-phalloidin-labeled actin filaments were observed under a fluorescent microscope (Diaphoto-TMD, NCF Fluor ×100 objective lens, NA = 1.3; Nikon, Tokyo) equipped with a SIT camera (C1000–12; Hamamatsu Photonics K. K., Hamamatsu, Japan) and were recorded on videotape. The video data were analyzed by a computer containing a video capture board (Centris 660AV, Apple Inc., CA). To check the enzymatic activity of S1, both the motility of actin filaments on the glass surface and the detachment of actin filaments from S1 were examined at 27 ± 1°C. For the motility, solution B was exchanged for solution C (i.e., solution B containing 1 mM ATP), and the sliding movement of actin filaments was observed. For the detachment, solution C was exchanged for a high-salt solution D (i.e., solution C containing 0.6 M KCl instead of 25 mM KCl), and the disappearance of fluorescent actin filaments was observed.

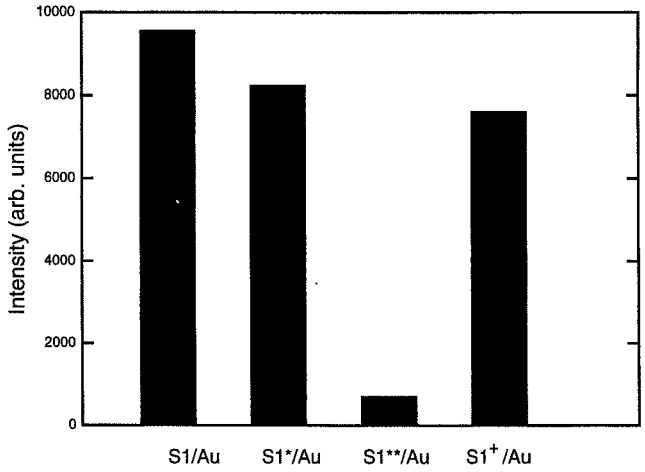

FIGURE 4 Population of ^{125}I-labeled S1 on the gold substrate after adsorption. S1/Au, S1*/Au, S1**/Au, and S1$^+$/Au, respectively, show the population of S1, S1*, S1**, and S1$^+$, the SH1 group of which was labeled with 5-eosinylmaleimide (EMI). The intensity of radiation of the ^{125}I-labeled S1s on the Au substrate was measured by pure Ge detector.

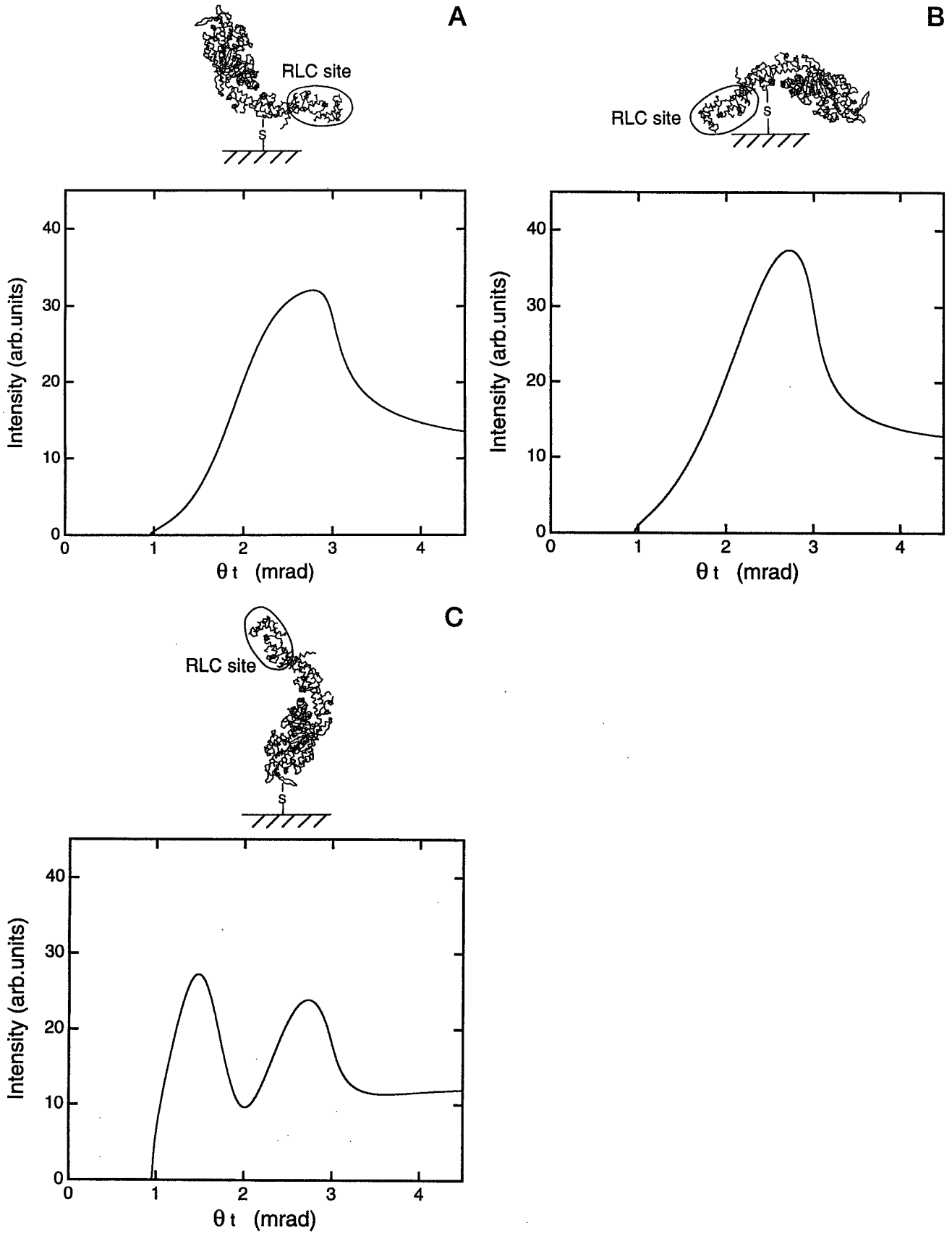

FIGURE 5 The calculated x-ray interference fringes from models *a*, *b*, and *c*. The values of total thickness (t), z_0 and δz for each model were (*a*) t = 10.0 nm, z_0 = 0.5 nm, δz = 1.0 nm; (*b*) t = 7.0 nm, z_0 = 1.0 nm, δz = 1.0 nm; (*c*) t = 14.0 nm, z_0 = 12.0 nm, δz = 3.0 nm. The illustration of S1 was taken from Rayment et al. (1993), but the location of the SH groups is not necessarily accurate.

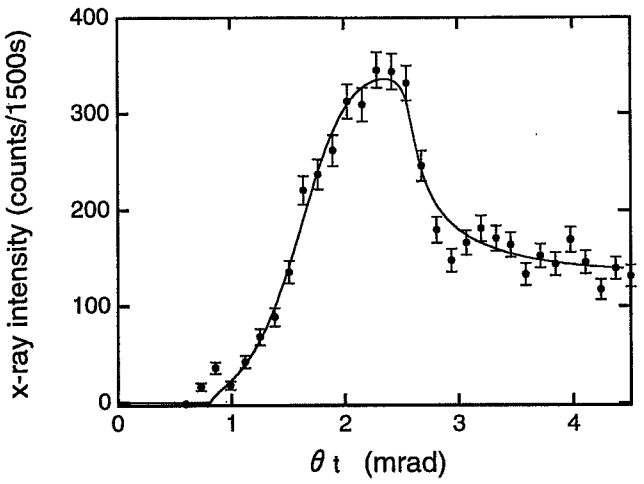

FIGURE 6 The measured angular distribution (*closed circles*) and theoretical one (*line*) of x-ray intensity from ^{125}I. The measured monochromatic radiation is the electron-capture x-rays (Te Kα) from ^{125}I. The statistical error rate for the experimental data was defined by the square root of the number of detected photons.

RESULTS AND DISCUSSION

Adsorption of S1 to a gold surface

First we checked whether the SH groups of the protein could be directly attached to the gold surface by the Au-S bonds. The selectivity in the adsorption of the gold surface was measured by the intensity of radiation from ^{125}I-labeled S1 molecules. Fig. 4 shows that the intensity of radiation from S1** was less than 1/10 of that from untreated S1, whereas that from S1* was nearly equal to that from untreated S1. In addition, we confirmed that SH1 is not the binding site for the Au substrate. These experimental results show that the adsorption of S1 on the gold surface occurs through SH groups other than those of RLC and SH1 of HC.

In additional experiments, we confirmed that the total amount of untreated S1 adsorbed on the Au substrate was approximately equal to that adsorbed on an HMDS-coated glass surface (data not shown). And we checked to see whether the reaction between the S1 and gold surface is the same as the S-S binding reaction. We found that the adsorbed S1 molecules were not removed from the gold surface by the reduced form of the glutathione, β-mercaptoethanol, or DTT. Thus S-Au binding seems to be more stable than S-S binding. These properties were important for the present experiments, because the buffer containing the reductants could be used to avoid the oxidation of the functional proteins adsorbed on the gold substrate.

Arrangement of S1 on a gold surface examined by the IPR method

We used the IPR method to obtain a vertical coordinate of the position of ^{125}I in the S1* monolayer on the Au substrate in an aqueous solution. The IPR method also revealed the vertical distribution of the RLC molecules in the S1* monolayer. The calculated angular distributions of x-ray intensity for assumed orientations of the adsorbed S1* molecules are shown in Fig. 5. In model a, the external SH site of ELC in S1* molecules (for example, Cys136 or Cys177) is directed toward the gold surface. In model b, the SH site of ELC (Cys136 or Cys177) located at the reverse side reacts with the gold surface. In model c the tip of the heavy chain (for example, Cys 402) is attached to the gold surface. In these model calculations we applied the structure of the S1 molecules according to Rayment's 3D structural data (Rayment at el., 1993). The IPRs for models a, b, and c have one and two fringes, respectively. In models a and b, the position of the first fringe peak is shifted to a lower take-off angle when the distance between the radioisotopes and the substrate surface becomes larger. In other words, the period of the calculated fringes is highly dependent on the distance between the radioisotopes and the gold surface. The orientation of the adsorbed S1 molecules can thus be determined by analyzing the interference fringes from the radioisotopes.

As shown in the interference pattern of Te Kα from ^{125}I (Fig. 6), there was one peak at 2–2.5 mradians. Below 0.7 mradians, the intensity of the x-rays could not be measured because of the x-ray refraction at the air-polyimide film interface. We calculated the theoretical interference fringes by χ^2 minimization fitting with Eq. 2. We assumed that $N(z)$ reached a maximum peak at $z = z_0$ and had a Gaussian distribution with a standard deviation σ, because the theoretical fringes are not so influenced by the fine structure of radiolabel distribution. We cannot assign each position of the radiolabeled sites from the experimental IPR when the radiolabeled sites are closer than about 1 nm. We obtained the theoretical curve in Fig. 6, in which a mean ^{125}I position $z_0 = 0.5 \pm 1.9$ nm, a Gaussian distribution width of 2σ (corresponding to δz shown in Fig. 2) = 1.0 ± 1.0 nm, and a total thickness of S1 monolayer = 10.0 ± 1.9 nm. The standard errors of z_0, 2σ, and the total thickness were obtained by χ^2 minimization fitting. Our experimental results indicated that the measured distribution of ^{125}I was Gaussian, with a width 2σ of 1.0 ± 1.0 nm. This value for the distribution of ^{125}I is much smaller than the total thickness (10.0 ± 1.9 nm) of the S1 monolayer. This value is also smaller than the size of RLC (2.4×5.2 nm). This indicates that the RLC sites are located close to the gold surface. We also obtained the position ($= 0.5 \pm 1.9$ nm) of the RLC subunit from the gold surface. The RLC subunit is located in the tail of the heavy chain. Thus we conclude that the orientation of the adsorbed S1 is as shown in model a of Fig. 5.

Considering both the structural data of S1 molecules (Rayment et al., 1993) and the above results, we infer that the binding site for the Au substrate is the cysteine in the α-helix of the heavy chain (Cys815) or in the essential light chain (Cys136 and/or Cys177). The cysteine in the α-helix of the heavy chain might be covered by the essential light chain. It is difficult to identify the binding site for the Au

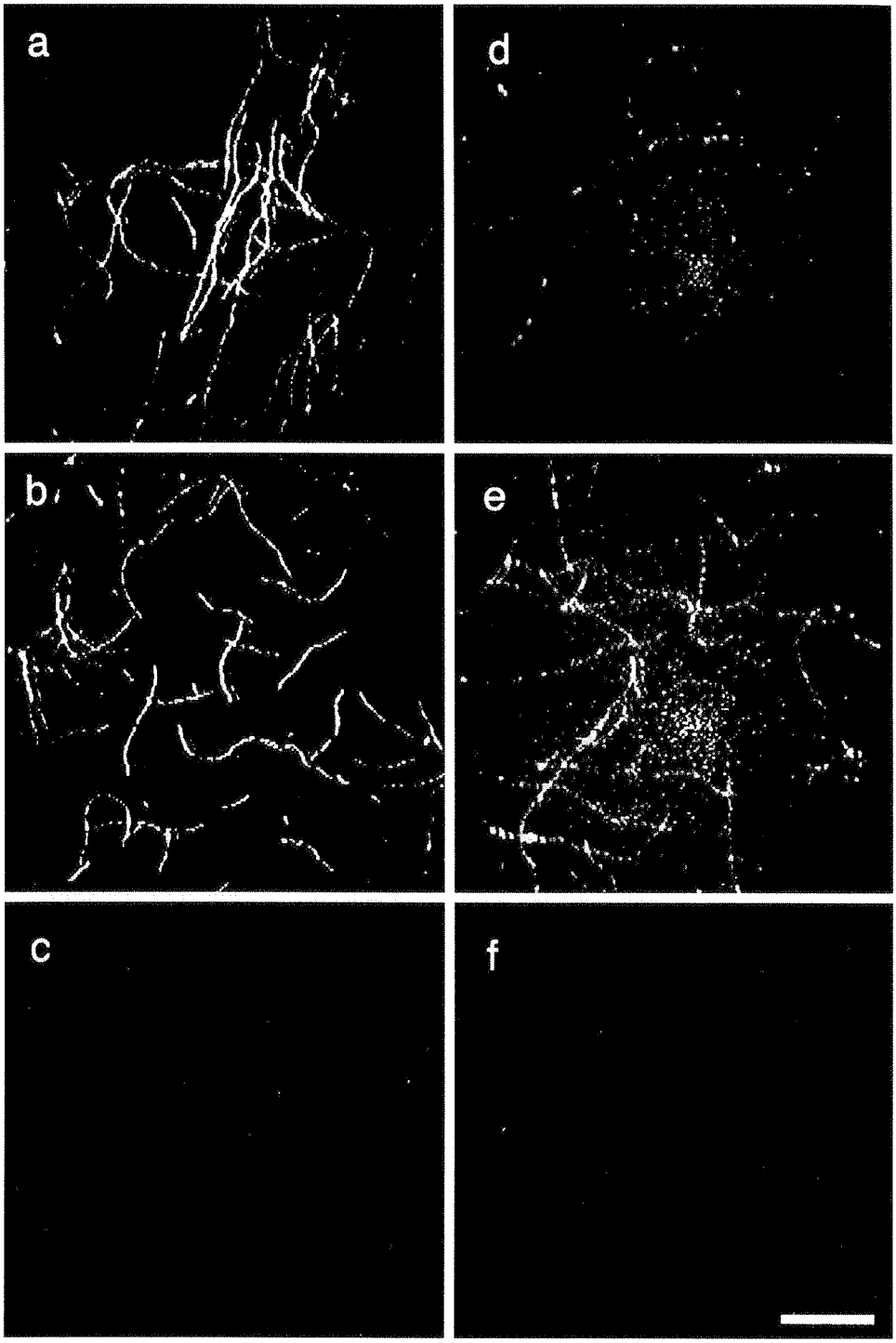

FIGURE 7 Fluorescent images of rhodamine phalloidin-labeled actin filaments. Rhodamine phalloidin-labeled actin filaments (0.5 μg/ml) (25 mM KCl, 25 mM imidazole HCl (pH 7.4), 4 mM $MgCl_2$, 1 mM EGTA, and 1 mM DTT) infused after 0.1 mg/ml S1 were introduced into the flow cell constructed from a HMDS-coated coverslip (*a–c*) or a 300.0-nm-thick Au-coated coverslip (*d–f*). (*a* and *d*) Images of actin filaments infused just after S1 was introduced under rigor conditions. (*b* and *e*) Images of actin filaments infused under the rigor condition after overnight incubation of S1 in the flow cell. (*c* and *f*) *b* and *e*, respectively, after the infusion of the high-salt solution containing ATP (0.6 M KCl, 25 mM imidazole HCl (pH 7.4), 4 mM $MgCl_2$, 1 mM EGTA, 10 mM DTT, and 1 mM ATP). In each preparation, 0.5 mg/ml BSA was infused before the introduction of actin filaments. Temperature, 27 ± 1°C. Scale bar, 10 μm. The BSA was infused into the cell to coat the bare surface to prevent the direct attachment of actin filaments to the surface.

substrate, because all of the atomic coordinates of S1 have not yet been published.

Interaction of actin filaments with S1 adsorbed on a gold surface

We examined the effects of Au-S bond formation on the physiological function of S1 by observing the interaction between the adsorbed S1 molecules and actin filaments. Although almost all actin filaments attached to the surface of the HMDS-coated glass surface (Fig. 7 *a*), none of them attached to the Au-coated glass surface (Fig. 7 *d*) under rigor conditions when the incubation time of S1 molecules was short. After overnight incubation of S1 solution, the extent of actin filaments attached to the Au-coated surface became similar to that of actin filaments attached to the HMDS-coated surface (Fig. 7, *b* and *e*). This indicates that the rate of attachment of the SH groups of S1 molecules on

the gold surface is very slow. This slow attachment was confirmed by the gradual increase in the population of attached S1 molecules (labeled with ^{125}I) (data not shown).

We examined the enzymatic activity of S1 molecules that attached to the gold surface by observing the motility of actin filaments and observing their detachment induced by the addition of high-salt solutions containing ATP. The actin filaments that attached to the gold surface on which S1 molecules had been incubated overnight in advance (Fig. 7 *e*) moved with the same velocity (about 2 μm/s) as that on the HMDS-coated surface. When a high-salt ATP solution was infused, as shown in Fig. 7, *c* and *f*, almost all of the actin filaments detached from both surfaces. Therefore, we conclude that the S1 molecules on the gold surface retain their enzymatic functions to an extent similar to that of S1 molecules on the HMDS-coated surface.

CONCLUSION

We could obtain structural and functional data concerning the monolayer array of the radioactively labeled S1 molecules on the Au substrate in an aqueous solution by analyzing the interference pattern from the radioisotopes and by using an in vitro motility assay. First, the orientation of the adsorbed S1 molecules could be determined from structural data. The IPR method thus makes it possible to obtain structural information about proteins adsorbed on a metal substrate, from a simple analysis of the interference fringes.

The advantage of the IPR method is not only that the instrumentation itself is simple, but also that the experimental analysis can be made under wet conditions without preparing single-crystal samples and without using outer primary beams. We also confirmed that the motor function of the S1 molecules is maintained when they are attached to a gold substrate. If the structural changes of the protein monolayer are synchronized with the enzymatic activity, they must be observed as the vertical movement of the position of radioactive atoms incorporated into a specific site of the protein molecules and as the changes in the total thickness of protein monolayer. In the present work we characterized the S1 monolayer on a gold surface under rigor conditions. The S1 monolayer should also be characterized in the presence of ATP and during its interaction with actin filaments.

Furthermore, we should mention that the binding reaction between Au surface and cysteine residue in the protein is stable. If cysteine residue is mutationally introduced into the outside of the protein as we like, we can control the orientation and characterization of the mutant proteins. In other fields, for example, this new covalent technique between colloidal gold probes and cysteine residue in the protein may also be useful for producing high-resolution labels that are visible in an electron microscope.

REFERENCES

Bolton, A. E., and W. M. Hunter. 1973. The labeling of proteins to high specific radioactivities by conjugation to a ^{125}I-containing acylating agent. *Biochem. J.* 133:529–539.

Caffrey, M., and J. Wang. 1995. Membrane-structure studies using x-ray standing waves. *Annu. Rev. Biophys. Biomol. Struct.* 24:351–377.

Chiang, C., H. Ishida, and J. L. Koenig. 1980. The structure of *g*-aminopropyltriethoxysilane on glass surfaces. *J. Colloid Interface Sci.* 74:396–404

Emoto, Y., T. Kawamura, and K. Tawada. 1985. Characterization of the ATPase active site in myosin subfragment-1 with the use of vanadate plus ADP as a reversible "affinity-labeling" reagent: evidence for heterogeneity in the active sites. *J. Biochem.* 98:351–377.

Hallmark, V. M., S. Chiang, J. F. Rabolt, J. D. Swalen, and R. J. Wilson. 1987. Observation of atomic corrugation on Au(111) by scanning tunneling microscopy. *Phys. Rev. Lett.* 59:2879–2882.

Harada, Y., K. Sakurada, T. Aoki, D. D. Thomas, and T. Yanagida. 1990. Mechanochemical coupling in actomyosin energy transduction studied by in vitro movement assay. *J. Mol. Biol.* 216:49–68.

Itakura, S., H. Yamakawa, Y. Y. Toyoshima, A. Ishijima, T. Kojima, Y. Harada, T. Yanagida, T. Wakabayashi, and K. Sutoh. 1993. Force-generating domain of myosin motor. *Biochem. Biophys. Res. Commun.* 196:1504–1510.

Kinosita, K. Jr., S. Ishiwata, H. Yoshimura, H. Asai, and A. Ikegami. 1984. Submicrosecond, and microsecond rotational motions of myosin head in solution, and in myosin synthetic filaments as revealed by time-resolved optical anisotropy decay measurements. *Biochemistry.* 23:5963–5974.

Kron, S. J., Y. Y. Toyoshima, T. Q. P. Uyeda, and J. A. Spudich. 1991. Assays for actin sliding movement over myosin-coated surfaces. *Methods Enzymol.* 196:399–416.

Moses, P. R., L. M. Wier, J. C. Lennox, H. O. Finklea, J. R. Lenhard, and R. W. Murray. 1978. X-ray photoelectron spectroscopy of alkylamine-silanes bound to metal oxide elctrodes. *Anal. Chem.* 50:576–585.

Muller, W., H. Ringsdorf, E. Rump, G. Wildburg, X. Zhang, L. Angermaier, W. Knoll, M. Liley, and J. Spinke. 1993. Attempts to mimic docking processes of the immune system: recognition-induced formation of protein multilayers. *Science.* 262:1706–1708.

Nishizaka, T., H. Miyata, H. Yoshikawa, S. Ishiwata, and K. Kinosita, Jr. 1995. Unbinding force of a single motor molecule of muscle measured using optical tweezers. *Nature.* 377:251–254.

Rayment, I., W. R. Rypniewski, K. Schmidt-Base, R. Smith, D. R. Tomchick, M. M. Benning, D. A. Winkelmann, G. Wesenberg, and H. M. Holden. 1993. The three-dimensional structure of myosin subfragment-1: a molecular motor. *Science.* 261:50–58.

Sasaki, Y. C., Y. Suzuki, and T. Ishibashi. 1994a. Fluorescent x-ray interference from a protein monolayer. *Science.* 263:62–64.

Sasaki, Y. C., Y. Suzuki, T. Ishibashi, and I. Satoh. 1995. Interference effect of electron-capture x-rays from an ^{125}I-labeled protein monolayer in an aqueous solution. *Anal. Sci.* 11:545–548.

Sasaki, Y. C., Y. Suzuki, Y. Tomioka, and A. Fukuhara. 1993. Observation of an interference effect for fluorescent x-rays. *Phys. Rev. B.* 48: 7724–7726.

Sasaki, Y. C., Y. Suzuki, Y. Tomioka, and T. Ishibashi. 1994b. Site determination of radioactive atoms from the interference effect of electron-capture x-rays. *Phys. Rev. B.* 50:15516–15518.

Suzuki, N., H. Miyata, S. Ishiwata, and K. Kinosita. Jr. 1996. Preparation of bead-tailed actin filaments: estimation of the torque produced by the sliding force in an in vitro motility assay. *Biophys. J.* 70:401–408.

Wagner, P. D. 1982. Preparation and fractionation of myosin light chains and exchange of the essential light chains. *Methods Enzymol.* 85:72–81.

Whitesides, G. M., and P. E. Laibinis. 1990. Wet chemical approaches to the characterization of organic surfaces: self-assembled monolayers, wetting, and the physical-organic chemistry of the solid-liquid interface. *Langmuir.* 6:87–96.

生体系材料の分子シンクロナイゼーション

石渡信一　早稲田大学・理工学部・物理学科

1．はじめに

様々な生体機能は，それに固有の酵素（群）によって担われている。それらの酵素は，酵素と相互作用するタンパク質を含めて，空間的に集合したり，あるいはさらに時間的に協調することによって，秩序だった生体機能を発揮する。例えば化学一力学エネルギー変換酵素が結晶状に配列した筋細胞では，入力信号に対して「全か無か（all or none）」の応答を示す。

一方，各酵素は，孤立した一分子のレベルでは確率的（stochastic）に機能する。酵素に結合した基質分子は，その酵素に特有の，修飾や分解などの化学変化を受けるが，それがいつ起こるかは予測できない。一般的にいって酵素反応の平均的時間は決定できるが，いちいち各酵素について反応時間を特定することはできない。従来，酵素作用のメカニズムの研究は，何兆個もの酵素分子からなる溶液系を用いて行われてきた。その結果，酵素反応が確率的に生じることを前提に，平均的な性質が明らかにされてきた。

ところが最近になって，主として蛍光顕微鏡法の進歩により，酵素一分子を“生きたまま”画像化したり，その機能を“見る”ことが出来るようになった[1)~3)]。その結果，酵素機能の確率的性質が実証された[2)]。ここでは，生体系として筋収縮系を取り上げ，運動性酵素（分子モーター）一分子のレベルから，それが高次構造へと組み上がる中で，収縮・運動機能が構成分子の機能の協調（分子シンクロナイゼーション）によってどのように組織化されるかを見ることにしよう。分子協調のメカニズムについては，未解明な点が多いこともあって具体的な形では述べない。ここで取り上げる題材のほとんどは，筆者の研究室と，協同研究先の研究室で得られた成果の中から選ぶことにする[4)~8)]。

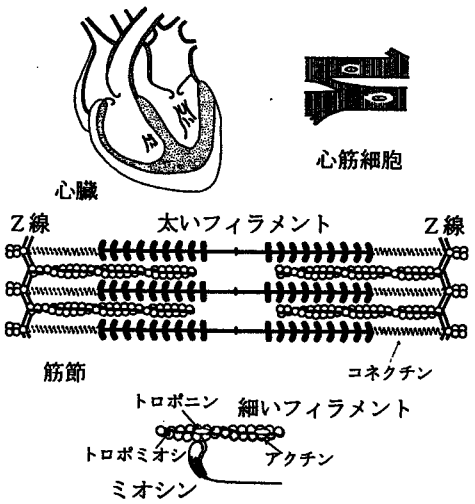

図1　心筋の階層構造

2．筋収縮系構造の階層性

本論に入る前に，まず筋収縮系の構造について概観しておこう[9)]。横紋筋の構造を心筋を例に示すと，図1のように10^{-1}mサイズの心臓という筋組織から10^{-8}mサイズの単一分子モーターに至る階層構造をなしている（赤池氏の論文中の図も参照）。筋収縮系における収縮要素は，ミオシン分子モーターと，これに相互作用するアクチン分子である。これらの収縮要素は，筋節の中でその機能を有効に加算的に発揮できるように，整然と規則的に配列している。すなわち，ミオシン分子とアクチン分子は，それぞれ繊維状に重合・集積して，長さの揃った太いフィラメントと細いフィラメントを形成している。筋節はさらに縦（直列）に繋がって一本の筋原線維を形成し，そして横方向（並列）にも整然と配列し横紋構造をなす。

細いフィラメント中のアクチンフィラメント（FA）には，制御タンパク質であるトロポミオシンとトロポニン（Ca^{2+}結合タンパク質）が周期的に結合している。一方，太いフィラメントの骨格をなすミオシンフィラメントに

も構造タンパク質が結合している。特に分子量300万の巨大タンパク質コネクチン（タイチンとも呼ばれる）が太いフィラメントの中央部からフィラメントに沿って結合し，さらに端から突き出てZ線に達して結合している。従って太いフィラメントは，コネクチン分子の弾性的な性質によって筋節の中央に繋ぎとめられていることになる。さらに骨格筋では，ネブリン（心筋には存在しない）とよばれる巨大タンパク質が，細いフィラメントに沿って引き延ばされた形で結合している。細いフィラメントの両端にはキャップタンパク質が結合しており，細いフィラメントの構造安定性に寄与している。このように筋細胞の中では，同じ種類のタンパク質が集合するだけでなく，それに何種類ものタンパク質が関与することによって，規則構造が形成され，それらが集積して階層構造をなしているのである。

3．分子モーターの一分子力学・熱力学特性の顕微解析

1）in vitro滑り運動系

ガラスなどの基板上に吸着させたミオシン分子の上を，FAはATP（化学エネルギーの供給源）を分解しつつ滑り運動する。FAは蛍光分子でラベルされているので，その動きは蛍光顕微鏡ー超高感度テレビカメラービデオシステムによって観察記録し，画像処理コンピューターによって解析することができる。このin vitro滑り運動系と呼ばれる実験系が開発されたことによって，一個の分子モーターや一本のFAの力学・運動特性を研究することが可能になった。ここで紹介する研究では，ミオシン分子としてその酵素活性断片であるHMM分子，あるいはSI分子を用いている。HMM分子は“頭部”と呼ばれる部分（FAとの結合部位と，ATPを加水分解する酵素活性部位を含む）を2個もち，SI分子はその“頭部”に相当する。いずれも，FAの滑り運動を引き起こす分子モーターとしての能力を保持している。

2）分子モーターの素動作，およびFAとの結合特性

レーザー光を集光することによって原子・分子・微粒子を捕捉するレーザー光ピンセット法と呼ばれる非接触捕捉法が開発され，生物学研究にも用いられるようになってきた。我々は，FAの後端に直径1 μmのプラスチックビーズを結合し，このビーズを光ピンセットで捕捉することによって，FAの顕微操作やFAに発生する滑り力の顕微計測を行っている。ビーズに作用する光ピンセットの捕捉力は，フックのバネのように捕捉中心からの距離に比例する[8]。

FAに結合したビーズを捕捉しつつ非常に低濃度のATPを加えたところ，ビーズにステップ状の動きがみられた。このビーズの動きは分子モーターそのものの動きに対応していると考えられる。ステップの大きさは平均約10 nmであったが，捕捉力を弱めると大きくなる傾向にあった。分子モーターは，外力の大きさに応じてその素動作を柔軟に調節しうるようなメカニズムを，単独で備えているようにみえる。逆に捕捉力を強めるとステップサイズは小さくなるが，あるサイズ以下にはならないようであった。基本的な最小ステップが存在するのかもしれない[9]。この極限の1ステップで一分子モーターが発生する力は数pNと見積もられた。このような分子モーターの素機能は，時間的にランダムに発現する。その第一の原因は，溶液中に存在するATP分子と分子モーターとの結合が，ランダムな拡散過程によっているためである。第二は，ATP分子が結合した後の，加水分解反応自体が確率的に生じるからである。このように，孤立して存在する分子モーターは，互いに独立に，しかも確率的に機能する。さらに，ATPの加水分解反応（化学素過程）と，分子モーターの素機能（力学素過程）とが歯車のように直結している（tight coupling）とは限らず，両者の間の連結がゆるい（loose coupling）可能性のあることが指摘されている。

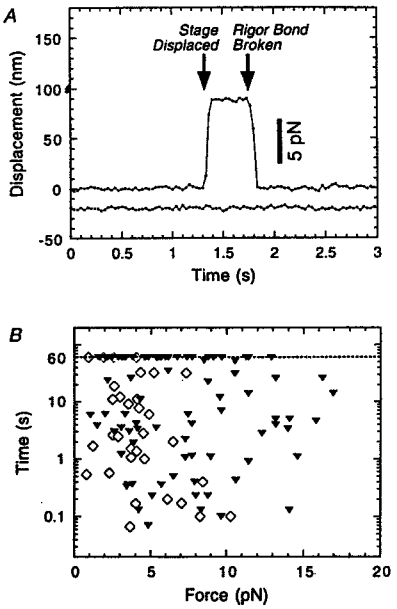

図2　単一のミオシンーFA間硬直結合の寿命に対する負荷の影響[8]

一方ATP非存在下では，ミオシン分子はFAと安定な“硬直結合”を形成する。我々は，in vitro滑り運動系（ただし，ATPが存在しないので滑り運動は生じない）を用いてこの結合一個の破断力を計測した[8]。FAの後端に結合したプラスチックビーズを光ピンセットで顕微操作することによって，硬直結合に最大約70 pNの負荷を加えることができる。負荷を大きくすると結合は破断し，FAはミオシン（HMM）分子から離れる（図2A）。沢山のHMM分子について，硬直結合の破断力を計測した結果，幅広い分布を示したが，平均は約9 pNであった[10]。最近の未発表データによれば，この幅広い分布には2つの山があり，それぞれのピークの値は，約7 pNと15 pNである。破断力の小さな方はHMM分子が単頭で結合したものに

対応し，大きな方は双頭結合に対応していると推測される。

そもそも硬直結合は，熱平衡状態にあって，結合・解離をランダムに繰り返しているものと考えられる。従って硬直結合には，解離の速度定数の逆数に対応する寿命が存在する。溶液系の実験によって，HMM-FA 間硬直結合の寿命が計測されており，約 1000 秒と報告されている。我々も顕微鏡下でこれを一分子計測し，約 2000 秒という値を得た（S 1-FA 間の硬直結合については約 150 秒であった）。硬直結合の寿命はこのようなものだが，これらの値はあくまでも平均値である。平均的にこのような時間で解離すると予測することはできるが，それぞれの結合がいつ解離するかを予測することは出来ない。事実，単一の HMM-FA 硬直結合に負荷を加えると結合の寿命は平均として減少するが，同じ負荷を加えても結合が解離するまでの時間は様々である（図 2 B の逆三角印；ダイヤモンド印は S 1-FA 硬直結合）[8]。

4．分子モーター集合体の収縮機能にみる分子協調

通常筋収縮系は，力を発生して収縮する（ON 状態）か，力を発生せずに弛緩する（OFF 状態）かの 2 状態をとる。ON 状態における平均の発生張力は，細いフィラメントと結合するモーター分子の数に比例する。力を発生して収縮する際には力学的エネルギーが消費されるが，そのためのエネルギー源は ATP が ADP と無機リン酸（Pi）に加水分解する際に解放される化学エネルギーである。また 2 状態間の転移は，遊離の Ca^{2+} 濃度の変化によって起こる。遊離の Ca^{2+} 濃度が 1 μM より高いと Ca^{2+} はトロポニン分子に結合し，低いと解離する。これに応じて細いフィラメントは ON か OFF の状態をとる。

ところで心筋の収縮系（筋原線維）の場合には，遊離の Ca^{2+} 濃度が ON/OFF 制御の中点にあたる 1 μM 付近で，筋節長あるいは発生張力が自発的に（自励）振動することが知られている（我々はこの現象を CaSPOC と呼ぶ）[6]。骨格筋（速筋）ではこのタイプの SPOC は見られないが，Ca^{2+} 非存在下でも ATP 濃度以上の ADP と Pi が共存すると，同じような自励振動現象が見られる（ADPSPOC と呼ぶ；図 3）ことを我々は発見した。このような自励振動現象については，その生理的意味も期待されるが，メカニズムについては不明な点が多い[11]。

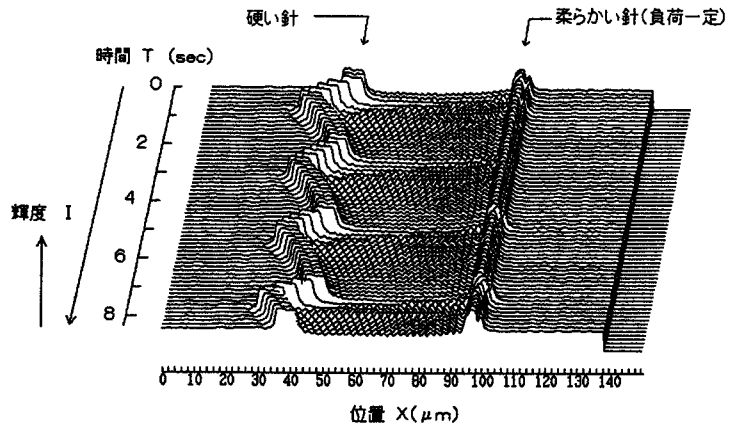

図 3　等張性SPOCにおける筋節の振動パターン

通常の ON 状態では，筋節が伸長すると発生張力は減少する。これは，FA と相互作用しているモーターの分子数が減少するからだと理解されている。ところが SPOC 状態では筋節長が自発的に短縮，伸長を繰り返し，どの断面をとっても同じ力を発生しているはずの一本の筋原線維中に，異なる長さの筋節が共存する。SPOC 現象で興味深いのは，このように，通常の収縮時には見られない動的安定性が見られる点である。さらに強調したいのは，骨格筋原線維の SPOC において，等張（フィードバック制御により張力を一定に保った）条件下で各筋節の長さ振動を顕微観察したところ，一本の筋原線維中で直列に繋がった数十個の全ての筋節がほぼ同位相で振動し始めたことである（図 3；筋原線維の一端を保持している柔らかいガラス微小針の平衡位置からの変位を一定に保つことによって，等張性を実現。そのために，硬い方の針を変動させている）[12]。つまり，張力を外部から制御することによって，筋原線維中の振動単位である筋節の振動パターンを制御できた。このように，分子モーター集合体における分子協調は外部パラメーターによって制御可能である。ここでは，複数個の分子モーターが関与することによ

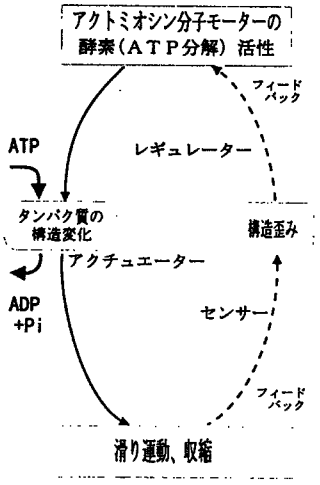

図 4　SPOCにおける分子モーターの機能と分子協調の仕組み（仮説）[11]

り，細いフィラメントのON，OFF状態，あるいは以下で述べるように分子モーターの機能そのものが，タンパク質構造の変化（歪み）を通じて協同的に制御されている可能性が高い（図4）。

5．収縮構造を作り替える

横紋筋の筋節構造にみられる規則性のもとには，まず第一に筋フィラメントの長さ制御の問題がある。その上に，筋フィラメントの配列という問題がある。そこで，FAの重合（脱重合）機構に着目し，これを，高次構造をもった筋収縮系の中で研究することを試みた。筋（原）線維の中で，既に出来上がっている筋フィラメントを選択的に解体（脱重合）する方法を探り，さらにその後，精製タンパク質を用いて筋フィラメントを構造的・機能的に再構築する方法を模索した。解体と再構築の手順を図5に模式的に示す[13]。

FAの解体には，FAを選択的に切断するゲルゾリンと呼ばれるタンパク質の性質を利用した。筋（原）線維をゲルゾリン処理するとFAはほとんど切断され除去されるが，Z線にFAの断片が残る。これをアクチン分子の重合成長の核として用いることにより，我々はFAの構造と機能の再構築に成功した。すなわち，光学顕微鏡レベルだけでなく，電子顕微鏡レベルにおいても本来のフィラメント構造（図1参照）が再現され，発生張力も本来のレベル（あるいはそれ以上）に達した。さらに，収縮・弛緩の制御をしている制御タンパク質（トロポミオシン・トロポニン複合体）を，FA再構成系に添加するだけで，Ca^{2+} イオンによる張力発生の制御能を完全に回復することもできた[13),14)]。

筋収縮系として骨格筋を用いた場合には，再構成されたFAの数は本来の20%程度で，張力回復も高々2，30%であった[14)]。しかし，心筋収縮系を用いると，FAの本数はほぼ元通りに回復し，しかも張力回復の程度は100%を越え，平均140%に達することがわかった[13)]。100%を越える張力回復の原因としては，心筋収縮系においては，元々FAの長さは厳密には揃っていず，短いものも沢山ある。従って，再構成によって過剰のアクチン分子が導入され，本来の長さ以上に重合成長したことが挙げられる。

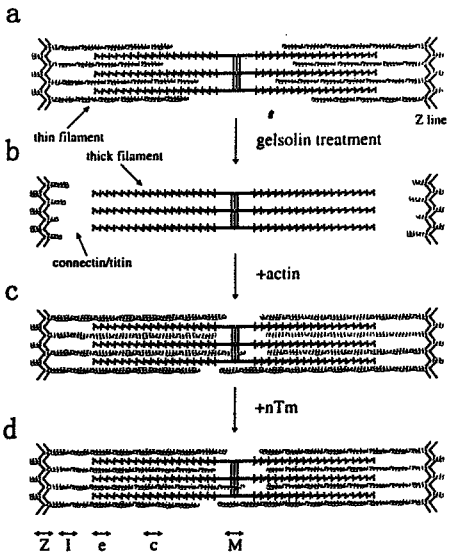

図5　筋節中の細いフィラメントの解体と再構成の手順[13)]

ところでFAの構造的・機能的再構築がなぜ心筋において成功し，骨格筋ではそれほどでなかったのか。その第一の原因は，再構成のために必須のアクチン重合核が，心筋においてはゲルゾリン処理によって損なわれることなく残っていたことである。Z線の構造が，心筋では二重構造となっており骨格筋と比べて堅牢である。第二に，骨格筋では，FAが切断除去されたことによってネブリン分子が宙ぶらりんになって残っており，これが再構成の邪魔をする可能性がある。骨格筋においては，おそらく筋収縮装置としての機能を十分に引き出すためにFAの長さを揃える必要があり，そのためにネブリンを必要としている。これが，我々のとった再構築の方法にはむしろ不都合であったとも考えられる。骨格筋の発生（形態形成）においては，この不都合を回避するために，FAの形成はネブリン発生の前か，あるいは同時に行われているかもしれない。いずれにしても，構造規則性が高い骨格筋では特に，タンパク質合成の厳密な時間的制御のもとに，タンパク質の自己集合能を十二分に生かした構造形成が行われているに違いない。

FA再構築モデル系の応用として，我々は自励振動（SPOC）現象を検討し，新しい性質を明らかにした。即ち，SPOC現象は，制御タンパク質が存在しない純粋なFA再構築系でも見られることを見いだしたのである（藤田英明，未発表データー）。このことは，SPOCという，一見制御タンパク質系が関与していると思われる現象が，アクチン，ミオシン固有の性質によるものであることを示すものである。しかし，SPOCのメカニズムは，一組のアクチン，ミオシン複合体の性質によっては理解しきれないかもしれない。つまり，分子モーターの性質の中には，集合体になることによって初めて現れるものがあり，それが生理機能にとっ

て意味を持つ，ということがあるのではなかろうか。そこでは，図4で指摘したように，分子モーターがアクチュエーターとしての機能だけでなく，センサー，レギュレーターとしての機能も兼ね備えており，それが顕著に現れる可能性が考えられる。

6．むすび

ここでは，ある意味では単純な階層性を持った筋収縮系を取り上げ，一分子から集合体へと階層を上るにつれてどのような“分子協調（シンクロナイゼーション）”が生じるか，その一面を紹介した。今後は，力学制御だけでなく，熱注入によるモーター機能の変調（熱変調）など，新しい機能制御方式を探り，分子機能協調の諸相を明らかにしていきたい。このようにして，「確率的にしか働かない分子が，集合することによって協調性を獲得し，全く新規な高次機能を発現するようになるメカニズムは何か」を明らかにしたいものである。

参考文献

1) 「生物物理」（日本生物物理学会誌）特集：生体におけるイメージング技術の発展一分子，細胞，組織の動態を可視化する— 36, No. 1 (1996).
2) T. Funatsu et al. Nature 374, 555-559 (1995).
3) I. Sase et al. Biophys. J. 69, 323-328 (1995).
4) 石渡信一「収縮装置を解剖する」生物物理のフロンティア（培風館）(1989).
5) 石渡信一「筋フィラメントの構造と機能」病態生理 10, 437-444 (1991).
6) 石渡信一「筋収縮系の力学特性」BME 9, 12-20 (1995).
7) 西坂崇之，石渡信一「分子モーターの力学・機能特性を見る」生物物理 36, 15-19 (1996).
8) 西坂崇之「アクトミオシン分子モーターの機能と力学特性の一分子顕微解析」早稲田大学理工学部博士論文 pp 160 (1996).
9) H. Miyata et al. Biophys. J. 68, 286s-290s (1995); J. Biochem. 115, 644-647 (1994).
10) T. Nishizaka et al. Nature 377, 251-254 (1995).
11) S. Ishiwata and K. Yasuda, Phase Transitions 45, 105-136 (1993).
12) K. Yasuda et al. Biophys. J. 70, 1823-1829 (1996).
13) H. Fujita at al. Biophys. J. 71, 2307-2318 (1996).
14) T. Funatsu et al. J. Muscle Res. Cell Motil. 15, 158-171 (1994).

早稲田大学　理工学部
〒169 東京都新宿区大久保 3-4-1
TEL 03-5286-3437
FAX 03-3200-2567

Proc. Natl. Acad. Sci. USA
Vol. 94, pp. 5646–5650, May 1997
Biophysics

Axial rotation of sliding actin filaments revealed by single-fluorophore imaging

(*in vitro* motility/molecular motor/force generation/fluorescence polarization/epifluorescence microscopy)

ICHIRO SASE*†, HIDETAKE MIYATA*‡, SHIN'ICHI ISHIWATA§, AND KAZUHIKO KINOSITA, JR.*¶

*Department of Physics, Faculty of Science and Technology, Keio University, Hiyoshi 3-14-1, Kohoku-ku, Yokohama 223, Japan; and §Department of Physics, School of Science and Engineering, Waseda University, Okubo 3-4-1, Shinjuku-ku, Tokyo 169, Japan

Communicated by Hugh E. Huxley, Brandeis University, Waltham, MA, March 25, 1997 (received for review December 2, 1996)

ABSTRACT **In the actomyosin motor, myosin slides along an actin filament that has a helical structure with a pitch of ≈72 nm. Whether myosin precisely follows this helical track is an unanswered question bearing directly on the motor mechanism. Here, axial rotation of actin filaments sliding over myosin molecules fixed on a glass surface was visualized through fluorescence polarization imaging of individual tetramethylrhodamine fluorophores sparsely bound to the filaments. The filaments underwent one revolution per sliding distance of ≈1 μm, which is much greater than the 72 nm pitch. Thus, myosin does not "walk" on the helical array of actin protomers; rather it "runs," skipping many protomers. Possible mechanisms involving sequential interaction of myosin with successive actin protomers are ruled out at least for the preparation described here in which the actin filaments ran rather slowly compared with other *in vitro* systems. The result also indicates that each "kick" of myosin is primarily along the axis of the actin filament. The successful, real-time observation of the changes in the orientation of a single fluorophore opens the possibility of detecting a conformational change(s) of a single protein molecule at the moment it functions.**

The actin filament is an array of actin protomers arranged in the form of two-start, right-handed helices with a pitch of ≈72 nm containing ≈13 protomers (1). If myosin tends to interact sequentially with one of the helical strands (the binding site on the other strand being on the opposite side), right-handed rotation of a sliding actin filament around its axis is expected. Indeed, in an *in vitro* motility assay in which the front end of a sliding filament was fixed on a surface, the middle part formed a left-handed superhelix, indicating right-handed rotation of the sliding rear part (2). However, in another assay where a marker (bead aggregate) was attached at the tail of a freely sliding filament, the filament slid over a long distance without rotating the tail beads (3). Quantitative resolution of this issue is important for the mechanism of motor function, because axial rotation is an indication of (*i*) sequential interaction of a myosin molecule with successive (or closely apposed) actin protomers, as stated above, and/or (*ii*) the presence of a genuine torque component in the individual myosin–actin interaction not necessarily related to the helical structure. In the first assay above (2) where the superhelix formation was observed, the number of axial rotations could not be determined in the video images of limited resolution. A complication with the bead-tailed actin (3) was that the beads produced a large rotational, but not translational, friction that may have impeded the axial rotation. Here we show that the amount of rotation is small even in the absence of the external asymmetric load. Neither *i* nor *ii* appear to be essential components of the actomyosin motor. Quantitative measurement of the axial rotation without an impeding marker was achieved by continuous, real-time detection of the orientation of individual fluorophores on actin, through fluorescence-polarization imaging on a microscope with extremely low background (4).

MATERIALS AND METHODS

Basic experimental procedures have been described (4). A brief summary and modifications are given below.

Motility Assay. Actin and heavy meromyosin (HMM) were prepared from rabbit skeletal muscle as described (4). Actin was labeled with pure 5-iodoacetamidotetramethylrhodamine (5) at a final ratio of 1 mol of the dye to 500 mol of actin, and polymerized into filaments (F-actin) in the presence of phalloidin (4). Into an observation chamber made of two quartz coverslips precleaned with KOH and ethanol, 1 mg/ml of poly-L-lysine was infused. After 60 s, the chamber was washed with distilled water and then with buffer A containing 25 mM imidazole/HCl (pH 7.5), 25 mM KCl, and 4 mM $MgCl_2$. This was followed by a series of 60-s incubations with washes indicated in brackets: (*i*) 80 μg/ml of HMM in buffer A [buffer A], (*ii*) 5 μM of unlabeled F-actin in buffer A [buffer A plus 2 mM ATP], and (*iii*) 5 nM of labeled F-actin in buffer A plus 2 mM ATP [buffer A plus 2 mM ATP]. All solutions were infused from the same side of the chamber. Buffers were degassed under reduced pressure immediately before use. The pretreatment of the chamber with unlabeled F-actin resulted in a smooth (constant speed), linear sliding of labeled F-actin parallel to the direction of infusion. The chamber was placed on a microscope stage such that the sliding direction was at ≈45° in the image plane. Measurements were made at 25 ± 2°C.

Fluorescence Microscopy. An inverted epifluorescence microscope (Diaphot TMD, Nikon) was modified to reduce its background luminescence by two orders of magnitude (4). Fluorescence was excited at 532 nm with a circularly polarized (by a quarter-wave plate) beam from an Nd/YAG laser (DPY425II, Adlas, Lübeck, Germany). The beam intensity was 8.5 mW over a sample area of 30 μm in diameter. For a fluorophore with a nondegenerate transition moment such as the tetramethylrhodamine used here, the circular excitation is equivalent with unpolarized excitation. That the excitation beam was isotropic in the image plane was confirmed by passing the beam through a polarizer placed on the sample

The publication costs of this article were defrayed in part by page charge payment. This article must therefore be hereby marked "*advertisement*" in accordance with 18 U.S.C. §1734 solely to indicate this fact.

0027-8424/97/945646-5$2.00/0
PNAS is available online at **http://www.pnas.org.**

Abbreviation: HMM, heavy meromyosin.

†Present address: Microscopes Development Department, Yokohama Plant, Nikon Corporation, Nagaodai-machi 471, Sakae-ku, Yokohama 244, Japan.
‡Present address: Physics Department, Graduate School of Science, Tohoku University, Aoba, Aramaki, Aoba-ku, Sendai 980-77, Japan.
¶To whom reprint requests should be addressed.

stage; rotation of the polarizer did not change the transmitted intensity. Fluorescence (>565 nm) was collected through a water immersion objective (60×, numerical aperture 1.20, WPlanApo60UV, Olympus, Tokyo), decomposed into vertically and horizontally polarized images in a dual-view apparatus (6), and detected with an image intensifier (KS1381, Video Scope International, Sterling, VA) coupled to an intensified charge-coupled-device camera (C3500, Hamamatsu Photonics, Hamamatsu, Japan). Images were rolling averaged in a digital image processor (C2000, Hamamatsu Photonics) with a half time of 2 frames (67 ms), and recorded on a Hi8 video recorder (EVO-9650, Sony, Tokyo). Recorded images were analyzed frame by frame in the digital image processor.

RESULTS

Fluorescence polarization of the actin filaments labeled with tetramethylrhodamine at high dye/protein ratios showed that the fluorophore was essentially immobile on actin and its transition moment lay at ≈45° to the filament axis. Thus, a suspension of 3% labeled filaments in a cuvette gave a fluorescence anisotropy of 0.32 (λ_{ex} = 532 nm, λ_{em} = 575 nm; measured in a Hitachi F-4010 spectrofluorometer), indicating that the wobbling of the fluorophore on actin was confined within a cone of semiangle <25° (7). When individual filaments labeled at 30% were examined on the fluorescence microscope, filaments lying parallel to the polarizer (analyzer) axis gave a polarization of 0.18 ± 0.04 (n = 12). This value, as analyzed in ref. 6 for unpolarized excitation and corrected in ref. 8 for the large numerical aperture of the objective of 1.2 (the effective aperture was much smaller for the excitation), indicates that the absorption and emission moments (assumed parallel) were at ≈45° from the filament axis. (When parallel absorption and emission moments are distributed on the surface of a cone of semiangle 46°, whose axis lies in the image plane, unpolarized or circularly polarized excitation with a beam perpendicular to the image plane will give rise to a fluorescence polarization, with respect to the cone axis, of 0.227. Observation through an objective with a numerical aperture of 1.2 will decrease the polarization value to 0.189.)

The results above allowed us to design an experimental protocol schematized in Fig. 1. Sparsely labeled (molar ratio = 0.2%) filaments were let slide on a glass surface coated with HMM, in the direction at ≈45° in the image plane. Fluorescent spots with an intensity corresponding to a single (or possibly double) fluorophore (4) were seen to move steadily from bottom right to top left, or in the reverse direction. The fluorescence was excited with circularly polarized light, and

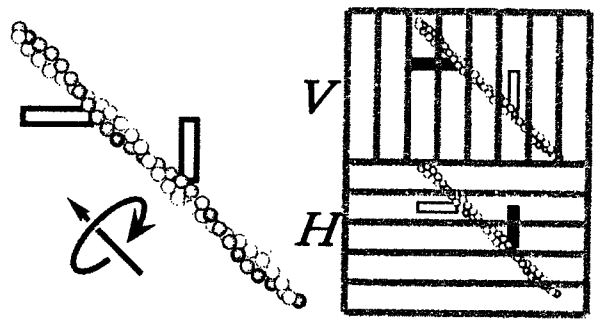

FIG. 1. Measurement of axial rotation through fluorescence-polarization imaging. An actin filament was sparsely labeled with fluorophores with their transition moment (shown as a thick bar) at ≈45° from the filament axis. Fluorescence was excited with circularly polarized light. The vertically polarized component of the fluorescence was projected onto the upper half of the detector plane, and the horizontal component onto the lower half, through a dual-view apparatus (6). Filament rotation will result in an alternate appearance of each fluorophore between the *V* and *H* images.

images of vertically (*V*) and horizontally (*H*) polarized fluorescence were acquired simultaneously. In this setup, axial rotation of sliding filaments should show up as alternation of the spot intensity between images *V* and *H* (Fig. 1 *Right*), as was indeed observed (Fig. 2*A*). Note that the alternating intensity is expected only when the fluorescence from a single (at most a few) fluorophore is resolved; a fully labeled filament in which the fluorophores are arranged with a helical symmetry will give rise to an averaged polarization that is insensitive to the axial rotation. The sudden disappearance (photobleaching) of the spot in Fig. 2 *A* (at ≈3.1 s) and *D* (at ≈1.7 s) is an indication (but not proof) that the spot represented a single fluorophore.

In principle, the alternation of spot intensity could also result from snake-like winding of the filament without axial rotation. Traces of the moving spots (Figs. 2*C* and 3*B*), however, were linear, and the polarization (= $[V - H]/[V + H]$) of the spot fluorescence alternated its sign quite regularly over a long distance (Figs. 2*B* and 3*A*). Also note, in Fig. 2*A* at 0–1 s, that two fluorophores, presumably on the same straight filament, flickered out of phase yet with a similar rhythm. In the absence of ATP, where actin binds to myosin tenaciously, the polarization remained relatively constant (Fig. 2 *D* and *E*), showing that the alternation of spot intensity did not originate from fluorophore rotation relative to actin nor from instrumental instability.

Fig. 4 summarizes the relation between the speed of axial revolution (estimated in the polarization plot) and sliding velocity. The sliding actin without an external load rotated by one turn per sliding distance of 1 μm, which is much longer than the helical pitch of the actin filament. In the superhelix formation by Nishizaka *et al.* (2), the end of the supercoil made at least four turns for a sliding distance of 5 μm. If they did not miss rapid rotation, their observation is consistent with ours.

DISCUSSION

The finding that the rotational pitch was much larger than the helical pitch has two major implications.

First, at least in our system described here, each myosin molecule does not maintain stereospecific interaction with an actin filament while the filament slides past the myosin. The force-generating (strong) interaction, in particular, is most likely to be stereospecific. Thus, the subsequent force-generating interaction of the same myosin molecule must be made on an actin protomer more than ≈36 nm (half pitch of the helix) apart; otherwise, an efficient axial rotation would be expected. Note that, even under "unloaded" conditions, a myosin molecule has to work against the "protein friction" (9) caused by other myosin molecules and thus has to generate force.

The long interval of >36 nm between successive force-generating interactions, longer than twice the physical size of a myosin head of ≈16 nm (10), rules out alternate bindings ("walk") of the two heads of myosin, a mechanism suggested for kinesin (11). In our system without an external load, myosin "runs" on actin, skipping many actin protomers. That myosin under unloaded conditions interacts with actin strongly only for a small fraction of the ATPase cycle has already been anticipated (see for example ref. 12), on the ground that the sliding velocity (several micrometers per second) divided by ATPase (≈10/s) yields the distance traveled by actin per cycle of >0.1 μm, much greater than the size of a myosin head. Implicit in this argument, however, is the assumption that strong binding of myosin and actin occurs only once in the ATPase cycle, a notion that has been challenged by Yanagida *et al.* (13), who claim that myosin under a small load undergoes multiple power strokes during one ATPase cycle. If multiple strokes occur in the motility system described here, and if each stroke requires a stereospecific interaction, the successive strokes in one ATPase cycle have to be separated by >36 nm.

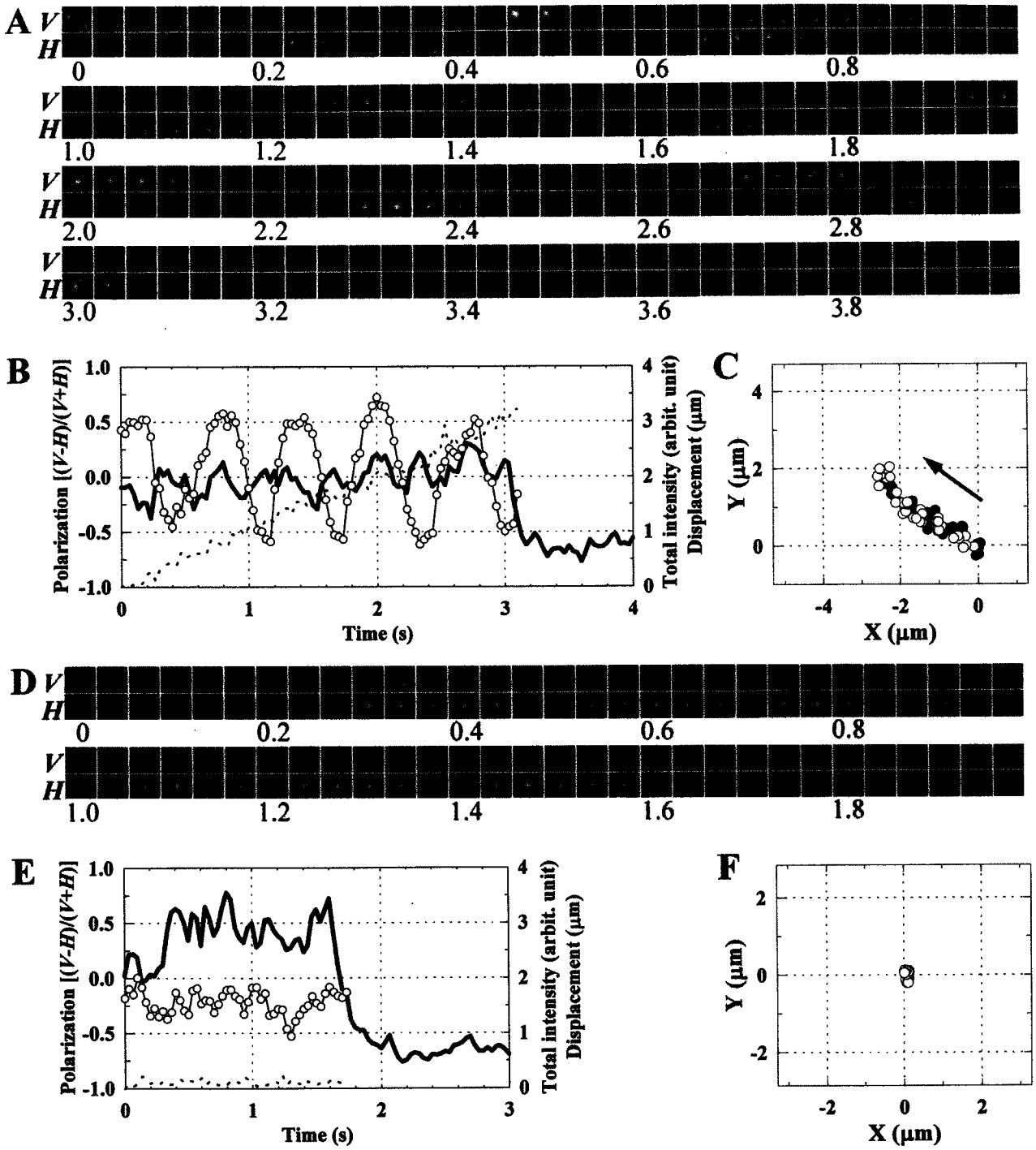

FIG. 2. Axial rotation detected in polarized fluorescence images. (*A*) Snapshots, at 33-ms intervals, of fluorescence from individual fluorophores on an actin filament sliding from bottom right toward top left. *V*, vertically polarized fluorescence; *H*, horizontally polarized fluorescence; numbers indicate time in seconds. Each image was spatially averaged over 3 × 3 pixels (0.66 × 0.66 μm^2), and corrected for shading (due mainly to inhomogeneous excitation). (*B*) Time courses of the polarized spot intensities. The peak intensity of the trailing spot in *A* (starting at bottom right at 0 s) was measured for *V* and *H*, from which the total intensity, $I = V + H$ (solid line), and polarization, $p = (V - H)/(V + H)$ (○) were calculated. Because the signal-to-noise ratio was not high, the peak intensities, *V* and *H*, were not corrected for the background intensity, which varied to some extent from sample to sample and amounted to, on the average, one-third of the spot intensity; the total intensity beyond 3.1 s (also beyond 1.7 s in *E*) represents the background intensity. The inclusion of the background intensity resulted in smaller values of *p*, but our primary concern is its time dependence. Broken line indicates the displacement of the spot peak from the position at time 0. If the absorption and emission moments (assumed parallel) of the dye make an angle θ with the filament axis, and if the filament rotates at an angular velocity of ω around its axis, which lies at 45° with *V* and *H* axes, the total intensity and polarization for circularly polarized excitation are given by $I = \cos^2\theta + \sin^2\theta\sin^2\omega t$ and $p = \sin 2\theta \sin\omega t/I$ (without correction for the large collection angle of the objective). Note that the theoretical *I* for a single fluorophore takes maximal values at times *t* when *p* passes either positive or negative peaks. The drop of the total intensity at ≈3.1 s resulted from photobleaching of the dye. (*C*) Trace of the trailing spot in *A*. (●), Spot positions where $p > 0$; (○), spot positions where $p < 0$. Arrow indicates the direction of sliding. The frame enclosing the trace represents the same area as each image in *A*. (*D–F*) Control experiment in the absence of ATP. The fluctuation of the spot intensity in this sample serves as a measure of the precision in *A–C*. The dye was photobleached at ≈1.7 s.

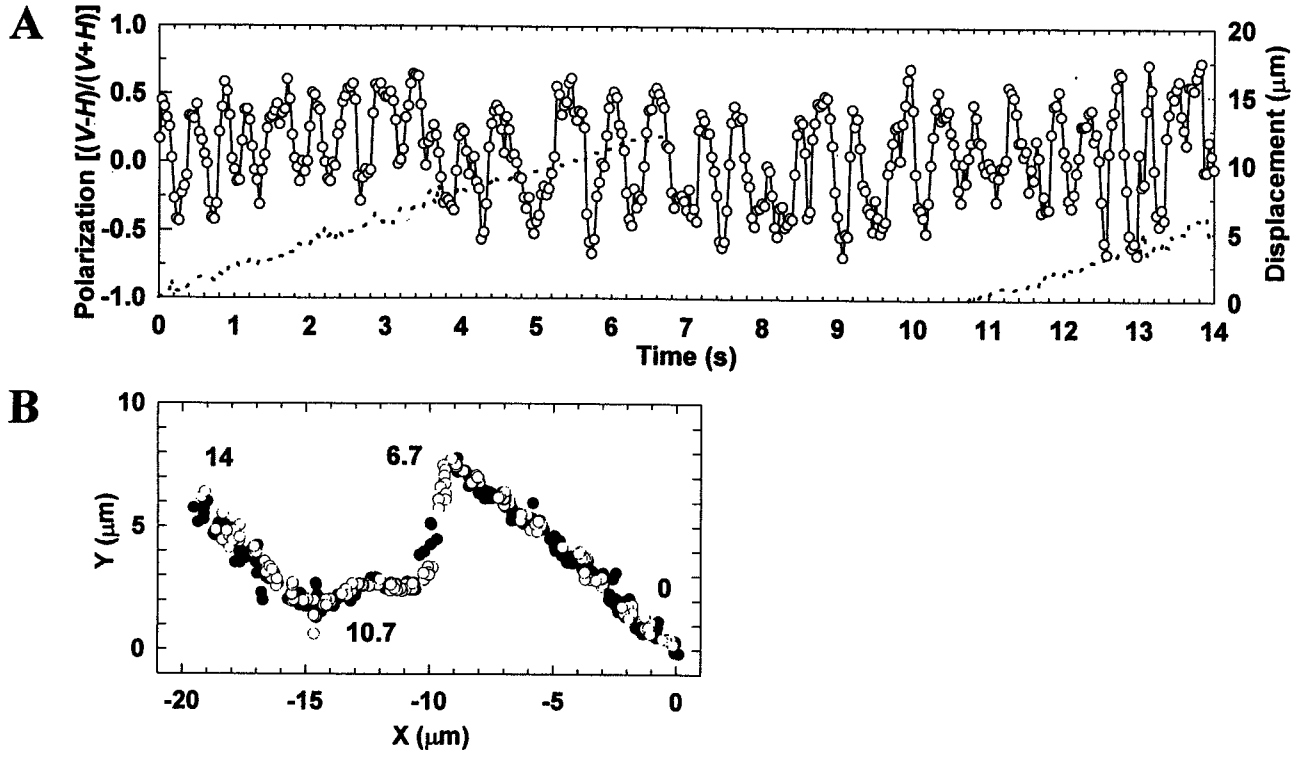

FIG. 3. The longest rotation record observed. See Fig. 2 for symbols. Between 6.7 and 10.7 s (−9 and −15 μm in *B*), the microscope stage was moved manually to keep the moving spot in the field of view.

Although multiple strokes are thus unlikely in our system, the sliding velocity was relatively low (see below). Multiple strokes (leading to efficient rotation) in a faster system cannot be ruled out.

In between the strongly bound states, myosin and actin are considered to interact "weakly," undergoing rapid cycles of association and dissociation (for a review see ref. 14). The nature of this weak interaction is not yet clear, but our results indicate that this interaction, too, cannot keep a myosin molecule on one strand of a sliding actin helix. Either the weak interaction also occupies only a small fraction of the ATPase cycle, or else the interaction is really weak and nonspecific, occurring indiscriminately over any part of the actin surface.

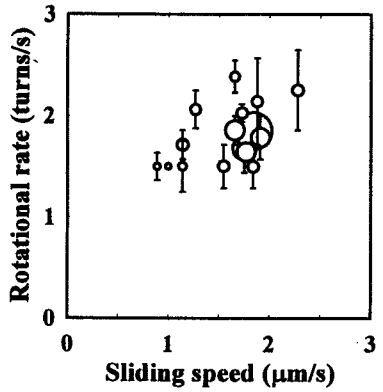

FIG. 4. The relationship between axial rotation and forward translocation. The sliding speed (abscissa) was estimated from the slope of the displacement record (broken lines in Figs. 2*B* and 3*A*). The rotational rate (ordinate) was calculated as the number of revolutions in a record divided by the total duration determined by photobleaching. The size of the symbols is proportional to the duration of the record. The average of the durations is 5.6 s, which is approximately twice the average lifetime of all single fluorophores (long-lived spots were selected for the analysis of rotation). Vertical bars indicate the uncertainty in the revolution count. In estimating the revolution count, peaks with a small amplitude or short duration (0.1 s or less) were judged as noises and ignored. In Fig. 3*A*, for example, the revolution count during the 14-s period was estimated to be between 27 and 29.

The other implication of our finding is that the individual myosin–actin interaction does not produce a significant rotational torque, compared with the sliding force parallel to the actin filament. If the interaction force is oblique to the filament axis and the perpendicular component contributes to the torque, the latter is likely to be <10% (72 nm/1 μm) of the parallel, sliding force. The experiment using bead-tailed actin also indicated that the torque component was much smaller than the sliding force (3).

The above estimate of torque rests on the assumption that the movement of myosin relative to actin was parallel to the oblique force. If the axial rotation was somehow hindered in our motility system, the torque component may be underestimated. The sliding velocity on the polylysine-coated glass (Fig. 4) was indeed low, compared with 3.5–4 μm/s at 25°C on nitrocellulose surfaces (3, 15) or 7.8 μm/s at 22°C on Sigmacoat (16), suggesting the presence of an impeding factor(s) in our system, probably myosin damaged on the surface. Normal myosin, too, exerts protein friction (9), which impedes the filament motion. Let us consider the impeding mechanism in detail. When a myosin molecule pulls the actin filament, it stretches the holding linkages of other myosin molecules, normal or damaged. A next myosin molecule may bind and pull, but it only increases strain of existing linkages. It is the release of holding myosin molecules that allows the filament to slide and rotate continuously. It is primarily the release rate that determines the extent of resistance. In this scheme, the impeding mechanism will affect the rotation and linear sliding more or less equally, unless the spring in the linkage is highly anisotropic. A decrease in the release rate (an increase in the number of holding molecules) will slow down rotation and sliding equally. A myosin molecule with internal flexible joints (17) is unlikely to be rigid only in the particular direction opposing the axial rotation. Denatured myosin is less likely to be rigid. Hindrance by possible binding of actin to polylysine

is also unlikely to be anisotropic. Thus, our contention that the torque component of individual myosin–actin interaction is small appears to be basically valid.

The small torque component in the actomyosin motor is contrasted to the case of *Tetrahymena* 14S (but not 22S) dynein, which caused axial rotation of a microtubule with a rotational pitch shorter than the helical pitch of the protofilaments of the microtubule (18). The 14S dynein produced a genuine torque component. The *ncd* motor on a microtubule also appears to produce a genuine torque (19). Among myosins, brush border myosin I may produce a genuine torque because the head of this myosin has been shown to swing around an actin filament upon release of ADP (20). In the skeletal myosin studied here, such a lateral swing is absent or, if it occurs, it does not generate enough torque to produce efficient axial rotation. The torsional stiffness of an actin filament has suggested that, in an intact skeletal muscle where actin filaments are bound at one end to the Z-disk, the actin filament of length 1 μm is twisted by only one turn even if 10% of the isometric contractile force contributes to the torque component (21). In a shortening muscle producing a much smaller force, myosin will not be able to follow the helical track of the fixed actin filament. A skeletal muscle is an asymmetric system, where the z-disk hinders rotation without impeding shortening.

Although the rotational pitch in our motility system was long, the sliding actin filament did rotate axially with a relatively constant pitch. This slow rotation may have been caused by a small torque generated in the myosin–actin interaction. Or, the rotation may have resulted from the right-handed helical structure of the actin filament: if the steps of running myosin are distributed such that the probability of landing within 36 nm is slightly greater than on further sites, a slow, right-handed rotation is expected. In this latter case, the genuine torque could be totally absent or could even be left-handed (the magnitude being small).

In conclusion, we note that the polarization imaging of single fluorophores as described here should be useful in detecting a conformational change(s) in a single protein molecule during function. Once a fluorophore is firmly attached to a particular site on the protein, reorientation of the fluorophore as a result of the conformational change will be detected as a change in the fluorescence polarization. Because individual protein molecules (molecular machines) always operate stochastically and cannot be synchronized in the rigorous sense, single-molecule observation is vital to the understanding of their mechanisms. Chemical reaction (ATPase) in a single molecule has already been imaged (22). A future challenge is the simultaneous observation of chemistry and conformational changes in a single protein molecule.

We thank Dr. J. E. T. Corrie and Mr. J. S. Craik for the pure rhodamine dye, which was essential in this work. We also thank Dr. A. Ikegami and Dr. Y. Inoue for support, and Mr. H. Itoh, Mr. M. Hosoda and Mr. K. Atsumi for help in developing the image analysis system. This work was supported by Grants-in-Aid from Ministry of Education, Science, Sports and Culture of Japan, a Keio University Special Grant-in-Aid for Innovative Collaborative Research Projects, and by CREST (Core Research for Evolutional Science and Technology) of Japan Science and Technology Corporation. I.S. was a Research Fellow of the Japan Society for the Promotion of Science.

1. Holmes, K. C., Popp, D., Gebhard, W. & Kabsch, W. (1990) *Nature (London)* **347,** 44–49.
2. Nishizaka, T., Yagi, T., Tanaka, Y. & Ishiwata, S. (1993) *Nature (London)* **361,** 269–271.
3. Suzuki, N., Miyata, H., Ishiwata, S. & Kinosita, K., Jr. (1996) *Biophys. J.* **70,** 401–408.
4. Sase, I., Miyata, H., Corrie, J. E. T., Craik, J. S. & Kinosita, K., Jr. (1995) *Biophys. J.* **69,** 323–328.
5. Corrie, J. E. T. & Craik, J. S. (1994) *J. Chem. Soc. Perkin Trans. 1,* 2967–2973.
6. Kinosita, K., Jr., Itoh, H., Ishiwata, S., Hirano, K., Nishizaka, T. & Hayakawa, T. (1991) *J. Cell Biol.* **115,** 67–73.
7. Kinosita, K., Jr., Kawato, S. & Ikegami, A. (1977) *Biophys. J.* **20,** 289–305.
8. Axelrod, D. (1979) *Biophys. J.* **26,** 557–574.
9. Tawada, K. & Sekimoto, K. (1991) *J. Theor. Biol.* **150,** 193–200.
10. Rayment, I., Rypniewski, W. R., Schmidt-Base, K., Smith, R., Tomchick, D. R., Benning, M. M., Winkelmann, D. A., Wesenberg, G. & Holden, H. M. (1993) *Science* **261,** 50–58.
11. Howard, J., Hudspeth, A. J. & Vale, R. D. (1989) *Nature (London)* **342,** 154–158.
12. Huxley, H. E. (1990) *J. Biol. Chem.* **265,** 8347–8350.
13. Yanagida, T., Harada, Y. & Ishijima, A. (1993) *Trends Biochem. Sci.* **18,** 319–324.
14. Brenner, B. (1987) *Annu. Rev. Physiol.* **49,** 655–672.
15. Anson, M. (1992) *J. Mol. Biol.* **224,** 1029–1038.
16. Harada, Y., Sakurada, K., Aoki, T., Thomas, D. D. & Yanagida, T. (1990) *J. Mol. Biol.* **216,** 49–68.
17. Kinosita, K., Jr., Ishiwata, S., Yoshimura, H., Asai, H. & Ikegami, A. (1984) *Biochemistry* **23,** 5963–5975.
18. Vale, R. D. & Toyoshima, Y. Y. (1988) *Cell* **52,** 459–469.
19. Walker, R. A., Salmon, E. D. & Endow, S. A. (1990) *Nature (London)* **347,** 780–782.
20. Jontes, J. D., Wilson-Kubalek, E. M. & Milligan, R. A. (1995) *Nature (London)* **378,** 751–753.
21. Yasuda, R., Miyata, H. & Kinosita, K., Jr. (1996) *J. Mol. Biol.* **263,** 227–236.
22. Funatsu, T., Harada, Y., Tokunaga, M., Saito, K. & Yanagida, T. (1995) *Nature (London)* **374,** 555–559.

Interhead Distances in Myosin Attached to F-Actin Estimated by Fluorescence Energy Transfer Spectroscopy

Shin'ichi Ishiwata,*# Masao Miki,§ Izumi Shin,* Takashi Funatsu,* Kenji Yasuda,¶ and Cristobal G. dos Remedios‖

*Department of Physics, School of Science and Engineering, #Advanced Research Institute for Science and Engineering, and Materials Research Laboratory for Bioscience and Photonics, Waseda University, Shinjuku-ku, Tokyo 169, Japan; §Department of Applied Chemistry and Biotechnology, Fukui University, Fukui-shi 910, Japan; ¶Advanced Research Laboratory, Hitachi Ltd., Saitama, Japan; and ‖Muscle Research Unit, Institute for Biomedical Research, Department of Anatomy and Histology, The University of Sydney, Sydney 2006, Australia

ABSTRACT Fluorescence resonance energy transfer (FRET) spectroscopy has been used to determine distances between probes attached to the most reactive sulfhydryl (SH1) group on individual myosin "heads." We measured intramolecular and intermolecular interhead distances as well as the distance between one head of heavy meromyosin (HMM) mixed with subfragment-1 (S1) heads attached to F-actin under rigor conditions. The SH1 cysteine was specifically labeled with either a donor (5-((((2-iodoacetyl)amino)ethyl)amino)naphthalene-1-sulfonic acid) or an acceptor probe (5-iodoacetamidofluorescein). In free solution, the distance between these probes was too large to allow significant FRET, but in the rigor complex with F-actin, intermolecular interhead distances between S1 molecules, HMM molecules, or S1 and HMM were determined to be 6.0–6.3 nm. The radial coordinate of the labels relative to F-actin was 5.0–6.4 nm. However, the intramolecular interhead distance in HMMs in which the two heads were labeled with D and A probes was estimated to be larger. The binding affinity of the second head of HMM(D/A) to F-actin may be reduced because of heterogeneous modification of the SH1 groups, such that the probability of single-head binding is increased.

INTRODUCTION

The attachment of myosin heads to F-actin is a key step in the molecular process involved in muscle contraction and the development of contractile force. Any investigation that reveals structural relationships between these two proteins would surely provide valuable insights into this molecular process. In recent years our understanding of the structure of actin (Kabsch et al., 1990; McLaughlin et al., 1993; Schutt et al., 1993) has advanced to the point where there is no longer room for reasonable doubt. The three-dimensional structure of subfragment-1 (S1) of myosin (Rayment et al., 1993b) has been resolved by x-ray crystallography such that we now have a clear picture of the separate proteins. This has naturally led to speculation as to the atomic structure of F-actin (Holmes et al., 1990; Lorenz et al., 1993; Tirion et al., 1995) and of the acto-S1 complex (Rayment et al., 1993a; Schröder et al., 1993; see dos Remedios and Moens, 1995a, for a full review).

The atomic structure of these complexes will remain unsolved until high-resolution data become available from F-actin and the acto-S1 complex when, and if, they are crystallized. However, electron microscopy of SH1-biotin-avidin-labeled S1 revealed that the most reactive SH1 cysteine (Cys707) and the ATP-binding sites are both located at a position approximately one-third the length of S1 from the tip of the head (Sutoh et al., 1984, 1986). Using the same technique, the geometrical relationships among the actin-binding site, ATP-binding site, and SH1 on S1 in the actin-tropomyosin-S1 complex were also investigated (Tokunaga et al., 1987; Toyoshima et al., 1985). These results are consistent with the more recent three-dimensional reconstruction of unstained S1-decorated F-actin observed by cryoelectron microscopy and with the known structure of S1 (Rayment et al., 1993a; Schröder et al., 1993).

Fluorescence resonance energy transfer (FRET) spectroscopy has been widely used to study the spatial relationships between specific sites in proteins. In particular, FRET has been employed to study distances between a large number of loci on myosin and actin (cf. dos Remedios et al., 1987; Miki et al., 1992; dos Remedios and Moens, 1995b). Among these, the SH1 residue is by far the most well characterized. It is located in a section of α-helix on the 20-kDa segment lying under the nucleotide-binding site pocket. Chemical modification of SH1 modifies the ATPase activity of S1 (Kielley and Bradley, 1956; Seidel, 1969). Thus we elected to study the acto-S1 (or heavy meromyosin, HMM) rigor complex without nucleotides.

An important innovation of the FRET technique is its capacity to determine the radial coordinate of a pair of loci with respect to the axis of the actin filament. This was first done by Taylor et al. (1981) for a donor and acceptor probe pair located at residue Cys374 on F-actin under conditions ensuring random assembly. Kasprzak et al. (1988) and Moens et al. (1994) studied this locus using different probe pairs. Besides Cys374, the radial coordinates of other loci

Received for publication 15 October 1996 and in final form 15 May 1997.

Address reprint requests to Dr. Shin'ichi Ishiwata, Department of Physics, School of Science and Engineering, Waseda University, 3-4-1 Okubo, Shinjuku-ku, Tokyo 169, Japan. Tel.: 81-3-5286-3437; Fax: 81-3-3200-2567; E-mail: ishiwata@mn.waseda.ac.jp.

Dr. Funatsu's present address is Yanagida Biomotron Project, ERATO, JRDC, 2-4-14 Senba-Higashi, Mino, Osaka 562, Japan.

0006-3495/97/08/895/10 $2.00

on F-actin have been determined, including Cys10, Gln41, Tyr69, and the nucleotide-binding site on F-actin (for a review, see Miki et al., 1992). These observations raised the possibility of determining the radial coordinates of SH1 on S1 in a rigor complex with F-actin, provided that the donor-acceptor probe pair does not exceed the outer limit imposed by the Förster (1965) critical distance (R_0) relationship. The probe pair used in this report effectively limits our measurements to ~7.5 nm.

In the absence of ATP, myosin forms a tight complex with F-actin, which saturates at one head per actin monomer. Assuming the above location of SH1 on the S1, determination of its radial coordinate would require that the donor-acceptor probe pair be able to sense distances longer than those used to determine the radial coordinates of loci on F-actin. Furthermore, the determination of the radial coordinate would only be possible if the next myosin "head" bound to the nearest-neighbor actin monomer under conditions in which a head is bound to all monomers in F-actin. Binding to any other monomer (e.g., one on the opposite strand of the two-start helix) would be too great a distance for the FRET method.

Herein we present evidence which strongly suggests that the two "heads" of myosin do indeed bind to adjacent actin monomers on the long-pitch helix of F-actin. In addition, we present a new insight into the binding mode of two heads, based on interpretation of the experimental data according to a model simulation.

Preliminary results were previously published as abstracts (Ishiwata et al., 1987b, 1988, 1996). The intermolecular distance between S1 molecules attached to F-actin was recently measured by Brown and Hambly (1996) with a similar technique.

MATERIALS AND METHODS

Chemicals

5-((((2-Iodoacetyl)amino)ethyl)amino)naphthalene-1-sulfonic acid (1,5-IAEDANS) and 5-iodoacetamidofluorescein (5-IAF) were purchased from Molecular Probes (Eugene, OR). DE52 was obtained from Whatman BioSystems (Maidstone, Kent, England), trypsin was from Sigma Chemical Co. (St. Louis, MO), and α-chymotrypsin was from Worthington Biochemical Co. (Freehold, NJ). Hydroxylamine hydrochloride was purchased from Wako Pure Chemical Industries (Osaka, Japan), and piperazine-*N*,*N*′-bis(2-ethanesulfonic acid) (PIPES) was from Sigma Chemical Co. or Dojindo Lab. (Kumamoto, Japan). All other chemicals were of analytical grade.

Protein preparations

Myosin and actin were prepared from rabbit back and leg white muscles as previously reported (Kinosita et al., 1984). Myosin was stored in 50% glycerol at −20°C. Glycerol was removed by precipitating myosin in 50 mM KCl and 5 mM PIPES (pH 7.0) (solution A) with low-speed centrifugation at 4°C just before use. In some preparations, myosin was chromatographed on DE52, but the results were indistinguishable from those obtained by using myosin prepared without column chromatography. F-actin was generated from G-actin by the addition of 50 mM KCl, 2 mM $MgCl_2$, and 50 mM PIPES (pH 7.0). Molecular masses used for calculating molar concentrations of proteins were 115 kDa for S1, 350 kDa for HMM, 480 kDa for myosin, and 42 kDa for actin. Protein concentrations were determined by the biuret method, as well as by using the extinction coefficients of $A^{1\%}_{290\,nm} = 6.3\ cm^{-1}$ for G-actin (Lehrer and Kerwar, 1972), $A^{1\%}_{280\,nm} = 7.5\ cm^{-1}$ for S1 (Weeds and Pope, 1977), and $6.0\ cm^{-1}$ for HMM (Margossian and Lowey, 1978).

Labeling of proteins

The following five different samples were prepared as schematically illustrated in Fig. 1 (see Table 1):

1. double-labeled HMM in which 9–15% of heads were labeled with IAEDANS (D) and 60–85% with IAF (A) (HMM(D/A));
2. labeled HMM in which 69–93% of heads were labeled with D (HMM(D)) or A (HMM(A));
3. labeled S1 in which 70–83% was labeled with D (S1(D)) or A (S1(A)).

Labeled HMM and S1 were prepared by chymotryptic digestion of labeled myosin as previously reported (Kinosita et al., 1984). For the preparation of HMM(D/A), 10 mg/ml (~42 μM heads) of myosin was first mixed with 4 or 8 μM IAEDANS (10–20% molar ratios of label/myosin heads) in solution A with 0.1 mM EDTA for 3 h. Free dyes were removed by repeatedly sedimenting myosin under low-salt conditions followed by dissolution at a high-salt concentration (0.6 M KCl, 20 mM PIPES, pH 7.0). IAEDANS-labeled myosin was mixed with a threefold molar excess of IAF in solution A with 0.1 mM EDTA for 16 h. The reaction was terminated by the addition of 1 mM dithiothreitol, and free dyes were removed by repeated sedimentation as described above. The final pellet was dissolved in the above high-salt solution, and undissolved aggregates were removed by ultracentrifugation at 100,000 × *g* for 1 h; then the supernatant was dialyzed against the same high-salt solution containing 1 mM $MgCl_2$. Probes were dissolved in dimethylformamide (DMF) and slowly added to the myosin solution with continuous stirring. The volume of DMF added did not exceed 1% (v/v) of the total volume. All procedures were carried out at 4°C in the dark. The fraction of heads labeled with D was estimated before the addition of A because the absorption coefficient of D is an order of magnitude smaller than that of A.

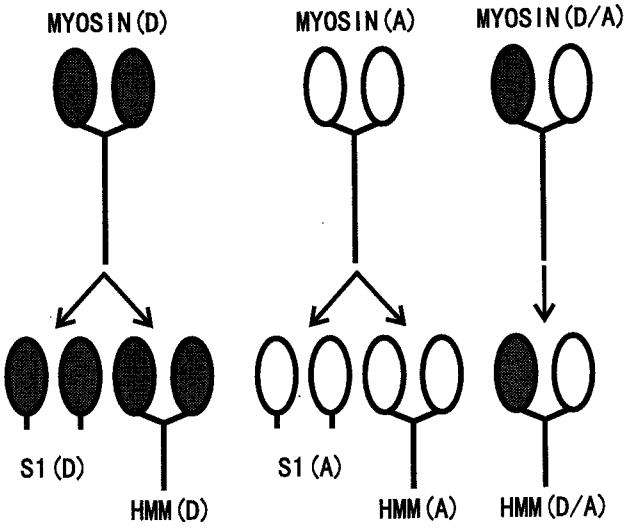

FIGURE 1 Protocol for labeling S1 and HMM with a fluorescence donor (D), IAEDANS, and a fluorescence acceptor (A), IAF. Cys707 (SH1) of myosin was labeled with either D (MYOSIN(D)) or A (MYOSIN(A)), or double-labeled with A after labeling with D (MYOSIN(D/A)). Then five different samples, S1(D), HMM(D), S1(A), HMM(A) and HMM(D/A), were prepared by chymotryptic digestion. Myosin heads labeled with D are represented by filled ovals, those labeled with A by unfilled ovals.

TABLE 1 Characterization of labeled myosin heads

Sample	Fraction of labeled heads*	Relative K^+-EDTA-ATPase rates#	Relative Ca^{2+}-ATPase rates§
S1 (unlabeled)	—	1	1 (1)
S1(D)	81.3	0.19 (81)	2.54 (2.98)
S1(A)	85.0	0.09 (91)	1.40 (2.93)
HMM(D)	79.0	0.30 (70)	2.39
HMM(A)	92.8	0.10 (90)	1.71
HMM(D/A)	15.0/80.0	0.07 (93)	2.35

*Expressed as a percentage of the ratio between molar concentrations of dyes and myosin heads. For details, see Materials and Methods.
#Relative values of ATPase rates measured in 0.45 M KCl, 5 mM ATP, 0.5 mM Tris-HCl (pH 8.0) and 1 mM EDTA at 20°C. Values in parentheses (%) are the fraction of labeled heads estimated by assuming that labeled heads lost their ATPase activity.
§Relative values of ATPase rates measured in 0.6 M KCl, 5 mM ATP, 0.5 mM Tris-HCl (pH 8.0) and 10 mM $CaCl_2$ at 20°C or 30°C (values in parentheses).

Molar labeling ratios of double-labeled HMM heads were, for example, 0.15 for D and 0.80 for A (Table 1). Here we assumed that the labeling occurs at random, such that the fraction of HMM(D/A) in which one head was labeled with D and the other with A was estimated to be 0.24 (0.15 × 0.80 × 2), the fraction in which both heads were labeled with D was 0.02 (0.15 × 0.15), that with A was 0.64 (0.80 × 0.80), and the fraction in which one of the two heads was unlabeled was 0.1. Extinction coefficients of 6,100 M^{-1} cm^{-1} at 338 nm for IAEDANS (Hudson and Weber, 1973) and 75,000 M^{-1} cm^{-1} at 490 nm for IAF (Takashi, 1979) were used to determine the labeling ratios.

Spectroscopic measurements

Absorption was measured with an ultraviolet/visible spectrophotometer, either a Philips PU 8800 or a Shimadzu UV 2100. Fluorescence intensity was measured with a photon counting SLM 8000 spectrofluorometer (Urbana, IL) operated in the ratio mode or with a Hitachi 240-60 spectrofluorometer (Hitachi Ltd., Tokyo). Light scattering intensity was measured at 550 nm at a 90° angle, using the latter spectrofluorometer. The temperature was maintained at 20°C.

Fluorescence resonance energy transfer

The efficiency (E) of FRET between probes was determined by measuring the fluorescence intensities (F) of the donor, in both the presence (F_{DA}) and the absence (F_D) of the acceptor, as given by

$$E = 1 - F_{DA}/F_D$$

E is related to the distance (R) between a donor and an acceptor and the Förster (1965) critical distance (R_0), at which E is equal to 0.5, as follows:

$$E = R_0^6/(R_0^6 + R^6)$$

R_0 (in nm) can be obtained by

$$R_0^6 = (8.79 \times 10^{-11})n^{-4}\kappa^2 Q_0 J$$

where n is the refractive index of the medium (taken to be 1.4), κ^2 is the orientation factor, Q_0 is the quantum yield of the donor in the absence of the acceptor, and J is the spectral overlap integral (in M^{-1} cm^{-1} nm^4) between donor emission and acceptor absorption. The quantum yield of IAEDANS bound to S1 was taken to be 0.44, as previously reported (Miki, 1987). κ^2 was assumed to be 2/3 for calculation of the distance R_0. In the present case, R_0 was calculated to be 4.81 nm. Thus the effective upper limit of R was ~7.5 nm.

SDS PAGE

To examine the specificity of labeling, sodium dodecyl sulfate (SDS)-polyacrylamide gel electrophoresis (PAGE) was performed according to the method of Laemmli (1970), with slight modifications (Kinosita et al., 1984). Acrylamide concentrations were 15% (w/v) for the separating gel and 5% (w/v) for the stacking gel. Coomassie Brilliant Blue R-stained SDS-PAGE gels were photographed with a Polaroid camera (600SE), using a positive/negative instant film (Polaroid 665). Fluorescent bands were photographed on a trans-illuminator (model TL-33 with 365 nm; Ultra-violet Products). SDS-PAGE in urea was performed, using 16% and 5% (w/v) acrylamide for the separating and stacking gels, respectively (Sutoh, 1981).

Other techniques

ATPase activities of unlabeled and labeled S1 and HMM were measured using a pH stat consisting of a Radiometer TTT2 titrator with a PHA943 titrigraph module, an ABU12 autoburette, and an SBR3 titrigraph assembly (Miki, 1987). The activities of labeled myosin fragments are reported relative to that of unlabeled S1 (or in the case of HMM, twice that of unlabeled S1). The binding of HMM to F-actin was determined from the protein concentration in the supernatant obtained after ultracentrifugation at 160,000 × g for 40 min at 20°C (TL-100, Beckman).

Data analysis and estimation of interhead distance

The FRET data were analyzed by model simulation. First we assumed that FRET occurs between adjacent (nearest-neighbor) S1 fragments and the heads of HMM bound to the long-helical strand of F-actin, because the FRET efficiency (E) would be negligibly small for second-nearest neighbors. Our experimental design did not require taking into account cooperative binding of S1 (or HMM) molecules to F-actin, at least at molar ratios of F-actin/S1 (or heads of HMM) below 1, because virtually all of the F-actin sites were occupied by bound S1 (and/or HMM). The actual degree of occupancy depends on the binding constant under rigor conditions. Under our experimental conditions, it could be assumed that the fraction of A-labeled heads adjacent to a D-labeled head on an F-actin is equal to the fraction of attached A-labeled heads. Thus we were able to analyze the data according to the binding equilibrium equations assuming random binding between S1 (and/or HMM) molecules and F-actin. The following exemplifies our approach.

1. Consider S1 binding to F-actin (FA):

$$\text{FA} + \text{S1} \leftrightarrow \text{FA-S1}: \quad K[\text{FA}][\text{S1}] = [\text{FA-S1}]$$

where we assumed that the binding constant K does not depend on whether S1 is labeled. The total concentrations of actin ($[FA_0]$) and S1 ($[S1_0]$) are

$$[\text{FA}_0] = [\text{FA}] + [\text{FA-S1}]$$

$$[\text{S1}_0] = [\text{S1}] + [\text{FA-S1}]$$

$$[\text{FA-S1}] = [\text{FA-S1(D)}] + [\text{FA-S1(A)}] + [\text{FA-S1(U)}]$$

$$[\text{S1}] = [\text{S1(D)}] + [\text{S1(A)}] + [\text{S1(U)}]$$

where S1(U) indicates unlabeled S1. By solving these equations, we determined the concentrations of each species.

Here the fluorescence intensity (F) of D is represented by the following equation:

$$F([\text{FA}_0], f) = [\text{S1(D)}] + a[\text{FA-S1(D)}]G(f)$$

where f is the fraction of actin-binding sites with attached S1(A), i.e., f = [FA-S1(A)]/[FA_0]; a is the ratio of fluorescence intensities of D in attached

and detached states in the absence of A, i.e., $a = F(\text{FA-S1(D)})/F(\text{S1(D)})$, which was determined to be 1.1. $G(f)$ is a factor contributing to a decrease in fluorescence intensity due to the FRET between each donor and adjacent acceptor(s) in the rigor complex with F-actin:

$$G(f) = (1-f)^2 + 2f(1-f)/\{1 + (R_0/R)^6\} + f^2/\{1 + 2(R_0/R)^6\}$$

where R_0 is the Förster critical distance (i.e., 4.81 nm) for the combination of IAEDANS and IAF. In practice, F was examined after normalization with the F of S1(D) measured in the absence of S1(A) at the same $[FA_0]$.

2. Next we briefly present the case of HMM:

$$\text{FA} + \text{HMM} \leftrightarrow \text{FA-HMM}: K'[\text{FA}][\text{HMM}] = [\text{FA-HMM}]$$

where we assumed that the binding constant K' does not depend on whether both heads of HMM are labeled with D (HMM(D)) or A (HMM(A)) or are unlabeled (HMM(U)), or only one head is labeled with either D or A, and the other head is unlabeled (HMM(D/U) or HMM(A/U), respectively). The total concentrations of actin ($[FA_0]$) and HMM ($[HMM_0]$) are

$$[FA_0] = [FA] + 2[\text{FA-HMM}]$$

$$[HMM_0] = [HMM] + [\text{FA-HMM}]$$

$$[\text{FA-HMM}] = [\text{FA-HMM(D)}] + [\text{FA-HMM(A)}] + [\text{FA-HMM(U)}] + [\text{FA-HMM(D/U)}] + [\text{FA-HMM(A/U)}]$$

$$[HMM] = [HMM(D)] + [HMM(A)] + [HMM(U)] + [HMM(D/U)] + [HMM(A/U)].$$

Other formulations are essentially the same as that for case 1, that is,

$$F([FA_0], f) = 2[HMM(D)] + [HMM(D/U)] + a\{2[\text{FA-HMM(D)}] + [\text{FA-HMM(D/U)}]\}G(f)$$

and

$$G(f) = (1-f) + f/\{1 + (R_0/R)^6\}$$

where $f = \{2[\text{FA-HMM(A)}] + [\text{FA-HMM(A/U)}]\}/[FA_0]$.

For data analysis, the above F was normalized by dividing it by the F of HMM(D), measured in the absence of HMM(A) at the same $[FA_0]$.

The interhead distance obtained in this study depended on the values of the chosen binding constants. The larger (or smaller) the value of the binding constants we assumed, the longer (or shorter) were the interhead distances. However, the maximum deviation of 0.1 nm was estimated for the interhead distances for binding constants ×2 or ×0.5 the assumed values. Taking into account the published binding constants (Marston and Weber, 1975; Highsmith, 1977, 1978; Margossian and Lowey, 1978; Miyanishi and Borejdo, 1989) and comparing the light scattering and simulated curves shown in Figs. 3–7, we determined that the combination of $K = 10^7/\text{M}$ and $K' = 5 \times 10^7/\text{M}$ best fits the data.

On the other hand, we assumed that the light scattering intensity increases in proportion to the attached S1 and HMM heads in which, for the sake of simplicity, their different contributions to the light scattering intensity were not taken into account.

By assuming a helical symmetry for SH1 groups around an actin filament (Fig. 2), their average radial coordinate, q, about the actin filament can be estimated (Taylor et al., 1981) by

$$R^2 = (2q \sin(\phi/2))^2 + P^2$$

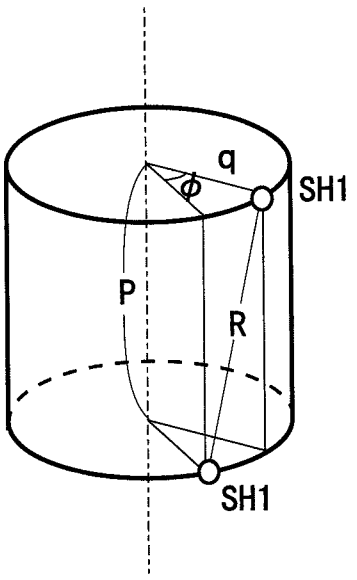

FIGURE 2 A schematic illustration of the geometry of the location of SH1 of myosin heads when attached to F-actin. The vertical broken line represents the central axis of F-actin; R, the distance between adjacent SH1 groups of myosin heads; P, the pitch of an actin molecule in F-actin, 5.5 nm; ϕ, 28°. We assumed that the arrangement of myosin heads around F-actin has helical symmetry and that SH1 is located on a cylinder with a radius (radial coordinate) of q.

where R is the distance between adjacent SH1 sites, q is the radial coordinate of the probe with respect to the actin filament axis, the angle ϕ (=28°) is the rotation of one monomer with respect to the next monomer along the same long-pitch strand, and P (=5.5 nm) is the pitch of an actin monomer along a long-pitch helical strand of F-actin. These parameters are defined in Fig. 2.

RESULTS

Characterization of labeled myosin

SDS PAGE showed that the labels were selectively incorporated into SH1 of myosin heavy chains (data not shown). Labeled S1 was digested with trypsin and further treated with hydroxylamine for 5.5 h at 45°C. Our observations were in accordance with those of Sutoh (1981), who previously showed the 20-kDa fragment of the S1 heavy chain, which contains the two "essential" thiol groups SH1 and SH2, to be fragmented by hydroxylamine treatment into a 13-kDa peptide containing SH1 and a 7-kDa peptide containing SH2. Only the 20-kDa and 13-kDa fragments were fluorescent, indicating that both labels are selectively attached to SH1.

The K^+-EDTA-ATPase and Ca^{2+}-ATPase activities of SH1-labeled S1 and HMM were compared with those of unlabeled S1 (Table 1). The decrease in K^+-EDTA ATPase activity of labeled S1 and HMM was consistent in relationship to the fraction of labeled heads estimated from spectroscopic data. On the other hand, the Ca^{2+}-ATPase activities of labeled S1 and HMM were greater than that of unlabeled S1. These results also indicated a specific labeling

of SH1 under our present experimental conditions (Sekine and Kielley, 1964; Seidel, 1969). It should be noted that the extent of the increase in Ca^{2+}-ATPase activity induced by SH1 labeling strongly depends on the species of labeling dyes and on the temperature (especially in the case of IAF) at which the ATPase measurements are carried out.

The shape of the absorption and emission spectra of HMM, double-labeled with IAEDANS (D) and IAF (A), was the superposition of the spectra of HMM labeled with either D or A. Throughout these experiments, the fluorescence intensity of IAEDANS was measured at 470 nm (the noise level was ~1% of the signal level), with excitation at 338 nm, the wavelength at which there was no contribution from the fluorescence of IAF (spectra, not shown).

FRET between intermolecular heads of S1(D) and S1(A) attached to F-actin

The change in fluorescence intensity of IAEDANS-labeled S1 (S1(D)) in the mixture with IAF-labeled S1 (S1(A)) after the addition of F-actin was measured under rigor conditions. As shown in Fig. 3, the normalized fluorescence intensity ($F_{DA}/F_D = 1 - E$) decreased as the molar ratios of actin to S1 increased up to 1, and then increased again to nearly the initial value. With this change, the light scattering intensity increased and saturated at a molar ratio of ~1. The recovery of fluorescence intensity at molar ratios of >1 can be attributed to a decrease in the fraction of neighboring S1(A) on the F-actin filaments. This is shown schematically in the inset in Fig. 3. Ultracentrifugation of the F-actin/S1 complex at a molar ratio of 1:1 showed that ~95% of S1 cosedimented with F-actin, demonstrating that 95% of the heads were attached to F-actin, leaving ~5% of S1 in the supernatant.

The data were analyzed according to the random attachment model described in Materials and Methods. Three curves superimposed on the data indicated that the average interhead distance (= distance between nearest-neighbor SH1s) is 6.2 nm (corresponding radial coordinate, q = 5.9 nm), although the data deviated from the simulated curve, especially at higher molar ratios of F-actin and S1. Here and below, we present a set of data obtained by using a preparation with a certain D/A labeling ratio, except in the case of HMM(D/A); although we did not obtain duplicate data for every point, some duplicate data suggest that the estimation error for donor-acceptor distances is within the range of the three calculated curves shown in the figures.

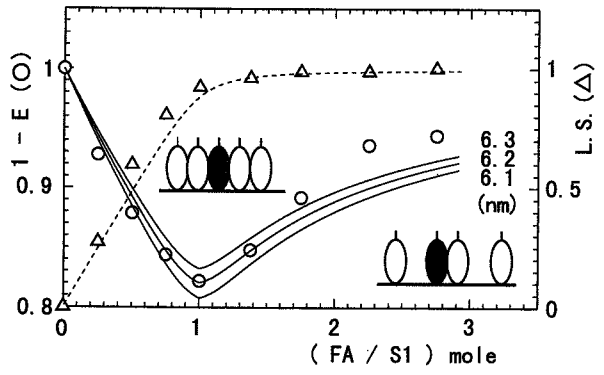

FIGURE 3 Change in FRET efficiency (E) between S1(D) and S1(A) induced by the addition of F-actin (○) under rigor conditions. The binding of S1 and F-actin was monitored by light scattering intensity (LS) at 550 nm (△). S1(D), 73% labeled with IAEDANS; S1(A), 70% labeled with IAF. A small volume of 7 mg/ml (167 μM) of F-actin solution (0.1 M KCl, 1 mM $MgCl_2$, 20 mM Tris-HCl, pH 8.0, 0.1 mM ATP) was added stepwise (final concentration 17 μM) to the solution containing 0.035 mg/ml (0.3 μM) S1(D) and 0.7 mg/ml (6 μM) of S1(A) dissolved in 0.1 M KCl, 1 mM $MgCl_2$, 20 mM Tris-HCl (pH 8.0) at 20°C. The fluorescence intensity was measured after hydrolysis of contaminant ATP. Dilution effects were taken into consideration. The inset illustrates schematically the binding of S1 to F-actin (see Fig. 1). The three curves obtained by model simulation are superimposed on the data. The distance between adjacent S1(D) and S1(A) used for obtaining each curve is shown on the right-hand side.

FRET between intermolecular heads of S1(D) and HMM(A) attached to F-actin

The FRET was determined for a mixture of S1(D) and HMM(A) in the presence of various amounts of F-actin under rigor conditions. As shown in Fig. 4, the normalized fluorescence intensity decreased with increasing molar ratios of F-actin to heads (S1(D) + heads of HMM(A)) up to 1 and then increased again to nearly the initial value. Note that the decrease in fluorescence intensity as the molar ratios approached 1 was convex upward, which contrasts with the S1(D)/S1(A) case in which the decrease was slightly concave (Fig. 3; a characteristic curve was also distinct in other preparations). The simulation curve can reproduce these characteristics. In addition, the average interhead distance was estimated to be 6.3 nm, which is nearly equal to that observed for the S1(D)/S1(A) case. On the other hand, the light scattering intensity increased linearly and saturated when the molar ratio of actin and heads

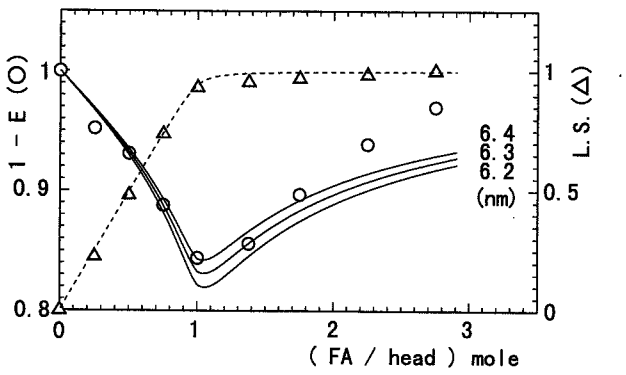

FIGURE 4 Change in FRET efficiency (E) between S1(D) and HMM(A) induced by the addition of F-actin (○) under rigor conditions. The binding of S1 and HMM to F-actin was monitored by light scattering intensity at 550 nm (△). Other conditions and experimental procedures were the same as in Fig. 3, except that 1.05 mg/ml (3 μM = 6 μM heads) of 69% labeled HMM(A) was used instead of S1(A). The abscissa shows the numerical ratio of added actin against S1(D) plus heads of HMM(A).

was 1, suggesting a 1:1 stoichiometry for myosin heads bound to F-actin, similar to the S1(D)/S1(A) case (Fig. 3). The major difference from this latter case is the steep curve around molar ratios of 1, indicating a large HMM binding constant.

FRET between intermolecular heads of HMM(D) and S1(A) attached to F-actin

Similar experiments were performed using mixtures of HMM(D) and S1(A). As shown in Fig. 5, the normalized fluorescence intensity decreased as the molar ratios of actin monomers to heads (S1(A) + heads of HMM(D)) increased up to 1, and then increased again to nearly the initial value. There is a clear concave, although smaller, decrease in fluorescence intensity (up to 0.9). Despite this, the calculated average interhead distance was similar, i.e., ~6.1 nm. In addition, the light scattering intensity data confirmed that binding stoichiometry occurs at a molar ratio of actin monomers to heads of ~1.

FRET between intermolecular heads of HMM(D) and HMM(A) attached to F-actin

Experiments were done for the fourth combination of heads, using a mixture of HMM(D) and HMM(A). As shown in Fig. 6, the normalized fluorescence intensity decreased with an increase in the molar ratios of actin monomers to total heads, and then increased above molar ratios of 1. The average interhead distance obtained by the model simulation produced a value similar to those of the above combinations, i.e., ~6.0 nm. Changes in light scattering intensity were similar to those of the other cases, although the data points were slightly more scattered and a gradual decrease was seen above molar ratios of 1.

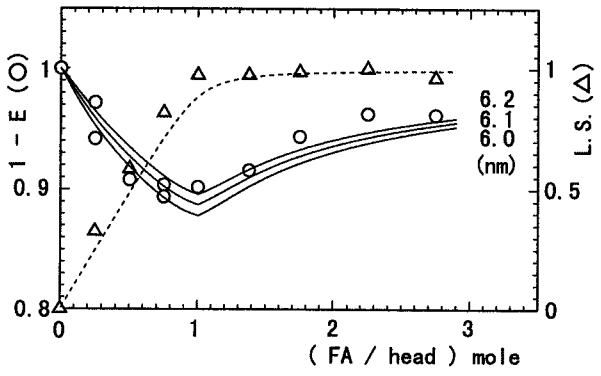

FIGURE 5 Change in FRET efficiency (E) between HMM(D) and S1(A) induced by the addition of F-actin (○) under rigor conditions. The binding of HMM and S1 to F-actin was monitored by light scattering intensity at 550 nm (△). Other conditions and experimental procedures were the same as in Fig. 3, except that 0.056 mg/ml (0.16 μM = 0.32 μM heads) of 78% labeled HMM(D) was used instead of S1(D). The abscissa shows the numerical ratio of added actin against S1(A) plus heads of HMM(D).

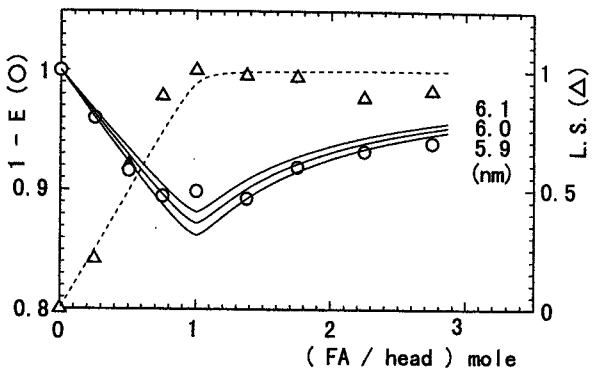

FIGURE 6 Change in FRET efficiency (E) between HMM(D) and HMM(A) induced by the addition of F-actin (○) under rigor conditions. The binding of HMM to F-actin was monitored by light scattering intensity at 550 nm (△). Other conditions and experimental procedures were the same as in Fig. 3, except that 0.056 mg/ml (0.16 μM = 0.32 μM heads) of 78% HMM(D) and 1.05 mg/ml (3 μM = 6 μM heads) of 69% labeled HMM(A) were used instead of S1(D) and S1(A), respectively. The abscissa shows the numerical ratio of added actin against heads of HMM(D) and HMM(A).

FRET between intramolecular heads in HMM attached to F-actin

Using the techniques described above, we designed experiments to determine the intramolecular interhead distance (R_{intra}) of HMM molecules attached to F-actin, complementing the intermolecular interhead distance (R_{inter}) obtained above. Fig. 7 summarizes the results of the fluores-

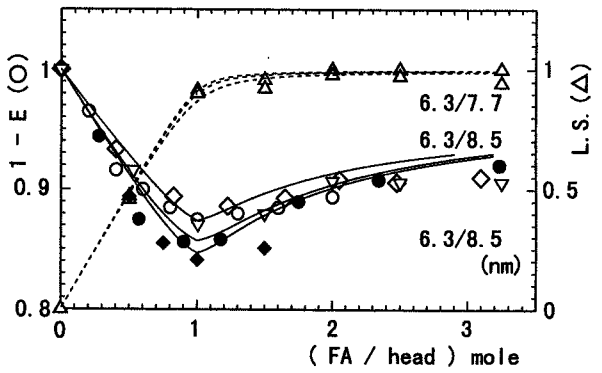

FIGURE 7 Change in FRET efficiency (E) within and between HMM(D/A) molecules induced by the addition of F-actin (●, ◆, ○, ◇, ▽) under rigor conditions. The binding of HMM to F-actin was monitored by light scattering intensity at 550 nm (△). Other conditions and experimental procedures were the same as in Fig. 6, except that double-labeled HMM(D/A) was used instead of HMM(D) and HMM(A). Three different HMM(D/A) preparations were examined: ●, ◆, 0.40 mg/ml (1.15 μM = 2.3 μM heads) HMM(D/A) containing 9% D and 85% A, F-actin was added stepwise up to 7.36 μM; ○, ◇, 0.175 mg/ml (0.5 μM = 1.0 μM heads) HMM(D/A) containing 15% D and 80% A, F-actin was added stepwise up to 3.2 μM; ▽, 0.30 mg/ml (0.86 μM = 1.7 μM heads) HMM(D/A) containing 15% D and 60% A, F-actin was added stepwise up to 5.2 μM. A model simulation was done for each preparation. The distance corresponding to each curve is shown on the right-hand side, with the intermolecular interhead distance (R_{inter}) being shown on the left-hand side and the intramolecular interhead distance (R_{intra}) on the right.

cence intensity and light scattering experiments with three different D/A ratios. A range of different protein concentrations was examined to test the suitability of the model simulations. We anticipated that the results (Fig. 7) would mirror those described above. However, the data unexpectedly resulted in an average interhead distance of 7.0 nm, rather than the 6.0–6.3 nm obtained above. The best fit of the simulation curves to the data is shown here (Fig. 7). We have made the reasonable assumption that the distance between heads on different molecules (R_{inter}) remained at 6.3 nm. Note that a similar interhead distance was obtained, irrespective of the fraction of donor-labeled and acceptor-labeled heads produced in the HMM population.

FRET between intramolecular heads in free HMM

These experiments were designed to distinguish between D/A labeled heads that were not constrained by binding to F-actin. Thus we attempted to determine whether FRET occurs between heads within free HMM molecules in the absence of F-actin. For this purpose, we compared the time course of fluorescence intensity changes in double-labeled HMM(D/A) molecules with that of HMM(D) after the addition of trypsin (Chantler and Tao, 1986). Had FRET occurred between the unattached heads of HMM, the ratio of the fluorescence intensities for HMM(D/A) and HMM(D) would presumably have increased, because the FRET efficiency would have decreased because of the separation of heads by limited tryptic digestion. The results (data not shown) revealed a decrease in fluorescence intensity of HMM(D/A) similar to that observed with HMM(D). Thus no appreciable change in the ratio of fluorescence intensities was detected.

DISCUSSION

Characteristics of SH1-labeled myosin

Since Sekine and Kielley (1964) first demonstrated that specific modification of SH1 on myosin heads with *N*-ethylmaleimide activates the Ca^{2+}-promoted ATPase activity of myosin while inhibiting the K^+-EDTA ATPase activity, many researchers have used this property to identify the specific labeling of this locus with fluorescent dyes (dos Remedios et al., 1987). Therein we have shown that the extent of the activation of the Ca^{2+}-ATPase activity by SH1 modification depends on the labeling dyes used and on the temperature at which the ATPase activity is measured (Table 1). This was also the case for the labeling of SH1 of S1 with IANBD, in which the Ca^{2+}-ATPase activity of IANBD-S1 was less than that of unlabeled S1 at 20°C and was 1.7 times that of unlabeled S1 at 38°C (Miki and Wahl, 1984). Thus these properties of the Ca^{2+}-ATPase activity must be considered for identifying the specific SH labeling.

Estimation of interhead distance by FRET

In the FRET analysis, κ^2 was assumed to be ⅔. The upper and lower bounds of this parameter were calculated according to the method of Dale et al. (1979). The limiting anisotropies of IAEDANS and IAF bound to SH1 were previously determined to be 0.283 (Takashi, 1979) and 0.285 (Miki and Wahl, 1984), respectively. The fundamental anisotropies of IAEDANS and IAF have been reported to be 0.328 (Hudson and Weber, 1973) and 0.4 (Chen and Bowman, 1965), respectively. These values give a maximum error range for the critical distance (R_0) calculated by using κ^2 = ⅔ of ~30%, i.e., the calculated range appears to be unacceptably large. It should be noted, however, that the extreme values of R_0 correspond to extreme cases in which the axes of the cones in which the donor and acceptor transition moments rotate rapidly are oriented entirely in unique directions, i.e., perpendicular or parallel to each other. In this calculation, depolarization due to segmental motions of macromolecules (in the time range of 10^{-8} to 10^{-6} s) are not taken into account in estimating the orientation of the transition moments.

Proteins are flexible rather than rigid macromolecules and, therefore, the directions of the transition moments of the probes are probably randomized because of segmental motions. Moreover, in the acto-S1(D) rigor complex, FRET will occur from the probe on SH1 of one S1(D) to its two neighboring S1(A), except in the presence of excess F-actin, which tends to average the range of possible κ^2-values. The real range of κ^2 is thus probably much narrower, and consequently we can expect a concomitant increase in the accuracy of the measured distances.

We have pointed out elsewhere (Miki et al., 1992) that reasonable agreement was obtained between intramolecular distances determined by FRET assuming κ^2 = ⅔. More recently, good agreement was reported between the radial coordinates of specific labels on F-actin and x-ray diffraction data from aligned F-actin (Holmes et al., 1990; dos Remedios and Moens, 1995a). Thus there is mounting evidence for agreement between FRET data, for which interprobe distances have been calculated assuming κ^2 = ⅔, and the same dimension determined by x-ray diffraction.

Experimental conditions for FRET measurements

In the titration experiments shown in Figs. 3–7, we added a small volume of concentrated F-actin stepwise to a D- and A-labeled S1 (and/or HMM) solution and measured the fluorescence intensity of the donor. Although we intended to measure the interhead distance in the rigor complex, a low concentration of ATP remained in the F-actin solution, which would have allowed repeated detachment and reattachment of heads, so as to randomize binding accompanying the hydrolysis of ATP every time F-actin was added. We believe this procedure was especially important for achieving random, nonclustered binding at molar ratios of F-actin to heads greater than 1.

As a consequence, there is a stepwise accumulation of the products of ATP hydrolysis such that at an actin:S1 molar ratio of 1, the ADP concentration would be $\sim 4 \times 10^{-6}$ M. However, the dissociation constant of ADP for the acto-S1 complex and myofibrils is $\sim 2 \times 10^{-4}$ M (White and Taylor, 1976; Greene and Eisenberg, 1980; Johnson and Adams, 1984). We estimate that only $\sim 2\%$ ($= 100 \times (4 \times 10^{-6})/(2 \times 10^{-4})$) of the rigor complex will have bound ADP. Thus we conclude that the actomyosin complexes in our experiments were exclusively in a rigor state.

Interhead distances between S1 and HMM attached to F-actin

No energy transfer was detected between probes on the two heads of HMM that were not attached to F-actin. Because the R_0 for our probe pair is 4.81 nm, the donor and acceptor probes cannot be closer than ~8 nm in solution. This result is consistent with previous reports that the interhead distance between homologous light chains located at the neck region of (scallop) myosin was too great to be detected by the FRET method (Chantler and Tao, 1986), and that the two heads of myosin in the thick filaments in the relaxed state are mobile (Kinosita et al., 1984; Ishiwata et al., 1987a). Consequently, two heads of myosin are, on average, widely separated in solution.

On the other hand, in the rigor complex, Katayama and Wakabayashi (1981) analyzed the three-dimensional image of the acto-HMM rigor complex and concluded that there is little difference in the conformations of the two heads of HMM and that both bind to the homostrand of the two-start F-actin helix (see also Craig et al., 1980). This is consistent with our data. We found that the calculated distances between two SH1 probes on HMM(D) and HMM(A), S1(D) and HMM(A), and S1(A) and HMM(D) were 6.0, 6.3, and 6.1 nm, respectively, being consistent with the 6.2 nm between S1(D) and S1(A) (Fig. 8). Thus the interhead distances did not appear to depend on whether the myosin head was free (S1) or attached to another head (HMM).

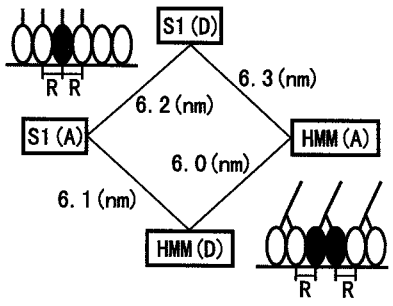

FIGURE 8 The distances between S1 molecules and the heads of HMM molecules attached to F-actin, estimated by model simulation. The binding geometry of S1 and HMM molecules is illustrated schematically in the upper left-hand and lower right-hand portions of the figure. S1 is shown as an oval with a short tail, and HMM is illustrated as two ovals connected by a Y-shaped tail. Filled and unfilled ovals represent D-labeled and A-labeled heads, respectively.

Taken together, these observations indicate that the two heads of HMM must bind to successive monomers along the same long pitch helix of F-actin and that there is no gross distortion in the two heads of HMM, at least around the tip portion containing SH1 groups, when they bind to F-actin. The only exception, as discussed below, is the case in which HMM contains both a donor and an acceptor.

It is noteworthy that, in the case of S1, the calculated curves deviated significantly from the data points when the concentration of actin exceeded that of S1 (Figs. 3–5). These results may be partly attributable to the existence of S1 heads that changed their position/orientation, leading to an increase in the donor-acceptor distance by 1) binding with an altered head orientation (Andreev and Borejdo, 1992; Xiao et al., 1995) and/or 2) bundling formation of actin filaments (Ando and Scales, 1985), both of which occur only at molar ratios of actin/S1 > 1. In contrast, the fit was much better for HMM (Fig. 6), suggesting that the altered head orientation may be characteristic of S1.

The radial coordinate, q (Fig. 2), was estimated from the interhead distances (R = 6.0–6.3 nm) to be 5.0–6.4 nm. The accuracy of this estimate is lower than that of R, e.g., a variation of 0.1 nm of R (at around 6.0 nm of R) corresponds to ~0.4 nm of q. It should also be noted that, were the position of SH1 to be distributed around the average position, the FRET distance would represent a lower bound because FRET efficiency depends on the inverse sixth power of R.

Intramolecular interhead distance of HMM attached to F-actin

The unexpected and most interesting consequence of our data is the estimate of the intramolecular interhead distance of HMM molecules attached to F-actin. To estimate this distance, we prepared HMM double-labeled with D and A. The model simulation showed that the average interhead distance was longer than the intermolecular interhead distance, R_{inter}, estimated using HMM(D) and HMM(A). This result was not anticipated because the intramolecular interhead distance, R_{intra}, was expected to be somewhat shorter. In fact, Onishi et al. (Onishi et al., 1989; Onishi and Fujiwara, 1990), using a cross-linking technique, demonstrated that intramolecular head-to-head contact occurs in the complex of smooth muscle HMM and F-actin.

Fig. 9 is a schematic interpretation of HMM results in which shaded and unshaded ovals represent donor-labeled and acceptor-labeled heads, respectively. HMM is shown as two oval heads connected by a Y-piece. In Fig. 9 *a*, the two heads of HMM are separated by a longer distance, R_{intra}, than R_{inter}. In this case, a straightforward interpretation is that the F-actin/HMM complex is distorted so as to make the R_{intra} longer than R_{inter}. This interpretation is realistic because some distortion of the molecule is expected to occur when the second head of an HMM molecule is bound to F-actin. However, in this case, the q and/or ϕ defined in

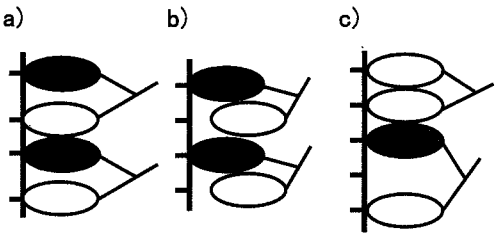

FIGURE 9 An illustration showing three possible interpretations of the model simulations of the binding geometry of HMM(D/A) to F-actin. The intramolecular interhead distance (R_{intra}) is longer than the intermolecular interhead distance (R_{inter}) because of (*a*) the distortion of the structure of an F-actin/HMM complex; (*b*) one-head binding; or (*c*) second-nearest neighbor binding. In the cases of *a* and *c*, R_{intra} is actually longer than R_{inter}. On the other hand, in the case of *b*, the average interhead distance (R_{intra} + R_{inter})/2) is longer than that in the F-actin-HMM (D or A) complex.

Fig. 2 should change, and such changes might be detectable by electron microscopy and/or x-ray fiber diffraction.

A second and more plausible interpretation of our data is illustrated in Fig. 9 *b*. In this scheme, the distances R_{intra} and R_{inter} do not differ, and the binding constant of the acceptor-labeled head for F-actin is effectively decreased because of the heterogeneous labeling. Thus the apparent binding constant of HMM(D/A) molecules will become different from that of HMM(D) or HMM(A). The slight curve observed between molar ratios of 0 and 1 in Figs. 3 and 6 can be more precisely simulated by assuming that the D-labeled heads have a binding constant a few times greater than that of both the A-labeled heads and the unlabeled heads. The tendencies of the data to be convex or concave, as shown in Figs. 4 and 5, are attributable mainly to the higher binding constant of HMM as compared to S1. Thus we speculate that in HMM, in which each head carries a donor or acceptor label (HMM(D/A)), the first head to bind is predominantly D-labeled and the binding equilibrium of the second A-labeled head is reduced, as shown in Fig. 9 *b*. Such single-head binding may be analogous to that previously suggested as the binding mode of HMM with F-actin in the presence of sub-mM PPi (Fujime et al., 1972).

A third interpretation is shown schematically in Fig. 9 *c*. The two heads of HMM(D/A) molecules are assumed to bind to F-actin, along a long strand, to every other actin molecule because of the heterogeneity of the labeled heads. If only 10% of HMM molecules attach to F-actin as shown in Fig. 9 *c*, such that the light scattering determination of the binding stoichiometry is not affected, this would explain the observed increase in the intra-HMM distances (because fluorescence is an average measurement).

CONCLUSIONS

We describe a new method for analyzing FRET data. This method is a potentially powerful tool for analyzing the separate contributions of intramolecular and intermolecular interhead distances from observed fluorescence intensities of S1 and HMM attached to F-actin.

We have demonstrated that under rigor conditions, the interhead distance between SH1 loci is very large in free solution and that the distance (6.0–6.3 nm) between HMM heads attached to F-actin is consistent with their sequential attachment to successive actin monomers along the long-pitch helix of the actin filament. This distance appears to be significantly greater when measured between the two heads of (double-labeled) HMM.

This structural approach was used to analyze the myosin heads interacting with F-actin in the absence of Mg-ATP and is applicable to other states in the kinetic cycle of Mg-ATP hydrolysis.

This paper is dedicated to the memory of Jack Seidel, one of the pioneers in the study of myosin sulfhydryl groups.

A preliminary but essential part of this work was performed in Sydney while one of the authors (SI) was participating in an exchange program for faculty members between the University of Sydney and Waseda University. We thank both universities. We are grateful to Dr. W. Gratzer for his helpful comments on a preliminary version of the manuscript. We also thank the reviewers for their valuable comments.

This work was partially supported by the Ministry of Education, Science, Sports and Culture of Japan, and CREST of Japan, and by a project grant from the National Health and Medical Council of Australia.

REFERENCES

Ando, T., and D. Scales. 1985. Skeletal muscle myosin subfragment-1 induces bundle formation by actin filaments. *J. Biol. Chem.* 260: 2321–2327.

Andreev, O. A., and J. Borejdo. 1992. Two different acto-S1 complexes. *J. Muscle Res. Cell Motil.* 13:523–533.

Brown, L., and B. Hambly. 1996. Distance between the alkali light chains of myosin subfragment-1 bound to F-actin measured using fluorescence spectroscopy. *Biophys. J.* 70:A264. (Abstr.)

Chantler, P. D., and T. Tao. 1986. Interhead fluorescence energy transfer between probes attached to translationally equivalent sites on the regulatory light chains of scallop myosin. *J. Mol. Biol.* 192:87–99.

Chen, R. F., and R. L. Bowman. 1965. Fluorescence polarization measurement with ultraviolet polarizing filters in a spectrophotofluorometer. *Science.* 147:729–732.

Craig, R., A. G. Szent-Györgyi, L. Beese, P. Flicker, P. Vibert, and C. Cohen. 1980. Electron microscopy of thin filaments decorated with a Ca^{2+}-regulated myosin. *J. Mol. Biol.* 140:35–55.

Dale, R. E., J. Eisinger, and W. E. Blumberg. 1979. Orientational freedom of molecular probes. Orientation factor in intramolecular energy transfer. *Biophys. J.* 26:161–194.

dos Remedios, C. G., M. Miki, and J. A. Barden. 1987. Fluorescence resonance energy transfer measurements of distances in actin and myosin. A critical evaluation. *J. Muscle Res. Cell Motil.* 8:97–117.

dos Remedios, C. G., and P. D. J. Moens. 1995a. Actin and the actomyosin interface: a review. *Biochim. Biophys. Acta.* 1228:99–124.

dos Remedios, C. G., and P. D. J. Moens. 1995b. Fluorescence resonance energy transfer spectroscopy is a reliable "ruler" for measuring structural changes in proteins. Dispelling the problem of the unknown orientation factor. *J. Struct. Biol.* 115:175–185.

Förster, T. 1965. Delocalized excitation and excitation transfer. *In* Modern Quantum Chemistry. O. Sinanoglu, editor. Academic Press, New York. 93–137.

Fujime, S., S. Ishiwata, and T. Maeda. 1972. F-actin-heavy meromyosin complex studied by optical homodyne and heterodyne methods. *Biochim. Biophys. Acta.* 283:351–363.

Greene, L. E., and E. Eisenberg. 1980. Dissociation of the actin-subfragment 1 complex by adenyl-5'-yl imidodiphosphate, ADP, and PPi. *J. Biol. Chem.* 255:543–548.

Highsmith, S. 1977. The effects of temperature and salts on myosin subfragment-1 and F-actin association. *Arch. Biochem. Biophys.* 180: 404–408.

Highsmith, S. 1978. Heavy meromyosin binds actin with negative cooperativity. *Biochemistry.* 17:22–26.

Holmes, K. C., D. Popp, W. Gebhard, and W. Kabsch. 1990. Atomic model of the actin filament. *Nature.* 347:44–49.

Hudson, E. N., and G. Weber. 1973. Synthesis and characterization of two fluorescent sulfhydryl reagents. *Biochemistry.* 12:4154–4161.

Ishiwata, S., K. Kinosita, Jr., H. Yoshimura, and A. Ikegami. 1987a. Rotational motions of myosin heads in myofibril studied by phosphorescence anisotropy decay measurements. *J. Biol. Chem.* 262: 8314–8317.

Ishiwata, S., M. Miki, and C. G. dos Remedios. 1987b. Measurement of inter-head distance of myosin using fluorescence energy transfer method. *Biophys. Suppl. (Japanese).* 27:S86. (Abstr.)

Ishiwata, S., M. Miki, T. Funatsu, and C. G. dos Remedios. 1988. Fluorescence energy transfer between heads of myosin bound to F-actin under rigor condition. Proceedings of the 2nd Japan-China Bilateral Symposium on Biophysics, pp. 293–294.

Ishiwata, S., M. Miki, I. Shin, T. Funatsu, K. Yasuda, and C. G. dos Remedios. 1996. Distance between myosin heads in rigor complex measured by fluorescence resonance energy transfer. *Biophys. J.* 70: A14. (Abstr.)

Johnson, R. E., and P. H. Adams. 1984. ADP binds similarly to rigor muscle myofibrils and to actomyosin-subfragment one. *FEBS Lett.* 174: 11–14.

Kabsch, W., H. G. Mannherz, D. Suck, E. F. Pai, and K. C. Holmes. 1990. Atomic structure of the actin:DNase I complex. *Nature.* 347:37–44.

Kasprzak, A. A., R. Takashi, and M. F. Morales. 1988. Orientation of the actin monomer in the F-actin filament: radial coordinate of glutamine-41 and effect of myosin subfragment-1 binding on the monomer orientation. *Biochemistry.* 27:4512–4522.

Katayama, E., and T. Wakabayashi. 1981. Three-dimensional image-analysis of the complex of thin filaments and myosin molecules from skeletal muscle. III. The multi-domain structure of actin heavy meromyosin complex. *J. Biochem.* 90:703–714.

Kielley, W. W., and L. B. Bradley. 1956. The relation between sulfhydryl groups and the activation of myosin adenosinetriphosphatase. *J. Biol. Chem.* 218:653–659.

Kinosita, Jr., K., S. Ishiwata, H. Yoshimura, H. Asai, and A. Ikegami. 1984. Submicrosecond and microsecond rotational motions of myosin head in solution and in myosin synthetic filaments as revealed by time-resolved optical anisotropy decay measurements. *Biochemistry.* 23:5963–5975.

Laemmli, U. K. 1970. Cleavage of structural proteins during the assembly of the head of bacteriophage T4. *Nature.* 227:680–685.

Lehrer, S. S., and G. Kerwar. 1972. Intrinsic fluorescence of actin. *Biochemistry.* 11:1211–1217.

Lorenz, M., D. Popp, and K. C. Holmes. 1993. Refinement of the F-actin model against x-ray fiber diffraction data by the use of a directed mutation algorithm. *J. Mol. Biol.* 234:826–836.

Margossian, S. S., and S. Lowey. 1978. Interaction of myosin subfragments with F-actin. *Biochemistry.* 17:5431–5439.

Marston, S., and A. Weber. 1975. The dissociation constant of the actin-heavy meromyosin subfragment-1 complex. *Biochemistry.* 14: 3868–3873.

McLaughlin, P. J., J. T. Gooch, H.-G. Mannherz, and A. G. Weeds. 1993. Structure of gelsolin segment 1-actin complex and the mechanism of filament severing. *Nature.* 364:685–692.

Miki, M. 1987. The recovery of the polymerization of Lys-61-labeled actin by the addition of phalloidin. *Eur. J. Biochem.* 164:229–235.

Miki, M., S. I. O'Donoghue, and C. G. dos Remedios. 1992. Structure of actin observed by fluorescence resonance energy transfer spectroscopy. *J. Muscle Res. Cell Motil.* 13:132–145.

Miki, M., and P. Wahl. 1984. Fluorescence energy transfer between points in acto-subfragment-1 rigor complex. *Biochim. Biophys. Acta.* 790: 275–283.

Miyanishi, T., and J. Borejdo. 1989. Differential behavior of two cysteine residues on the myosin head in muscle fibers. *Biochemistry.* 28: 1287–1294.

Moens, P. D. J., D. J. Yee, and C. G. dos Remedios. 1994. Determination of the radial coordinate of Cys-374 in F-actin using fluorescence resonance energy transfer spectroscopy: effect of phalloidin on polymer assembly. *Biochemistry.* 33:13102–13108.

Onishi, H., and K. Fujiwara. 1990. The rigor configuration of smooth muscle heavy meromyosin trapped by a zero-length cross-linker. *Biochemistry.* 29:3013–3023.

Onishi, H., T. Maita, G. Matsuda, and K. Fujiwara. 1989. Evidence for the association between two myosin heads in rigor acto-smooth muscle heavy meromyosin. *Biochemistry.* 28:1898–1904.

Rayment, I., H. M. Holden, M. Whittaker, C. B. Yohn, M. Lorenz, K. C. Holmes, and R. A. Milligan. 1993a. Structure of the actin-myosin complex and its implications for muscle contraction. *Science.* 261:58–65.

Rayment, I., W. R. Rypniewski, K. Schmidt-Base, R. Smith, D. R. Tomchick, M. M. Benning, D. A. Winkelmann, G. Wesenberg, and H. M. Holden. 1993b. Three-dimensional structure of myosin subfragment-1: a molecular motor. *Science.* 261:50–58.

Schröder, R. R., D. J. Manstein, W. Jahn, H. Holden, I. Rayment, K. C. Holmes, and J. A. Spudich. 1993. Three-dimensional atomic model of F-actin decorated with *Dictyostelium* myosin S1. *Nature.* 364:171–174.

Schutt, C. E., J. C. Myslik, M. D. Rozycki, N. C. W. Goonesekere, and U. Lindberg. 1993. The structure of crystalline profilin-β-actin. *Nature.* 365:810–816.

Seidel, J. C. 1969. Similar effects on enzymic activity due to chemical modification of either of two sulfhydryl groups of myosin. *Biochim. Biophys. Acta.* 180:216–219.

Sekine, T., and W. W. Kielley. 1964. Enzymic properties of *N*-ethylmaleimide modified myosin. *Biochim. Biophys. Acta.* 81:336–345.

Sutoh, K. 1981. Location of SH1 and SH2 along a heavy chain of myosin subfragment 1. *Biochemistry.* 20:3281–3285.

Sutoh, K., K. Yamamoto, and T. Wakabayashi. 1984. Electron microscopic visualization of the SH1 thiol of myosin by the use of an avidin-biotin system. *J. Mol. Biol.* 178:323–339.

Sutoh, K., K. Yamamoto, and T. Wakabayashi. 1986. Electron microscopic visualization of the ATPase site of myosin by photoaffinity labeling with a biotinylated photoreactive ATP analog. *Proc. Natl. Acad. Sci. USA.* 83:212–216.

Takashi, R. 1979. Fluorescence energy transfer between subfragment-1 and actin points in the rigor complex of acto subfragment-1. *Biochemistry.* 18:5164–5169.

Taylor, D. L., J. Reidler, J. A. Spudich, and L. Stryer. 1981. Detection of actin assembly by fluorescence energy transfer. *J. Cell Biol.* 89: 362–367.

Tirion, M. M., D. ben-Avraham, M. Lorenz, and K. C. Holmes. 1995. Normal modes as refinement parameters for the F-actin model. *Biophys. J.* 68:5–12.

Tokunaga, M., K. Sutoh, C. Toyoshima, and T. Wakabayashi. 1987. Location of the ATPase site of myosin determined by three-dimensional electron microscopy. *Nature.* 329:635–638.

Toyoshima, C., K. Yamamoto, K. Sutoh, T. Sekine, and T. Wakabayashi. 1985. Three-dimensional image analysis of the actin-tropomyosin-myosin subfragment-1 complex: location of specifically reactive thiol SH1. Proceedings of Yamada Conference XI on Energy Transduction in ATPases. Y. Mukohata, M. F. Morales, and S. Fleischer, editors. Yamada Science Foundation, Osaka. 162–163.

Weeds, A. G., and B. Pope. 1977. Studies on the chymotryptic digestion of myosin. Effects of divalent cations on proteolytic susceptibility. *J. Mol. Biol.* 111:129–157.

White, H. D., and E. W. Taylor. 1976. Energetics and mechanism of actomyosin adenosine triphosphatase. *Biochemistry.* 15:5818–5826.

Xiao, M., Andreev, O. A., and J. Borejdo. 1995. Rigor cross-bridges bind to two actin monomers in thin filaments of rabbit psoas muscle. *J. Mol. Biol.* 248:294–307.

カバー写真の説明

表紙：心筋（上段）および骨格筋（下段）の共焦点蛍光顕微鏡画像。ローダミン・ファロイジンという蛍光色素によってアクチン分子を選択的に染色。ただし，右側はそれぞれ化学固定後に蛍光色素を加えることによって，筋線維中のすべてのアクチンフィラメントをほぼ均等に染色。左側は，無固定での染色。心筋は固定染色と変わらないが，骨格筋ではアクチンフィラメントの両端だけが染色されている。矢じりはZ線の位置を示す。その下の横棒に沿って筋原線維が配向している（序章参照）。(Yasuda, K. *et al.*, *Proc. Jap. Acad.*, **70**, 151-156, 1994)

裏表紙・そで：アクチンフィラメントとミオシン分子との分子間結合力の計測の様子を示す蛍光画像。アクチンフィラメントの端に結合したポリスチレンビーズをレーザー光ピンセットによって捕捉し，異なる方向に負荷を加えている様子（序章参照）。(Nishizaka, T. *et al.*, *Nature*, **377**, 251-254, 1995)

〔説明：石渡信一〕

序章

分子モーター研究の新展開

石渡信一

生体運動の分子レベルでの仕組み（分子メカニズム）は，半世紀にわたる多角的な研究にもかかわらず，いまだに解明されていない[1-5]。ところが，この10年間の研究の歩みは，それまでとは質的に異なる様相を見せている。生体運動を担う分子モーターを，1分子レベルで見て操作できるようになったこと，しかも，分子の立体構造が解かれ，遺伝子操作によるタンパク質構造の改変技術がその真価を発揮し始めたことなどによって，いよいよ分子モーターの仕組みが解明されるのではないかという機運が生じている[6]。分子モーターの研究は，新たな展開の時期を迎えた。

はじめに

分子モーターとは

モーターというと，まず回転するモーターを連想する。生体運動の研究の歴史は長いが，ごく最近まで，生物モーターといえば細菌の鞭毛回転モーター[7]のことをさしていた。筋収縮を担っているミオシン分子や，真核生物の鞭毛（1-2，1-3参照），繊毛の波打ち運動を担っているダイニン分子は，モーターとは呼ばれてこなかった。

ところが，10年ほど前に，*in vitro* motility assay（本書では，*in vitro* 滑り運動測定系と呼ぶことにする。p.30とp.48のCOLUMN，3-1，3-3，4-1，4-2参照）と呼ばれる人工的な実験系が考案され，タンパク質フィラメントが滑り運動（Key Word参照）する様子を光学顕微鏡下で直接見ることができるようになった。このこととレーザー光ピンセット法（COLUMN，p.57のCOLUMN）の開発[8]

や，顕微計測技術と画像処理技術[9,10]の進歩が相まって，運動性タンパク質によるピコニュートン（pN）オーダーの発生力やナノメーター（nm）オーダーの動きが計測されるようになった[6]（3-2，4-2参照）。その一方で，アクチン分子の構造[11,12]や，ミオシン頭部（S1）[13,14]や，キネシン[15]，ncd[16]のATP結合部位の構造がX線結晶構造解析によって解かれた（2-1，2-2参照）。こうして，これらに共通する構造と機能とが鮮明になるにつれて，見かけは異なるが生体運動を担っているタンパク質分子を総称して，分子モーターと呼ぶようになった。分子モーターは，狭義には，「ATPがADPと無機リン酸（Pi）に加水分解される際に解放される化学的エネルギーを，仕事（運動）という力学的エネルギーに変換するタンパク質分子機械」の総称である。しかしこの定義だと，アクチン系と微小管系の分子モーターしか含まれないことになる。エネルギー源をATPに限定せず，しかも生体機能を力発生や運動に限定せず，分子モーターを広義にとらえると，生体分子モーター群は表1のようにまとめられる。

生物モーターとして従来から認知されてきた細菌の鞭毛モーターは，細胞内外のpH（水素イオンの濃度）差をエネルギー源として，細胞外から細胞内への水素イオン（H^+）の拡散過程に応じて回転し，鞭毛に推進力を与える[7]。エネルギー源としてATPを使わない点や，回転運動が本質的である点などから，アクチン系や微小管系の分子モーターとはその運動の分子メカニズムが異なるように見える。ところがごく最近になって，ミトコンドリア膜内外のpH差をエネルギー源としてATPを合成するF_1-ATP合成酵素が，ATP存在下で回転することが*in vitro*実験系で証明された（1-4参照）。この酵素系の場合には，ATPを回転のエネルギー源にしてはいるが，鞭毛モーターと違ってその生体機能は回転することではない。回転運動は，この酵素系の構造上，効率のよいH^+輸送のための1つの手段にすぎない。その点では，F_1-ATP合成酵素を分子モーターの一員に加えるのはためらわれるが，1-4で述べられているように，運動の分子メカニズムについては，アクチン系や微小管系の分子モーターと共通の基盤がありそうである。そういう意味で，この膜タンパク質系も回転モーターの1つに加えよう。

さらに，従来からDNAポリメラーゼやRNAポリメラーゼ，それにmRNAに結合しリボソームの並進運動を引き起こしつつタンパク質合成（アミノ酸添加）に寄与する伸長因子（EF-G）なども，化学

Key Word

滑り運動

分子モーターと基質フィラメントとの間の運動は，通常の条件ではフィラメントがその長軸方向になめらかに運動することから，滑り運動（sliding motion）と呼ばれる。そもそも，1954年に2人のハックスレー（A.F. HuxleyとH.E. Huxley）によって独立に提唱された筋収縮の分子メカニズムが，滑りメカニズムと呼ばれたことに始まる。すなわち筋線維中では，ミオシン分子の繊維状重合体である太いフィラメントと，アクチン分子の繊維状重合体である細いフィラメントとが，その長さを変えることなく相互の位置をずらすことによって収縮（短縮）することが実験的に証明された。このことによって，当時有力な仮説であった筋フィラメント自体の短縮（折り畳み）による収縮というメカニズムが否定された。当時は2種類の筋フィラメントの相対的位置の変化が何によって生じるのかがわからず（今でも決定的な証明はなされていないが），クロスブリッジ（Key Word参照）の存在も知られていなかったので，あたかも2種類の筋フィラメントが滑るように見え，そのように呼ばれるところとなった。

HMMとS1分子

ミオシン分子は分子量約48万で，ミオシン頭部と呼ばれる2つの分子モーター機能部位（ATP結合部位とアクチン結合部位からなる）と，互いに重合してフィラメントを形成する尾部からなっている。キモトリプシンやパパインなどのタンパク質分解酵素によって頭部の根元を切断すると，分子量約12万のSubfragment 1（S1：エス，ワンと読む）と呼ばれる頭部2個と，Rod（ロッド）と呼ばれる尾部に分断される。異なる条件でこの限定分解を行うと，尾部の中程で切断することができ，2個の頭部を持ちミオシンと等価なモーター活性を保持している，分子量約35万のHeavy Meromyosin（HMM：エイチ，エム，エムと読む）と重合能を保持しているLight Meromyosin（LMM：エル，エム，エムと読む）に分断される。HMM分子もS1分子もフィラメント形成能を失っており，生理的環境下で1分子に分散されやすいので，*in vitro*滑り運動系や1分子計測系に好んで用いられる。

表 1　分子モーターの分類

運動様式	モーターシステム		エネルギー源	生体機能
	レール分子*1	分子モーター*1（運動の向き）		
リニアモーター	アクチン	ミオシン(+端)ファミリー*2	ATP	力発生 (2-4, 4-1, 4-2 参照)，滑り運動 (3-1, 3-3, 4-1, 4-2 参照)，アメーバ運動，細胞内物質輸送 (1-1 参照) など
		I		
		II		筋収縮 (2-2, 2-3, 3-3 参照)，細胞分裂，原形質流動 (1-1 参照) など
	微小管	ダイニン(−端)ファミリー	ATP	力発生，滑り運動，細胞内物質輸送，繊毛，鞭毛 (1-2, 1-3, 3-2 参照) など
		キネシン(+，−端)ファミリー	ATP	滑り運動 (4-2 参照)，細胞内物質輸送 (2-1, 3-1 参照) など
		キネシン（+端）		
		ncd（−端）		
	DNA	ポリメラーゼ	NTP	DNA 複製
	RNA	ポリメラーゼ	NTP	RNA 複製
		伸長因子 (EF-G)	GTP	タンパク質合成
回転モーター*3	細菌の鞭毛モーター（純，逆回転）		H^+ の濃度勾配	鞭毛の回転運動による推進力発生
	F_1-ATP 合成酵素*4			
	（純回転）		H^+ の濃度勾配	ATP 合成 (1-4 参照)
	（逆回転）		ATP	H^+ の能動輸送 (1-4 参照)

*1：ここでは，運動を引き起こす能動素子と考えられる方を“分子モーター”と呼ぶ。モーターとして働くためには回転子（ローター）の他に固定子（ステーター）も必要であるし，正しくは回転子と固定子の1セットをモーターと呼ぶべきだろう。その点，たとえばミオシン分子モーターと呼ぶよりも，アクトミオシン分子モーターと呼ぶ方が適切かもしれない (2-4 参照)。しかも，生体分子モーターシステムにおいて，現在レールタンパク質と呼ばれているものが，センサーやレギュレーターとしてだけでなく能動素子として機能している可能性も残されている。本書でも 4-2 などに，これを支持する研究成果が述べられている。分子モーターの（運動の向き）は，レール分子のプラス（+）端あるいはマイナス（−）端 (p.43 の Key Word 参照) 方向への運動性を示す。

*2：現在ミオシンファミリーは，系統発生学的にミオシン I からミオシン XII まで分類されている[22,23]。その中で I と II，とくに II が重要である。1930 年代に最初に筋肉から抽出精製されたのはミオシン II の方であり，ミオシン I は 1970 年代になってからアメーバより抽出されたものである。その際，分子量が小さく，単頭のミオシンと見られたことからミオシン I と名付けられた。その後，従来のミオシンは双頭であることもあって，ミオシン II と呼ばれるようになった。

*3：回転モーターは，エネルギー源である H^+ 濃度勾配の向きの違い（鞭毛モーターの場合）や，エネルギー源の種類の違い（F_1-ATP 合成酵素の場合）によって，同じモーターでも回転の向きを変えることができる。この点リニアモーターの場合には，同じモーターであって滑り運動の向きが+（−）端から−（+）端に変わる条件は見いだされていない。滑り運動の向きは，モーターの種類によって決まっているように見える。

*4：ATP を分解・合成する酵素部位は，回転子としての γ サブユニットではなく，固定子としての α と β サブユニットの方にある (1-4 参照)。この点は，NTP（ここで N は A, G などの任意の核酸塩基を表す）分解酵素の方が能動素子として機能しているように見えるリニアモーターとは見かけ上異なる。

エネルギーを仕事に変換するという意味で（といっても，力学的仕事そのものはこれらのタンパク質分子の機能ではないが），分子モーターと見られてきた[6]。

また，GTP を結合しその加水分解を情報伝達メカニズムに利用しているGタンパク質と呼ばれるタンパク質群が存在する（伸長因子：EF-G，はGタンパク質群にも属しているが，一般のGタンパク質とは異なり，運動する）。ところが分子モーターの立体構造が解明されてみると，このGタンパク質群の構造との共通性が注目されるようになった。しかも，ATP や GTP（総称して NTP と呼ぶ）の結合にともなう構造変化に共通性があることがわかってきた。こうして，一方は運動性，他方は情報伝達，という機能の違いこそあれ，構造機能連関（機能発現のための分子内構造変化）に関する共通性や，分子進化と機能分化の関連などについて，これまでにはない新しい視点からの問題提起がなされるようになってきた。本書では DNA，RNA ポリメラーゼやGタンパク質，それに細菌鞭毛モーターは取り上げないが，「生体分子モーターの仕組み」として，タンパク質レベルではすべてに共通する原理が存在するかもしれないという視点を忘れないことにしよう。分子モーターの仕組みの解明にとって，思わぬ方向からのアプローチが有効になることもあるだろう。また，分子モーター群として表 1 のメンバーがさらに豊富になることも大いにあり得ることである。

❶——これまでの分子モーター研究

分子モーターの研究は，1930 年代に筋肉組織からミオシン分子が抽出され，それが ATPase（ATP 分解酵素）であることが認識されたことに始まる。その後 1940 年代になって，ミオシン分子と相互作用して，筋収縮を引き起こすアクチン分子が精製され，筋収縮の分子メカニズムの研究が本格化した。ここで筋収縮研究の歴史をひもとくつもりはないが，こうしてごく最近に至るまで，「生体分子モーター

の仕組み」は，筋収縮の分子メカニズムの研究を中心に進められてきた[3]。電子顕微鏡技術や光学顕微鏡技術の進歩に支えられた筋生理学・筋構造学によって，まず，筋収縮系がミオシン，アクチンという2種類の筋タンパク質からなる筋フィラメントから構成されているこ

COLUMN

筋収縮系の階層構造

筋収縮系はミオシン分子モーターの繊維状重合体である太いフィラメントと，アクチン分子の繊維状重合体である細いフィラメントが互いに入り組んでできあがった筋フィラメント格子構造に始まり，図Aのような階層性を持っている。この図Aは，横紋構造を持った骨格筋・心筋収縮系の階層構造を示す模式図である。ミオシン分子については頭部と呼ばれる部分（S1とも呼ぶ）の結晶構造が解明されており（2-1，2-2参照），アクチン分子についても立体構造が明らかになっている（2-3参照）。これを図Bにまとめた。

このような筋フィラメントによる格子構造体は筋節（サルコメア）と呼ばれる構造を形成する（通常は，太さ約1 μm，長さ約2 μmである。長さは筋線維の種類によって，およそ2 μmから8 μmまでの幅がある）。それが直列につながって筋原線維をなし，それが横方向に束ねられて単一筋線維（これが筋細胞であり，細胞膜に包まれている），さらには筋組織を形成する。横方向に筋節の位置が揃うと，筋線維全体にわたって横紋が観察されることになる。筋収縮機構の研究は主として，この（単一）筋線維を用いて行われてきた。とくに，細胞膜を力学的あるいは化学的に除去したモデル筋（たとえば，それぞれ名取の筋線維，グリセリン処理筋に代表される）を用いた研究が活発に行われてきた。また，筋原線維レベルまでは光学顕微鏡で観察でき顕微操作もできるので，筋線維を用いた筋生理学と同等の研究もできる。筋節中の筋フィラメントの格子構造となると，光学顕微鏡で見ることはできない。電子顕微鏡を用いて初めて観察することができる。ところが，筋節を解体して1本の筋フィラメントのレベルになると，かえって暗視野顕微鏡や蛍光顕微鏡を用いて観察することができるようになる。溶液中の筋フィラメントを電子顕微鏡で観察することは難しいが，光学顕微鏡では，タンパク質機能を保持したままの生きた状態にある筋フィラメント，あるいは分子モーターを溶液中で見ることができる[4]。暗視野顕微鏡の場合には希薄溶液でしか観察できないが，蛍光顕微鏡を使えば，蛍光色素でラベルしたものだけが画像化されるので，ラベルしていないものを共存させることによって濃厚溶液中での目的の分子のふるまいを画像化することもできる。

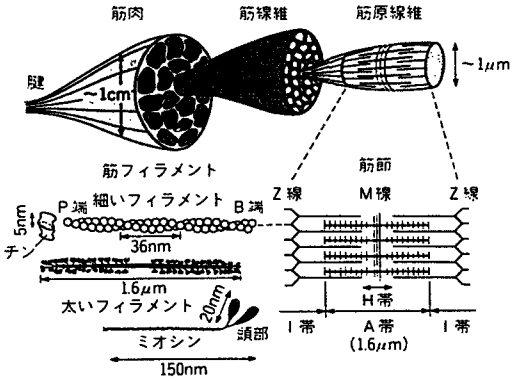

図A　横紋筋収縮系の階層構造の模式図

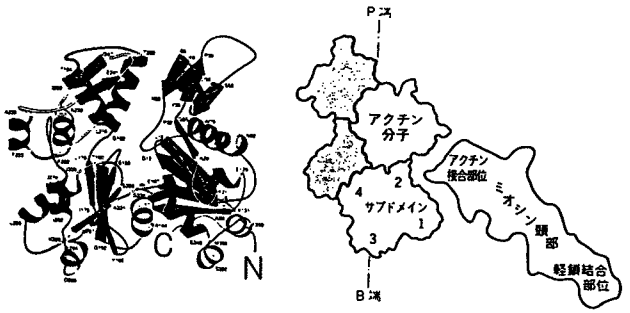

図B　アクチン分子の立体構造とフィラメント構造[11,12]およびミオシン頭部（S1）の概形[13,14]
アクチン分子とミオシン頭部との大きさの比は実寸比ではない。

とが明らかになった。そして，筋収縮はこの2種類の筋フィラメントが相互作用しつつ互いの相対的な位置をずらす，いわゆる滑り運動によって生じるという，滑り運動メカニズムの概念が提案された。これは1950年代に入ってからのことである。しかし滑り運動メカニズムが確立するまでのその後の経緯は，決して平坦なものではなかった。現在では確立したといえるが，ごく最近までこのメカニズムに異を唱える論文が現れていたような状況である。このような状況が続いていること自体，いかに分子モーターの本質を解明することがやっかいなことか，その難しさが映し出されていよう。

1960年代になると，ミオシン分子の形態や，アクチンフィラメントのらせん状構造が，主として電子顕微鏡観察によって明らかになった。ミオシン分子は2つの頭部を持ち，その頭部の先端でアクチンフィラメントに結合して，矢じりのような電子顕微鏡像を与える。60年代は，この程度の空間分解能での分子構造の研究や，生化学による酵素活性の研究を中心としたタンパク質物理化学の時代であった。60年代の後半になって，滑り運動メカニズムにおけるクロスブリッジ（Key Word参照）の概念が定着した上に，クロスブリッジの首振り運動（Key Word参照）説が提唱されるようになった。この10年は，筋収縮制御におけるCa^{2+}の本質的な役割の解明や，Ca^{2+}を結合するトロポニンの発見など，分子モーター機能の制御を司る分子システムが明らかになった時期でもある。

1970年代の初頭には，ミオシンATPaseのキネティックスが簡潔な形でモデル化され，広く受け入れられるようになった。こうして酵素化学の一里塚が築かれた。図1のような形で，分子モーターの酵素反応のスキーム（2-2も参照）がまとめられるに至った。この酵素反応スキームと，分子モーターによる力発生過程との対応づけの試みは，主として単一モデル筋線維を用いた筋生理の研究に，ケージドATPを用いたフラッシュ・フォトリシス法を導入するなどして，今日に至るまで続けられている。この対応づけについては，4-2でも述

Key Word

クロスブリッジ

筋収縮系において，細い（アクチン）フィラメントに結合したミオシン頭部のこと。架橋と訳される。電子顕微鏡像を見ると，まさしく細いフィラメントと太い（ミオシン）フィラメントとの間を繋ぐ架橋構造として見える。クロスブリッジの概念は筋収縮機構の研究の中から生まれ，クロスブリッジというと筋肉の分野でしか使われないようである。

首振り運動

ミオシン頭部はある特定の角度でアクチンフィラメントに結合する（矢じり構造：2-2，2-3参照）。そこでこの結合角度がATPの加水分解にともなって変化すれば，ミオシン分子モーターとアクチンフィラメントとは互いに滑り合うことになる。このようにボートのオールを漕ぐような動作をミオシン頭部が繰り返せば，滑り運動が生じるだろう。これを滑り運動のミオシン首振り説と呼ぶ。昆虫の飛翔筋の中で，この動きを示唆する電子顕微鏡写真が得られたのは1965年のことである。1969年にH.E. Huxleyが具体的にこの説を図解して取り上げ，以後滑り運動（筋収縮運動）の分子メカニズム解明のための作業仮説として重視されてきた（教科書的には長いこと証明されたかのごとく扱われてきた）。90年代に入ってミオシン頭部（S1）の立体構造が解明されたことや，頭部の特定の部位に結合した蛍光ラベルやスピンラベルの向きに関する詳細な分光学的解析の結果，ミオシン頭部先端部とアクチンとの結合角度は変化せず，分子内屈曲によって首根っこ部分（あるいは，しっぽ部分で，αらせんからなる部分：2-1，2-2参照）が振れる，という状況証拠が集まりつつある。

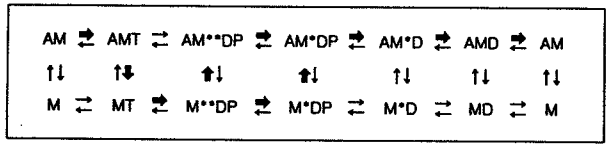

図1　ミオシンおよびアクチン・ミオシン複合体によるATPの加水分解反応スキーム

Aはアクチン，Mはミオシン，TはATP（アデノシン三リン酸），DはADP（アデノシン二リン酸），Pは無機リン酸（Pi）を表す。*と**はミオシンの状態が異なることを示す（2-2参照）。太い矢印が最も確率の高い反応経路を表す。ミオシン，アクチンの代わりにそれぞれをキネシン，微小管とした場合も，同様の反応スキームに従うものと考えられるが，アクトミオシン系ほどには詳細に検討されていない。ただしキネシン・微小管系の特徴は，ATPを結合したキネシンが解離しにくい代わりに，ADPを結合したキネシンが解離しやすいことである。

べられているように，1分子レベルでの研究が90年代になって可能になり，現在活発に研究が行われている。

COLUMN

硬直結合の1分子顕微計測

ミオシン分子モーターとアクチンフィラメントとの1対1の硬直結合（p.160のKey Word参照）の結合力と結合の寿命に対する負荷の影響が，光ピンセット法を用いて計測されている[34]。図のようにガラス表面上にまばらに吸着したHMM分子に，アクチンフィラメントを結合する。その際，アクチンフィラメントの後端（滑り運動の先端はP端，後端はB端と呼ばれる。アクチンフィラメントの重合速度の違いから，微小管と同じようにP端をマイナス（−）端，B端をプラス（+）端と呼ぶこともある）には，B端結合タンパク質であるゲルソリンを表面に結合した直径1 μmのポリスチレンビーズを結合する。このビーズを光ピンセットによって顕微操作し負荷を加える。その結果，約10 pN/sの割合で負荷を加えていくと，硬直結合の破断力ヒストグラムは数pNから20数pNにわたる広い分布を示し，平均9 pNであることがわかった。最近では，原子間力顕微鏡による計測もなされ，約15 pNと約25 pNに2つのピークを持つ，やはり広い分布を示すことが見いだされている[35]。

一方，負荷を加えなくても，硬直結合は自然に解離する。すなわち，多数の硬直結合について解離過程を観測すると，解離は自然に，確率的に生じ，同じ硬直結合であってもある場合には早く，またある場合には遅いことがわかる。このようにして，解離は熱揺らぎによる確率過程であることが，1個1個の硬直結合を観測することによって実証された。一方多数個の硬直結合の解離過程の観測から平均の解離速度が求められるが，その逆数が硬直結合の平均寿命である。上と同じ顕微実験系を用いて計測されたHMM分子による硬直結合の寿命は，約2000秒であった。S1分子の寿命は，その約十分の1であった。この違いは，双頭結合と単頭結合の差に帰せられる。

つぎに，一定の負荷を急激に加えることによる結合の寿命の変化が，ビーズを後端に結合したアクチンフィラメントを用いて計測された。その結果，HMM分子，S1分子ともに，10 pNの負荷によって寿命は2桁小さくなった。負荷を加えることによってアクチン，ミオシン頭部間の結合のポテンシャルが変化し，熱揺らぎによる解離の確率が，負荷の大きさに対して指数関数的に増大したものと考えられる。このようにして，一対のタンパク質分子間結合の熱力学的な解析が可能になった。

1970年代の後半から80年代の前半にかけては，分子モーターメカニズムの研究という点からは，ある意味では停滞期であったかもしれ

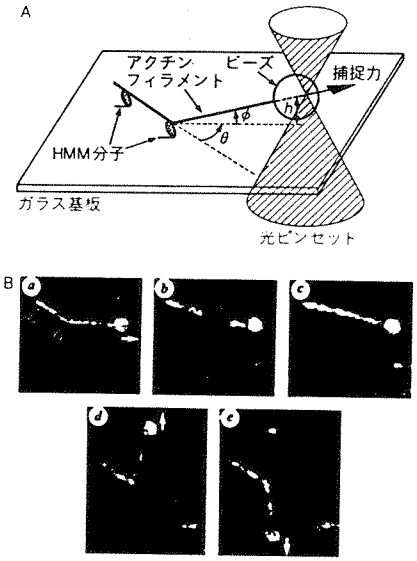

図　光ピンセットによるアクチンフィラメント・ミオシン分子モーター（実験に用いたのはHMM分子）間の硬直結合の1分子計測
A：実験系の模式図。光ピンセットによって，アクチンフィラメントの後端に結合したポリスチレンビーズを捕捉し，顕微操作する。ビーズには，ビーズの重心とレーザーの捕捉中心（焦点）の距離に比例する復元力が加わる。私たちの装置では，レーザーの捕捉中心に対して半径200 nmの円内で最大70 pNの負荷を加えることができる。この装置を用いて，一定の割合で負荷を加えていったときの結合破断力や，瞬間的に一定の負荷を加えたことによる結合寿命の減少などを調べることができる。h：ビーズの高さ，ϕ：アクチンフィラメントとガラス面の間の角度（10°程度に抑えてある），θ：HMM分子に対する負荷の方向。B：実際に得られた蛍光顕微鏡画像。a，アクチンフィラメントに結合したビーズ（黒矢印）を，光ピンセットで捕捉しつつ右方へ引く（白矢印）。b，ある大きさの負荷が加わったところでHMM分子との間の硬直結合（a図の右側の矢じり）が破断する。c，アクチンフィラメントは2個目の硬直結合（a図の左側の矢じり）によってガラス基板につなぎとめられている。dとe，光ピンセットを操作することによって，再び同じHMM分子との間に硬直結合を作ることができ，繰り返し破断力を計測することができる。しかも，加える負荷の方向（θ）をおよそ±90°の範囲で変えることができた（文献34））。横棒は5 μm。

ない。この時期爆発的に研究が進んだのは，非筋細胞における運動性タンパク質の研究である。とくにアクチン・ミオシン系を中心に，細胞骨格の構造・機能を調節するさまざまな，次への飛躍の準備となるような研究が進められていた[18]。このころまでは，分子モーターの仕組みの研究となると，筋生理・筋タンパク質物理化学の研究分野が他をリードしていたが，それに対する新しい方法論，実験手法に対する模索が，生物物理学や生理学の分野に限らず，細胞生物学の分野においても始まっていた。

1980年代になると，それまでの研究状況を打破しようとする動きが具体的に出始めた。その1つが1分子観察，1分子解析への指向である。光学顕微鏡下での生体高分子の直接観察という面からは，古くは大腸菌のフラジェラ（鞭毛）線維の運動の観察，そして，その多型

COLUMN

光ピンセット法の生物学への応用

レーザー光ピンセット法が初めて生物研究に応用されたのは，1980年代の後半である。原子・分子の捕捉手段としてこの方法を開発したアシュキン(Ashkin, A.)[9]のグループが，たまたま応用が容易な実験系として微粒子（タバコモザイクウイルス―これが生体物質系への最初の応用例といえる―やポリスチレンビーズなど）を選び，その捕捉実験をしている際に，非常に強い散乱強度を持つ粒子が捕捉されることに気づき，調べたところ，それが大腸菌であったということである。これが生き物を光ピンセットで捕捉した最初の例となった。生物研究への応用は，こうして偶然のことから始まった。その際，可視光を使ったのでは生体系のダメージが大きいが，波長1 μmの近赤外光を用いると何時間でも生きたまま捕捉できることがわかった。光ピンセットの捕捉力を生かした本格的な生物研究は，大腸菌の鞭毛モーターが発生するトルクの大きさを，菌体を捕捉することによって計測した実験によって始まった。分子モーターへの応用は，キネシン分子モーター[24]について1993年に，そして，ミオシン分子モーター[25,26]に関しては1994年に最初の成果が発表された。

性・多型変換の直接観察に始まり，精子の鞭毛などの真核生物の鞭毛を構成する微小管1本の直接観察が行われた。これらは，線維が太いことから，光散乱能が大きく，暗視野顕微鏡観察が可能であった。アクチンフィラメントの場合には，束になれば暗視野観察できたが，1本となるとミオシン（HMM：Key Word参照）分子を硬直結合（p.160のCOLUMN参照）させて光散乱強度を高める必要があった。こうして溶液中における繊維状重合体のブラウン運動が直接観察されるところとなった。

さらにこの時期には，細胞生物学において蛍光顕微鏡の威力が一層大きなものになってきた[19]。細胞膜を通過した後に蛍光性を獲得する蛍光指示薬が開発され，細胞内における遊離のCa^{2+}やpHなど，さまざまな細胞内の環境変化が画像化されるようになった。共焦点顕微鏡などの，細胞内観察を可能にする光学顕微鏡技術の進歩もあった。1分子とまではいかなくても，細胞内における特定の分子（集団）のダイナミクス（離合，集散，運動）を細胞機能との関連で可視化したいという機運が現実のものとなりつつあった。一方，分子モーターの分野では，1本のアクチンフィラメントが蛍光像として可視化され，そのブラウン運動が直視できたこと，それに対するミオシンや，制御タンパク質の作用が顕微解析されたこと，そして80年代後半には，1本のアクチンフィラメントに発生するpNオーダーの滑り力が初めて顕微計測されたこと[20,21]などを通して，1分子研究への動きが本格化した[6]。

その上，それまで微小管上を滑り運動するモーター分子としては，ダイニンしか知られていなかったが，ダイニンとは逆向きに滑り運動するキネシン分子とそのファミリーが次々に見いだされた。ミオシン分子ファミリーも非筋細胞から続々見いだされた[22,23]。こうして分子モーターの世界が，それまでの筋収縮系を中心とする細胞運動という概念ではとらえきれないほどの広がりを見せるようになった。

そしていよいよ90年代に入り，光ピンセット法，*in vitro* 滑り運動系を用いて，微小管上での1個のキネシン分子の8 nmのステップ

状運動[24]や，ミオシン（HMM）分子によるアクチンフィラメントの10 nmの変位と，1 pNオーダーの滑り力の顕微計測[25,26]が行われた。また，DNAポリメラーゼの運動や，メッセンジャーRNA上でのリボソームの滑り運動，さらにはミトコンドリア膜にあるF_1-ATP合成酵素の回転運動（1-4参照）など，運動でありながら必ずしも同じ範疇の問題としてはこれまでとらえられてこなかった生体運動機能の分子メカニズムが，共通の視点から研究されるようになってきた。さらに，NTP結合部位の立体構造の共通性から，分子進化の過程でNTP結合タンパク質が，あるものは分子モーターとして進化し，あるものは情報伝達素子として進化したという可能性が生じた。分子モーターの研究が分子モーター分野だけに収まらず，またその逆に，他分野の研究成果が分子モーター研究に関連するという状況が生まれている。まさしく「分子モーター研究の新展開」と呼ぶにふさわしい時代を迎えたことになる。

COLUMN

筋収縮研究はどこへ行くのか

さて，1分子顕微解析が進む一方で，筋（原）線維を用いた筋収縮（筋生理）研究はどこへ行くのだろうか。大げさに聞こえるかもしれないが，筋収縮研究に未来はあるだろうか。この問いは，長年筋収縮系を中心に研究してきたものには避けて通れない。私見を述べれば，それはまったくないわけではない。まず，横紋筋構造の規則性を生かして，分子モーターの特定の場所に蛍光色素などのプローブを導入することができ，実験条件を工夫することができれば，1分子計測では得られないSN比で分子モーターの動きを検出できる可能性がある。事実この方向での研究は第一線の研究として現在でも評価されている。

その一方で，分子モーターの滑り運動は，首振り運動（あるいは，現在有力視されているしっぽ振り運動：Key Word参照）の所産か，とは問わず，筋収縮系というシステムの動特性のメカニズムに視点を移すことである。そうすれば，筋収縮の研究にも未来はある。骨格筋だけでなく心筋も，構造上は横紋筋に属し，その階層性を持った秩序構造の美しさは見事である（COLUMN参照）。分子モーターが秩序構造の中に置かれたとき，1分子レベルとは異なる特性を発揮することは当然予測される。筋フィラメントの形態や配置が異なる平滑筋では，また別の特性があるだろう。たとえば3-3で述べたような，自励振動現象の出現に見られるように，分子モーター間の協同性，協調性による新たな機能発現があるはずである。通常の筋収縮においても，分子モーター間の協調性によって，システムのダイナミックな安定性が保証されている可能性がある。トランジスターの物理がわかっても，ラジオはできないように，またエンジンの熱力学がわかっても自動車の動く仕組み（車輪が回転する仕組み）はわからないように，分子モーター1個の働きはわかっても，直列に筋節が繋がった筋収縮系がダイナミックに安定に収縮する仕組みや，精子の鞭毛の波打つ仕組みには，興味深い未知のものが残されている。とくに心筋収縮系の場合には，収縮振動はまさしく生理機能そのものであり，分子モーター集合体のダイナミクスを明らかにすることには生理学としての意義がある。もちろん，生体構造の構造形成メカニズムを研究するための素材としても，筋収縮系は依然として魅力的である。

❷——分子モーター研究の新展開——現状と将来

「分子モーター研究の新展開」は，1分子直視，1分子解析手法の開発をきっかけに，分子モーターとその基質タンパク質の立体構造の解明や遺伝子操作手法によるモーター分子の構造・機能改変技術の導入を通じ，さらにはすべての細胞運動，細胞内輸送などの細胞生物学における諸問題に対する関心に支えられて引き起こされた。前者の3つの要素技術の中で遺伝子技術は分子生物学からの貢献だが，残りの2つについては「生物物理学」の貢献が大きいだろう。

分子モーター研究の過程で開発された手法や，解明された分子メカニズムは，分子モーター以外の，生体機能を担う分子機械のメカニズムの解明にも貢献するだろう。1分子生理学，1分子構造機能学の始まりである。現在までに開発されたり導入された技術を，本書で取り上げたセクションの番号とともに列挙すると：

1分子蛍光可視化技術[27,28]（新規の蛍光色素の合成，エバネッセント場（4-2）や2，3光子励起などによる局所照明法），*in vitro* 滑り運動系（1-1，1-3，3-3，4-1），光ピンセット法などの顕微操作技術

(序章のCOLUMN，4-2)，原子間力顕微鏡などの走査型顕微鏡技術(2-4)，nm・pN顕微計測技術（3-2，4-2)，ビデオ画像解析法[10,29]，

COLUMN

分子モーター研究の成果を示す雑誌の表紙

この数年間に，分子モーター研究の成果が *Nature* や *Science* をはじめとする一般科学雑誌に数多く発表されているが，その表紙を飾るものも少なくない。上段左から右へ，*Science* 誌に発表されたミオシン分子頭部の立体構造*1 (2-1，2-2参照)，*Nature* 誌に発表された1分子顕微解析のためのアクチンフィラメントの蛍光像*2 (COLUMN，3-3，4-2参照) と，キネシン分子，ncd分子のATP結合部位の立体構造*3 (2-1参照) を示す。また，筋収縮系の研究にも新展開が見られる。ただし，モーターの機能という面よりも，横紋構造の形成メカニズムという観点からの研究成果を示す。下段左から，*Nature* 誌の表紙を飾った心筋横紋構造の蛍光像*4 と，*Biophysical Journal* (米国生物物理学会誌) に発表された心筋収縮系内のアクチンフィラメントの解体と再構築を示す蛍光像*5。

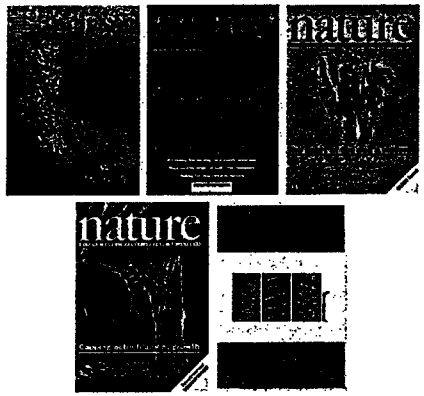

*1：*Science*，2 July，1993の表紙
*2：*Nature*，10 March，1994の表紙
*3：*Nature*，11 April，1996の表紙
*4：*Nature*，7 September，1995の表紙
*5：*Biophys.*，J.，71 (No.5)，1996の表紙

顕微局所励起（光）・摂動（熱）技術，結晶構造解析（アクチン，ミオシン，キネシンなど(2-1)），電子顕微鏡技術(2-3)，X線小角散乱法(2-2)，遺伝子組換え技術による機能改変モーター(3-1)あるいは機能解析用モーター系(1-4)の作成，突然変異体を用いたモーターの構造・機能解析系の開発(1-2)

などである。

さて分子モーター研究の近未来と遠未来はどのようなものだろうか。上で述べたように，分子モーターの働きが1分子レベルで研究される中で，分子モーター内部（頭部やレバー（首根っこ）部など）の動き（構造変化，分子内屈曲）や，その動きとATP加水分解との関係，1個のATP分解にともなう分子モーターの運動とその負荷依存性などについては，すでに活発な研究が行われている(4-2参照)。さらに分子モーターとレール分子との間の結合力，結合ポテンシャルなどの1分子解析（COLUMN参照）を含めて，より詳細な実験的研究が行われるだろう。その一方で，分子モーターの仕組みについて，理論面からのアプローチも盛んになろう[6]。

以下に，これ以外の今後解決すべき諸問題を列挙し，簡単に解説しよう。

(1) **分子モーターの双頭構造の意味**：古くて新しい問題。キネシンは1分子で機能するが，単頭の分子1個では滑り運動性を失い，双頭でのみ滑ることができる。双頭運動の協同性，ATP分解のタイミングと，滑り運動との関係を明らかにしたい。分子モーターは，協同的な分子変形そのものが生理機能に直結し，一方の頭部の分子変形がもう一方の頭部の酵素活性に影響するといった，運動性アロステリック酵素という見方ができる。また（4）で指摘するように，分子間の協同性という点では，微小管や，アクチンフィラメントなどの，レール分子の構造変化にも興味深いものがある。

微小管上でのキネシン分子の運動はhand-over-handメカニズム(キネシン分子の2つの頭部が，微小管を構成するチューブリン分子の上を交互に，結合・解離を繰り返しながら，歩くように動く。ATP

分解サイクルも，それに応じて2つの頭部が協調して互いの位相関係を適当にずらす）といわれているが，その際に2つの頭部のうちの結合した頭部が自転して，前方のチューブリン分子への，もう一方の頭部の結合を促すとするモデルが提案されている[30]。バクテリアの鞭毛モーターやF_1-ATP合成酵素のみならず，従来型の分子モーターも「回転モーター」ではないか，という提案である。今後は，このような統一的な視点が有効になるだろう。

（2） **歩くモーター(キネシン)と，走るモーター(ミオシン，ダイニン)とで，構造・機能の何が違うか**：単に，ATP分解時間に占める，レール（基質）タンパク質との結合時間の割合（duty ratio）が長いか，短いかの違いであるかもしれない。しかし，前者は1分子でもレールから解離せずに長距離にわたって方向性運動を行うことができるのに対して，後者は何らかの束縛を受けていないと長距離にわたる運動を行うことができない。双頭間の協同性に違いがあるように見える。キネシン分子は，細胞内にあって1個あるいは少数個で物質輸送を担っており，微小管以外の構造体によってはその運動が束縛されていない。そのために，歩くモーターとして進化したのかもしれない。それに対して，筋フィラメント格子構造の中で滑り運動するミオシン分子と，鞭毛（9+2）システムの中で鞭毛の曲げ運動を引き起こすダイニン分子の場合には，運動が束縛されているだけでなく，複数（多数）個で機能する。レールとの接触時間が短ければ，他のモーターに対して余計な負荷にならない。こうして走るモーターとして進化したのかもしれない。しかしこのことは逆に，互いの接触時間を適当に制御すると，異なる分子間協調性が出現する可能性を示唆する。分子モーター集合体システムとしての動的安定性は，このような分子間協調のメカニズムを介して行われているのではないか（3-3参照）。

（3） **滑り運動の方向性は何が決めているか**：キネシンとncdは，そのATP結合部位周辺（モーター領域）の立体構造はほとんど区別できないほど似ている（ミオシンとも似ている：2-1参照）。それにもかかわらず，同じ微小管上をキネシンは＋端側に滑り，ncdは

COLUMN

1分子計測でわかること，わかったこと

わざわざ1分子で計測したことの意味はどこにあるのだろうか。1分子計測によって初めてわかったことは何だろうか。COLUMNで紹介した硬直結合の破断力や，結合の寿命の負荷依存性については，その平均的性質ならば，筋線維を用いても同じ量を計測したという報告がある。しかし現実には，硬直結合力の場合には，他の分子間結合力に比べて小さくはないので，筋線維に負荷を加えて行くと硬直結合が破断するとともに他のタンパク質分子間結合も破断されてしまい，高次構造が保てないという問題が生じる。したがって，たくさんあるタンパク質間結合の中でどれが破断したのかを決めることが原理的に難しい。たとえ硬直結合だけが破断するような条件が見つかったとしても，計測にかかった硬直結合の数は1万個を下回ることはない。したがって，得られた数値はあくまでも何万個かの結合の平均値なのである。上のコラムで指摘したような，硬直結合の確率的性質は決して明らかにはならない。

筋線維などの細胞の中ではミオシン分子モーターは1個では機能せず，少なくとも100個（1本のアクチンフィラメントと相互作用するクロスブリッジの数）以上はまとまって機能していると考えられる。ならば，何も1個の性質がわからなくともよい，という見方もあるかもしれない。平均的な性質がわかれば十分だという見方もあろう。しかし，その見方には限界がある。自動車が何気筒のエンジンを搭載していようとも，その集合としての性質を知るだけでなく，1個のエンジンの働きを知らなければ，自動車が動く仕組みを完全に理解したことにはならない。それと同じことである。分子モーターの場合には，一般に互いに同調して機能してはいないといわれている。だからこそ，運動機能は平均化されてなめらかな滑り運動が発現するともいえよう。ただし，昆虫の飛翔筋の場合には，ミオシン分子モーターがある程度同調する（同位相で機能する）といわれている。この同調性を生かした研究が行われているが，1分子特性にたどりつくのは難しい。

nmサイズの分子レベルになると，分子運動は熱揺らぎにさらされることになる。分子モーターがいかに同調して機能していたとしても，多数個の働きを調べたのでは，熱揺らぎの作用は平均化され，1個の分子モーターに対する熱揺らぎの作用を抽出することはできない。こうして，熱揺らぎと分子モーター機能との関わりを明らかにすることは，1分子解析の究極の目標であるといえる。

一端側に滑る（表1参照）。この運動方向決定のメカニズムを分子構造をもとに明らかにしたい。ところでキネシンのモーター領域はアミノ酸配列のN末端側にあり，ncdのそれはC末端側にある。しかし滑り運動の方向性はそれでは決まらないという報告があったが[31]，ごく最近，ncdのモーター領域のC端側にキネシン由来の“しっぽ”を結合したところ＋端に動くようになったことが報告され[32,33]，研究の進展が見られた。この問題は，分子モーターの運動メカニズムそのものと密接に関連している。

（4） **アクチンや微小管は単なる“レール”か**：分子モーター単独では酵素活性は低い。分子モーターの機能に必要な酵素活性は，レール（基質）分子との相互作用によって初めて現れる。この点だけでも，単純なレールとはいえない。では，レール分子の役割は分子モーター機能の活性化と機能制御に限定されているのか。あるいは，複数個の分子モーター間の機能協調にも関与しているか。また，それ以上に，滑り運動機能そのものに関与しているのか。それらの可能性を示唆する構造変化などの状況証拠は，タンパク質溶液系や *in vitro* 滑り運動系の実験からいろいろと得られている。しかし，分子モーターのメカニズムに直結する確証はない。

（5） **エネルギー変換の分子メカニズム**：ATP由来のリン酸結合のエネルギーはどこに，どのような形で蓄えられるか。これは，NTP分解酵素に共通する分子内構造基盤にかかわる問題を含んでいる。ここでは，分子間結合の物理化学的基盤に対する1分子計測からのアプローチに期待がかかる。分子内，分子間でのH^+やイオンの流れや移動にも注目したい。このような課題は，分子モーターにとどまらず，タンパク質構造・機能学における中心課題の1つである。

（6） **モーターが複数（多数）個集まったときに現れる高次機能**：分子協調，タンパク質高次集合体における構造・機能連関の問題。各種の自励振動現象（微小管・ダイニン系については3-2，筋原線維については3-3参照）の分子メカニズムなど，興味深い問題を含む。

（7） **各生体運動系に固有の問題**：たとえば，筋収縮系（骨格筋，心筋，平滑筋）における収縮特性，制御機構の問題（筋線維の種類によって，タンパク質も異なれば，制御方式も微妙に異なる），非筋細胞における運動方式の違い。分子モーターやレールタンパク質の集合状態の違いや，その離合・集散のダイナミクスと細胞機能との関係。分子モーターの仕組みとともに，細胞生物学としての応用問題は数多く存在する。

（8） **分子モーターファミリーの構造と機能についての共通性と多様性**：分子進化，構造・機能分化の遺伝子的基盤を解明するための研究素材となる。比較分子生物学の格好の研究対象である。

（9） **水の構造とモーター機能との関係**：ATP分解にともなう水分子の結合・解離，水の構造変化が，モーター分子の運動性に直接関与しているというアイデアがある。分子モーターに固有の問題であると同時に，タンパク質1分子熱力学という新たな生物物理的課題を提供している。

おわりに

1分子解析については，まだ10年の歴史もないが，1分子生理学への期待が膨らむ一方で，以前の研究とどのように質的に異なる成果が得られたのか，という問いがすでに投げかけられている。これは，新しい技術や概念を生み出す際の産みの苦しみの，ひとつの現れであろう。しかし，1分子解析によって初めてわかることは何か，それを評価することは大切なことである。1分子解析によってしかわからないこと，しかもそれが分子モーター学（広くは生物学）の重要課題であること，それを解いてみせる必要がある。分子モーターの研究は新たな展開を見せているが，生物物理学からのこの分野への真の意味での貢献は，今後の研究いかんにかかっている。

文 献

1) 日本生物物理学会 編：生物物理の最前線（ブルーバックス），講談社（1990）
2) 郷 信広・若林健之・松本 元 編：生物物理のフロンティア，培風館（1989）
3) 丸山工作：筋肉のなぞ（岩波新書），岩波書店（1980）
4) 神谷 律・丸山工作：細胞の運動，培風館（1992）
5) 御橋廣眞：筋肉の動きを探る（パリティ物理学コース），丸善（1994）
6) 日本生物物理学会 編：ナノピコスペースのイメージング―生物分子モーターのメカニズムを見る―(生物物理から見た生命像3)（柳田敏雄・石渡信一 編），吉岡書店（1997）
7) 相沢慎一：原子（もの）が生命（いのち）に転じるとき，カッパサイエンス（1993）
8) Ashkin, A.: Optical trapping and manipulation of neutral particles using lasers. *Proc. Natl. Acad. Sci. USA.*, **94**, 4853-4860 (1997)
9) 宮本 宏・石渡信一 編：特集「生体におけるイメージング技術の発展―分子，細胞，組織の動態を可視化する―」，生物物理，**36**, No.1 (1996)
10) Inoué, S.: Video microscopy. pp.584, Plenum Press (1986)
11) Kabsch, W., Holmes, K.C. *et al.*: Atomic structure of the actin: DNase I complex. *Nature*, **347**, 37-44 (1990)
12) Holmes, K.C., Kabsch, W. *et al.*: Atomic model of the actin filament. *Nature*, **347**, 44-49 (1990)
13) Rayment, I., Holden, H.M. *et al.*: Three-dimensional structure of myosin subfragment-1: A molecular motor. *Science*, **261**, 50-58 (1993)
14) Rayment, I., Milligan, R.A. *et al.*: Structure of the actin-myosin complex and its implications for muscle contraction. *Science*, **261**, 58-65 (1993)
15) Kull, F.J., Vale, R.D. *et al.*: Crystal structure of the kinesin motor domain reveals a structural similarity to myosin. *Nature*, **380**, 550-555 (1996)
16) Sablin, E.P., Fletterick, R.J. *et al.*: Crystal structure of the motor domain of the kinesin-related motor ncd. *Nature*, **380**, 555-559 (1996)
17) Vale, R.D.: Switches, Latches, and Amplifiers: Common themes of G proteins and molecular motors. *J. Cell Biol.*, **135**, 291-302 (1996)
18) 丸山工作：アクチンと調節タンパク質（UPバイオロジー），東京大学出版会（1986）
19) 宝谷紘一・木下一彦 編：限界を超える生物顕微鏡－見えないものを見る，日本分光学会（1991）
20) Kishino, A., Yanagida, T.: Force measurements by micromanipulation of a single actin filament by glass needles. *Nature*, **334**, 74-76 (1988)
21) Ishijima, A., Yanagida, T. *et al.*: Sub-piconewton force fluctuations of actomyosin *in vitio*. *Nature*, **352**, 301-306 (1990)
22) Mooseker, M.S., Cheney, R.E.: Unconventional myosins. *Ann. Rev. Cell Dev. Biol.*, **11**, 633-675 (1995)
23) Sellers, J.R., Goodson, H.V., Wang, F.: A myosin family reunion. *J. Musc. Res. Cell Motil.*, **17**, 7-22 (1996)
24) Svoboda, K., Block, S.M. *et al.*: Direct observation of kinesin stepping by optical trapping interferometry. *Nature*, **365**, 721-727 (1993)
25) Finer, J.T., Simmons, R.M., Spudich, J.A.: Single myosin molecule mechanics: piconewton forces and nanometre steps. *Nature*, **368**, 113-119 (1994)
26) Miyata, H., Ishiwata, S. *et al.*: Stepwise motion of an actin filament over a small number of heavy meromyosin molecules is revealed in an *in vitro* motility assay. *J. Biochem.*, **115**, 644-647 (1994)
27) Funatsu, T., Yanagida, T. *et al.*: Imaging of single fluorescent molecules and individual ATP turnovers by single myosin molecules in aqueous solution. *Nature*, **374**, 555-559 (1995)
28) Sase, I., Kinosita, Jr. K. *et al.*: Real time imaging of single fluorophores on moving actin with an epifluorescence microscope. *Biophys. J.*, **69**, 323-328 (1995)
29) 石渡信一 編：実験生物物理，丸善（1993）
30) Howard, J.: The movement of kinesin along microtubules. *Annu. Rev. Physiol.*, **58**, 703-729 (1996)
31) Stewart, R.J., Thaler, J.P., Goldstein, L.S.B.: Direction of microtubule movement is an intrinsic property of the motor domains of kinesin heavy chain and *Drosophila* ncd protein. *Proc. Natl. Acad. Sci. USA.* **90**, 5209-5213 (1993)
32) Henningsen, U., Schliwa, M.: Reversal in the direction of movement of a molecular motor. *Nature*, **389**, 93-96 (1997)
33) Case, R.B., Vale, R.D. *et al.*: The directional preference of kinesin motors is specified by an element outside of the motor catalytic domain. *Cell*, **90**, 959-966 (1997)
34) Nishizaka, T., Kinosita, Jr. K. *et al.*: Unbinding force of a single motor molecule of muscle measured using optical tweezers. *Nature*, **377**, 251-254 (1995)
35) Nakajima, H., Ando, T. *et al.*: Scanning force microscopy of the interaction events between a single molecule of heavy meromyosin and actin. *Biochem. Biophys. Res. Comm.*, **234**, 178-182 (1997)

第3章

3 ミオシン分子モーターの特殊な機能

石渡信一

分子モーターの機能は，ATPを分解しつつ力を発生し，基質フィラメントに一方向性の滑り運動を引き起こすことである。ところが分子モーターには，これ以外に特殊な運動モードが存在することがわかってきた。ここではまず，ミオシン分子モーターによるアクチンフィラメントの回転滑り運動と，その結果形成されるアクチンフィラメントの超らせん構造について述べる。これは微小管・ダイニン系でも見られたものである（1-3参照）。さらに，ミオシン分子が多数集まった筋収縮系に見られる，自励振動現象について簡単に述べる。このような特殊な運動モードの生理的な意義は不明だが，まだ私たちの目の届かないところで何らかの役割を担っているのではなかろうか。

はじめに

分子モーターの機能は，基質フィラメントに滑り運動を引き起こすことである。基質フィラメントがその長軸方向に動けば，あるいは逆に分子モーターが基質フィラメントの長軸に沿ってスムーズに運動できれば，それだけで収縮や物質輸送などの生体機能を発揮することができる。ところが1-3で述べられているように，*in vitro* 滑り運動系で調べたところ，微小管系のモーターの機能の中にはなかなか面白いものがあることがわかった。たとえば，ある種のダイニン分子は，微小管に回転滑り運動を引き起こす。あるいはキネシン分子は，ある条件下では微小管に長軸方向の1次元的なブラウン運動を誘起する。滑り運動の場合には微小管はプラス端（＋端）あるいはマイナス端（－端）（p.43のKey Word参照）の方向にしか運動しないが，この条件下では運動の異方性が失われ，拡散過程と似て運動は等方的になる。キネシン分子は，微小管にとってあたかもロープを引っ掛ける輪のような働きをする。

こうしてみると，分子モーターと基質フィラメントとの結合モードは単一ではなく，少なくとも次の3つに分類されることがわかる。まずATP存在下で形成される，① 滑り運動をもたらす結合モード（力発生結合モード）と，② 単にフィラメントをつなぎ止めるだけの弱い結合モード（弱結合モード），そして，ATPが存在しないときに形成される，③ 硬直結合（Key Word参照）モードである（硬直結合の1分子計測についてはp.10のCOLUMN参照）。この中のどの結合モードが優位になるかによって，分子モーター・基質フィラメント運動系はさまざまな様相を呈することになる。たとえば，力発生結合モードが優位にある通常の活性条件下では，基質フィラメントは方向性を持ったスムーズな滑り運動をする。弱結合モードが優位になる条件は一般には弛緩条件だが，*in vitro* 滑り運動系では1次元的なブラウン運動の様相を見せることもある。さらに以下で述べるように，3種類の結合モードがすべてほどほどに存在するような条件下では，自発的な（収縮・弛緩）振動を引き起こす。ATP濃度を非常に下げると，①と③が共存し，基質フィラメントの動きは階段状になる。また，1本の基質フィラメントの上で①と③が不均一に分布するような条件下では，部分的に基質フィラメントは捻れ，超らせん（Key Word参照）を形成する。このセクションでは，分子モーター・基質フィラメント系は，単なる滑り運動発生装置ではなく，多様な運動モードを持ち，多彩な顔を持っていることを強調しよう。多様な運動モードを解析することを通じて，分子モーターの構造と機能，基質フィラメントとの相互作用モードについて新しい視点が得られるかもしれない。一方，このような分子モーターの多彩な顔のすべてが生体中で生かされているか否かについては，何ともいえない。今後の研究を待つほかはないが，まだ私たちの目の届かないところで何らかの役

割を担っているものと期待する。

このセクションではまず，ミオシン分子モーターの場合にも，微小管・ダイニン系とまったく同様な，特殊な運動モードが存在することを述べる。すなわち，ミオシン分子モーターが発生する滑り力には，アクチンフィラメントの長軸に平行な成分だけでなく，垂直な成分が含まれている。その結果アクチンフィラメントにトルクが働き，フィラメントは回転しつつ滑り運動することになる。さらに，フィラメントの一部が固定されると，その後部が回転滑り運動する結果，フィラメントの中間部が超らせんを形成する。この一連の現象をまとめよう。最後に，ミオシン分子が多数集まった筋収縮系に見られる自励振動現象について簡単に述べる。1分子レベルではタンパク質間相互作用は確率的な様相を呈するが，分子が集合するとともに組織化され，秩序立った機能が発現されることになる。

Key Word

超らせん
らせん構造を持ったフィラメントがつくる，高次のらせん構造のこと。アクチンフィラメントの場合には，それ自体右巻きの2重らせん構造をとっているが，これがさらに大きならせんを形成する場合がある。遺伝子DNAは有名な2重らせん構造をとっているが，これがさらに捩れることによって，超らせん（supercoil）構造をとることが知られている。その構造はここで述べたアクチンフィラメントに見られる超らせん構造と類似のものである。

トルク
物体に回転運動を引き起こす力の作用。ここでは，1個の分子モーターが発生する滑り力ベクトルがアクチンフィラメント（あるいは微小管）の長軸に完全には平行でなく，ある角度で傾いていることにより，フィラメントに長軸回りの回転運動を引き起こすようなトルク成分（滑り力ベクトルの横成分 × フィラメントの半径）が存在する。フィラメントには同時に多数の分子モーターが働いているので，フィラメントに加わるトルクは，働いている分子モーターの数だけ大きくなる。

硬直結合
ATPが存在しない条件下でミオシン分子とアクチンフィラメントとの間に形成される分子間結合のこと。ATPが数mM存在する生理的条件下では，ほとんど形成されないといってよい。生体においては，死後硬直時に形成される。

❶——分子モーターはトルクを発生する

A．トルク発生をどうやって証明するか

分子モーターがトルクを発生するか否かを証明する方法はいくつか考えられる。まずは，①直接トルクを計測することである。しかもトルクが右巻きか左巻きかを区別したい。しかし，この直接計測はちょっと難しい（いまだに誰もやっていない）。そこで間接的だが，②トルクが発生すればアクチンフィラメントは長軸の回りに回転するはずなので，その回転運動を見る，という方法がある。しかし，ただ見ただけではだめで，以下に改めて述べるように，特殊な工夫を必要とする。微小管・ダイニン系の場合には，たまたま微小管の一部が2本鎖となっており，勾玉のような形をしていたので，その回転運動を見ることができた（1-3参照）。この方法は，微小管が硬い棒状構造であったために成功したが，アクチンフィラメントのように柔軟なフィラメントの場合にはなかなか難しい。たとえ勾玉状の構造物をアクチンフィラメントの後端部に結合できたとしても，それが回転しているのか，単にフラフラと揺らいでいるだけなのか，を区別することが難しいのである。そこでさらに間接的だが，③もしトルクが発生しているのなら，柔軟なアクチンフィラメントの捻れが見えてもよかろうと，私たちはまず考えた。フィラメントが柔らかいという性質を逆手にとって，それを利用しようと考えたのである。

そのために，私たちは図1Aに示したような手順で，アクチンフィラメントの先端部をガラス表面に固定し，先端部は滑りも回転もしないような実験系を工夫した[1]。フィラメントの中央部と後端部とはトラック状に並んだミオシン分子（実験では，HMM分子を用いた）の上を滑り運動するようにする。先端部が固定されているのに後端部が滑り運動すると，中央部は座屈（バックリンク）して横に飛び出るだろう。そこで後端部が長軸の回りに回転しながら滑り運動し続けると，座屈した部分は超らせんを形成するのではないか[2]。その超

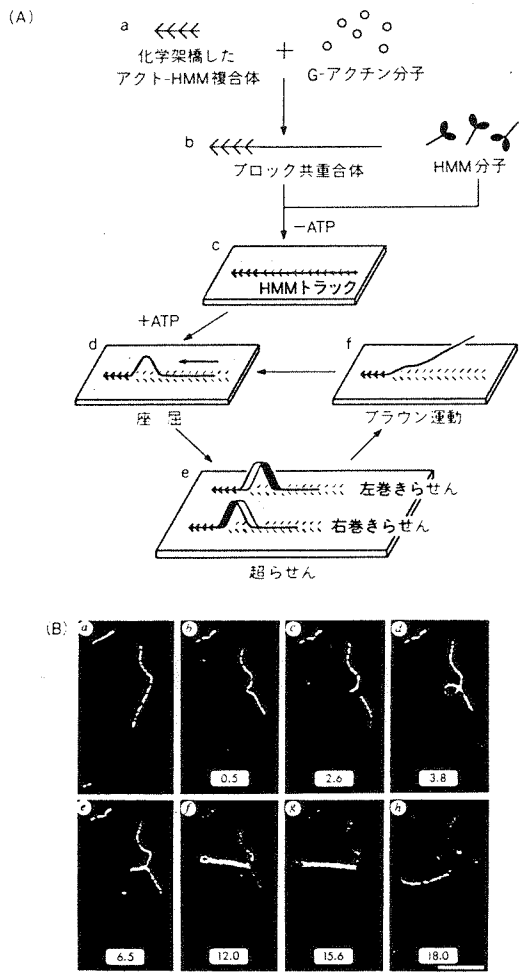

図 1　アクチンフィラメントの回転滑り運動と超らせん形成を証明するために工夫された実験系の模式図（A）と得られた蛍光顕微鏡写真（B）

(A) アクチンフィラメントの先端部だけをガラス表面に固定して滑り運動を抑えるために，まずアクチンフィラメント断片にミオシン（HMM）分子を化学架橋した(a)。次に，このフィラメント断片を重合核としてアクチン分子を重合成長させ（ブロック共重合体），成長した部分に正常な HMM 分子を結合した(b)。この複合体をガラス表面に結合したのち(c)，ATP を加えた。重合成長したフィラメント部分は HMM トラックの上を滑り運動

らせんが右巻きか，左巻きかを光学顕微鏡で決められればよい。そう，私たちは考えた。何か適当なひもを手にとって確かめてみるとよいが，超らせんが右巻きならば，後端部は左巻きの回転滑り運動をしているはずだし，逆に超らせんが左巻きならば，後端部は右巻きの回転滑り運動をしていることになる。そう考えて行った実験の結果は私たちの予想以上のものだった。

100 例近い実験例の中で，はっきりしない数例を除いて，その他の超らせんはすべて左巻きであった[1]。このことは，後端部の滑り運動は，右ねじが進むような，右巻きに回転しながらの運動であることを示唆している。私たちの予想を超えていたのは，図 1 B に見られるように，1 重の超らせんができた後，それが倒れてループを形成し，さらにその後で多重の超らせんへと移行したことである[1,3]。この多重の超らせんは先端部にある小さなループを回転させながら徐々に成長した。そして，フィラメントの後端が HMM トラックからはずれた瞬間にほどけた。この過程が何度でも繰り返された。ここで見られる多重の超らせんの構造は，電話線のコードで日常的に見ることのできるものと同じものである。このような超らせん構造は遺伝子 DNA ではよく知られているが，タンパク質で見いだされたのはこれが最初である。

B．トルクの大きさを見積もる

次に，「はじめに」で述べた②の方法によって，アクチンフィラメントの回転運動を間接的に観察し，その上でトルクの大きさを見積も

図 1 つづき
するので，フィラメントの中央部は押されて座屈する(d)。もし分子モーターが右巻きトルクを発生していれば，座屈した部分は左巻きの超らせんを形成するはずである(e)。トルクが左巻きならば，形成される超らせんは逆に右巻きのはずである(e)。アクチンフィラメントの後端部はあるところまで滑ると HMM トラックからはずれ，ブラウン運動をするであろう。そして再び HMM トラックに結合すると，同じ過程が繰り返されることになる。(B) その結果は，蛍光写真の c に見られるように，まず 1 重の超らせんが形成され，それは左巻きであった。さらにループ d を経て，e から g のような多重の超らせんが形成された。数字の単位は秒（文献 1）から改変）。白い横棒は 5 μm。

るための実験系が考案された[4]。滑り運動するアクチンフィラメントの後端にポリスチレン球を結合する。それも，微小管運動で用いられた勾玉状の構造物と類似のものにするために，ポリスチレン球を2個結合し，その回転運動を観察しようというものである。トルクの大きさは，2球の有効回転半径の3乗と，回転の角速度，それに溶媒の粘性に比例する粘性抵抗力を計算することによって見積もることとした。その結果，観測時間内に2球が完全に1回転することはなかった。このことから回転速度の上限値，したがってトルクの上限値が5 pN·nmと見積もられた。分子モーターの個数を正確に見積もることが難しいので，分子モーター1個あたりのトルクを正確に求めることは難しい。しかし，アクチンフィラメントの長軸に垂直な，トルクに寄与する滑り力成分は，長軸に平行な滑り力成分の10%を越えることはなさそうである。このようにして，トルクをもたらす力成分は滑り力と比べて決して大きな割合を占めてはいないことがわかった。しかしその程度であっても，アクチンフィラメントを捻るには十分であり，さらに超らせんの形成（COLUMN参照）には十分である。

C. 分子の回転運動を直接見る——1分子計測の利用

さて，このようにして間接的な証拠から，アクチンフィラメントは（右巻き）回転滑り運動をすることが強く示唆された。ではこの回転運動を直接見ることはできないだろうか。4−2でも述べられている

COLUMN

アクチンフィラメントはリングや超らせんを形成する

ここで述べた一連の実験の過程で，偶然のことからアクチンフィラメントはリング（左図）にもなることが見いだされた[2]。しかも，図1の実験系の場合にはしばしば8の字型のリング（中央図）やクローバー型のリング（右図）が見られた[3]。三つ葉のクローバー型の捩れリング（右図）は，フィラメントが捩れたのちにリングが形成され，その結果，捩れがリングの中に蓄積されたままになったものと考えられる。そもそも，アクチンフィラメントがリングを形成するということは，先端部と後端部とが結合することであって不可能なことではない。この実験系では，通常の *in vitro* 滑り運動系と同様に，蛍光色素ローダミンをアクチンフィラメントに特異的に導入する目的で，ローダミン·ファロイジンという物質を用いている。キノコ毒であるファロイジンは，アクチンフィラメントに選択的に結合するだけでなく，アクチン分子間の結合を強固にしてフィラメント構造を安定化する糊（のり）として働いている。リングが容易に形成されたのも，この糊があってこそである。

ところで，超らせん構造はアクチンフィラメントの専売特許ではなかった。その後，驚いたことに，微小管でも図1Bとまったく同じ形態の超らせんが形成されることが発見された[14]（アクチンの場合と違って，微小管の（捩れ）リング構造はまだ見いだされていない）。なぜ驚いたかというと，微小管はアクチンフィラメントのようには柔らかくない（ヤング率は1桁大きいと見積もられている）ので，直感的に，このように曲率の大きなループはできないだろうと予想していたからである。何事も真実は私たちの想像を超えていることを痛感させられた。一方，遺伝子であるDNAの場合には，このような超らせん構造の研究は盛んに行われており，標準的な教科書にも記載されているほどである。環状DNAの場合には，アクチンフィラメントで見られたのとまったく同型の捩れ多重リングの形成がよく知られている。しかも，DNAの場合には捩れを作ったり解いたりする酵素（トポイソメラーゼ）の存在も知られており，超らせんの多型性と遺伝子機能との関連性が注目を集めている。今のところ，タンパク質フィラメントの超らせんの生理的な意義はわからない。もちろん，フィラメント構造の捩れを調節するような酵素の存在など知られていない。しかし，生物界は私たちの想像を超えて広く深い。未知のものの中に，タンパク質フィラメントによる超らせん形成の生理的意義が隠されている可能性はある。

図　本文中の図1の実験の過程で偶然に見いだされたアクチンフィラメントのリング構造とリング状の超らせん構造を示す蛍光像
アクチンフィラメントはローダミン蛍光色素でラベルしてある（文献3）より転載）。横棒は5 μm。

ように，最近になって蛍光1分子が顕微鏡下で見えるようになった。しかも，1分子の偏光まで画像化できるようになった[5,6]。蛍光の偏光（つまり蛍光分子の向き）を画像化できれば，蛍光色素が結合したタンパク質分子の向きを決めることができる。したがって分子の回転を見ることもできるのである。ところが，らせん対称性を持つアクチンフィラメントや微小管の場合には，その構成要素（アクチン分子やチューブリン分子）のすべてに蛍光色素を結合してしまうと，偏光は平均化されてしまって，各分子の向きをモニターすることができない。フィラメントが長軸の回りに回転しても偏光は何ら変化しない。そこで1分子の偏光を画像化することができれば，この平均化の難点は解消される。この問題に1分子偏光画像化の手法が応用された[7]。その結果を図2にまとめる。この解析から，外からの負荷が加わらない条件で自由に滑り運動しているアクチンフィラメントは，およそ1 μm 進んで1回転することがわかった。ただし，この観察からは，右巻きか左巻きかを判定することはできない。

ところで，アクチンフィラメントは約70 nm の周期の，右巻きの2重らせん構造をとっている。もしミオシン分子モーターがこのらせんを厳密にたどるように動くとすると，70 nm 進んで1回転するはずで

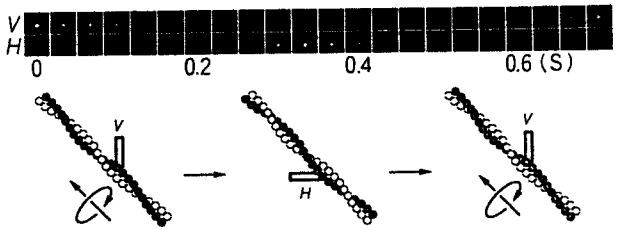

図2　滑り運動中のアクチンフィラメントに結合した1個の蛍光色素の蛍光偏光画像

縦偏光（*V*）と横偏光（*H*）とが交互に画像化されていることから，各模式図に見られるように，アクチンフィラメントはその長軸の回りに自転しつつ滑り運動していることがわかる（文献7）から改変）。

ある。実験結果は，ミオシン分子モーターは2重らせん構造に沿って力を発生するが，らせんをたどるようには運動しないことを強く示唆している。このミオシン分子モーターの性質は，微小管の上を歩くように動くキネシン分子モーターとは大いに異なったものである。このことは，キネシン分子がATP加水分解サイクルのほとんどの時間，微小管に結合しているのに対して（ATP加水分解の1サイクルに要する時間の中で，力発生時間の占める割合：duty ratio，が1に近い），ミオシン分子の場合には，ほとんどの時間，アクチンフィラメントから解離している（duty ratioが1に比べて小さい）という，ATP分解のキネティックスの解析から予想された結果と矛盾しない。このようなモーター機能の特徴から，キネシン分子は *porter*（運び手），ミオシン分子は *rower*（漕ぎ手）であるともいわれる。

❷—分子モーターが集合すると自発的な振動現象が生じる

さて，ミオシン分子モーターは，生体中では1分子で働くことはない。筋線維（筋細胞）の中にあっては何兆個もの集団で機能しているし，横紋筋の最小構造単位である1 μm^3 ほどの大きさの筋節（p.6のCOLUMN参照）の中でさえ，10万個のモーター分子が働いている。それほど多くなくても，モーター分子が複数個集合することによって集団運動や協調運動が現れないだろうか。

分子モーターはそれ1個でも十分に複雑な構造を持ち，人工的な構築が困難なナノスケールの世界で，力発生・滑り運動という驚くほど精妙な機能を発現しているナノマシーンである。力発生に際しては，構造を変化させているらしい。その結果，外部に対して力学的な仕事をすることになる。そこで外部から負荷が加われば，分子モーターの構造は受動的に歪むはずである。力学酵素としての分子モーターであってみれば，このような構造歪みによって，酵素活性を変調することもできるのではないか。それでこそ化学-力学エネルギー変換酵素

である。このような力学過程を取り込んだ自己触媒機構というものが，分子モーターには備わっていてよい。このような特性は1分子レベルで発現されてもよいが，集合体となればより顕著に発現されるであろう。そうであれば，同じ分子モーターであっても，置かれた環境や集合の仕方によって，多彩な機能を発現することができるだろう。分子モーターの協調化（シンクロナイゼーション）による機能の多彩化・多様化，そういう図式が成り立つのではないだろうか[8]。

分子モーターの協調運動の例と見られる現象を1つ紹介しよう。筋収縮系の通常の機能は，力を発生して収縮するか，弛緩するかのいずれかである。生理的にはエネルギー源であるATP存在下で，遊離のCa^{2+}濃度がおよそ1 μM以上になると収縮，逆に1 μM以下になると弛緩，この2状態のうちのいずれかをとる。ところが弛緩の溶液条件であっても，ATPと同等かそれ以上の濃度のADPが共存すると，筋収縮系は力を発生してゆっくりと収縮する。そこにさらに無機リン酸（Pi）が共存すると，図3と4に見られるように，自発的に各筋節が鋸波状の振動を始める。このような性質が，細胞膜を取り除いた単一筋線維と筋原線維で見いだされた[9-11]。この現象を，私たちはSPOCと呼ぶことにする（自発的振動収縮の英訳である，SPontaneous Oscillatory Contractionから）。

SPOCにおいては，1本の筋原線維の中に長さの異なる筋節が共存する。つまり，各筋節ごとに働いている分子モーターの数が異なる。それにもかかわらず，各筋節（正確には，半筋節：序章のCOLUMN参照）の発生する力はどれも同じと見なせるので（力の伝達速度は非常に早く，数十 μmの長さの筋原線維の一端から他端まで力が伝達する時間はマイクロ秒（μs）以下である），短縮している筋節中の分子モーター1個あたりに加わる負荷は大きいはずである。つまり，分子モーターはそれに加わる負荷の大きさに応じて，自在に発生力を調節することができるのではないか，と推測される。各筋節の振動の位相は一般には揃わない。それにもかかわらず，振動周期や振動波形はどの筋節もほぼ同じであ

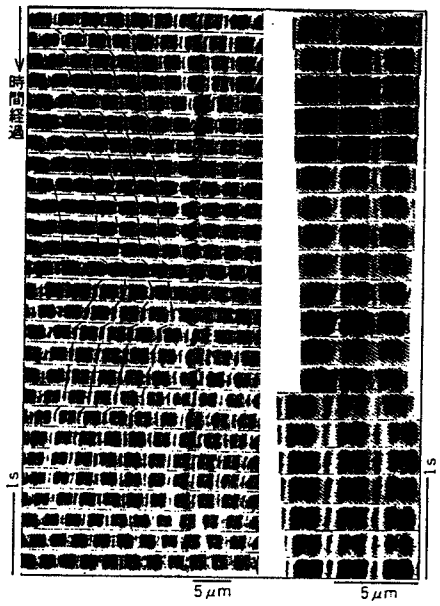

図3 ウサギ骨格筋から調製した筋原線維で見られるSPOC波形（位相差顕微鏡像）

この画面では見えないが，筋原線維の両端はガラス表面に固定されているので，筋原線維の全長は一定に保たれている（等尺性（isometric）条件）。各筋節はほぼ一定の周期で，ゆっくりとした収縮（短縮）相と，急激な伸長相からなる鋸波状に収縮・伸長を繰り返す。しかし，互いに遠く離れた筋節間の振動には決まった位相関係（相関）はない。図4の条件下でのSPOC波形とは対照的であることに注意（文献9）から転載）。

る（等尺性条件でのSPOC波形について，図3参照）。図4Aにあるように，長さも負荷もともに変化する条件では，隣接する筋節の振動の位相差がほぼ一定になるように，筋節の伸長相が筋原線維の一端から他端に伝播するので，筋原線維全体の振動はmetachronalな様相を呈する。さらに図4Bに見られるように，フィードバック制御によって筋原線維に加える負荷を一定に保つようにすると（等張性条件），

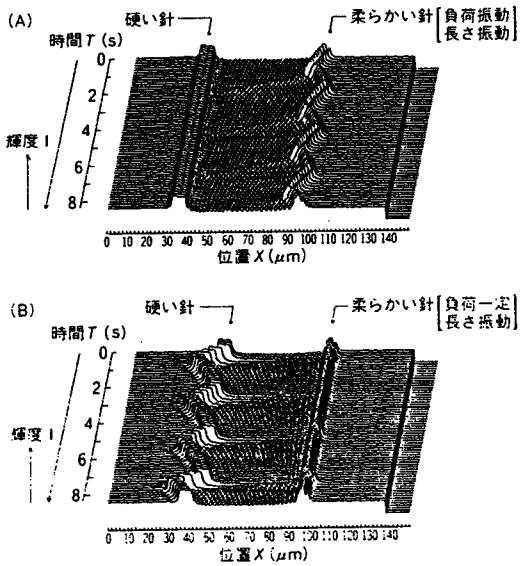

図 4　ウサギ骨格筋から調製した筋原線維で見られる SPOC 波形（位相差像の輝度表示）

筋原線維の両端は 2 本のガラス微小針に巻き付けてある。筋原線維が力を発生して収縮すると，柔らかい方のガラス微小針が撓む。その撓みの程度を画像解析することによって発生張力を計測することができる。また，各筋節が鋸波状の振動を繰り返していることが見てとれる。筋原線維の長さも負荷もともに変化するこの例では，右側の筋節から順々に伸長相が伝播していることがわかる（A）。このような自励振動を metachronal SPOC と呼ぶことにする。ところが，柔らかい方のガラス微小針の変位が常に一定になるように，硬い方の針の位置をフィードバック制御すると（この条件を等張性（isotonic）条件という），全部の筋節がほぼ同調して振動するようになる（B）。これを synchronous SPOC と呼ぶ[10]。

長さ振動のみ発生し，すべての筋節の振動がほぼ同調するようになる。このように，SPOC における筋節振動は，外部のパラメータを通じて制御することができる。

SPOC の分子メカニズムについては，いまだによくわからない点が多い。ただ，SPOC 発生の条件が，単に弛緩条件と収縮条件の中間にあるというだけでなく，弛緩から収縮への状態の転移が緩やかであることが必須なことから，集団としてのミオシン分子モーターの状態が，「はじめに」で述べた①〜③の 3 状態のどれもが同程度存在することが必要ではないか，という推測にたどり着く[11]。これは少なくとも SPOC 発生のための必要条件である。どの状態も同程度に存在する方が，分子モーター集団として外部パラメータの変動に対して追随しやすいことは明らかである。

さて，以上のような推論はできるし，理論的研究[12,13]もあるが，SPOC 発生の分子メカニズムとなると確たることは何もいえない。実験的に明らかにしたいことはたくさんある。最近の光明は，制御タンパク質の結合していない純粋なアクチンフィラメント再構築筋でも SPOC が発生することが発見されたことである（藤田・石渡：未発表）。つまり，SPOC 現象には制御タンパク質系を通じての制御のメカニズムは本質的でないことがわかった。自励振動現象は，アクチン・ミオシン分子モーター系それ自体に備わった性質である。分子モーターそれ自体に，ある種の調節機能も備わっていることになる。分子モーターは，力を発生し，滑り運動を引き起こす分子機械であるが，その力を感知しそれに応じて機能を自己調節することもできる，それ自体センサーやレギュレーターにもなりうるインテリジェントな分子機械である。この結果に勇気を得て，近い将来は *in vitro* 滑り運動系で純粋なアクチン・ミオシン系を用いて，分子モーターの数を調節しつつ，自励振動特性の分子メカニズムを明らかにしたいと考えている。分子モーターの持つこの自己調節特性は，通常の条件下での滑り運動発生の分子メカニズムにも密接に関与していると期待するからである。

おわりに

このセクションで紹介した分子モーターの特殊な機能や現象は，あ

くまでも細胞膜を取り除いた筋収縮系や，精製タンパク質による *in vitro* 滑り運動系で発現されたものである。生体中では，発現されたにしてもさして重要でないかもしれない（生体中で容易に見つからないところを見ると，その可能性はある。私たちは重要であることを願ってはいるが）。しかし，これらの機能が分子モーターの特性であることに変わりはない。このような一見特殊に見える特性を解析することから，分子モーター機能の発現のメカニズムについて，いまだ知られざる本質に迫れる可能性もある。また，分子モーター集団の示す協調運動は，その生理的意義の大きさいかんにかかわらず，生物物理学が解明すべき興味深い研究対象であろう。生体分子を人工的に組み合わせ，あるいは人工的に改変することによって，人工系を機能構築しようとするような工学指向の研究にとっては，1つの道しるべとなるかもしれない。

文 献

1) Nishizaka, T., Ishiwata, S. *et al.*: Right-handed rotation of an actin filament in an *in vitro* motile system. *Nature*, **361**, 269-271 (1993)
2) Tanaka, Y., Ishijima, A., Ishiwata, S.: Super helix formation of actin filaments in an *in vitro* motile system. *Biochim. Biophys. Acta*, **1159**, 94-98 (1992)
3) 西坂崇之：アクトミオシン分子モーターの機能と力学特性の一分子顕微解析，早稲田大学理工学部博士論文，pp.160 (1996)
4) Suzuki, N., Kinosita, Jr., K. *et al.*: Preparation of bead-tailed actin filaments: Estimation of the torque produced by the sliding force in an *in vitro* motility assay. *Biophys. J.*, **70**, 401-408 (1996)
5) Sase, I., Miyata, H. *et al.*: Real time imaging of single fluorophores on moving actin with an epifluorescence microscope. *Biophys. J.*, **69**, 323-328 (1995)
6) 佐瀬一郎：超高感度蛍光顕微鏡による単一分子および単一微小細胞のリアルタイムイメージング，慶應義塾大学理工学部博士論文，pp.156 (1996)
7) Sase, I., Kinosita, Jr., K. *et al.*: Axial rotation of sliding actin filaments revealed by single-fluorophore imaging. *Proc. Natl. Acad. Sci. USA*, **94**, 5646-5650 (1997)
8) 石渡信一：生体系材料の分子シンクロナイゼーション，ポリファイル，**37**, 25-29 (1997)
9) Ishiwata, S., Okamura, N. *et al.*: Spontaneous oscillatory contraction (SPOC) of sarcomeres in skeletal muscle. *Adv. Biophys.*, **27**, 227-235 (1991)
10) Yasuda, K., Shindo, Y., Ishiwata, S.: Synchronous behavior of spontaneous oscillations of sarcomeres in skeletal myofibrils under isotonic conditions. *Biophys. J.*, **70**, 1823-1829 (1996)
11) Ishiwata, S., Yasuda, K.: Mechano-chemical coupling in spontaneous oscillatory contraction of muscle. *Phase Transitions*, **45**, 105-136 (1993)
12) Smith, D.A., Stephenson, D.G.: Theory and observation of spontaneons oscillatory contractions in skeletal myofibrils. *J. Muscle Res. Cell Motil.*, **15**, 369-389 (1994)
13) Jülicher, F., Prost, J.: Spontaneous oscillations of collective molecular motors. *Phys. Rev. Lett.*, **78**, 4510-4513 (1997)
14) Mimori, Y., Miki-Noumura, T.: Extrusion of rotating microtubules on the dynein-track from a microtubule-dynein γ-complex. *Cell Motil. Cytoskel.*, **30**, 17-25 (1995)

♡

第1章

5 光ピンセット
——1分子を見て操作する

木下一彦・宮田英威・石渡信一

たった1個の分子が働く様子を直接見てやろう。さらに1分子に操作を加えることにより，分子の働く仕掛けを明らかにしてやろう。こんな夢のようなことが，光学顕微鏡の下でできるようになってきた。見るのはもちろん光，操作を加えるにも，光を使うのである。タンパク質でできた分子モーターの仕組みに迫る試みを通じて，1分子生理学の幕開けを紹介したい。

はじめに

光を使ってものを摘まむことができる。低温・真空の物理学の世界では，すでに原子1個を捕まえての実験が盛んである。常温・水中の生き物の世界では原子や分子を直接摘まむことはできないが，細胞をつかんでぐるぐる回したり，光だから細胞に穴を開けずに中まで“手”をつっこんで細胞内の粒子を摘まんだり，光ピンセットと呼ばれて重宝がられている[1,2]。

ここでは，この光ピンセットを使って生体分子機械の動作原理の解明を目指す仕事を紹介する。生物を構成するタンパク質分子は，たった1分子で精緻な機能を発揮するため，分子機械と呼ばれる。この分子機械に，摘まみやすいよう大きな粒子を付けてやり，顕微鏡下の光ピンセットでとらえると，分子機械を自在に操れる。それだけでなく，分子機械のわずかな動きや力を測ることができるようになる。

たった1個の分子が働く様子を，目の前にすることができるのである。

分子機械全体の動きを見るには大きな粒子が便利であるが，特定の小部分に注目したいときには，その部分に分子機械よりずっと小さな蛍光色素分子を結合させ，その蛍光から動きを探る。蛍光法[3]と光ピンセットを併用できれば，分子機械の仕組みの解明のための有力な武器となろう。

❶—光ピンセットとは

強力なレーザー光を1点に絞り込むと，焦点に向かって引力が生じる。これが光ピンセットである。引力の原因は，次のように考えられる。すなわち，光は電磁波だから，焦点では電場も大きくなる。すべての誘電体は，電場の大きなところに引き寄せられる，と大学1年生の電磁気学で教わったのを覚えておられるだろうか？

もう忘れた，という方のために，図1にもうひとつの説明を示す。焦点から外れたところに屈折率の大きな（＝誘電率の大きな）球があるとする。この球に入射した光線は図のように屈折し，最終的に太矢印の分だけ向きを変える。この反作用として，球は反対向きの力を受ける。図中の2本の太矢印に対する反作用を合成すると，いずれも球を焦点に引き付ける力になることがわかる。

生物試料を光ピンセットで摘まむときは，波長1 μm近辺の赤外光を用いる。波長の短い光は生物試料が吸収し，1 μm以上では水の吸

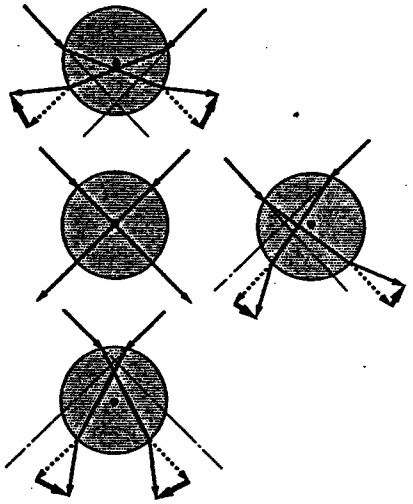

図1　光ピンセットの原理
球により屈折させられた光は，その反作用として球を光束の焦点に引き戻す。

COLUMN 1

光ピンセットの力を測る[1]

光ピンセットでプラスチックビーズをとらえたとき，ビーズは完全に静止するわけではなく，光ピンセットの引力のポテンシャルの中でブラウン運動を続ける。ビーズの位置を次々と測定してプロットしてみると，図のaのように焦点を中心に分布する。位置rにおけるビーズの存在確率$P(r)$はボルツマン分布$P(r) \propto \exp[-V(r)/k_BT]$に従うと考えられるので，図のaから得られる$P(r)$の対数をとれば，引力のポテンシャル$V(r)$が求まる（$k_B$はボルツマン常数，$T$は絶対温度）。これを$r$で微分すれば引力が求まる。焦点付近ではポテンシャルは図のbのように放物線となり，引力は単純なバネ型となる。

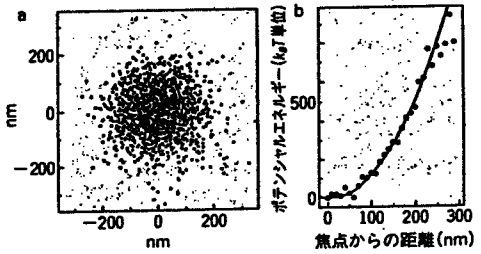

収が大きくなるので，強いレーザー光による損傷が問題となり得るからである。1 μm 近辺の光に対しては細胞は透明なので，細胞内に透過した光でミトコンドリアなどの細胞内器官を摘まむことも可能である。

❷──分子モーターを操る

常温では，光ピンセットで分子1個をとらえるのは難しい。分子1個に対する引力は弱いので，分子のブラウン運動のほうが勝ち，逃げていってしまうのである。直径1 μm くらいのプラスチックビーズだと，簡単に捕まる。ビーズに分子を結合させてやれば，分子も操れる。ここでは，分子モーター（Key Word 参照）を操る話を紹介する。

筋肉の主成分であるミオシンとアクチンというタンパク質をとってくる。双葉の形をしたミオシン分子をガラス面上に少量吸着させる(図2)。アクチン分子のほうは，生理条件下では二重らせん状に会合してアクチン線維を形成するが，これをミオシンをまぶしたガラス面上に置き，エネルギー源として ATP を加える。すると，アクチン線維がミオシンの上を，あたかもリニアモーターのようにスルスルと滑り出す。筋肉が縮むときには，筋肉の中で同じことが起きているのである[4]。

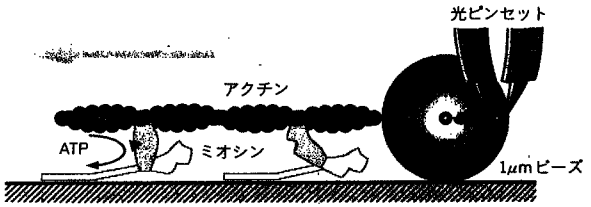

図 2　分子モーターと光ピンセットの綱引き
ガラス面上のミオシン分子（双葉形）は，ATP（赤三角）を分解しながらそのエネルギーを使ってアクチン線維を太矢印方向に滑らせる。一方，アクチン線維の後端に結合させたビーズを光ピンセットが引き戻そうとする。

アクチン線維にはちゃんと前と後があって，いつも同じ方向に滑る。後端のほうにプラスチックビーズを付けておくと，ビーズを引きずって滑る。このビーズを光ピンセットでとらえると，アクチンの滑りを止めたり，さらに逆向きに引っ張ったり，あるいはガラス面上から水中に持ち上げてしまったりといった操作をすることができる。光ピンセットとミオシンにアクチンの綱引きをさせると，その勝ち負けから，ミオシンがアクチンを引っ張る力を見積もることができる。1分子のミオシンの出す力は，ピコニュートン（pN，Key Word 参照）のオーダーである。

❸──分子モーターの歩みを測る

図2のように光ピンセットとミオシンに綱引きをさせるとき，ミオシン分子の数を減らして数個にし，ATP 濃度も十分下げてたまにしか ATP がやってこないようにすると，個々のミオシン分子の単位動作が見えてくる。ビーズが，ときどきぴくりと動くのである。ナノ

Key Word

ナノメートル（nm）とピコニュートン（pN）
1 nm は 10^{-9} m すなわち 1/10 億 m，原子が数個並ぶ長さである。タンパク質分子1個の大きさは 10 nm 前後。一方，1 pN は力の大きさで 10^{-12}N，ほぼ 1/100 億 g（10^{-10} g）のおもりに働く重力に等しい。1 pN の力で 4 nm 動いたとすると，そのときした仕事が 4 pN·nm で，ちょうど常温での熱エネルギー k_BT に等しい。ATP 1分子を分解して得られるエネルギーは，約 100 pN·nm=25 k_BT である。

分子モーター
線維状の構造物に沿って動き，必要に応じて力も出すリニアモーター型の分子モーターとして，アクチンの上を走るミオシンの他に，微小管の上を歩くキネシンや ncd，同じくダイニン（歩くのか走るのかは不明）などが知られており，最近 DNA 上を歩く RNA ポリメラーゼが仲間に加わった。一方，回転型のモーターは，長い間バクテリアのべん毛モーターが唯一の例であったが，つい最近，ATP 合成酵素がたった1分子よりなる回転型モーターであることがわかった[14]。

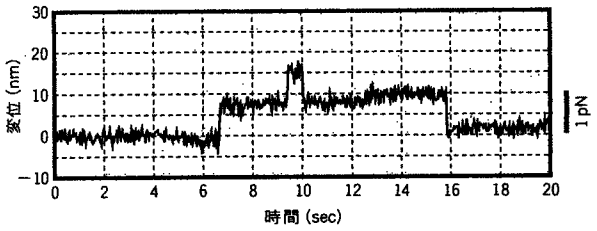

図 3　ミオシンモーターの単位動作
図 2 の系で，ビーズの動きをナノメートル精度で測定した（COLUMN 2 参照）。数秒に 1 回の割合でミオシンに ATP が結合する条件下での測定。光ピンセットのバネ常数（COLUMN 1 参照）は，10 nm 当たり 1 pN。

メートル（nm，Key Word 参照）精度でビーズの動きを測ると，図 3 のようなデータが得られる。プラスの変位はアクチンの前進，マイナスは後退に相当し，いずれも歩幅は数 nm である。図では，2 歩前進した後，2 歩後退している。前進するときは，1 pN くらいの力を出している。光ピンセットの引き戻す力が強い場合には，それに応じてミオシンも頑張り，5 pN くらいまでの力が出せるようである[5~7]。

生物学の教科書によると，ミオシン分子のアクチンに結合する部分（図 2 の赤の濃い網掛け部分）は ATP のエネルギーを利用して垂直結合（図 2 左側）から斜め結合（右側）へと構造変化を起こし，あたかも舟を漕ぐようにしてアクチンを引っ張ることになっている[4]。この説の直接証拠は今のところ何もないが，もし本当だとすると，図 3 に見られる変位はミオシン分子の構造変化を直接測ったものということになる。舟漕ぎ説の真偽はともかく，アクチンという紐を介してビーズという大きな目印を結合させることにより，1 分子の構造変化をナノメートル精度でとらえる技術がすでに確立されたことになる。

❹──分子間力を測る

ミオシンに結合した ATP が分解され，分解産物がミオシンから解離するにつれ，ミオシンとアクチンの結合が強くなっていくことがわかっている。分子モーターの出す力の源は，この結合力変化にあるという考え方もある。そこで，一番結合力の大きな状態，すなわち ATP も分解産物もまったく結合していないミオシンとアクチンの結合力を，光ピンセットを用いて直接測ってみた。ちなみに，死後硬直と呼ばれる現象は，筋肉中から ATP がなくなり，ミオシンとアクチンが強く結合したままになってしまった状態をいう。

結合力を測るには，図 2 で ATP なしの状態から，ビーズをゆっくりと右に動かして，右側のミオシンとの結合が切れる瞬間に光ピンセットのバネがどれだけ伸びているか（ビーズの中心と光ピンセット

COLUMN 2

光学顕微鏡でナノメートル（nm）を測る

光学顕微鏡の分解能は光の波長程度（緑の光で 500 nm）と教科書に書いてあるのに，どうしてナノメートル精度で位置測定ができるのか。波長よりずっと小さな物体の像は，下図の赤実線のように波長（λ）程度に広がってしまう。すぐそばにもうひとつ物体があり赤破線のような像を与えるとすると，両者は重なって見分けがつかない。これが教科書にいう分解能である。しかし，ただひとつの物体が実線から破線のように位置を変える場合は，強度分布を精密に測りさえすれば，そのずれから移動量を知ることができる。ポイントは，強度分布のずれの原因が移動以外にないことがわかっていることで，ビーズのように変形しない球形粒子（向きの変化で分布が変化しない）を用いる必要がある。十分な光強度があれば精密に分布を測定できるので，0.1 nm 精度の測定も可能である。蛍光色素 1 分子の場合は，信号が弱く，これだけの精度は出ない。

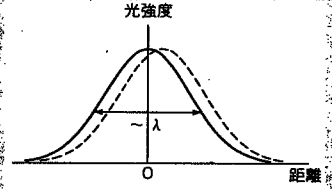

の中心がどれだけずれているか）を見ればよい。100個以上のミオシン分子ひとつひとつにつき測定していった結果，平均約10 pNの力でアクチンから剝がせることがわかった。ミオシンが前進するときに出す力，5 pNより強くなくては“足が滑って”しまうわけだから，ほどよい結合力といえるかもしれない。

1個のミオシン分子を相手に，何度もアクチンを結合させては剝がすという測定を繰り返してみたところ，分子に見かけ上の“個性”があることがわかってきた。すなわち，あるミオシンは常に強い力をかけないとアクチンから離れないが，別のミオシンはいつも弱い力で離れてしまう。個性があったのでは“分子”の定義に背くが，これはガラス面との接触の仕方の違いによるものであろう。微環境の差により，同一種の分子や原子の性質が異なることがわかってきたのは，つい最近のことである。結合力の測定からは他にもいろいろ情報が得られるが，それらは文献に譲る[8]。

❺——蛍光を使って分子の向きを知る

図3の変位が仮にミオシン分子の構造変化を表すものだとしても，分子のどこがどのように変化したのかを，このデータだけから知ることはできない。特定部分の構造変化をとらえるには，蛍光偏光が有効な方法のひとつである。

蛍光は，色素分子が光を吸収して励起され，再び光を放射する現象である。溶液中では発光波長が励起波長より長くなるため，発光波長だけを通すフィルターを介して観察することにより，暗闇の中に目的とする蛍光だけが浮かび上がる。顕微鏡自身が蛍光を出したりしないように注意を払えば，蛍光色素たった1分子が水溶液中を動き回る様子を連続観察することもできるようになった[9,10]。

蛍光は，色素分子の発光軸の方向（発光にかかわる電子の振動方向）に沿って偏光する[3]。そこで，図4aのように縦向きの偏光子を通した像（V）と横偏光（H）の像を同時にカメラに映し出すと，色

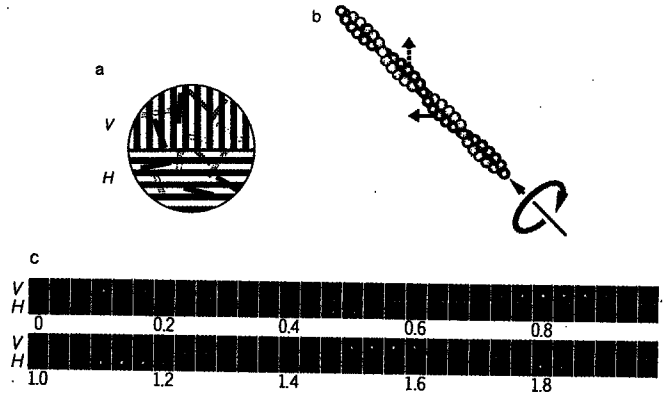

図4 蛍光色素1分子の向きの測定
a：縦向き（V），横向き（H）それぞれの偏光板を通した蛍光像を上下に並べてカメラに映し出すと，発光軸（図中の長方形）が縦を向いた色素は上の画面で，横を向いた色素は下の画面で強く光る。b：斜め45°方向に滑るアクチン線維に蛍光色素（矢印）を結合させておき，その向きの変化からアクチンの線維軸まわりの回転をとらえる。c：bの系でaの測定をした結果の連続写真[11]。数字は秒。わずかではあるが輝点の位置が左上方向に移動していくことに注意。

素分子（の発光軸）が縦を向いていればVの画面に明るく映り，横向きならHの画面に映る。すなわち，色素1分子からの蛍光を縦・横2つの偏光成分に分けることにより，その分子がどちらを向いているのかを連続的に観察できる。

例を示そう。アクチン線維は図4bのようにらせん構造をしているから，ミオシンの上を滑るとき，線維軸のまわりに回転しながら前進することが期待される。しかし，直径たった10 nmのアクチン線維の回転を直接とらえるのはなかなか難しい。そこで，アクチン線維に1個か2個の蛍光色素分子を，約45°の角度をなすようにしっかりと結合させる（図4bの赤い矢印）。すると，アクチン線維が画面上を斜め45°の方向に回転しながら滑るとき，色素分子は交互に縦を向いたり横を向いたりする。すなわち，図4aの分割画面上では交互に上側（V）と下側（H）で光るはずである。実際，図4cに示すように，

画面右下から左上に向かって動く輝点は交互に V 側と H 側で強く光った[11]。

こうして，アクチン線維は回転しながら滑ることが実証された。しかし，観察された回転の周期はらせんのピッチから予想されるよりはるかに長く，らせんがミオシンをなぞりながら進むわけではないこともわかった。ミオシンの立場から見ると，ミオシンはらせんに沿って“歩く”のではなく，たくさんのアクチン分子を飛び越えながらほとんどまっすぐ“走って”いくことがわかったのである。

図4cは，色素1分子の回転（向きの変化）を連続的に観察した初めての例である。ミオシン分子のここぞと思う場所に蛍光色素を結合させれば，ミオシン分子の構造変化も，色素分子の向きの変化としてとらえられるはずだということがおわかりいただけると思う。

COLUMN 3

蛍光色素1分子のイメージング

色素1分子のイメージングが難しいのは，1分子からの蛍光が弱いからというよりは，背景光を減らすのが難しいことによる。およそ世の中にあるものは何にでも，蛍光性の不純物が混入あるいは付着しており，目的の色素からの蛍光が不純物の蛍光に埋もれてしまうのである。できるだけ余計なところを照らさないようにするのがこつで[10]，不純物だらけの市販の顕微鏡でも光路に工夫を加えれば1分子が見える[9]。今や，試料そのものに含まれる不純物が最大の敵である。

水溶液中では，よい色素を選ぶと1分子から 10^6 個オーダーの光子を出させることができる。このくらい励起を繰り返すと，色素分子が「死んで（漂白して）」しまうのである（図4cの1，8番以降）。顕微鏡の下で検出できるのは，この光子の1割程だから，光子数の揺らぎが背景光とともに測定を左右する問題となる。強い励起光を用いれば単位時間当たりのS/Nが向上するが，寿命が早くなるため観察時間が短くなる。特にTVのビデオ機構をしようとすると，現状では観察時間1分程度が限界である。

1分子イメージングの応用としては，位置（融合）および向き（回転）の検出の他に，化学反応や分子間距離の測定などがある[10]。

なお，アクチン線維の回転を見るには，アクチン線維自身[8]，あるいはアクチン線維に付けたビーズ[12]を大きな目印として用いる方法もある。とくに，光ピンセットを用いて2個のビーズを互いに吸着させたものを目印に用いると，回転角が精度よく求まる[13]。

おわりに

1分子生理学へ向けて

ビーズのように大きな目印を用いて，あるいは蛍光色素のような小さな目印を頼りに，タンパク質分子がどのような構造変化を起こして機能を発揮するのか，すなわち生体分子機械がどのような仕掛けで働くのかを，1分子を相手に測定できるようになった。分子機械は常に確率的に働くので（図3の例でいうと前進・後退のタイミングが気まぐれにしか決まらない），たくさんの分子機械を完全に同期させることはできない[9]。構造変化をきちんととらえるには，どうしても1分子測定をしなくてはならないのである。

大きな目印からは強い信号が得られるので，空間分解能，時間分解能ともに高い測定をすることができる。一方，小さな目印のほうは精度がやや劣るが，特定の部分に起こる構造変化を他と区別して知らせてくれる。両者をうまく使いこなして，分子モーターに限らずあらゆる分子機械の働きを解明していきたい。タンパク質1分子の生理学ともいうべき，新しい学問を育てたい。

文 献

1) 鈴木直哉・木下一彦：光ピンセット．生体の科学，44，159-165（1993）
2) Svoboda, K., Block, S.M.：Biological applications of optical forces. *Annu. Rev. Biomol. Struct.*, **23**, 247-285 (1994)
3) 木下一彦・御橋廣眞（編）：蛍光測定－生物科学への応用，学会出版センター（1983）
4) 石渡信一（編）：生体分子モーターの仕組み，シリーズ・ニューバイオフィジックス④，共立出版（1997）

5) Finer, J.T. *et al.*: Single myosin molecule mechanics: piconewton forces and nanometre steps. *Nature*, **368**, 113-119 (1994)
6) Miyata, H. *et al.*: Mechanical measurements of single actomyosin motor force. *Biophys. J.*, **68**, 286 s-290 s (1995)
7) Ishijima, A. *et al.*: Single-molecule analysis of the actomyosin motor using nano-manipulation. *Biochem. Biophys. Res. Commun.*, **199**, 1057-1063 (1994)
8) 西坂崇之・石渡信一：分子モーターの力学・機能特性を見る．生物物理，**36**, 15-19 (1996)
9) 佐瀬一郎・吉川　博・宮田英威・木下一彦：「1個」を見る．生物物理，**36**, 20-24 (1996)
10) 船津高志：1分子イメージング，1分子ナノ操作－1分子モーターの運動と酵素反応を観る－．生物物理，**36**, 5-9 (1996)
11) Sase, I. *et al.*: Axial rotation of sliding actin filaments revealed by single-fluorophore imaging, *Proc. Natl. Acad. Sci. USA*, **94**, 5646-5650 (1997)
12) Suzuki, N. *et al.*: Preparation of bead-tailed actin filaments: estimation of the torque produced by the sliding force in an *in vitro* motility assay. *Biophys. J.*, **70**, 401-408 (1996)
13) Yasuda, R. *et al.*: Direct measurement of the torsional rigidity of single actin filaments. *J. Mol. Biol.*, **263**, 227-236 (1996)
14) Noji, H. *et al.*: Direct observation of the rotation of F_1-ATPase. *Nature*, **386**, 299-302 (1997)

8 The use of fluorescent probes

Shin'ichi Ishiwata

Current Methods in Muscle Physiology

Advantages, Problems, and Limitations

Prepared under the auspices of the International Union of Physiological Sciences

Edited by

Haruo Sugi

Chairman of the IUPS Commission on Muscle Physiology

8.1 Introduction

Muscle contraction is attributed to the microscopic (to be more precise, nanoscopic) structural changes in protein motors. However, we have not yet succeeded in observing these critical structural changes despite nearly half a century of anticipating this breakthrough.

At present, it is possible to directly observe single actin filaments under fluorescence microscopy by labelling actin protomers with fluorescent probes (Yanagida *et al.* 1984; Honda *et al.* 1986). Moreover, the sliding movement of actin filaments can be visualized on a myosin-coated glass surface in real time (*in vitro* motility assay system) (Kron and Spudich 1986) and the active tension developed in single actin filaments can then be measured (Kishino and Yanagida 1988; Finer *et al.* 1994; Miyata *et al.* 1994, 1995). The sliding movement of actin filaments clearly shows a mutual displacement of actin and myosin. However, this does not necessarily mean that the structural changes occur within the motor (myosin) molecules. Does the motor actually change its structure? The answer to this question cannot be obtained only by observing sliding movement (Yanagida *et al.* 1993; Spudich 1994).

Structural changes in the constituents may not even be a prerequisite for motor function. Were the sliding movement to occur according to a mechanism similar to that of a man-made linear motor, structural changes would not be required. There would be, instead, a flow of small molecules such as protons and ions. Thus, to study the molecular mechanism of biological motors, it is essential to detect critical structural changes.

Spectroscopies such as fluorescence (phosphorescence), absorption, circular dichroism (CD)/optical rotatory dispersion (ORD), light scattering, X-ray scattering, neutron scattering, electron paramagnetic resonance (EPR) and nuclear magnetic resonance (NMR), are very powerful tools for studying structural changes in proteins (Cantor and Schimmel 1980). Among these, the fluorescence method is especially useful because not only quantitative time-resolved analysis is possible, but also imaging of the organized structure under fluorescence microscopy; in addition, different information can be imaged at the same time by using dual- or multi-view microscopy (Kinosita *et al.* 1991). For monitoring the spatio-temporal changes in the structure of a particular protein in an organized system,

the fluorescent probe method is superior to that of other spectroscopies. If an epi-fluorescence dye is incorporated into a specific site on a particular protein, it is possible to selectively monitor information on the state (and dynamic structure) of the labelled protein. Furthermore, various kinds of fluorescent probes are now available (Haugland 1996) and can monitor local and gross structural changes in proteins, hydrophobicity (polarity) and charge distributions around binding sites, the concentrations of ions such as Ca^{2+}, Mg^{2+} and inorganic phosphates and so on (see concise description on environmental sensitivity of fluorescence by Johnson 1996). Thus, the fluorescent probe method has various advantages which overcome the disadvantages and limitations characteristic of labelling methods.

In this section, I would like to introduce fluorescent (and phosphorescent) probe studies reported over the past decade. However, this is not a comprehensive review. Preliminary results obtained in my laboratory are also described. I recommend that readers refer to the reviews of Cooke for research up to about 1980 (Cooke 1982) and of Thomas for that up to about 1986 (Thomas 1987). The following sections deal with the spin probes of Arata (1997) and, subsequently, the nucleotide fluorescent analogues of Bagshaw (1997), concisely and comprehensively reviewing not only nucleotide fluorescent analogues but also general fluorescence techniques and principles, including fluorescence resonance energy transfer (FRET), fluorescence quenching and so on. As to the FRET method, which is widely used in muscle research, the reviews by dos Remedios and colleagues (dos Remedios *et al.* 1987; dos Remedios and Moens 1995) and Miki *et al.* (1992) also are useful.

8.2 Methods and results

The fluorescence labelling method is not complicated. The most important point is incorporating the label at the specific site (amino acid side chains for covalent bonds or the micro environment for non-covalent bonds) on the protein by selecting environmental conditions (pH, temperature, ionic strength, ion species and so on) suitable for the labelling reaction (for the actual labelling method for each probe, see references below and the next section, also Arata 1997).

The most difficult challenge is maintaining the physiological functions of the labelling proteins; functions are modified to some extent by labelling. It is thus important to characterize labelled proteins, for comparison with unlabelled proteins, and then determine the limitations of interpreting the data obtained. To incorporate probes at a specific site in order to monitor structural changes directly coupled to physiological functions without modification of functions entails two seemingly contradictory tasks. We must overcome the disadvantages inherent in probe methods by developing innovative experimental methods and systems.

Here, I will describe examples of fluorescent probe methods applied to the muscle system: actin, myosin and regulatory proteins. Further elaboration on applications to the muscle fibre (fibril) system is provided below.

Actin

Phallodin, a toxin extracted from the mushroom *Amanita phalloides*, is a useful substance for monitoring and visualizing the structure of actin, even in association with other organized elements, because it is selectively incorporated into actin filaments (Wieland and Faulstich 1978; Wulf *et al.* 1979). Observation of single actin filaments under fluorescence microscopy was made possible by labelling with fluorescent-dye conjugated phalloidin (Yanagida *et al.* 1984) or stabilization of the polymer structure of actin with phalloidin, upon labelling with fluorescein isothiocyanate (FITC) (Honda *et al.* 1986) and other SH-reactive fluorescent probes. Recently, the location of the binding site of phalloidin was determined to be the boundary region of actin protomers (Lorenz *et al.* 1993). Applying a FRET method to fluoresceinisothiocyanatophalloidin-labelled and tetramethylrhodamineisothiocyanatophalloidin-labelled actin filaments, Heidecker *et al.* (1995) reported that the distance between adjacent phalloidins measured about 3.7 nm with a radial co-ordinate of 1.45 nm, which was consistent with the atomic model.

The only problem with incorporating the fluorescent-phalloidin into actin filaments in muscle fibres is that the binding is disturbed by nebulin (Yasuda *et al.* 1994) and probably some other proteins as well. In practice, in skeletal muscle, where nebulin is one of the constituents of thin filaments, the binding site of phalloidin is limited to the ends of the thin filaments (Yasuda *et al.* 1994) (see also Fig. 8.2). Some investigators have reported that prolonged incubation of phalloidin can induce specific binding to a broader thin filament region (Szczesna and Lehrer 1993; Bukatina *et al.* 1996). On the other hand, in cardiac muscle phalloidin immediately attaches to the entire thin filament, probably because nebulin is absent (Yasuda *et al.* 1994).

This technique was first applied to muscle fibres by Prochniewitz-Nakayama *et al.* (1983). Although they did not observe the binding region of FITC-phalloidin in sarcomeres, they showed that the concentration of incorporated FITC-phalloidin coincided with that of actin. Based on the results of fluorescence polarization of the attached FITC under rigor, relaxing and contracting conditions, they suggested that the orientation of actin molecules changes with the activation of muscle. The results were consistent with the flexibility changes in reconstituted thin filaments previously obtained by solution experiments (Fujime and Ishiwata 1971; Ishiwata and Fujime 1971, 1972). Here and below, the fluorescence polarization, P, is defined as follows, unless stated otherwise:

$$P_{\parallel} = ({}_{\parallel}I_{\parallel} - {}_{\parallel}I_{\perp})/({}_{\parallel}I_{\parallel} + {}_{\parallel}I_{\perp}),$$

$$P_{\perp} = ({}_{\perp}I_{\perp} - {}_{\perp}I_{\parallel})/({}_{\perp}I_{\perp} + {}_{\perp}I_{\parallel}),$$

where ${}_{\parallel}I_{\parallel}$, ${}_{\parallel}I_{\perp}$, ${}_{\perp}I_{\perp}$, ${}_{\perp}I_{\parallel}$ are the intensities of four components of polarization. The subscripts on the left and right, respectively, show the directions of polarization of

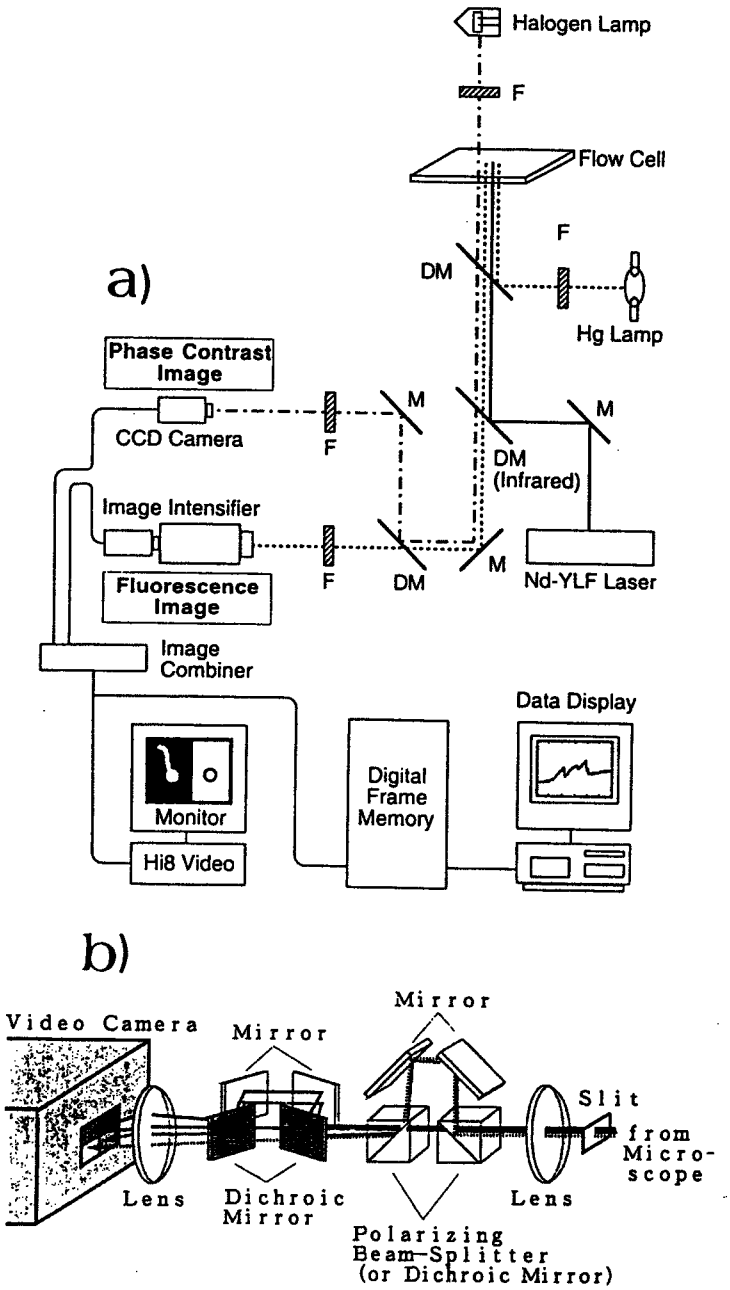

Fig. 8.1 Schematic illustration of a multi-view microscope equipped with optical tweezers. (a) Dual-view microscopic system (Kinosita *et al.* 1991) used for nanometer–piconewton measurements in an *in vitro* motility assay. Infrared laser light serves as the light source of the optical tweezers used to manipulate small particles. F, optical filter; DM, dichroic mirror; M, mirror; Flow Cell, sample stage. Taken from doctoral thesis of Nishizaka (1996). (b) Optical system for multi-view microscopy. The optical system shown at the *upper left* in (a) can be replaced by this system. Different images (four images in this illustration) can be observed simultaneously according to the direction of polarization or the wavelength. Taken from Suzuki *et al.* (1995).

incident and emitted light relative to the fibre axis; ∥ and ⊥, respectively, show the directions parallel and perpendicular to the fibre axis.

The same technique was used for detecting changes in the orientation of actin protomers in single actin filaments in an *in vitro* motility assay system (Kinosita *et al.* 1991). The fluorescence polarization of rhodamine-phalloidin attached to single actin filaments was measured with dual-view microscopy (Kinosita *et al.* 1991; Suzuki *et al.* 1995) (cf. Fig. 8.1). Here, the fluorescence polarization, P, was defined as $P=(V-H)/(V+H)$, where V and H, respectively, indicate the intensities of the vertical and horizontal polarization components of fluorescence obtained under isotropic excitation. No difference in the fluorescence polarization of rhodamine was detected between in rigor and sliding conditions. That is, the average orientation of rhodamine molecules attached to hundreds of actin protomers did not change upon activation.

Recently, Heidecker *et al.* (1995) used a FRET method to show that the distance between adjacent phalloidin binding sites does not change during sliding movement in and *in vitro* motility system, which supports our results (Kinosita *et al.* 1991).

Thus, there are two avenues of research which are inconsistent with each other; either the orientation of actin protomers changes or it does not change (or, more precisely, is undetectable) under different conditions. It is not clear at present whether this apparent discrepancy is attributable to differences among fluorescent dyes or experimental systems. This important point awaits clarification, as interest focuses on the role of structural changes in actin filaments in the molecular mechanism of contraction.

On the other hand, it recently became possible to image single fluorophores not only by fluorescence intensity (Funatsu *et al.* 1995; Sase *et al.* 1996) but also by fluorescence polarization (Sase 1996; Sase *et al.* 1997). Therefore, it is possible to image changes in the orientation of each actin protomer in single actin filaments. Sase *et al.* (1997) found that a single rhodamine-phalloidin rotates at a nearly constant rate accompanying sliding movement of an actin filament in an *in vitro* motility assay system (Sase 1996; Sase *et al.* 1997). This result supports the previous finding that a sliding actin filament, of which the front portion is fixed on a glass surface, forms a left-handed supercoil at the middle portion, suggesting that right-handed rotation around the filament axis occurs with sliding movement (Tanaka *et al.* 1992; Nishizaka *et al.* 1993).

The fluorescent dye-conjugated phalloidin could be used not only for studying structural changes in actin filaments as described above but also for monitoring changes in the local environment (such as pH, the concentrations of free ions, hydrophobicity, electrostatic potential and so on). Recently, we synthesized SNAFL-phalloidin for the purpose of monitoring and imaging the pH value around the phalloidin binding site (Kato *et al.* 1995). SNAFL (Haugland 1996) is a pH-sensitive dye, of which the excitation spectrum changes around pH 7.0. Figure 8.2 shows fluorescent images of skeletal myofibrils labelled with SNAFL-phalloidin in a rigor solution of different pH values (Kato *et al.* 1995; Kato 1996).

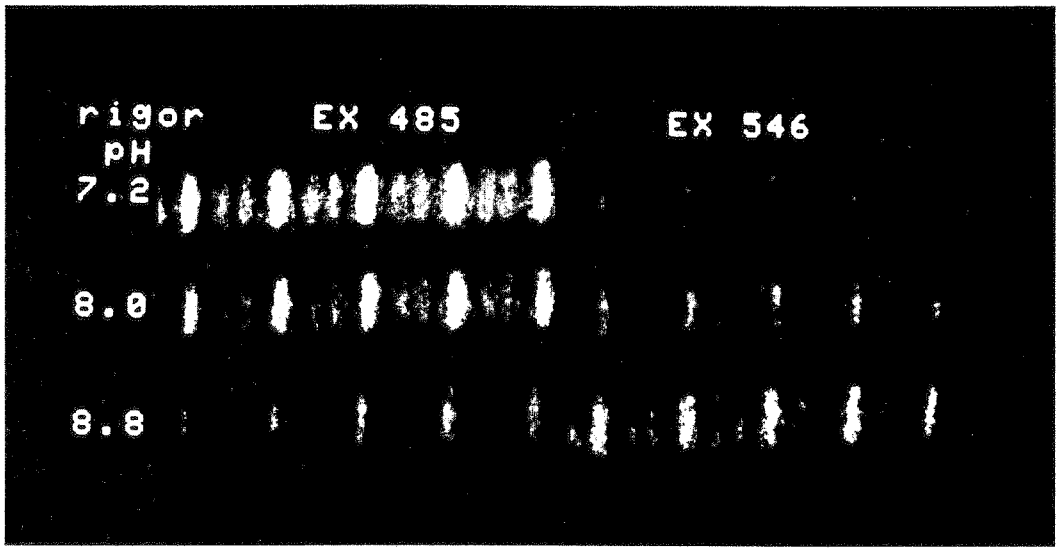

Fig. 8.2 Fluorescence images of a single skeletal myofibril obtained with SNAFL-phalloidin labelling (taken from Kato 1996). Only the ends of thin filaments are clearly labelled. The vertical lines with stronger and weaker fluorescence intensity, respectively, correspond to the Z line and the free ends of thin filaments. The images were taken at the excitation (Ex) wavelength of 485 nm (*left*) or 546 nm (*right*) and at an emission wavelength of about 590 nm. The pH value in the rigor solution was raised from 7.2 to 8.0 and finally to 8.8. As the pH value was raised, the fluorescence intensity at Ex. 485 nm decreased, whereas that at Ex. 546 nm increased. Thus, from the intensity ratio, the pH value around the phalloidin binding site in the myofibrils could be imaged and determined.

To apply dual-view microscopy and obtain real-time imaging of probe-labelled protein systems, it is convenient to use fluorescent probes of which the emission, but not excitation, spectrum is sensitive to the environment, allowing excitation at a single wavelength and imaging at two different wavelengths (Fig. 8.1a) or through vertical and horizontal polarization components (Fig. 8.1b). Recently, we custom-ordered Molecular Probes Inc. to synthesize SNARF-phalloidin of which the emission spectrum changes in response to pH changes. Experiments like those shown in Fig. 8.2 but using dual-view microscopy, are now possible.

Both association and dissociation rate constants were measured by monitoring changes in the fluorescence intensity of rhodamine phalloidin, which increases several-fold upon binding to actin filaments (De La Cruz and Pollard 1994). (Note: the binding constant of phalloidin with actin filaments is in the order of 10^7/M according to Haugland 1996). We found that both rate constants increased with increasing temperature, between 25 and 45 °C with an activation enthalpy in the order of 10^5 J/mol (Hotta and Ishiwata 1996). This approach, using environment-sensitive fluorescent dye-conjugated phalloidin, yields valuable information about the local environment of actin filaments.

Ando and associates recently examined the electrostatic potential around the phalloidin binding site using the 'diffusion-enhanced FRET' method (Yamamoto *et al.* 1994). For this purpose, they synthesized terbium (Tb)-diethylenetriamine-N,N,N′,N″,N″-Pentaacetic acid (DTPA)-phalloidin to serve as the fluorescent donor. They found that the electrical potential around the phalloidin binding site was negative and that this negative potential was slightly reduced by the binding of S1 (Ando *et al.* 1993).

The extent of modification of the structure and function of actin filaments by phalloidin labelling is not known; there is reportedly a tension–pCa curve shift to the left, i.e. the regulatory mechanism is modified by the attachment of phalloidin (Bukatina *et al.* 1996). We have confirmed that the maximum tension itself does not change appreciably with the binding of phalloidin to thin filament-reconstituted cardiac muscle fibres (Fujita *et al.* 1996).

As is well known, there is one reactive SH group in actin, i.e. Cys374, located near the actin filament surface (Holmes *et al.* 1990). Because SH-reactive reagents can be preferentially incorporated into Cys374, among the five cysteines in actin, the SH-reactive fluorescent probes have been widely used for specific labelling of actin molecules. Among these probes, N-(1-pyrene) iodoacetamide (PIA) appears to have been the most successful for monitoring structural changes in actin molecules, i.e. the fluorescence intensity is enhanced by more than 20-fold upon polymerization of actin (Kouyama and Mihashi 1981). Such an extraordinarily large change in fluorescence intensity is exceptional; this study is a typical demonstration of the remarkable potential uses of fluorescent probes.

In general, the fluorescence intensity of the probe incorporated into Cys374 is sensitive not only to the polymerization–depolymerization of actin (for tetramethylrhodamine-iodoacetamide (IATR) labelling, see Tait and Frieden 1982), but also to the interaction of actin filaments with myosin and regulatory proteins. For example, the fluorescence intensity of pyrene, incorporated into Cys374 of actin filaments, decreased to 1/3–1/5 with S1 binding (Geeves 1989). However, few studies taking this approach have been reported recently.

The labelling with PIA and N-((2-(iodoacetoxy)ethyl)-N-methyl)amino-7-nitrobenz-2-oxa-1, 3-diazole (IANBD) of actin (Ishiwata and Funatsu 1985) minimally affected polymerizability and the interaction with myosin. However, in general, the properties of actin filaments are modified to some extent with labelling at Cys374. Although rhodamine, for example, is a useful dye in the sense of slow photobleaching, large quantum yield and so on, tetramethylrhodamine-maleiamide (MTR) and IATR labelling reduces the polymerizability of actin. However, polymerizability is restored by co-polymerization with unlabelled actin (Ishiwata, unpublished observation). Needless to say, the attachment of phalloidin also stabilizes these fluorescent dye-labelled filaments, allowing application to an *in vitro* motility assay.

Other than Cys374, there are several sites of potential fluorescent probe labelling, such as Cys10, Gln41 (Kasprzak *et al.* 1988), and Lys61 and Tyr69

(see review, Miki *et al.* 1992). These sites have been used mainly as loci for FRET measurements. It has been shown that the polymerizability of actin was impaired by the labelling of, e.g. Lys61, but was restored with the addition of phalloidin (Miki 1987). The motion of subdomain 2 in actin filaments, in which Lys61 is located, was detected upon binding of S1, i.e. via changes in the distance between Lys61 and the adenine moiety (Miki and Kouyama 1994).

Thus, several studies have been done in solution but relatively few in an organized system that is relevant to the contraction mechanism. The main reason is that there has been no way to selectively incorporate the fluorescent dyes into a particular residue, such as Cys374, while maintaining the organized structure of muscle fibres or myofibrils. The only option, currently available, is to use a reconstitution system as described below in Section 8.4 on future prospects.

Myosin

Phallotoxin has no counterpart that specifically attaches to myosin molecules (or filaments) without modifying the structure and function of myosin. The most popular way to incorporate fluorescent dyes into myosin is the use of reactive cysteine residues called SH1 (Cys707) and SH2 (Cys697) present in the main chain (Reisler 1982) or SH groups in the light chain such as Cys177 on the alkali light chain (Trayer and Trayer 1988) or Cys127 and 156 (skeletal), and Cys108 (gizzard) on the regulatory light chain (LC2) of myosin.

There is an established method of labelling SH1 selectively (Reisler 1982). Figure 8.3 shows that both *N*-(iodoacetyl)-*N'*-(1-sulfo-5-napthyl)-ethylenediamine (5-(2-iodoacetylaminoethyl) aminonaphthalene-1-sulfonic acid (IAEDANS) and 5-(iodoacetamido) fluorescein (IAF) are incorporated into SH1 (Ishiwata, unpublished data). However, a serious problem exists in the labelling of SH1 and SH2, i.e. ATPase activities are to some extent modified (Root and Reisler 1992). As is well known, the K^+-ATPase activity of myosin is lost by labelling of SH1 (or SH2) with SH reagents such as N-ethylmaleimide (NEM) (Sekine and Kielley 1964; Seidel 1969). The actin-activated Mg^{2+} ATPase activity, which is essential for motor function, is also damaged and actin filaments remain attached to the labelled myosin even in the presence of ATP. Interestingly, these labelling effects are highly dependent on the label species. For most labels, however, the actin-activated Mg^{2+} ATPase is reduced so that the sliding movement of actin filaments is somewhat modified (Root and Reisler 1992). It would still be overly hasty to assert that SH1 (or SH2) labelling studies are useless. In fact, if an appropriate label is selected, important characteristics of intact myosin, for example, the dissociation from actin filaments on addition of ATP and binding affinity in the absence of ATP, are preserved. Using such labels, one can examine the dynamic structure of myosin in the attached and detached states.

In this respect, we selectively introduced eosin-maleimide into SH1 of myosin in myofibrils and studied the rotational motion of myosin heads in the presence

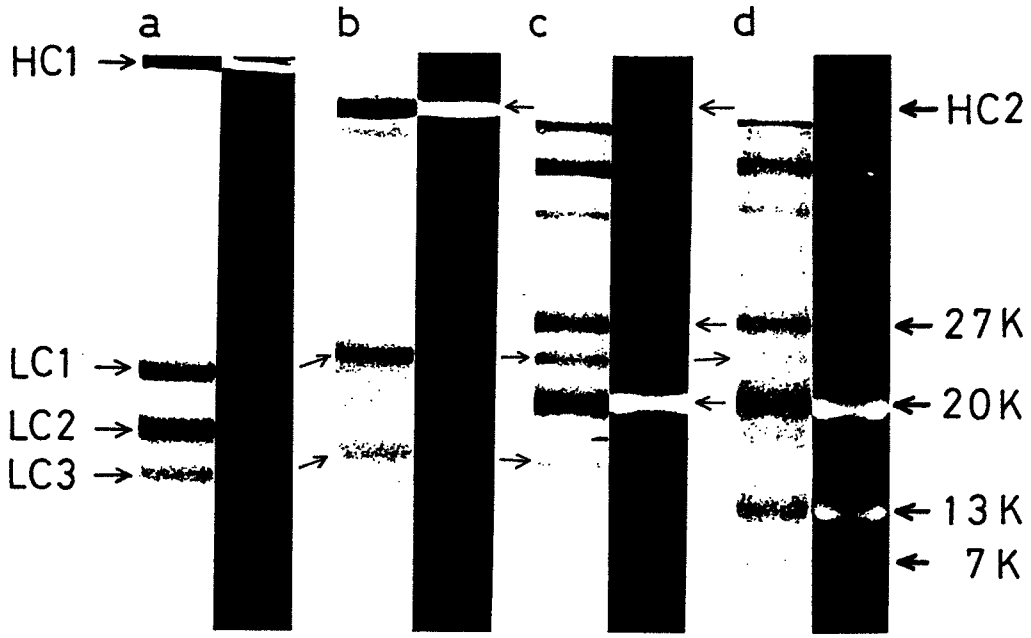

Fig. 8.3 An SDS PAGE pattern of SH1-labelled myosin and its derivatives separated on a 16% acrylamide gel. Approximately 10 μg of protein were loaded onto each lane. In each pair of photographs, the *left lane* shows proteins stained with Coomassie Brilliant Blue R, the *right line* shows fluorescence before staining. (a) Doubly-labelled HMM, where HC1, LC1, LC2 and LC3, respectively, indicate heavy chain and the three light chains of myosin (Ishiwata *et al.* 1996, 1997). The doubly-labelled HMM was prepared by labelling first with IAEDANS (fluorescence donor), then with IAF (fluorescence acceptor). (b) S1 separated from doubly-labelled myosin, where HC2 indicates heavy chain of S1. (c) Products of digestion of S1 (b) by trypsin at 25 °C. (d) Hydrolysis of S1 with hydroxylamine for 5.5 h at 45 °C (Sutoh 1981). 27 K, 20 K, 13 K and 7 K, respectively, indicate the 27, 20, 13 and 7 kDa fragments. The observation of fluorescence only at 13 kDa fragments indicates that the label was specifically incorporated into SH1 (Sutoh 1981). Similar results were reported by Miyanishi and Borejdo (1989) for the labelling of SH1 with IATR, or SH2 with MTR.

and absence of ATP using the phosphorescence anisotropic decay method (Ishiwata *et al.* 1987, 1988). Under rigor conditions, the anisotropy did not decay within milliseconds (at a minimum). This observation indicated that the rotational motion of myosin heads was suppressed. Under relaxing conditions, on the contrary, anisotropic decay was observed; the decay curve was decomposed into two exponentials having respective relaxation times of sub-microseconds and a few microseconds. We interpreted these results according to the double-cone model (Kinosita *et al.* 1977): the detached myosin heads rotate in sub-microseconds and, additionally, slow motion is superimposed because one end of the heads is connected to the movable neck portion. This result is not peculiar to a condensed system such as that of muscle fibres; similar results were obtained for myosin

filaments in dilute solution (Eads *et al.* 1984; Kinosita *et al.* 1984; Ludescher *et al.* 1987; Mendelson and Wilson 1987; Ludescher and Thomas 1988).

To introduce eosin-maleimide specifically into SH1 in myofibrils, we adopted the method developed by Duke *et al.* (1976). After pre-treatment with NEM under rigor conditions, i.e. blocking reactive SH residues (such as Cys374 in actin) other than SH1 in advance, the label was introduced under relaxing conditions with pyrophosphate (Ishiwata *et al.* 1987); the same technique was previously used for spin-labelling (Ishiwata *et al.* 1986). We noticed the problem that ATPase activity under relaxing conditions tended to approach that under activating conditions, making relaxation difficult to achieve. The labelling method we used was the best available at that time but, at present, removable SH blocking reagents should be used instead of NEM. For example, SH-reactive reagents, such as thimerosal (Emoto *et al.* 1985), are recommended [recently, 5,5′-dithiobis-(2-nitrobenzoic acid) (DTNB) has also been used; see next section and Arata 1997]. The SH-reactive reagents can be removed after selective labelling using S–S bond reductants, such as dithiothreitol. The aforementioned side-effects will thus be avoided. Pre-treatment of S1 with thimerosal was recently adopted to block undesirable SH residues from reacting with the Au (gold) surface and to allow creation of a mono-layer of S1 molecules on the Au surface (Sasaki *et al.* 1997). Thus, the selective labelling method can be improved by choosing an appropriate labelling procedure and using different types of reagents.

On the other hand, contractile function is not damaged by LC2 labelling. Physiological functions may be essentially unchanged, despite the sliding velocities in an *in vitro* motility assay system being diminished by removal of, not only alkali light chains (LC1 and LC3), but also regulatory light chains (LC2) (Lowey *et al.* 1993). Caution should be exercised in applying the same technique to other muscle systems, such as smooth and molluscan muscle, in which regulatory light chains are especially important for regulation.

It is now believed that the tip, i.e. the SH1 (Thomas *et al.* 1995), and nucleotide binding regions (Yanagida 1981; Tanner *et al.* 1992) of the myosin head do not rotate during force generation; rather, it may be that the neck portion of the head changes its orientation. For these two reasons, research interest has focused on how to detect changes in the orientation of the neck portions of myosin heads.

The LC2 of chicken gizzard muscle contains only one SH residue (Cys108), although there are two SH residues (Cys127 and 156) in the LC2 of rabbit skeletal muscle. Thus, a new method has been developed, in which the intrinsic LC2 or rabbit skeletal muscle fibres (or fibrils) is substituted for the extrinsic chicken gizzard LC2 of which Cys108 has been labelled beforehand. Recently, Irving *et al.* (1995) expressed wild-type chicken gizzard LC2 in *Escherichia coli* and labelled its Cys108 with 6-IATR, thereby measuring the polarization (Q) of the label under contraction, relaxation and rigor conditions, to investigate changes in response to quick release and stretch of the fibre. They found that, during contraction, $Q_{\parallel}$ increased and $Q_{\perp}$ decreased simultaneously on quick release of

the fibre, whereas $Q_{\parallel}$ decreased and $Q_{\perp}$ increased simultaneously on quick stretch of the fibre (definitions of $Q_{\parallel}$ and $Q_{\perp}$ differ slightly from those of $P_{\parallel}$ and $P_{\perp}$). On the other hand, with rigor, the direction of polarization change was opposite that of contraction. The orientation of the fluorescence dipole was estimated according to a model calculation (Irving 1996). They concluded that, 'the average probe orientations in the two states are on opposite sides of the plane at 90° to the filament axis' (see Fig. 4 in Irving *et al.* 1995). This appears to provide direct evidence for the tilting mechanism of force generation. The only problem is that the estimated degree of the tilting angle, i.e. less than 3° on average, is too small to account for the angle predicted in cross-bridge tilting models.

As pointed out by A.F. Huxley (1995), 'there are still many uncertainties in the interpretation', an ever-present feature of fluorescence polarization methods. First the orientation of the dipole relative to the long axis of myosin heads is unknown; second, myosin heads may have different orientations and so on.

More recently, the above study has been extended by combining X-ray diffraction with fluorescence microscopic observation (Ling *et al.* 1996) and flash photolysis of caged-ATP and ADP (Allen *et al.* 1995, 1996). The changes in LC2 orientation observed under different conditions could not be detected when sarcomeres were stretched up to 4.0 μm, where there was no overlap between thick and thin filaments (Ling *et al.* 1996).

Some of the difficulties recognized in the above studies might be overcome, if the orientation of a single fluorophore could be followed over time in the fibre system. This is not an unrealistic idea, because the first step in such an approach has already been taken in an *in vitro* motility assay system (Sase 1996; Sase *et al.* 1997).

Instead of labelling LC2, the conventional method of monitoring changes in the orientation of SH1 and SH2 regions in muscle fibres (or fibrils) has recently been re-examined by measuring fluorescence polarization (Cooke 1982; Thomas 1987). The time courses of changes in polarization and fluorescence intensities of labels incorporated into SH1 in skeletal muscle fibres were examined together with that of tension development following flash photolysis of caged nucleotides (Tanner *et al.* 1992; Berger *et al.* 1995, 1996). Tanner *et al.* found that the orientation of rhodamine fluorophores changed before force generation. However, the IATR they used was a mixture of 5 and 6 isomers, such that the estimated values of polarization contained some ambiguity. Furthermore, these isomers appear to have different reactivities to the labelling sites in muscle fibres (Ajtai *et al.* 1992). Accordingly, Berger *et al.* (1995, 1996) re-examined the same properties using either the 5 or the 6 isomer (Corrie and Craik 1994) and confirmed the previous results. They suggested that the observed changes may be related to nucleotide binding but not cross-bridge rotation because the fluorescence changes occurred before cross-bridge detachment.

Recently, Thomas *et al.* (1995) re-examined the time-resolved phosphorescence anisotropic decay technique to refine earlier results and have confirmed the

microsecond rotational motions of the cross-bridges in SH1-labelled or LC2-labelled muscle fibres and fibrils. Erythrosin iodoacetamide and eosin maleimide were again used as the phosphorescent dyes. They recognized disordered rotational motions of both portions, instead of the ordered tilting motions hypothesized in the classical cross-bridge model, and have proposed that sliding force is generated in association with a disorder–order transition in the rotational motion of myosin heads.

Borejdo and associates used a fibre system to arrange the orientation of labels incorporated into either SH1 or SH2 of S1: the labelled S1 was diffused into glycerinated fibres and the orientation of labels was assessed based on the absorption dichroism (Borejdo and Burghardt 1987). The absorption dipole of IATR on SH1 was oriented at 65° with respect to the fibre axis under rigor conditions and at 51° in the presence of MgADP, in agreement with previous results, while that of MTR on SH2 was oriented at 42° regardless of MgADP, suggesting that the two SH sites behave differently (Miyanishi and Borejdo 1989).

The fluorescent dyes incorporated into SH1 and SH2 residues are sensitive to environmental changes. For example, Hiratsuka has shown that the binding of nucleotides increases the fluorescence intensity of 2-(4′-maleimidylanilino)-naphthalene-6-sulfonic acid (MIANS) attached to SH2 (Hiratsuka 1992*a*), while decreasing that of 4-fluoro-7-sulfamoylbenzofurazan (ABDF) attached to SH1 (Hiratsuka 1993). This suggests that the SH2 region moves toward the surface, the less hydrophobic region, whereas the SH1 region moves toward the interior of the protein. Fluorescence quenching studies with acrylamide and KI supported this conclusion (Hiratsuka 1992*a*, 1993). Measuring the fluorescence intensities of the IAF-labelled SH1 and IANBD-labelled SH2 in S1 showed that both sites behave differently depending on the species of bound nucleotides and phosphate analogues (Phan *et al.* 1996). It has thus been suggested that the SH1 and SH2 regions play essential roles in the communication pathway between nucleotide and actin binding sites (Botts *et al.* 1989; Berger *et al.* 1995, 1996).

Also, both SH1 and SH2 have been used extensively for distance measurements with FRET, especially under rigor conditions, because the capacity of rigor complex formation is maintained, allowing the assumption that the geometrical relationship is not greatly modified by the labelling. For an extensive review, see dos Remedios and Moens (1995) and Miki *et al.* (1992). Herein, I will briefly discuss our recent studies (Ishiwata *et al.* 1996, 1997).

We have used FRET to measure the distances between probes attached to SH1 on myosin (HMM), between those on adjacent S1s and between those on an HMM head and S1, and so on, when attached to F-actin under rigor conditions. The SH1 was specifically labelled with either IAEDANS employed as a fluorescent energy donor (D) or with IAF as an acceptor (A). We confirmed that, in free solution, the distance between SH1s on two HMM heads was too large to be measured by FRET. However, in the rigor complex with F-actin, the intermolecular distances between S1 molecules (S1(D) and S1(A)) and the heads of

HMM molecules (HMM(D) and HMM(A)) were determined to be 6.0–6.3 nm, whereas the intramolecular inter-head distance of HMM determined using doubly-labelled HMM (D and A) was larger than the values obtained above. We interpreted this to mean that the binding constant of the rigor bond is diminished for the second head of doubly-labelled HMM (D and A) molecules due to heterogeneous chemical modification of the SH1 groups. In any case, this is apparently the first report estimating the intramolecular distance between two HMM heads in complex with F-actin by spectroscopy.

Intrinsic fluorophores, such as the tryptophan residue, can be used as a fluorescence donor for FRET measurements. Hiratsuka (1992*b*) has shown that fluorescence energy is transferred from intrinsic tryptophan to MIANS attached to SH2, indicating a distance of 2.7 nm. He proposed that Trp510 is the most probable candidate for this energy transfer. Such an inspection, based on the results of fluorescence labelling techniques, must be reconciled with the three-dimensional structure of S1 (Rayment *et al.* 1993*a*) and the acto-S1 complex (Rayment *et al.* 1993*b*; Schröder *et al.* 1993).

Are there any other sites or techniques involving fluorescence labelling? As a possible means of overcoming limitations, site-directed mutagenesis may open a new approach to incorporating probes into specific sites of proteins. Saraswat and Lowey have succeeded in inserting cysteine residues into LC2, which are reactive to SH reagents (Saraswat and Lowey 1991). Very recently, Hopkins *et al.* (1996) attempted to detect tilting motions in the LC2 region by labelling five different SH sites introduced at positions 2, 73, 94, 126 or 155 by genetic engineering. Although the results were similar to those described above, such trials will ultimately yield valuable results.

Regulatory proteins

The conformational changes in TnC accompanying Ca^{2+} binding have been examined using labels incorporated into either Cys84 or Cys35 (Ingraham and Hodges 1988; Fuchs *et al.* 1989; Dong and Cheung 1996). It was suggested that Cys84 of cardiac TnC (cTnC), into which 2-(4′-(iodoacetamido)anilino)naphthalene-6-sulfonic acid (IAANS) or 6-acrylol-2-(dimethylamino)naphthalene (acrylodan) had specifically been incorporated, became externalized upon Ca^{2+} binding (Dong and Cheung 1996).

Miki measured the distance between Cys133 in troponin-I (TnI) and Lys61 in actin in reconstituted thin filaments, of which the filament structure had been stabilized with phalloidin (Miki 1990; Miki and Iio 1993). Either IAEDANS or 4-acetamido-4′-maleimidylstilbene-2,2′-disulfonic acid (AMS) was labelled at Cys133 in TnI, as a fluorescent donor, and FITC was labelled at Lys61 in actin, as a fluorescent acceptor. The kinetics of structural changes in the reconstituted thin filaments, which occurred co-operatively at a pCa of 6.25, were examined based on changes in the distance between TnI and actin by combining the FRET technique with a stopped-flow method (Miki and Iio 1993).

As to selective labelling of regulatory proteins in muscle fibres, the replacement of troponin and troponin-C (TnC) with the labelled counterparts is frequently used because selective removal and reconstitution of these proteins are relatively easy, with reliability similar to that of LC2 (see review of Moss 1992). Replacement is achieved by incubating the fibre or fibrils in rigor solutions without divalent cations. Accompanying this treatment, a portion of the LC2 molecules usually dissociates, necessitating reconstitution of LC2 together with troponin (or TnC).

For example, TnC labelled with 5-dimethylaminonaphthalene-1-sulfonyl aziridine was exchanged for TnC in muscle fibre and the structural changes upon Ca^{2+} binding were studied (Zot and Potter 1987). The same label was used for Met25 in TnC by Allen *et al.* (1992) to distinguish the bindings of Ca^{2+} to high and low affinity binding sites; they confirmed that muscle contraction was triggered by TnC structural changes that occured upon Ca^{2+} binding to the low affinity binding site. Hannon *et al.* (1992) introduced cTnC, in which Cys84 had been primarily labelled and Cys35 partly labelled with IAANS (sensitive to hydrophobicity), into cardiac or skeletal muscle fibres. The correlation between changes in fluorescence intensity and tension development (reflecting strong cross-bridge attachment) was examined. Liou and Fuchs (1992) examined cardiac myofibrils in which two Cys residues in TnC had been labelled with N-(1-pyrene)maleimide (PMA) or N-(1-pyrene)iodoacetamide (PIA).

As to tropomyosin, Cys190 is the usual labelling site (Ishii and Lehrer 1991). Either PIA (Ishii and Lehrer 1990), PMA (Ishii and Lehrer 1987, 1991) or 1,5-IAEDANS (Borovikov *et al.* 1993) can be labelled to detect local conformational changes around the SH residue of tropomyosin. Stopped-flow experiments have shown that structural changes occur in the tropomyosin–troponin complex within several tens of milliseconds after Ca^{2+} binding. The excimer fluorescence of PIA incorporated into Cys190 of two chains of skeletal tropomyosin molecules has allowed monitoring of intramolecular chain–chain interactions in reconstituted thin filaments (Ishii and Lehrer 1990).

Physico-chemical studies on regulatory proteins in which SH groups are genetically mutated started several years ago (for TnC, see Grabarek *et al.* 1990 and Fujimori *et al.* 1990 and for a review of TnC studies, see Grabarek *et al.* 1992). Genetically engineered regulatory proteins have since been used for fluorescence labelling of TnC and tropomyosin. For example, Zhao *et al.* (1995) have used a genetically introduced tryptophan residue of troponin-T (TnT) fragments as a fluorescent donor and dansyl aziridine or IAEDANS attached to TnC or TnI, in which a single Cys was genetically introduced at positions 9, 96 or 117, as a fluorescent acceptor site. They found that the distance between these sites in the complex of TnT–TnC or TnT–TnI changes upon binding of Ca^{2+} or Mg^{2+} to TnC. On the other hand, Dong and colleagues (Dong *et al.* 1996; Dong and Cheung 1996) prepared a mono-cysteine mutant of cardiac TnC, which contains only Cys84 (Cys35, one of two intrinsic cysteines, had been replaced with Ser), and labelled Cys84 with IAANS. They investigated the kinetics of the

conformational changes in the regulatory domain of TnC, which accompany the association and dissociation of Ca^{2+} and Mg^{2+}.

8.3 Problems and limitations

The problems and limitations of the fluorescent probe method are the same, in many respects, to those of the spin probe method described in the next section (Arata 1997). The weakness of the fluorescent probe method is the difficulty of incorporating a bulky, hydrophobic probe into the functionally important site or, at least, a region close to that site, in order to monitor the structural changes tightly coupled to function. Chemical modification of the functional site inevitably affects the function being studied. Thus, the incorporation of probes into the functionally important site is, in principle, incompatible with the requirement that the physiological function not be modified.

In contrast to the spin probe method, the sensitivity of the fluorescence probe method is extremely high, such that the probe concentration necessary for measurements is several orders of magnitude smaller. In the fluorescence method, imaging and spectroscopy at the single fluorophore level are now possible (Funatsu *et al.* 1995, 1996; Sase 1996; Sase *et al.* 1995, 1997). The fluorescence intensity (spectrum) usually reflects only local conformational and/or environmental changes around the labelling site, i.e. secondary changes, such that the interpretation becomes sometime difficult. Thus, the fluorescence probe method needs many-sided control experiments.

To monitor the rotational motions (orientation changes) of the labelled protein using fluorescence (phosphorescence) (de)polarization measurements (either static or dynamic), rigid binding is essential. The orientation of the probes against the protein is also important. In such measurements, however, the labelling site can be a physiologically insignificant site, such as the SH residues in LC2. If the tilting motion of myosin heads in actually essential to the molecular mechanism of muscle contraction, one should be able to detect a sizeable rotational angle. It is ironic that the largest problem in the fluorescent probe approach to muscle research is that no probe has yet been found which reflects structural changes essential for motor function. This critical breakthrough in muscle research must be made.

One must be cautious in that probes usually contain hydrophobic residues, making dissolution in aqueous solution difficult (especially, at high probe concentrations) and forming non-specific complexes (especially, in muscle fibres and fibrils). The fluorophores frequently form dimers in solution or at the binding site (Ajtai *et al.* 1992), which may produce excimer fluorescence.

It is also possible for probes to be incorporated into binding sites non-randomly, i.e. the binding at one site may affect the affinity of subsequent binding to adjacent sites. In fact, there is a report suggesting that the binding of phalloidin to actin filaments is co-operative (Moens *et al.* 1994). Similarly, one must be careful when

labelling two myosin heads, and in the exchange of LC2 and TnC. Whether or not co-operative binding occurs should be examined in each case. Imaging and spectroscopy of single fluorophores (Funatsu *et al.* 1995, 1996; Sase *et al.* 1995, 1997; Sase 1996) will overcome some of these difficulties.

8.4 Future prospects

As described above, various fluorescent probe techniques have been developed. How can we optimally apply these techniques to future muscle research? I consider the next advance in the application of probe methods to depend on the development of reconstitution techniques for the muscle (motor) contractile system. Needless to say, the reconstituted *in vitro* motility assay systems widely used nowadays are powerful investigative tools. On the other hand, in the contractile system, the incorporation of labelled proteins is limited to a few cases, such as TnC and LC2. In this sense, our thin(actin)-filament reconstitution system is attractive (Funatsu *et al.* 1994; Fujita *et al.* 1996). Labelled actin and regulatory proteins (even genetically engineered) can be incorporated into thin filament-free fibres (fibrils), allowing measurement of the contractile function and, at the same time, monitoring of the dynamics of labelled proteins and the local environment of labelling sites. Unfortunately, we have not yet devised an appropriate way to reconstitute thick (myosin) filaments in the contractile apparatus using purified proteins (Ishiwata 1980).

On the other hand, phalloidin is a unique substance: the binding to actin is highly specific, such that the aforementioned reconstitution of actin filaments is not required for incorporating into specific muscle fibre sites. Furthermore, many useful fluorescent-probe conjugates have been synthesized. Unfortunately, monitoring structural changes closely related to the molecular mechanism of contraction has not yet been achieved. I look forward to the development of a new fluorescent phallotoxins, which will reveal essential information on the structure of actin.

Finally, I would like to point out that the future of fluorescent probe methods is still bright. Chemical techniques allowing incorporation of fluorescent probes into specific sites have not yet reached an impasse. Genetic engineering has just been introduced to this field. Innovative fluorescent probes, e.g. temperature-sensitive (Kato *et al.* 1997), stress-sensitive and specific-ion sensitive probes, are anticipated. I also expect that new techniques will be devised that allow different protein states to be distinguished, monitoring of ion flow in organized structures, and so on. Moreover, we can expect technological advances in optics, microscopy, image-processing and high-speed cameras suitable for detecting the properties of individual fluorophores. The combination of these technologies will make it possible to detect the key event, which must occur in a single molecule, underlying muscle contraction and its regulation.

8.5 Conclusion

In this short review, I have focused on a limited range of topics pertaining to the application of fluorescent probe techniques. Although the use of fluorescent probes has inevitable problems, I believe that the potential of these techniques has not yet been fully developed. The future possibilities of innovative techniques and applications remain to be explored.

Acknowledgments

I acknowledge my colleagues, especially, Mr H. Kato, for permitting the use of unpublished data; unpublished data described herein were obtained mainly in my laboratory and partly in collaboration with other laboratories. A part of the unpublished data was obtained in the Advanced Research Laboratory of the Graduate School of Science and Engineering, Waseda University. I thank Dr M. Miki of Fukui University and Dr Y. Ishii of ERATO for their valuable discussions, and Dr H. Sugi (editor) of Teikyo University for his encouragement in completing this manuscript. I also thank Drs C.R. Bagshaw and T. Arata for having sent me their preprints, which were very useful in preparing this manuscript. Finally, I thank Dr K. Kinosita, Jr. for his continuous co-operation of fluorescence techniques. The unpublished studies described herein were partly supported by Grants-in-Aid for Scientific Research from the Ministry of Education, Science, Sports and Culture of Japan and CREST.

References

Ajtai, K.P., J.K. Ilich, A. Ringler, S.S. Sedarous, D.J. Toft and T.P. Burghardt (1992) Stereospecific reaction of muscle fiber proteins with the 5' or 6' isomer of (iodoacetamido) tetramethylrhodamine. *Biochemistry* **31**, 12 431–40.

Allen, T.S.C., L.D. Yates and A.M. Gordon (1992) Ca^{2+}-dependence of structural changes in troponin-C in demembranated fibers of rabbit psoas muscle. *Biophys. J.* **61**, 399–409.

Allen, T.S.C., C. Sabido-David, N. Ling, M. Irving and Y.E. Goldman (1995) Transients of fluorescence polarization in skeletal muscle fibers labeled with rhodamine on the regulatory light chain. *Biophys. J.* **68**, 81s–86s.

Allen, T.S.C., N. Ling, M. Irving and Y.E. Goldman (1996) Orientation changes in myosin regulatory light chains following photorelease of ATP in skinned muscle fibers. *Biophys. J.* **70**, 1847–62.

Ando, T., N. Kobayashi and E. Munekata (1993) Electrostatic potential around actin. *Adv. Exp. Med. Biol.* **332**, 361–76.

Arata, T. (1997) The use of spin probes. In this volume, Chapter 9, pp. 223–40.

Bagshaw, C.R. (1997) The use of fluorescent nucleotides. In this volume, Chapter 4, pp. 91–132.

Berger, C.L., J.S. Craik, D.R. Trentham, J.E.T. Corrie and Y.E. Goldman (1995) Fluorescence polarization from isomers of tetramethyl rhodamine at SH-1 in rabbit psoas muscle fibers. *Biophys. J.* **68**, 78s–80s.

Berger, C.L., J.S. Craik, D.R. Trentham, J.E.T. Corrie and Y.E. Goldman (1996) Fluorescence polarization of skeletal muscle fibers labeled with rhodamine isomers on the myosin heavy chain. *Biophys. J.* **71**, 3330–43.

Borejdo, J. and T.P. Burghardt (1987) Cross-bridge order and orientation in resting and active muscle fibers studied by the linear dichroism of fluorescence. In *Optical studies of muscle cross-bridges* (ed. R.J. Baskin and Y. Yeh), pp. 99–121. CRC Press, Boca Raton, FL.

Borovikov, Y.S., E. Nowak, M.I. Khoroshev and R. Dabrowska (1993) The effect of Ca^{2+} on the conformation of tropomyosin and actin in regulated actin filaments with or without bound myosin subfragment 1. *Biochim. Biophys. Acta* **1163**, 280–6.

Botts, J., J.F. Thomason and M.F. Morales (1989) On the origin and transmission of force in actomyosin subfragment 1. *Proc. Natl. Acad. Sci. (USA)* **86**, 2204–8.

Bukatina, A.E., F. Fuchs and S.C. Watkins (1996) A study on the mechanism of phalloidin-induced tension changes in skinned rabbit psoas muscle fibres. *J. Musc. Res. Cell Motil.* **17**, 365–71.

Cantor, C.R. and P.R. Schimmel (1980) *Biophysical chemistry*. W.H. Freeman, San Francisco.

Cooke, R. (1982) Fluorescence as a probe of contractile system. *Meth. Enzymol.* **85**, 574–93.

Corrie, J.E.T. and J.S. Craik (1994) Synthesis and characterisation of pure isomers of iodoacetamidotetramethyl rhodamine. *J. Chem. Soc. Perkin Trans.* **1**, 2967–73.

De La Cruz, E.M. and T.D. Pollard (1994) Transient kinetic analysis of rhodamine phalloidin binding to actin filaments. *Biochemistry* **33**, 14 387–92.

Dong, W.-J. and H.C. Cheung (1996) Calcium-induced conformational change in cardiac troponin C studied by fluorescence probes attached to Cys-84. *Biochim. Biophys. Acta* **1295**, 139–46.

Dong, W.-J., S.S. Rosenfeld, C.-K. Wang, A.M. Gordon and H.C. Cheung (1996) Kinetic studies of calcium binding to the regulatory site of troponin C from cardiac muscle. *J. Biol. Chem.* **271**, 688–94.

dos Remedios, C.G. and P.D.J. Moens (1995) Actin and the actomyosin interface: a review. *Biochim. Biophys. Acta* **1228**, 99–124.

dos Remedios, C.G., M. Miki and J.A. Barden (1987) Fluorescence resonance energy transfer measurements of distances in actin and myosin. A critical evaluation. *J. Musc. Res. Cell Motil.* **8**, 97–117.

Duke, J., R. Takashi, K. Ue and M.F. Morales (1976) Reciprocal reactivities of specific thiols when actin binds to myosin. *Proc. Natl. Acad. Sci. (USA)* **73**, 302–6.

Eads, T.M., D.D. Thomas and R.H. Austin (1984) Microsecond rotational motions of eosin-labeled myosin measured by time-resolved anisotropy of absorption and phosphorescence. *J. Mol. Biol.* **179**, 55–81.

Emoto, Y., T. Kawamura and K. Tawada (1985) Characterization of the ATPase active site in myosin subfragment-1 with the use of vanadate plus ADP as a reversible 'affinity-labeling' reagent: evidence for heterogeneity in the active sites. *J. Biochem.* **98**, 351–77.

Finer, J.T., R.M. Simmons and J.A. Spudich (1994) Single myosin mechanics: piconewton forces and nanometer steps. *Nature* **368**, 113–19.

Fuchs, F., Y.M. Liou and Z. Grabarek (1989) The reactivity of sulfhydryl groups of bovine cardiac troponin-C. *J. Biol. Chem.* **264**, 20 344–9.

Fujime, S. and S. Ishiwata (1971) Dynamic study of F-actin by quasielastic scattering of laser light. *J. Mol. Biol.* **62**, 251–65.

Fujimori, K., M. Sorenson, O. Herzberg, J. Moult and F.C. Reinach (1990). Probing the calcium-induced conformational transition of troponin C with site-directed mutants. *Nature* **345**, 182–4.

Fujita, H., K. Yasuda, S. Niitsu, T. Funatsu and S. Ishiwata (1996) Structural and functional reconstitution of thin filaments in the contractile system of cardiac muscle. *Biophys. J.* **71**, 2307–18.

Funatsu, T., T. Anazawa and S. Ishiwata (1994) Structural and functional reconstitution of thin filaments in skeletal muscle. *J. Musc. Res. Cell Motil.* **15**, 158–71.

Funatsu, T., Y. Harada, M. Tokunaga, K. Saito and T. Yanagida (1995) Imaging of single fluorescent molecules and individual ATP turnovers by single myosin molecules in aqueous solution. *Nature* **374**, 555–9.

Funatsu, T., Y. Ishii, Y. Harada, A. Iwane, T. Wazawa, J. Watai *et al.* (1996) Imaging and spectroscopy of single bio-molecules. *Biophysics* (*Japanese*) **36** (Supplement), S216 (Abstract).

Geeves, M.A. (1989) Dynamic interaction between actin and myosin subfragment 1 in the presence of ADP. *Biochemistry* **28**, 5864–71.

Grabarek, Z., R.-Y. Tan, J. Wang, T. Tao and J. Gergely (1990) Inhibition of mutant troponin C activity by an intra-domain disulphide bond. *Nature* **345**, 132–5.

Grabarek, Z., T. Tao and J. Gergely (1992) Molecular mechanism of troponin-C function. *J. Musc. Res. Cell Motil.* **13**, 383–93.

Hannon, J.D., D.A. Martyn and A.M. Gordon (1992) Effects of cycling and rigor crossbridges on the conformation of cardiac troponin C. *Circ. Res.* **71**, 984–91.

Haugland, R.P. (1996) *Handbook of fluorescent probes and research chemicals.* Molecular Probes Inc., Eugene, OR.

Heidecker, M., Y. Yan-Marriott and G. Marriott (1995) Proximity relationships and structural dynamics of the phalloidin binding site of actin filaments in solution and on single actin filaments on heavy meromyosin. *Biochemistry* **34**, 11017–25.

Hiratsuka, T. (1992*a*) Movement of Cys-697 in myosin ATPase associated with ATP hydrolysis. *J. Biol. Chem.* **267**, 14941–8.

Hiratsuka, T. (1992*b*) Spatial proximity of ATP-sensitive tryptophanyl residue(s) and Cys-697 in myosin ATPase. *J. Biol. Chem.* **267**, 14949–54.

Hiratsuka, T. (1993) Behavior of Cys-707 (SH1) in myosin associated with ATP hydrolysis revealed with a fluorescent probe linked directly to the sulfur atom. *J. Biol. Chem.* **268**, 24742–50.

Holmes, K.C., D. Popp, W. Gebhard and W. Kabsch (1990) Atomic model of the actin filament. *Nature* **347**, 44–9.

Honda, H., H. Nagashima and S. Asakura (1986) Directional movement of F-actin *in vitro*. *J. Mol. Biol.* **191**, 131–3.

Hopkins, S.C., C. Sabido-David, L.D. Saraswat, Y.E. Goldman, M. Irving and S. Lowey (1996) Tilting motions of rhodamine probes at five different sites on the myosin regulatory light chain (RLC) following length steps in contracting muscle fibers. *Biophys. J.* **70**, A17.

Hotta, M. and S. Ishiwata (1996) Temperature dependence of association and dissociation kinetics of rhodamine phalloidin with actin filaments. *Biophysics* (*Japanese*) **36**(Supplement), S12.

Huxley, A.F. (1995) Crossbridge tilting confirmed. *Nature* **375**, 631–2.

Ingraham, R.H. and R.S. Hodges (1988). Effects of Ca^{2+} and subunit interactions on surface accessibility of cysteine residues in cardiac troponin. *Biochemistry* **27**, 5891–8.

Irving, M. (1996) Steady-state polarization from cylindrically-symmetric fluorophores undergoing rapid restricted motion. *Biophys. J.* **70**, 1830–5.

Irving, M., T.S.C. Allen, C. Sabido-David, J.S. Craik, B. Brandmeier, J. Kendrick-Jones *et al.* (1995) Tilting of the light-chain region of myosin during step length changes and active force generation in skeletal muscle. *Nature* **375**, 688–91.

Ishii, Y. and S.S. Lehrer (1987) Fluorescence probe studies of the state of tropomyosin in reconstituted muscle thin filaments. *Biochemistry* **26**, 4922–5.

Ishii, Y. and S.S. Lehrer (1990) Excimer fluorescence of pyrenyliodoacetamide-labeled tropomyosin: a probe of the state of tropomyosin in reconstituted muscle thin filaments. *Biochemistry* **29**, 1160–6.

Ishii, Y. and S.S. Lehrer (1991) Two-site attachment of troponin to pyrene-labeled tropomyosin. *J. Biol. Chem.* **266**, 6894–903.

Ishiwata, S. (1980) *Partial destruction and reconstruction of an ordered structure in striated muscle.* Sixth Taniguchi International Symposium on Biophysics, Santa City, The Taniguchi Foundation, pp. 262–93.

Ishiwata, S. and S. Fujime (1971) Effect of Ca^{2+} on dynamic properties of muscle proteins studied by quasielastic light scattering. *J. Phys. Soc. Japan* **31**, 1601.

Ishiwata, S. and S. Fujime (1972) Effect of calcium ions on the flexibility of reconstituted thin filaments of muscle studied by quasielastic scattering of laser light. *J. Mol. Biol.* **68**, 511–22.

Ishiwata, S. and T. Funatsu (1985) Does actin bind to the ends of thin filaments in skeletal muscle? *J. Cell Biol.* **100**, 282–91.

Ishiwata, S., B.A. Manuck, J.C. Seidel and J. Gergely (1986) Saturation transfer electron paramagnetic resonance study of the mobility of myosin heads in myofibrils under conditions of partial dissociation. *Biophys. J.* **49**, 821–8.

Ishiwata, S., K. Kinosita, Jr., H. Yoshimura and A. Ikegami (1987) Rotational motions of myosin heads in myofibril studied by phosphorescence anisotropy decay measurements. *J. Biol. Chem.* **262**, 8314–7.

Ishiwata, S., K. Kinosita, Jr., H. Yoshimura and A. Ikegami (1988) Optical anisotropy decay studies of the dynamic structure of myosin filaments. *Adv. Exp. Med. Biol.* **226**, 267–76.

Ishiwata, S., M. Miki, I. Shin, T. Funatsu, K. Yasuda and C.G. dos Remedios (1996) Distance between myosin heads in rigor complex measured by fluorescence resonance energy transfer. *Biophys. J.* **70**, A14.

Ishiwata, S., M. Miki, I. Shin, T. Funatsu, K. Yasuda and C.G. dos Remedios (1997) Inter-head distances in myosin attached to F-actin estimated by fluorescence energy transfer spectroscopy. *Biophys. J.* **73**, No. 2, in press.

Johnson, I.D. (1996) Introduction to fluorescence techniques. In *Handbook of fluorescent probes and research chemicals*, (ed. R.P. Haugland), pp. 1–6. Molecular Probes Inc., Eugene, Oregon.

Kasprzak, A.A., R. Takashi and M.F. Morales (1988) Orientation of the actin monomer in the F-actin filament: radial coordinate of glutamine-41 and effect of myosin subfragment-1 binding on the monomer orientation. *Biochemistry* **27**, 4512–22.

Kato, H. (1996) *Imaging of mechano-chemical coupling in the contractile system of muscle by using pH-sensitive fluorescent dyes.* Master thesis. Department of Physics, School of Science and Engineering. Tokyo, Waseda University.

Kato, H., M. Kawase, T. Nishizaka, K. Someya, G. Marriott, K. Kinosita, Jr. *et al.* (1995) Imaging of mechanochemical coupling of muscle contractile system by pH-sensitive fluorescent dyes. *J. Musc. Res. Cell Motil.* **16**, 337–8 (Abstract).

Kato, H., T. Nishizaka, T. Iga, K. Kinosita, Jr. and S. Ishiwata (1997) Thermal activation of actomyosin motors with temperature-pulse microscopy. *Biophys. J.* **72**, A183 (Abstract).

Kinosita, K. Jr., S. Kawato and A. Ikegami (1977) A theory of fluorescence polarization decay in membranes. *Biophys. J.* **20**, 289–305.

Kinosita, K. Jr., S. Ishiwata, H. Yoshimura, H. Asai and A. Ikegami (1984) Submicrosecond and microsecond rotational motions of myosin head in solution and in myosin synthetic filaments as revealed by time-resolved optical anisotropy decay measurements. *Biochemistry* **23**, 5963–75.

Kinosita, K. Jr., H. Itoh, S. Ishiwata, K. Hirano, T. Nishizaka and T. Hayakawa (1991) Dual-view microscopy with a single camera: real-time imaging of molecular orientations and calcium. *J. Cell Biol.* **115**, 67–73.

Kishino, A. and T. Yanagida (1988) Force measurements by micromanipulation of a single actin filament by glass needles. *Nature* **334**, 74–6.

Kouyama, T. and K. Mihashi (1981) Fluorimetry study of N-(1-pyrenyl) iodoacetamide-labeled F-actin. Local structural change of actin protomer both on polymerization and on binding of heavy meromyosin. *Eur. J. Biochem.* **114**, 33–8.

Kron, S.J. and J.A. Spudich (1986) Fluorescent actin filaments move on myosin fixed to glass surfaces. *Proc. Natl. Acad. Sci. (USA)* **83**, 6272–6.

Ling, N., C. Shrimpton, J. Sleep, J. Kendrick-Jones and M. Irving (1996) Fluorescent probes of the orientation of myosin regulatory light chains in relaxed, rigor and contracting muscle. *Biophys. J.* **70**, 1836–46.

Liou, Y.-M. and F. Fuchs (1992) Pyrene-labeled cardiac troponin C. Effect of Ca^{2+} on monomer and excimer fluorescence in solution and in myofibrils. *Biophys. J.* **61**, 892–901.

Lorenz, M., D. Popp and K.C. Holmes (1993) Refinement of the F-actin structure against X-ray fiber diffraction data by the use of a direct mutation algorithm. *J. Mol. Biol.* **234**. 826–36.

Lowey, S., G.S. Waller and K.M. Trybus (1993) Skeletal muscle myosin light chains are essential for physiological speeds of shortening. *Nature* **365**, 454–6.

Ludescher, R.D. and D.D. Thomas (1988) Microsecond rotational dynamics of phosphorescent-labeled muscle cross-bridges. *Biochemistry* **27**, 3343–51.

Ludescher, R.D., T.M. Eads and D.D. Thomas (1987) Triplet anisotropy studies of restricted rotational motion in myosin monomers and filaments. In *Optical studies of muscle cross-bridges*, (ed. R.J. Baskin and Y. Yeh), pp. 33–65. CRC Press, Boca Raton, FL.

Mendelson, R. and M.G.A. Wilson (1987) Fluorescence polarization studies of myosin and muscle cross-bridges. In *Optical studies of muscle cross-bridges*. (ed. R.J. Baskin and Y. Yeh) pp. 67–98. CRC Press, Boca Raton, FL.

Miki, M. (1987) The recovery of the polymerization of Lys-61-labeled actin by the addition of phalloidin. *Eur. J. Biochem.* **164**, 229–35.

Miki, M. (1990) Resonance energy transfer between points in a reconstituted skeletal muscle thin filament. *Eur. J. Biochem.* **187**, 155–62.

Miki, M. and T. Iio (1993) Kinetics of structural changes of reconstituted skeletal muscle thin filaments observed by fluorescence resonance energy transfer. *J. Biol. Chem.* **268**, 7101–6.

Miki, M. and T. Kouyama (1994) Domain motion in actin observed by fluorescence resonance energy transfer. *Biochemistry* **33**, 10171–7.

Miki, M., S.I. O'Donoghue and C.G. dos Remedios (1992) Structure of actin observed by fluorescence resonance energy transfer spectroscopy. *J. Musc. Res. Cell Motil.* **13**, 132–45.

Miyanishi, T. and J. Borejdo (1989) Differential behavior of two cysteine residues on myosin head in muscle fibers. *Biochemistry* **28**, 1287–94.

Miyata, H., H. Hakozaki, H. Yoshikawa, N. Suzuki, K. Kinosita Jr., T. Nishizaka *et al.* (1994) Stepwise motion of an actin filament over a small number of heavy meromyosin molecules is revealed in an *in vitro* motility assay. *J. Biochem.* **115**, 644–7.

Miyata, H., H. Yoshikawa, H. Hakozaki, N. Suzuki, T. Furuno, A. Ikegami, K. Kinosita, Jr., T. Nishizaka and S. Ishiwata (1995). Mechanical measurements of single actomyosin motor force. *Biophys. J.* **68**, 286s–90s.

Moens, P.D.J., D.J. Yee and C.G. dos Remedios (1994) Determination of the radial coordinate of Cys-374 in F-actin using fluorescence resonance energy transfer spectroscopy: effect of phalloidin on polymer assembly. *Biochemistry* **33**, 13 102–8.

Moss, R. (1992) Ca^{2+} regulation of mechanical properties of striated muscle. Mechanistic studies using extraction and replacement of regulatory proteins. *Circ. Res.* **70**, 865–84.

Nishizaka, T. (1996) *Microscopic analysis of function and mechanical properties of single actomyosin motors with optical tweezers.* Doctoral thesis, p. 160. Department of Physics, School of Science and Engineering. Waseda University, Tokyo.

Nishizaka, T., T. Yagi, Y. Tanaka and S. Ishiwata (1993) Right-handed rotation of an actin filament in an *in vitro* motile system. *Nature* **361**, 269–71.

Phan, B.C., P. Cheung, W.F. Stafford and E. Reisler (1996) Complexes of myosin subfragment-1 with adenosine diphosphate and phosphate analogs: probes of active site and protein conformation. *Biophys. J.* **59**, 341–9.

Prochniewicz-Nakayama, E., T. Yanagida and F. Oosawa (1983) Studies on conformation of F-actin in muscle fibers in the relaxed states, rigor, and during contraction using fluorescent phalloidin. *J. Cell Biol.* **97**, 1663–7.

Rayment, I., W.R. Rypniewski, K. Schmidt-Base, R. Smith, D.R. Tomchick, M.M. Benning *et al.* (1993*a*) Three-dimensional structure of myosin subfragment-1: a molecular motor. *Science* **261**, 50–8.

Rayment, I., H.M. Holden, M. Whittaker, C.B. Yohn, M. Lorenz, K.C. Holmes *et al.* (1993*b*) Structure of the actin-myosin complex and its implications for muscle contraction. *Science* **261**, 58–65.

Reisler, E. (1982) Sulfhydryl modification and labeling of myosin. *Meth. Enzymol.* **85B**, 84–93.

Root, D.D. and E. Reisler (1992) Cooperativity of thiol-modified myosin filaments. ATPase and motility assays of myosin function. *Biophys. J.* **63**, 730–40.

Saraswat, L.D. and S. Lowey (1991) Engineered cysteine mutants of myosin light chain 2. Fluorescent analogues for structural studies. *J. Biol. Chem.* **266**, 19 777–85.

Sasaki, Y.C., K. Yasuda, Y. Suzuki, T. Ishibashi, I. Satoh, Y. Fujiki *et al.* (1997) Two-dimensional arrangement of a functional protein by cysteine-gold substrate interaction: Enzyme activity and characterization of a protein monolayer on a gold substrate. *Biophys. J.* **72**, 1842–8.

Sase, I. (1996) *Real time imaging of single fluorophores and single small cells with high-sensitive epifluorescence microscope.* Doctoral thesis, p. 156. Department of Physics, Faculty of Science and Technology. Keio University, Yokohama.

Sase, I., H. Miyata, J.E.T. Corrie, J. Craik and K. Kinosita, Jr. (1995) Real time imaging of single fluorophores on moving actin with an epifluorescence microscope. *Biophys. J.* **69**, 323–8.

Sase, I., H. Miyata, S. Ishiwata and K. Kinosita, Jr. (1997) Axial rotation of sliding actin filaments revealed by single-fluorophore imaging. *Proc. Natl. Acad. Sci. (USA)* **94**, 5646–50.

Schröder, R.R., D.J. Manstein, W. Jahn, H. Holden, I. Rayment, K.C. Holmes *et al.* (1993) Three-dimensional atomic model of F-actin decorated with *Dictyostelium* myosin S1. *Nature* **364**, 171–4.

Seidel, J.C. (1969) Similar effects on enzymic activity due to chemical modification of either of two sulfhydryl groups of myosin. *Biochim. Biophys. Acta* **180**, 216–9.

Sekine, T. and W.W. Kielley (1964) Enzymic properties of N-ethylmaleimide modified myosin. *Biochim. Biophys. Acta* **81**, 336–45.

Spudich, J.A. (1994) How molecular motors work. *Nature* **372**, 515–8.

Sutoh, K. (1981) Location of SH1 and SH2 along a heavy chain of myosin subfragment 1. *Biochemistry* **20**, 3281–5.

Suzuki, K., Y. Tanaka, Y. Nakajima, K. Hirano, H. Itoh, H. Miyata *et al.* (1995) Spatiotemporal relationships among early events of fertilization in sea urchin eggs revealed by multiview microscopy. *Biophys. J.* **68**, 739–48.

Szczesna, D. and S.S. Lehrer (1993) The binding of fluorescent phallotoxins to actin in myofibrils. *J. Musc. Res. Cell Motil.* **14**, 594–7.

Tait, J.F. and C. Frieden (1982) Polymerization-induced changes in the fluorescence of actin labeled with iodoacetamidotetramethylrhodamine. *Arch. Biochem. Biophys.* **216**, 133–41.

Tanaka, Y., A. Ishijima and S. Ishiwata (1992) Super helix formation of actin filaments in an *in vitro* motile system. *Biochim. Biophys. Acta* **1159**, 94–8.

Tanner, J.W., D.D. Thomas and Y.E. Goldman (1992) Transients in orientation of a fluorescent cross-bridge probe following photolysis of caged nucleotides in skeletal muscle fibers. *J. Mol. Biol.* **223**, 185–203.

Thomas, D.D. (1987) Spectroscopic probes of muscle crossbridge rotation. *Ann. Rev. Physiol.* **49**, 691–709.

Thomas, D.D., S. Ramachandran, O. Roopnarine, D.W. Hayden and E.M. Ostap (1995) The mechanism of force generation in myosin: a disorder-to-order transition, coupled to internal structural changes. *Biophys. J.* **68**, 135s–41s.

Trayer, H.R. and I.P. Trayer (1988) Fluorescence resonance energy transfer within the complex formed by actin and myosin subfragment 1. Comparison between weakly and strongly attached states. *Biochemistry* **27**, 5718–27.

Wieland, T. and T. Faulstich (1978) Amatoxins, phallotoxins, phallolysin, and antamanide: the biologically active components of poisonous Amanita mushrooms. *CRC Crit. Rev. Biochem.* **5**, 185–260.

Wulf, E., A. Deboben, F.A. Bautz, H. Faulstich and T. Wieland (1979) Fluorescent phallotoxin, a tool for the visualization of cellular actin. *Proc. Natl. Acad. Sci. (USA)* **76**, 4498–502.

Yamamoto, T., S. Nakayama, N. Kobayashi, E. Munekata and T. Ando (1994) Determination of electrostatic potential around specific locations on the surface of actin by diffusion-enhanced fluorescence resonance energy transfer. *J. Mol. Biol.* **241**, 714–31.

Yanagida, T. (1981) Angles of nucleotides bound to cross-bridges in glycerinated muscle fiber at various concentrations of e-ATP, e-ADP and e-AMP.PNP detected by polarized fluorescence. *J. Mol. Biol.* **146**, 539–60.

Yanagida, T., Y. Harada and A. Ishijima (1993) Nano-manipulation of actomyosin molecular motors *in vitro*: a new working principle. *TIBS* **18**, 319–24.

Yanagida, T., M. Nakase, K. Nishiyama and F. Oosawa (1984) Direct observation of motion of single F-actin filaments in the presence of myosin. *Nature* **307**, 58–60.

Yasuda, K., H. Fujita, Y. Fujiki and S. Ishiwata (1994) Length regulation of thin filaments without nebulin. *Proc. Jap. Acad.* **70**(Ser. B), 151–6.

Zhao, X., T. Kobayashi, H. Malak, I. Gryczynski, J. Lakowicz, R. Wade *et al.* (1995) Calcium-induced troponin flexibility revealed by distance distribution measurements between engineered sites. *J. Biol. Chem.* **270**, 15507–14.

Zot, A.S. and J.D. Potter (1987) The effect of $[Mg^{2+}]$ on the Ca^{2+} dependence of ATPase and tension development of fast skeletal muscle. The role of the Ca^{2+}-specific sites of troponin C. *J. Biol. Chem.* **262**, 1966–9.

特集■生命にとって時間とは何か

心筋の収縮と超分子の自己組織化

化学振動から生物リズムへ2

石渡信一

われわれの期待は，横紋構造をもつ心筋収縮系は単なるポンプではなく，ペースメーカーによる心拍支配に自在に適応しうるような自己調節機能を保持しているのではないかというものである．この点は，心拍機能の中ではこれまでほとんど注目されてこなかった．ここでは，1分子では確率的にしか働かない分子モーターが組織化されることによって，自励振動*というまったく新規の高次機能を発現するようになる分子協調現象を取り上げよう．

心臓の拍動と筋収縮系

われわれの心臓は1秒間におよそ1回の割合で休みなく拍動する．心筋収縮系はペースメーカーの生み出す電気信号に応じてリズミカルに収縮・弛緩を繰り返す．心臓の拍動においては，ペースメーカーが支配者であり，筋収縮系はこれに従属するだけの働き手のようにみえる．確かに，筋収縮系の機能は信号に応じて力を発生し収縮するか，弛緩して引きのばされるか，基本的にはこの二つだといってよい．しかし，心筋収縮系は単なる受け身の“ポンプ”でしかないのだろうか．

ところで心拍数は，休んでいるか動いているかなどの個体の状態の違いによって，数倍も変動する．また，一見周期的とみえる休息時の拍動も，揺らいでいる．心拍は一定不変のものではなく，自発的に揺らぎ，かつ環境の変化に適応して変動する．

心拍機能にみられる柔軟な適応性は，ペースメーカーだけでなくペースメーカーから心筋細胞(膜系)を経て収縮系に至る階層構造の中に，さまざまな形で存在するであろう．われわれはその中で，最終的に拍動を担っている筋収縮系の収縮特性に注目したい．ここで筋収縮系というのは，アクトミオシン分子モーター[1][2](ATP(アデノシン三リン酸)加水分解酵素であるミオシン分子と，それと相互作用して滑り運動するアクチン分子との複合体)が集合してでき上がった超分子システムのことである．

収縮・弛緩の制御と自励振動現象

生体中では，骨格筋，心筋をとわず，筋収縮系のon(収縮)/off(弛緩)は遊離のカルシウムイオン(Ca^{2+})濃度によって制御されている．すなわち，図1に示すように，Ca^{2+}濃度が1 μM以上になると収縮し，それ以下では弛緩する．弛緩状態で筋細胞内の内部膜系に蓄えられているCa^{2+}は，細胞膜が電気的な刺激を受けると，一連の信号伝達機構を介して放出される．放出されたCa^{2+}はアクチンフィラメント上の制御タンパク質トロポニンに結合し，アクトミオシン分子モーターが働き始める．逆に刺激が止むと，Ca^{2+}は再び内部膜に取り込まれ，遊離のCa^{2+}濃度が1 μM以下になるので，Ca^{2+}はトロポニンから解離し，分子モーター機能は再び抑制される．

このように心臓の拍動は，筋収縮系のレベルでみると，遊離Ca^{2+}の濃度の増減による収縮・弛緩の繰り返しという点で，化学振動とみることができる．このみかたは正しいが，ことはそれほど単純ではない．生体中の心筋細胞では，遊離のCa^{2+}濃度は骨格筋と異なってそれほど高くならず，収縮と弛緩の中間程度にしかならないといわれている．そして1 μM程度のCa^{2+}濃度では，心拍数かそれよりもいくぶん遅い振動数で自励振動する特性を，心筋収縮系はもっているのである[3][4][5](図1参照)．

* 一定の力によって励起される自発的振動．

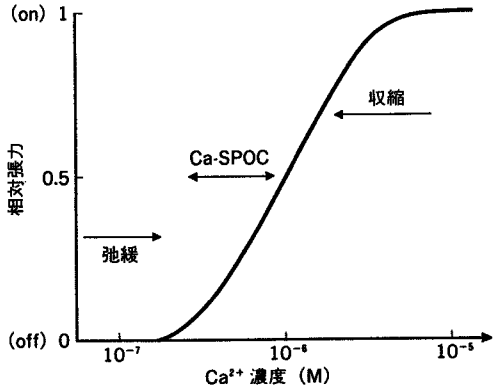

図1　心筋収縮系の状態の Ca^{2+} 濃度依存性. 筋収縮系は，遊離の Ca^{2+} 濃度が1 μM より低いと弛緩し，高いと収縮する．この点は，心筋と骨格筋に共通する性質である．心筋収縮系の特徴は，中間の Ca^{2+} 濃度で自励振動することである(Ca-SPOC)．すなわち，筋節の長さと発生張力が自発的に振動する．われわれはこれを，SPOC(SPontaneous Oscillatory Contraction(自発的振動収縮))と呼ぶ．SPOCは，細胞膜を取り除いた除膜筋モデル系でみられる．生体中でCa-SPOCが機能しているかどうかは，はっきりしない．

イオン環境が変動しなくとも，膜系を取り除いた筋収縮系それ自体に，リズムを生み出す自励振動能が備わっている[6]．こう結論できる根拠は，太さが1 μm と非常に細く，したがってATPやADP(アデノシン二リン酸)，それに Ca^{2+} などの化学物質の濃度変動がないと考えられる筋原線維において，自発的振動収縮(SPOC)がみられることにある(図2参照)．われわれはSPOCを溶液条件の違いによって二つに分類している．一つは，上で述べた，Ca^{2+} 濃度が1 μM 程度で発生するCa-SPOCである(図1)．もう一つは，ATPにADPとPi(無機リン酸)が共存し，Ca^{2+} を除去した条件下で生じるADP-SPOCである[6]．

図2にADP-SPOCの振動波形を示す．この実験では新鮮な溶液を流し続けているので，筋原線維内のイオン濃度が変動することはない．つまり，SPOCは化学振動ではないのである．しかも，図2bにみられるように，負荷の加わり方に応じて振動パターンが変化する[7][8]．SPOCは力学的な外部環境の変化に適応しうるのである．このことは，筋収縮系の自励振動特性が，心拍機能に一役買っていることを期待させる．超分子システムが示すこのような自励振動の例として，鞭毛運動を担う微小管・ダイニン分子モーター系における高速(数百Hz)微小振動を挙げておこう[9]．

分子モーターだけで自励振動する

最近心筋収縮系において，アクチンフィラメントの全置換が可能になった[10]．膜系を除去した心筋線維に，ゲルゾリンと呼ばれるアクチンフィラメント切断タンパク質を作用させると，フィラメントの断片を残してすべてのアクチンが取り除かれる．こうして得られたアクチン除去収縮系は収縮能を完全に失っている．そこで，精製したアクチン分子を適当な条件下で添加すると，残存する断片を重合核としてアクチンフィラメントは重合成長し，元の長さ以上に再構築される．しかも，この再構築筋は元のもの以上に大きな力を発生する．しかし，Ca^{2+} 感受性は失われている．これに制御タンパク質を添加すると，Ca^{2+} による収縮・弛緩の制御機能も完全に回復する．

そこでわれわれは，純粋なアクチンフィラメントによって再構築された心筋収縮系を用いて，SPOC現象がみられるかどうかを検討した．制御タンパク質を含まない再構築筋には Ca^{2+} 感受性がないので，Ca-SPOCやADP-SPOCの条件ではSPOCは発生しない．そこで，収縮・弛緩の中間状態を安定に実現するための別の溶液条件を探索し，ATP, ADP, Pi共存下に，BDM(2, 3-butanedione monoxime)という筋弛緩剤を添加して張力レベルを低下させたところ，自励振動がみいだされた．こうして，SPOCには制御タンパク質は必ずしも必要でないことがわかった(藤田・石渡: 未発表データ)．つまり，自励振動特性は，あくまでもアクトミオシン分子モーターそれ自体に備わった特性なのである(最近，この考えに沿ったSPOCの理論が発表された[11])．

収縮振動はタンパク質分子間協調によって生じる

筋収縮系の自励振動はアクトミオシン分子モーターのどのような機能特性によって生じるのだろ

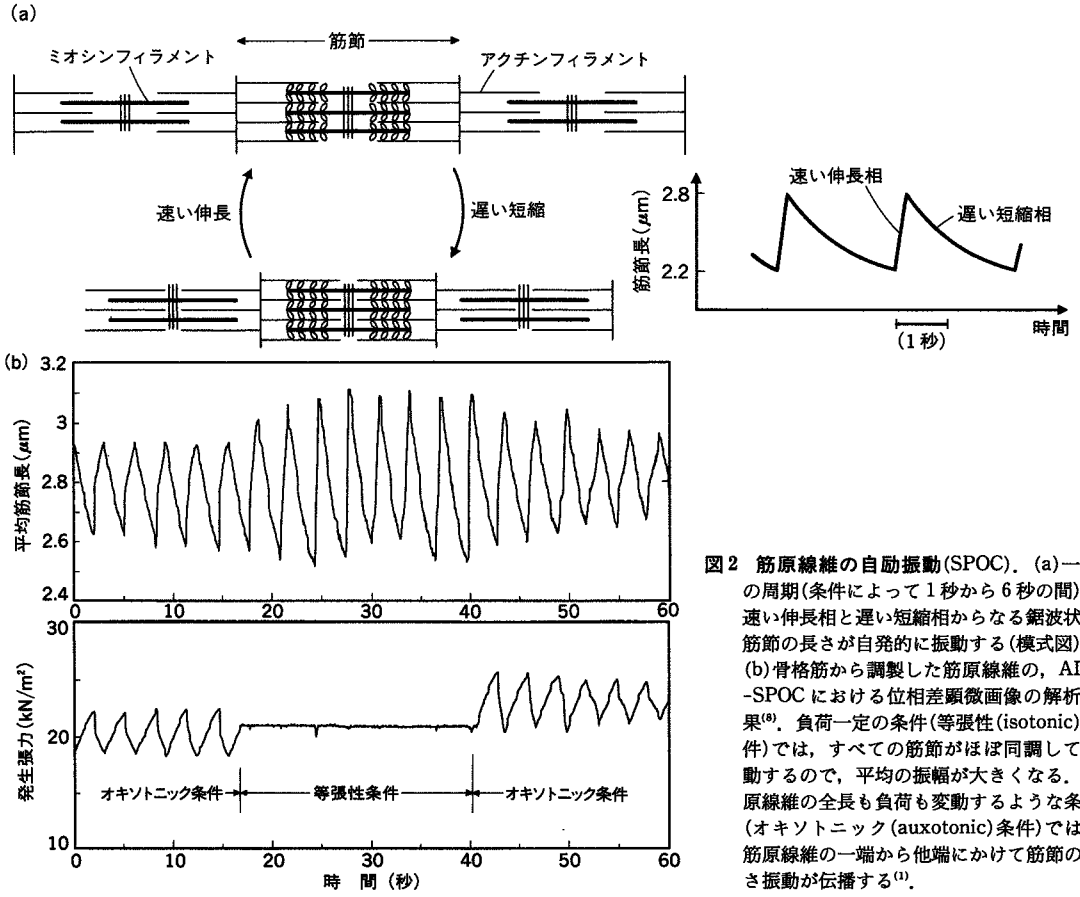

図2 筋原線維の自励振動(SPOC). (a)一定の周期(条件によって1秒から6秒の間)で,速い伸長相と遅い短縮相からなる鋸波状に筋節の長さが自発的に振動する(模式図). (b)骨格筋から調製した筋原線維の,ADP-SPOCにおける位相差顕微画像の解析結果[8]. 負荷一定の条件(等張性(isotonic)条件)では,すべての筋節がほぼ同調して振動するので,平均の振幅が大きくなる. 筋原線維の全長も負荷も変動するような条件(オキソトニック(auxotonic)条件)では,筋原線維の一端から他端にかけて筋節の長さ振動が伝播する[1].

うか. 最近光学顕微鏡下で,1個の分子モーターの運動機能(滑り運動変位,滑り力など)を空間分解能1nm(ナノメートル)以下,力に換算して1pN(ピコニュートン)以下,時間分解能1ms以下で画像解析できるようになった[1][2]. そこで明らかになったことは,分子モーターは1個では確率的に働くナノマシンである,ということである[1][2].

エネルギー源であるATP分子は確率的にしか結合しないし,結合したとしても,ある決まった一定の時間の後に力を発生するというものでもない. 化学・力学エネルギー変換機構における一連の化学反応ステップは,確率的に生じる. その積み重ねの後にパルス的に数pNの力が発生するが,いつ力を発生するかについては,平均的な時間を予測することしかできない. 1個のミオシン分子とアクチンフィラメントとの硬直結合(ATP非存在下での結合で,アクトミオシン結合の中で最も安定だと考えられる)がいつ解離するかについても,平均の寿命を予測することしかできない[12]. 1組のアクトミオシン分子モーターの示す,運動・結合特性の中には,拍動という生体リズムを生み出すような協調性はなにも存在しないようにみえる.

ところが多数の分子モーターが集合した超分子システムとなると,自発的な収縮振動を生み出すことができる. アクトミオシン分子モーター系におけるSPOC現象がそれであり,微小管ダイニン分子モーター系における高速微小振動現象がそれである. 化学物質の濃度が変動しない中で,どのような仕組みでタンパク質集合体は自励振動できるのか. そこには,多数の分子が集合したことによって分子間に生じる協調メカニズムが存在するに違いない.

このアイデアをまとめると,図3のようになる. つまり,心筋を構成するアクトミオシン分子モーターは,エネルギー源であるATPを,ADPと

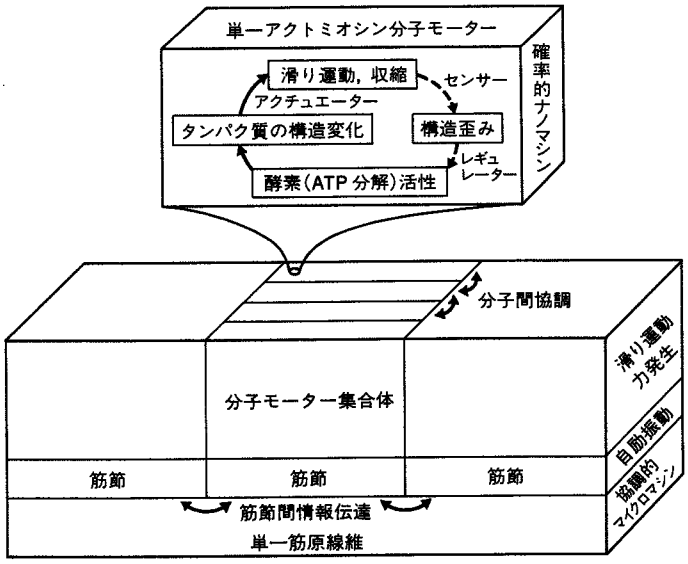

図3 分子モーター機能の分子間協調性に関するメカノケミカル・カップリング(仮説). 筋収縮系の各階層と階層間で化学過程(ATP 分解)と力学過程(力発生)を介した分子間協調メカニズムが存在すれば，自発的な振動が生み出される．

Pi に加水分解する酵素であり，化学・力学エネルギー変換の分子メカニズムによって力を発生し，収縮運動する．ところがこれに伴って，自分自身だけでなく他の分子モーターも(受動的かつ協同的に)構造歪み(変化)を受ける．そのことによって分子モーターの酵素活性が変調を受けるのではないか．このようなフィードバック特性こそ，生体分子モーターが化学・力学酵素と呼ばれるゆえんである，とわれわれは考える．分子モーターはそれ自体，アクチュエーターであるだけでなくセンサーでもあり，レギュレーターでもあるのである．それゆえ，アクトミオシン分子モーターは，化学過程と力学過程を分子モーター間でやり取りしつつ，集団として振動する．このようなスキームが浮かび上がる．

心臓組織はペースメーカー細胞や心筋細胞の集合体であり，心筋細胞は筋原線維の集合体であり，筋原線維は筋節が直列に繋がった構造体であり，そして筋節はアクトミオシン分子モーターの集合体である．心筋細胞という超分子システムの中に，このような階層構造が幾重にも存在する．そして，ここで紹介した SPOC 現象はアクトミオシン分子モーター集合体内での分子間協調の結果である可能性が高い．そうであってみれば，心臓の拍動は，分子モーター系のもつ分子間協調特性によって支えられているともいえよう．

最後の結論は，今後の実験的な検証を必要としている．心臓の拍動という生体リズムにおいて，分子モーター系の自励振動特性が重要な役割を演じていることを，何とかして実験的に証明したいものである．そして，それを通してタンパク質とその集合体が，生体にとって基本的なリズムを生み出しうる，柔軟かつ多様な機能を備えたシステムであることを明らかにしたいと考える．

(Shin'ichi ISHIWATA 早稲田大学理工学部)

文 献

(1) 石渡信一編: 生体分子モーターの仕組み，共立出版(1997)
(2) 柳田敏雄・石渡信一編: ナノピコスペースのイメージング——生物分子モーターのメカニズムを見る，吉岡書店(1997)
(3) A. FABIATO & F. FABIATO: J. Gen. Physiol., **72**, 667(1978)
(4) W. A. LINKE et al.: Circ. Res., **73**, 724(1993)
(5) N. FUKUDA et al.: Pflug. Arch., **433**, 1(1996)
(6) S. ISHIWATA & K. YASUDA: Phase Transi., **45**, 105(1993)
(7) K. YASUDA et al.: Biophys. J., **70**, 1823(1996)
(8) 新藤嘉明: 早稲田大学理工学研究科 1996 年度修士論文
(9) S. KAMIMURA & R. KAMIYA: Nature, **340**, 476(1989); J. Cell Biol., **116**, 1443(1992)
(10) H. FUJITA et al.: Biophys. J., **71**, 2307(1996)
(11) F. JULICHER & J. PROST: Phys. Rev. Lett., **78**, 4510(1997)
(12) T. NISHIZAKA et al.: Nature, **377**, 251(1995)

Cell, Vol. 93, 21–24, April 3, 1998, Copyright ©1998 by Cell Press

F_1-ATPase: A Rotary Motor Made of a Single Molecule

Minireview

Kazuhiko Kinosita, Jr.,*† Ryohei Yasuda,*† Hiroyuki Noji,† Shin'ichi Ishiwata,‡† and Masasuke Yoshida§†
*Department of Physics
Faculty of Science and Technology
Keio University
Yokohama 223-8522
Japan
†CREST (Core Research for Evolutional Science and Technology)
"Genetic Programming" Team 13
Teikyo University Biotechnology Research Center 3F
Nogawa, Kawasaki 216-0001
Japan
‡Department of Physics
School of Science and Engineering
Waseda University
Tokyo 169-8555
Japan
§Research Laboratory of Resources Utilization
Tokyo Institute of Technology
Yokohama 226-8503
Japan

The bacterial flagellar motor (DeRosier, 1998) has long been the sole rotary mechanism known in the biological world. While we might call some movements in the body "rotation", the continuous nature of our joints does not allow true rotation, which requires separation of the two parts in order to achieve sliding of one part against the other over all angles. At the level of molecules, however, sliding is commonly encountered, and repeated use of identical subunits often leads to formation of helical structures, including cylinders and rings, which can support rotational motions. A helical actin filament sliding past myosin, for example, has been shown to rotate (Nishizaka et al., 1993), albeit inefficiently (Sase et al., 1997). It is quite possible that rotating molecular machines have simply been overlooked, due to the technical difficulties of detecting molecular rotations. Recently, a new face has joined the class of circularly rotating machines, second to the bacterial flagellar motor. A single molecule of F_1-ATPase, a portion of ATP synthase, is by itself a rotary motor in which a central rotor, made of a γ subunit, rotates over unlimited angles against a surrounding stator cylinder of an $\alpha_3\beta_3$ hexamer (Noji et al., 1997; Figure 1). At a size of ~10 nm, it is the smallest rotary motor ever found.

ATP Synthase

ATP, a major currency of energy, is synthesized by ATP synthase. This enzyme is composed of a membrane-embedded, proton-conducting portion, F_0, and a protruding portion, F_1 (Figure 1). When protons flow through F_0, ATP is synthesized in F_1. The synthase is fully reversible in that hydrolysis of ATP in F_1 drives reverse flow of protons through F_0. Isolated F_1 catalyzes only hydrolysis of ATP, and hence is called the F_1-ATPase.

How is the proton flow through F_0 coupled to the synthesis/hydrolysis of ATP in F_1? Almost 20 years ago Paul Boyer made a radical proposal that the two reactions are mechanically coupled by rotation of a common shaft penetrating F_0 and F_1 (see Boyer, 1997). Part of his reasoning was that F_1 contains three catalytic sites, one on each β, which participate on average equally in ATP synthesis/hydrolysis. The γ subunit, known to be adjacent to β, lacks 3-fold symmetry. For γ to touch the three β's impartially, therefore, it has to rotate. F_0 may also be a rotary motor if likened to the bacterial flagellar motor which is driven by the flow of protons. In this view, the ATP synthase comprises two motors, one ATP-driven and the other proton-driven, with a common shaft of which γ is a major part. Rotation in one direction produces ATP, and ATP hydrolysis causes reverse rotation.

Boyer's model gained support when a crystal structure of F_1 was solved by John Walker and colleagues (Abrahams et al., 1994). Importantly, the three β's carried different nucleotides in the crystal, AMPPNP (an ATP analog), ADP, and none in the clockwise order when viewed from the F_0 side (Figure 1, bottom). If hydrolysis were to proceed, the order in the next step would be ADP, none, and ATP. A face of γ opposing the empty β, for example, would thus turn counter-clockwise. In the crystal, the conformation of empty β was noticeably different from those bearing a nucleotide.

Cross-linking and spectroscopic studies have since given strong evidence favoring rotation of γ (Junge et al., 1997, and references therein): a residue on γ could be cross-linked to different β's only when ATP was hydrolyzed/synthesized, and an optical probe attached to

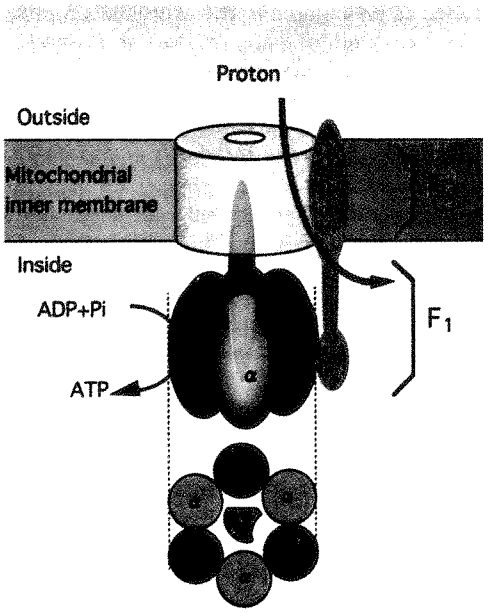

Figure 1. Simplified Structure of ATP Synthase

F_1 consists of $\alpha_3\beta_3\gamma\delta\epsilon$ (δ and ϵ are not shown), and the simplest composition of F_0 (not mitochondrial) is $ab_2c_{9\text{-}12}$. The gray portion indicates a suggested location of δab_2.

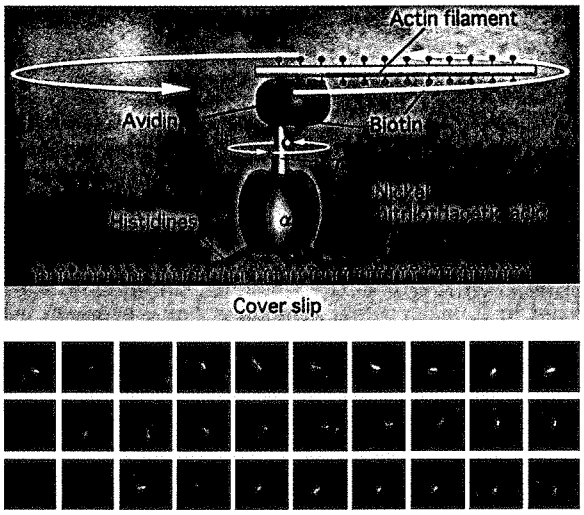

Figure 2. Observation of F_1 Rotation
Video images of a rotating actin filament at intervals of 133 ms are shown at the bottom.

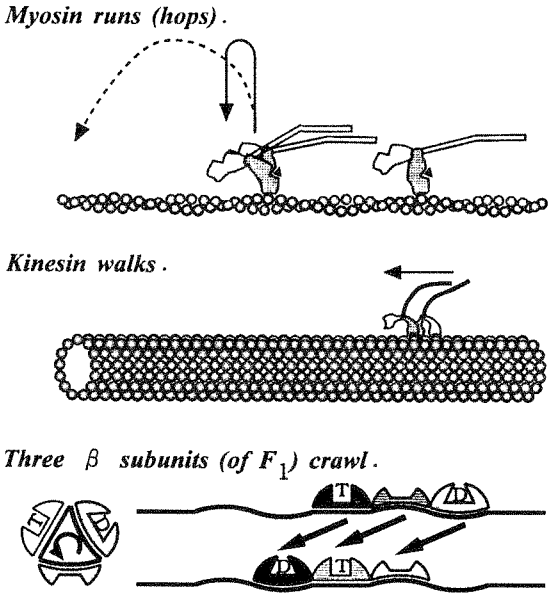

Figure 3. Mode of Operation of Various Molecular Motors
See text for further description. T, ATP; D, ADP. The β subunits of F_1 slide across unrolled γ with the forefoot in front and the hindfoot at back. Note that the different colors of the three β's indicate differences in the bound nucleotide and their nucleotide-dictated conformations (and not their identity). The surfaces of γ that would match the three β's conformations are colored accordingly. The heavy, medium, and light stippling of the β subunits indicate their respective identity. All three β's move simultaneously as shown by the arrows. The scheme here is simplified and the bound nucleotides on the three β's may not change simultaneously. In addition to its bound nucleotide, the conformation of each β should depend on the surface of γ it faces (and indirectly the conformations of the other two β's).

γ underwent large-amplitude rotations. However, the questions of whether γ continues to rotate in one direction, and, if so, its direction, were not addressed in these studies.

Rotation of F_1 Has Been Videotaped

One way of detecting molecular rotation is to attach a large tag that is readily visible under an optical microscope. Noji et al. (1997) attached a fluorescently labeled actin filament to the γ subunit of F_1 (lacking δ and ε subunits) through a streptavidin-biotin link (Figure 2). The β subunits were bound to a glass surface through histidine tags engineered at the N termini. When ATP was added, the filament rotated, invariably counterclockwise as anticipated from the crystal structure. The rotation continued for many minutes at a speed of several revolutions per second. Based on the rate of ATP hydrolysis measured in solution (on the order of 10^2/s), and the assumption of the hydrolysis of three ATP molecules per revolution, the rotational speed might have been predicted to be much higher.

The observed rotational speed was, in fact, quite high when taking into account the hydrodynamic friction against the rotating actin filament. If F_1 were scaled to the size of a person, the person would be standing at the bottom of a large swimming pool rotating an ~500 m rod at several revolutions per second! The F_1 was really working at full throttle. The torque the molecular F_1 produced to overcome the friction amounted to ~40 pN · nm over a broad range of rotational speed (Noji et al., 1997). This torque times $2\pi/3$ (=120°), ~80 pN · nm, is the mechanical work done in one third of a revolution. This work is comparable to the free energy of hydrolysis of one ATP molecule of ~80 pN · nm. If one ATP is consumed per 120° as one may anticipate from the make of this motor, the efficiency of our F_1 is nearly 100%, far superior to a Honda V6. A model by Oosawa and Hayashi (1986) has predicted such a high efficiency.

F_0 Awaits Experimental Proof of Rotation

Relatively little is known about the putative proton-driven motor F_0. In *E. coli*, the subunit composition of F_0 is believed to be ab_2c_{9-12} (the number of c subunits is yet uncertain). Models have been proposed (Junge et al., 1997; Elston et al., 1998) in which a ring of c_{9-12} is attached to γ and the two together constitute the common shaft; ab_2, bound to $\alpha_3\beta_3$ through δ, extends to the c ring and serves as the stator for ring rotation (Figure 1, gray part). Supportive (but not yet conclusive) evidence exists, but the models detract from the elegance in the Boyer's proposal in that the presumably symmetric ring of c's is attached to the asymmetric γ, and δab_2 rests on one side of the symmetric $\alpha_3\beta_3$. Whether the c ring really rotates with γ remains to be seen (videotaped?).

Comparison of Nucleotide-Driven Molecular Motors

In Figure 3, we compare the different ways that molecular motors use their multiple "feet." Myosin is a linear motor that "runs" along actin, in that its two feet (the two globular parts of myosin usually referred to as "heads") are detached from actin for most of the time (Sase et al., 1997). In fact, myosin can run, skipping many actin monomers in a step, if other myosin molecules pull the actin filament while the first one is detached. If only one myosin molecule interacts with actin, it simply hops and will not move relative to actin while detached (except for random diffusion). Kinesin, on the other hand, appears to "walk" along a microtubule, without detaching its two feet simultaneously and probably using

Table 1. Comparison of Nucleotide-Driven Motors

Motor/Rail	Step Size	Max. force	Max. Efficiency	Processivity	Mode
Myosin/Actin	variable	3–5 pN	~20%	none–poor	runs (hops)
Kinesin/Microtubule	8 nm	5 pN	~50%	good	walks
RNA polymerase/DNA	0.34 nm?	14 pN	~20%	excellent	crawls?
$F_1\beta/F_1\gamma$	120°	40 pN · nm	~100%	perfect	crawls
(at the radius of 1 nm)	(2 nm)	(40 pN)			

its two feet in an alternate fashion (Block, 1998, and references therein). F_1 could be unrolled, conceptually, to make it a linear motor (Figure 3). The three β's (and α's) then "crawl" on repeats of unrolled γ in that they never detach from γ (they would slide on γ by pushing and/or pulling actions) and, in contrast to the presumed walking of kinesin, the forefoot always remains in front and the hindfoot at the back. (If unrolled γ is considered to slide along repeats of unrolled $\alpha_3\beta_3$, the γ would "walk" in that it uses the three feet alternately. Figure 3 conforms to the prevailing custom of regarding only the molecule that hydrolyzes a nucleotide as the "motor" and its partner a passive rail.)

The three motors above and another linear motor, RNA polymerase (Gelles and Landick, 1998), are compared in Table 1. The F_1 motor most likely makes 120° steps, because the asymmetric conformations of the three β's, presumably dictating the orientation of γ, are stable in the crystal structure. Short pauses at 120° orientations were not resolved in the video images of Noji et al. (1997) at the resolution of 33 ms; however, measurements at low ATP concentrations could reveal such steps. RNA polymerase is expected to step by 0.34 nm, the distance between base pairs. Kinesin's 8 nm steps have been measured. All these step sizes represent intervals of the structural repeats. Myosin's so-called "unitary step" measured in vitro is a different quantity, in most cases representing movement made while a foot of myosin is attached to actin. It is believed by many to be related to the size of a conformational change that occurs in attached myosin (Goldman, 1998). Genuine steps of running myosin are expected to be multiples of 5.5 nm, the distance between neighboring actin monomers.

The four motors differ in efficiency, the mechanical work divided by the free energy of nucleotide hydrolysis. Because the motors can move without an external load (efficiency 0%), maximal efficiencies are quoted in Table 1. The near 100% efficiency of F_1 accords with the fully reversible nature of this motor; net synthesis of nucleotide triphosphate has not been reported for the other motors. The efficiency of the myosin/actin system quoted here is the work produced in a "unitary step" divided by the free energy of ATP hydrolysis. The myosin efficiency appears low in vitro, the quoted value being on the higher end in the literature (Ishijima et al., 1995), although the efficiency of intact muscle is generally considered to be higher.

Motor Mechanism: Bending versus Binding

Nucleotide-driven motors, including F_1, share common structural motifs near the nucleotide-binding site (Vale, 1996; Noji et al., 1996), suggesting that these motors might employ common principles in some aspects of their mechanisms. As a general principle, we propose that the distinction between bending and binding is important.

Bending (conformational change) of a motor protein alone could produce motion and force relative to its rail, the latter serving merely as a base that securely holds the "sole" of the "foot" of the motor. Myosin is considered to bend its leg forward when attached to actin, producing the "unitary step" (Figure 3, pink myosin on the left; Goldman, 1998). The machinery for bending could all be in myosin, because isolated myosin changes its conformation depending on the bound nucleotide (Gulick and Rayment, 1997). The free-energy changes associated with myosin ATPase, however, indicate that myosin alone would be unable to produce a large amount of work. Moreover, when myosin interacts with actin, as much as half of the free energy of ATP hydrolysis is used for unbinding of myosin from actin. Subsequent rebinding thus liberates energy. If myosin is to work at high efficiency, it should convert the energy gained during rebinding to mechanical output, by cooperation with actin.

A model by A. F. Huxley (1957) is on the other extreme: that binding alone produces motion and force. Myosin fluctuates thermally, and when it fluctuates in the correct direction, it binds to actin resulting in displacement and pull. In binding-alone models, thermal diffusion brings the motor and rail close to the binding configuration, and binding energy is used to stabilize that configuration. Work has to be done in the diffusion process, and can be done as shown below. Diffusive displacement of a particle of diameter d over a distance L takes a time of the order of $(L^2/2) \cdot (3\pi\eta d/k_BT)$, which is ~1 μs for $L = d = 10$ nm at room temperature (thermal energy $k_BT \approx 4$ pN · nm) in water (the viscosity $\eta \approx 10^{-3}$ N · s · m^{-2}). If this displacement is to produce work W (against a load), the time for displacement is multiplied by $\sim\exp(W/k_BT)$, which is 2×10^4 for $W = 10\ k_BT \approx 40$ pN · nm and 5×10^8 for $W = 20\ k_BT \approx 80$ pN · nm. Thus, work below $10\ k_BT$ can be done if the frequency of motor operation is below ~10^2/s. Binding models also require a mechanism that ensures correct choice of a binding site, or proper directional biasing of diffusion. The mechanism is not specified in the Huxley model.

An elegant interplay between bending and binding has been proposed for kinesin and its cousin ncd (Hirose et al., 1996). When one foot of kinesin (or ncd) is bound to a microtubule (rail), the other foot is unbound and undergoes thermal motion. They have shown that the unbound foot of kinesin, which walks toward the plus end of a microtubule, swings toward the plus end presumably by bending of the bound leg (Figure 3, pink

kinesin), and the unbound foot of minus-directed ncd swings toward the minus end. The bending biases the Brownian search of the unbound foot for the next binding site, for the plus direction for kinesin, and minus for ncd. The 8 nm step of kinesin (yet unresolved for ncd), and associated force, are produced when the foot lands on the binding site. A substep(s) and partial force may be produced by the bending, but the major mechanical output of this motor likely comes from the binding of the motor to its rail.

The three-foot F_1 (Figure 3) could in principle operate by binding alone, stepping among the three stable configurations with the correct direction being dictated by the bound nucleotide. ("Binding" for the case of F_1 should be interpreted as a transition to the most stable configuration between β's and γ, and might involve repulsive rather than attractive interactions.) The large mechanical output of $\sim 20\ k_BT$ per step, however, cannot be achieved by a purely diffusive process because it would be too infrequent to account for the observed rate of rotation. Probably, the effective potential between β's and γ is downhill toward the next stable configuration, thus assisting the diffusion against an external load. The work per step would be determined by the total height of the potential slope, which is not dependent on the rotational speed. Bending of the three β's alone is unlikely to rotate γ by 120° because of the obstruction by intervening α subunits.

Of course the distinction between bending and binding becomes less obvious as one inquires more deeply into the mechanism. What we wish to stress here is that molecular motors must work through close cooperation of the two partners. The rail, in particular, is not a simple support, and binds and unbinds its nucleotide-hydrolyzing partner, supplying binding energy and controlling hydrolysis. The two aspects, bending and binding, should be useful in analyzing the mechanism of cooperation. The F_1 motor in which the two partners never detach from each other provides a wonderful opportunity to explore the details of the cooperation experimentally.

Selected Reading

Abrahams, J.P., Leslie, A.G.W., Lutter, R., and Walker, J.E. (1994). Nature *370*, 621–628.

Block, S.M. (1998). Cell *93*, this issue, 5–8.

Boyer, P.D. (1997). Annu. Rev. Biochem. *66*, 717–749.

DeRosier, D.J. (1998). Cell *93*, this issue, 17–20.

Elston, T., Wang, H., and Oster, G. (1998). Nature *391*, 510–513.

Gelles, J., and Landick, R. (1998). Cell *93*, this issue, 13–16.

Goldman, Y.E. (1998). Cell *93*, this issue, 1–4.

Gulick, A.M., and Rayment, I. (1997). Bioessays *19*, 561–569.

Hirose, K., Lockhart, A., Cross, R.A., and Amos, L.A. (1996). Proc. Natl. Acad. Sci. USA *93*, 9539–9544.

Huxley, A.F. (1957). Progr. Biophys. Biophys. Chem. *7*, 255–318.

Ishijima, A., Harada, Y., Kojima, H., Funatsu, T., Higuchi, H., and Yanagida, T. (1995). Biochem. Biophys. Res. Commun. *199*, 1057–1063.

Junge, W., Lill, H., and Engelbrecht, S. (1997). Trends Biochem. Sci. *22*, 420–423.

Nishizaka, T., Yagi, T., Tanaka, Y., and Ishiwata, S. (1993). Nature *361*, 269–271.

Noji, H., Amano, T., and Yoshida, M. (1996). J. Bioenerg. Biomemb. *28*, 451–457.

Noji, H., Yasuda, R., Yoshida, M., and Kinosita, K., Jr. (1997). Nature *386*, 299–302.

Oosawa, F., and Hayashi, S. (1986). Adv. Biophys. *22*, 151–183.

Sase, I., Miyata, H., Ishiwata, S., and Kinosita, K., Jr. (1997). Proc. Natl. Acad. Sci. USA *94*, 5646–5650.

Vale, R.D. (1996). J. Cell Biol. *135*, 291–302.

Estimation of the Hydrophobicity in Microenvironments by Pyrene Fluorescence Measurements: *n*-β-Octylglucoside Micelles

Hiroyasu Itoh,*,† Sayoko Ishido,‡ Masashi Nomura,‡ Tsuyoshi Hayakawa,† and Shigeki Mitaku‡

Tsukuba Research Laboratory, Hamamatsu Photonics K.K., Tokodai 5-9-2, Tsukuba, Ibaraki, 300-26, Japan, and Department of Material Systems Engineering, Faculty of Technology, Tokyo University of Agriculture and Technology, Nakamachi 2-24-16, Koganei, Tokyo 184, Japan

Received: December 11, 1995; In Final Form: February 26, 1996[⊗]

A simple and reliable method was developed for estimating the hydrophobicity of microenvironments, such as the internal region of aqueous detergent micelles, using a fluorescence probe, pyrene. The partition coefficient of pyrene between hydrophobic environments and water was used as a measure of the hydrophobicity. To validate our method, the partitioning of pyrene between organic solvents of various dielectric constants (*n*-hexane, 1-octanol, 1-propanol, ethanol, and methanol) and water was measured. This calibration set was then used to estimate the hydrophobicity of the internal region of *n*-β-octylglucoside micelles. Combining the spectral changes of pyrene as a function of the *n*-β-octylglucoside concentration with a theoretical model of the micellization process, the partitioning of pyrene between the internal region of the micelles and the surrounding water was calculated. The partition coefficient of pyrene was calculated to be about 1.5×10^4 based on an assumed aggregation number of 90 for the aqueous *n*-β-octylglucoside micelles. Our results demonstrate that the interior of the micelle becomes very hydrophobic once the structure forms.

1. Introduction

Hydrophobic interactions are known to play an important role in the structural formation of polymers and amphiphiles in aqueous media. From a biological point of view, this interaction must contribute greatly to the transformation of the constituent molecules of living matter into complex structural entities such as cell membranes and proteins.[1−3] There is some direct and indirect evidence that indicates the importance of this interaction. For example, biological membranes and detergent micelles are formed mainly due to hydrophobic interactions.[4] The internal region of biological membranes can become very nonpolar, with dielectric constants in the region of 2−4.[5] If the hydrophobic interactions of the structural entities can be measured easily, systematic studies of the transformation mechanisms of the constituent molecules should become possible. To date, there are no methods for evaluating easily and systematically the hydrophobicity inside the biological structures. To estimate the hydrophobicity of microenvironments in terms of a thermodynamically well-defined physical parameter, the measurement of the partition coefficient of a probe is useful because it allows us to obtain an index for the hydrophobicity of microenvironments. This is possible because the partition coefficient, which is described by the ratio of the concentration of the probe between the microenvironment and water, can be correlated with the free energy of transfer of the probe molecules. As a result, the hydrophobicity in the microenvironment can be expressed as a physical quantity.

Pyrene has several advantages as a probe molecule. First, as a fluorescence probe, pyrene shows relative changes in the fine structure of the fluorescence spectrum in response to the polarity of the microenvironment.[6−8] Because the fine structure of the pyrene fluorescence spectrum is not affected by factors other than the polarity of the environment, evaluation of the partition coefficient based on the measurements of the fine structure of the pyrene fluorescence is more reliable than those based simply on the fluorescence intensity. The second advantage is that the efficiency of excimer formation, which can be monitored by the fluorescence spectrum of pyrene around 480 nm, can be used to determine if a single molecule of pyrene is in a micelle. The third advantage is that the small size of pyrene leads to only small perturbations of the microenvironment. Finally, the fourth advantage is that pyrene does not contain any hydrophilic parts that would tend to attract it to interfaces. Pyrene can penetrate into the hydrophobic interior of structures. There are no other fluorescence probe molecules that can rival pyrene on these four advantages.

To validate and calibrate the hydrophobicity measurements, detergent micelles may be the simplest model for analyzing the microenvironment formed in aqueous systems. Detergent molecules are amphiphilic and self-assemble in water with their hydrophilic parts exposed to the bulk water and the hydrophobic parts incorporated into the internal region. Because the interior of micelles is composed of hydrocarbon chains, it is expected that the microenvironment is as hydrophobic as the inside of the membranes themselves. The fluorescence measurement of the partition coefficient of a hydrophobic molecular probe in micelles has significance from two aspects. First, it establishes the validity of the method for evaluating quantitatively the hydrophobicity of microenvironments in terms of the partition coefficient measurement. The second important aspect is that this is the first quantitative evaluation of the hydrophobicity of the interior of micelles.

In this work, we have estimated the partition coefficient of the fluorescence probe pyrene for various organic solvents and their mixtures with water. The values were compared to that for the interior of *n*-β-octylglucoside micelles. There are two reasons why *n*-β-octylglucoside was selected from among the various kinds of detergents. First, the thermodynamic param-

* Address correspondence regarding this article to this author. Address reprint requests to Dr. Shigeki Mitaku. Tel: +81-423-88-7048. Fax: +81-423-87-6591.

† Hamamatsu Photonics K.K.

‡ Tokyo University of Agriculture and Technology.

⊗ Abstract published in *Advance ACS Abstracts,* May 1, 1996.

S0022-3654(95)03682-3 CCC: $12.00

eters of the *n*-β-octylglucoside micelle, such as the critical micelle concentration (cmc), the size or the aggregation number, etc., have been well studied by means of surface tensiometry, light scattering, and NMR measurements.[9-12] In our investigations, the parameters are also obtained simultaneously with the partition coefficient. The accuracy of the values strongly impacts the reliability of our method. Second, *n*-β-Octylglucoside is considered to be a mild detergent that is often used for the solubilization of membrane proteins. The physical properties of the detergent are closely related to its activity and its mildness as a solubilizing detergent. The partition coefficient of pyrene in the *n*-β-octylglucoside micelle is about 10^4, which is as large as that of pure organic solvents. From a technical viewpoint, the present work provides a simple and reliable method for evaluating the hydrophobicity of microenvironments.

2. Materials and Methods

2.1. Chemicals. Pyrene was purchased from Wako Pure Chemical (Osaka, Japan), and *n*-β-octylglucoside from Sigma Chemical (St. Louis, MO) as specially prepared reagents. All organic solvents were spectrograde or special grade reagents.

2.2. Spectral Measurements. Absorption and fluorescence spectra were recorded on a Hitachi 557 spectrophotometer and a Hitachi F3000 fluorescence spectrophotometer (Hitachi, Tokyo, Japan), respectively. All experiments were done with the sample temperature controlled at 25 °C by using a refrigerated bath circulator RTE-9 (Neslab Instruments, Newington, NH).

2.3. Measurement of the Partition Coefficient of Pyrene between Bulk Organic Solvents and Water. The partition coefficient of pyrene between water and various organic solvents was measured by two methods, depending on the characteristics of the organic solvents. When the organic solvents were immiscible with water, such as *n*-hexane, a simple, conventional method was used.[13] Pyrene at various concentrations of pyrene (0.04, 0.35, 1.8, and 3.8 mM) to the total volume of the system was mixed in the binary system of *n*-hexane and water (50% v/v) and equilibrated overnight. Each phase was isolated and the fluorescence intensity of the peak around 373 nm was measured. For determining the concentrations of pyrene, a calibration set was prepared by dissolving weighed amounts of pyrene into *n*-hexane and water, respectively. The ratio of the concentration of pyrene in each phase was calculated to determine the partition coefficient.

On the other hand, when the organic solvents are miscible in water, such as alcohols like methanol, the solubility of pyrene in each solvent was used to measure the partition coefficient. The partition coefficients of pyrene were measured for various alcohols (methanol, ethanol, 1-propanol, and 1-octanol) and methanol solutions of water at various concentrations from 0 to 100%. First, pyrene solutions in water, pure alcohols, and aqueous alcohol solutions were prepared with concentrations of pyrene of more than 60 mM. These were equilibrated overnight at room temperature. Then, the solution was centrifuged at 12 000 rpm for 1 h to remove the undissolved pyrene crystals. The supernatant fluid was diluted and used for the absorbance measurements. For determining the concentrations of pyrene, standard solutions were prepared by dissolving weighed amounts of pyrene in each alcohol and in water to estimate the molar extinction coefficient in each solution. The solubility of pyrene in the organic solvents and water was measured from the absorbance around 335 nm. The ratio of the solubility in the organic solvent and water gives the partition coefficient of pyrene, κ.

$$\kappa = C_H/C_W \tag{1}$$

Here, C_H and C_W are the concentration of pyrene in the organic solvent and water, respectively.

2.4. Measurement of Pyrene Fluorescence in *n*-β-Octylglucoside Solutions. Because detergent micelles are completely dispersed in water, it is impossible to separate the signal of the pyrene fluorescence in the aqueous environment from that in the hydrophobic microenvironment of micelles. Therefore, we measured the detergent concentration dependence of the fluorescence spectra in detail to determine the partition coefficient (the method of data analysis is described in the next section). These experiments were done at a constant concentration of pyrene (1.5 μM), while the concentration of the *n*-β-octylglucoside was varied. To keep the concentration of pyrene constant in these experiments, an *n*-β-octylglucoside solution containing pyrene was exchanged with the same amount of the 1.5 μM pyrene solution.

3. Theoretical Analysis

We need to consider the following three aspects in regard to determining the partitioning of fluorescent probes between solvents and micelles: (1) formation of micelles by detergent molecules, (2) penetration of probe molecules into micelles, and (3) fluorescence of pyrene in micelle solutions.

3.1. Formation of Micelles by Detergent Molecules. The micellization process of detergents in water has been studied in terms of the equilibrium thermodynamics of the aggregate and monomer states.[14] As shown in Figure 1, the chemical potential of molecules in both the monomer and aggregate states is expressed by the standard chemical potential μ°, the concentration in the unitary scale X, and the activity coefficient γ.

$$\mu_1 = \mu_1^\circ + k_B T \ln X_1 + k_B T \ln \gamma_1 \tag{2}$$

$$\mu_N = \mu_N^\circ + \frac{k_B T}{N} \ln \frac{X_N}{N} + \frac{k_B T}{N} \ln \gamma_N \tag{3}$$

Here, the subscripts 1 and N represent the monomer and aggregate states, respectively, and N is the aggregation number of the micelles. The constant k_B is Boltzmann's constant and T is temperature. Under actual experimental conditions, the activity coefficient can be set equal to zero because of the very low concentration of the detergents or micelles. When the monomer and aggregate states are in equilibrium (i.e., $\mu_1 = \mu_N$), the concentration of the aggregate state of the detergent can be described as follows.

$$X_N = N\left\{X_1 \exp\left(\frac{\mu_1^\circ - \mu_N^\circ}{k_B T}\right)\right\}^N = N(X_1 \exp \alpha)^N \tag{4}$$

At low concentrations of detergent, most of the molecules in the solution will exist as isolated monomers. However, when the concentration of the detergent increases, X_1 and X_N should approach specific critical values because X_N can never exceed unity. Here, $\exp(-\alpha)$ corresponds to the monomer concentration when a finite value of 1 is assumed for the total concentration of the detergent, X_T ($=X_1 + X_N$). We denote $\exp(-\alpha)$ as X_C (the relationship between this value and the cmc will be addressed in the Discussion).

When the concentration of the detergents is low enough (compared to the mole concentration of water), the relationship between the mole fraction and the mole concentration is as follows.

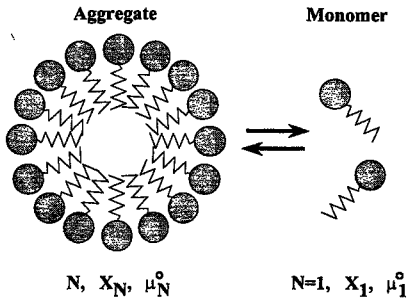

Figure 1. Detergent micelles, completely dispersed in water and in equilibrium with the monomer. All parameters needed to describe the thermodynamic equilibrium state of aqueous micelles are denoted.

$$X_1 = \frac{D_1}{\frac{1000}{M_W} + D_1 + D_N} \cong \frac{D_1}{55.5} \tag{5}$$

$$X_N = \frac{D_N}{\frac{1000}{M_W} + D_1 + D_N} \cong \frac{D_N}{55.5} \tag{6}$$

Here D_1 and D_N are the concentrations of the monomer and aggregated detergent, respectively. The value M_W is the molecular weight of water. Therefore, eq 5 can be rewritten as follows.

$$D_N = 55.5N\left(\frac{D_1}{55.5}\exp\alpha\right)^N \tag{7}$$

The values of D_1 and D_N can be solved numerically for each D_T (the total concentration of the detergent) from eqs 4 or 7 by a conventional method of least squares, the *Newton–Raphson method*,[15] leading to the values of α and N.

3.2. Penetration of Probe Molecules into Micelles. The chemical potential of a reference probe in an environment is one of the most fundamental thermodynamic parameters for characterizing the hydrophobicity of the environment. The chemical potential of a probe in a hydrophobic environment, in water, and in the solid state may be written in terms of the standard chemical potential μ°, the concentration in the unitary scale X, and the activity coefficient γ as follows.

$$\mu_H = \mu_H^\circ + k_B T \ln X_H + k_B T \ln \gamma_H \tag{8}$$

$$\mu_W = \mu_W^\circ + k_B T \ln X_W + k_B T \ln \gamma_W \tag{9}$$

$$\mu_S = \mu_S^\circ \tag{10}$$

Here, the subscripts H, W, and S represent the hydrophobic environment, water, and the solid state, respectively. Under actual experimental conditions, $k_B T \ln \gamma$ can be safely set equal to zero because of the very low concentrations of the probe.

When the organic and water phases are in equilibrium (Figure 2A), the chemical potentials of the probe in each phase become equal ($\mu_H = \mu_W$) for the equilibrium state. From eqs 8 and 9, the mole fraction ratio of the probe molecule can be expressed as follows.

$$\frac{X_H}{X_W} = \exp\left(-\frac{\mu_H^\circ - \mu_W^\circ}{k_B T}\right) \tag{11}$$

The left term of eq 11 is rewritten by using the mole concentration of the probe.

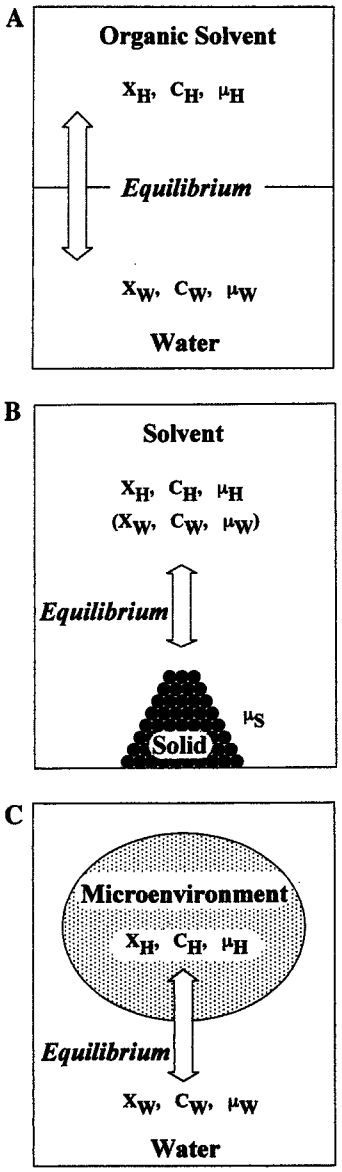

Figure 2. Three different equilibrium schemes for the probe molecule depending on the characteristics of the environment (A) When the organic solvent is immiscible in water, clear phase separation appears under equilibrium conditions. The distribution of the probe molecule depends on the partition coefficient between the organic solvent and water. (B) When the organic solvent is miscible in water, the solubility of the probe may be used to evaluate the partition coefficient. (C) The detergent molecules in aqueous micellar systems are in equilibrium between the aggregate and monomer states.

$$\kappa = \frac{C_H}{C_W} = A\exp\left(-\frac{\mu_H^\circ - \mu_W^\circ}{k_B T}\right) \tag{12}$$

$$A = M_H \rho_W / M_W \rho_H \tag{13}$$

Here, C is the mole concentration of the probe in each phase, where M is the molecular weight of the solvent and ρ is the density of the solvent. The concentration ratio, C_H/C_W, is defined as the partition coefficient κ of the probe between the hydrophobic environment and water. Usually, the concentration of the probe molecules can be directly obtained, for example from the absorbance measurement of the probe, because one of the phases is easily separated from the other.

When the organic solvents are miscible with water (e.g., small polar alcohols), the solubilities of the probe in both the organic solvents and in water are used to calculate the partition coefficient (Figure 2B). Furthermore, the partition coefficient of the aqueous organic solvent (e.g., mixtures of methanol and

water) can be obtained. This system is convenient for systematically varying the characteristics of the hydrophobic environment, such as the dielectric constant. Also, this calibration set can be used as a series of reference solvents to evaluate the hydrophobicity of the microenvironment.

Finally, we will discuss the situation of isolated microenvironments such as the internal region of micelles that are dispersed in the aqueous medium (Figure 2C). Although an analogous method to that described above for determining microproperties can be considered for these systems also, the core cannot physically be separated under actual experimental conditions. Thus, the probe concentration in the core cannot be obtained directly because unknown parameters still exist in the system.

For micelle systems, the hydrophobic fluorophore is incorporated spontaneously into the micellar phase. From the law of conservation of mass, the total concentration of the hydrophobic probe, F_T, can be expressed as follows.

$$F_T = \phi F_m + (1 - \phi)F_W \tag{14}$$

Here, F_m and F_W are the concentrations of the fluorophores contained in the micellar and aqueous phases, respectively. The parameter ϕ represents the volume fraction of the hydrophobic core of the micelles and is defined as follows.

$$\phi = D_N NM/1000\rho_m \tag{15}$$

Here, the molecular weight and the density of the hydrophobic moiety of the micelles is denoted as M (1/mol) and ρ_m (g/mL), respectively. From eqs 14 and 15 we can define the fraction of the hydrophobic probe pyrene, f, between the micellar phase and water as follows.

$$f = \frac{\phi F_m}{(1 - \phi)F_m + \phi F_m} \tag{16}$$

The parameter κ can be calculated as follows.

$$\kappa = F_m/F_W \tag{17}$$

Thus, eq 15 can be written as follows.

$$f = \frac{\kappa\phi}{\kappa\phi + (1 - \phi)} \approx \frac{1}{1 + \frac{1}{\kappa\phi}} \quad (\text{for } f \ll 1) \tag{18}$$

Therefore, if f and ϕ are determined experimentally, we can calculate the value of κ.

3.3. Fluorescence of Pyrene in Micelle Solutions. The pyrene monomer fluorescence spectrum has five major peaks that can be used to monitor the micellization of the detergents (see Figure 4). The intensity ratio of peak 3 (I_3) to peak 1 (I_1) is dependent of the solvent polarity.

$$R = I_3/I_1 \tag{19}$$

The fluorescence spectrum of pyrene in aqueous detergent solution must be the sum of the spectra from the three states of pyrene: (1) pyrene in water, (2) pyrene incorporated in the hydrophobic core of micelles, and (3) pyrene interacting with preaggregated *n*-β-octylglucoside. The former two states contribute the most to the intensity ratio. On the basis of this fact, we can estimate the partition coefficient of pyrene between the hydrophobic core of micelles and water. However, the last state shows small but significant contribution to the intensity ratio, so it may not be neglected in the quantitative analyses. In practice, the intensity ratio below the cmc gradually increases as the detergent concentration is raised. Therefore, we added a small correction term for the preaggregated state to the intensity ratio. This effect was reported by Fischer for *non*ionic detergents, such as *n*-β-octylglucoside below the cmc.[12] Although the behavior of nonionic detergent below the cmc is not clear, we assume a linear relationship between the total concentration of the detergent and the preaggregated state in the system because the fraction of this state is small. Therefore, the base line of the intensity ratio can be written as in the following equation.

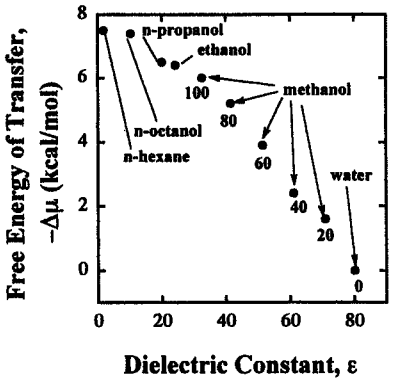

Figure 3. Free energy of transfer for the solvents tested. The values were calculated by using eqs 12 and 13. All the parameters for the calculations are listed in Table 1.

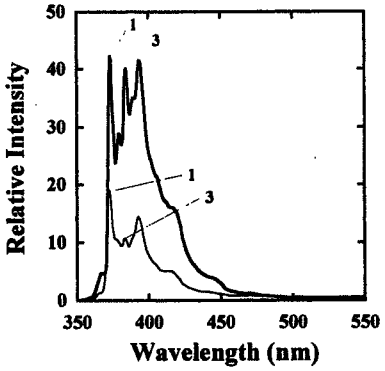

Figure 4. Fluorescence spectra of pyrene (pyrene concentration 1.5 μM) in *n*-β-octylglucoside solutions at 25 °C. The concentration of *n*-β-octylglucoside was 6 mM (thin line) and 35 mM (thick line).

$$R_{min} = R_0 + R_1 D_1 \tag{20}$$

Here, R_0 is the intensity ratio of pyrene in water (i.e., $f = 0$) and R_1 is a coefficient that denotes the contribution to the fluorescence intensity ratio due to the interaction of pyrene with the preaggregated state of the detergent. The intensity ratio of pyrene outside the micelle core is represented by R_{min}. Using this equation for the base line, the intensity ratio above the cmc can be expressed by using f as follows.

$$R = R_{min} + (R_{max} - R_{min})f \tag{21}$$

Here, R_{max} is the intensity ratio, based on the condition that X_T is equal to 1. Combining eqs 18 and 21, we obtain an equation for the equilibrium thermodynamics of detergent micellization based on parameters that can be measured experimentally.

$$R = R_{min} + (R_{max} - R_{min})\frac{1}{1 + \frac{1}{\kappa\phi}} \tag{22}$$

To evaluate the value of κ, all the parameters in eqs 15, 20, and 22 have to be determined in a consistent manner.

TABLE 1: Partition Coefficients of Pyrene between Organic Solvents and Water Measured by Different Methods Depending on the Miscibility with Water[a]

solvent	ρ_m (g/mL)	M (g/mol)	ϵ	solubility (μM)	partition coeff, κ	free energy of transfer, $\Delta\mu$ (kcal/mol)
water	1.0	18	80.4	2.1		
methanol						
20 % (v/v)[b]	0.959	21	71.0	25	12	−1.6
40%	0.918	24	61.2	82	38	−2.4
60%	0.876	26	51.5	860	400	−3.9
80%	0.835	29	46.5	6500	3000	−5.2
100%	0.794	32	32.4	19000	9800	−6.0
ethanol	0.793	46	24.6	30000	13000	−6.4
1-propanol	0.802	60	20.3	26000	12000	−6.5
1-octanol	0.820	130	10.3	59000	26000	−7.4
n-hexane	0.655	86	1.89		40000	−7.5

[a] ρ, density of the solvent; M, molecular weight; and ϵ, dielectric constant. [b] The volume fraction (v/v) denotes the binary system of an organic solvent and water.

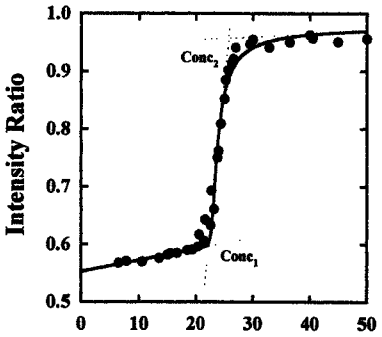

Figure 5. Intensity ratio plotted as a function of the concentration of n-β-octylglucoside. The line through the data points was calculated by the method of least squares assuming an aggregation number of 90. All the parameters used for the calculations are summarized in Table 2.

3. Results

The partition coefficients of pyrene between organic solvents of various dielectric constants and water were measured by one of the two methods described in section 2.3, depending on the miscibility with water (Table 1). The dielectric constants adopted for the organic solvents used here were taken from the literature.[16] The partition coefficient is directly related to the free energy for the transfer from water to the organic solvents as expressed by eq 11. The free energies obtained for transfer of pyrene from water to the organic solvents, assuming that the activity of the medium is unity, are also listed in Table 1. Figure 3 shows the free energy of transfer for each organic solvent as a function of its dielectric constant. The free energy of transfer decreased systematically as the dielectric constant of the solvents was increased.

The partition coefficient of pyrene between the hydrophobic core of the n-β-octylglucoside micelles and water was estimated based on the analysis of the spectral change of the pyrene fluorescence as a function of the n-β-octylglucoside concentration. It is worth noting that excimer formation of pyrene can be monitored by the fluorescence intensity around 480 nm and that no excimer formation appeared under the experimental conditions used (data not shown). Figure 4 shows the fluorescence spectra of pyrene at two different concentrations of n-β-octylglucoside (pyrene concentration is 1.5 μM). The ratio of the intensity of peak 3 to that of peak 1, which are indicated in the figure, can be used to analyze the pyrene partitioning into micelles. Figure 5 shows the (peak 3)/(peak 1) ratio of pyrene as a function of the n-β-octylglucoside concentration obtained by the spectral measurements. The sigmoidal curve that was obtained shows that the pyrene is transferred from water to the nonpolar environment as the n-β-octylglucoside concentrations increases. To investigate this transferring process quantitatively, numerical calculations were done based on the theoretical analysis described in section 3. Equation 22 can be used to fit the sigmoidal curve that was obtained as a function of the n-β-octylglucoside concentration. All the parameters used for the calculations are summarized in Table 2. Figure 6A−C shows some of the results from the calculations in which the parameter set of κ, D_C, and R_{max} was varied to fit the data based on the assumption of an aggregation number of 90. We obtained κ = 14 814, D_C = 27.8 mM, and R_{max} = 0.979 (the validity of the aggregation number of 90 will be discussed later). The curve through the data points in Figure 5 was calculated by the method of least mean squares for the data.

TABLE 2: Summary of All the Parameters Used for the Calculations To Fit the Data Based on Eq 22[a]

density of hydrophobic moiety, ρ_m (g/mL)	1.0
molecular weight, M (g/mol)	100
intensity ratio of pyrene in water, R_0	0.553
contribution of intensity ratio of pyrene interacting with preaggregated state of the detergent, R_1 (M^{-1})	1.96×10^3

[a] The values of ρ_m and M were estimated based on considerations of the size and shape of the micelles.[18] The values of R_0 and R_1 were estimated from the intensity ratio by the method of linear least squares below the cmc based on the relationship between D_T (or D_1).

5. Discussion and Conclusions

In this paper we mainly addressed the following two points: (1) the evaluation of the hydrophobicity of microenvironments based on the partition coefficient of the hydrophobic probe, pyrene, and (2) the validation of our method. In this study, we made a reference set of materials to evaluate the partition coefficient of pyrene between various organic solvents and water. The results of our work allow us to arrive at two key conclusions: (1) the partition coefficient for the interior of nonionic detergent micelles made from n-β-octylglucoside were determined to be 1.5×10^4, which corresponds to values for pure organic solvents, and (2) the partition coefficient of the reference probe, pyrene, provides information that allows us to determine the degree of the hydrophobicity of the core region.

The hydrophobicity of molecules is usually estimated in terms of the free energy of transfer of molecules from water to a pure hydrocarbon solvent.[3] This physical quantity clearly represents the hydrophobicity. For microenvironments, such as that inside the n-β-octylglucoside micelles used in this work, the hydrophobicity can thus be estimated by the sum of the free energy of transfer of the constituent molecules. Although our new method described here represents the local area around the probe, the measurement of the partition coefficient allows us to obtain the direct measurements of the thermodynamic properties of microenvironments. We proved that the partition coefficient of the reference probe between a microenvironment and water provides the same information as the free energy of transfer of the constituent molecules. A conventional method for determining the partition coefficient, however, becomes very difficult because specific structures cannot be isolated. Our new method thus represents the first method for estimating the hydrophobicity of microenvironments such as the interior of the core region of micelles.

All the parameters in eqs 14, 19, and 21 can in principle be determined exactly because the equations are fairly perfect representations of the penetration process of pyrene into detergent micelles, as shown in Figure 5. Because n-β-octylglucoside is a mild nonionic detergent, it is widely used

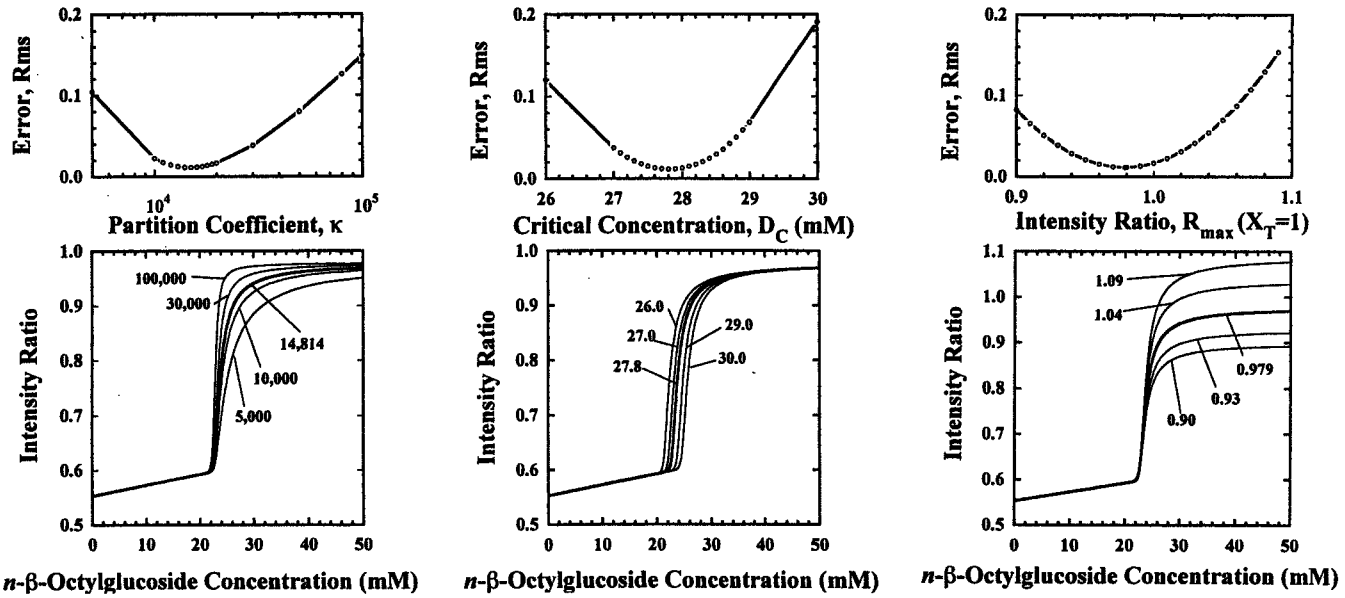

Figure 6. Based on an assumed aggregation number of 90 for the *n*-β-octylglucoside micelles, the best fit curve was determined for the curve of the intensity ratio as a function of the partition coefficient κ, the value α, and the aggregation number, N. All lines are plotted as functions of the following: (A, left) partition coefficient, κ, (B, center) critical concentration, D_C, (C, right) intensity ratio ($X_T = 1$), R_{max}. The thick lines show the best fit data, which were obtained by the method of least squares. The upper curves show the root mean square values between the experimental data and eq 22.

for membrane protein chemistry. In our investigation, it provided a simple system that did not have any electrolyte effects in the aqueous media. The physical properties, such as the cmc and the aggregation number, have been well studied by others.[9-12] The accuracy of these values strongly impacts on the reliability of our method. Although the Newton–Raphson method is powerful for solving the nonlinear formula, the adjusted parameters do not yield the best fit to the data for actual experiments. Under actual experimental conditions, we restricted the study to a narrower and lower concentration region of *n*-β-octylglucoside than the theoretical treatment for R_{max} and D_C. Therefore, we fixed the aggregation number to decrease the ambiguity of the analyses, and then the other parameters were adjusted to fit the data. In the following parts we will discuss the meaning of the partition coefficient of 1.5×10^4 obtained here and then discuss the reliability of the parameters in comparison to the previous values obtained by others.

Partition Coefficient of Pyrene between Detergent Micelles and Water. The calibration set for the partition coefficient of pyrene between organic solvents with various dielectric constants and water was established to evaluate the hydrophobicity of microenvironments. A pure hydrocarbon liquid was used in our experiments. Several alcohols and the aqueous methanol solutions were also used to vary the dielectric constants of the solution in a systematic manner. The free energy of transfer of each alcohol was calculated from κ based on eqs 12 and 13. Although a small inflection appeared on the calibration set in Figure 4, a linear relationship between the free energy of transfer and the dielectric constants was found. For the organic solvents, parameter A of eq 13 is in the range of 0.1–1. The free energy of transfer of pyrene from water to *n*-hexane was calculated to be −7.5 kcal/mol, because the value of A is 0.137 for *n*-hexane. The free energy of transfer obtained above corresponds to the value of the free energy of transfer for carbon atoms of 25 cal/(mol/Å^2).[17] Based on this value and the estimated surface area of a pyrene molecule (about 236 Å^2 calculated at a distance of 1.5 Å from the pyrene surface, the distance of closest approach for the center of a water molecule to the surface), the free energy of transfer of pyrene is estimated to be −5.9 kcal/mol. On the other hand, the partition coefficient of 1.5×10^4 corresponds to the free energy of transfer of −6.8 kcal/mol obtained by the calculation based on eqs 12 and 13 assuming the aggregation number of 90. This agreement thus confirms the accuracy of our method and that the partition coefficient should be as large as 10^4 in order of magnitude. The partition coefficient of pyrene between the internal region of *n*-β-octylglucoside micelles and water approximately corresponds to the value for pure organic solvents. The interior of the micelles appears to be quite nonpolar, with an estimated dielectric constant of 20–30.

Relationship between D_C and the Critical Micelle Concentration. The value of 25.0 mM for the cmc for *n*-β-octylglucoside micelles was determined first by Shinoda et al. based on the surface tensiometry.[9] The value obtained by Kameyama et al. of 25.3 mM as measured by light scattering[10] was in good agreement with that reported by Shinoda. In our investigations, a value for X_C (or D_C) of 27.8 mM was adjusted to fit the data. Based on the definition by Islaelachvili,[14] this value is the cmc for the *n*-β-octylglucoside micelles studied here. As with other methods, we had expected that there would be a drastic change appearing in the plot of the intensity ratio of pyrene and that this would serve as the critical concentration of the micelle formation. Although the conventionally used term of cmc reflects the aggregated structure of the detergent, there is some ambiguity in defining the cmc for actual experiments. Figure 7 shows the relationship of X_1 and X_N to X_T based on eq 7 when the following assumptions are made: $D_C = 25$ mM and $N = 90$. The cmc may be defined in three ways: (1) the onset of the formation of aggregate structures, (2) the concentration at which the monomer detergent concentration levels off, and (3) the concentration of monomer at which the total concentration of detergent (X_T) equals unity. If the detergent micellization is thermodynamically ideal, the three critical values described above might be equal to the value of the cmc. The three sections in Figure 5, which are indicated by two critical concentrations of *n*-β-octylglucoside ($conc_1$ and $conc_2$), clarify some of the ambiguity described above. The region between the two critical concentrations (where there is a rapid increase in the peak ratio) can be ascribed to the start of micelle formation. If the starting point (lower concentration of detergent, $conc_1$) at 22.1 mM is just at the onset of the formation of the aggregate structures, then the value appears to be slightly smaller than that reported in the literature. Kalyanasundaram[7]

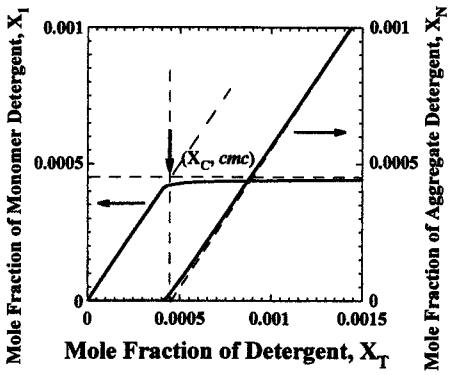

Figure 7. Monomer and aggregate concentrations as a function of the total concentration of n-β-octylglucoside. The calculations are based on eq 4. X_T is the mole fraction of the total detergent in water. The value of D_C was 25.0 mM and N was 90. From the relationship between the mole fraction and the mole concentration (eqs 5 and 6), a value for X_C of 0.000 45 was obtained. The dashed lines indicate the cmc defined in three ways: the monomer state, the aggregate state, and the infinite concentration when X_1 becomes unity.

also reported the upper value (second critical point in Figure 5, $conc_2$) as the cmc for sodium dodecyl sulfate micelles. If the upper value in our data (25.6 mM) is the cmc, it is in good agreement with that of the literature.[9,10] If we use the method of Israelachvili[14] to determine the value of cmc, the cmc of our system is equal to X_C at which the intensity ratio asymptotically approaches R_{max}. These differences may be due to a distribution in the aggregation number of the various nonionic detergents, such as n-β-octylglucoside[14] or due to a distribution in the number of pyrene molecules that are incorporated into micelles according to Poisson's law.[8] To clarify the ambiguity associated with the definition of cmc, we must consider the dynamic mechanism of the micelle formation around the cmc. This distinction, however, is not normally of significance to biochemists when they remove the detergent after solubilizing membrane proteins.

Intensity Ratio at the Finite Value of 1 Assumed for X_T (R_{max}). Pyrene is suitable for our purpose because the intensity ratio of parts within the fine structure is sensitive to the polarity of the microenvironment in the solution and such a measurement is not dependent on the fluorescence intensity. For hydrocarbons such as n-hexane, the intensity ratio is 1.65, while it is 0.63 in water.[7] When the finite value of 1 was assumed for the total concentration of the detergent (X_T), and R_{max} value of 0.979 was adjusted to fit the data. The curve in Figure 5 shows three sections (1) below the cmc (no micelles present, pyrene fluorescence spectrum almost corresponds to that in water, and the intensity only gradually increases as a function of the n-β-octylglucoside concentration), (2) rapid increase in the peak ratio around the cmc, and (3) above the cmc (here the (peak 3)/(peak 1) ratio reaches a steady value (0.96) that is independent of the detergent concentration in this region). Although the intensity ratio is sensitive to the polarity of the environment, the relationship to the hydrophobicity is unclear. It is not yet known whether pyrene in the micelle is located closer to the micellar surface or in the inner core region. The intensity ratio of the pyrene in the n-β-octylglucoside micelle system is, however, higher than it is in other detergent micelle systems,[7] so the pyrene molecules appear to be incorporated in the inner core region where no water molecules exist. In actual experiments, the intensity ratio above the cmc might be used to estimate the hydrophobicity of the microenvironments.

Aggregation Number. Kameyama also estimated that the aggregation number for n-β-octylglucoside micelles in distilled water was 87.[10] We obtained an aggregation number of about 95 based on the static and dynamic fluorescence quenching measurements.[18] In our experiments, narrower and lower concentration ranges of n-β-octylglucoside were used. Therefore, the adjusted parameters do not yield the best data fit for the actual experiments as mentioned above. We used an aggregation number of 90 for simplicity in the calculations. The error should be almost negligent in our approximations in eq 21, because the term in parentheses should be smaller than 1.

In conclusion, we found that the nonpolar moiety in the core of n-β-octylglucoside micelles is maintained even in aqueous media. In other words, hydrophobic interactions play a very important role in the formation of nonionic detergent micelles and in the maintenance of their structures once formed. Our investigations also provide a method for evaluating the thermodynamic properties of detergent micelles, such as cmc, R_{max}, and the aggregation number. Although we were unable to estimate the errors for these parameters, the error values are insignificant compared to the actual values derived from the experiments. The molten globule state of proteins is now becoming a hot issue in discussions on the structural formation of proteins.[19,20] Our new method opens the way to quantitative investigations of such intermediate states of proteins and provides means to study the structural formation of proteins. Applications based on our method will find wide use in the study of the structural formation mechanisms of proteins.[21]

Acknowledgment. We thank Dr. R. Lewis (Tsukuba Research Consortium) for critically reading the manuscript. We also thank Mr. T. Hiruma (President of Hamamatsu Photonics K.K.) for his support and encouragement of this work. Mr. T. Hirokawa helped us to estimate the surface area of pyrene on the workstation. This work was partially supported by a Grant-in-Aid from the Ministry of Education, Science and Culture of Japan.

References and Notes

(1) Kauzman, W. *Adv. Protein Chem.* **1959**, *14*, 1.
(2) Tanford, C. *J. Phys. Chem.* **1972**, *76(21)*, 3020.
(3) Tanford, C. *The Hydrophobic Effect*, 2nd ed.; John Wiley & Sons: New York, 1980.
(4) Bruning, W.; Holtzer, A. *J. Am. Chem. Soc.* **1961**, *83*, 4865.
(5) Kano, K.; Goto, H.; Ogawa, T. *Chem. Lett.* **1981**, *1981*, 653.
(6) Nakajima, A. *J. Lumin.* **1976**, *11*, 429.
(7) Kalyanasundaram, K.; Thomas, J. K. *J. Am. Chem. Soc.* **1977**, *99*, 72039.
(8) Kalyanasundaram, K. *Photochemistry in Microheterogeneous Systems*, 1st ed; Academic Press: New York, 1987.
(9) Shinoda, K.; Yamaguchi, T.; Hori, R. *Bull. Chem. Soc. Jpn.* **1961**, *34*, 237.
(10) Kameyama, K.; Takagi, T. *J. Colloid Interface Sci.* **1990**, *137(1)*, 1.
(11) De Grip, W. J.; Bovee-Geurts, P. H. M. *Chem. Phys. Lipids* **1979**, *23*, 231.
(12) Fischer, T. H. *Mol. Cryst. Liq. Cryst.* **1983**, *92*, 7.
(13) Mitaku, S.; Wright, J. K.; Best, L.; Janig, F. *Biochim. Biophys. Acta* **1984**, *776*, 247.
(14) Israelachvili, J. N. *Intermolecular and Surface Forces*, 2nd ed; Academic Press: New York, 1989; Chapter 15.
(15) For example: *Numerical Recipes, The Art of Scientific Comuting. (Fortran version)*; Cambridge University Press: Cambridge, 1989; Chapter 9.
(16) Japan Chemical Society *Kagaku Binran Kisohen II*, 3rd ed.; Maruzen: Tokyo, 1984; Chapter 13.3.
(17) Eisenberg, D.; Geselowitz, A. R.; Lesser, G. J.; Lee, R. H.; Zehfus, M. H. *Science* **1985**, *229*, 834.
(18) Itoh, H., unpublished data.
(19) Kuwajima, K. *Proteins* **1989**, *6*, 87.
(20) Mitaku, S.; Suzuki, K.; Odashima, S.; Ikuta, K.; Suwa, M.; Kukita, F.; Ishikawa, M.; Itoh, H. *Proteins* **1995**, *22*, 350.
(21) Mitaku, S.; Ishido, S.; Hirano, Y.; Itoh, H.; Kataoka, R.; Saito, N. *Biophys. Chem.* **1991**, *40*, 217.

JP953682Z

Use of a gain modulating framing camera for time-resolved imaging of cellular phenomena

Hiroyasu Itoh, Ariella Evenzahav[a], Katsuyuki Kinoshita, Yoshinori Inagaki, Hiroshi Mizushima, Akira Takahashi, Tsuyoshi Hayakawa, and Kazuhiko Kinosita, Jr.[b]

Tsukuba Research Laboratory, Hamamatsu Photonics K.K., Tokodai, Tsukuba, Ibaraki, 300-26, Japan
[a]Department of Chemistry, Columbia University, NY. USA
[b]Department of Physics, Faculty of Science and Technology, Keio University, Yokohama 223 Japan

ABSTRACT

A gain modulating framing camera and its application towards the study of real time cellular phenomena will be described. Based on a unique operating principle, this framing camera can be modulated by over 90% at 1 GHz. The camera consists of an image converter with a pair of deflection electrodes and a rectangular aperture. Since a sinusoidal electric field is applied to the deflection electrodes, the photoelectron image-forming beam is continuously deflected and swept on the aperture. A bias is applied to center the sweep of the photoelectron beam on the edge of the aperture. The gain modulating with high depth can hence be accomplished. We are now constructing a fluorescence lifetime imaging microscope system employing this gain modulating framing camera based on the phase domain method. Such high depth modulation enables us to achieve frequency signals as low as 1 Hz in heterodyne operation. We will describe examples of application of the system towards the observation of various cellular phenomena.

Keywords: Fluorescence lifetime imaging microscopy (FLIM), framing camera, frequency domain, phase-resolved, cellular phenomena, dual-view assembly.

1. INTRODUCTION

The use of fluorescence lifetime imaging microscopy is now becoming possible for the study of molecular events with spatial distributions in a microscope image.[1,2] Lifetime measurements have been traditionally carried out using two methods, (1) the pulse method, and (2) the phase-domain method. Fluorescence lifetime imaging microscopy follows this trend. To accomplish the lifetime measurement, developments of an optical device with a certain spatial resolution and a pico- to nanosecond temporal resolution are required. Fluorescence lifetime imaging microscopy might be accelerated by the development of image detectors, such as an image intensifier, which has a nanosecond time resolution. Gating (100 % on/off) or continuously modulating the gain of the image intensifier has been possible for the nanosecond lifetime imaging. It is difficult to compare the advantages and disadvantages of both methods because both methods have theoretically the same abilities and the applications to fluorescence microscopy so far as few. It is expected that the choice be made depending on the experiment, or that will be left to the preference of the researchers. However, regarding the optical device, the image intensifier, some problems still exists with respect to its abilities, for example, shutter speed and repetition rate of gating, or frequency and depth of modulation, which are caused by the inherent capacitance and resistance of the image intensifiers.

Streak camera technology based on a photoelectric effect and electron beam manipulation in an image converter have been improved and extended into the femtosecond world.[3] The streak camera has been basically used only for one-dimensional measurements. For imaging, scanning methods must be employed. The first time-resolved imaging (not lifetime) study with a framing camera based on this technology succeeded in obtaining a series images of fast, irreversible cellular phenomena.[4] The framing camera technology, furthermore, has been employed in pico- to nanosecond time-resolved imaging.[5,6,7] The latest version of the framing camera can be gated with a 480 psec shutter at a 4 MHz repetition rate based on a unique operating principle.[8] We also found that the gain of the camera can be modulated to 500 MHz with high modulation depth. The deflection electrodes were modified to accomplish a modulation frequency to 1 GHz.[3,9]

additional author information: phone 81-298-47-5161, fax 81-298-47-5266, e-mail hiritoh@hpk.trc-net.co.jp

In this report, we will introduce our efforts to develop the fluorescence lifetime imaging under a microscope utilizing the phase-domain method. Such high modulation depth will enable us to obtain a cross-correlation signal as low as 1 Hz in heterodyne operation. The signal can be continuously read out by a conventional CCD camera. Some ideas to carry out real-time imaging of cellular phenomena will be shown, and some examples of application of the system will be described.

2. GAIN MODULATING FRAMING CAMERA

A framing camera whose gain can be continuously modulated over a wide range of frequency (- 1 GHz) with a high depth of modulation (90% -) was developed based on a unique operating principle, which originates in a high-repetition framing camera described elsewhere.[5,6,7,8] Figure 1A shows the operating principle of the gain modulating framing camera. The camera is basically an image converter with a pair of deflection electrodes and a rectangular aperture. An incident optical image is first converted to a photoelectron image at the photocathode. The photoelectron image-forming beam is accelerated, and hits the output phosphor screen. The emerged image on the output window can be multiplied by a proximity focused image intensifier coupled with an optical fiber plate, and is then read out by a conventional CCD camera via a tapered optical fiber plate. A sinusoidal electric field is applied externally to the electrodes. The photoelectron image is thus continuously deflected and swept on the aperture. The photoelectron beam arriving from the center of the rectangular aperture to the exterior results in the gain modulation (Fig. 1B). Since a focusing electrical lens rigidly maintains the image position of the photoelectron image on the phosphor screen, the emerged image does not move even when the photoelectron image is swept by the deflection electrodes. The meander-type traveling wave deflection electrodes with a low impedance (100 W) and a wide band width (1 GHz) is designed to transmit such high repetition voltage.[3,9] Figure 2 shows the system response function of the gain modulating framing camera. At 900 MHz, modulation of over 90% was obtained, but at 500 MHz, the modulation depth decreases to 70%. This might be caused by an inherent resonance effect of the framing camera.

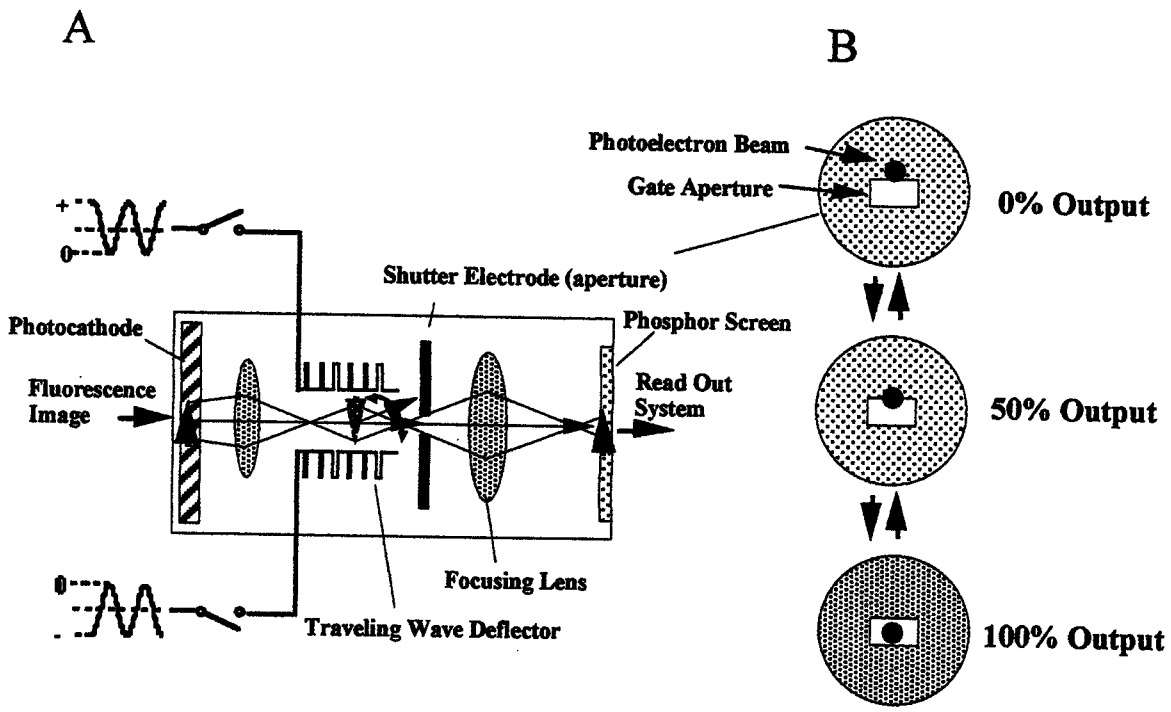

Fig. 1 A: Operating principle of the gain modulating framing camera. An electric field (sinusoidal voltage) is applied to the deflection electrode. B: The beam continuously swept by the deflection electrode is brought back to the center of the aperture to carry out the gain modulation.

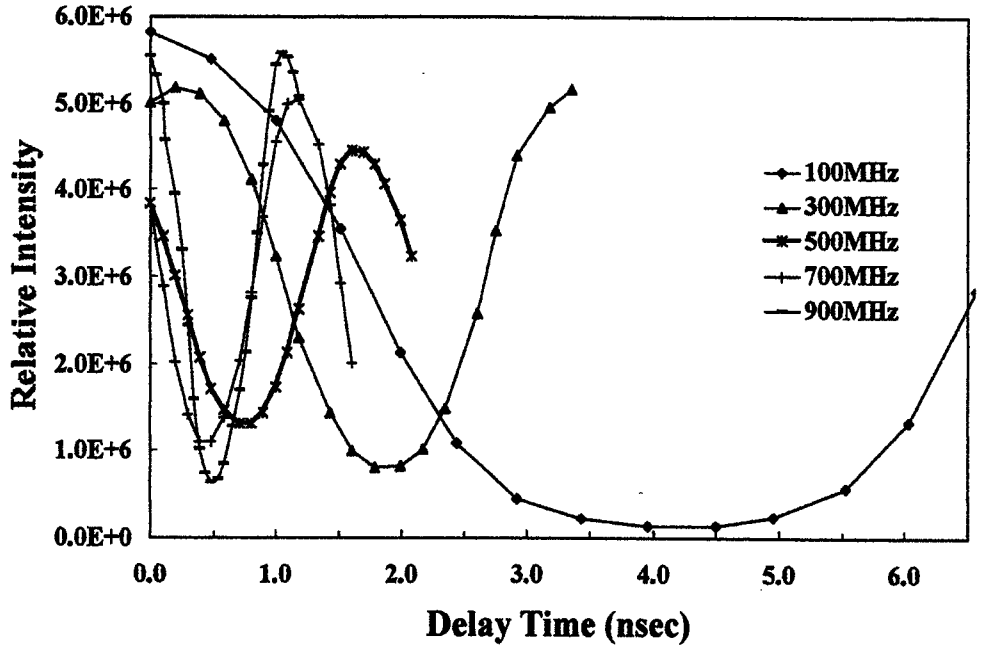

Fig. 2 The system response function of the gain modulating framing camera. A pulse laser (100 psec, FWHH, 1 MHz) was synchronously triggered by a pulse controller with a certain electric delay. The response is shown as a function of the delay time.

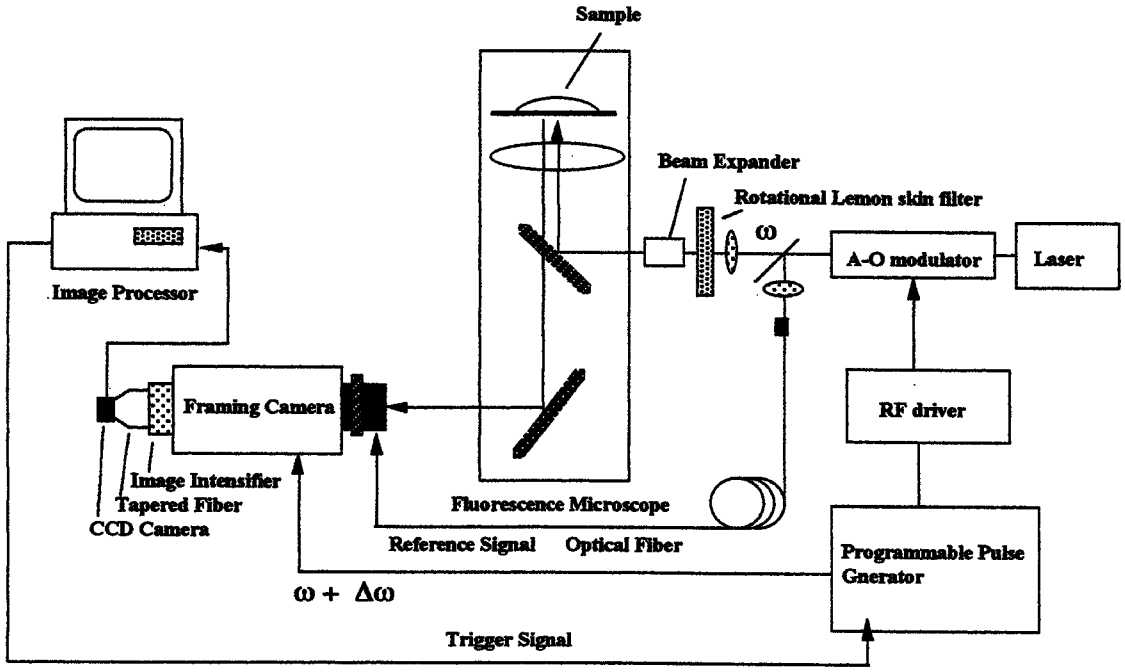

Fig. 3 A schematic diagram of our fluorescence lifetime imaging microscope system based on the modulating framing camera.

3. FLUORESCENCE LIFETIME IMAGING MICROSCOPE SYSTEM

Figure 3 shows a schematic diagram of our fluorescence lifetime imaging microscope system. The instrument consists of (a) a frequency-doubled Nd/YAG laser as an excitation light source, (2) an acousto-optical modulator, (3) an epi-fluorescence microscope, (4) a gain modulating framing camera with an image intensifier and a CCD camera, and (5) a programmable signal generator. The excitation light source modulated by the acousto-optical modulator (100 MHz) was focused onto a rotating diffuser disk (lemon-skin filter) and introduced into the microscope through a beam expander to illuminate the entire field of a view. The programmable signal generator can produce two synchronous signals. The difference of frequency and phase angle in the two signals can be controlled and swept with high accuracy of ±0.1 Hz or ±0.1°.

Lifetime measurements of fluorescent samples (detection and analysis) using the frequency domain method have been described extensively in the literature.[10] In the heterodyne method, a low frequency signal ($\Delta\phi$), which is produced by the cross-correlation between high frequency optical signals (ϕ) and high frequency gain modulation ($\phi + \Delta\phi$) of a detector, can be manipulated for the analysis of the lifetime measurements. In our system, the modulation frequency of the excitation light and the gain modulation is same. The heterodyne operation was carried out by sweeping the phase angle of the light modulation to the gain modulation of the camera.[11] The fluorescnece lifetime is determined ralative to the phase delay of scattering of the excitation light. In our system, the measurements were initiated by a trigger signal produced by the computer. The trigger signal has an inherent jitter of about 100 msec, so that the cross-correlation frequency of 0.1Hz was temporally used. This will be improved in the new version as described later, in which the reference signal for analysis of phase delay and modulation depth can be captured simultaneously in the view of the respective image.

A sensitivity test of our system was carried out using an optical delay (a dual-view assembly described elsewhere[8]). A chevron-type mirror was set upside and down, and placed in the microscope. For this measurement, a cutoff filter was removed. The reflection beam from the mirror was first passed through the rectangular slit in order to select a certain area of the view, and was then introduced into the dual-view assembly. The beam was separated into two images. One of the components was passed through an optical delay path, and the difference of the delay time between the two images was therefore produced in the dual-view assembly. The two images were then focused on the framing camera side by side. One of the images had a certain delay time determined with great accuracy by the measurable optical path length. The modulation phase of the excitation light source was swept at 2° / 10 msec. The images (512 x 512 pixels at 30Hz) were stored into the frame memory of a computer for the analysis. Signals with very low frequency, which correspond to the frequency of the phase sweep (1/1.8 Hz) appeared on the figures. Figure 4 shows average intensities of 200 x 200 pixels as a function of time (the rate of video frame). From a mathematical analysis based on a sin curve, the delayed phase angle produced by the optical delay can be calculated. Figure 5 shows the optical delay length calculated from the delayed phase angles as a function of the measured optical path lengths (The phase angle of 360° corresponds to the 10 nsec at the frequency of 100 MHz, and the delay path length of 30 cm causes a delay of 1 nsec). The slope of the 0.97 indicates the accuracy of our system. Analytical errors and heterogeneous modulation of the view in the camera might result in a small error.

A sensitivity test of the imaging system was also carried out using a homogeneous fluorescent sample. The fluorescent dye, calcium orange, in various calcium buffers was used. Figure 6 shows the phase and modulation curve of the cross-correlation signals of the dye. The lifetimes based on the phase angle and the modulation were well resolved by the analysis of the sin curve fitting (Fig. 7). The modulation frequency should be comparable to the decay rate to obtain measurable values of the phase and the modulation, and in order to determine the multiple components of the lifetime, several frequencies must be examined Although only the modulation frequency of 100 MHz is available in the present version of our system, the lifetimes obtained here are comparable to the value (an average lifetime) reported in the literature.[12]

The phase and modulation analysis for a living cell (human melanoma, HMM, stained with a fluorescent dye, Acridine Orange) was preliminary carried out by using our fluorescence microscope system. The dye interacts with DNA and RNA by intercalation or electrostatic attractions. The dye has an emission maximum of 525 nm when bound to DNA. Upon association with RNA, its emission is shifted to 650 nm.[13] In this measurement, a cutoff filter of 600 nm was used, so that the lifetime of the probe bound to RNA could be exclusively observed. The analysis of the lifetime imaging has not yet been completed. Fig. 8 shows the cross-correlation signals of the small area in the cell. The lifetimes obtained here were summarized in Table 1.

As described above, both the measurements of the references and samples were initiated by a trigger signal from the computer, which has a relatively large jitter of 100 msec in the present version of our system. We are now developing a monitor system of the reference with the respective image. A small diffusive material irradiated by the reference light splitted from the excitation light via an optical fiber is placed in the optical path where the intermediary image is formed. The reference signals for the phase and gain can be obtained simultaneously in the respective image. The duty cycle of the measurement will be extremely reduced. We are now preparing the system which can be inserted directly into the input optics of the camera (shown in the figure).

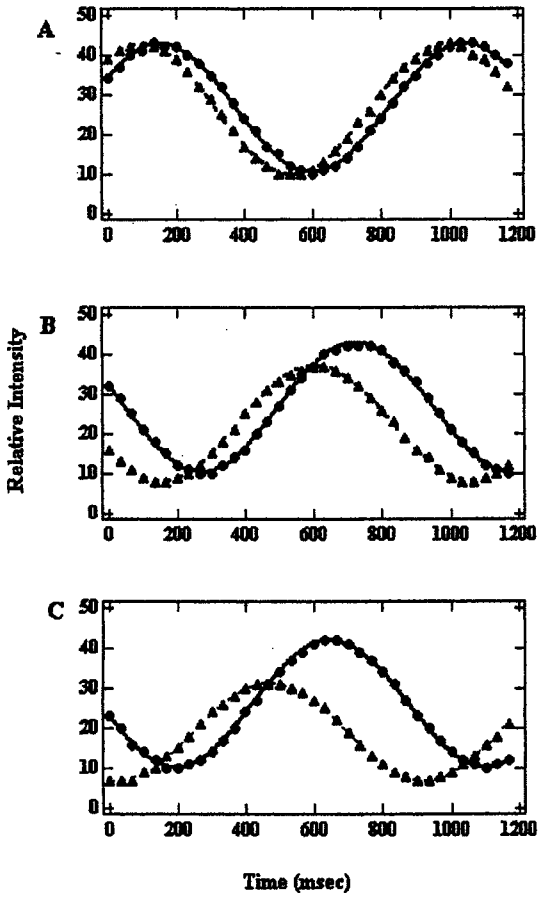

Fig. 4 Cross-correlation signals obtained by our system. The procedure of the measurements is described in the text. The optical delay length produced by the dual-view assembly is A: 20 cm, B: 40 cm, and C: 60 cm, respectively. The circle denotes the average intensity of the straight image, and the triangle the intensity of the delayed images. The curves are calculated by the mathematical analysis based on the sin curve.

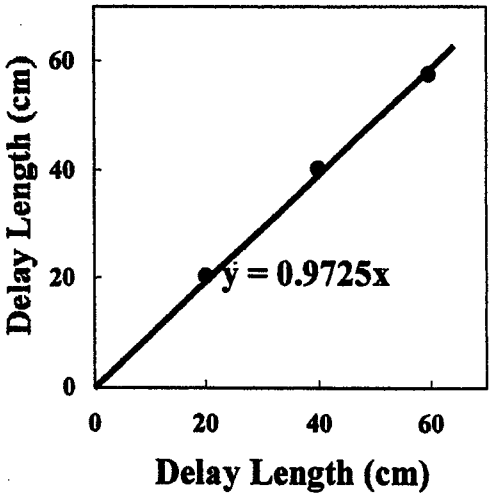

Fig. 5 The optical delay length calculated from the phase angle as a function of the measured delay length. The slope of 0.975 was obtained.

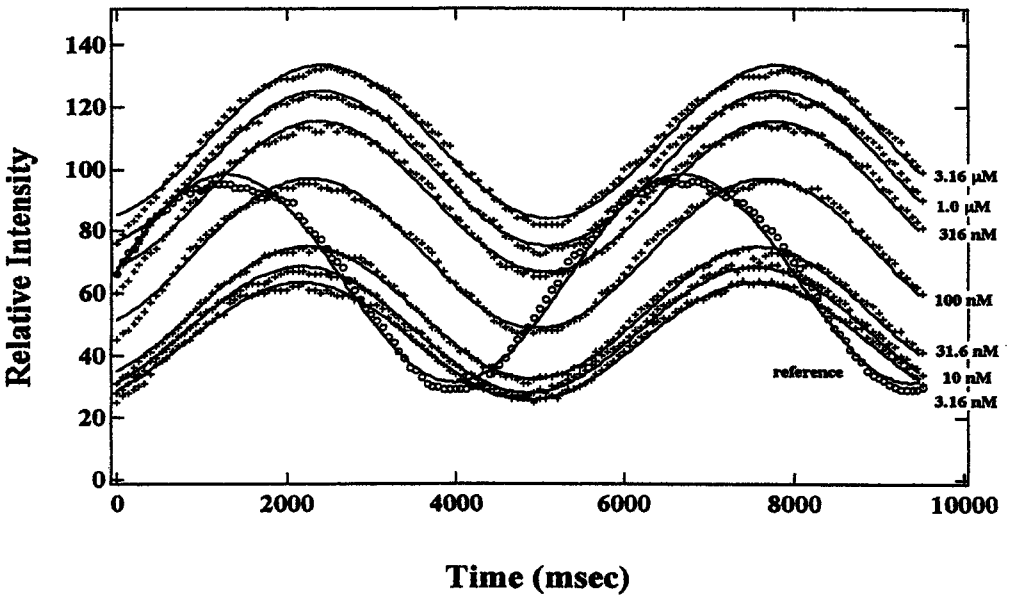

Fig. 6 Cross-correlation signals of the Calcium Orange as a function of free calcium ion concentrations

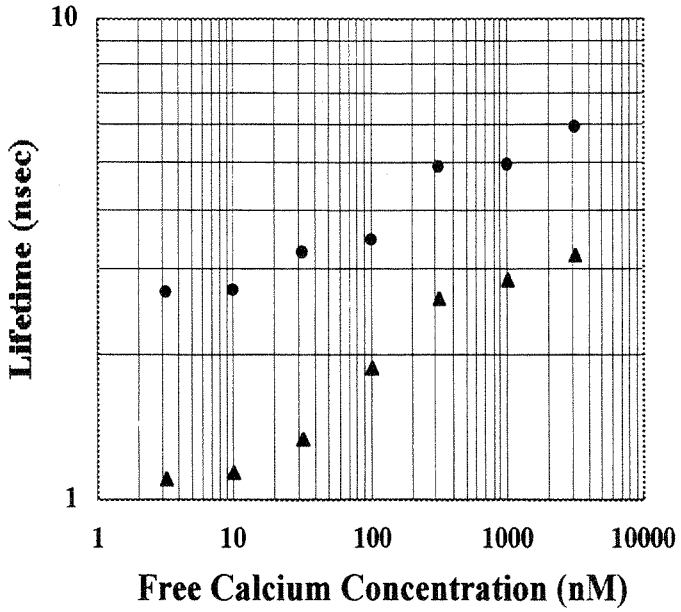

Fig. 7 Calculated lifetime of the calcium orange from the phase (●) and the modulation(▲).

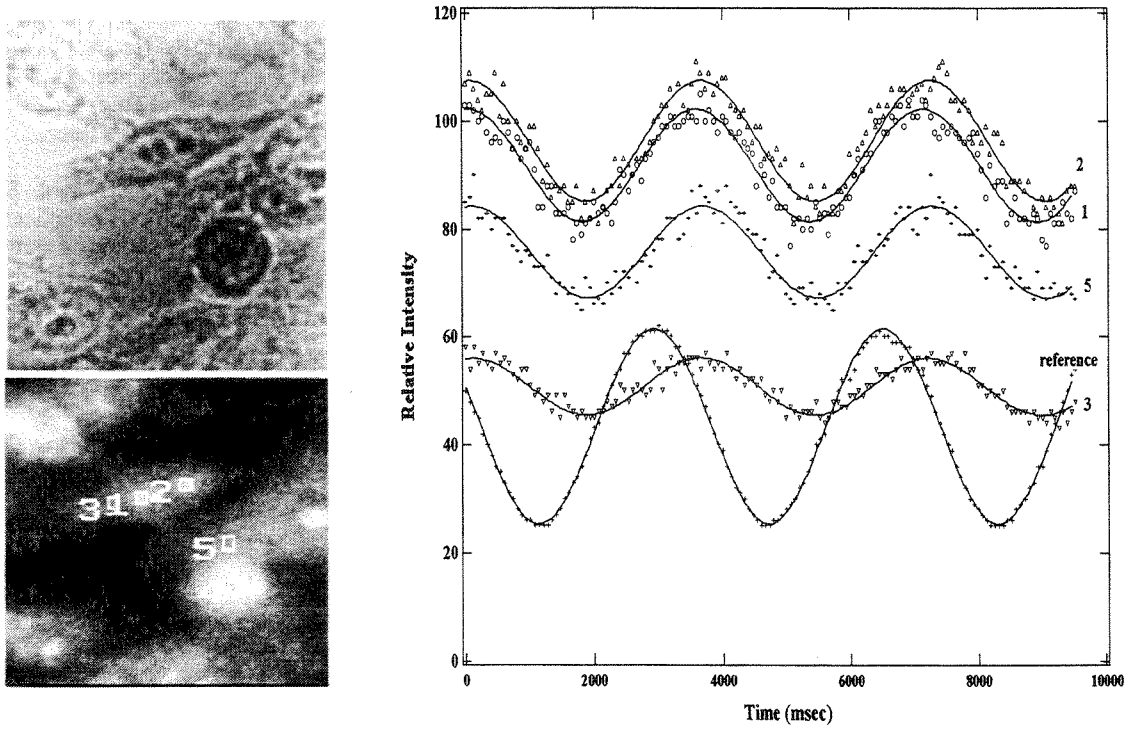

Fig. 8 Phase contrast image of cell (upper left), fluorescence image (lower left), cross correlation signals of the cell (human meranoma). The cell was stained with 20 μM of Acridine Oorange, and incubated for 1 hour.

738

	τ (phase)	τ (modulation) nsec
1	4.69	5.61
2	5.28	5.28
3	6.66	6.66
4	-	-
5	7.00	7.00

Table 1 Lifetime measurement of small areas of the cell. The numbers were indicated in the fluorescence image of Fig. 7. Flurescence intensity of area 4 was saturated .

4. DISCUSSION AND CONCLUDING REMARKS

We developed a gain modulating framing camera to construct a fluorescence lifetime imaging microscope system. The camera can be modulated by over 90% at 1 GHz based on a unique operating principle. The reference signal, which is necessary for analysis of the phase delay and modulation depth, can be simultaneously obtained in the respective image. The duty cycle of the measurement would be extremely shortened. The phase of 360° was measured in 1 sec. Since only several images are sufficient for analyzing the lifetime image, the further improvement can be expected, when the mathematical analysis is added.

We are currently in the process of improving the system. In the present version of our system, the frequency is restricted at 100 MHz due to the frequency of the acousto-optics ability. Therefore, the application of the system is limited and the accuracy of the measurement is relatively low. We are now planning to introduce pulsed lasers (psec and fsec) as a light source. Mutifrequency measurements will be carried out for the lifetime measurement of multiple component of a fluorescent dye.[14]

In this report, we described our efforts towards developing a fluorescence lifetime imaging microscope system. Because the framing camera can be modulated to 1 GHz (although modulation up to 2 GHz is theoretically possible). The application can be extended to other fields, such as the time resolved imaging of a thick tissue[15] or the measurement of photon migration in brain science.[16] The technology of the framing camera will play a major role in the ultrafast time-resolved imaging fields.

ACKNOWLEDGEMENTS

We thank Mr. T. Hiruma (President of Hamamatsu Photonics K.K.) for his support and encouragement of this work. We also thank Dr. N. Miyoshi (Fukui Medical School) for cell preparation. Participation in this project by Ms. A. Evenzahav, was supported by the Summer Institute Student program of the National Science Foundation (NSF) and the Japan International Science and Technology Exchange Center (JISTEC). This work was supported in part by the Japan Science and Technology Corporation (JST).

REFERENCES

1. T. Oida, Y. Sako, and A. Kusumi, "Fluorescence lifetime imaging microscopy (flimscopy): Methodology development and application to studies of endosome fusion in single cells", Biophys. J., Vol. 64, pp. 676-685, 1993.
2. R. M. Clegg, B. Feddersen, E. Gratton, and T. M. Jovin, "Time resolved imaging microscopy", Proc. SPIE, Vol. 1640, pp. 448-460, 1992.
3. A. Takahashi, M. Nishizawa, Y. Inagaki, M. Koishi, and K. Kinoshita, "New femtosecond streak camera with temporal resolution of 180 fs", Proc. SPIE, Vol. 2116, pp. 275-284, 1994.

4. H. Itoh, M. Hibino, M. Shigemori. M. Koishi, A. Takahashi, T. Hayakawa, and K. Kazuhiko, Jr., "Multi-shot pulsed laser fluorescnece microscope system", Proc. SPIE, Vol. 1024, pp. 49-53.
5. K. Kinoshita, "New picosecond electronic framing camera", Proc. SPIE, Vol. 569, pp. 2-8, 1985.
6. K. Kinoshita, Y. Inagaki, and T. Nakamura, "Picosecond electronic framing camera", Proc. SPIE, Vol. 693, pp.2-8 , 1986.
7. K. Kinoshita, Y. Inagaki, S. Yamabe, A. Takahashi, H. Itoh, M. Koishi, H. Mizushima, and T. Hayakawa, "High-repetition shutter camera", Proc. SPIE, Vol. 2513, pp. 41-49, 1994.
8. H. Itoh, A. Evenzahav, K. Kinoshita, Y. Inagaki, H. Mizushima, A. Takahashi, and T. Hayakawa, "Fluorescence lifetime imaging microscopy with a high repetition gated camera and a dual-view assmbly for the real time measuremtn",Advances in Fluorescence Sensing Technology in Clinical Diagnostics III, Conference Chairs: Joseph R. Lakowicz, Proc. SIPE, 1997.
9. M. Suyama, K. Kinoshita, T. Okada, and M. Ito, "Streak tube having ultra-heigh deflection sensitivity", Proc. SPIE, Vol. 1757, pp. 19- 31, 1992.
10. R. D. Spencer, and G. Weber, "Measurement of subnanosecond fluorescence lifetimes with a cross-correlation phase fluorometer", Ann. N.Y. Acad. Sci. Vol. 158, pp. 361-376, 1969.
11. J. R. Lakowicz, "Principles of fluorescence spectroscopy", Plenum Press, New York, 1983.
12. J. R. Lakowicz, H. szmacinski, and M. L. Johnson, "Calium imaging using fluorescence lifetimes and long-wavelength probes", J. Fluorescence, Vol. 2, pp. 47-62, 1992,
13. R. P. Haugland, "Handbook of fluorescent probes and research chemicals", 6th Ed., Molecular Probes.
14. E. Gratton, "Multifrequency phase fluorometry using pulsed sources: Theory and applications"
15. J. Lakowicz, I. Gryczynski, H. Szmacinski, K. Nowaczyk, "Advances in frequency-domain fluorometry; Gigahertz instrumentation, Time-dependent photo migration and fluorescence lifetime imaging", Proc. SPIE, Vol. 1599, pp. 227-243, 1991.
16. Y. Tsuchiya, and T. Urakami, "Photon migration model for turbid biological medium having various shapes", Jpn. J. Appl. Phys. Vol. 34, pp. 79-81, 1995.

Fluorescence lifetime imaging microscopy with a high repetition gated camera and a dual-view assembly for the real time measurement

Hiroyasu Itoh, Ariella Evenzahav[a], Katsuyuki Kinoshita, Yoshinori Inagaki, Hiroshi Mizushima
Akira Takahashi, Tadashi Fukami, Tsuyoshi Hayakawa, and Akihiro Kusumi[b]

Tsukuba Research Laboratory, Hamamatsu Photonics K.K., Tokodai, Tsukuba, Ibaraki, 300-26, Japan

[a]Department of Chemistry, Columbia University, NY. USA.
[b]Department of Pure and Applied Science, The University of Tokyo Meguro, Tokyo, 153, Japan.

ABSTRACT

A novel method for real-time imaging of fluorescence lifetimes employing a new framing camera will be introduced. Based on a unique operating principle, this framing camera can be gated with a 480 picosecond shutter. The camera consists of an image converter with a pair of deflection electrodes and an aperture. As the photoelectron image passes through the deflection electrodes, an electric field is applied externally. The photoelectron image is thus deflected, and swept on the aperture. High speed gating can hence be accomplished. We are now constructing a fluorescence lifetime imaging microscope system employing this framing camera whereupon the repetition rate has been increased to 4 MHz. Although application of this method requires multiple acquisitions at different delay times, it enables us for the first time to observe real-time intracellular phenomena. This is achieved by combining the system with a dual-view assembly, composed of a pair of beam splitters and mirrors which produce a certain delay, hence enabling us to capture two time-resolved images simultaneously in a single operation of the framing camera. These two images have different delay times, each of which can be set from 300 picoseconds to 2 nanoseconds. The two images are used for the analysis based on the assumption that the decay is single exponential. We will describe an example of application of the system towards the observation of cellular phenomena.

Keywords: Fluorescence lifetime imaging microscopy (FLIM), framing camera, high repetition, gating, cellular phenomena

1. INTRODUCTION

Fluorescence lifetime-resolved imaging microscopy (FLIM) is a relatively new fluorescence imaging technique, which enables us to obtain the spatial variations of fluorescence lifetimes in single cells as a source of image contrast.[1,2,3] Time-resolved fluorescence measurement has been widely used for research in biophysics, biochemistry, cell biology and medicine. Excited-state lifetimes of fluorescent probes can provide information pertaining to dynamic processes occurring in microenvironments, such as molecular rotation, solvent relaxation, quenching mechanism, reactions, and energy transfer. The recent research move towards the development of fluorescence microscope imaging in cell research has been accelerated by the requirements of direct measurements of molecular events in single cells. Although fluorescence imaging is sensitive, some uncertainty still remains in the steady-state measurement. Complex corrections are necessary for spatial variations in path length, light scattering, and the number of fluorophores. In fact, the excited-state lifetime would be the only physical observable, the absolute value of which could be precisely determined by fluorescence microscopy.

Further author information: H. I. (correspondence): E-mail: hiritoh@hpk.trc-net.co.jp, Phone: 81-298-47-5161, Fax: 81-298-47-5266

SPIE Vol. 2980 • 0277-786X/97/$10.00

The determination of fluorescence lifetimes is traditionally carried out by two techniques: (1) the time-domain pulse method and (2) the frequency domain or phase-resolved method.[4,5] Although fluorescence lifetime imaging microscopy was expected to become a powerful and valuable tool for observation of molecular events in single cells, it has not yet evoked the interest and attention of researchers in applications of cell research. Not only is the system complex, but also the real-time measurement is difficult to carry out because the several time-resolved images at various delay times or with different phase angle would be required for the analysis. It takes several seconds for accumulation of the image with higher S/N ratio, including the setup of the fixed delay time or phase angle and the transferring of the image to the computer.

In this report, we will introduce our efforts to accomplish the real-time fluorescence lifetime imaging under microscope based on the pulse method. A framing camera with a unique operating principle has been developed for this purpose.[6,7,8] The camera can be gated with a 480 psec shutter at a 4 MHz repetition rate. The gate width must be sufficient to resolve prompt fluorescence, and the repetition rate can be fixed with a conventional pulsed laser under a cavity-dumper or a pulse selector. The temporal resolution and S/N ratio was remarkably improved for time-resolved imaging. Although the fluorescence lifetime requires multiple acquisitions at different delay times, it enables us for the first time to observe real-time intracellular phenomena. This is achieved by combining the system with a dual-view assembly which was developed for capturing two time-resolved images simultaneously in a single operation of the framing camera. These two fluorescence images with different delay times can be used for the analysis based on the assumption that the decay is single exponential. An example of application of the system towards the observation of cellular phenomena will be described.

2. A HIGH-REPETITION FRAMING CAMERA

A high-repetition framing camera was previously shown elsewhere.[6,7,8] The camera is basically an image converter with a pair of deflection electrodes and an aperture (Fig. 1A). An incident optical image is first converted to a photoelectron image at the photocathode. The photoelectron image-forming beam is accelerated, and hits the output phosphor screen. The emerged image on the output window can be multiplied by a proximity focused image intensifier coupled with an optical fiber plate, and is then read out by a conventional CCD camera via a tapered optical fiber plate. As the photoelectron beam passes through the deflection electrodes, an electric field is applied externally to the electrodes. The photoelectron image is thus deflected and swept on the aperture. Since a focusing electrical lens rigidly maintains the position of the photoelectron image on the phosphor screen, the emerged image does not move even when the photoelectron image is swept by the deflection electrodes . To cut off the retrace photoelectron beam, the beam is shifted and reswept to the waiting position by applying the electric fields to the another deflection electrodes (Fig. 1B). High speed gating can hence be accomplished. The driving electronics of the framing camera was modified in order to increase the repetition rate to 4 MHz in this study.

The period during which the photoelectron beam can pass through the aperture corresponds to the gate width or the shutter speed. The period is a function of the deflection sensitivity[9,10] and the aperture size (alternatively, if the photoelectron beam diameter is small, the same effect can be expected). If the fluorescence signal is so weak, a longer gate width would be preferred to obtain the image with a higher S/N ratio. The deflection sensitivity can be controlled by the slope of the externally applied voltage to the deflection electrodes, which corresponds to the amplitude of the voltage. Figure 4 shows the system response function of the framing camera. The amplitude of the voltage applied to the deflection electrode was varied from ± 150 to ± 75 V. The gate width of 480 psec was obtained at ± 150 V when the repetition rate was 4 MHz.

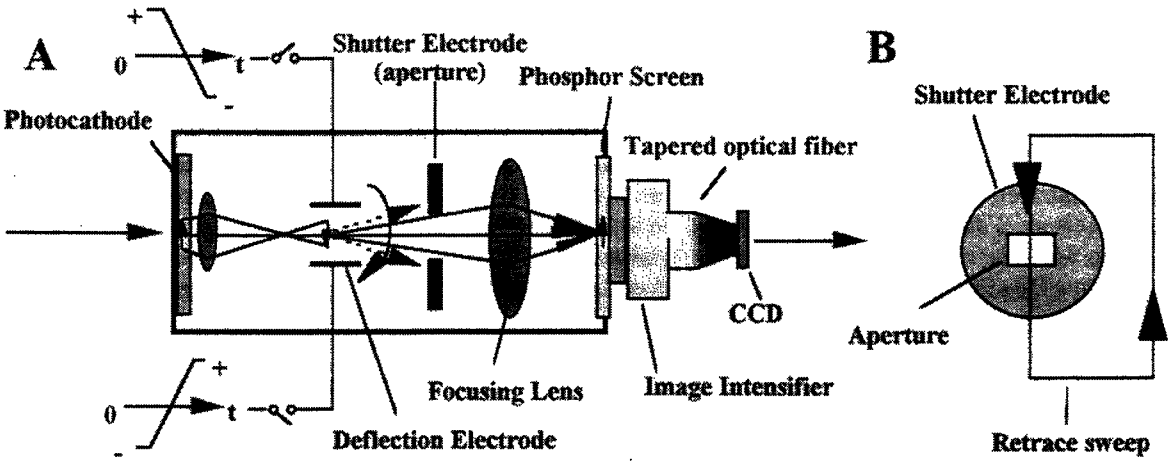

Fig. 2 A: A schematic diagram of the framing camera and procedure of the operation. Electric fields (ramp-shaped voltage) are applied to the pair of deflection electrodes, simultaneously (push-pull methods). B. Blanking procedure for retrace sweep. The beam swept by the deflection electrodes is shifted by the other deflection electrodes (not shown here), then reshifted back to the waiting position for the next sweep.

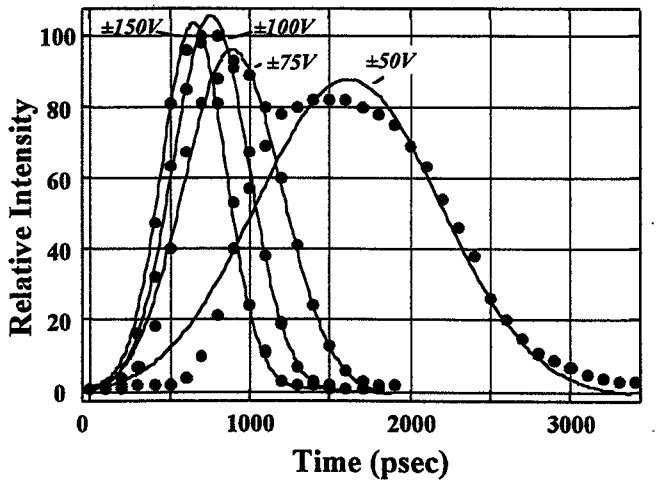

Fig.2 The system response function of the high-repetition framing camera. The gate of 480 psec at a 4 MHz repetition rate was obtained when the electric field of ±150 V was applied externally to the deflection electrodes. The gate width can be controlled by the amplitude of the applied electric field. The solid curves were drawn based on the assumption of a gauss response curve.

3. DUAL-VIEW ASSEMBLY

Dual-view microscopy, termed " W-microscopy" is the technique which can be used to observe two different images of an object simultaneously, and continuously through a single video camera.[11,12] In the former versions, a beam separator inserted between the microscope body and the camera was used to split the image-forming beam into two component beams, which can be separated based on the wavelength or direction of polarization. We recently developed the dual-view assembly to obtain two different images which have different delay time. Figure 3 shows a schematic diagram of the

14

assembly for producing two time-resolved images by utilizing the shutter camera. The microscopic fluorescence image excited by a pulsed laser at first passes through the depolarizer and is introduced into the polarizing beam splitter. One of the optical beam components is deflected by two mirrors and focused onto a slightly shifted position of the framing camera. The other component can be passed through the next beam splitter and focused on the side. A certain delay time between two images thus can be produced. The optical delay can be determined simply by measuring the optical path length between the center of the polarizing beam splitter cubes to the reflection mirror (L cm) with great accuracy. Variation of the delay time can be adjusted from 300 psec to 2 nsec, because the setting of L = 30 cm results in a delay of 1 nsec (delay time = 2 * L /30 nsec).

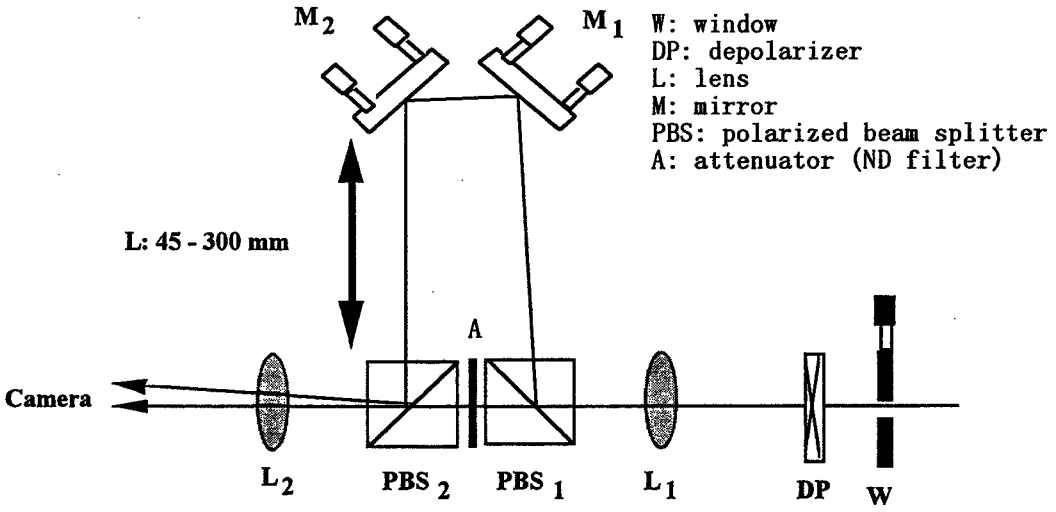

Fig. 3 A schematic diagram of a dual-view assembly. The delay is introduced by sliding two aluminized mirror in order to increase the light path by a known distance.

4. REAL-TIME FLUORESCENCE LIFETIME IMAGING MICROSCOPY

Figure 4 shows a schematic diagram of our fluorescence lifetime imaging microscope system. The instrument consists of (a) a pulsed light source, (b) epi-fluorescence microscope, (c) a dual-view assembly, (d) a high-repetition framing camera with an image intensifier and a CCD camera, and (e) a computer for controlling the experiments and for analyzing the fluorescence image. Figure 5 shows a schematic diagram of the two images produced by the dual-view assembly and captured in a single operation of the framing camera.

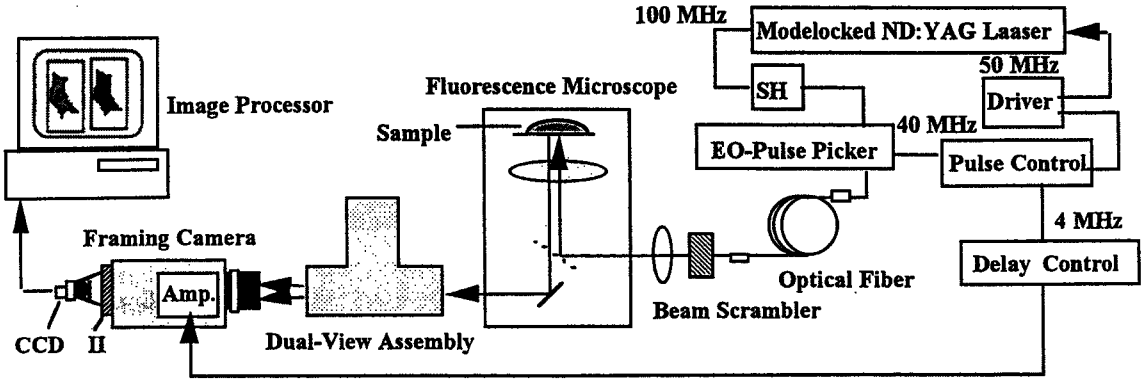

Fig. 4 A schematic diagram of the fluorescence lifetime imaigng microscope system.

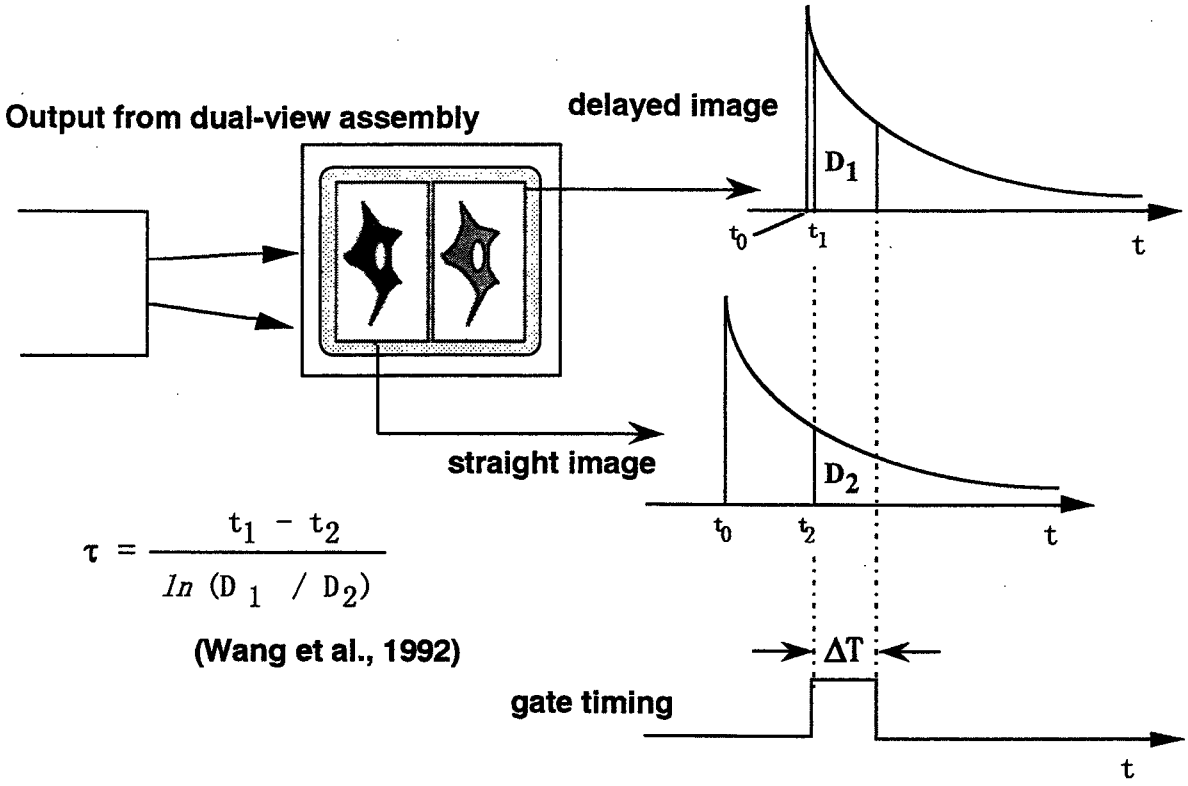

Fig. 5 Two images derived from the dual-view assembly can be captured at different time windows by a single framing camera simultaneously, then used for the analysis based on the assumption that the decay is single exponential.

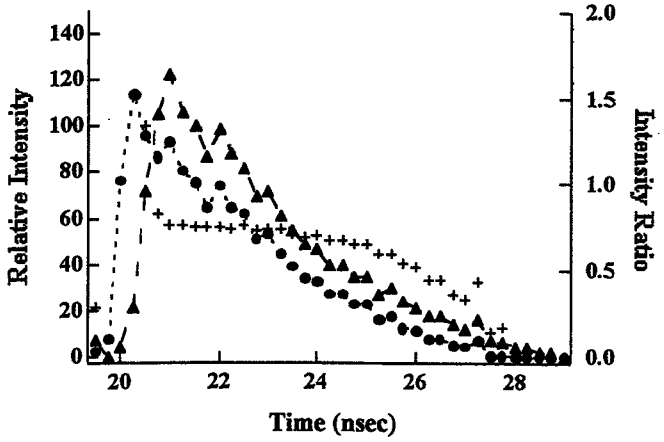

Fig. 6 Temporal profile of the rhodamine B solution in ethanol obtained under the fluorescence lifetime imaging microscope system. The average intensities of 200 x 200 pixels are presented, straight image (●), delayed image(▲), and the ratio(+).

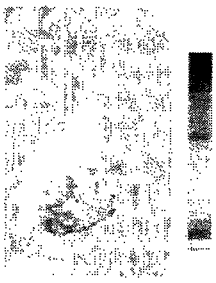

Hela cell stained with Rhodamine123

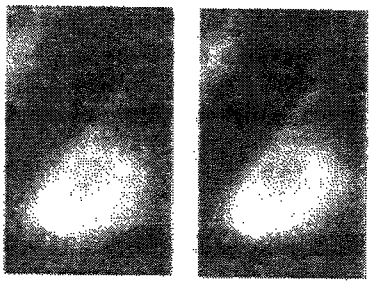

Fig. 7 A dual view image of a Hela cell stained with rhodamine 123 (0.1 mg/ml). This dye can penetrate into mitochondria in the cell. The lower left is a straight fluorescence image , and the lower right is a delayed fluorescence image. The upper image is a phase contrast image of the cell, which is superimposed on the intensity ratio image (not lifetime image, only the calculation of straight / delayed was carried out) after a certain threshold was given. The gray scale shows steps 1 to 2.

Preliminary examinations were carried out using rhodamine B solution in ethanol and a living cell. Temporal profiles of the decay for the average intensity (in an area of about 200 x 200 pixels) of rhodamine B solution are shown in Fig. 6. The delay was varied using a electrical delay controller. The two profiles were obtained simultaneously by using our system. A lifetime of approximately 4 nsec was calculated based on a mathematical analysis of each profile. The temporal profile of the intensity ratio, which is a function of lifetime, is also shown in the figure. The profile seems to be too complex to explain. The intensity ratio drastically decreased when the delay time increased. The lifetime of 2.3 nsec was calculated from the intensity ratio at the maximum and the relative plateau region (as an average value of 0.75 was used at the small delay time). Because our system is still unstable, the jitter is relatively large (about 500 psec jitter for 120 psec laser pulse, FWHH), so that corrections of image distortions and shadings are required for the image analysis of two windows in an image. A living cell also examined (Fig. 7). The two images with different delay times are shown in the figure. The delay time was adjusted to 0.67 nsec (L = 10 cm). The analysis of the lifetime measurements has not yet been completed. The program for accurate correction of distortion and shading for the two image is now under preparation.

5. DISCUSSION AND CONCLUDING REMARKS

In this report, we described our efforts towards developing a real-time fluorescence lifetime microscope system. The high-repetition gated camera and the dual-view assembly were developed for this purpose. The camera with a unique operating principle can be gated with a 480 psec shutter at a 4 MHz repetition rate. The gate width would be sufficient to resolve the lifetime of conventional fluorescent probes, and the S/N ratio of the image should be favorable due to a high repetition rate. The dual-view assembly enabled us to obtain two time-resolved images at different delay times simultaneously. The two images can be used for the analysis based on the assumption that the decay is single exponential.

We expect that this novel method will greatly rouse interest in the field of cell research.

We are currently in the process of improving the system. The real-time imaging of fluorescence lifetime should be feasible based on the concept of the dual-view assembly. Clegg et al[4] proposed a convenient method based on the suppression of fluorescence components with particular lifetime. This is easily accomplished by subtracting two images taken at phase settings 180° with respect to another. It is possible to apply our method to such frequency domain method, because the delay angle can be produced when the high repetition rate is required to measure the lifetime. This method can be applied fields other than biology, such as surface chemistry. The framing camera described here also can be used for a gain modulating camera with significant depth (>90%). The camera will be utilized for the alternative method, the frequency domain method. The outline of the system will be described in another paper.[13]

The framing camera described here utilizes streak camera technology based on a photoelectric effect and electron beam steering in the image converter. Our method would accomplish real-time imaging of fluorescence lifetime. Lifetime measurement based on the pulse method, in which accumulation of signal is carried out in a selective window, causes loss of almost all the information. We are now developing a new framing camera to produce several images at different time windows in a single operation (a multi-format framing camera). This camera will accumulate several images simultaneously, and reduce loss of information. The technology of the framing camera will play a major role in the ultrafast imaging fields.

6. ACKNOWLEDGEMENTS

We thank Mr. Hiruma (President of Hamamatsu Photonics K.K.) for his support and encouragement of this work. We also thank Mr. M. Yanagisawa (OPTO-DESIGN) and Mr. K. OTA (Luminex) for the design and building of the home-made laser system, and Mr. M. Takada (SIGMA KOKI) for the dual-view assembly. Participation in this project of Ms. A. Evenzahav, was supported by the Summer Institute Student program of the National Science Foundation (NSF) and the Japan International Science and Technology Exchange Center (JISTEC). This work was supported in part by Special Coordination Funds of the Science and Technology Agency of the Japanese Government.

7. REFERENCES

1. J. R. Lakowicz, I. Gryczynski, H. Szmacinski, K. Nowaczyk, "Recent advances in the uses of light in physics, chemistry, engineering, and medicine", Proc. SPIE, Vol. 1559, pp. 227-246, 1991.
2. R. M. Clegg, B. Feddersen, E. Gratton, and T. M. Jovin, "Time resolved imaging microscopy", Proc. SPIE, Vol. 1640, pp. 448-460, 1992.T. Oida, Y. Sako, and A. Kusumi, "Fluorescence lifetime imaging microscopy (flimscopy): Methodology development and application to studies of endosome fusion in single cells", Biophys. J., Vol. 64, pp. 676-685, 1993.
3. X. F. Wang, A. Periasamy, and B. Herman, D. M. Coleman, "Fluorescence lifetime imaging microscopy (FLIM): Instrumentation and applications", Critical Reviews in Anal. Chem., Vol. 23, pp. 369-395, 1992.
4. T. W.J. Gadella, Jr., Thomas M. Jovin and R. M. Clegg, "Fluorescence lifetime imaging microscopy (FLIM): Spatial resolution of microstructures on the nanosecond time scale", Biol. Chem., Vol. 48, pp. 221-239, 1993.
5. K. Kinoshita, "New picosecond electronic framing camera", Proc. SPIE, Vol. 569, pp. 2-, 1985.
6. K. Kinoshita, Y. Inagaki, and T. Nakamura, "Picosecond electronic framing camera", Proc. SPIE, Vol. 693, pp.2- , 1986.
7. K. Kinoshita, Y. Inagaki, S. Yamabe, A. Takahashi, H. Itoh, M. Koishi, H. Mizushima, and T. Hayakawa, "High-repetition shutter camera", Proc. SPIE, Vol. 2513, pp. 41-49, 1994.
8. M. Suyama, K. Kinoshita, T. Okada, and M. Ito, "Streak tube having ultra-heigh deflection sensitivity", Proc. SPIE, Vol. 1757, pp. 19- 31, 1992.
9. A. Takahashi, M. Nishizawa, Y. Inagaki, M. Koishi, and K. Kinoshita, "New femtosecond streak camera with temporal resolution of 180 fs", Proc. SPIE, Vol. 2116, pp. 275-284, 1994.
10. K. Kinosita, Jr., H. Itoh, S. Ishiwata, K. Hirano, T. Nishizaka, and T. Hayakawa, "Dual-view microscopy with a single camera: real-time imaging of molecular orientations and calsium", J. Cell Biol. Vol. 115, pp. 67-73, 1991.

11. K. Suzuki, Y. Tanaka, Y. Nakajima, K. Hirano, H. Itoh, H. Miyata, T. Hayakawa, and K. Kinosita, Jr., "Spatiotemporal relationships among early events of fertilization in sea urchin eggs revealed by multiview microscopy", Biophys. J., Vol.68, pp. 739-748, 1995.
12. H. Itoh, A. Evenzahav, K. Kinoshita, Y. Inagaki, H. Mizushima, A. Takahashi, and T. Hayakawa, "Use of a gain modulating framing camera for time-resolved imaging of cellular phenomena", Optical Tomography and Spectroscopy of Tissue: Theory, Instrumentation, Model, and Human Studies II, Conference Chairs: Britton Chance, Proc. SIPE, 1997.

Corrections

7. REFERENCES

1. J. R. Lakowicz, I. Gryczynski, H. Szmacinski, K. Nowaczyk, "Recent advances in the uses of light in physics, chemistry, engineering, and medicine", Proc. SPIE, Vol. 1559, pp. 227-246, 1991.
2. R. M. Clegg, B. Feddersen, E. Gratton, and T. M. Jovin, "Time resolved imaging microscopy", Proc. SPIE, Vol. 1640, pp. 448-460, 1992.
3. T. Oida, Y. Sako, and A. Kusumi, "Fluorescence lifetime imaging microscopy (flimscopy): Methodology development and application to studies of endosome fusion in single cells", Biophys. J., Vol. 64, pp. 676-685, 1993.
4. X. F. Wang, A. Periasamy, and B. Herman, D. M. Coleman, "Fluorescence lifetime imaging microscopy (FLIM): Instrumentation and applications", Critical Reviews in Anal. Chem., Vol. 23, pp. 369-395, 1992.
5. T. W.J. Gadella, Jr., Thomas M. Jovin and R. M. Clegg, "Fluorescence lifetime imaging microscopy (FLIM): Spatial resolution of microstructures on the nanosecond time scale", Biol. Chem., Vol. 48, pp. 221-239, 1993.
6. K. Kinoshita, "New picosecond electronic framing camera", Proc. SPIE, Vol. 569, pp. 2-, 1985.
7. K. Kinoshita, Y. Inagaki, and T. Nakamura, "Picosecond electronic framing camera", Proc. SPIE, Vol. 693, pp.2- , 1986.
8. K. Kinoshita, Y. Inagaki, S. Yamabe, A. Takahashi, H. Itoh, M. Koishi, H. Mizushima, and T. Hayakawa, "High-repetition shutter camera", Proc. SPIE, Vol. 2513, pp. 41-49, 1994.
9. M. Suyama, K. Kinoshita, T. Okada, and M. Ito, "Streak tube having ultra-heigh deflection sensitivity", Proc. SPIE, Vol. 1757, pp. 19- 31, 1992.
10. A. Takahashi, M. Nishizawa, Y. Inagaki, M. Koishi, and K. Kinoshita, "New femtosecond streak camera with temporal resolution of 180 fs", Proc. SPIE, Vol. 2116, pp. 275-284, 1994.
11. K. Kinosita, Jr., H. Itoh, S. Ishiwata, K. Hirano, T. Nishizaka, and T. Hayakawa, "Dual-view microscopy with a single camera: real-time imaging of molecular orientations and calsium", J. Cell Biol. Vol. 115, pp. 67-73, 1991.
12. K. Suzuki, Y. Tanaka, Y. Nakajima, K. Hirano, H. Itoh, H. Miyata, T. Hayakawa, and K. Kinosita, Jr., "Spatiotemporal relationships among early events of fertilization in sea urchin eggs revealed by multiview microscopy", Biophys. J., Vol.68, pp. 739-748, 1995.
13. H. Itoh, A. Evenzahav, K. Kinoshita, Y. Inagaki, H. Mizushima, A. Takahashi, and T. Hayakawa, "Use of a gain modulating framing camera for time-resolved imaging of cellular phenomena", Optical Tomography and Spectroscopy of Tissue: Theory, Instrumentation, Model, and Human Studies II, Conference Chairs: Britton Chance, Proc. SIPE, 1997.

Journal of Muscle Research Cell Motility
Vol. 17, 281 (1996) Abstr.

Regulation of sliding movement of reconstituted thin filaments in an *in vitro* motility assay system

Y. FUJIKI and S. ISHIWATA
Department of Physics, School of Science and Engineering, Waseda University, 3-4-1 Okubo, Shinjuku-ku, Tokyo 169, Japan

Muscle contraction is regulated by the concentration of free Ca^{2+}. The Ca^{2+}-binding to troponin switches on the state of thin filaments (Ebashi & Endo, *Prog. Biophys. Mol. Biol.* 18, 123–83, 1968). It is known that even in the absence of Ca^{2+}, 'switching on' occurs by lowering the concentration of ATP (Weber & Murray, *Physiol. Rev.* 53, 612–73, 1973) or by adding high concentrations of ADP (Shimizu *et al., Biophys. J.* 61, 1087–98, 1992). To study this regulatory mechanism, we examined the effect of the number of cross-bridges on pCa-sliding velocity relation in an *in vitro* motility assay system (Solution A; 50 mM ionic strength, 1 mM ATP, 3 mM free Mg^{2+}, 20 mM imidazole-HCl (pH 7.0), 10 mM DTT, 0.5 mg ml^{-1} BSA, 27° C) using the reconstituted thin filaments composed of F-actin, tropomyosin and troponin. The experiments were carried out under the following conditions of various concentrations of HMM, MgATP, MgADP, free Ca^{2+} (pCa = 5.4–9.0) and Pi: (1) the concentration of HMM perfused into a glass surface, 30–200 μg ml^{-1}; (2) the concentration of MgADP, 0–4 mM; (3) the concentration of MgATP, 10 μM–1 mM; (4) 5 mM Pi in the presence of 0.5 mM MgATP and 2 mM MgADP. In the absence of MgADP, the increase in the HMM concentration slightly shifted the pCa-velocity relation to the high pCa side and slightly decreased the cooperativity (Hill coefficient, n_H). In the presence of 1 mM MgATP and 4 mM MgADP, the increase in the HMM concentration shifted pCa-velocity relation to the high pCa side, such that the Ca^{2+}-sensitivity was increased, whereas the cooperativity was decreased (30 μg ml^{-1} HMM, $pCa_{50} = 6.6$, $n_H = 2.3$; 100 μg m^{-1} HMM, $pCa_{50} = 7.1$, $n_H = 1.4$; 200 μg ml^{-1} HMM, $pCa_{50} = 7.3$, $n_H = 1.1$). The similar results could be also obtained by the decrease of the MgATP concentration at 200 μg ml^{-1} HMM in the absence of MgADP (1 mM MgATP, $pCa_{50} = 6.6$, $n_H = 2.8$; 0.2 mM MgATP, $pCa_{50} = 6.7$, $n_H = 2.6$; 50 μM MgATP, $pCa_{50} = 6.8$, $n_H = 1.6$; 10 μM MgATP, $pCa_{50} = 7.2$, $n_H = 1.2$). The addition of 5 mM Pi in the presence of 0.5 mM MgATP and 2 mM MgADP shifted the pCa-velocity relation to the lower pCa side, such that the Ca^{2+}-sensitivity was decreased, whereas the cooperativity was increased. But under the condition of SPOC (Okamura & Ishiwata, *J. Muscle Res. Cell Motil.* 9, 111–19, 1988) (1 mM ATP in solution A was replaced with 0.2 mM MgATP, 4 mM MgADP, 5 mM Pi), the pCa-velocity relation became nearly independent of pCa. Thus, the increase in the number of strong binding cross-bridges appears to increase the Ca^{2+} sensitivity, whereas decreased the cooperativity in the regulation of sliding movement. The number of interacting cross-bridges under each condition should be directly measured by microscopic manipulation of thin filaments with optical tweezers in future (see Nishizaka *et al., Nature*, 377, 251–4, 1995).

Journal of Muscle Research Cell Motility
Vol. 17, 282 (1996) Abstr.

Structure of acto-myosin rigor complex analysed by fluorescence resonance energy transfer

I. SHIN[1], K. YASUDA[2] and S. ISHIWATA[1]
[1]*Department of Physics, School of Science and Engineering, Waseda University, 3-4-1 Okubo, Shinjuku-ku, Tokyo 169 and* [2]*Advanced Research Laboratory, Hitachi Ltd., Hatoyama, Saitama 350-03, Japan*

Fluorescence resonance energy transfer (FRET) spectroscopy has been used to estimate the distance between heads of myosin (subfragment-1 (S-2) or heavy meromyosin (HMM)) which are attached to F-actin (FA) or F-actin-tropomyosin (FA-TM) complex under the rigor condition (0.1 M KCl, 1 mM $MgCl_2$, 20 mM Tris-HCl (pH 8.0), 20° C). Each sulfhydryl group (SH1; Cys 707) on myosin heads was labelled with either N-(iodoacetyl)-N'-(1-sulfo-5-naphthyl)-ethylenediamine (IAEDANS) employed as a fluorescence energy donor (D) or with 5-(iodoacetamido)fluorescein (IAF) as a fluorescence energy acceptor (A). Then, the fluorescence intensity of IAEDANS and the light scattering intensity of the solution were measured simultaneously every time after FA (or FA-TM) was stepwise added to the solution containing the mixture of either S-1 (D) and S-1 (A), S (D) and HMM (A), HMM (D) and S-1 (A), of HMM (D) and HMM (A). The inter-molecular distances between the heads of S-1 or HMM were estimated to be about 6 nm according to the model calculation, in which the binding constant of S-1 (HMM) and FA was assumed to be 10^7 (5×10^7)/M that was confirmed to simulate the change in the light scattering intensity. Then intra-molecular inter-head distance between the two heads of HMM was estimated using the HMM molecule which was heterogeneously labelled with IAEDANS and IAF. The inter-molecular distances between HMM molecules thus examined were about 6.1 nm, equal to the values estimated above. On the other hand, intra-molecular inter-head distance, about 7.7 nm, was appreciably longer than this value. There will be at least the following two ways to interpret this result: (1) the intra-molecular distance is in fact longer than the inter-molecular distances because of the distortion of the structure of the FA-HMM rigor complex, and (2) this is only apparent and the binding constant between HMM and FA was lowered when the heads were heterogeneously labelled with two different probes. Next, we applied the above technique S-1 and FA-TM complex; the data of FRET and the light scattering intensity could be explained by assuming that the binding constant of S-1 and FA-TM complex is five times greater than that of S-1 and FA, while the distance between S-1 molecules attached to the FA-TM complex is the same, i.e. about 6 nm, as that in the absence of TM. This technique is useful to study of the inter-molecular and the intra-molecular inter-head distances of myosin molecules attached to FA under various conditions.

Journal of Muscle Research Cell Motility

Vol. 18, 491 (1997) Abstr.

Temperature dependence of association and dissociation rate constants of rhodamine phalloidin with actin filaments

M. HOTTA[1] and S. ISHIWATA[1,2]

[1]*Department of Physics, School of Science and Engineering and* [2]*Advanced Research Institute for Science and Engineering, Waseda University, 3-4-1 Okubo, Shinjuku-ku, Tokyo 169, Japan*

Phalloidin, a heptapeptide toxin extracted from the mushroom *Amanita phalloides*, binds tightly and specifically to polymerized actin, and fluorescent derivatives of phalloidin are frequently used to visualize single actin filaments in various studies. Recently, we have studied the effects of temperature on the sliding movement of F-actin in an *in vitro* motility assay system (Kato *et al.*, *Biophysics* (Japanese) 36 suppl., S71, 1996), where the temperature on F-actin was estimated from thermal quenching of the fluorescence intensity of rhodamine phalloidin (RhPh). Accordingly, understanding of the temperature dependence of kinetics of RhPh binding to F-actin has become indispensable. In the present study, the effects of temperature on the binding between F-actin and phalloidin have been studied in solution A (25 mM KCl, 4 mM $MgCl_2$, 1 mM EGTA, 1 mM ATP, 25 mM imidazole-HCl, pH 7.4) according to de la Cruz and Pollard (*Biochemistry* 33, 14387–92, 1994). First, we have determined the dissociation rate constant (k_-) of RhPh from F-actin at various temperatures. The time course of the decrease in the fluorescence intensity was measured after the addition of non-fluorescent phalloidin (200-fold molar excess of RhPh). The decrease in the fluorescence intensity was attributed to the dissociation of RhPh from F-actin. Temperature was changed in the range between 25 and 45° C, and the effects of bound heavy meromyosin (HMM) or tropomyosin (TM) in solution A without ATP were also examined. Second, we have determined the association rate constant (k_+) of RhPh with F-actin at various temperatures. The time course of the increase in the fluorescence intensity was measured after the addition of RhPh to F-actin. In this case, the molar ratio of actin and RhPh was 100–500. A second-order reaction could be analysed as a pseudo-first-order process, $k_{obs} = k_+[A] + k_-$, where k_{obs} is the experimentally observed rate constant and [A] is the concentration of actin. Temperature was changed in the range between 20 and 40° C. With increasing temperature, both dissociation and association rate constants increased, which were fitted to the Arrhenius equation. The association rate constant increased from 6×10^3 M^{-1} s^{-1} at 20° C to 5×10^4 M^{-1} s^{-1} at 40° C, and the dissociation rate constant increased from 2×10^{-4} s^{-1} at 25° C to 3×10^{-3} s^{-1} at 45° C. The rate of the decrease in the fluorescence intensity due to the dissociation of RhPh every 10 s exposure at 45° C was estimated to be at most 3%. Binding of HMM and TM and the presence or absence of ATP did not affect the dissociation rate constants. The binding constant estimated from the ratio of the association and dissociation rate constants was about 6×10^7 M^{-1} at 25° C and decreased to about 3×10^7 M^{-1} at 40° C.

Biophysical Journal
Vol. 72, A183 (1997) Abstr.

Tu-Pos260

THERMAL ACTIVATION OF ACTOMYOSIN MOTORS WITH TEMPERATURE-PULSE MICROSCOPY. ((H. Kato[1], T. Nishizaka[1], T. Iga[1], K. Kinosita,Jr.[2], S. **Ishiwata**[1,3])) Department of Physics, School of Science and Engineering, Waseda University, 3-4-1 Okubo, Shinjuku-ku, Tokyo 169, Japan[1]; Department of Physics, Faculty of Science and Technology, Keio University, 3-14-1 Hiyoshi, Kohoku-ku, Yokohama 223, Japan[2]; Advanced Research Institute for Science and Engineering, Waseda University, Japan[3].

Microscopic real-time imaging of temperature on sliding actin filaments in an in vitro motility assay system (heavy meromyosin (HMM) was used as motor proteins) has been achieved by monitoring the fluorescence intensity of rhodamine phalloidin attached to actin filaments. Temperature pulse could be locally and reversibly introduced by illuminating metal particles with an infrared laser light (λ = 1.053 μm) by splitting the laser beam used for the optical tweezers. Combining these techniques (temperature-pulse microscopy: TPM), reversible increase and decrease of an order of magnitude of sliding velocity and tension generation were observed with repetitive temperature modulation between about 20 ℃ and 45 ℃. An abrupt displacement of sliding actin filaments as large as 2 to 0.2 μm occurred following temperature pulse (from 18 to 45 ℃ on average) in a duration as short as 1/16 to 1/128 s, respectively, which corresponds to the sliding velocity of 26 to 32 μ m/s. Judging from the fact that Q_{10} of ATPase per head of HMM is larger than 2, several to only a few ATPase cycles (even a fraction of cycle) appear to occur during these short pulses. This may imply that the displacement is proportional to the number of ATPase cycles even to a fraction of cycle. The TPM should be applicable to the studies on spatio-temporal response of supramolecules, organelles and living cells over a wide range of thermal modulation.